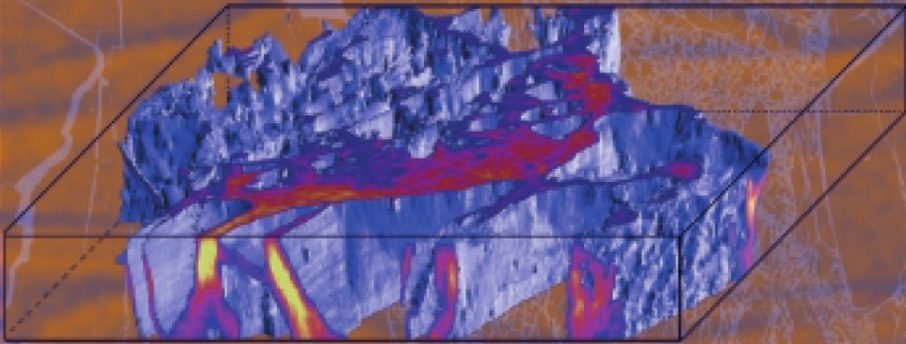


Mervyn S. Paterson  
Teng-fong Wong

# Experimental Rock Deformation – The Brittle Field



Second Edition

 Springer

---

Mervyn S. Paterson

Teng-fong Wong

**Experimental Rock Deformation – The Brittle Field**

---

Mervyn S. Paterson  
Teng-fong Wong

# **Experimental Rock Deformation – The Brittle Field**

Second, Completely Revised and Updated Edition

With 87 Figures

 Springer

---

## Authors

### Dr. Mervyn S. Paterson

Research School of Earth Sciences  
The Australian National University  
Canberra 0200  
Australia

### Dr. Teng-fong Wong

Department of Geosciences, ESS Building  
State University of New York at Stony Brook  
Stony Brook, NY 11794-2100  
USA

The first edition of this book was published by Springer-Verlag in 1977 within the book series 'Minerals and Rocks' (ISBN 3-540-08835-0).

Library of Congress Control Number: 2004117900

ISBN-10 3-540-24023-3 Springer Berlin Heidelberg New York  
ISBN-13 978-3-540-24023-5 Springer Berlin Heidelberg New York

This work is subject to copyright. All rights are reserved, whether the whole or part of the material is concerned, specifically the rights of translation, reprinting, reuse of illustrations, recitations, broadcasting, reproduction on microfilm or in any other way, and storage in data banks. Duplication of this publication or parts thereof is permitted only under the provisions of the German Copyright Law of September 9, 1965, in its current version, and permission for use must always be obtained from Springer. Violations are liable to prosecution under the German Copyright Law.

**Springer is a part of Springer Science+Business Media**

springeronline.com

© Springer-Verlag Berlin Heidelberg 2005

Printed in The Netherlands

The use of general descriptive names, registered names, trademarks, etc. in this publication does not imply, even in the absence of a specific statement, that such names are exempt from the relevant protective laws and regulations and therefore free for general use.

Cover design: Erich Kirchner, Heidelberg

Typesetting: Büro Stasch (stasch@stasch.com), Klaus Häring, Bayreuth

Production: Luisa Tonarelli

Printing: Krips bv, Meppel

Binding: Litges & Dopf, Heppenheim

Printed on acid-free paper 32/2132/LT – 5 4 3 2 1 0

---

## Preface

This monograph deals with the part of the field of experimental rock deformation that is dominated by the phenomena of brittle fracture on one scale or another. Thus a distinction has been drawn between the fields of brittle and ductile behaviour in rock, corresponding more or less to a distinction between the phenomena of fracture and flow. The last chapter deals with the transition between the two fields. In this new edition an attempt has been made to take into account new developments of the last two and a half decades. To assist in this project, the original author greatly appreciates being joined by the second author.

The scope of the monograph *is* limited to the mechanical properties of rock viewed as a material on the laboratory scale. Thus, the topic and approach is of a “materials science” kind rather than of a “structures” kind. We are dealing with only one part of the wider field of rock mechanics, a field which also includes structural or boundary value problems, for example, those of the stability of slopes, the collapse of mine openings, earthquakes, the folding of stratified rock, and the convective motion of the Earth’s mantle. One topic thus excluded is the role of jointing, which it is commonly necessary to take into account in applications in engineering and mining, and probably often in geology too. Shock phenomena have also not been covered.

We attempt to bring out the principal aspects of brittle behaviour, with special attention to the fundamental physical aspects. We hope, in doing so, to provide also a useful introduction to the basics of rock properties for engineering and earth science applications. We have tried to present the material in a way that will enable advanced students and others not specialized in this field to grasp the context, or to guide them to where relevant background material is to be found (for example, many references have been made to appropriate sections in Jaeger and Cook (1979)). Thus *we* hope that the monograph will be useful to students and non-specialists as well as to those actively engaged in research in this field.

The primary aim of the book is to set down the state of current knowledge of the *brittle* mechanical properties of rock as determined in laboratory experiments, covering also the history of the developments leading to this state and giving a fairly comprehensive listing of the published material. The presentation has therefore something of the character of a guided tour of the literature, and it is hoped that it will serve enduringly as a reference source.

For the new edition one entirely new chapter (Chapt. 6) has been added to deal with theoretical developments that mainly post-date the first edition. Extensive revision has also been done in Chapters 5, 8 and 9, while the remaining chapters have

been revised in minor ways, incorporating new references. The first edition covered the period up to about 1977 with an attempt to give a comprehensive coverage of the literature on the main topics. In view of the exponentially expanding publication rate, it has not been feasible to attempt anything approaching complete coverage of the literature since 1977 in the new edition. However, we have attempted to include what have appeared to us to be the main contributions that have appeared in the interim. We apologize for omissions or important papers that we have overlooked.

As far as possible, we have referred to publications that are generally available in libraries and have avoided reference to theses and reports not having wide distribution. We have also, on the whole, avoided reference to abstracts of papers presented to meetings but we have made a general exception in the case of EOS (Transactions of the American Geophysical Union) where the material is of particular interest and we have been unable to trace its publication in full.

The S. I. system of units is used and conversion has been made to these units where necessary in presenting data. The quantity most often quoted is stress, for which the most convenient unit is the meganewton per square metre, called the megapascal (MPa). One megapascal is equal to 10 bars, so to convert from MPa to bars simply add one zero. Useful conversions are:

$$\begin{aligned}
 1 \text{ MPa} &= 10 \text{ bar} = 145 \text{ lb in}^{-2} \\
 100 \text{ MPa} &= 1 \text{ kbar} = 6.47 \text{ imperial ton in}^{-2} \\
 4.18 \text{ kJ mol}^{-1} &= 1 \text{ kcal mol}^{-1} = 0.0434 \text{ eV atom}^{-1} \\
 1 \text{ J m}^{-2} &= 1000 \text{ erg cm}^{-2}
 \end{aligned}$$

The sign convention adopted for stress and strain is that compressive stress is positive and shortening strain is positive. Thus, if  $l$  is the length and  $\Delta l$  is a small increase in the length, we define the infinitesimal strain as  $\epsilon = \Delta l/l$ . Similarly if  $v$  is the volume and  $\Delta v$  a small increase in volume, we define the volumetric strain  $\epsilon_v$  as  $\epsilon_v = \Delta v/v$ . By adopting these conventions in both stress and strain, the elastic constants and moduli remain positive quantities.

We are grateful to Drs. W. F. Brace, E. T. Brown, M. Friedman, R. C. Liebermann, S. A. F. Murrell, and E. H. Rutter for critical reading of the original individual chapters and to Drs. N. Beeler, B. Evans, P. Meredith and J. Rudnicki for reviews of the new material. We are also grateful to our colleagues for many useful discussions and criticisms. Finally special thanks go to our wives for their understanding, forbearance and support during the rather long gestation of this revision.

*Canberra and Stony Brook, September 2004*      *M. S. Paterson*  
*Teng-fong Wong*

---

# Contents

<b>1</b>	<b>Introduction</b>	<b>1</b>
<b>2</b>	<b>Experimental Procedures</b>	<b>5</b>
2.1	The Triaxial Test	5
2.1.1	Principle and Terminology	5
2.1.2	Triaxial Testing Apparatus	7
2.1.3	Preparation and Jacketing of Specimens	12
2.1.4	Measurements, Control, and Data Reduction	13
2.2	Other Types of Tests	15
<b>3</b>	<b>Experimental Studies on the Brittle Fracture Stress</b>	<b>17</b>
3.1	Introduction	17
3.2	Types of Fractures	18
3.3	Observed Stresses at Brittle Failure	21
3.4	Influence of Strain Rate, Temperature, and Time	27
3.5	Size and Shape Effects	30
3.6	Influence of Intermediate Principal Stress	35
3.7	Anisotropy	38
3.7.1	Observations	38
3.7.2	Theoretical Analysis	41
<b>4</b>	<b>Griffith Theory of Brittle Failure</b>	<b>45</b>
4.1	Introduction	45
4.2	Uniaxial Tension	46
4.3	Uniaxial Compression and Biaxial Stresses	49
4.4	Triaxial Stresses	51
4.5	Modified Griffith Theory (Closed Cracks)	53
4.6	Extension of the Griffith Approach to Other Modes of Localized Inelastic Failure	55
4.6.1	Shear Failure	55
4.6.2	Compressive Failure	55
4.7	General Comment on Griffith-Type Theories	56

<b>5</b>	<b>Evolution of Physical Properties during Brittle Failure</b>	59
5.1	Introduction	59
5.2	Pre-peak and Post-peak Behaviour	60
5.2.1	Role of the Testing Machine	60
5.2.2	Complete Force-Displacement Curves	62
5.3	Volume Changes	68
5.4	Elastic Wave Speeds and Attenuation	76
5.4.1	General	76
5.4.2	Background Theory and Observation	77
5.4.3	Stress-Induced Changes in Elastic Wave Speeds	81
5.4.4	Attenuation	87
5.5	Transport Properties	88
5.6	Acoustic Emission	93
5.7	Microscopical Observations	99
5.7.1	General	99
5.7.2	Observational Methods	99
5.7.3	Initial Structure	101
5.7.4	Effects of Stressing	105
5.8	A Synoptic View of Brittle Failure	111
<b>6</b>	<b>Micromechanics of Brittle Fracture</b>	115
6.1	Introduction	115
6.2	Micromechanical Theory for Compact Rock	116
6.2.1	Initiation of Stress-Induced Microcracking	116
6.2.2	Microcrack Propagation and Stability	119
6.2.3	Microcrack Interaction and Damage Mechanics of Brittle Failure	120
6.2.4	General Comments on Micromechanics-Based Damage Mechanics Models for Compact Rock	127
6.2.5	Stochastic Model of Brittle Failure in Compact Rock	130
6.2.6	Time-Dependent Failure of Compact Rock	133
6.3	Micromechanical Theory for Porous Rock	134
6.3.1	General	134
6.3.2	Strongly Cohesive Porous Rock	134
6.3.3	Weakly Cohesive Porous Rock	135
6.4	Localization Theory	137
6.4.1	Application of Plasticity Theory and Bifurcation Analysis	137
6.4.2	Comments on Localization Theory	143
<b>7</b>	<b>The Role of Pore Fluids</b>	147
7.1	Introduction	147
7.2	The Notion of Effective Stress	148
7.3	Elastic Properties of Porous Media	149
7.3.1	Linear Poroelasticity	149
7.3.2	Experimental Measurement of Poroelastic Properties	152
7.4	Brittle Failure – Experimental	155
7.4.1	Drained Tests	155



7.4.2	Undrained Tests .....	158
7.4.3	Chemical Effects .....	160
7.5	Brittle Failure – Theory of Pore Pressure Effects .....	161
<b>8</b>	<b>Friction and Sliding Phenomena .....</b>	<b>165</b>
8.1	Introduction .....	165
8.2	Coefficient of Friction .....	166
8.2.1	General .....	166
8.2.2	Influence of Variables .....	168
8.3	Phenomenology of Frictional Behaviour .....	173
8.3.1	General .....	173
8.3.2	Time Dependence of Static Friction .....	173
8.3.3	Velocity Dependence of Kinetic Friction .....	176
8.3.4	Rate- and State-Dependent Friction .....	183
8.3.5	Experimental Observations on the Occurrence of Stick-Slip .....	188
8.3.6	Influence of Friction Constitutive Behaviour and Machine Stiffness on Stick-Slip .....	194
8.3.7	Nucleation and Propagation of Dynamic Shear Rupture .....	196
8.4	Physical Aspects of Rock Friction .....	198
8.4.1	Frictional Slip, Wear and the Formation of Gouge .....	198
8.4.2	Gouge Deformation .....	200
8.4.3	Physical Factors Determining the Frictional Strength .....	203
8.4.4	Physical Basis for the Direct Effect (Velocity Parameter $a$ ) .....	205
8.4.5	Physical Basis for the Ageing and Evolution Effects (Parameters $\beta$ and $b$ ) .....	207
<b>9</b>	<b>Brittle-Ductile Transition .....</b>	<b>211</b>
9.1	Introduction .....	211
9.2	Experimental Observations .....	212
9.2.1	Role of Confining Pressure .....	212
9.2.2	Role of Temperature and Strain Rate .....	217
9.2.3	Physical Properties and Pressure Sensitivity .....	219
9.2.4	Microstructural Observations .....	221
9.3	Physical Basis of the Brittle-Ductile Transition .....	222
9.3.1	Preliminaries .....	222
9.3.2	Brittle-Ductile Transition with Increasing Pressure .....	225
9.3.3	Continuum Models and Localization Analysis .....	228
9.3.4	Influence of Temperature, Strain Rate and Water .....	232
9.4	Ductile to Brittle Transitions .....	233
9.4.1	High Pressure Embrittlement .....	233
9.4.2	High Temperature Embrittlement .....	234
<b>A1</b>	<b>Appendix 1 • Fracture Mechanics .....</b>	<b>239</b>
A1.1	Stress Intensity Analysis .....	239
A1.2	Critical Parameters for Failure .....	242
A1.3	Dynamic and Kinetic Effects .....	244

<b>A2 Appendix 2 · Plasticity Theory and Localization Analysis</b> .....	247
A2.1 Introduction .....	247
A2.2 Constitutive Relations for a Material without Pressure Dependence or Dilatancy .....	248
A2.3 Constitutive Model for Dilatant, Pressure-Sensitive Materials .....	250
A2.4 Bifurcation, Instability and Shear Localization .....	254
<b>A3 Appendix 3 · Constitutive Relations for Friction</b> .....	257
A3.1 Introduction .....	257
A3.2 Friction Law .....	258
A3.3 Evolution Law .....	259
A3.4 Time-Dependent Evolution during Stationery Contact .....	261
A3.5 Analysis of Frictional Stability – Stick-Slip .....	262
A3.6 Influence of Normal Stress and Temperature .....	263
<b>References</b> .....	267
<b>Index</b> .....	335

## Introduction

A knowledge of the mechanical properties of rocks is fundamental to several branches of both Earth science and engineering. However, depending on the environmental conditions and on the scale in space and time, many different aspects of mechanical behaviour may be involved. This diversity ranges from effects associated with the very small, short-term, essentially elastic strains in earthquake waves to the large, slow, irreversible deformations of the Earth's crust and mantle that are involved in the gross tectonic processes of ocean-floor spreading and continental evolution.

Because of the variety of viewpoints, research on the mechanical behaviour of rocks has tended to develop somewhat independently in several directions not closely related to each other. In particular, there has tended to be a separation between studies undertaken because of interest in civil engineering and mining and studies aimed at geologic understanding. There are also important aspects of rock behaviour that involve porosity of the rock and the movement of fluids through the pore structure, with applications to fields such as petroleum engineering, nuclear waste storage and environmental pollution problems (Committee on Fracture Characterization and Fluid Flow 1996).

In the engineering fields the problems are commonly concerned with possible failure to support a load, e.g., in a mine opening or slope, or with the avoidance of excessive displacement, as in the case of a dam foundation. In either case, it is rare that large strains are involved, but a knowledge of fracture properties is usually vital. Thus, engineering rock mechanics tends to be preoccupied with brittle behaviour.

In the Earth sciences, brittle behaviour is also of interest, as in faulting and the mechanics of earthquakes. However, now there is a wide range of phenomena, extending from the small-scale penetrative deformation studied by the geologist in the hand specimen to the large-scale deformations involved in major tectonic processes, which depend on the ability of rock to undergo large plastic deformations. So the rock mechanics problems in the Earth sciences often also involve those of ductile behaviour. Thus, the fields of engineering and geologic rock mechanics are not exclusively distinguished by their respective concerns with brittle and ductile behaviour, and any research on mechanical properties may be potentially of interest in either field.

The task of establishing the mechanical properties of rocks is undertaken mainly in the laboratory. It constitutes an important branch of materials science, both for the potential practical applications and for the intrinsic scientific interest of exploring

other classes of materials, especially where silicon-oxygen bonding or pore structure is involved. However, attention should be drawn to an important constraint of scale in applying laboratory results to practical situations.

In most bodies of rock there are structural features, notably joints, on a coarser scale than the scale of specimens used in laboratory tests, and these features often have an important influence on the mechanical behaviour of the body of rock. In the extreme, the strength of the rock mass may be determined almost entirely by the properties of the joints, the blocks between the joints behaving largely as rigid elements. This circumstance leads to a distinction being made between the behaviour of the “rock material” and the behaviour of the “rock mass” (cf. Jaeger and Cook 1979). The laboratory tests normally give information about the properties of the rock material itself but other steps may have to be taken to determine the properties of the rock en masse. Whether such a distinction between rock material and rock mass need be made in particular cases in practice has to be decided in the individual situation; it may not always be of significance, especially where the processes involved are pervasive down to a fine scale, as with microcracking or crystal plasticity. The effects of scale tend, in general, to be of greater importance in brittle behaviour than in ductile but must always be borne in mind in extrapolating to practical situations.

In treating the laboratory study of inelastic behaviour of rocks, the major division of the subject is naturally that into the brittle and ductile fields. The distinction between brittle and ductile behaviour is in the first place a macroscopic one, depending on whether or not the rock is capable of undergoing a substantial permanent strain without macroscopic fracture. The distinction is not in all respects a sharp one, especially when microscopic processes are also taken into account, but it is nevertheless a very useful one. At the same time, it is important to bear in mind that brittleness or ductility depends in a vital way on the environmental conditions, such as pressure, temperature, and strain rate; the same rock may be brittle under some circumstances and ductile under others.

The present volume deals only with the field of brittle behaviour. The main emphasis will be on the results of laboratory and related theoretical investigations on the mechanical properties of rock under the conditions in which it behaves as a brittle material, although the factors leading to the brittle-ductile transition are also considered in the concluding chapter. In brief, the aim is to review here what we know about rock as a relatively brittle material. In many cases, a broad distinction will be made between compact and porous rocks. The former are often of igneous or metamorphic origin, although some well-cemented sediments also fall into this category, while the latter are often sedimentary rocks. *Compact rocks* are those of very small porosity, less than a few percent, whose properties tend largely to depend on the crack-like nature of their pore space. *Porous rocks* are those with a substantial amount of pore space of more or less equant dimensions, especially as intergranular space; their properties often involve a role of the pore space in the destruction of cohesion between grains or in compaction.

After a preliminary chapter on apparatus, there are two chapters dealing with the stress at which brittle fracture occurs. These chapters treat what may be described as the classical approach to brittle fracture, which regards it as a discrete event and records

---

only the peak stress. The next two chapters deal with the development of events that precede the peak in the load-displacement curve and continue into the post-peak region, and with the theoretical treatment of the brittle behaviour at the micromechanical level. The role of pore fluid pressure on brittle behaviour is then dealt with, followed by a chapter on friction, which is of importance wherever there is sliding on fracture surfaces. Finally, the transition to ductile behaviour with increase in confining pressure and temperature is discussed.

## Experimental Procedures

In the mechanical testing of metals, the applied stress is usually uniaxial, two of the principal stresses remaining zero during a test. However, in the case of rocks, as also in the case of soils, experiments on the mechanical properties are commonly made with all three principal stresses non-zero, and usually compressive. To some extent, this practice has arisen because, with triaxial stress, practical situations involving overburden are more effectively simulated. But, more fundamentally, it reflects the fact that the failure criteria for rock and soil depend strongly on both the normal and shear components of stress, at least where brittle or cataclastic behaviour is concerned. This situation is in contrast to the situation with metals where the yielding depends very little on the mean normal stress. In this chapter, we review briefly the various experimental arrangements that have been used for studies on the brittle behaviour of rocks, mostly at room temperature.

### 2.1 The Triaxial Test

#### 2.1.1 Principle and Terminology

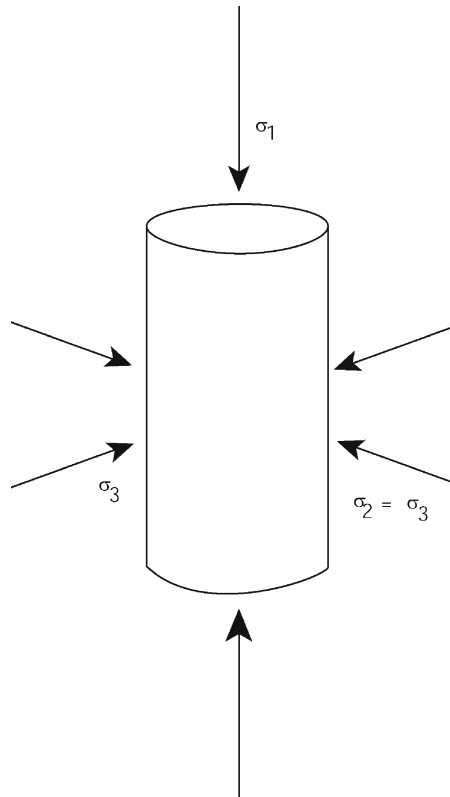
The simplest and most commonly used procedure for achieving a triaxial state of stress in a laboratory test is to superimpose a hydrostatic pressure and a uniaxial stress, that is, in effect to carry out a uniaxial test in an environment of hydrostatic pressure. Such a test is usually referred to simply as a “triaxial test”, following the nomenclature of soil mechanics, and we follow this convention here. Of course, this test, more accurately described as an axisymmetric triaxial test, involves only a special case of triaxial stress in which the intermediate principal stress is always equal to one or other of the extreme principal stresses, but the term is widely used without qualification to refer to these conditions. As a result, the term has to be qualified when a general triaxial stress is involved, that is, when all three principal stresses are varied independently; such a general triaxial test is often referred to as a “true triaxial test”.

At this point, it is useful to define some further terms and concepts relating to experimental conditions, particularly to triaxial tests. Since, in these tests, cylindrical specimens are subjected to simple compression or extension in the presence of a superposed hydrostatic pressure, the state of stress in the specimen ideally consists of

two equal principal stresses normal to the compression or extension axis and a third principal stress parallel to it. Adopting the convention common in geologic and rock mechanics literature that compressive stress is positive, and designating the greatest, intermediate, and least principal stresses as  $\sigma_1$ ,  $\sigma_2$ ,  $\sigma_3$ , respectively, the stress state in a triaxial compression test is therefore normally assumed to be that shown in Fig. 1. The two equal principal stresses have the same magnitude as the superposed hydrostatic pressure, while the third principal stress departs from it. The superposed hydrostatic pressure is called the *confining pressure* since it is the pressure in the medium surrounding the specimen (note that this is not the same as the mean stress in the specimen, which, in the triaxial compression test, is  $(\sigma_1 + 2\sigma_3)/3$ ).

The amount by which the axial stress component departs from the confining pressure in a triaxial test is commonly called the “*differential stress*”. This jargon term is, in origin, peculiar to the rock mechanics literature, although it has also become widely used in geological literature. It should not be confused with the deviatoric stress or stress deviator, as defined in mechanics (Fung 1965, Ch. 3; Engelder 1994). In the ideal triaxial situation assumed above, the differential stress is identical with the “*stress difference*”, which is the classic term for the difference between the greatest and least principal stresses,  $\sigma_1 - \sigma_3$ , that is, twice the maximum shear stress (Love 1910). How-

**Fig. 1.**  
System of stresses in the conventional triaxial compression test;  $\sigma_3$  is the confining pressure



ever, in practice, due to factors such as anisotropy or misalignment of the specimen, the axial stress component may not exactly represent the maximum principal stress. Therefore, we retain the term “differential stress” for use in the direct reporting of triaxial test results but suggest that the term “stress difference” be used when referring to the principal stresses.

The force applied by the loading piston to the specimen in the triaxial test can be resolved into two components, one corresponding to the confining pressure itself and one equal to an additional or *net axial force* (we now prefer the term “*net axial force*” to the term “*differential load*” used in the first edition). The net axial force is the force measured by an internal load cell.

### 2.1.2 Triaxial Testing Apparatus

The essential elements of a triaxial testing apparatus are shown schematically in Fig. 2. The cylindrical specimen is surrounded by a fluid, commonly liquid in the present applications, which is raised to a high pressure to provide the confining pressure. The confining pressure is normally held constant during the experiment. The piston can be advanced to apply the net axial force to the specimen. The confining pressure and axial force can normally be controlled independently of each other, and means are provided for measuring the axial force and the displacement during the test.

Many practical designs for triaxial testing apparatus have been described in the literature. No attempt is made to review them comprehensively here but several will

**Fig. 2.**  
Schematic representation of the elements of a conventional triaxial compression testing machine, including optional arrangements for pore fluid pressure

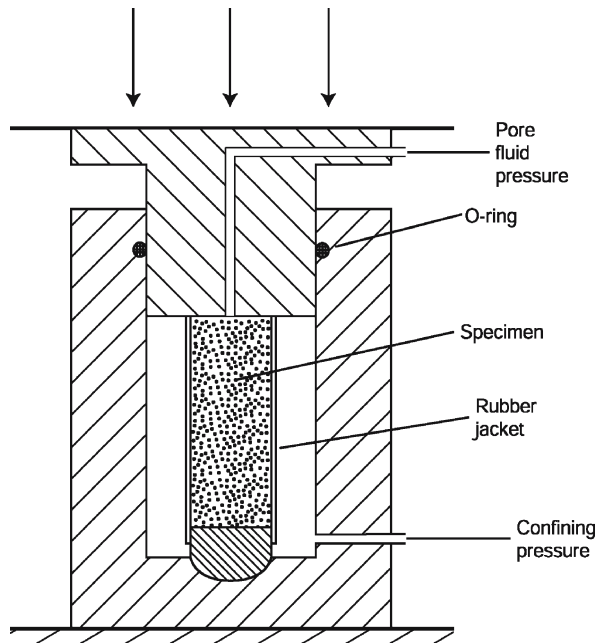
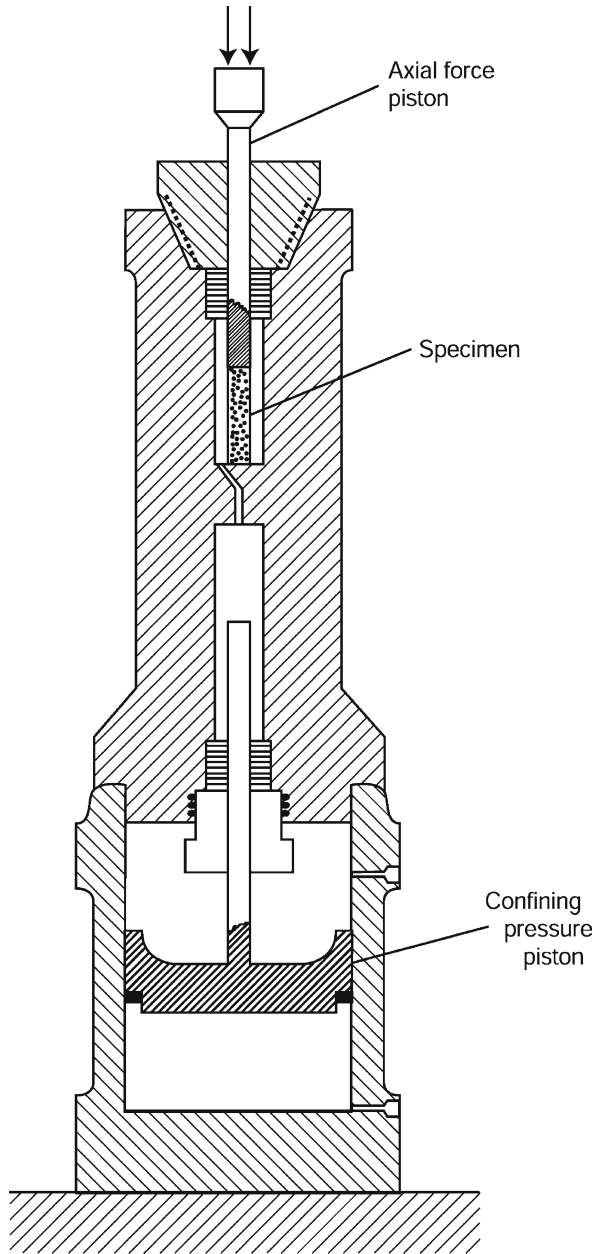




**Fig. 3.**  
Triaxial testing apparatus of  
von Kármán (1911), slightly  
simplified



be mentioned to illustrate particular developments. The pioneering apparatus of von Kármán (1911) already contained all the essentials just listed and served as a prototype for later apparatus (Fig. 3). Simple examples are those of the U.S. Bureau of

Reclamation (Balmer 1953), Donath (1966, 1970a), and Hoek and Franklin (1968) (see also Robertson 1955; Brace 1964a; Murrell 1965; Smith et al. 1969).

The first apparatus of Griggs (1936; see also Griggs and Miller 1951) introduced the innovation of using two pistons of equal diameter, connected by a yoke so as to undergo identical movements. Only one of the pistons contacts the specimen and applies force to it while the other performs two compensating functions: (1) it maintains constant volume (apart from a small elastic distortion effect deriving from the net axial force) and hence avoids change in confining pressure due to piston movement during straining; (2) it counterbalances the piston load due to the confining pressure alone, so that the external loading device only has to apply the net axial force itself plus the friction on the two pistons, which is a much smaller net force than would otherwise be the case when the confining pressure is high. The same arrangement has been used by Paterson (1964b, 1970), and an equivalent arrangement has been used by Donath (1970a). An alternative way of achieving the same end is, using appropriate seals, to connect the pressure fluid to the annular area on a stepped single piston to provide the compensating force (Murrell and Ismail 1976a; Tullis and Tullis 1986; Paterson 1990a), as shown in Fig. 4.

Nearly all triaxial testing apparatus for rock mechanics operate within the 1000 MPa pressure range and, even within this range, most have been restricted to pressures of up to 300–500 MPa. Although pressures higher than 1000 MPa and at least up to 3000 MPa have been used to some extent in triaxial testing in metallurgy (see e.g., Bridgman 1952; Ryabinin et al. 1958; Brandes 1970), the use of such pressures is unusual in rock mechanics at room temperature. Exceptions include the 2000 MPa apparatus of Bergues et al. (1974), an apparatus designed by Heard and used by him and co-workers up to 2200 MPa (Schock, Heard and Stephens 1973), and the cubic press of Shimada (Shimada 1981; Shimada and Yukutake 1982; Shimada 2000).

Carrying out extension tests in triaxial testing apparatus does not generally present special difficulties provided that there are means of making positive attachments to each end of the specimen assembly. Gripping the specimen is very simple if it is jacketed and if the stress difference is numerically smaller than the confining pressure. The tensile net axial force can then in effect be applied to the ends of the specimen by suction relative to the confining pressure when the piston is allowed to move out of the cylinder. All three principal stresses are, of course, still compressive in this case. If net tensile stress is to be applied or if end effects from friction are to be minimized, grips can be attached to suitably shaped specimens such as the “dogbone” specimens used by Brace (1964a; see also Mogi 1966b).

The adaptation of triaxial testing apparatus for use at elevated temperatures is relevant mainly to studies in the ductile field but the influence of temperature on brittle behaviour has been studied to some extent. In brief, for moderate temperatures, up to around 800 K, an external furnace can be used to heat the whole pressure vessel and contents, while for higher temperatures and for greater flexibility in operation the furnace is placed inside the pressure vessel and an inert gas becomes essential as a pressure fluid. For examples of apparatus in these categories, see Griggs et al. (1951), Handin (1953), Griggs, Turner and Heard (1960), Heard (1963), Heard and Carter (1968), Paterson (1970), Goetze (1971), Heard and Duba (1978), Tullis and Tullis (1986), Kohlstedt and Chopra (1987), Durham (1990) and Paterson (1990a).

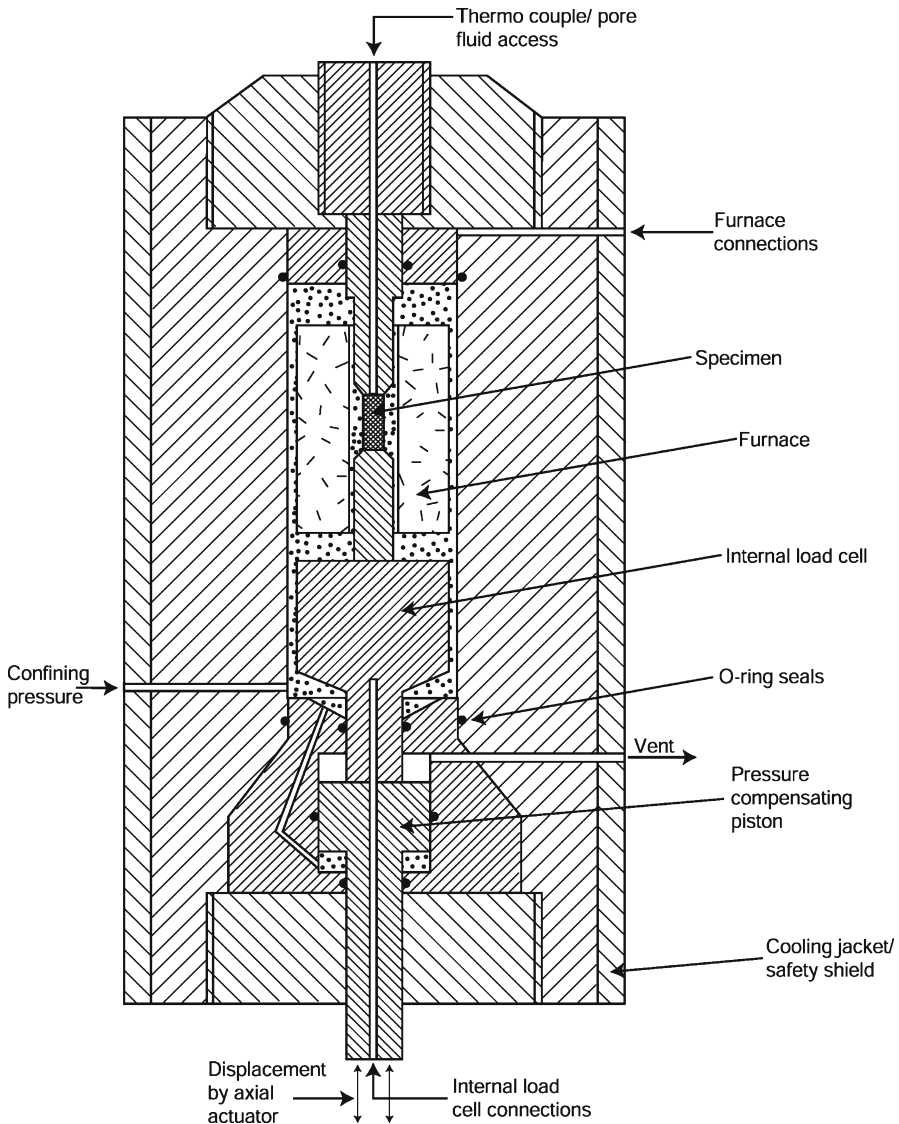


**Fig. 4.** Schematic representation of a high-pressure high-temperature triaxial testing apparatus, incorporating compensating piston and showing specimen set-up for a compression test. Details of the internal load cell and displacement-measuring arrangements not shown (after Paterson 1990a)

Pore fluid pressure is often an important experimental variable in rock mechanics. Pore fluid pressure can be independently controlled in a jacketed specimen attached to the loading piston if the piston is drilled so that the pore fluid, often water, can be introduced inside the jacket from an independent external pressure generator. It may

be desirable to interpose a porous pad between the specimen and the piston to give a better distributed access of the pore fluid to the specimen while preventing extrusion of the specimen, but in the case of strong rocks it is important to use material for the pad that has, at the same time, adequate strength and adequate permeability. Brace and co-workers have used zirconium carbide powder for this purpose (Brace, Orange and Madden 1965; Brace, Walsh and Frangos 1968) but suitable porous ceramic discs are now available commercially. Another problem, discussed in Chapt. 7, is that a long period of time is required for achieving pressure equilibrium within the pore space in a rock of very low permeability. In some experimental situations, a hollow piston open to atmosphere is useful for ensuring that the pore pressure is zero; this expedient can be especially useful in cases where there is a question of whether effective jacket sealing is being achieved.

There are many other refinements or modifications in triaxial testing apparatus that have been introduced for special purposes and which will be dealt with where appropriate in later chapters. These innovations include devices for measuring dilatancy or velocity of elastic waves and the use of servo-controlled or especially stiff machines. Another optional feature, common even in the simplest apparatus, is the use of a spherical seat in compression testing to help ensure better initial concentricity of loading. Safety in operation should also not be overlooked and adequate shielding of highly stressed parts is important. Even with liquids, quite high stored energy is involved at a few hundred megapascals and failure in hardened pistons or tubing connections can give rise to dangerous missiles. A code of safe practice has been published by the High Pressure Technology Association (Cox and Saville 1975).

The design of pressure vessels has been the subject of considerable study, although some of the problems relate to larger vessels than are normally used for laboratory triaxial apparatus; see, e.g., Davidson and Kendall (1970), Turner (1974), Mraz and Nisbett (1980), Bednar (1985), Bonn and Haupt (1995) and the proceedings of two conferences organized by the Institution of Mechanical Engineers (1968, 1977). References to the problem of fatigue life of pressure vessels will also be found in the latter proceedings.

A pressure fluid commonly used at room temperature is kerosene but many other low viscosity liquids are also suitable. The viscosity of kerosene becomes very high as 1000 MPa is approached, and if low viscosity is important lower hydrocarbon mixtures such as petroleum ether or even pure isopentane can then be used. Tables of the influence of pressure on viscosity of lubricating fluids published by the American Society of Mechanical Engineers (1953) may be used in selecting pressure fluids of suitable viscosity. Some liquids can also be used at moderately high temperatures, especially under high pressure; thus, Handin (1953), Yukutake and Shimada (1995) and Ohnaka et al. (1997) used silicone fluid and perfluoro-polyether oil up to 773 K.

Many types of commercially available pumps are suitable for generating pressures of up to the order of 100 MPa or so. Compressed air-driven pumps can be especially convenient and versions of these are available with which much higher pressures can be reached. However, intensifiers have usually been used for the highest pressures, backed up by a suitable priming pump. For pressure measurement, Bourdon gauges or pressure gauges based on sensing the distortion of a container by means of strain gauges or displacement transducers are available commercially for pressures up to at least 700 MPa. However, manganin resistance gauges are convenient and still widely

used over the whole pressure range (for use of manganin and other gauges, see Babb 1970; Peggs 1983).

Conventional seals of many types from commercial hydraulic practice can be used at lower pressures, at least below 100 MPa. For the higher pressures, the “unsupported area” seal of Bridgman (1949a) has been widely used in the past for both closure and piston seals and various modifications of it have also been used (e.g., Heard 1963). Lower friction can be achieved with the “controlled clearance” seal (Handin 1953; Johnson and Newhall 1953; Newhall 1957) and with O-ring seals. Conventional O-ring seals are especially convenient to use both for static and piston seals but anti-extrusion rings are needed at high pressures. Examples of reliable O-ring piston seal design are shown in Fig. 5. The choice of an O-ring compound with good low temperature properties helps to avoid brittle failure of the O-ring above the glass transition (Paterson 1964a).

### 2.1.3 Preparation and Jacketing of Specimens

Specimens are usually obtained by diamond core drilling, the thin-walled glass-working drills being especially convenient and economical for this purpose. A drilling machine with minimal vibration is desirable for reducing breakage of cores. The ends of the cores can be squared off with abrasive paper or by diamond grinding, as appropriate, using a V-block or similar jig to aid in getting the ends square to the specimen axis. It is important that the ends be parallel within a small tolerance, say, 0.01 mm or less. In geotechnical applications, it is often important to preserve the original water content, which may require special procedures (Brown 1981). In geophysical applications, it is more often important to test under controlled moisture conditions, such as

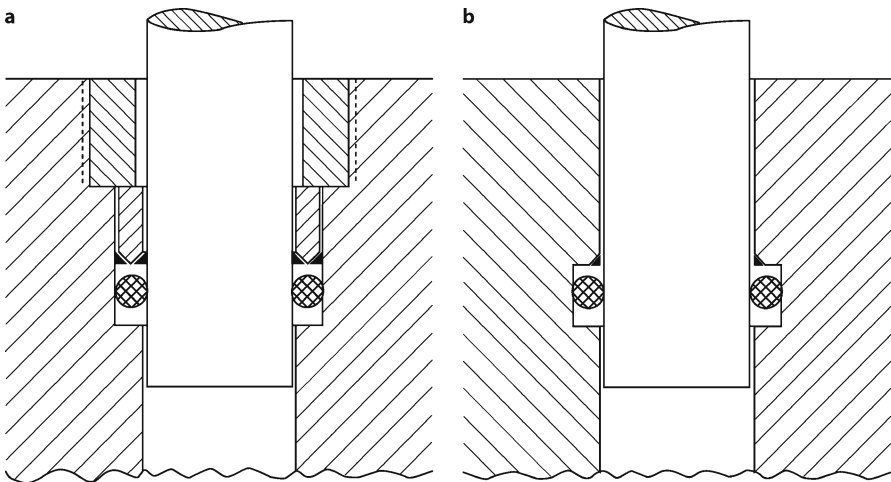


**Fig. 5.** Examples of O-ring seals with anti-extrusion rings, suitable for piston seals. **a** With separate retaining sleeve, after Paterson (1962); **b** simpler version, suitable when the diameter is large enough that the anti-extrusion ring can be flexed into position

saturated or dry. Although air drying is often used, a more thorough or controlled drying, such as in a vacuum oven, is good practice. For a study of the importance of the various factors in specimen preparation, see Podnieks et al. (1972).

The jacketing of the specimen in an impervious jacket is a very important factor in the experimental conditions in triaxial testing of rocks. The jacket prevents the pressure fluid from entering pores or cracks and its use greatly influences the strength. In general terms, its action is to enable the confining pressure effectively to inhibit the opening of cracks or sliding on existing crack surfaces. At room temperature, tubing of rubber, polyurethane, or similar materials is widely used for jacketing, the ends being sealed by devices such as a hose-clip or a stretched ring of the same material, or “heat-shrink” tubing can be used. Although these types of jackets are very convenient, it should be realized that elastomers may become quite strong and apply appreciable constraint to the specimens if the glass transition pressure (commonly 200–500 MPa) is exceeded (Paterson 1964a; Weaver and Paterson 1969a,b). Therefore, even at room temperature, jacketing is often better done with thin-walled tubing of metal such as copper or indium, sealing the ends with rubber tubing or an O-ring (Donath 1966, 1970a). At elevated temperatures, metal jackets can be sealed with press-fitted rings of the same material as the pistons (Handin 1953), or a long jacket covering also the loading pistons can be used, sealed with O-rings at the cool ends of the pistons (Paterson, Chopra and Horwood 1982).

#### **2.1.4 Measurements, Control, and Data Reduction**

The two primary measurements to be made during a triaxial test at constant confining pressure are those of net axial force and axial displacement, from which a plot of differential stress versus axial strain can be derived. In some applications, the change of volume of the specimen is also measured.

For measurement of the force externally to the pressure vessel a suitable load cell, chosen from the wide range commercially available, can be used, or the force can be obtained by measuring the oil pressure in the loading jack. These approaches are, however, only satisfactory if the net axial force is large compared with the piston friction, for which correction must be made. Otherwise, an internal load cell is desirable since friction can be notoriously variable or unpredictable and the corrections correspondingly inaccurate.

A suitable internal load cell can be made from an elastic element to which electric resistance strain gauges are attached, as first used by Haasen and Lawson (1958; see also Pugh and Gunn 1964; Mogi 1965; Davis and Gordon 1968; Paterson 1970), although Bridgman (1952) measured the change in resistance of the element itself. Alternatively, some form of displacement transducer can be used to measure the distortion of the elastic element (Robertson 1955; Heard 1963; Gelles 1968; Paterson 1990a), although some of these arrangements have the disadvantage of being fairly sensitive to changes in confining pressure as well as to the net axial force. In the case of the first type, attachment of electric resistance strain gauges with epoxy resin tends to be short-lived at the higher pressures because of the difference in compressibility of the resin and the metal substrate; this difficulty can be reduced by the use of ceramic strain gauge cements or sprayed coatings normally intended for high-temperature use. The

chief problem in achieving high precision with internal load cells is to calibrate them under pressure in order to allow for any small effects of the confining pressure that there may be on their sensitivity – for some methods, see Pugh and Gunn (1964), Davis and Gordon (1968), Gelles (1968), Paterson (1970, 1990a), and Fung (1975).

The axial strain in the specimen is commonly obtained from measurements of piston displacement made outside the pressure vessel and corrected for apparatus distortion. The linear variable differential transformer (LVDT or DCDT) is very convenient for this purpose. Electric resistance strain gauges can be used on the specimen itself (see, e.g., Brace 1964a,b; Schock and Duba 1973) or other types of strain transducers devised (Serdengecti and Boozer 1961; Smith et al. 1969; Hardy and Kim 1970; Fung 1975; Tullis and Tullis 1986; Brown and Heuze 1979; Spetzler 1987).

Measurement of volume change that occurs in response to the application of both hydrostatic and deviatoric stress is also often of interest, especially in porous rocks. Procedures for measurement of volume changes are discussed in Chapt. 5.

The simplest and commonest way of carrying out a test is to operate the machine at a constant displacement rate (or constant drive-motor speed), except in simple creep tests where constant force is maintained after the initial loading. However, servo-control loading systems were introduced in the 1970's (Houpert 1970; Rummel and Fairhurst 1970; Hudson, Brown and Fairhurst 1971; Hardy, Stefanko and Kimble 1971; Rummel 1975) and are now in general usage. In these systems, the property of specimen behaviour to be controlled, for example, the axial strain, is measured by a suitable transducer, whose signal is monitored by the control system; the control system, in turn, adjusts the driving device in such a way as to make the signal follow a programmed course. This course may be a set strain rate or loading rate, a constant force or strain, or any other desired course such as a cycling force. The application of such systems to the study of the later stages of fracture development is discussed in Chapt. 5.

The axial force and displacement data are now commonly acquired and reduced digitally, but a visual output on a strip-chart recorder may also be desirable for following the progress of the test. For early application of computers, see Donath and Güven (1971), Güven and Donath (1971) and Hardy et al. (1971).

In reducing the data the following steps are usually involved:

- *Strain*: The measured piston displacements are corrected for apparatus distortion, which is normally proportional to the force, although non-linearity may have to be taken into account at small forces. The strain is then commonly calculated as  $\varepsilon = \Delta l/l_0$  where  $l_0$  is its initial length and  $\Delta l$  is the decrease in length of the specimen (under the convention of shortening strain being positive). If the strain is large, the “natural strain”  $\varepsilon = \ln(l_0/l)$  is often used, where  $l$  is the current length.
- *Stress*: If an external load cell is used, the friction correction has to be subtracted from the recorded force; this correction is usually obtained from observations made during piston advance before the specimen is contacted, neglecting further friction associated with the axial force. Any force known to be supported by the jacket must also be subtracted from the measured force. At small strains, the differential stress is calculated from the corrected force, using the initial cross-sectional area of the specimen; a “true stress” is more appropriately calculated using the current cross-sectional area (usually assuming that the specimen is deforming at constant volume and remaining cylindrical).

## 2.2 Other Types of Tests

The *uniaxial compression test* is widely used in engineering practice and is also often used in research. It has the advantage of being simple in principle, and of requiring minimal sophistication in equipment. A further advantage is that it most readily allows the carrying out of auxiliary measurements, for example, of lateral strain, dilatancy, or velocity of elastic waves. New potentialities in the use of the uniaxial compression test have also been opened up recently with the advent of servo-control (Sect. 2.1.4 and 5.2.1). For a comprehensive review of the uniaxial compression test, see Hawkes and Mellor (1970) and Vutukuri et al. (1974).

The *uniaxial tension test*, the most common test in metallurgy, is used only minimally for rocks. A major reason for its avoidance lies in the difficulty of gripping relatively short specimens in such a way that reproducible behaviour can be achieved. For methods of overcoming this difficulty, see Fairhurst (1961), Hardy and Jayaraman (1970), Hawkes et al. (1973), Barla and Goffi (1974), and Okubo and Fukui (1996). More commonly, indirect testing methods involving inhomogeneous stress states are applied in attempting to characterize the tensile strength of rock in a reproducible way.

The main use of inhomogeneous stress tests is, in fact, that of obtaining data on the tensile strength of rocks. There are many such methods based variously on bending, torsion, indentation, diametral compression, hoop-stress loading from internal pressure in hollow cylinders, etc., often involving application of line loads or point loads. For an introduction to these test methods and for further references on them, see Jaeger (1965, 1967), Jaeger and Cook (1979, p. 160 et seq.), Hardy and Jayaraman (1970, 1972), Mellor and Hawkes (1971), Broch and Franklin (1972), Barla and Innaurato (1973), Lawn and Wilshaw (1975a), Cox and Scholz (1988), Santarelli and Brown (1989), Ewy and Cook (1990a,b), and Suárez-Rivera et al. (1990).

The *shear test* is sometimes used in rock mechanics in a form similar to that common in soil mechanics (Lambe and Whitman 1969); the machine of Obert et al. (1976) is such an example but with arrangements for varying its normal stiffness. However, the main application of the shear test has been for friction or joint studies (e.g., Goodman and Ohnishi 1973; Ross-Brown and Walton 1975; Dieterich 1972a; Dieterich 1981; Linker and Dieterich 1992; Cox 1990). The disadvantage of inhomogeneous stress in the simple shear test can be reduced by the use of torsion of hollow cylinders (Christensen, Swanson and Brown 1974; Durand and Comes 1974; Kutter 1974; Durand 1975; Tullis and Weeks 1986; Biegel et al. 1992; Beeler et al. 1996). For an analysis of the stress conditions and other aspects of the torsion test, see Paterson and Olgaard (2000).

For “true” triaxial testing, independent loading of the three pairs of opposite faces of a cubic specimen is usually used. Severe difficulties are encountered in reducing friction at the loaded faces to obtain a good approximation to homogeneous stress, but considerable progress has been made. References are listed in the further discussion of such tests in Sect. 3.6.

There are also various tests in which the specimen’s dimensions are constrained in some degree. The simplest of these is the *uniaxial strain test* in which the specimen is constrained to retain the same diameter during deformation with the intention of simulating certain situations in the Earth (for examples of studies in uniaxial strain,



see Swanson and Brown 1971b; Brace and Riley 1972; Walsh and Brace 1972; Schock, Heard and Stephens 1973; Spiers et al. 1990; Teufel, Rhett and Farrell 1991). It follows that the volume changes significantly during such a test. Another case is that of the *biaxial strain test* in which the specimen is constrained to undergo plane strain (for example, Maso and Lerau 1980; Ord, Vardoulakis and Kajewski 1991; Labuz, Dai and Papamichos 1996; Yumlu and Ozbay 1995).

## Experimental Studies on the Brittle Fracture Stress

### 3.1 Introduction

In the simplest view, the brittle fracture of a rock is a discrete event in which the failure of the rock occurs, without significant prior deformation and without warning, at a particular stress. In later chapters it will be shown that this view is oversimplified and is, in particular, inadequate for an understanding of the physical mechanisms of fracture. However, it is often sufficient from a phenomenological point of view, and it is a view that has underlain a great deal of research on the factors that affect the gross brittle behaviour of rocks. The present chapter and the following one deal with these studies, in which, apart from noting the gross nature of the fracture, the only quantity of interest is the peak stress (“brittle fracture stress”). Such studies, often essentially empirical in approach, provide much of the basis for applied rock mechanics in engineering and mining, as well as for the analysis of geologic faulting.

This chapter deals with experimental studies on the various factors (except pore pressure) that affect the brittle fracture stress and the gross nature of the fracture. Fracture is described as “brittle fracture” when it is not preceded by any appreciable amount of permanent deformation, although the microscopic and other pre-failure observations described in Chapt. 7 show that the behaviour is by no means purely elastic prior to the macroscopic fracture. There is, indeed, some latitude in defining what is a brittle fracture. Sometimes it may refer to failure following amounts of inelastic strain that are small compared with the elastic range; in other cases, fracture following several percent of inelastic strain is still taken as brittle (e.g., Heard (1960) defined fractures as brittle if the strain did not exceed 3% prior to the fracture).

Many types of tests have been used in the experimental study of brittle fracture in rocks. We shall consider mainly the results from the uniaxial compression test and the conventional triaxial test, described in Chapt. 2. These tests have the advantage of being the simplest to interpret because, at least in principle, they involve only homogeneous stress. Tests such as torsion, bending, and diametral compression (“Brazilian”) tests involve inhomogeneous stress distributions, and their interpretation then tends to rest on the generally dubious assumption that the stress distribution prior to fracture corresponds to that of the purely elastic state. Some of the latter tests have advantages of practical convenience, as in assessing the relative tensile strengths of different rocks at atmospheric pressure, but we shall not consider them in detail here (for references, see Sect. 2.2).

### 3.2 Types of Fractures

It is useful, following Griggs and Handin (1960), to distinguish two principal modes of brittle failure (Fig. 6):

1. Shear fracture, in which the relative displacement is parallel to the fracture surface, the latter being generally inclined at an angle of less than  $45^\circ$  to the maximum compressive principal stress.
2. Extension fracture, characterized by separation normal to the failure surface, which is generally oriented normal to the least principal stress (compression positive).

The *shear fracture* is the dominant mode of macroscopic brittle failure in triaxial compression tests at all but the lowest confining pressures. Shear fracture also predominates in triaxial extension tests above a higher threshold of confining pressure. In general, the fractures in both cases occur at a fairly well-defined angle to the direction of the greatest compressive principal stress, usually between  $20^\circ$  and  $30^\circ$ . However, there is often a tendency for the angle to increase slightly with increase in confining pressure (e.g., Paterson 1958). Also, in extension tests it has been shown that there tends to be a gradual change in orientation of the failure surface in the transition from extension fracture to shear fracture with increasing confining pressure in the transition range (Brace 1964a; Hoskins 1969b).

As the brittle-ductile transition is approached with increasing confining pressure, the shear failure tends to become a zone of intense deformation and fine-scale frac-

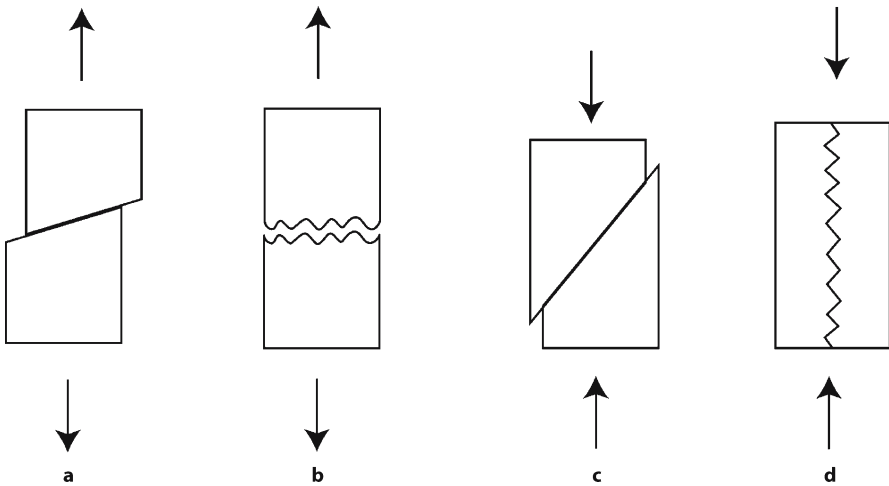


**Fig. 6.** Types of fractures. **a** Shear fracture in extension test (least principal stress vertical, compression positive); **b** extension fracture in extension test; **c** shear fracture in compression test (greatest principal stress vertical); **d** extension or “axial splitting” fracture in compression test

turing, rather than a discrete shear fracture, and separation may not then take place readily at the failure zone after the test. The term “fault” is sometimes applied to shear failures to cover both the discrete shear fracture and such a shear zone of concentrated cataclasis, but Jaeger and Cook (1979, p. 92) have suggested that this term be restricted to geologic use. At confining pressures near the brittle-ductile transition, conjugate shear failures sometimes occur, but this effect seems to depend on there being constraint on rotation of the ends of the specimen; thus, single shears have been observed when a spherical seat was used and two conjugate shear, or more, with rigid end platens under otherwise identical conditions (Paterson 1958; Jaeger 1960a).

More detailed discussion on the genesis and development of shear failures will be given in Chaps. 5 and 9. The remainder of this section will deal only with the topic, sometimes rather enigmatic, of extension fractures.

The *extension fracture* is best known from its occurrence in the uniaxial tension test as a parting of the specimen normal to the direction of the tensile stress. However, extension fractures can also occur under predominantly compressive conditions, as is observed in several types of tests. In the classic “embracing” or “pinching-off” experiment of Föppl (1900) and Bridgman (1912, 1952), a cylindrical rod of brittle material is loaded by fluid pressure on the cylindrical surface while the free ends project from the pressure vessel and are restrained only by the friction at the packings; the failure is usually by extensile fracturing normal to the axis of the rod (see also Gurney and Rowe 1948a, 1948b; Jaeger and Cook 1963; Secor and Montenyohl 1972). Extensile fractures are also commonly observed in triaxial tests in extension when all the macroscopic principal stresses are compressive (Handin 1953; Heard 1960; other references given by Griggs and Handin 1960), and they have been observed in confined Brazilian tests under similar circumstances (Jaeger and Hoskins 1966a). Further, in compression tests at or near atmospheric pressure, there frequently occur extension fractures in the form of splitting parallel to the compression axis, analogous to the fractures observed in biaxial compression by Föppl (1900).

The apparent paradox of extension fractures occurring in the absence of macroscopic tensile stress has given rise to a good deal of speculative discussion. One view is that the fracture occurs when a certain critical extensile strain is exceeded (maximum extensile strain criterion of failure, e.g., Bridgman 1938). However, this is not a very satisfying explanation from a physical point of view, although Bridgman has attempted to defend it against such criticism. In terms of physical processes, an extension fracture presumably must involve failure of bonds under local tensile stress, even if this only occurs at the molecular or atomic scale (cf. Gurney and Rowe 1948a,b). It seems most likely that the fractures originate in response to local tensile stresses around flaws or cracks on a microscopic scale, arising as described below in relation to axial splitting (see also Scholz, Boitnott and Nemat-Nasser 1986).

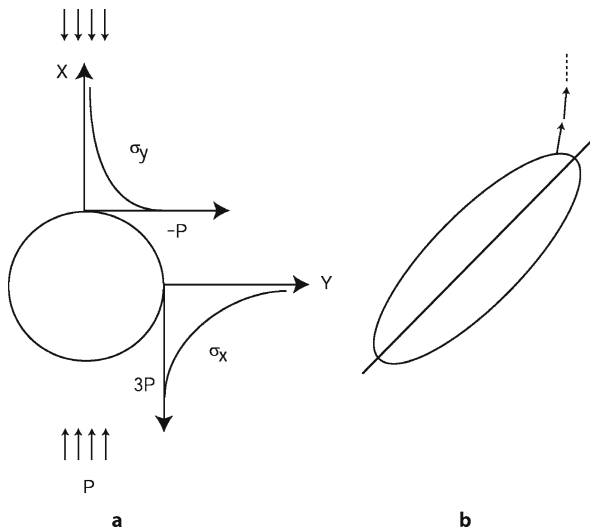
The nature and magnitude of local stresses around microscopic flaws will be strongly affected by whether fluid or other material under pressure has access to them. This consideration leads to the distinction, emphasized by Brace (1964a), between *intrusion fractures* and *internal fractures*. Intrusion fractures are said to occur when the surrounding material (pressure medium, jacket material, or even a wedge-shaped fragment of the specimen itself) penetrates cracks that are open to the surface. Such

fractures can therefore occur when all the macroscopic principal stresses are compressive, and they probably account for many of the extensile failures observed under these conditions. In contrast, internal fractures can only be expected when there is a net tensile component of stress in the region through which the crack is propagating, arising independently of the injection of material. The essential difference between intrusion and internal fractures, therefore, lies in whether or not normal forces act on the crack faces after separation.

The “axial splitting” or “axial cleavage” fracture is common in uniaxial testing but it is suppressed by the addition of relatively low confining pressures, even by a few megapascals in some cases (Griggs 1936; Paterson 1958; Heard 1960; Jaeger 1960a; Wawersik and Fairhurst 1970; Wawersik and Brace 1971). The axial splitting probably normally originates from local transverse tensile stresses at flaws or heterogeneities in the material. Thus, in uniaxial compression tests, Wawersik and Fairhurst (1970) have noted a reduced tendency to axial splitting in the more nearly homogeneous or finer-grained materials such as lithographic limestone.

The manner in which local transverse tensile stresses can arise at flaws is illustrated in the two-dimensional analysis of stresses around a circular hole in an elastic medium (Jaeger and Cook 1979, pp. 249–252). This analysis (Fig. 7a) shows that, under a uniform uniaxial loading applied at a large distance from the hole, there is not only an intensification of the axial compressive stress component  $\sigma_x$  in the neighbourhood of the end of the transverse diameter of the hole but there arises also a transverse tensile stress  $\sigma_y$ , of peak magnitude equal to that of the mean compressive applied stress, in the neighbourhood of the end of the diameter parallel to the direction of loading. A qualitatively similar situation arises at an elliptical hole or crack with the major diameter parallel to the uniaxial compressive loading direction (Jaeger and Cook 1979, pp. 266–277). This transverse local tensile stress component is reduced or completely suppressed by the addition of a compressive transverse loading of the body (e.g., by

**Fig. 7.**  
**a** Distribution of stresses around a hole in uniaxial compressive loading (two-dimensional case);  $\sigma_y$  is the lateral stress at points along the  $x$  axis,  $\sigma_x$  the longitudinal stress along the  $y$  axis, and  $P$  the average applied compressive stress. **b** Direction of propagation of a crack from an inclined flaw under compressive loading applied vertically



applying a confining pressure). Thus, qualitatively we can expect local transverse tensile stresses to arise at the ends of any axially oriented flaws in brittle rock specimens if the confining pressure is not too high, thus favouring propagation of a crack parallel to the specimen axis from the flaw. When the flaws are inclined to the specimen axis, the maximum tensile stress component no longer occurs at the end of the major diameter but at a point where the normal to the flaw surface is more nearly parallel to the specimen axis. Then the flaw will tend not to propagate in its own plane but to swing into an orientation more nearly parallel to the axis of loading, as shown in Fig. 7b (Brace and Bombolakis 1963; Bombolakis 1964; Hoek and Bieniawski 1965). More detailed analysis in the context of the wing crack model and linear elastic fracture mechanics will be discussed in Chapt. 6 and Appendix 1.

The local, induced tensile stresses of the type just described have therefore been invoked to explain why cracks often propagate parallel to the direction of compressive loading, for example, by Gramberg (1965, 1970), Fairhurst and Cook (1966) and Holzhausen and Johnson (1979). Somewhat related notions are found also in the explanations of Ros and Eichinger (1949), Trollope and Brown (1966), Brown and Trollope (1967), Trollope (1968) and Karihaloo (1979). A microdynamical theory of axial splitting has been given by Nemat-Nasser and Horii (1982) and by Horii and Nemat-Nasser (1985, 1986); see Chapt. 6. An energy-based model of compressive splitting was also proposed by Bhattacharya (1998).

### 3.3 Observed Stresses at Brittle Failure

There is no universal simple law governing the level of stress at which a given rock fractures because, (1) this level involves all principal components of the stress and, (2) it probably depends on the mode of fracture. To express the failure conditions in the most general way, it is usual to seek an appropriate function of the three principal stresses  $\sigma_1$ ,  $\sigma_2$ ,  $\sigma_3$ , which takes on the same characteristic value for any combination of the principal stresses at which fracture occurs. This condition, often for convenience written in the form

$$\sigma_1 = f(\sigma_2, \sigma_3)$$

is known as a *criterion of failure*. The function  $f$  includes at least one parameter, the value of which is characteristic of the particular material. However, it cannot be assumed that a given simple form of the function  $f$  will necessarily apply to more than one particular mode of fracture unless it is shown that the underlying physical mechanisms are the same; in particular, it is possible that extension and shear fractures may be controlled by different criteria of failure.

The question of establishing criteria of failure for rocks under general conditions of stress will be taken up later in this chapter. Here, we shall only discuss the stresses at macroscopic failure in the situations most commonly dealt with experimentally. These involve extension fracturing and shear fracturing in the conventional uniaxial and triaxial tests, and so the immediate interest centres on the uniaxial strengths and on their modification by the addition of the confining pressure.

It is not feasible to present here a compendium of all existing room temperature data from uniaxial and triaxial tests, so we shall only present a broad summary of the trends. Important compilations of data have been given by Hirschwald (1912, pp. 75–82), Ros and Eichinger (1949), Balmer (1953), Wuerker (1956, 1959), Handin (1966, esp. Tables 11-3 to 11-5), Lama and Vutukuri (1978), Hoek and Brown (1980), and Singh (1981). Useful summary plots including some of the same data have been given by Hoek and Bieniawski (1965); see also Jaeger and Cook, (1979, p. 154), Mogi (1966a), Ohnaka (1973b), Hoek and Brown (1980), and Lockner (1995). Measurements on sedimentary rocks (mostly arenaceous and argillaceous) has been published by Handin and Hager (1957, 1958), Hoshino et al. (1972), Hoshino (1974), and Vernik et al. (1993); see also Jones and Preston (1987). Very broadly, the compressive fracture stresses for various rocks at room temperature can be categorized as:

1. *Igneous and high-grade metamorphic rocks*: uniaxial compressive strengths generally in the range 100–200 MPa, sometimes higher, especially in fine-grained rocks; at a confining pressure of 100 MPa, differential stresses at fracture often around 500–800 MPa, sometimes higher; at a confining pressure of 500 MPa, differential stresses at fracture usually above 1000 MPa and sometimes above 2000 MPa.
2. *Low-porosity sedimentary and low to medium-grade metamorphic rocks* (including calcite limestones and marbles): uniaxial compressive strengths in the range 50–100 MPa; at a confining pressure of 100 MPa, differential stresses at fracture of 200–300 MPa, if still brittle.
3. *High-porosity sedimentary and some low-grade metamorphic rocks*: uniaxial compressive strengths of 10–50 MPa.
4. *Low-porosity dolomites and quartzites*: very high uniaxial compressive strengths, up to 300 MPa or more; at 100 MPa confining pressure, differential stress at fracture in range 500–1000 MPa, or even higher in quartzite.

The uniaxial tensile strengths tend to be of the order of one-tenth of the uniaxial compressive strengths, but in triaxial tests the differential stresses for shear fracturing in extension are of a similar order of magnitude to those in compression.

The strength variations above reflect many factors that cannot be analysed in detail in a general treatment. These factors include mineral composition, porosity, state of alteration or weathering, and prior history affecting microstructural details such as the density and distribution of microcracks. For systematic studies on the influence of porosity, see Dunn, La Fountain, and Jackson (1973), Hoshino (1974), Friedman (1976), Logan (1987), Scott and Nielsen (1991), Vernik, Bruno and Bovberg (1993), Hatzor, Zur and Mimran (1997) and Wong, David and Zhu (1997).

We shall now summarize the broad trends that have been deduced for the macroscopic fracture stress as influenced by variation in the confining pressure, a variation that corresponds to variation in the ratio of the extreme principal stresses. We distinguish between the extension and shear modes of fracturing and, for the present, only isotropic behaviour is considered.

*Extension fracturing* is often said to occur when the least principal stress (compressive stresses reckoned positive) is equal to the uniaxial tensile strength (e.g., Murrell 1967a; Hoek 1968). The most important data for rocks in support of this con-

clusion are those of Brace (1964a) and Murrell (1965), although it is also supported by data for other materials such as cast iron and concrete (see Murrell 1967a). However, this conclusion, while probably valid within rough limits, needs to be qualified in several respects:

1. The accurate determination of the uniaxial tensile strength is notoriously difficult, both because of the experimental problem of achieving a macroscopically uniform tensile stress and because of the inherently large scatter in tensile strength of most rocks. Consequently, there is a general preference for obtaining the uniaxial tensile strength from an indirect test such as the diametral compression (“Brazilian”) test, which gives more consistent results, but, as commented previously (Sect. 3.1), this approach rests on certain assumptions about stress distribution.
2. The range of combinations of principal stresses over which the preceding conclusion can be tested is severely limited because in the triaxial test there is a fairly narrow range of confining pressures in which clearly internal extensile fractures occur. With increasing confining pressure, a transition is soon made to shear fracturing but, even before that transition, complications enter, especially because of intrusion fractures in which the macroscopic stress field is perturbed by loading on the crack faces as the fracture propagates; then the foregoing simple rule is no longer directly applicable. This non-applicability is most obvious for the extension fractures that occur with all principal stresses compressive (cf. Sect. 3.2). A similar exception probably should also be made for the axial splitting type of extension fracturing that occurs in uniaxial compression or at very low confining pressures, although difficulties may again stem from uncertainty about the true stress distribution.

The failure stresses in case of *shear fracturing* are known in much greater detail than those in case of extension fracturing. The measurement of the former comprises the bulk of triaxial testing, carried out on many rocks and over a wide range of confining pressures. It is found that the maximum differential stress,  $\sigma_1 - \sigma_3$ , preceding a brittle shear failure always depends markedly on the confining pressure (Fig. 8). Within the limits of uncertainty set by the normal scatter of results from rocks, this dependence can often be represented, at least over a moderate range of confining pressure  $p$ , by the linear relation

$$\sigma_1 - \sigma_3 = \sigma_0 + p \tan \psi \quad (3.1)$$

where  $\sigma_0$  is a constant, equal to the uniaxial compressive strength if the relation is obeyed down to zero confining pressure, and  $\tan \psi$  is another constant with a value usually between 1 and 10;  $p = \sigma_3$  in a compression test and  $p = \sigma_1$  in an extension test. The same relationship can be expressed in terms of a Mohr diagram (Jaeger 1969, p. 9) by the straight-line envelope

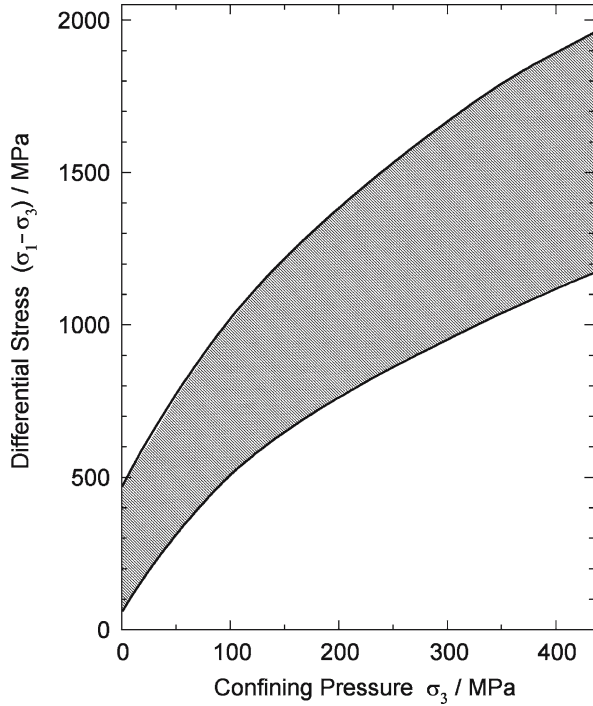
$$|\tau| = \tau_0 + \sigma \tan \varphi \quad (3.2)$$

where  $\tan \varphi$  is another constant, the slope of the envelope. The constants in Eqs. 3.1 and 3.2 are related as follows:



**Fig. 8.**

Dependence of differential stress on confining pressure for a wide range of igneous rocks; limits from the compilation of Ohnaka (1973b)



$$\tau_0 = \frac{\sigma_0}{2\sqrt{1 + \tan \psi}}; \quad \tan \varphi = \frac{\tan \psi}{2\sqrt{1 + \tan \psi}}; \quad \sin \varphi = \frac{\tan \psi}{2 + \tan \psi}$$

$$\sigma_0 = 2\tau_0 \tan\left(\frac{\pi}{4} + \frac{\varphi}{2}\right) = 2\tau_0 \left(\sqrt{1 + \tan^2 \varphi} + \tan \varphi\right) = \frac{2\tau_0 \cos \varphi}{1 - \sin \varphi}$$

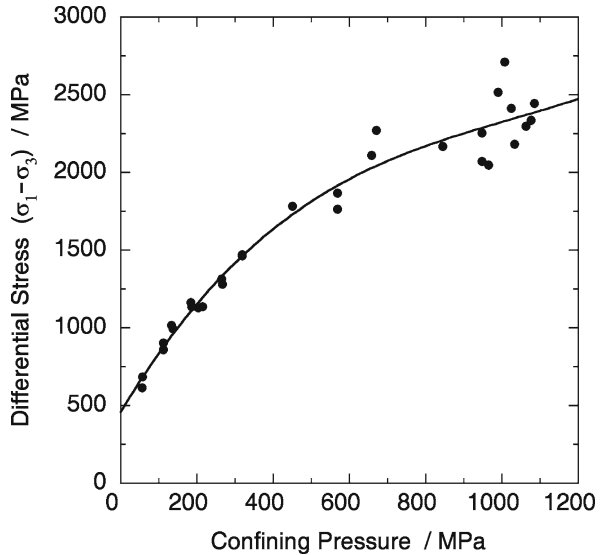
$$\tan \psi = \tan^2\left(\frac{\pi}{4} + \frac{\varphi}{2}\right) - 1 = 2 \tan \varphi \left(\sqrt{1 + \tan^2 \varphi} + \tan \varphi\right) = \frac{2 \sin \varphi}{1 - \sin \varphi}$$

The stresses  $\tau$  and  $\sigma$  corresponding to the points on the Mohr envelope (Eq. 3.2) are the maximum shear stress and the normal stress, respectively, acting on the plane inclined at the angle  $\theta = \pi/4 \pm \varphi/2$  to the specimen axis (minus sign for compression, plus sign for extension). The above relationships follow from the analysis given by Jaeger and Cook (1979, pp. 95–97)).

When Eq. 3.2 is used as a criterion of failure in rocks under general states of stress, it is known as the *Coulomb criterion* (the terms Coulomb-Navier criterion and Coulomb-Mohr criterion have also been used but the attribution to Coulomb is now widely accepted as preferable (Paul 1968, p. 447; Handin 1969; Jaeger and Cook 1979, p. 95)). In the Coulomb criterion, only the greatest and least principal stresses are taken into account, neglecting any influence of the intermediate principal stress. The term  $\tau_0$  is called the “*cohesion*” and  $\tan \varphi$  the “*coefficient of internal friction*”, in analogy with the

**Fig. 9.**

Dependence of differential stress at failure in compression on confining pressure for granite, illustrating non-linearity (after Byerlee 1967a)



usage in soil mechanics.  $\tan \phi$  cannot be interpreted directly as a coefficient of friction in a real physical sense (cf. Handin 1969) although it does have values that usually lie in the range 0.5 to 1.5 (Sangha and Dhir 1975; Mogi 1966a; Lockner 1995), in general agreement with but often slightly higher than the coefficients of friction for sliding between rock surfaces (Chapt. 6). However,  $\tan \phi$  is identified with a real coefficient of friction in the modified Griffith theory of failure (Chapt. 4) or in similar interpretations of brittle behaviour in terms of microcracks (Mogi 1974a; Savage, Lockner and Byerlee 1996).

There are a great many cases where the dependence on confining pressure of the maximum differential stress preceding shear failure is clearly non-linear (Fig. 9), usually in the sense of being concave toward the confining pressure axis, and it may be that a curved relationship is, in general, better for fitting experimental results than the linear Coulomb relation. Often a curved plot can definitely be attributed to the brittle-ductile transition being approached, that is, to there being a change in mechanism with pressure. However, this does not seem to be always the explanation. Moreover, there are theories, such as the simple Griffith theory (Chapt. 4), that predict non-linear pressure dependence even without change of mechanism. There are also suggestions that there is a gradual increase in the degree to which cracks are closed by the confining pressure as the confining pressure is increased, leading to a change in the slope of the Mohr envelope (Murrell 1971; Mogi 1972b, 1974a). Therefore, the non-linearity of Mohr envelopes in cases of shear failure can be of considerable fundamental importance in theoretical interpretation and may prove to be the rule rather than the exception. However, the Coulomb relation remains important because of its mathematical simplicity; sometimes it may be genuinely valid and in other cases it may be applicable as a first approximation, especially over a limited range of pressure.

Many forms of non-linear relations have been proposed for the fitting of experimental data when it is wished to take the non-linearity into account. Mohr (1900)

proposed that failure occurs on a given plane when the shear stress  $\tau$  and normal stress  $\sigma$  on it satisfy a relation  $\tau = f(\sigma)$ , leaving the function  $f$  non-explicit. This hypothesis carries the implication that the failure conditions are independent of the intermediate principal stress and that the orientation of the failure surface will contain the direction of the intermediate principal stress. Within the same limitation that the intermediate principal stress does not influence the failure, the two simplest explicit forms of non-linear failure criteria are

$$\tau^2 = c_0 + c_1 \sigma$$

$$\tau = c_0 + c_1 \sigma^n \quad (\text{cf. Murrell 1971})$$

Similar, but not necessarily identical, forms have also been proposed in terms of the principal stresses, such as

$$\sigma_1 = c_0 + c_1 \sigma_3^n$$

$$\sigma_1 - \sigma_3 = c_0 + c_1 \sigma_3^n$$

$$\sigma_1 - \sigma_3 = c_0 (\sigma_1 + \sigma_3)^n \quad (\text{cf. Franklin 1971a, 1971b; Mogi 1972b})$$

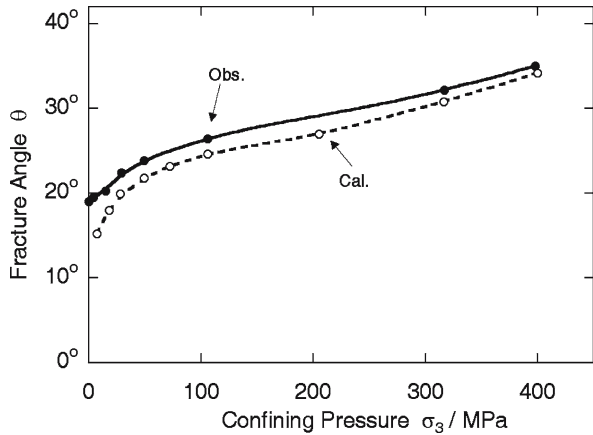
$$\sigma_1 - \sigma_3 = c_0 \sqrt[m]{m \frac{\sigma_3}{c_0} + 1} \quad (\text{Hoek and Brown 1980, 1997; Hoek, Kaiser and Bawden 1994})$$

In these expressions,  $c_0$ ,  $c_1$ ,  $m$  and  $n$  are material constants (not identical in the different expressions). For other forms, see also Yudhbir, Lemanza and Prinzl (1983), Singh, Ramamurthy and Rao (1989), Sheory, Biswas and Choubey (1989) and Lockner (1995). Forms of failure criteria that include some dependence on the intermediate principal stress are given later (Sect. 3.6).

As implied by the Mohr fracture theory cited above (see Paul 1968; Jaeger 1969, p. 80; Jaeger and Cook 1979, p. 99 for a fuller exposition), the actual shear failure surface is usually observed to have an orientation roughly equal to that of the plane inclined at an angle  $\theta = \pi/4 \pm \varphi/2$  to the direction of the maximum compressive principal stress, where  $\tan \varphi$  is the slope of the Mohr envelope (equal to the coefficient of internal friction in the particular Coulomb case); again, the minus sign refers to compression and the plus sign to extension. However, the correspondence is not always exact, as is seen in Fig. 10 and from other results given by Mogi (1966b), Hoshino et al. (1972, p. 114), and Woronow (1975), and there is some evidence that the discrepancy is greater in extension tests (Mogi 1967b). It has even been suggested that the orientation of the shear fractures in uniaxial compression tests is determined mainly by a tendency for the fracture to run diagonally across the specimen from one end to the other (Paul and Gangal 1967; Paul 1968, p. 445), thus also drawing attention to a possible influence of stress heterogeneity associated with end effects. Moreover, since the studies described in Chapt. 5 reveal that the macroscopic shear fracture usually only develops after the point of maximum stress has been passed, any relation of the fracture orientation to the slope of the Mohr envelope at the maximum stress must be an indirect one.

**Fig. 10.**

Relation between confining pressure and inclination  $\theta$  of shear fracture to compression direction in Westerly granite; *closed circles*: observed angles; *open circles*: angles calculated from coefficient of internal friction  $\tan \phi$  according to  $\theta = \pi/4 - \phi/2$  (after Mogi 1966b)



### 3.4 Influence of Strain Rate, Temperature, and Time

Although, in general, brittle fracture is relatively insensitive to changes in strain rate or temperature compared with behaviour in the ductile field, there are quite significant effects. We consider first the effect of strain rate, which has been studied extensively at room temperature.

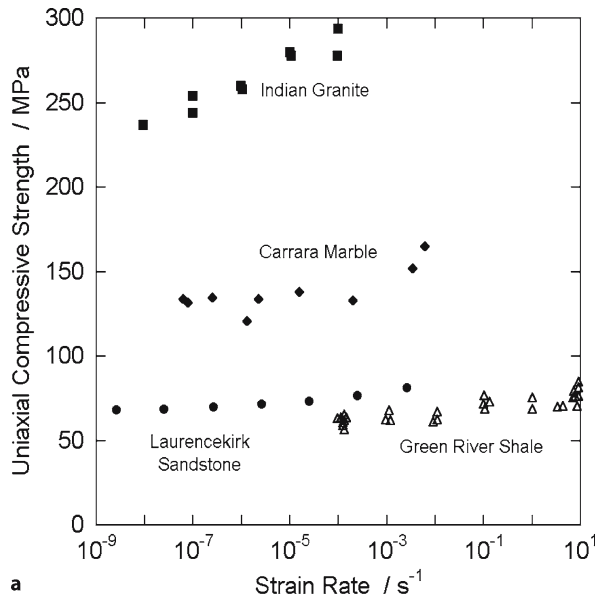
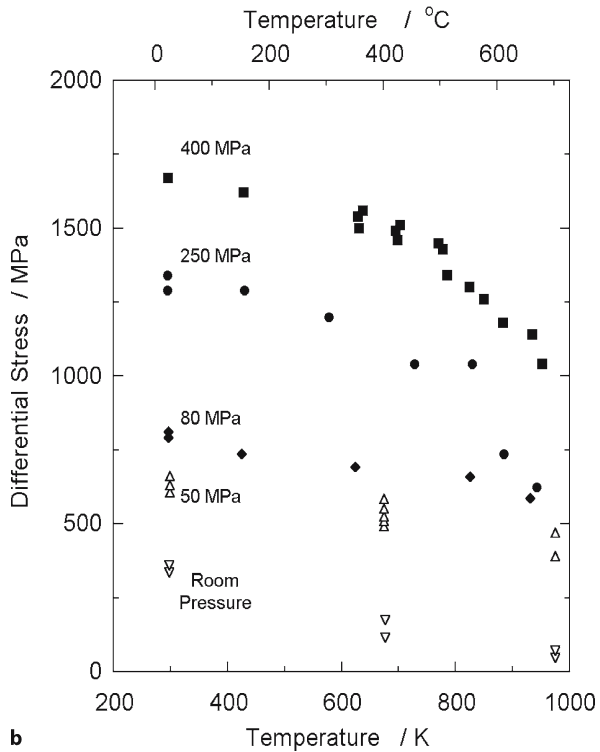
In triaxial tests on limestone and several igneous rocks at *strain rates* of  $10^{-1} \text{ s}^{-1}$  or less, Serdengecti and Boozer (1961), Brace and Martin (1968), Stowe and Ainsworth (1972), Masuda, Mizutani and Yamada (1987) and Masuda (2001) found increases in fracture stress of around 10% for  $10^3$ -fold increase in strain rate. This effect is similar to that noted in uniaxial tests on a marble and a granite by Mogi (1959, 1962c) and on oil shale by Chong et al. (1980). Comparable effects were also found in uniaxial tests on granite, marble, shale, and tuff (Peng 1973; Sano, Ito and Terada 1981; Costin and Mecholsky 1983; Chong et al. 1980; Olsson 1991; Li, Zhao and Li 1999); some of these results are shown in Fig. 11a. Sangha and Dhir (1975) found an effect of similar magnitude in a sandstone in a uniaxial test but a smaller effect in triaxial tests, which also diminished at lower strain rates. Donath and Fruth (1971) found no significant influence of strain rate on the shear fracture strength of a sandstone and a siltstone under a confining pressure of 100 MPa. In contrast, rather large strain rate effects are found in weak porous rocks such as mudstone (Wichter 1979; Chiu, Johnston and Donald 1983; Swan et al. 1989).

For compact rocks, similar strain rate sensitivity is found in uniaxial tests carried to higher strain rates, except for a marked increase in strain rate sensitivity as very high (shock loading) rates are approached (Kumar 1968, on granite and basalt; Perkins, Green and Friedman 1970, on tonalite; Goldsmith, Sackman and Ewart 1976, on granite; Olsson 1991, on tuff; see also Grady et al. 1977; Lankford 1977, 1981). Brace and Jones (1971) suggest that the sharp increase at the highest strain rates is due to a transition to uniaxial strain conditions in shock loading (the relationship between uniaxial straining tests and shock loading is explored further by Schock and Heard 1974).

**Fig. 11.**

**a** Uniaxial compressive strength as a function of strain rate for four different rock types. The marble and sandstone data are from the compilation of Sano, Ito and Terada (1981). The granite and shale data are from Masud, Mizutani and Yamada (1987) and Chong et al. (1980), respectively.

**b** Influence of temperature on peak differential stress at confining pressures shown. The data for room pressure and 50 MPa are for Charcoal granodiorite at a strain rate of  $10^{-4} \text{ s}^{-1}$  (Friedman et al. 1979). The data for 80 MPa, 250 MPa and 400 MPa are for Westerly granite at a strain rate of  $10^{-5} \text{ s}^{-1}$  (Wong 1982b)

**a****b**

However, Grady and coworkers (1980, 1987) argue that this high strain rate sensitivity is due to the fracture dynamics of fragmentation, while Chong et al. (1980) interpret such an effect in oil shale by a nonlinear viscoelastic model. Green and Perkins (1972), Green et al. (1972), and Logan and Handin (1971) also found a relatively high strain rate sensitivity in Westerly Granite at intermediate strain rates, this trend being accentuated under elevated confining pressures, and Lindholm et al. (1974) observed a similar effect in basalt. However, Blanton's (1981) dynamic analysis of his triaxial compression apparatus indicates that such an apparently high strain rate sensitivity can result from machine inertia and need not reflect an intrinsic increase in the rock strength; taking inertia into account, he concluded that the actual failure stresses of Charcoal granodiorite, Indiana limestone and Berea sandstone are relatively independent of strain rate between  $10^{-2}$  and  $10$   $s^{-1}$ . Strain rate sensitivity in fracture strength has also been demonstrated under other types of loading (Price and Knill 1966; Willard and McWilliams 1969; Lipkin, Grady and Campbell 1977; Lipkin and Jones 1979).

The influence of *temperature* on brittle failure stresses for various minerals and rocks in triaxial compression tests at strain rates of the order of  $10^{-4}$   $s^{-1}$  is summarized in the compilations by Handin (1966), Heuze (1983), and Lockner (1995). Further observations are found in the following papers: Tullis and Yund (1977); Friedman et al. (1979); Bauer, Friedman and Handin (1981); Lockner and Byerlee (1980); Caristan (1982); Wong (1982a); Schrodtt and Holder (1983); Fischer and Paterson (1989); Gottschalk et al. (1990); Tullis and Yund (1992); Hirth and Tullis (1994) and Ohnaka et al. (1997). These observations show that there is some decrease in strength with increase in temperature. There is also some tendency for the inclination of the shear fracture to the compression axis to increase with increase in temperature (Handin 1966; Handin, Heard and Magouirk 1967) but the tendency is not very marked, and where it occurs it may be reflecting approach to the brittle-ductile transition (Chapt. 9). Figure 11b summarizes observations on granites which show that the decrease in strength is relatively small at moderate temperatures; a more marked decrease at higher temperatures may be reflecting possible effects of thermal cracking and partial melting. The conclusion that, in the absence of changes of mechanism, brittle fracture has a relatively small temperature sensitivity is further supported by uniaxial tests by Kumar (1968) on basalt and granite and by Perkins, Green and Friedman (1970) on tonalite, including at temperatures below at room temperature (note, however, that the progressive freezing of water films as rock is cooled below 273 K can also contribute to substantial increases in strength down to approximately 150 K; cf. Mellor (1973), and further references given by him).

Thus, there is generally some influence of strain rate, temperature and time on brittle fracture, which may vary with the material and the experimental conditions. This observation points to there being some participation of thermally activated processes in brittle fracture. However, if the effect is assumed to follow an Arrhenius law, the apparent activation energies are low; for example, Kumar (1968) deduces values of 0.8–2  $\text{kJ mol}^{-1}$ , while the "heats of activation" quoted by Serdengecti and Boozer (1961) are equivalent to even lower values of activation energy. The same processes presumably will give rise to some creep at stresses below the fracture stress (Kranz 1979a; Lockner and Byerlee 1980; Carter et al. 1981; Kranz, Harris and Carter 1982; Okubo, Nishimatsu and Fukui 1991), or to static fatigue, and they may include the stress-cor-

rosive effect of water (Scholz 1968c, 1972; Martin 1972). Various fracture mechanics models based on the kinetics of subcritical crack growth have been developed to interpret the creep behavior and strain rate sensitivity of brittle strength (Spetzler, Sondergeld and Getting 1981; Costin and Mecholsky 1983; Lockner and Madden 1991b; Kemeny 1991; Yoshida and Horii 1992). Details will be discussed in Chapt. 6.

### 3.5 Size and Shape Effects

A dependence of fracture stress on *size* or *scale* is well known in materials such as glass and brittle metals. It has also been widely reported in rocks, where it is of particular importance because of the large span in scale between laboratory test specimens and the bodies of rock involved in engineering practice.

Size dependence has commonly been related to a statistical distribution in the severity of the flaws at which fracture is initiated. In this case, it should also be intimately connected with the scatter in strength between specimens in identical tests. Several “weakest link” theories have been developed in which, depending on the form of the distribution function assumed, various types of size dependencies have been predicted (Epstein 1948; Saibel 1971). The theory of Weibull (1939, 1951, 1952) predicts a fracture stress proportional to  $V^{-1/\beta}$  where  $V$  is the volume (the number of defects is assumed to be proportional to the volume) and  $\beta$  is a constant. This theory has received considerable attention and some support (see, e.g., Skinner 1959; Bernaix 1969; Hudson and Fairhurst 1971; Jaeger and Cook 1979). Other types of distributions have been considered which give a  $(\log V)^{-1/\alpha}$  dependence (Epstein 1948), where  $\alpha$  is a constant, or a  $-\log V$  dependence (Kostak and Bielenstein 1971), while Protodyakonov (1964) obtained yet another form of size dependence based upon an average spacing of discontinuities in a body of rock. However, the weakest link theories imply a simple failure model such as one of the simple Griffith type (Chapt. 4) and probably should only be applied in cases of uniaxial tension (Brown 1971), although Lundborg (1972, 1974) has proposed an extension of the Weibull theory to compressive conditions. Brady (1969c), in particular, has suggested that weakest link theories cannot be applied to fracture of rock under general states of stress, and he has proposed instead a statistical theory based on the proliferation of microcracking and assumes that failure occurs “when the volumetric strain due to microcracking attains a critical value” (cf. also Wiebols and Cook 1968). Hudson and Fairhurst (1971) also point to the need for a more general approach than that of Weibull’s theory, and Pretorius (1972) proposed a modification in which correlation between the strengths of adjacent volume elements is taken into account. McClintock and co-workers have developed a statistical approach which includes re-evaluating the stress distribution resulting from the presence of the already-formed stable microcracks at each stage before predicting the formation of the next crack, thus introducing another realistic element (McClintock and Zaverl 1979). Brown and Gonano (1975) have also emphasized the importance of basing theories of the size effect on realistic models of the microcrack structure of real rocks.

The experimental observations of size dependence in rocks have been made primarily in uniaxial compression (Fig. 12a) or in Brazilian tests. In general, they show a decrease in fracture stress with increase in dimensions (Burchartz and Saenger 1931,

and earlier work quoted by them; Dreyer 1958; Evans and Pomeroy 1958; Skinner 1959; Evans, Pomeroy and Berenbaum 1961; Mogi 1962a; Koifman 1963; Habib and Vouille 1966; Jahns 1966; Lundborg 1967, 1968; Bieniawski 1968a, 1972; Bernaix 1969; Kostak and Bielenstein 1971; Pratt, Brown and Brace 1971; Wagner and Schümann 1971; Herget and Unrug 1974; Heuze 1980; Dey and Halleck 1981). Hoek and Brown (1980) give an approximate rule that the uniaxial compressive strength varies inversely as  $d^{0.18}$  in the range 10 to 100 mm diameter, while Bazant and Kazemi (1990) suggest an inverse proportionality to  $(d_0 - d)^{1/2}$  where  $d$  is the diameter and  $d_0$  is a constant. Sometimes the size effect has been found to be negligible or very small (e.g., Obert, Windes and Duvall 1946; Hodgson and Cook 1970; Swolfs 1983) or to become negligible above a certain size (see under in situ tests below). However, these conclusions must be qualified in several respects.

First, size dependence is notably more marked where stress gradients exist, as in Brazilian or punching tests. Where the stress is homogeneous as, for example, in simple compression, the size effect may generally be relatively small (Durelli and Parks 1962; Jaeger and Hoskins 1966b; Lundborg 1967; Hodgson and Cook 1970; Brown 1971; Brown and Gonano 1975). In statistical theories, the greater size effect in heterogeneously stressed specimens is usually related to the relatively small volume in which the highest stresses occur, although Hodgson and Cook (1970) give an explanation of the observed size effect in punching tests in terms of the different diameter dependences of the work done by the punch and the work required for fracture. Sirieys and Saint Leu (1969) have done experiments on the role of stress gradients in fracture in marble, and Lajtai (1971, 1972) relates the size effect to stress gradients by applying a critical local tensile stress criterion at a point that is a fixed absolute distance from the point of theoretically greatest stress concentration, somewhat after the manner of Neuber (1958). It has also been shown that the fluctuations in measured strain with increasing measurement base or “gauge length” become negligible beyond a certain gauge length, 60 mm in the granite studied (Gustkiewicz 1975). The relevance of statistical effects is supported by the observations of Bernaix (1969) that the magnitude of the size effect in Brazilian tests is correlated with the degree of scatter. However, other factors may also be involved.

Thus, second, it has been suggested by Glucklich and Cohen (1967, 1968) that, in materials where there is an appreciable increase in stress between the initiation of local cracking and the occurrence of complete fracture, the fracture stress also depends on the available elastic strain energy in the specimen and hence on its dimensions. They have demonstrated this effect in plaster specimens. Einstein et al. (1970) experimented with plaster, too, and similarly concluded that, while the stress for the start of stable crack propagation only shows a statistical size dependence, the stage of unstable crack propagation leading to complete failure is affected by the available elastic strain energy.

Third, application of confining pressure is said to reduce the size effect and the scatter, based on triaxial tests on marble (Habib and Bernaix 1966; Habib and Vouille 1966; Bernaix 1969). This observation is attributed to the closing of microcracks, but the situation is complicated by the brittle-ductile transition in the pressure range concerned (up to 100 MPa).

By the use of in situ tests the experimental study of the influence of specimen size on strength has also been extended to sizes beyond those used in laboratory tests



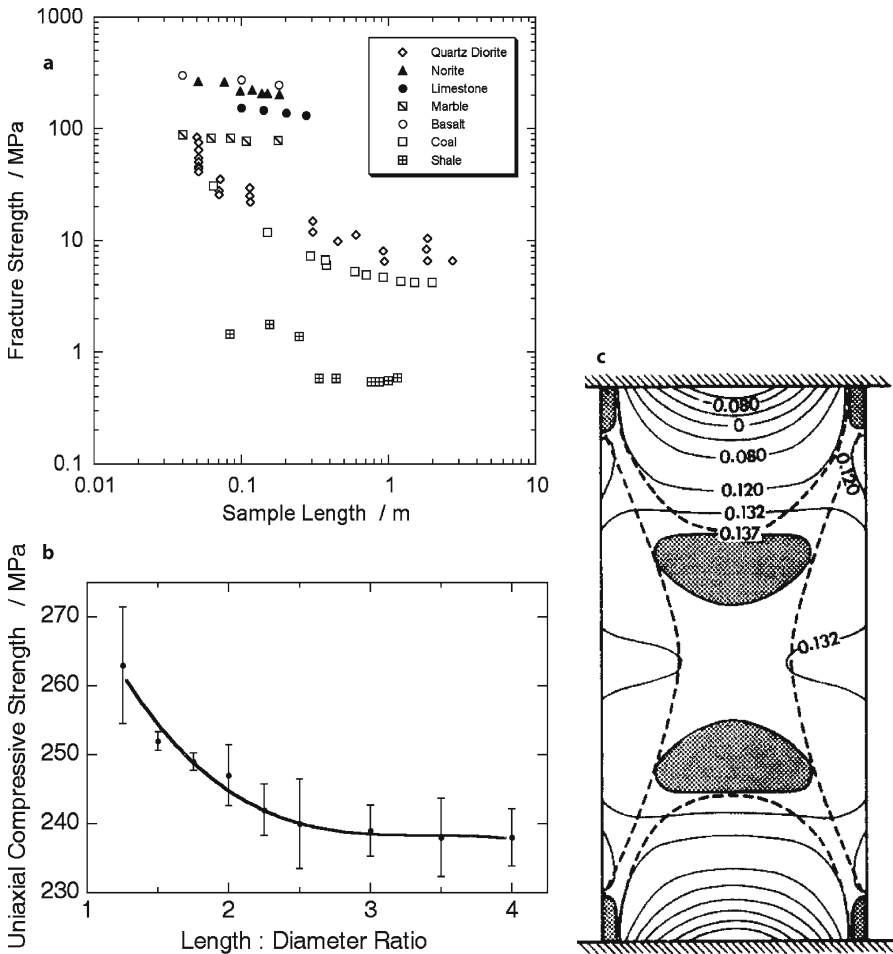


**Fig. 12.** **a** Effect of sample size on peak differential stress at fracture (after Lockner 1995). **b** Dependence of uniaxial compressive strength on length: diameter ratio for Westerly granite (after Mogi 1966). **c** Analysis of elastic stress distribution in uniaxial compression specimen with complete radial constraint at the ends: the contours represent relative intensity of stressing on the modified Griffith criterion of failure with closed cracks (Chapt. 4), the shaded areas being those most severely stressed (after Hawkes and Mellor 1970)

(Fig. 12a). This development is of special relevance to the question of the applicability of laboratory tests in engineering practice. From in situ tests so far carried out, it would appear that little further decrease in strength can be expected for sizes beyond the order of a metre in unjointed rock (Pratt, Brown and Brace 1971; Pratt et al. 1972; and Pratt, Black and Brace 1974, for work on diorite; Bieniawski and van Heerden 1975; Cook and Heard 1981, for further papers; Pinto da Cunha 1990, for a general review).

*Grain size* is another factor that is well known to influence the fracture strength of brittle materials. Experimental study of this factor is difficult because other microstructural, as well as compositional, differences tend to accompany difference in grain size and possibly to obscure the influence of the latter. However, the general trend seems established that finer grain size leads to higher fracture stress (Handin and Hager 1957; Paterson 1958; Skinner 1959; Brace 1961, 1964a; Dreyer 1966, 1967, 1972; Hugman and Friedman 1979; Freiman 1988; Fredrich, Evans and Wong 1990; Wong, Chau and Wang 1996; Hatzor, Zur and Mimran 1997; Prikryl 2001). This trend has been rationalized in terms of Griffith theory (Chapt. 4) by identifying the Griffith crack size with the maximum grain size (Skinner 1959; Brace 1961, 1964a), and similarly in the wing crack model (Chapt. 6).

*Shape* can influence fracture strength in several ways. In practice, most of the research on the role of specimen shape has been concerned with the ratio of length to diameter ("*l/d* effect") in compression or extension tests, especially in relation to end or grip effects. A second role of shape enters through the elastic strain energy effect mentioned above, probably most clearly in special situations such as in bending tests on notched beams of various lengths in which all other dimensions are fixed (Glücklich and Cohen 1967). Where surface damage is significant, shape may also be important in small specimens since it affects the ratio of surface area to volume. Mogi's observations (1962a) indicate a damaged surface layer of the order of one grain diameter in depth. However, no clear practical importance of this in shape (or size) effects appears to have been demonstrated. Here, we shall only discuss the *l/d* effect in relation to end effects.

It has been widely observed in materials testing that in uniaxial compression tests in which platens substantially wider than the specimen diameter are used the brittle fracture stress decreases, at a diminishing rate, as the length:diameter ratio is increased. This effect is also well documented in rocks (Obert, Windes and Duvall 1946; Hobbs 1964a; Herel 1966; Mogi 1966b; Hawkes and Mellor 1970; Bordia 1971; Green and Perkins 1972; Starfield and Wawersik 1972; Dhir and Sangha 1973); see Fig. 12b. Consequently, it is usually recommended that in practical testing the length:diameter ratio should not be less than 2:1 or, preferably, 2.5:1 (Hawkes and Mellor 1970; International Society for Rock Mechanics Commission on Standardization of Laboratory and Field Tests 1978, 1979; Brown 1981). Jaeger (1973) also showed that the length:diameter ratio affects the crushing strength under various conditions of non-uniform loading.

The chief reason for the *l/d* dependence clearly lies in the perturbation of the nominally homogeneous stress field by boundary effects at the contact with the platens, frictional constraint being one of the most important factors; Peng (1971) demonstrated such heterogeneity by strain measurements on granite and steel with different end conditions. This explanation is supported by theoretical analyses of the stress and strain fields that arise in an elastic cylinder in compression under various assumptions such as zero lateral displacement or specific friction conditions at the ends (Filon 1902; Pickett 1944; D'Appolonia and Newmark 1951; Balla 1960; Kotte et al. 1969; Hawkes and Mellor 1970; Brady 1971a–c; Peng 1971; Brady and Blake 1972; Al-Chalabi and Huang 1974). Bordia (1971) made a similar analysis using Prandtl plasticity theory, while Albert and Rudnicki (2001) performed a finite element analysis using non-associated elastic-plastic theory. Using Balla's calculated stresses and the McClintock-Walsh failure criterion (Chapt. 4), Hawkes and Mellor deduced that the most critically stressed regions are those shown shaded in Fig. 12c, that is, that cracking will commence in these regions. Using alterna-

tively a maximum extensile strain criterion of failure, in conjunction with their own calculations, Kotte et al. predicted a somewhat similar pattern, and they were able to correlate observed orientations of microcracks in granite specimens with predicted orientations of extensile strains (see also Peng and Johnson 1972; Peng and Ortiz 1973). These studies therefore show that important departures from uniform stress can be expected for distances of up to roughly half a diameter from the ends when the behaviour is substantially elastic; thus, specimens must have  $l/d$  considerably in excess of 1 in order to approximate a uniform stress in the main part of the specimen, especially when the ends are effectively clamped.

In designing uniaxial compression tests various attempts have been made to reduce or to eliminate the end effects. A detailed discussion of these is given by Hawkes and Mellor (1970); see also Jaeger and Cook (1979, p. 144) and Peng (1971). Briefly, they have included the following devices:

1. Insertion of thin layers of suitable material (e.g., molybdenum disulphide, stearic acid plus talc, Teflon, cardboard, thin metal sheet) between the specimen face and the platen (Föppl 1900; Hardy 1967; Labuz and Bridell 1993). Care has to be taken with this approach to avoid over-compensation, as discussed below. The use of hydraulic loading of the specimen ends (Schock and Duba 1972) or the use of “brush platens” (bundles of flexible steel pins: Brown 1974; Brown and Gonano 1974) overcomes this problem.
2. Matching the properties of the platens more closely to those of the specimens. In practice this involves choosing end pieces having the same value of  $\nu/E$  as the specimen itself, where  $\nu$  = Poisson’s ratio and  $E$  = Young’s modulus. Peng (1971) showed that in granite in the elastic range nearly uniform stressing results from the use of thick steel end pieces of the same diameter as the specimen; see also Hallbauer et al. (1973).
3. Adoption of special specimen shape, for example, slightly conical ends to compensate for frictional constraint, or a “dog-bone” shape with enlarged ends.

In triaxial compression tests, end constraint also exists, as shown by the barrelling that occurs in ductile specimens, but in the brittle field the end effects are found to be less serious in triaxial tests than in unconfined tests and  $l/d = 2$  appears to be satisfactory (Mogi 1966b). This conclusion is supported by theoretical analysis of the elastic stress field along the same lines as mentioned above, which shows that the addition of confining pressure leads to a more nearly uniform stress distribution (Balla 1960; Kotte et al. 1969; Brady 1971a,c).

There has been considerable controversy about the role of end effects in the occurrence of macroscopic brittle fractures parallel to the direction of maximum compressive loading, the so-called *axial splitting* or “axial cleavage” fracture (see Sect. 3.2). This type of fracture is markedly sensitive to the platen or end conditions. For example, either axial splitting or shear fracture has been produced in norite and quartzite in uniaxial tests, depending on whether the platens are similar to the specimen in diameter or are much larger (Bieniawski 1967a). In the latter case, the larger platens presumably give greater constraint at the specimen ends, modifying the stress distribution sufficiently to suppress the longitudinal splitting. However, restraint at the ends

is not always effective in this way, as shown by the experiments of Seldenrath and Gramberg (1958) in which clamping rings were fitted around the ends of the specimens; axial splitting still occurred but at a higher stress. However, Seldenrath and Gramberg had used special pads at the ends of the specimens to reduce friction. The use of too-soft end pads or of a lubricant tends to promote axial splitting by introducing transverse tensile stresses (Brady 1971b,d; Peng and Johnson 1972; Jaeger 1973). Also, initial conical shear failure leads to transverse tensile stresses being generated during further straining because of its wedging action (Griggs 1936; Seldenrath and Gramberg 1958; Griggs and Handin 1960). However, such secondary causes of axial splitting are not always evident, and it appears that, although end effects may promote, modify, or tend to suppress axial splitting, it is an intrinsic mode of initial failure in very brittle material in response to macroscopically homogeneous compressive stress (cf. Wawersik and Fairhurst 1970; Wawersik and Brace 1971).

### 3.6 Influence of Intermediate Principal Stress

It is implicit in the widely used Coulomb and Mohr criteria of failure that the value of the intermediate principal stress  $\sigma_2$  does not affect the brittle fracture strength; in particular, the Mohr envelopes for failure in triaxial compression and extension tests should coincide. Some observations have, within experimental accuracy, been consistent with this (e.g., Brace 1964a) but usually there is some discrepancy in the sense that the failure stresses in extension tend to be slightly higher than would be predicted from compression measurements (Boeker 1915; Ros and Eichinger 1949; Heard 1960; Murrell 1965; Handin, Heard and Magouirk 1967; Mogi 1967b). It would, therefore, appear that the relative value of  $\sigma_2$  does influence the brittle strength, that is, that the Coulomb and Mohr criteria of failure are not strictly valid.

In undertaking investigations on this question, several precautions and qualifications should be mentioned. Thus, it is important that the different stress situations being compared involve the same type of failure, since it is possible that different types of relations will exist between the stress components for different types of failures, depending on the physical mechanisms involved. Also, unless isotropy of strength is being assumed, the anisotropy must be taken into account. Finally, apart from uncertainties due to scatter, the comparison of compressional and extensional triaxial tests has the limitation that  $\sigma_2$  is always equal to one or another of the extreme principal stresses, and more general tests are needed to investigate a full range of relative values of  $\sigma_2$ .

Studies aimed specifically at defining the role of all three principal stresses in brittle failure have mainly used the following types of experimental arrangement:

1. Torsion under confining pressure, combined with additional axial loading, and preferably using hollow cylindrical specimens in order to achieve more nearly homogeneous stress (Boeker 1915; Handin, Higgs and O'Brien 1960; Handin, Heard and Magouirk 1967; Durand 1975; Tullis and Tullis 1986; Paterson and Olgaard 2000); alternatively, differential diametral loading of a hollow cylinder combined with axial loading (Robertson 1955; Jaeger and Hoskins 1966a; Mazanti and Sowers 1966; Hoskins 1969b).

2. Compressive loading on two or three opposite pairs of faces of cubic specimens, referred to respectively as biaxial and “true triaxial” or “polyaxial” tests, in which special precautions are taken to minimize frictional constraint at the loading platens (Mogi 1967b; Wawersik 1971; Wawersik and Swenson 1972; Brown 1974, for biaxial tests; Kvapil and Luffer 1960; Dreyer and Borchert 1962; Niwa and Kobayashi 1967; Niwa, Kobayashi and Koyanagi 1967; Hojem and Cook 1968; Bieniawski, Denkhaus and Vogler 1969; Mogi 1971a,b,1977; Atkinson and Ko 1973; Alexeyev, Osiika and Todoseychuk 1974; Alexeyev, Nedodaev and Chekhova 1974; Gau, Cheng and Zhuo 1983; Amadei and Robison 1986; Esaki and Kimura 1989; Crawford et al. 1995; Smart 1995; Haimson and Chang 2000; Chang and Haimson 2000, for triaxial tests); also Akai (1967) quoted by Mogi (1971a).
3. Brazilian and punching tests under confining pressure, in which it is possible that stress gradients play a complicating role (Robertson 1955; Jaeger and Hoskins 1966a; Handin, Heard and Magouirk 1967).

The general conclusion from the experimental studies reported in the preceding papers is that the value of the maximum principal stress  $\sigma_1$  in cases of brittle *shear* fracture is affected by the value of  $\sigma_2$  as well as by  $\sigma_3$  (Fig. 13). However, there is no general agreement about the form of the  $\sigma_2$  dependence. Handin et al. plotted octahedral shear stress

$$\tau_{\text{oct}} = \frac{1}{3} \sqrt{(\sigma_2 - \sigma_3)^2 + (\sigma_3 - \sigma_1)^2 + (\sigma_1 - \sigma_2)^2}$$

against mean stress  $(\sigma_1 + \sigma_2 + \sigma_3)/3$  and found different relations for the different types of tests, so this procedure did not give a useful failure criterion. On the other hand, Mogi has variously fitted results to criteria of the following forms:

$$\sigma_1 - \sigma_3 = f(\sigma_1 + \sigma_3 + \alpha\sigma_2) \quad \text{where } \alpha \text{ is around } 0.1 \text{ to } 0.2 \quad (\text{Mogi } 1967\text{b})$$

$$\tau_{\text{oct}} = f(\sigma_1 + \sigma_3 + \alpha\sigma_2) \quad \text{or} \quad \tau_{\text{oct}} = f(\sigma_1 + \sigma_3) \quad (\text{Mogi } 1971\text{b})$$

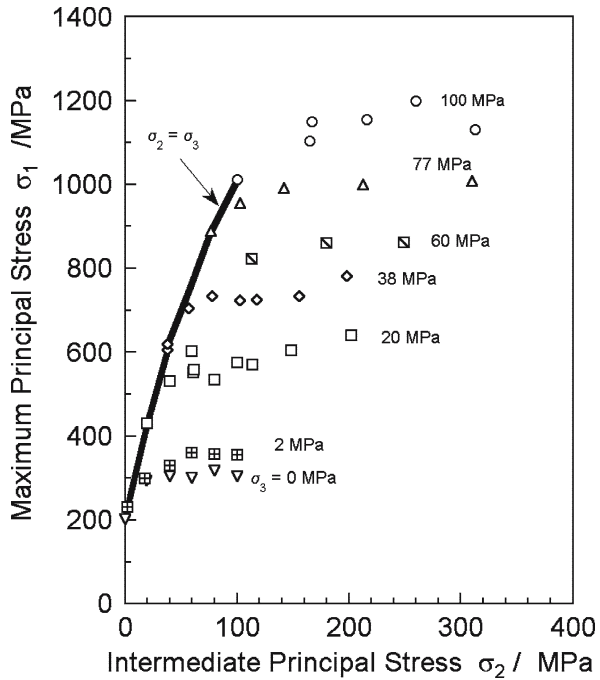
$$\tau_{\text{oct}} \approx A(\sigma_1 + \sigma_3)^n \quad (\text{Mogi } 1972\text{a}; \text{ Chang and Haimson } 2000; \text{ Haimson and Chang } 2000)$$

where  $A$  and  $n$  are constants ( $n$  varying from 0.56 for Solnhofen limestone to 0.89 for a granite). Green et al. (1972) also found the last form to fit data for limestone and granite, with  $n = 1$ . This form represents a modification of the von Mises failure criterion (Jaeger 1969, p. 92) such that the limiting value of the octahedral shear stress (or elastic shear strain energy) at which failure occurs increases as the mean normal stress on the potential shear failure plane increases. However, for unjacketed amphibolite, Haimson and Chang (2002) found that a linear relationship between octahedral shear stress and octahedral normal stress gave a better representation of the failure condition.

It is also found that the angle  $\theta$  between the shear failure plane and the maximum compressive principal stress increases as the relative value of  $\sigma_2$  increases (Heard 1960; Handin, Heard and Magouirk 1967; Mogi 1972a). In particular, the  $\theta$  values in extension

**Fig. 13.**

Data from “true” triaxial tests of Westerly granite, plotted as the peak value of  $\sigma_1$  as function of  $\sigma_2$  at  $\sigma_3$  values shown. Data points connected by the solid line were from conventional triaxial tests (after Haimson and Chang 2000)



tests are less than those in compression tests. The failure plane is always parallel to the  $\sigma_2$  direction (cf. Sect. 3.7.1 for anisotropic materials). Ductility is also found to decrease with increase in the relative value of  $\sigma_2$  (Heard 1960; Handin, Heard and Magouirk 1967; Mogi 1971a,b, 1972a).

There is less experimental information relating specifically to the influence of  $\sigma_2$  on *extension* failures. Handin, Heard, and Magouirk (1967) concluded that extension fracturing in different types of tests on Solnhofen limestone occurred at approximately the same value of least compressive principal stress regardless of the values of both the other principal stresses and that, because of the different mechanisms, there was no point in attempting to correlate this with the shear failure cases. On the other hand, Hoskins (1969b), in agreement with Brace (1964a), concluded that there is a smooth transition from failure by extension fracture to failure by shear, with correspondingly no sharp transitions in the failure conditions in terms of the principal stresses; this may mean that the intermediate principal stress has much the same influence on failure stresses regardless of whether the final fracture is an extension fracture or a shear fracture.

The explanation of the role of the intermediate principal stress probably lies in factors involved in the propagation of the fracture rather than in its initiation. In the simple Griffith picture (Chapt. 4) of the initiation of cracking at a critical flaw, analyses of elastic stress distributions show that the applied intermediate principal stress should not affect crack initiation, which will occur in a plane parallel to the  $\sigma_2$  axis (Murrell and Digby 1970). The same prediction arises from the Coulomb notion that a crack will

propagate in the plane in which the macroscopic shear stress first overcomes the “friction” from the normal stress across the plane. However, as various workers have pointed out (Brady 1969a–d, 1970; Murrell and Digby 1970; Mogi 1971a), the actual fracture surface is irregular and not everywhere parallel to the  $\sigma_2$  axis. Thus, the development of the macroscopic failure in practice involves fracture locally on surfaces not exactly parallel to  $\sigma_2$ , the normal and shear stresses on which will include a component of  $\sigma_2$ , so that the development of the cracking will be influenced by  $\sigma_2$ . Prediction of this influence follows in statistical or strain energy theories of the failure condition (Wiebols and Cook 1968; Brady 1970; Lundborg 1972, 1974; see Chapt. 4 for further details of these approaches). Fjaer and Ruistuen (2002) have proposed a failure probability model based on the concept that the stress state has a lower symmetry when the intermediate principal stress is unequal to either of the extreme principal stresses and then there are fewer potential failure planes available.

## 3.7 Anisotropy

### 3.7.1 Observations

So far, we have assumed isotropic behaviour in considering failure conditions such as the Coulomb relation and the  $\pi/4 - \phi/2$  failure angle (Sect. 3.3). This assumption is only valid for rocks that do not have a preferred orientation of planes of weakness or other pronounced fabric. However, in many rocks, for example, in jointed rock masses or in slates and schists, anisotropy in brittle behaviour can be important. It is expressed as a variation of the fracture stress with orientation of the principal stress axes relative to the fabric of the rock; also, shear fractures may depart markedly from the  $\pi/4 - \phi/2$  orientation.

Four examples of anisotropy of fracture stress in slates and shales are illustrated in Fig. 14 from triaxial compression tests by Donath (1972a) and McLamore and Gray (1967). Other triaxial studies have been made by Jaeger (1960b), Donath (1961, 1962, 1964, 1972b), Dayre and Sirieys (1964), Hobbs (1964b), Hoek (1965), Chevenert and Gatlin (1965), Avramova and Stancheva (1966), Deklotz, Brown and Stemler (1966), Sirieys (1966), Youash (1966), Fayed (1968), Akai, Yamamoto and Arioka (1970), Masure (1970), McGill and Raney (1970), Pomeroy, Hobbs and Mahmoud (1971), Attewell and Sandford (1974), McCabe and Loerner (1975), Gottschalk et al. (1990), Vernik, Lockner and Zoback (1992), Shea and Kronenberg (1993), Niandou et al. (1997), Rawling, Baud and Wong (2002), and others. The range of behaviour shown in Fig. 14 is typical of other foliated rocks as well (including amphibolite, gneiss, phyllite and schist). The minimum in strength occurs when the maximum principal compressive stress is inclined at around  $30^\circ$ , or somewhat more, to the plane of foliation. In some cases, especially in weakly anisotropic rocks and in slates, schists and gneisses, the strength versus orientation curve is concave upwards over its whole range; in other cases, such as singly jointed rock or rock with prominent bedding, the curve tends to have flat “shoulders” near the extreme orientations (especially near the  $90^\circ$  orientation). Rais-

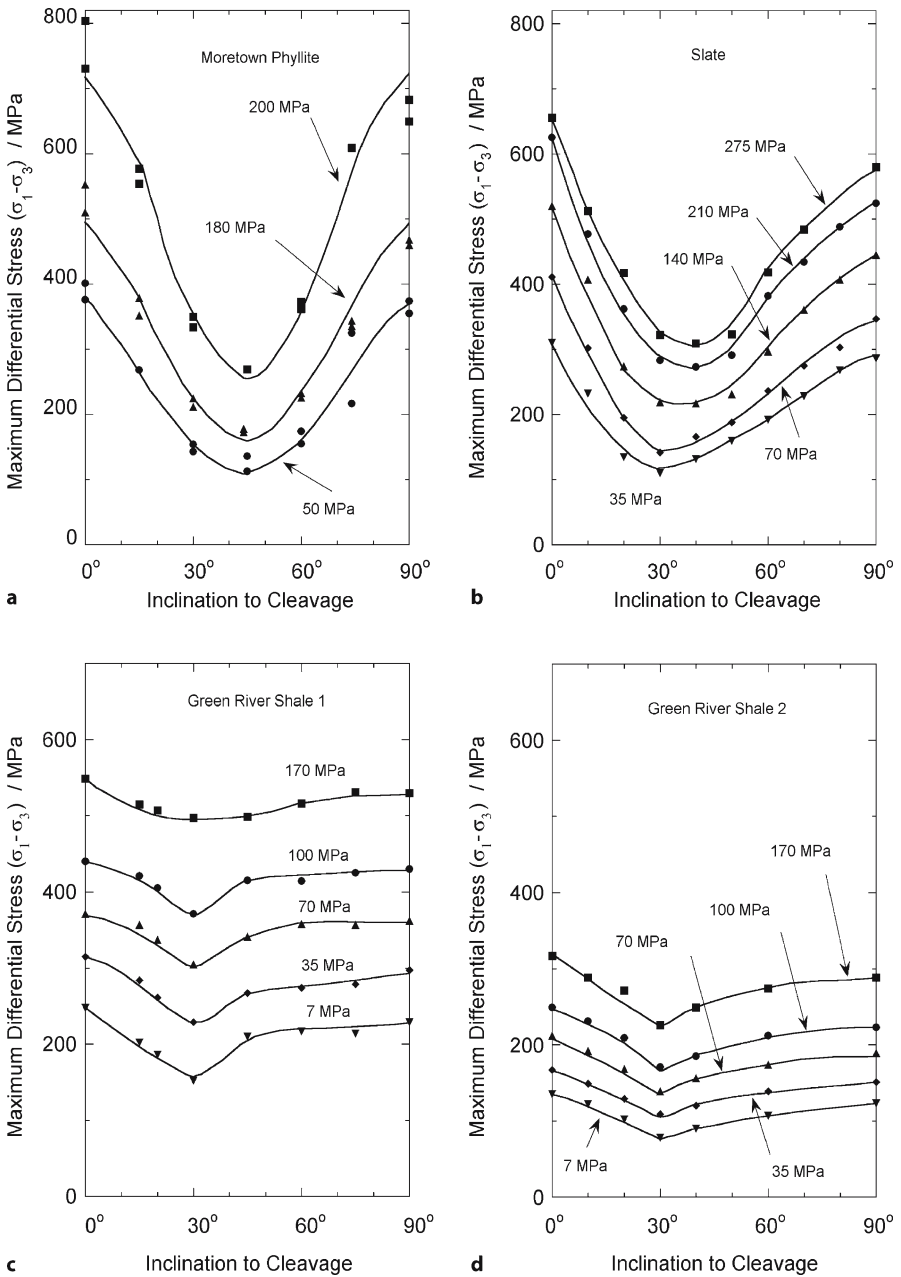


**Fig. 14.** Dependence of differential stress at failure in triaxial compression on the inclination of the cleavage plane to the compression axis for foliated rocks at confining pressures shown. **a** Phyllite (after Donath 1972a); **b-d** a slate and two shales (after McLamore and Gray 1967)



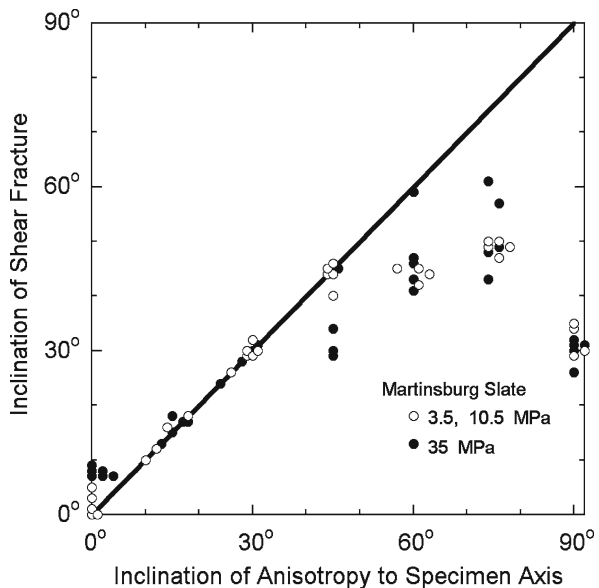
ing the confining pressure may enhance or diminish the degree of anisotropy in different cases. Also, the strength in compression parallel to the foliation plane may be greater or less than that normal to it.

The representation of the anisotropy in diagrams like Fig. 14, or in the equivalent polar diagrams sometimes used (cf. Fig. 16b below), is only adequate if the strength is approximately isotropic in the foliation plane and axially symmetric about the normal to this plane. In more general cases, a three-dimensional representation of the anisotropy is required. Rodrigues (1966, 1970) and Rodrigues and Aires-Barros (1970) showed that quadratic or quartic surfaces can be fitted to strength measurements in these cases, and they present experimental results for granites, diabases, slates, and schist. Stereographic projection can be a convenient aid in depicting data that require three-dimensional representation (Jaeger and Rosengren 1969).

Shear fractures in foliated rock tend to coincide with the plane of lowest shear strength for a range of intermediate orientations but, for the more extreme orientations, the fractures either occur at the  $\pi/4 - \phi/2$  inclination of roughly  $30^\circ$  (as in isotropic rocks, Sect. 3.3) or at an inclination intermediate between this and the plane of lowest shear strength. The orientations of shear fracture in a slate shown in Fig. 15 illustrate this. Also the fracture plane need no longer contain the intermediate principal stress axis (Jaeger 1964).

An orientation dependence of failure stress like that possessed by some anisotropic rocks can be simulated in confined compression tests on specimens of isotropic rock containing a sawcut or similar single plane of weakness (Jaeger 1959; Handin and Stearns 1964; Lane and Heck 1964; More, quoted by Sirieys 1966; Okusa 1971). Over a wide range of orientations, failure occurs by sliding on the cut rather than on

**Fig. 15.** Inclination of shear fracture to compression axis for different inclinations of the cleavage plane to the compression axis in triaxial compression tests on slate at the confining pressures shown. Note that for small inclinations the shear fractures followed the cleavage (after Donath 1961)



the  $\pi/4 - \varphi/2$  plane expected for the intact rock while, for orientations of the cut near to  $90^\circ$  to the compression axis, and sometimes near  $0^\circ$ , failure occurs through the intact rock. This leads to flat shoulders on the strength versus orientation curve similar to those mentioned previously. The study of specimens with cuts has been pursued in part as an aid to understanding the behaviour of jointed rock in engineering situations and leads to experiments with models of jointed rock.

### 3.7.2 Theoretical Analysis

Theories of brittle failure of rocks with planar anisotropy (that is, axially symmetric in symmetry) fall broadly into two groups. Those in the first group, which may be called plane-of-weakness theories, give a treatment that is equivalent to taking as a model the isotropic rock with a sawcut, described in the previous paragraph. Thus, assuming one set of values of cohesion and internal friction,  $\tau'_0$  and  $\tan \varphi'$ , for the plane of weakness and another set  $\tau_0$ ,  $\tan \varphi$  for failure on any other plane, Jaeger (1960b) used Coulomb theory to calculate the resistance to failure on the plane of weakness and on the most favoured plane intersecting it, in terms of the principal stresses. This leads to the type of dependence of compressive strength on orientation depicted in Fig. 16. In region B, the shear failure follows a plane of weakness and occurs when

$$\sigma_1 - \sigma_3 = \frac{1}{\cos(\varphi' + \alpha) \sin \alpha} (\tau'_0 \cos \varphi' + \sigma_3 \sin \varphi')$$

where  $\alpha$  is the inclination of the plane of weakness to the maximum principal compressive stress direction (Jaeger 1971; Jaeger and Cook 1979, p. 106); the minimum strength occurs when  $\alpha = \pi/4 - \varphi'/2$ . In region A, failure occurs more easily on a plane

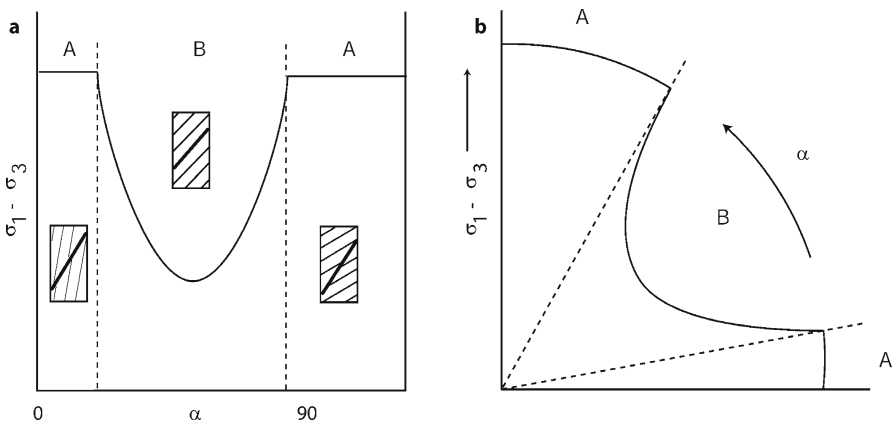


**Fig. 16.** The dependence of the differential stress  $\sigma_1 - \sigma_3$  at failure on the orientation  $\alpha$  for the single-plane-of-weakness model of anisotropic rock (see text for details). **a** Cartesian plot; **b** polar plot

other than the plane of weakness and since all other planes are assumed equivalent in strength, the failure occurs at the Coulomb stress (Sect. 3.3)

$$\sigma_1 - \sigma_3 = \sigma_0 + \sigma_3 \tan \psi = \frac{2}{1 - \sin \varphi} (\tau_0 \cos \varphi + \sigma_3 \sin \varphi)$$

and the predicted failure plane is oriented at  $\pi/4 - \varphi/2$ , independently of the orientation of the plane of weakness. Relations identical to the above have been derived from an equivalent Griffith crack model in which it is assumed (1) that there are two populations of cracks, long cracks lying parallel to a given plane (the “plane of weakness”) and short cracks randomly oriented, and (2) that the cracks are closed and subject to friction in the relative sliding of their surfaces (Hoek 1965; Walsh and Brace 1964; see also Barron 1971a).

The behaviour modelled by the plane-of-weakness theories (Fig. 16) is represented very roughly in practice by that of some rocks, for example, the shales of Fig. 14c and 14d or the slate studied by Hoek (1965), but in general the development of shoulders is not as marked as predicted, and the strengths parallel to and normal to the foliation are not equal, as in the simple theory. Walsh and Brace (1964) discussed modification of the Griffith theory in which a distribution of the sizes of the long cracks is assumed which would lead to more general types of behaviour. Kobayashi (1970) also discussed several modifications to the single plane-of-weakness theories, including assumption of planes of weakness of more than one orientation and assumption of a quadratic dependence on normal stress in place of the linear Coulomb relation. However, in the absence of more detailed knowledge of the actual mechanisms of failure, the introduction of additional parameters in this way is likely to be more of curve-fitting value than of physical significance. Nevertheless, Attewell and Sandford (1974) have explored the application of Griffith analysis further, using an anisotropic crack distribution derived from X-ray measurements on the preferred orientations of the platy minerals in a slate and applying the analysis to cracks as existing just prior to final failure.

The theories of the second group are more empirically based but are more versatile and, in particular, are probably more suitable for modelling cases of moderate anisotropy. These models allow a gradation in behaviour with orientation rather than the two sharply distinguished modes of failure considered in the simple plane-of-weakness models.

As a first move, Jaeger (1960b) took the purely empirical step of generalizing the Coulomb theory by expressing the cohesion term as a function of orientation of the form

$$\tau_0 = \tau'_0 - \tau''_0 \cos 2\omega$$

where  $\omega$  is the angle between the plane of shearing and the plane of minimum shear strength, and  $\tau'_0$ ,  $\tau''_0$  are constants (the same form of orientation dependence of the cohesion had previously been proposed by Casagrande and Carrillo 1944). The resistance to shearing on the plane is then given by

$$\tau'_0 - \tau''_0 \cos 2\omega + \sigma_n \tan \varphi$$

where  $\sigma_n$  is the normal stress acting on the plane and  $\tan \varphi$ , the coefficient of internal friction, is assumed to be independent of orientation. In a triaxial test in which the maximum principal compressive stress  $\sigma_1$  is applied at an angle  $\alpha$  to the plane of minimum shear strength, failure is then predicted to occur on the plane on which the quantity

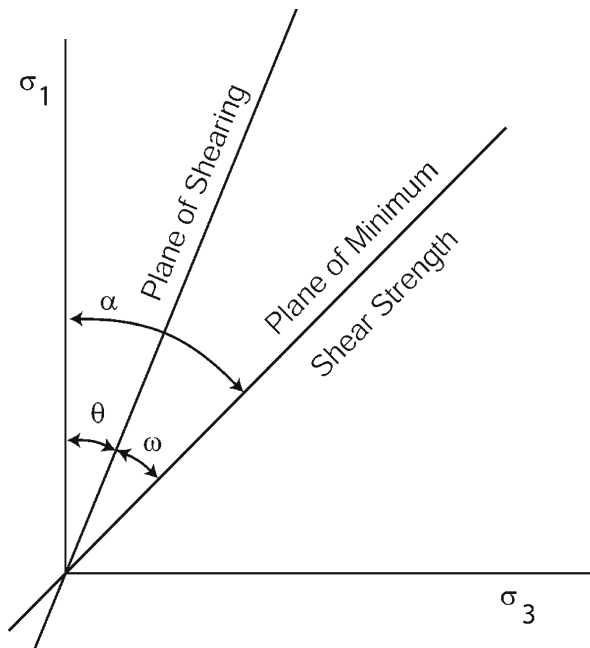
$$\tau - \sigma_n \tan \varphi + \tau''_0 \cos 2\omega$$

first reaches the value  $\tau'_0$ , where  $\tau$  is the shear stress on the plane. Putting  $\omega = \alpha - \theta$  (Fig. 17), expressing  $\tau$  and  $\sigma_n$  in terms of the principal stresses  $\sigma_3$ , and maximizing this quantity with respect to variation in  $\theta$ , it follows that fracture is predicted on the plane whose inclination  $\theta$  to  $\sigma_1$  is given by

$$\tan 2\theta = \frac{(\sigma_1 - \sigma_3) + 2\tau''_0 \sin 2\alpha}{(\sigma_1 - \sigma_3) \tan \varphi + 2\tau''_0 \cos 2\alpha}$$

It can then be shown that only when  $\alpha = \pi/4 - \varphi/2$  is fracture predicted at  $\theta = \pi/4 - \varphi/2$ , and only for this orientation does the predicted failure plane coincide with the plane of minimum shear strength. In all other orientations, shear failure is predicted to deviate from the orientation  $\pi/4 - \varphi/2$  in the sense of towards that of the

**Fig. 17.**  
Definition of angular relationships for anisotropic rock



plane of minimum shear strength. The relation between the principal stresses at fracture can now be derived from the equation

$$\tau - \sigma_n \tan \varphi + \tau_0 \cos 2(\alpha - \theta) = \tau'_0$$

by using the value of  $\theta$  derived above; this leads to

$$[(\sigma_1 - \sigma_3) + 2\tau'_0 \sin 2\alpha]^2 + [(\sigma_1 - \sigma_3) \tan \varphi + 2\tau''_0 \cos 2\alpha]^2 = [(\sigma_1 + \sigma_3) \tan \varphi + 2\tau'_0]^2$$

which can be re-arranged to give equivalent but cumbersome expressions relating differential stress to confining pressure or describing the Mohr envelope in a Mohr plot.

Compared with the single plane of weakness theory, this theory gives a less sharply developed minimum in the variation of strength with orientation and an absence of shoulders at the extreme orientations. Other distinctive properties are:

1. The exact shape of the dependence of differential stress at failure on orientation, and the values of the failure angle  $\theta$ , now depend on the level of the stresses themselves (e.g.,  $\tan 2\theta$  is shown as a function of  $\tau''_0/(\sigma_1 - \sigma_3)$  above).
2. The differential stress has a non-linear dependence on confining pressure and the Mohr envelope is correspondingly curved.
3. The predicted strengths parallel to and normal to the foliation are different, that parallel to the foliation always being the lesser.

The last prediction is often not realized in practice, the strength parallel to the foliation sometimes being the greater. This suggests that  $\tan \varphi$  also varies with orientation and that  $\tan \varphi$  is sometimes greater for loading parallel to the foliation than for normal (Jaeger 1964). Casagrande and Carrillo (1944) considered the case where  $\tan \varphi$  also varies with orientation. McLamore and Gray (1967) analysed the behaviour of a shale and a slate in terms of variable  $\tau_0$  and variable  $\tan \varphi$  but they also used different values of the constants ( $\tau'_0$ , etc.) in the ranges of inclination  $\alpha$  below and above an intermediate value. Further, McLamore and Gray used a  $\cos^n 2\omega$  form of variation in  $\tau_0$  and  $\tan \varphi$ , where  $n$  is given values up to 5 or more, to reproduce the observed tendency towards the development of "shoulders" in the plot strength versus orientation (there seems to be some confusion in their paper between specifying failure orientations relative to the foliation plane and to the orientation of the maximum principal compressive stress; also, it is not clear how they calculated the failure stresses  $\sigma_1 - \sigma_3$  from  $\tau_0$  and  $\tan \varphi$ ).

## Griffith Theory of Brittle Failure

### 4.1 Introduction

There have been classically two different approaches to developing a theory of brittle failure of rocks that will predict the macroscopic fracture stress. The first approach consists essentially of empirical attempts to state criteria of failure that are consistent with the observed failure conditions in particular types of experiments but whose main function is to provide a basis for calculating failure conditions in practical situations involving more general states of stress. Although such theories may be discussed in physical terms, such as limits on stresses on certain planes or limits on strain energy, they say very little about the physical mechanisms of failure. The best-known of such failure criteria are those of Coulomb and Mohr (Paul 1968; Jaeger 1969); see Sect. 3.3. These criteria are given in terms of stresses but do not depend on the intermediate principal stress  $\sigma_2$ . However, evidence has also been given that  $\sigma_2$  does influence the failure, and some forms of failure criteria taking  $\sigma_2$  into account have been mentioned in this connection (Sect. 3.6). Other forms of criteria in terms of stresses have been given by Cherry, Larson and Rapp (1968), Lundborg (1968, 1972, 1974), and Franklin (1971b). Commonly a separate criterion, such as the critical maximum tensile stress criterion (Sect. 3.3), is applied to extensile failure, and this may be combined with the Coulomb criterion as “tension cut-offs” (see Paul 1961, 1968). In other cases (e.g., Cherry, Larson and Rapp 1968), a single form of criterion is applied to all types of failures.

Attempts have also been made to express brittle failure criteria in terms of strains. The simplest version, that failure occurs at a critical value of the maximum extensile strain, has already been mentioned (Sect. 3.2; cf. also Trollope 1968). Hatano (1969) also takes up the critical maximum extensile strain criterion but suggests that the critical strain is subject to some variability in accordance with a Weibull statistical distribution. In the case of shear failure, it has also been proposed that fracture will occur on planes on which critical shear strain is first reached (Becker 1893; see comments by Griggs 1935; and Jaeger 1969, p. 86). However, this criterion has found little favour.

The second approach to developing a brittle failure theory attempts to set up a physical model of the brittle fracture process that is amenable to theoretical treatment. Although a degree of empiricism may still be involved, the model is intended to represent essential aspects of the actual physical mechanism of fracture and provide a firmer basis for establishing criteria of failure applicable to general states of stress. This approach is epitomized in the application to rocks of the Griffith theory of brittle fracture.

One of the most significant advances in the theory of fracture was Griffith's proposal in 1920 that the strength of brittle materials is governed by the initial presence of small cracks. There is abundant evidence for the existence of crack-like flaws in many brittle materials. In particular in rocks the presence of microcracks within grains and at grain boundaries has been well established (Chapt. 5) and there are, in addition, larger-scale cracks such as joints. Therefore, Griffith's model is physically plausible and has been intensively studied and developed to derive macroscopic criteria of failure under combined stresses. For the application of the Griffith theory in rock mechanics, Jaeger and Cook (1979, pp. 101–106, 277–282, 337–347) give a general introduction, and more details of this application will be found in papers cited below, especially the papers by Brace, Walsh, Murrell and Hoek and their co-workers. The mechanistic study of the brittle fracture processes, dealt with later, will reveal severe limitations to the direct application of Griffith's theory to the macroscopic fracture stress and will highlight the need for a micromechanical approach. However, Griffith's theory has also given rise to the subject of linear elastic fracture mechanics (see Appendix 1) which has extensive application in the micromechanics of brittle failure (Chapt. 6). It is therefore of importance to deal briefly with the theory here.

The basis of Griffith's theory in its biaxial form (Griffith 1924) is that failure occurs when the most vulnerably oriented crack in a population of randomly oriented cracks begins to extend under the applied stress. The extension of the crack is assumed to occur when the maximum tensile stress component at any point around the crack reaches the critical value needed to overcome the interatomic cohesion of the material. To make the calculation of the stress distribution tractable, Griffith also assumed that the cracks were of cylindrical shape with a flattened elliptical cross-section and he dealt only with the two-dimensional problem in the plane of this cross-section, using the classical theory of linear elasticity to calculate the local stress distribution around a crack. The problem has been generalized in later treatments, as described below. However, as an introduction, we shall first discuss Griffith's preliminary calculation of the influence of a crack on the tensile strength of a brittle material.

## 4.2 Uniaxial Tension

To calculate the brittle tensile strength, Griffith (1920) introduced an energy argument which has often been used since in discussing crack propagation. This approach in effect uses the surface energy as a measure of the local cohesive strength of the material. The criterion of failure, based on the principle that the potential energy of a system will tend to a minimum, is that the crack will propagate if in doing so the sum of the following three terms is zero or negative:

1. the surface energy of the new crack surface created;
2. the change in the elastic strain energy of the body;
3. the change in the potential energy of the loading system.

Since in the absence of any other changes this sum represents the change in the Gibbs potential, the energy criterion is equivalent to requiring the Gibbs potential to

be minimized, and it is therefore sometimes referred to as the thermodynamic criterion of failure (e.g., Murrell 1964; Murrell and Digby 1972).

In the case of an applied uniaxial macroscopic tensile stress  $\sigma$ , the energy criterion predicts failure at the stress

$$\sigma = T_0 = \sqrt{\beta \frac{E\gamma}{c}} \quad (4.1)$$

where  $E$  is Young's modulus,  $\gamma$  is the specific surface energy, and  $2c$  is the crack length (i.e., the major diameter of the elliptical cross-section, the minor diameter being assumed to be negligibly small). The quantity  $\beta$  is a numerical constant of the order of unity. The exact value of  $\beta$  depends on assumptions made in calculating the local elastic stress distribution around the crack. If plane strain is assumed

$$\beta = \frac{2}{\pi(1-\nu^2)}$$

where  $\nu$  is Poisson's ratio; if generalized plane stress is assumed,  $\beta = 2/\pi$  (see Sih 1967; Sih 1968, for calculations of these values of  $\beta$  and for values of  $\beta$  in the cases where the minor axis of the ellipsoidal cross-section is not negligibly small). A similar result is obtained for penny-shaped ellipsoidal cracks, with  $\beta = \pi/[2(1-\nu^2)]$  (Sack 1946; Sneddon 1946). It is implicit that the crack is normal to the applied stress. If there is a random distribution of the orientations of cracks with the given length  $2c$ , the crack that will first begin to extend when the stress satisfies Eq. 4.1 will be the one whose major axis lies normal to the direction of the applied stress.

Several comments will now be made on the significance of Eq. 4.1 in relation to (1) the shape of the crack and singularity problems, (2) the local failure criterion, (3) the significance of the surface energy term, and (4) dynamic aspects:

1. *Shape of the crack.* The assumption that the ellipsoidal crack is of negligible width normal to the plane of the crack implies that the radius of curvature at the crack tip is effectively zero and the maximum stress therefore infinite in the elasticity calculation. The existence of this singularity is glossed over by saying either that the region affected is negligibly small or that the radius of curvature cannot be smaller than atomic or molecular dimension (e.g., Orowan 1949); indeed, the crack surfaces must be slightly separated to prevent surface forces from closing the crack (Elliott 1947; Murrell 1964). The value of  $\beta$  in the Griffith formula (Eq. 4.1) is not very sensitive to the exact shape of the crack, provided that its width normal to its plane is small compared with its length  $2c$ .
2. *Local failure criterion.* Griffith's energy approach to the derivation of Eq. 4.1 does not explicitly consider the magnitudes of the local stresses at the crack tip but Griffith did draw attention to the facts that the maximum local tensile stress component will be approximately  $2\sigma \sqrt{c/r}$ , where  $r$  is the radius of curvature at the crack tip and  $\sigma$  is the applied macroscopic tensile stress normal to the crack (Inglis 1913) and that when reasonable values of  $r$  are inserted, this expression implies very high local tensile stresses, probably of an order corresponding to interatomic



forces. This raises the question of trying to define more precisely the local conditions of failure at the crack tip. Orowan (1949) gave an order of magnitude calculation of the maximum stress at the crack tip using an argument similar to Griffith's energy argument but applied only to the vicinity of the crack tip; this led to the following relationship between the surface energy and the interatomic cohesive strength  $\sigma_T$  of the material:

$$\sigma_T \approx 2\sqrt{\frac{E\gamma}{a}}$$

where  $a$  is the interatomic spacing. In more sophisticated approaches (Elliott 1947; Barenblatt 1959, 1962; Blekherman and Indenbom 1974; Lawn and Wilshaw 1975b, Ch. 7; Atkinson and Meredith 1987b; Lawn 1993, Ch. 6), the implicit assumption of a smooth contour at the atomic scale has been abandoned and explicit models for the interatomic cohesive forces in a cusp-shaped crack tip have been used, applying linear elasticity theory only outside the crack tip region; these approaches also yield essentially the same result as the Griffith formula (Eq. 4.1). However, in practice, non-elastic effects probably can be normally expected at the crack tips; these effects throw serious doubt on how far it is worth pursuing the idealized picture so far discussed, and they lead one to the next point.

3. *Significance of the surface energy term.* The specific surface energy  $\gamma$  of a solid can be estimated approximately on theoretical arguments from the elastic constants (Gilman 1960; Brace and Walsh 1962) or from the specific energy of evaporation (Pugh 1967); the predicted values are of the order of magnitude of  $0.1\text{--}1 \text{ J m}^{-2}$  for most materials. Experimental determinations of  $\gamma$  have been made by measuring the force needed for propagating a crack of known dimensions and then applying the Griffith energy argument. In favourable cases, not complicated by local plastic deformation or multiple fracturing at the crack tip, especially in single crystals, the experimentally derived values of  $\gamma$  agree reasonably well with theoretically predicted values, thus lending support to Griffith's theory; see Brace and Walsh (1962), Santhanam and Gupta (1968), Oglesby, Gutshell and Phillips (1976) and Atkinson (1987, Table 11.1) for observations on minerals, and Berry (1960, 1963) and Raasch (1971) for refinements in the method of calculating  $\gamma$  from the force measurements. However, in the majority of materials, especially when polycrystalline, the values of  $\gamma$  determined in this way from the work of fracture are much higher than theoretically predicted, commonly by an order of magnitude or more. Typical values of  $\gamma$  of the order  $10 \text{ J m}^{-2}$  have been reported for ceramics (Clarke, Tattersall and Tappin 1966) and rocks (Summers, Corwine and Chen 1971; Friedman, Handin and Alani 1972), and values of the order of  $100 \text{ J m}^{-2}$  or more are common in rocks (early measurements are given by Perkins and Bartlett 1963; Perkins and Krech 1966; Hoagland, Hahn and Rosenfield 1973; Krech 1974; Swain and Lawn 1976; and an extensive compilation is given in Table 11.2 in Atkinson 1987). High values are also reported in jade (Bradt, Newnham and Biggers 1973; Rowcliffe and Frühauf 1977). This apparent discrepancy with theoretical expectations has led to the recognition that, in addition to the provision of the surface energy of new surface, there are

other important processes of energy absorption in a spreading crack, leading to the concept of the “process zone” (Appendix 1). These processes include plastic deformation in the vicinity of the crack tip in response to the very high stresses there (Irwin 1948; Orowan 1949; Olsson 1975), the proliferation of microcracking accompanied by the relaxation of internal stresses (Friedman, Handin and Alani 1972; Hoagland, Hahn and Rosenfield 1973), and possibly other processes such as acoustic and thermal losses (Hasselmann et al. 1972). Therefore, in the general application of the Griffith formula (Eq. 4.1), the quantity  $\gamma$  should be interpreted as a specific energy absorption term in which all forms of energy absorption at the crack tip or in its vicinity are included, the value of this term normally being obtained empirically. This view of the Griffith theory forms the basis of the concept of critical strain energy release rate  $G_c$  in linear elastic fracture mechanics (see Appendix 1).

4. *Dynamic Aspects.* The energy considerations underlying the Griffith formula (Eq. 4.1) refer only to a stationary crack. To extend the treatment to moving cracks, the energy balance must take into account the kinetic energy absorbed when the material on one side of the new crack surface is set in motion relative to that on the other side (Mott 1948; Yoffe 1951; Berry 1960; Craggs 1960; Dulaney and Brace 1960; Kostrov and Das 1988; Freund 1990). This consideration sets an upper limit to the crack velocity (Bieniawski 1968b); see summary by Jaeger and Cook (1979, pp. 345–347). The stress field around the crack is also modified at high crack velocities (see references in Appendix 1).

### 4.3

## Uniaxial Compression and Biaxial Stresses

In the application of Griffith’s energy argument in deriving formula (Eq. 4.1) for the uniaxial tensile strength, it is implicitly assumed that the crack will spread in its own plane. This assumption permits a unique calculation of the energy changes resulting from extension of the crack. However, in applying Griffith’s theory to more complicated stress states and, in particular, to stress states of predominantly compressive character (defined more precisely later), two difficulties arise:

1. It can no longer be assumed that the crack will extend in its own plane, and there is, indeed, evidence to the contrary (Brace and Bombolakis 1963; Erdogan and Sih 1963; Hoek and Bieniawski 1965). Hence, an unambiguous calculation of the energy changes cannot be made without introducing a criterion to determine the direction of extension of the crack.
2. If the crack is of negligible width, it will tend to close under predominantly compressive conditions and it can no longer be assumed that the crack faces are not loaded. Moreover, normally under these conditions, no contribution to energy change can result from any relaxation of the elastic stress field during crack extension that would result in displacement of opposite crack faces towards each other. Only relative displacements parallel to the crack face can then come into consideration (cf. the modes II and III crack extension of fracture mechanics; see Appendix 1) and, if

there is frictional resistance to such displacements, the work of friction must also be taken into account.

Griffith (1924) avoided the second problem by considering only open cracks, and he avoided the first problem by changing to a critical maximum local tensile stress criterion of failure. Although he discussed the value of the maximum stress at the crack tip in the uniaxial tensile test, he did not give an explicit justification for this change of failure criterion in the general case but seemed to imply that the stress criterion was equivalent to the energy criterion. Most writers who apply Griffith crack theory in rock mechanics have used the critical local tensile stress criterion of failure, and it has sometimes been commented that the energy criterion, while necessary, is insufficient (e.g., Murrell 1964; Murrell and Digby 1972). However, to attribute this insufficiency to the elastic strain energy being independent of whether the strains are tensile or compressive misses the points contained in the two difficulties listed above, namely, that in applying the energy criterion in its simplest form the direction of crack propagation must also be prescribed, and that elastic energy associated with compressive elastic strains at crack tips is not available if points on opposite sides of a potential extension of the crack normal to the greatest compressive stress cannot move towards each other (the latter restriction no longer holds in porous material in which a zone of crushing is extending; cf. comment in Sect. 4.6.2). For further comment on the thermodynamics of cracking, see Eftis and Liebowitz (1976).

In the writings on fracture mechanics (Appendix 1), it is commonly agreed that the critical energy release rate and critical local tensile stress criteria of failure are equivalent (e.g., Irwin, Kies and Smith 1958; Sanders 1960; Sih and Liebowitz 1968, p. 106), although Swedlow (1965) points to cases of more complicated loading where, because of cross-terms in the stresses in the failure criterion, this equivalence no longer holds. However, in applying either type of criterion, the two factors mentioned above must be taken into account. Consequently, in the final analysis, it will usually be found that the underlying assumption has been made that the crack will spread in the direction normal to the maximum local tensile stress near its tip, although Lawn and Wilshaw (1975b, p. 67) set out a more sophisticated approach.

The Griffith (1924) theory for a biaxially stressed body with randomly oriented cracks of a given length proceeds in the following steps (for details, see Odé 1960):

1. From the elastic stress distribution around an elliptical cavity with free faces, the maximum tensile stress component is obtained for an arbitrary orientation of the cavity with respect to the applied stresses.
2. The cavity orientation is determined for which this maximum local tensile stress is greatest, and the applied stresses are then calculated for a critical value of the maximum local tensile stress thus obtained.
3. The critical value of the local tensile stress is obtained from the uniaxial test and is expressed in terms of the uniaxial tensile strength.

This procedure leads to the macroscopic criterion of failure, generally known simply as the *Griffith criterion* and expressed in terms of the biaxial principal stresses  $\sigma_1$ ,  $\sigma_2$  and the magnitude of the uniaxial tensile strength  $T_0$ , as follows:

$$(\sigma_1 - \sigma_2)^2 - 8T_0(\sigma_1 + \sigma_2) = 0 \quad \text{if } \sigma_1 > -3\sigma_2 \quad (4.2a)$$

$$\sigma_2 = T_0 \quad \text{if } \sigma_1 < -3\sigma_2 \quad (4.2b)$$

(compressive stresses being taken as positive). The condition  $\sigma_1 > -3\sigma_2$  defines the stress states of “predominantly compressive character” mentioned at the beginning of this section. Criterion 4.2 can also be expressed in terms of the shear stress  $\tau$  and the normal compressive stress  $\sigma_n$  acting on the plane containing the major axis of the elliptical cavity, as follows

$$\tau^2 - 4T_0\sigma_n = 4T_0^2 \quad (4.3)$$

Equation 4.3 is then the Mohr envelope corresponding to failure (Murrell 1958).

It follows from Eq. 4.2a,b that the Griffith criterion of failure predicts a value of the uni-axial compressive strength eight times the value of the uniaxial tensile strength. This ratio is smaller than the ratio commonly measured for rocks (McClintock and Walsh 1962; Wagner 1969).

It also follows from the theory leading to Eq. 4.2a that the orientation of the elliptical cavity at which the failure is initiated is given by

$$\cos 2\theta = \frac{1}{2} \frac{\sigma_1 - \sigma_2}{\sigma_1 + \sigma_2}$$

where  $\theta$  is the angle between the major axis of the ellipse and the maximum principal stress  $\sigma_1$ . However, since the maximum local tensile stress does not occur exactly at the end of the major axis and is not normal to the major axis, the cracking will develop in an orientation inclined to the major axis of the ellipse and more nearly parallel to the maximum macroscopic principal stress  $\sigma_1$ . This tendency for a crack to propagate out of its own plane under predominantly compressive conditions has been demonstrated experimentally (Brace and Bombolakis 1963; Erdogan and Sih 1963; Hoek and Bieniawski 1965).

Koide (1972) derived a criterion for the initiation of crack propagation that is essentially equivalent to Griffith's but is generalized to include crack initiation at an inclusion of different elastic properties.

#### 4.4 Triaxial Stresses

Orowan (1949, p. 201) argued that the Griffith criterion (Eq. 4.2 or 4.3) can be applied to general states of stress because normal or shear stresses acting on the plane perpendicular to the edge of the crack will not appreciably influence the failure condition. For this reason, or often without any such supporting argument, the Griffith criterion (Eq. 4.2 or 4.3) for biaxial stresses has been applied directly to triaxial tests in the form

$$(\sigma_1 - \sigma_3)^2 - 8T_0(\sigma_1 + \sigma_3) = 0 \quad \text{if } \sigma_1 > -3\sigma_3 \quad (4.4a)$$

$$\sigma_3 = -T_0 \quad \text{if } \sigma_1 < -3\sigma_3 \quad (4.4b)$$

where  $\sigma_1$  and  $\sigma_3$  are the greatest and least principal stresses (compression positive) and  $T_0$  is the magnitude of the uniaxial tensile strength. This form, which involves no influence of  $\sigma_2$ , is the one most commonly used as the “Griffith criterion” in analysing conventional triaxial test results.

Murrell (1963, 1965) made an alternative suggestion that the biaxial criterion can be generalized in triaxial stress as a paraboloid, introducing a dependence on  $\sigma_2$ :

$$(\sigma_2 - \sigma_3)^2 + (\sigma_3 - \sigma_1)^2 + (\sigma_1 - \sigma_2)^2 - 24T_0(\sigma_1 + \sigma_2 + \sigma_3) = 0$$

(for details, see Jaeger and Cook 1979, pp. 103–106). However, there seems to be no a priori reason for selecting this triaxial criterion except on empirical grounds. Another empirical extension of the Griffith failure criterion to triaxial stresses has been proposed by Niwa and Kobayashi (1967).

The complete solution of the three-dimensional Griffith problem of a body under general stress, containing randomly oriented ellipsoidal cavities of given dimensions, was obtained by Murrell and Digby (1970), following several treatments of the stress fields around three-dimensional ellipsoidal cavities or elliptical flat cracks and application of Griffith theory to such cases for simple types of loading; see Kassir and Sih (1967), or Sih and Liebowitz (1968, pp. 131–166, and earlier references given by them); also Key (1969) and Smith (1971). Proceeding in the same steps as outlined above for the biaxial Griffith theory, Murrell and Digby deduced a general triaxial failure criterion, which for predominantly compressive conditions has the form

$$(\sigma_1 - \sigma_3)^2 - \alpha T_0(\sigma_1 + \sigma_3) = \beta T_0^2$$

where  $\alpha$  and  $\beta$  are constant factors containing as parameters Poisson’s ratio and the axial ratios of the ellipsoids. In the particular case of “penny-shaped cavities” (two principal axes of the ellipsoid equal and much greater than the third), the criterion of failure becomes

$$(\sigma_1 - \sigma_3)^2 - 2(2 - \nu)^2 T_0(\sigma_1 + \sigma_3) = \nu(4 - \nu)(2 - \nu)^2 T_0^2 \quad \text{for } \sigma_1 > -A^* \sigma_3 \quad (4.5a)$$

and

$$\sigma_3 = -T_0 \quad \text{for } \sigma_1 < -A^* \sigma_3 \quad (4.5b)$$

where  $A^*$  is a constant factor involving Poisson’s ratio  $\nu$  and having the value 1.0 when  $\nu = 0.3$  and 2.5 when  $\nu = 0.1$ . Formulas were also obtained for the equivalent Mohr envelopes and for the corresponding orientations of the cavity at which failure will first occur. It is noteworthy that even in the general triaxial case the Griffith failure condition is independent of the intermediate principal stress and that the predicted ratio of uniaxial compressive to tensile strengths is still rather low, lower in fact than in the biaxial case. Because of discrepancies with observations such as these, modifications to the classical Griffith model must be considered.

## 4.5 Modified Griffith Theory (Closed Cracks)

An important property of the classical Griffith model is that the crack-like cavities are open and contain no fluid under pressure. The influence of pore fluid pressure is discussed in Chapt. 7. We now consider the effects of the closing of the cracks under load and of the frictional effects that can then arise. In experiments under moderate confining pressure, it is likely that many of the cracks in a rock will close under the action of the applied stress component normal to their plane. An indication of this closure is the increase in velocity of sound waves with applied hydrostatic pressure, an increase which flattens out at high pressures, say, beyond 100 or 200 MPa; see, e.g., Birch (1960, 1961). The attenuation of sound waves gives a similar indication of crack closure (e.g., Birch and Bancroft 1938a), as does often the initial part of the stress-strain curve; for further evidence, see Brace (1972b) and Chapt. 5.

After closure, the crack faces will exert a normal force on each other and, since the only relative displacement of crack faces during spreading of the crack is then sliding, a tangential loading will also be introduced on the crack faces. Taking these effects into account under the simple assumption of uniform distribution of the forces on the crack faces, McClintock and Walsh (1962) calculated the conditions for crack extension under biaxial stress for a model similar to Griffith's except that the cracks are assumed to close under a certain value  $\sigma_c$  of the macroscopic normal stress component perpendicular to the crack. This theory is known as the *modified Griffith theory*. Murrell (1964) developed an identical theory and Murrell and Digby (1970) extended the theory to the general three-dimensional problem with closed cracks.

In both biaxial and triaxial cases, when the cracks are closed, the initiation of failure is governed by the criterion

$$\left(\sqrt{1+\mu^2}-\mu\right)(\sigma_1-\sigma_3)=\alpha'T_0\sqrt{1+\frac{\sigma_c}{T_0}}+2\mu(\sigma_3-\sigma_c) \quad (4.6)$$

or the equivalent Mohr envelope

$$\tau=\frac{\alpha'}{2}T_0\sqrt{1+\frac{\sigma_c}{T_0}}+\mu(\sigma_n-\sigma_c) \quad (4.7)$$

In these expressions,  $\sigma_1$  and  $\sigma_3$  are the greatest and least principal stresses (compression positive), and  $\tau$  and  $\sigma_n$  are the maximum shear stress and the normal stress on the plane of the crack at which failure is initiated, namely, the plane containing the intermediate principal stress axis and inclined at angle  $\theta$  to the  $\sigma_1$  axis where  $\tan 2\theta=1/\mu$ ;  $\mu$  is the coefficient of friction on the crack faces and  $\sigma_c$  is the critical macroscopic compressive stress perpendicular to the crack that is needed for closing the crack. In the general triaxial case, the constant  $\alpha'$  is a complicated function of Poisson's ratio  $\nu$  and the axial ratios of the crack (Murrell and Digby 1970); for the penny-shaped crack it reduces to  $\alpha'=2(2-\nu)$ . In the biaxial case,  $\alpha'=4$  (McClintock and Walsh 1962; Murrell 1964). It is to be noted that in both biaxial and triaxial cases,

the predicted criterion of failure is again independent of the intermediate principal stress. However, in contrast to the parabolic form of the criterion for open cracks, the criterion for closed cracks is linear in the stresses  $\sigma_1$  and  $\sigma_3$ , and therefore has the same form as the Coulomb criterion (Sect. 3.3), with a “cohesion”  $\tau_0$  equal to

$$(\alpha'/2)T_0\sqrt{1 + (\sigma_c/T_0)} - \mu\sigma_c$$

and a “coefficient of internal friction”  $\tan \phi$  equal to the coefficient of friction  $\mu$  for sliding on the crack faces.

The theory leading to Eqs. 4.6 and 4.7 is only valid provided all cracks are closed under the applied stresses. McClintock and Walsh (1962), Murrell (1964), and Murrell and Digby (1970) have discussed the transition in failure criterion from open crack conditions to closed crack conditions. This transition is rather complicated to describe in general because under certain conditions there can be an intermediate region.

It is also not very clear what values can be given to  $\sigma_c$  in practice. Brace (1960) argued that for long narrow cracks  $\sigma_c$  will be very small. More detailed discussion of the stress for crack closure has been given by Murrell (1964), Berg (1965), Walsh (1965a,b), and Digby and Murrell (1976). Digby and Murrell calculated on the basis of an assumed atomic cohesive strength that the crack closure stress will be about  $10T_0$  and concluded that this is consistent with observations.

However, using the relation between the uniaxial compressive strength  $C_0$  and the cohesion  $\tau_0$  (Sect. 3.3), it follows that the uniaxial compressive strength predicted by the modified Griffith theory when closed crack conditions are met is

$$C_0 = \left( \sqrt{1 + \mu^2} + \mu \right) \left( \alpha' \sqrt{1 + \frac{\sigma_c}{T_0}} - 2\mu \frac{\sigma_c}{T_0} \right) T_0 \quad (4.8)$$

For values of  $\alpha'$  between 3 and 4 and  $\mu$  between 0.5 and 1, the maximum possible values of  $C_0$  when  $\sigma_c/T_0$  is varied fall in the range  $6T_0$  to  $10T_0$  and the corresponding values of  $\sigma_c/T_0$  are between 3 and zero. These values of  $C_0$  are similar to those predicted on the classical Griffith theory for open cracks and so do not reflect a marked effect from the crack closing.

When  $\sigma_c$  is negligibly small, closed crack conditions apply under all compressive stress states, and the Eqs. 4.6 and 4.7 become

$$\left( \sqrt{1 + \mu^2} - \mu \right) (\sigma_1 - \sigma_3) = \alpha'T_0 + 2\mu\sigma_3 \quad (4.9)$$

$$\tau = \frac{\alpha'T_0}{2} + \mu\sigma_n \quad (4.10)$$

That is, they are then identical with a Coulomb criterion of failure in which the cohesion  $\tau_0$  is equal to  $\alpha'T_0/2$ , or  $2T_0$  in the biaxial case. However, the predicted cohesion  $\tau_0$  becomes negative when  $\sigma_c$  becomes large compared with  $T_0$  unless  $\mu$  is small. A large value of  $\sigma_c$  would imply a very marked upturning of the Mohr envelope beyond the transition to closed crack conditions with normal values of  $\mu$ , and this

transition would only be achieved when the minimum principal stress is already a fairly large compressive stress.

## 4.6

### Extension of the Griffith Approach to Other Modes of Localized Inelastic Failure

So far, we have considered only failure originating by the propagation of local tensile or cleavage fracture from a crack-like flaw, which is the essential feature of the Griffith theory. However, the stress field around a flaw will contain concentrations of shear stress and of compressive stress in addition to the concentration of tensile stress focussed upon by Griffith. Some studies have considered the initiation of shear and compressive modes of localized failure at these stress concentrations.

#### 4.6.1

##### Shear Failure

Using an approach similar to that for failure initiation by tensile fracture at an ellipsoidal cavity when a theoretical cleavage strength  $\sigma_{\max}$  is exceeded, Digby and Murrell (1975b) developed the theory of failure initiation by inelastic shear failure due to the maximum shear stress exceeding a theoretical shear strength  $\tau_{\max}$ . They treated the general triaxial case and also extended the treatment to the case of closed cracks (Digby and Murrell 1975a). It is shown that the potential sites of local tensile and shear failure occur at different places on a given crack and that, for open cracks but not for closed cracks, the critical sites often occur on cracks of different orientations. The relative precedence of tensile and shear failure initiation is explored as a function of the ratio  $\sigma_{\max}:\tau_{\max}$  and has implications for the brittle-ductile transition (Chapt. 9).

#### 4.6.2

##### Compressive Failure

In experiments on plaster-of-Paris models with artificial cavities of macroscopic dimensions, Nemetova and Lajtai (1973) and Lajtai and Lajtai (1974) observed local failures that occur approximately normal to the applied compressive stress, as well as the usual local extension failures. The local compression failures, described confusingly as “normal shear fractures”, are shown to occur at sites of maximum compressive stress concentration predicted from elastic theory. Presumably these failures represent some sort of crushing or collapse involving local volumetric compaction as well as local shortening and are only to be expected in a material of rather high porosity. The inhomogeneous failure of sandstone described by Edmond and Paterson (1972) and the “compaction bands” observed in sandstone in the field by Mollema and Antonellini (1996) and in the laboratory by Olsson (1999) and Wong, Baud and Klein (2001) may have something of this character (see further in Sect. 6.4.1). An analogous “anti-crack” effect arising from volume change has been evoked by Green and co-workers (Green and Burnley 1989, 1990; Green et al. 1990; Burnley, Green and Prior 1991; Green and Zhou 1996) in connection with phase transformations that may lead to deep-focus earthquakes.



## 4.7 General Comment on Griffith-Type Theories

The Griffith theory and its closed-crack modification have been discussed at some length because they represent first steps towards a physically realistic model of the failure process. However, although the grosser aspects of observed behaviour are accounted for, perhaps better on the modified theory if the confining pressure is not very low, both theories meet difficulties when compared carefully to observations, in the following respects:

1. The predicted ratios of uniaxial compressive strength to uniaxial tensile strength tend to be too low, unless, in the modified theory, the coefficient of friction is given an unrealistically high value of around 1.5 (cf. Sect. 8.2.1).
2. The observed influence of the intermediate principal stress is not accounted for (cf. Sect. 3.6).
3. The predicted slope of the Mohr envelope does not agree closely with that observed. The actual slope tends to be greater than the coefficient of friction (modified theory), or there is sometimes a degree of curvature intermediate between the predictions of the two theories (cf. Mogi 1972b).

The way to the resolution of these apparent discrepancies is opened when it is realized that the theories are only directly concerned with the initiation of failure on the scale of the cracks whereas the strength observations refer to the final or macroscopic failure. This point has been made from time to time (e.g., Brace 1960; Brace and Bombolakis 1963; Hoek and Bieniawski 1965; Bieniawski 1967a) but it only slowly became widely appreciated. Under tensile conditions, the spreading of a crack often leads to catastrophic failure without significant further increase in load and so failure initiation theories have tended to dominate the subject of fracture mechanics as developed in metallurgy and related material sciences for ordinary engineering applications. However, under predominantly compressive conditions such as are usually involved in experimental rock deformation work, the initiation of failure at an individual flaw is commonly observed to occur considerably below the macroscopic failure stress (Chapt. 5). The rise in stress during the progression of the failure immediately explains the tendency for the macroscopic fracture stress in uniaxial compression to be higher relative to the uniaxial tensile strength than predicted from the Griffith-type failure theories. However, the detailed consideration of the development of the failure and the prediction of the macroscopic failure stress under predominantly compressive conditions are complex. The following factors are likely to be important:

1. The initial cracks tend to spread out of their plane, as mentioned earlier (Sect. 3.2), in such a way as requires increased stress for further propagation (see summary by Jaeger and Cook 1979, p. 342). Paul and Gangal (1967; also Paul 1968) have referred to this requirement as “fracture hardening” and have attempted to give a quantitative description of it.

2. Because of this rise in stress, other cracks will also begin to spread. The final fracture then presumably results from some sort of linking up of local cracks rather than the propagation of a single crack across the specimen (cf. Brace and Bombolakis 1963; Bombolakis 1964; Hoek and Bieniawski 1965; Murrell 1971), although it may still be possible to describe or model the penultimate microcrack structure as a single new effective Griffith crack propagating through material already modified by earlier microcracking activity. In the later stages of failure, the local stress pattern will be complicated by the interaction of the fields from individual cracks and the frictional resistance will be a complicated summing of the effects of closure in individual cracks. Thus, the resultant frictional effect may not be represented by the same value of  $\mu$  as for simple sliding.
3. Among the other cracks brought into activity by the rise in stress there will probably be some that are inclined to the  $\sigma_2$  axis. The spreading of these will therefore be affected to some extent by  $\sigma_2$  and hence the macroscopic fracture stress can be expected to show some influence of the intermediate principal stress (Brady 1969a–d, 1970; Murrell and Digby 1970).
4. A spread in initial crack sizes and departure from random orientation are likely to contribute to size effects, scatter in strengths and anisotropy (e.g., Brady 1969a–d; Attewell and Sandford 1974).

Early attempts to augment or extend the Griffith-type theories to take into account the proliferation of local microcracking prior to a macroscopic failure while otherwise retaining the principles of Griffith's approach have been made by Wiebols and Cook (1968), Brady (1969a–d) and Barron (1971a). However, in each case, a criterion of macroscopic failure has to be introduced on rather empirical grounds and, as pointed out by Attewell and Sanford (1974), these theories retain the essential character of simple Griffith theory, and they offer little to the physical understanding of the final unstable propagation of a macroscopic fracture.

Clearly, in place of the model of an isolated crack in an elastic continuum, it is essential to have a realistic structural description of the rock as a basis for further theoretical developments, and to consider the evolution of the structure during the progression of the failure. Physical property and microstructural observations bearing on this evolution are dealt with in the next chapter and related theoretical studies in the following chapter.

## Evolution of Physical Properties during Brittle Failure

### 5.1 Introduction

The experimental studies reviewed in Chapt. 3 were concerned only with brittle fracture from a macroscopic point of view. Brittle fracture was viewed as a singular event, occurring after an unrelated, essentially elastic deformation and characterized uniquely by the peak stress (“ultimate strength” or “fracture stress”). The theoretical approach of Chapt. 4 also set out from this viewpoint, but concluded that it was too simplistic, especially for predominantly compressive conditions. Thus it becomes evident that brittle failure has to be seen as the culmination of a progressive development of cracking during loading rather than the catastrophic spread of a single crack at a peak stress.

In this chapter, we review observations on behaviour in the brittle field that throw light on the evolution of microcracking and thus on the mechanism of brittle failure. We shall now be concerned with the complete progression of events as the whole stress-strain or force-displacement curve is followed. This progression includes both pre-peak and post-peak parts of the force-displacement curve, that is, the parts before and after the point of maximum axial force in the triaxial test.

The pre-peak behaviour already commonly shows significant departures from strictly elastic behaviour, especially in the upper part of the axial force range. In general, such effects can result either from localized plastic yielding or from microfracturing. The former is known to be of considerable importance in the mechanism of crack initiation in metals and ceramics (Stokes, Johnston and Li 1959; Clarke, Sambell and Tattersall 1962; Argon and Orowan 1964; Congleton and Petch 1966; Tetelman and McEvily 1967, Ch. 6; Lawn 1993). However, it is unclear to what extent localized plastic microstrain plays a similar role in rocks, either in crack initiation or in crack propagation. Microcracks tend to be ubiquitous in rocks and the need for a mechanism of crack initiation is perhaps less than in other materials. In quartz, Joshi and Paul (1976) found evidence for the nucleation of cracks as a result of slip but Martin and Durham (1975) did not, while, in marble, Olsson and Peng (1976) have described several microcrack nucleation mechanisms that depend on plastic strain. In contrast to the equivocal situation with plastic microstrain, there are many studies pointing to an extensive development of pre-peak microfracturing. The experimental evidence for the growth of microfracturing comes to a large degree from observations on dilatancy, acoustic emission, transport properties, and change in elastic wave speed in the course of loading. However, before discussing these observations, we shall consider in more detail the shape of the complete force-displacement curve in triaxial compression tests and some experimental aspects of its determination.

## 5.2 Pre-peak and Post-peak Behaviour

### 5.2.1 Role of the Testing Machine

Before the peak of the force-displacement curve is reached in a triaxial test, work must always be done on the combined specimen-machine system in bringing about an increment of deformation in the specimen. The system is, in this case, inherently stable mechanically. However, beyond the peak, because potential energy is released from the machine as the force decreases, it is possible that the work needed for further deformation of the specimen can be fully provided from within the specimen-machine system, so that the deformation process can continue spontaneously and uncontrollably, preventing the load-bearing capacity of the specimen from being readily assessed as a function of the deformation and leading rapidly to the destruction of the specimen. This situation is normal with the brittle failure of a rock specimen in a conventional “soft” testing machine, especially a machine with hydraulic loading.

The important features of this situation are brought out by considering Fig. 18a. The curve A represents the load-bearing capacity of a specimen as a function of its change of length (displacement). Consider the behaviour of the machine at a point X at or just past the peak force. In the absence of the specimen, the machine would relax elastically with release of force along a line XY, the negative slope of which may be referred to as the stiffness  $k$  of the machine (analogous to the stiffness of a spring). This relaxation is opposed by the specimen and cannot occur spontaneously as long as the force-displacement characteristic of the specimen has a lower negative slope than XY. However, in the case of brittle rock specimens and a conventional testing machine, a point X' is reached soon after the peak where the load-bearing capacity of the specimen falls off more rapidly than the force available from the machine and so uncontrolled failure

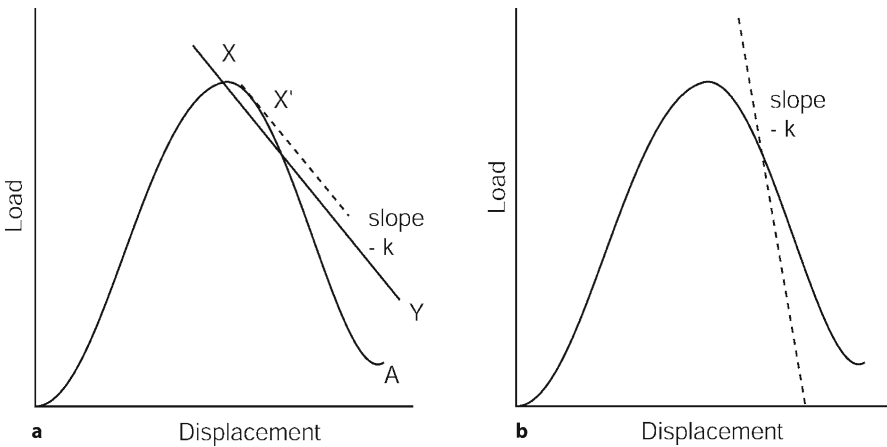


**Fig. 18.** Relationships between machine stiffness and specimen characteristics; details in text

occurs. The point  $X'$  is determined as the point at which the force-displacement curve has the slope  $-k$ . For a more detailed discussion of this situation, see Jaeger and Cook (1979, p. 177) and Hudson, Crouch, and Fairhurst (1972).

To study the complete progression of the failure process beyond the peak force, two experimental approaches have been made to overcome the limitation just described. One is to use a “stiff” testing machine, the other to use a servo-controlled machine.

1. *Stiff testing machines.* The complete force-displacement curve can be followed at will if the stiffness  $k$  of the machine corresponds to a slope that is steeper than the most steeply descending part of the force-displacement curve of the specimen (Fig. 18b). This approach was first exploited in rock mechanics by Cook (1965); cf. a similar approach in concrete testing by Barnard (1964). Various stiffening devices have been used (Cook 1981). Apart from the obvious step of massive construction of the machine for stiffness, these include the following:
  - a Loading an elastic element such as a steel tube or bar in parallel with the specimen; force is, in effect, transferred to the elastic element as the load-bearing capacity of the specimen diminishes (e.g., Cook 1965; Brace, Paulding and Scholz 1966; Bieniawski, Denkhaus and Vogler 1969; Brady, Duvall and Horino 1971; Maranhão 1974).
  - b Locking the moving platen after applying some force, then raising the force to the fracture level by allowing the pre-heated columns of the machine to contract thermally, or by heating the specimen support (Cook and Hojem 1966; Wawersik and Fairhurst 1970; Hustrulid and Robinson 1973).
  - c The use of mercury as hydraulic fluid (Hojem, Cook and Heins 1975).
2. *Servo-control.* In the servo-control of a testing machine for post-peak studies, positive steps are taken to unload the specimen when less force is required for its further deformation, without relying on the stiffness of the machine to follow a prescribed displacement sequence. Then, if the displacement at the specimen begins to run ahead of the prescribed course, the servo-control reduces the force being applied by the machine. In early studies, the control was done manually (Wawersik and Fairhurst 1970; Wawersik and Brace 1971), but automatic servo-control is now readily available, giving a much shorter response time and hence more effective control; see Houpert (1970) and Rummel and Fairhurst (1970) for early applications. Peng (1973) has described the transient interaction between machine and specimen that occurs when the rate of specimen failure becomes comparable with the response rate of the servo-control. Rummel and Fairhurst (1970) pointed out that the possibility of following and controlling the progress of fracture with a servo-system having a response time of the order of tens of milliseconds rests on the fact that the average rate of propagation of cracks in the materials studied is slow compared with sonic speeds; the same comment would apply even with the response time of 2 ms quoted by Hudson (1971).

Within the limitations set by the relative rates of specimen failure and machine response, it is thus possible with servo-control to follow the complete force-displacement curve, even in cases impossible to control with a stiff machine alone in which the specimen actually lengthens during fracture in compression (see, e.g., Wawersik and Brace 1971). However, in the latter cases, the feed-back for servo-control must

derive from a quantity that is changing monotonically throughout the test, such as the lateral specimen dimension (Kiyama et al. 1996; Kawakata et al. 1999), the rate of acoustic emission (Terada, Yanagitani and Ehara 1984; Lockner et al. 1991), or a suitable linear combination of strain and stress (Okubo and Nishimatsu 1985; Okubo, Nishimatsu and He 1990). For further discussion of the optimization of the control in servo-tests, see Hudson, Brown and Fairhurst (1971), summarized by Hudson, Crouch and Fairhurst (1972) and Fairhurst and Hudson (1999).

It is to be noted that the use of “stress-strain” curves should be avoided in the primary reporting of results in the post-peak region. Even the term “complete stress-strain curve” (Fairhurst and Hudson 1999) is somewhat misleading. Since the specimen tends to be disintegrating and to have very different stresses and strains in its different parts, it is more logical to report the results of complete tests as force-displacement curves, although these may later be analysed in terms of constitutive behaviour.

### 5.2.2

#### Complete Force-Displacement Curves

Some general properties of the force-displacement curve will now be reviewed. Brown and Hudson (1971) set down some broad conclusions about the role of the type of rock, pointing to steeper post-peak curves for finer-grained and less porous rocks (cf. also Bieniawski, Denkhaus and Vogler 1969). The post-peak region also has practical importance in mining where, despite the occurrence of fracturing, the “failed rock” is still capable of supporting considerable load, especially when there is lateral constraint (Brady and Brown 1985; Hoek and Brown 1980, pp. 236–239).

**Shapes of curves.** The pre-peak force-displacement curve often shows an initial increase in slope, followed by a more or less linearly elastic section. The initial toe is usually attributed to the closure of pre-existing cracks or the collapse of pores but needs to be carefully distinguished from “settling down” effects in the testing machine. The elastic section is normally followed by bending-over of the curve due to pre-fracture inelastic behaviour, with a strain hardening which diminishes in slope as the straining continues. Eventually a peak force is reached beyond which there is a weakening and ultimate failure of the specimen (Fig. 18). In rocks with substantial porosity, the initial toe is especially prominent and the “elastic” section may be very short or absent, there being simply a transition or inflection from being downward convex to being upward convex.

Pronounced differences in the character of the post-peak force-displacement curve appear in the published results. Many of the curves reported from stiff machines are very smooth, for example, Fig. 19a from Bieniawski, Denkhaus and Vogler (1969), and Fig. 19b from Brady, Duvall and Horino (1971), often with negative slopes of roughly the same magnitude as the positive, pre-failure slopes. On the other hand, with servo-controlled machines, more irregular shapes appear, especially in the manually controlled tests of Wawersik and Fairhurst (1970), and Wawersik and Brace (1971) – see Fig. 20 and compare this curve for Tennessee marble with that in Fig. 19b for an unspecified marble. At first sight, it might appear that the type of machine exerts an in-

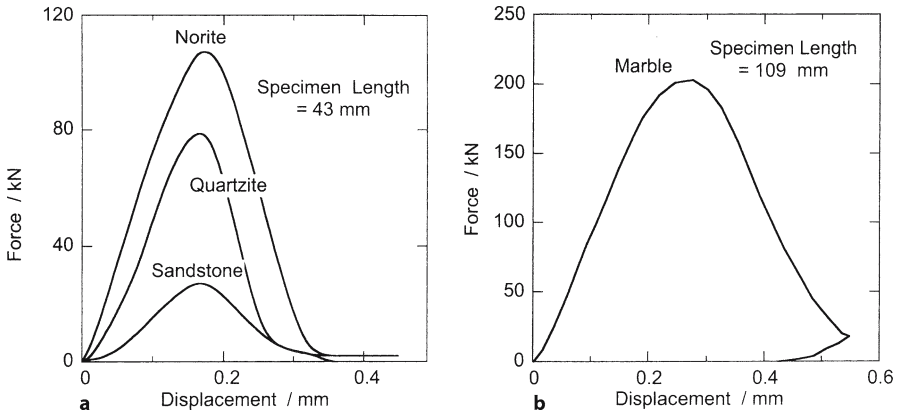
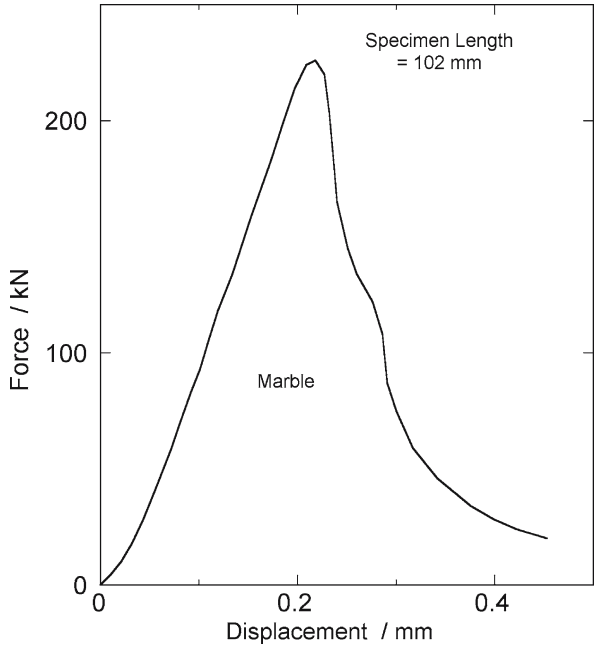


**Fig. 19.** Complete load-displacement behaviour in uniaxial compression tests in stiff testing machines. **a** Norite, quartzite and sandstone specimens of 21.5 mm diameter (after Bieniawski, Denkhaus and Vogler 1969); **b** marble specimen of 54 mm diameter (after Brady, Duvall and Horino 1971)

**Fig. 20.**

Complete load-displacement behaviour of Tennessee marble in uniaxial compression in a manually controlled testing machine (after Wawersik and Fairhurst 1970)



fluence, but other observations, for example, the relatively smooth curves obtained from servo-controlled machines by Peng (1973) and Hudson and Brown (1973) – see Fig. 24 – suggest that such a correlation is illusory. Variable success in achieving complete control in servo-controlled machines probably explains some of the effects, but variation in the intrinsic behaviour of the rock also clearly exists (E. T. Brown, pers. comm., 1973).

A characteristic of the more irregular type of curve (Fig. 20) is the tendency to alternate between steeply dropping parts and much flatter parts (“ledges”); possible correlation of this alternation with stages in the progress of failure has been suggested.

A distinction has often been made between two types of post-peak behaviour (Fig. 21a), designated Class I and Class II by Wawersik and Fairhurst (1970). In Class I, the slope of the post-peak force-displacement curve is always negative. In Class II, there is actual reversal of length change after passing the peak, the curve turning over so far that its slope becomes positive again. From the discussion in Sect. 5.2.1, Class II behaviour cannot be controlled with a stiff machine but if the fracture propagation rates are not too high it can be followed with servocontrol using appropriate feedback.

The post-peak behaviour can be analysed in terms of a “slip weakening” model in which it is assumed that a shear failure occurs, resulting in permanent deformation being concentrated in a shear surface or narrow shear zone sandwiched between two elastic blocks. The analysis of this situation by Rice (1980) and Wong (1982c) can be expressed as follows. The transition to Class II behaviour (Fig. 21b) occurs when the incremental change of length  $d\lambda$  becomes negative for an incremental change in axial force  $dF$ , that is, when

$$d\lambda = d\lambda^p + d\lambda^e < 0 \quad \text{or} \quad d\lambda^p < -d\lambda^e \quad (5.1)$$

where  $d\lambda^p = du \cos \theta$  is the permanent change of length resulting from a relative shear displacement  $du$  on a failure surface inclined at angle  $\theta$  to the specimen axis, and

$$d\lambda^e = \frac{dF}{AE} l$$

is the elastic change of length,  $l$  being the length of the specimen,  $A$  its cross-sectional area, and  $E$  its Young’s modulus. Since the increment in shear force is  $dS = dF \cos \theta$  and the increment in shear stress is  $d\tau = (dF/A) \cos \theta \sin \theta$  on the failure surface, the condition of Eq. 5.1 leads to

$$\frac{dS}{du} < -\frac{AE}{l} \cos^2 \theta \quad \text{or} \quad \frac{d\tau}{du} < -\frac{E}{l} \cos^2 \theta \sin \theta \quad (5.2)$$

Thus the distinction between the two classes is not a fundamental one but simply derives from the relative rates of strength loss and elastic stress relaxation during the test.

According to the slip weakening model, the structural response of the failed sample with a shear fracture is dependent on its size and shape. In the post-peak stage, an incremental decrease of the axial force induces the overall length to change by an increment that is the sum of the sample extension due to elastic relaxation and the shortening due to slip along the shear band (Kimura et al. 1987; Labuz 1991; Labuz and Biollzi 1991). The relation between displacement and force can be expressed as

$$\frac{d\lambda}{dF} = \frac{l}{EA} + \frac{\cos^2 \theta \sin \theta}{A} \frac{du}{d\tau} \quad (5.3)$$



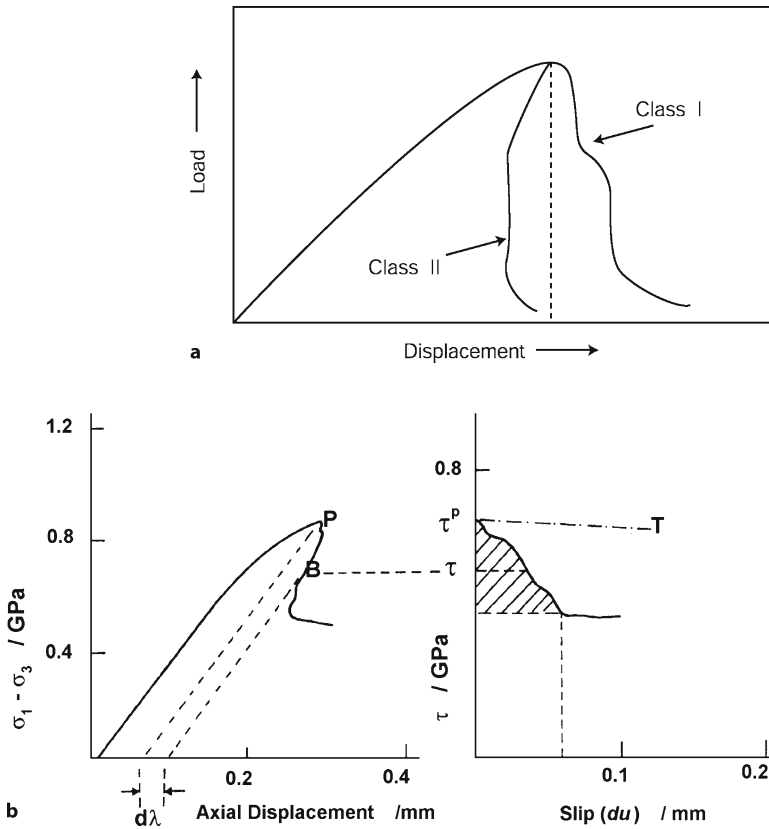


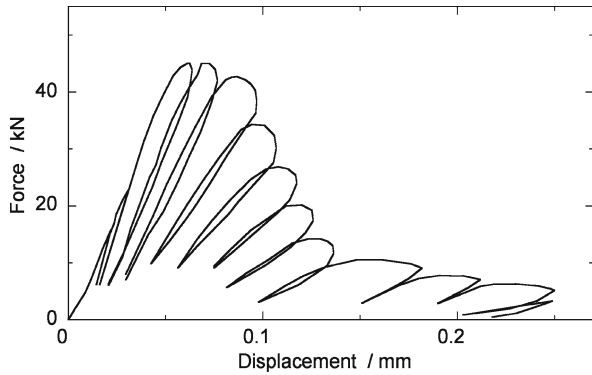
**Fig. 21. a** Two types of post-failure load-displacement behaviour (after Wawersik and Fairhurst 1970). **b** Transformation of post-peak data from a triaxial experiment to infer the resolved shear stress as a function of relative shear displacement used in a “slip-weakening” model. The dash-dotted line marked *T* indicates the transition slope from Class I to Class II behaviour in accordance with Eq. 5.2 (the loads have been normalized with respect to cross-sectional area and represented by stresses; after Wong 1982c)

Even if the slip weakening behaviour (characterized by  $d\tau/du$ ) is a material response, the force-displacement curve will be dependent on the sample shape because the elastic response depends on the ratio  $l/a$ , and on sample size because both the elastic and slip weakening responses are dependent on  $A$ . If the shear failure is assumed to occur in a narrow shear zone of thickness  $h$  instead of on a discrete surface, the analysis of Ortiz (1989) can be applied to determine the constitutive behaviour in the shear zone.

As fracturing progresses and the fraction of intact rock decreases, the elastic stiffness of the specimen correspondingly decreases. This effect is made evident if the force is cycled in the post-peak region (Bieniawski 1971; Brady, Duvall and Horino 1973; Ofoegbu and Curren 1992; Martin and Chandler 1994; see Fig. 22). Brady, Duvall and Horino measured the intact cross-section area at successive stages and showed

**Fig. 22.**

Deformational behaviour of fine-grained sandstone in cycling uniaxial compression, showing the diminishing stiffness of the specimen in the post-failure region. Diameter of specimen 21.5 mm, length unspecified (after Bieniawski 1971)



that the post-peak curve in various rock types can be explained in terms of the decreasing effective load-bearing area.

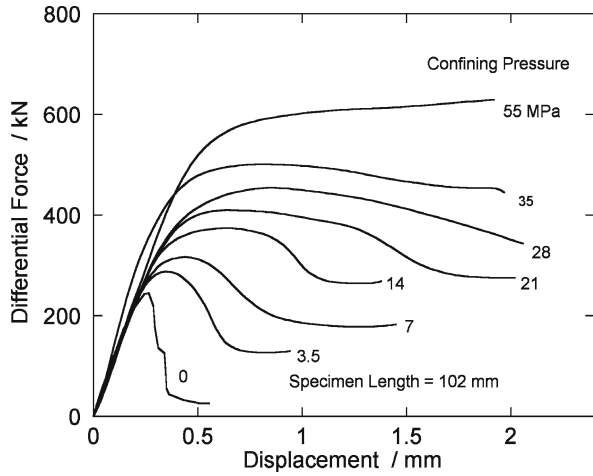
Post-peak force-displacement curves have been determined in extension by Krech (1974), Peng (1975) and Labuz, Shah, and Dowding (1983). Also, stiff and servo-controlled testing machines have been used for post-peak studies in types of tests other than uniaxial or triaxial compression tests, such as indentation and bending tests; for example, see Wagner and Schümann (1971), Brown et al. (1972), Hudson, Brown, and Rummel (1972), Rummel (1972), Wiebols, Jaeger, and Cook (1972), and Hudson, Hardy, and Fairhurst (1973). Finally, Crouch (1972a) has shown that the actual locus of the post-peak force-displacement curve is not obviously dependent on the path by which a given combination of confining pressure and axial force is reached.

**Influence of confining pressure and temperature.** Apart from the expected increase in force needed under higher confining pressures, increase in confining pressure also leads to the peak force occurring at a larger displacement and, often, to a less steep post-peak curve, as illustrated in the results of Rummel and Fairhurst (1970) on marble (Fig. 23). This figure also shows how some of the inflections become less marked as the brittle-ductile transition is approached. Similar effects of confining pressure have been demonstrated by Crouch (1970, 1972b), Wawersik and Fairhurst (1970), Bieniawski (1971), Wawersik and Brace (1971), Wiebols, Jaeger and Cook (1972), Kovári and Tisa (1975) and Wong (1982a). In granite it was also found that the post-failure slope became gentler at higher temperatures (Wong 1982a; Kato, Ohnaka and Mochizuki 2003).

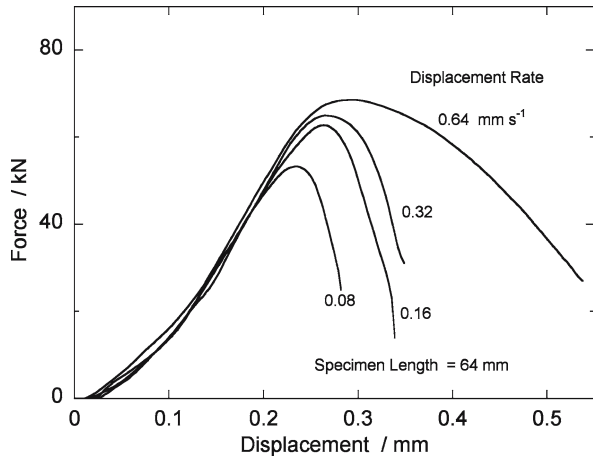
**Time effects.** It has been generally noted that the post-peak part of the force-displacement curve is more sensitive to time effects than the pre-peak part. This observation applies both to controlled strain rate and to creep and relaxation tests. Figure 24 illustrates the very marked strain rate dependence of the post-peak curve in the case of a sandstone studied by Peng (1973), using a servo-controlled testing machine. There are three principal effects as the displacement rate is decreased: (1) the peak force is reached at a lesser amount of shortening; (2) the post-peak curve tends to fall more steeply; (3) the maximum stress supported is lower at lower displacement

**Fig. 23.**

Complete load-displacement behaviour of Tennessee marble in triaxial compression in servo-controlled testing machine at confining pressures shown. Diameter of specimen 51 mm; displacement rate  $10^{-3} \text{ mm s}^{-1}$  (after Rummel and Fairhurst 1970)

**Fig. 24.**

Influence of deformation rate on post-failure behaviour of Arkose sandstone in uniaxial compression in a servo-controlled testing machine. Diameter of specimen 32 mm (after Peng 1973)



rates. These effects have also been observed in various other types of rocks, including granites, limestones, and marbles (Rummel and Fairhurst 1970; Peng and Podnieks 1972; Peng 1973, 1975; Wawersik 1973; Houpert 1974b), and they would be consistent with a simple model in which the time-dependence of cracking becomes more evident as the cracking proliferates (Hudson and Brown 1973; Houpert 1974b). However, the situation is not always as simple as this because other marbles and sandstones have been found to show the opposite of these effects (Bieniawski 1970; Houpert, Tisot and Thomas 1971; Hudson and Brown 1973; Houpert 1974b). Also, the servo-control in the more brittle rocks tends to be more effective at smaller deformation rates (Peng 1973; Houpert 1974b), implying that the post-peak curve is then falling less steeply, again in opposition to the second effect described above. Possibly some peculiarities of machine-specimen interaction are involved here, such as, for example, a fast propa-

gation of individual cracks which predominates and leads to uncontrollable behaviour in fast deformation while in slower deformation a more generalised proliferation of cracking occurs that is controllable.

Despite these differences in influence of deformation rate found by different workers, there are consistent results from relaxation tests made at various points along the post-peak force-displacement curve (Bieniawski 1970; Hudson 1971; Hudson and Brown 1973; Houpert 1972, 1974b; Peng 1973). Relaxation occurs until a lower curve is reached which represents the force that the failed specimen can support indefinitely. The amount of force drop to this curve appears to reach a maximum at some point of the force-displacement curve beyond the maximum force and often somewhere near the point of greatest downwards slope. Constant-force creep tests have also been done, beginning at various points along the post-peak curve (Peng 1973); these tests give a time to complete rupture that increases for points down the curve.

**Size and shape effects.** In uniaxial compression tests on various rocks it has been found that as the length:diameter ratio of the specimen is decreased, not only in the peak stress raised, as is well known (Chapt. 3), but the shortening attained at the peak stress in increased, and also the post-peak part of the force-displacement curve tends to take on a flatter slope (Bieniawski 1971; Hudson, Crouch and Fairhurst 1972; Hudson, Brown and Fairhurst 1972; Hustrulid and Robinson 1973). Hudson and coworkers also found that, for a given aspect ratio, decreasing the size of the specimen also tended to lead to a flatter post-peak curve; they point to a number of factors contributing to these effects. As suggested by Labuz (1991), these size and shape effects can be explained by the slip weakening model using Eq. 5.3 above. However, it should also be noted that the slip weakening behavior (as characterized by the slope  $d\tau/du$ ) may be quite variable from sample to sample.

### 5.3 Volume Changes

In the absence of phase transformations, the density of the solid components of a rock are not significantly changed during deformation except for elastic effects. Inelastic volume changes therefore reflect changes in the microstructure of the rock associated with the deformation processes that involve pores or cracks. Inelastic volume change is designated as *dilation* or *compaction* depending on whether there is volume increase or decrease, respectively. Under simple hydrostatic pressure, inelastic dilation is unlikely to occur, and inelastic compaction is only to be expected in porous rock. However, under deviatoric stress, dilation is often observed and the term *dilatancy* is used to refer to the development of the volume change during the resulting inelastic deformation. In the case of porous rock, there is also the possibility of compaction being associated with the inelastic deformation, the development of which may be designated as negative dilatancy or *compactancy*.

Dilatancy has long been known to be an important aspect of the deformational behaviour of granular aggregates such as soils and so it has been much studied in soil mechanics (e.g., Schofield and Wroth 1968; Lambe and Whitman 1969; Wood 1990). In such materials, the dilatancy can usually be attributed to changes in packing of the

grains during their relative movement and the macroscopic strains involved are often large compared with the elastic range. However, Bridgman (1949b) and Matsushima (1960a) and, in more detail, Brace, Paulding and Scholz (1966) showed that dilatancy occurs in compact rock prior to macroscopic failure when the rock is loaded under conditions conducive to brittle fracture. The total strains in this case are only of the order of the elastic range and the dilatancy can be attributed to microcracking occurring prior to the macroscopic failure. Crouch (1970, 1972b) has also shown that, for quartzite and norite, the dilation that begins prior to the peak force continues in a more marked degree in the post-peak region (also Houpert, Tisot and Thomas 1971; Thill 1973). However, before discussing these and later similar observations on dilatancy in the brittle field, a general resumé of the experimental methods for observing dilatancy is given.

There have been three main experimental approaches to measuring dilatancy:

1. The volumetric strain can be determined from the displacement of fluid if the deformation is done while the specimen is enclosed in a dilatometer. The dilatancy can then be obtained by subtracting the elastic volumetric strain calculated from elastic constants determined at lower stresses at which dilatancy can be assumed to be zero. This method was used at atmospheric pressure by Bridgman (1949b) but it is not easy to obtain high sensitivity in applications under confining pressure. Edmond and Paterson (1972) developed a pressure-compensated dilatometer for use in a pressure vessel at confining pressures up to 800 MPa but used it mainly for observations at relatively large strains in the ductile field. In an alternative approach at lower pressures, Crouch (1970) used the pressure vessel itself as the dilatometer, relying on precise pressure control and volume monitoring of the pressure medium; Wawersik (1975) described this procedure in more detail; see also Farran and Pérami (1974), Alheid (1982) and Elliot and Brown (1985).
2. In the case of sufficiently permeable rock, measurement of the amount of fluid moving in or out of a saturated specimen during deformation gives a measure of the volumetric strain associated with the accessible pores or cracks. After correction for elastic changes in pore volume, if significant or appropriate (Chapt. 7), the dilatancy can then be obtained. This method is the one commonly used in soil mechanics and it has been applied to rocks (e.g., Handin et al. 1963; Brace and Orange 1968; Cogan 1976; Scholz and Koczyński 1979; Chiu, Johnston and Donald 1983; Fischer and Paterson 1989; Marone, Raleigh and Scholz 1990; Olsen, Brandon and Gordon 1995). However, as pointed out by Handin et al. (1963), the method is of limited applicability to hard rocks because of the requirement that the permeability be adequate to maintain saturation during the experiment; it is also only applicable where the pore fluid is chemically inert with respect to the rock.
3. The most convenient method at present for obtaining the small volumetric strains that occur prior to brittle failure is to use electric resistance strain gauges to measure both the longitudinal and lateral strains in the specimen (e.g., Matsushima 1960a; Brace, Paulding and Scholz 1966; Blacic et al. 1981). Most of the results mentioned below have been obtained by this method, although other types of strain gauges have sometimes been used instead of electric resistance strain gauges (e.g., Bordia 1971; Brace 1978; Tullis and Tullis 1986).

In obtaining the dilatancy from the measured volumetric strain, a virtual elastic reference line has to be defined. This is usually an extrapolation of the approximately linear part of the curve relating volumetric strain to stress (or to longitudinal strain) which is observed at relatively low stresses, ignoring any initial non-linear behaviour associated with initial crack closing. However, in materials of appreciable porosity or previous microcracking history, there may be no truly linear portion of this curve and the choice of reference elastic line is more difficult and subjective. The solution adopted

**Table 1.** Dilatancy at brittle fracture

Rock	Initial porosity	Confining pressure (MPa)	Inelastic dilatational strain at peak stress $-\varepsilon_v^{\text{peak}}$	Reference
Wadhams anorthosite	0.002	150	0.006	Brace and Orange 1968
Spruce Pine dunite	0.002	150	0.014	Brace and Orange 1968
Cape granodiorite	0.003	150	0.006	Brace and Orange 1968
Rutland quartzite	0.004	150	0.004	Brace and Orange 1968
Witwatersrand quartzite	0.005	3 10 30	0.013 0.014 0.019	Crouch 1970
Westerly granite	0.007	160 300 500	0.002 0.003 0.004	Brace and Orange 1968
Climax granodiorite	0.007	20	0.002	Schock, Heard and Stephens 1973
KTB amphibolite	0.007	100 150	0.003 0.005	Chang and Haimson 2000
Carrara marble	0.007	5	0.003	Fredrich, Evans and Wong 1989
Blair dolomite	0.009	100 300	0.012 0.013	Heard et al. 1973
Pottsville sandstone	0.025	100	0.007	Brace and Orange 1968
Solnhofen limestone	0.029	50	0.002	Baud, Schubnel and Wong 2000
Lance sandstone	0.08	100	0.008	Schock, Heard and Stephens 1973
Bund sandstone	0.15	5 10 20 30 40	0.003 0.003 0.003 0.003 0.003	Gowd and Rummel 1980
Berea sandstone	0.17	5 10 20 30 40	0.007 0.006 0.006 0.006 0.003	Jamison and Teufel 1979
Adamswiller sandstone	0.226	5 40	0.005 0.003	Wong, David and Zhu 1997

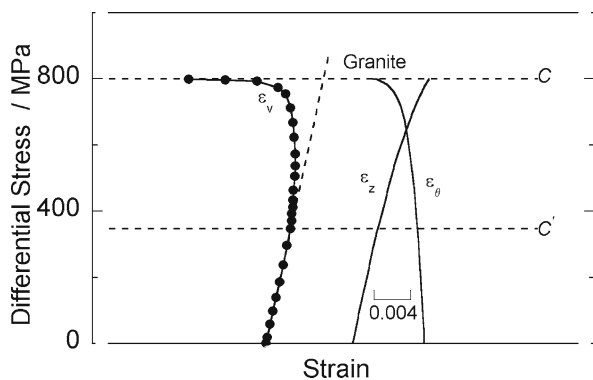
by Schock, Heard and Stephens (1973) is to define the dilatancy as the departure of the volumetric strain observed at a given mean stress from that observed in hydrostatic loading to the corresponding pressure. This approach has been adopted in later studies (e.g., Brace 1978; Jamison and Teufel 1979; Shimada and Yukutake 1982; Wong, David and Zhu 1997). It could in general be expected to give a more meaningful definition of the onset of dilatancy than that adopted by Sangha and Dhir (1972), namely, the point at which the observed instantaneous Poisson's ratio exceeds 0.5, although Sangha and Dhir argue in favour of the latter.

Bridgman (1949b) observed inelastic increases in volume prior to fracture in uniaxial compression tests on soapstone, marble, and dolerite. In a prescient comment, he attributed this dilatancy to "alterations in the structure" that are precursors to the macroscopic fracture. Matsushima (1960a) made similar observations of dilatancy in granite and showed, further, that the effect also occurred under confining pressure, although with increasing pressure its magnitude decreased and the range of truly elastic behaviour increased; he discussed the influence of confining pressure in terms of reduction in porosity. Handin et al. (1963) also observed a diminution in dilatancy with increasing confining pressure in dolomite in its brittle field. In contrast, Brace, Paulding and Scholz (1966) found that the dilatancy just prior to macroscopic fracture in granite, marble, and aplite did not decrease markedly with increase in confining pressure in the ranges of brittle behaviour in these rocks, although the magnitude of the effect varied considerably from one type of rock to another. Table 1 gives a compilation of the values of the inelastic dilational strain at peak stress, for a number of rock types, with initial porosities ranging from 0.002 to 0.226. Data for the compact rocks are mostly from the compilation of Brace (1978). We have also added recent data for porous rocks with a failure mode specified to be shear fracture. It is interesting to note that the values for compact and porous rocks all fall within the relatively narrow range of 0.002 to 0.019.

The work of Brace, Paulding and Scholz (1966) was the first detailed study of dilatancy at high confining pressures made with a view to elucidating the stages of development of microcracking leading up to macroscopic fracture. Some of their results are plotted in Fig. 25. Figure 26 gives further examples from the work of Bieniawski (1967a) firstly on quartzite in uniaxial loading and secondly on norite under confin-

**Fig. 25.**

Dilatancy in Westerly granite in triaxial test at 100 MPa confining pressure.  $\epsilon_v$  represents the volumetric strain,  $\epsilon_z$  the axial strain and  $\epsilon_\theta$  the circumferential strain; in each case relative dimensional decrease is taken as positive, so volume increases to the left.  $C$  is the macroscopic failure stress and  $C'$  the stress at the onset of dilatancy (after Brace, Paulding and Scholz 1966)



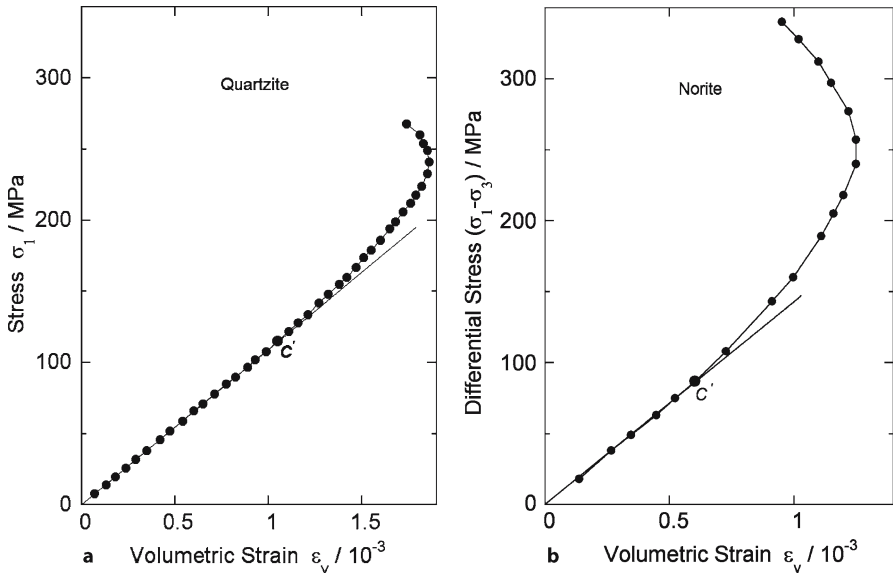


**Fig. 26.** Dilatancy in: **a** quartzite in uniaxial compression; **b** norite in triaxial compression with ratio of axial stress to confining pressure equal to 38:1; symbols and conventions as in Fig. 25 (after Bieniawski 1967a)

ing pressure, with constant ratio of greatest to least principal stress. Observations of a similar nature under both uniaxial and triaxial loading have been published by many workers, including Morgenstern and Phukan (1966, 1969), Scholz (1968d), Cook (1970), Saint Leu and Sirieys (1970), Bordia (1971), Green et al. (1972), Tomashevskaya and Khamiduulin (1972), Sangha and Dhir (1972), La Fountain and Dunn (1973), Schock, Heard and Stephens (1973), Thill (1973), Ui (1976), Mogi (1977), Jamison and Teufel (1979), Teufel (1981), Raleigh and Marone (1986), Fredrich, Evans and Wong (1989), Marone, Raleigh and Scholz (1990) and Peach and Spiers (1996). In fact, the phenomenon of dilatancy prior to macroscopic fracture in compression appears to be a general feature of most fairly compact brittle polycrystalline materials since it is also observed in such materials as concrete – e.g., Berntsson, Hedberg and Malinkowski (1971), Newman and Newman (1971), and several papers in Te'eni (1971); earlier references will be found in these papers – ice (Gold 1960), and cast iron (Coffin 1950). It has also been observed in extension tests (Hawkes, Mellor and Garipey 1973), but the work reviewed here refers to dilatancy observed in compression tests.

The stress level of the onset of dilatancy, commonly designated  $C'$  following Brace and co-workers, is usually observed to be between one-third and two-thirds of the macroscopic fracture stress, although in some cases dilatancy may be detected earlier or, in the case of porous rocks, only very near the fracture stress (Brace 1978). As illustrated in Fig. 27, the principal stresses at the onset of dilatancy for a given rock follow an approximately linear trend. Hadley (1973) showed that, in granite and gabbro below a certain confining pressure,  $C'$  is approximately equal to the stress for



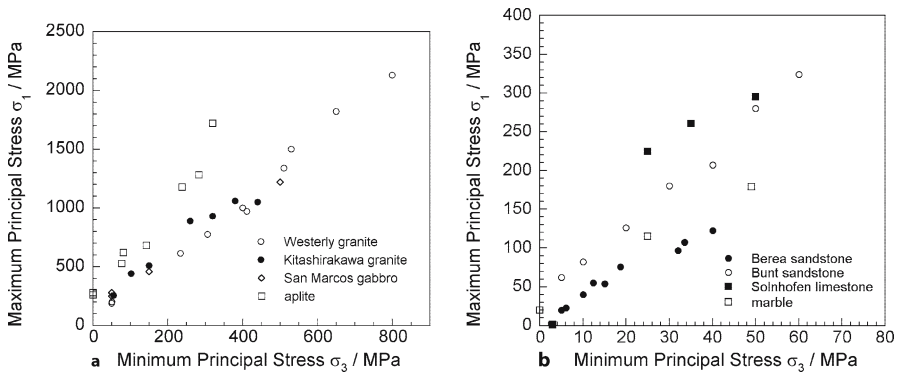


**Fig. 27.** Maximum and minimum principal stresses at the onset of dilatancy in (a) compact, and (b) porous rocks. The data for Westerly granite, aplite and marble are from Brace, Paulding and Scholz (1966), and those for Kitashirakawa granite, San Marcos gabbro, Berea sandstone, Bunt sandstone and Solnhofen limestone are from Matsushima (1960a), Hadley (1976b), Wong, David and Zhu (1997), Gowd and Rummel (1980), and Baud, Schubnel and Wong (2000), respectively

sliding on a shear failure. With porous rocks, the definition of  $C'$  may be complicated by the prior occurrence of some compaction due to collapse of pores under the deviatoric stress (Edmond and Paterson 1972; Green et al. 1972; Ingles, Lee and Neil 1973; Schock, Heard and Stephens 1973; Zoback and Byerlee 1975a,b). In this case, dilatancy can be defined somewhat subjectively by a significant reversal of the trend in volume change. As discussed above, a more objective approach is that proposed by Schock, Heard and Stephens (1973) whereby the onset of dilatancy is marked by the stress state at which the volumetric strain observed at a given mean stress deviates from that observed in hydrostatic loading to the corresponding pressure.

Dilatancy is influenced by temperature and by strain rate or time. Thus, Hadley (1975b) reports that increase in temperature up to 400 °C increases the amount of dilatation and sharply decreases the threshold stress  $C'$  in granite. There have been few studies of the temperature effect on other materials (Tan and Wu 1989). Dilatancy has also been observed to increase with time at a given applied force (Matsushima 1960a; Scholz 1968c; Hardy et al. 1970; Scholz and Kranz 1974; Wawersik 1974; Wu and Thomsen 1975; Cogan 1976; Kranz and Scholz 1977; Kranz 1980; Lajtai, Schmidtke and Bielser 1987; Lockner 1993a). Correspondingly, decrease in loading rate or strain rate can lead to greater dilatation at a given strain and can lower the detected threshold stress  $C'$  (Brace, Paulding and Scholz 1966; John 1974; Sano, Ito and Terada 1981; Masuda, Mizutani and Yamada 1987). However, this trend is sometimes preceded by a reverse influence of strain rate at the smaller strains (Perkins, Green and Friedman 1970; Sangha and Dhir 1972). Water-saturated rocks in uniaxial compression show more marked dilatancy at lower stresses than do dry rocks but a lesser effect at stresses approaching fracture (Tomashevskaya and Volodina 1976).

Studies have also been made of dilatancy in subsequent loading cycles (for a discussion on the choice of elastic reference line for subsequent cycles, see Hadley 1976b). At zero or small confining pressures,  $C'$  decreases with increasing number of cycles (Saint

Leu and Sirieys 1971; Haimson 1974; Scholz and Kranz 1974; Zoback and Byerlee 1975a), but at high confining pressures the effect decreases and may become unobservable (Zoback and Byerlee 1975a; Hadley 1976b). Also of interest is the shape or area of the hysteresis loop of volumetric strain plotted against axial strain (or stress); at moderate stress levels, this area can decrease with increasing number of cycles, approaching a stable condition, or it may increase as failure is approached in cycling to higher loads (Saint Leu and Sirieys 1971; Peng, Podnieks and Cain 1974; Scholz and Kranz 1974). These trends may be only notable at zero or very low confining pressures since Zoback and Byerlee (1975a) only found permanent strain accumulation in granite in the first cycle at confining pressures of 50 MPa and above, with fairly stable hysteresis loops thereafter. However, there is evidently in general a level of stress amplitude above which some progressive damage always accumulates since dynamic fatigue failure is observed in rocks in a way analogous to that in metals (Burdine 1963; Hardy and Chugh 1971; Morlier 1971b; Attewell and Farmer 1973; Cain, Peng and Podnieks 1974; Haimson and Kim 1972; Haimson 1974; Montoto 1974; Scholz and Koczyński 1979). Several types of hysteresis loops have been distinguished by Nishimatsu and Heroesewojo (1974), who give a discussion in terms of viscoelastic models; a more mechanistic model to account for dilatancy and the hysteresis has been developed by Brace, Paulding and Scholz (1966), Scholz and Kranz (1974) and Zoback and Byerlee (1975a).

By measuring the changes in both the inside and outside diameters of a hollow cylindrical specimen, Cook (1970) showed that dilatancy is a pervasive property of the rock. However, detailed measurements, especially with the aid of more precise measuring devices, show that the lateral strain component, and presumably the volumetric strain, become heterogeneous as fracture is approached, and the incipient development of shear zones suggests itself (Spetzler and Martin 1974; Spetzler, Sobolev and Getting 1989; Hadley 1975a; Liu and Livanos 1976; Soga, Martin and Spetzler 1976; Tomashevskaya and Volodina 1976).

It has become widely accepted that the stress threshold  $C'$  for dilatancy marks the initiation of microcrack propagation or proliferation, as first suggested by Brace, Paulding and Scholz (1966) and Bieniawski (1967a). The increase in linear compressibility in the lateral direction observed by Brace et al. indicates that the microcracks that are opening are predominantly oriented parallel to the specimen axis. Also measurements by Mogi (1977) under conditions of general triaxial stress show dilatancy to be notably anisotropic in a way that corresponds to microcracks opening predominantly normal to the least principal compressive stress. This picture of the onset of microcrack propagation is consistent with microscopic and other observations to be reviewed later in this chapter.

Several proposals have been made for extending the microcrack dilatancy concept to general stress states, treating the material as a continuum obeying an explicit non-linear constitutive relation (Morgenstern and Phukan 1969; Stuart and Dieterich 1974; Nur 1975; Cherry, Schock and Sweet 1975; Schock 1976). It may be noted here that the "shear-dilatancy" effect discussed theoretically by Freudenthal (1975) would seem to be essentially a non-linear elastic effect, not directly related to microcrack dilatancy – see also White (1976), on elastic dilatancy. The validity of these approaches rests somewhat tenuously on demonstrations that, within a limited range of conditions, the di-

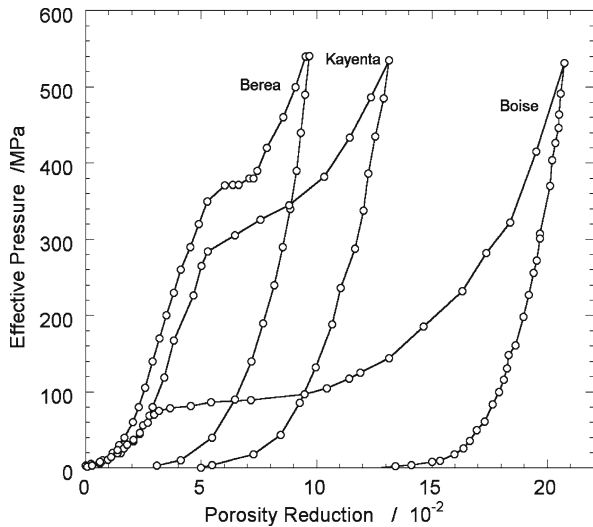
latant behaviour of rock under general states of stress is roughly independent of the path by which the state of stress is approached (Morgenstern and Phukan 1969; Swanson and Brown 1971a,b; Brace and Riley 1972; Schock, Heard and Stephens 1973). Alternatively, plasticity theory can be used to model the general inelastic behaviour of a dilatant-frictional material (Appendix 2).

Apart from throwing light on the processes of brittle failure, the phenomenon of dilatancy in rocks is potentially of considerable practical importance. Much of the early research on dilatancy has been stimulated by the hypothesis of its central role in the mechanism of earthquakes (Nur 1972; Scholz, Sykes and Aggarwal 1973) and its association with possible premonitory signs for earthquakes, such as changes in elastic wave speeds or in the levels of the Earth's surface or the water table; for dilatancy-diffusion models, see Nur (1972) and Scholz, Sykes and Aggarwal (1973), and for the dry crack proliferation models, see Mjachkin et al. (1972, 1975), Brady (1974, 1975, 1976), Mogi (1974b) and Stuart (1974). A comparison of the two types of models is given by Mjachkin et al. (1975). Recent reviews have been given by Crampin, Evans and Atkinson (1984), Scholz (1990) and Sibson (1994). However, dilatancy may also be of considerable importance in geologic processes, for example, in facilitating metasomatism or other processes dependent on the permeability of the rock, such as ore deposition (see, e.g., Dandurand et al. 1972a,b).

The dilatancy phenomena so far described are most obvious in compact rock where initial porosity does not play a significant role. The situation is more complex in porous rock where volume changes can occur during both hydrostatic and deviatoric stressing. Under hydrostatic loading, there is often observed to be an inflection point  $P^*$  in the hydrostat (the plot of porosity change versus effective pressure) which reflects the onset of inelastic compaction (Fig. 28) (Brace 1978; Wong 1990a; Zhang, Wong and Davis 1990b; Menéndez, Zhu and Wong 1996). The mechanism of such compaction in

**Fig. 28.**

Hydrostatic compression of three sandstone samples saturated with water. The hydrostats show inflection points that correspond to the onset of inelastic grain crushing at effective pressures of 75 MPa, 300 MPa and 380 MPa, respectively, for the Boise, Kayenta and Berea sandstones (Zhang, Wong and Davis 1990b)



sandstones has been shown to involve mainly grain crushing as a result of Hertzian contact stresses (Borg et al. 1960; Gallagher et al. 1974; McEwen 1981; Zhang, Wong and Davis 1990b; Menéndez, Zhu and Wong 1996).

Under the deviatoric stressing of porous rock, the collapse of porosity during deformation tends to counterbalance the tendency to dilatancy considered above and so porous rock commonly shows compactancy, or negative dilatancy. This effect is often called “shear-enhanced compaction” to distinguish it from the initial compaction that results simply from the application of hydrostatic pressure (Curran and Carroll 1979; Zhang, Wong and Davis 1990a). It is also not uncommon for rocks to show an early stage of compactancy followed by dilatancy at larger strains (Edmond and Paterson 1972; Schock, Heard and Stephens 1973; Elliot and Brown 1985; Baud, Schubnel and Wong 2000; Fossum and Fredrich 2000; Popp, Kern and Schulze 2001). The mechanisms of compaction during deformation may be broadly distinguished as involving either brittle grain crushing or ductile plastic collapse of the pores (Borg et al. 1960; Hirth and Tullis 1989; Menéndez, Zhu and Wong 1996; Renner and Rummel 1996; Wong, David and Zhu 1997; Papamichos 1999; Risnes and Flaageng 1999; Wong and Baud 1999; Baud, Schubnel and Wong 2000; Shimada 2000). However, Baud, Schubnel and Wong (2000) emphasize that the compaction and dilation processes occurring during deformation should not be viewed as mutually exclusive processes, since that there can be an evolution from one to the other.

When the compaction during deformation of a porous rock is localized, a “compaction band” is said to be formed. Compaction bands are discussed further in Chapt. 6.

## 5.4 Elastic Wave Speeds and Attenuation

### 5.4.1 General

The measurement of elastic properties has often been used to give information about the structural properties of a rock. The magnitudes of the elastic constants are sensitive to the mineralogic assemblage and are affected by the shapes, distribution, and preferred crystallographic orientation of the components. In addition, they are affected to an important degree by the presence, size, and orientation of defects such as pores and cracks, in a way that also depends on the presence or absence of interstitial fluids.

Elastic properties may be determined from static measurements of stress and strain or by dynamic methods. In the latter case, elastic wave speeds (“seismic velocities”) are commonly measured, using methods based on the resonant modes of the specimens or on the propagation of elastic waves in the specimens; for a review of dynamic methods, see Anderson and Lieberman (1968), Schreiber, Anderson and Soga (1973), Winkler and Plona (1982), Christensen (1985), Weidner (1987), and Christensen and Wepfer (1989). Although the first important evidence for cracks influencing elastic properties came from static measurements (Adams and Williamson 1923; Zisman 1933b,c), it is difficult to apply the static method at stresses low enough to avoid an influence of the probing stress itself on the properties of the specimen (cf. Zisman 1933a; Simmons and Brace 1965). Nevertheless, important refinements of static measurement technique have been

made by McKavanagh and Stacey (1974), Brennan and Stacey (1977) and Jackson and Paterson (1993). As a result of the difficulties with static methods, dynamic measurements, especially of ultrasonic elastic wave speeds using the pulse-transmission and pulse-echo methods, have mainly been used in microcrack studies. Another property of elastic wave propagation that is sensitive to the presence of cracks and to their degree of fluid saturation is the *attenuation*, as indicated by the relative amplitude of the received waves or pulses (Toksöz and Johnston 1981; Jackson 1993). In this section we review these studies, in which the state of microcracking of specimens and the influence of stress on it are inferred from the measured elastic wave speeds.

### 5.4.2

#### Background Theory and Observation

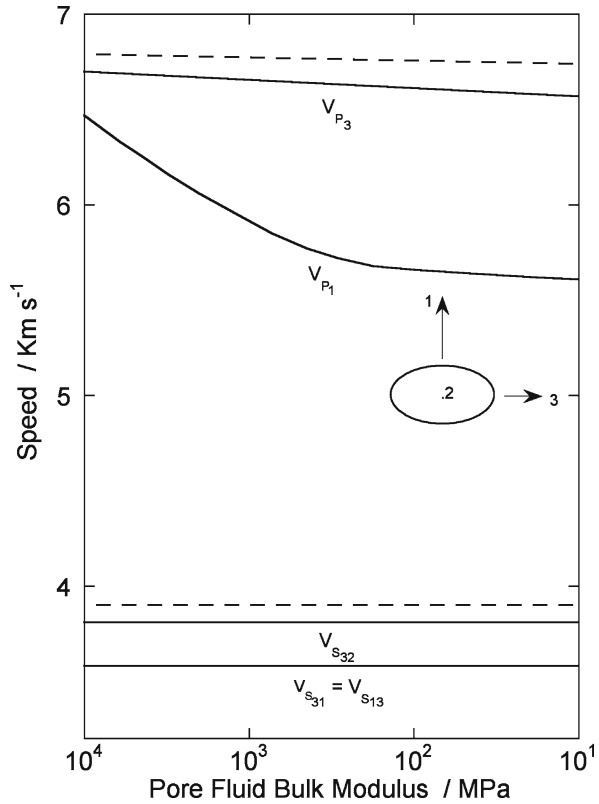
The theory on which interpretation must be based has been well developed in a number of papers (see compilations in Wang and Nur 1992; Winkler and Murphy 1995; Mavko, Mukerji and Dvorkin 1998). Some of these papers represent more or less direct developments from the basic elastic theory of Eshelby (1957), treating the static deformation of a dilute crack population, that is, assuming no interaction between cracks (e.g., Walsh 1965a,b, 1968, 1969, 1980; Nur 1971; Anderson, Minster and Cole 1974; Stiller, Wagner and Vollstädt 1977). The effect of interaction between cracks in the case of higher crack densities has been allowed for to a first approximation using self-consistent and similar schemes (O'Connell and Budiansky 1974, 1977; Bruner 1976; Budiansky and O'Connell 1976; McLaughlin 1977; Cleary, Chen and Lee 1980; Walsh 1980; Henyey and Pomphrey 1982; Mukerji et al. 1995; Guéguen, Chelidze and Le Ravalec 1997). Similar results have been obtained by Garbin and Knopoff (1973, 1975a,b) and by Kuster and Toksöz (1974) by applying scattering theory in the long wavelength limit; see also Toksöz, Cheng and Timur (1976), Hudson (1981), Berge, Fryer and Wilkens (1992), La Fountain and Dunn (1973) and Davis and Knopoff (1995). Elastic anisotropy due to preferentially oriented crack populations has also been considered (Nur 1971; Anderson, Minster and Cole 1974; Hoenig 1979; Piau 1980; Nishizawa 1982; Crampin 1984; Hudson 1990, 1994; Sayers and Kachanov 1991; Cheng 1993; Sayers 1993). Most of the analyses are for a cracked medium that is transversely isotropic. The results of these theoretical studies on the influence of cracks on elastic wave speeds in rocks can be summarized as follows:

1. *Dry rocks.* The compressional wave speed  $V_p$  and the shear wave speed  $V_s$  are both markedly decreased by the presence of dry cracks.  $V_p$  is affected more than  $V_s$  so the ratio  $V_p/V_s$  tends also to be decreased. These trends apply for all directions of propagation when there is no preferred orientation of the cracks.

When there is preferred orientation of the cracks, wave speed anisotropy arises, the fundamental nature of which is most simply illustrated in the case of a planar preferred orientation of cracks, as considered by Anderson, Minster and Cole (1974) – see Fig. 29, in which the behaviour with low pore fluid bulk modulus corresponds to that for dry rock with air-filled pores. The influence of the cracks on  $V_p$  is very strong for a propagation direction normal to the preferred plane of the cracks and is relatively small for propagation in this plane. The influence on  $V_s$  is also appre-

**Fig. 29.**

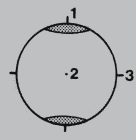
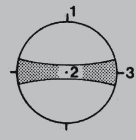
Compressional and shear wave speeds  $V_p$  and  $V_s$  in model granite with aligned oblate spheroidal cracks of axial ratio 20:1 and porosity 0.01, showing dependence on bulk modulus of fluid filling the cracks. *Inset* shows orientation of frame of reference and of cracks; *first suffix number* on speed symbol represents the direction of propagation and, in the case of shear waves, *second number* represents the direction of vibration; *broken lines* represent  $V_p$  and  $V_s$  for the granite matrix (after Anderson, Minster and Cole 1974)



ciable for propagation normal to the preferred plane (although rather less than on  $V_p$ ), and the same effect appears in  $V_s$  for propagation in the preferred plane if the direction of vibration is normal to this plane. For propagation in the preferred plane and with vibration direction also lying in it,  $V_s$  is very little affected by the cracks. These relative effects are summarized in qualitative terms in Table 2A, where the trends in  $V_p/V_s$  are also given.

The case of planar preferred orientation of cracks just considered, which can be represented by a single point maximum in a stereographic projection of the normal to the cracks (Table 2A), is a particular case of axial symmetry. Another important case of axial symmetry is that in which the cracks tend to be parallel to the unique rotation axis but are without preferred orientation in azimuth about this axis, as in the case of cracks forming parallel to a uniaxial stress in an otherwise statistically isotropic material. The behaviour in this case can be deduced qualitatively from that of the first case by superposition and is shown in Table 2B. The symmetry of the wave speeds is the same in both cases, although the degree of anisotropy exhibited will be less in the second case for a given degree of preferred orientation. In either case, of course, the degree of anisotropy also depends on the strength of the preferred orientation. Cases of lower symmetry are also possible,

**Table 2.** Influence on elastic wave velocities of crack distributions having preferred orientations

A. Planar case					
					
Propagation normal to preferred plane			Propagation in preferred plane		
	$V_{p_1}$	$V_{s_{12}} = V_{s_{13}}$	$V_{p_3}$	$V_{s_{31}}$	$V_{s_{32}}$
dry	{ large	medium (large decrease in $V_p/V_s$ )	small	medium (medium increase in $V_p/V_s$ )	very small (small decrease in $V_p/V_s$ )
wet	{ small	medium (small decrease in $V_p/V_s$ )	very small	medium (medium increase in $V_p/V_s$ , more than dry)	very small (very small decrease in $V_p/V_s$ , less than dry)
B. Cylindrical case					
					
Propagation parallel to axis			Propagation normal to axis		
	$V_{p_1}$	$V_{s_{12}} = V_{s_{13}}$	$V_{p_3}$	$V_{s_{31}}$	$V_{s_{32}}$
dry	{ small	small (small increase in $V_p/V_s$ )	medium	small (medium decrease in $V_p/V_s$ )	medium (small decrease in $V_p/V_s$ )
wet	{ very small	small (small increase in $V_p/V_s$ )	small	small (small increase in $V_p/V_s$ )	medium (medium increase in $V_p/V_s$ )

*Explanations:* a) The terms “small”; “large” etc. refer to the amount of decrease in the velocities due to introducing the cracks, relative to the velocities in uncracked material. b) The suffix on  $V_p$  and the first suffix on  $V_s$  specify the direction of propagation; the second suffix on  $V_s$  specifies the direction of vibration (the shear waves are assumed to be plane-polarized).

for example, with elongated cracks having a preferred orientation of the direction of elongation as well as of their planes.

It is pertinent to note that in all cases of wave speed anisotropy there will, in general, be birefringence or double refraction of shear waves (or near-shear waves), often referred to as “shear wave splitting”, except for special directions of propaga-

tion such as along the axis of rotational symmetry in the cases elaborated above. For further details, see Stoneley (1949), Musgrave (1970), and Nur (1971) on the theory, and Nur and Simmons (1969c), Todd, Simmons, and Baldrige (1973), Bonner (1974), Hadley (1975c), Sayers and van Munster (1991), Peacock et al. (1994) and Sayers and Kachanov (1995) for observations.

2. *Wet rocks.* When the cracks are filled with a fluid of relative low compressibility, such as liquid water, the effect of the cracks in reducing  $V_p$  as described for dry rocks is to a large extent removed, while the smaller effects of the cracks on  $V_s$  are little changed. Consequently, in rocks with randomly oriented cracks saturated with a low compressibility fluid (“wet rocks”), the ratio  $V_p/V_s$  tends to be somewhat higher than in the absence of cracks, the reverse of the trend in dry rocks.

In the anisotropic case with planar preferred orientation of the cracks (axisymmetric), the  $V_p$  values are considerably modified from those for dry rocks but the  $V_s$  values are unaffected – see Table 2A, again derived from Anderson et al. (1974), and Fig. 29. The  $V_p/V_s$  figures are therefore substantially different from those for the dry rocks, and comparison of the wet and dry cases shows that, with a given crack population, saturating the cracks leads to an increase in  $V_p/V_s$  for both directions of propagation and polarization. The corresponding, similar effects for the cylindrical preferred orientation are also shown in Table 2B.

Partial saturation or saturation with a fluid of intermediate compressibility gives effects intermediate between the “dry” and “wet” cases described above. Also the effects are dependent on the crack density, and at higher crack densities the picture may become more complicated (see, e.g., O’Connell and Budiansky 1974). With saturated rocks, the pressure in the fluid itself can be expected in general to have little direct influence on the wave speeds, but indirect effects may arise through changes in compressibility of the fluid (e.g., Anderson and Whitcomb 1973; Hadley 1975c; Spencer and Nur 1976). The viscosity of the fluid may also be important (Nur and Simmons 1969b).

These predictions for the behaviour of the wave speeds in dry and wet rocks with isotropic or planar preferred orientations of cracks are at least qualitatively consistent with the experimental observations on natural rocks, although in most cases only data for P waves have been obtained (e.g., Wyllie, Gregory and Gardner 1956, 1958; Birch 1960, 1961; Volarovich and Bayuk 1960; Christensen 1965, 1966, 1982; Volarovich 1965; Nur and Simmons 1969a; Thill, Willard and Bur 1969; Tourenq, Fourmaintraux and Denis 1971; Todd and Simmons 1972; Ramana and Venkatanarayana 1973; Thill, Bur and Steckley 1973; Wang and Lin 1974; Wang, Lin and Wenk 1975; Hadley 1976a; Bonner and Schock 1981; Nur and Wang 1989; Christensen and Wepfer 1989; Wang and Nur 1992, 2000). A comparison is made possible by the data of Wang et al. (1975) for a gneiss; these data include the speeds of the P waves and both polarizations of S waves, measured under dry conditions as a function of pressure and under water-saturated conditions at one atmosphere. If we take the measurements at high pressure and dry as a basis reflecting the behaviour in the absence of open cracks and compare the measurements made at low pressures both dry and wet with this basis, it is seen that the observed effects of the cracks correspond very well to the trends expected for a planar preferred orientation parallel to the foliation plane (Table 2A), except that the values of  $V_{S32}$  are relatively somewhat more affected than would be expected, due



possibly, at least in part, to the incompleteness of the preferred orientation. The variations in both P and S speeds with change in temperature over a range of confining pressures and pore water pressures have also been explored in detail by Spencer and Nur (1976).

Quantitative agreement between measured and predicted wave speeds has at various times been claimed in relation to given theories, the comparison being made either directly, when the crack geometry is taken to be known, or implicitly, when it is shown that the crack geometry required for agreement is reasonable (e.g., Nur 1971; Kuster and Toksöz 1974; O'Connell and Budiansky 1974; Toksöz, Cheng and Timur 1976; Soga et al. 1978; Seya, Suzuki and Fujiwara 1979; Sayers, van Munster and King 1990; Peacock et al. 1994; Ayling, Meredith and Murrell 1995; Takei 2002). However, as Hadley (1976a) points out, these tests of the theoretical models have not really been very discriminating. Critical comparison between observation and theory requires both an adequate mode of description of the assemblage of cracks and careful microscopical measurements. The porosity itself is an insufficient measure because, as shown for example by Walsh (1965a), the elastic behaviour also depends on the aspect ratio of the cracks (note that, in contrast to the practice in many other fields of defining the aspect ratio of an elongate cross-section as length:width, in the literature on cracks this term has commonly been defined in a reciprocal way as the ratio of the minimum to maximum dimensions, as applied to an axisymmetric crack). A convenient single parameter that incorporates both properties and fully represents the crack assemblage in this context is the "crack density parameter"  $\varepsilon$  of O'Connell and Budiansky (1974). For an isotropic assemblage of  $N$  thin ellipsoid cracks of area  $A$  and perimeter  $P$ , and using  $\langle \rangle$  to indicate the mean value, the crack density parameter is

$$\varepsilon = \frac{2N}{\pi} \left\langle \frac{A^2}{P} \right\rangle$$

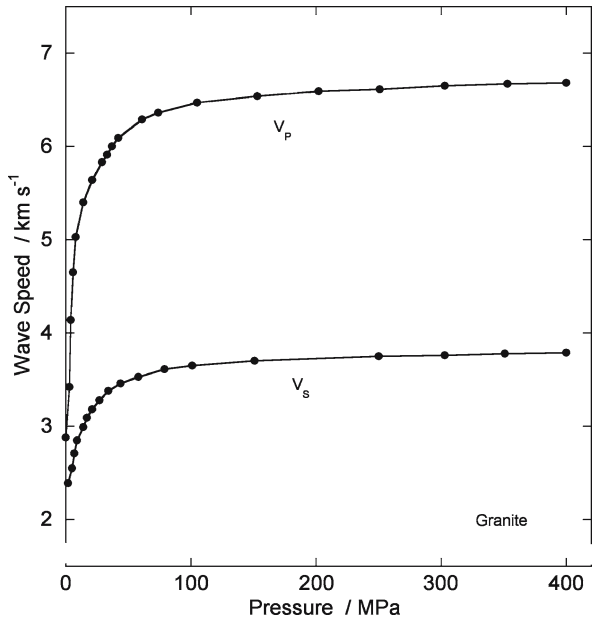
reducing to  $\varepsilon = N\langle a^3 \rangle$  for circular cracks of radius  $a$  (Walsh 1965b); for further discussion and practical measures of  $\varepsilon$  see Budiansky and O'Connell (1976), and for the description of anisotropic assemblages see Nur (1971). Hadley (1976a) has made careful measurements of crack geometry using the scanning electron microscope and has shown that the use of this geometry combined with an independently determined porosity leads to fairly close prediction of observed wave speeds, under hydrostatic conditions, on the theories both of Kuster and Toksöz and of O'Connell and Budiansky, but fails to discriminate between them.

### 5.4.3 Stress-Induced Changes in Elastic Wave Speeds

On the basis of the preceding preliminaries, we can now discuss the use of elastic wave speed measurements in exploring the state of microcracking within rock specimens as a function of applied stress. It is well established that the application of a hydrostatic pressure of a few hundred megapascals closes the cracks in dry rock and raises the wave speeds to those for the crack-free state (note that equidimensional pores may be little affected by these pressures); see e.g., Birch and Bancroft (1938a,

**Fig. 30.**

Influence of hydrostatic pressure on compressional and shear wave speeds,  $V_p$  and  $V_s$ , in dry Casco granite (after Nur and Simmons 1969a)



1940), Birch (1960, 1961), and Fig. 30, although Carlson and Gangi (1985) found that pressures in excess of 500 MPa were needed to close all cracks in some rocks.

A corresponding increase is commonly observed in the value of  $V_p$  measured in the axial direction when small compressional stress differences are applied to dry rock at zero or relatively low confining pressure (Shimozuru 1955; Volarovich et al. 1963a,b; Balakrishna and Ramana 1964; Balakrishna and Gowd 1965; Balakrishna 1967; Nur and Simmons 1969c; Hardy and Kim 1971a,b; Podnieks, Chamberlain and Thill 1972; Rao and Gogte 1972; Bonner, Benzing and Schock 1973; Gupta 1973; Thill 1973; Gramberg 1974; Rao and Ramana 1974; Rummel 1974; Jones and Murrell 1989). An initial increase is also often observed in  $V_p$  measured normal to the stress axis but the magnitude of the effect tends to be less (e.g., Nur and Simmons 1969c; Gupta 1973; Thill 1973; Gramberg 1974). However, at higher compressional stress differences, above roughly half the macroscopic failure stress, the value of  $V_p$  normal to the stress axis usually tends to show a marked decrease (Shimozuru 1955; Tocher 1957; Matsushima 1960b; Wolters 1971; Tomashevskaya and Khamidullin 1972; Gupta 1973; Hadley 1975; Lockner, Walsh and Byerlee 1977). With marble, this decrease has also been shown to continue beyond the peak stress, or in the case of loading in the ductile field, beyond the yield stress (Inami, Ibrahim and Mizutani 1969; Thill 1973; Rummel 1974). The values of  $V_p$  measured along the stress axis at the higher stress differences may either show further increase, or some decrease, but lesser in amount than in the normal direction. These changes may be inhibited in the presence of a high confining pressure (same references as for  $V_p$  normal to stress axis). Thus, in dry rock under stress a strong anisotropy in  $V_p$  tends to develop, much stronger in degree at the higher stress differences than at the lower, and with the sense of  $V_p$  being larger parallel to

the stress axis than normal to it. Such an effect is consistent with, first, closing cracks lying normal to the stress direction (cf. reverse of Case A, Table 2) and second, at higher stresses, opening cracks parallel to the stress direction (cf. Case B, Table 2). A similar effect is observed in concrete, for example, Jones (1952), and it is probably general in brittle polycrystalline materials; thus, Shamina, Pavlov, and Kopnichev (1973) and Shamina and Pavlov (1974) have observed wave speed changes in alabaster and “hyposulfite” during the development of cracking.

We now turn to the fewer cases in which  $V_S$  has been measured, usually in conjunction with  $V_P$ . The first such measurements are those of Nur and Simmons (1969c) who measured  $V_P$  and  $V_S$  as a function of angle to the force in diametrically loaded cylinders of dry granite, including both polarizations for the S waves. Although the stress is markedly heterogeneous in such loading, they observed the development of an appreciable anisotropy of wave speeds corresponding, with some deviation in the case of  $V_{S_{32}}$ , to the reverse of that set out for the dry planar crack distribution in Table 2A. Thus the effects they observed would be explained by the closing of cracks lying predominantly normal to the direction of loading, the stage of relatively low stresses described in connection with  $V_P$  in the previous paragraph (cf. also Nur 1971).

Gupta (1973) measured both  $V_P$  and  $V_S$  (no polarization specified) up to the point of fracture, both parallel and normal to the maximum compressive stress direction, in limestone under biaxial compression. Above about half the fracture stress, there was pronounced decrease in both  $V_P$  and  $V_S$  normal to the maximum compression direction and only small changes parallel to it; also  $V_P/V_S$  decreased markedly for the former direction and was little affected in the latter. In this case, both the  $V_P$  and  $V_S$  observations are consistent with what would be expected to result from the opening of cracks parallel to the direction of maximum compressive stress and normal to the direction of minimum stress, thus adding confidence to the deductions made above from  $V_P$  only. For dry granodiorite, Bonner, Benzing, and Schock (1973) briefly reported similar effects except that  $V_S$  was more markedly affected than  $V_P$  for propagation normal to the axis of compression and therefore  $V_P/V_S$  increased in this direction. The reason for the latter discrepancy from Gupta's result is not clear but it may involve difference in polarization of S waves or in azimuthal preferred orientation of the axial cracks. King, Shakeel and Chaudry (1997) have measured all nine wavespeed components in true triaxial tests on sandstones.

The development of axial cracking, postulated to explain the observed changes in wave speeds in dry rock at stresses above about half the fracture stress, is also consistent with that already postulated in previous sections to explain observations on dilatancy and acoustic emission but it adds stronger evidence on the orientation of the cracks. The correlation between dilatancy and wave speed changes has been demonstrated directly in dry rock by Bonner (1974) and Hadley (1975c) – see Figs. 31 and 32; in these figures, the wave speeds have been so labelled that the specimen axis ( $\sigma_1$ ) corresponds to the axis of symmetry, 1, of the cylindrical model of Table 2B. It is seen that qualitatively the correlation is very good, extending to both polarizations of  $V_S$  as well as to  $V_P$ ; the correlation also applies to subsequent loading cycles although there is a hysteresis (Hadley 1975c). See also Rothman, Greenfield, and Hardy (1975, 1976), Wang, Goodman, and Sundaram (1975), Lockner, Walsh, and Byerlee (1977), Soga et al. (1976), Rai and Hanson (1988), and Wu, King and Hudson (1991).

**Fig. 31.** Variation in volumetric strain and in shear wave speeds in course of loading dry Westerly granite to fracture in triaxial test at confining pressures of 20 MPa. Nomenclature and conventions as in Figs. 25 and 29; stress normalized to fracture stress; *error bar* indicates precision of wave speed measurements (Bonner 1974)

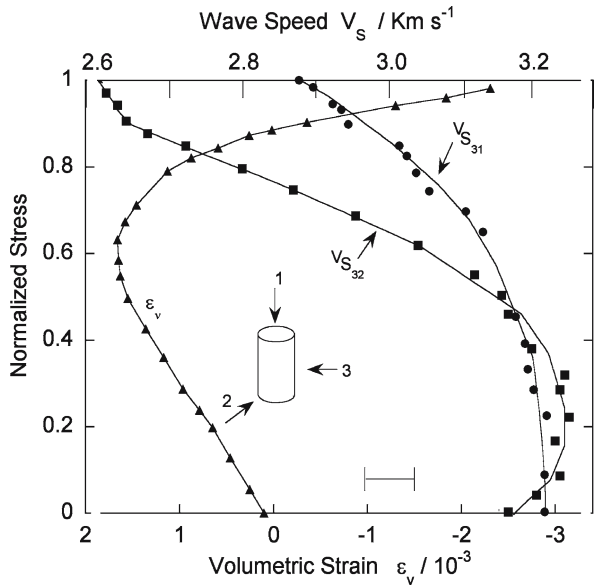
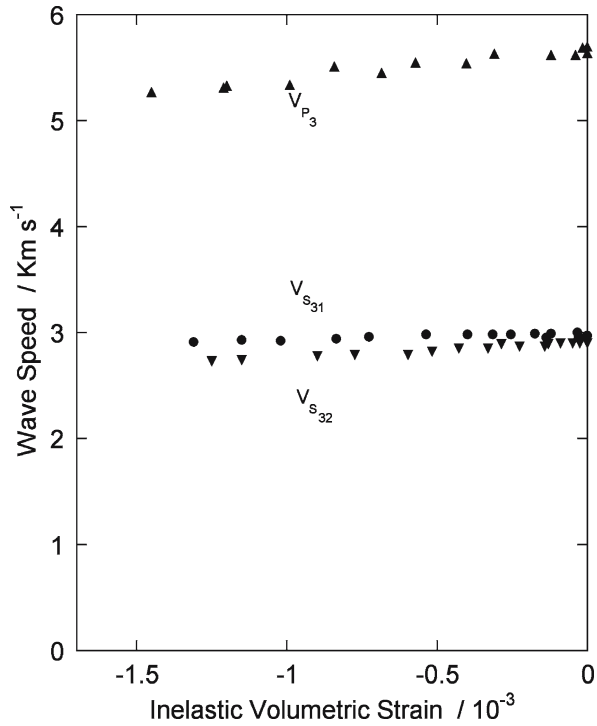


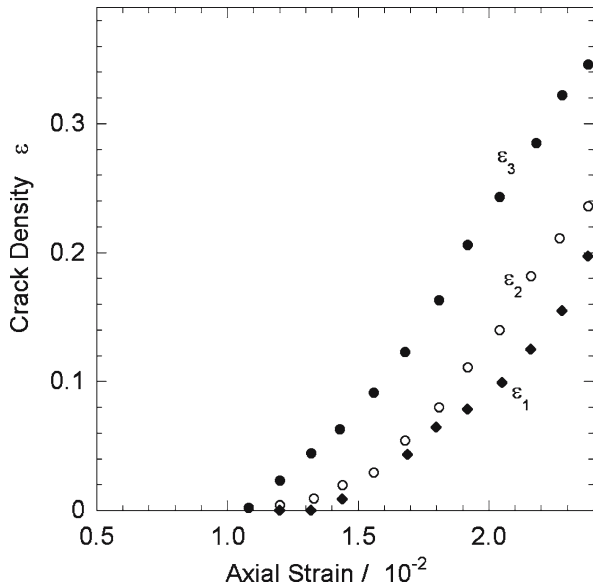
**Fig. 32.** Change in compressional and shear wave speeds with dilatation in dry Westerly granite in triaxial test at confining pressure of 39 MPa. Nomenclature and conventions as in Figs. 25 and 29 (Hadley 1975c)



Hadley (1975c) has also shown that when the rock is saturated with fluid at a pore pressure nearly equal to the confining pressure, the value of  $V_p/V_s$  measured normal to the specimen axis rises significantly as the rock dilates, in contrast to the fall that occurs in dry rock, and again consistent with the model of Table 2B. Bonner (1975) found similar consistency for measurements made parallel to the specimen axis, although he points out that the effect could be explained as well by a decrease in the thickness : length ratio of pre-existing axial cracks as by a proliferation of similar ones.

A number of quantitative studies have been conducted on dry samples to relate the sonic velocity data to the evolution of stress-induced microcracking and dilatancy. Soga et al. (1978) measured the speeds of compressional and shear waves propagated along two orthogonal directions perpendicular to the maximum compression axis of a rectangular prism of Westerly granite. They adopted the model of Anderson, Minster and Cole (1974), with the additional assumptions that the crack density  $\varepsilon$  can be expressed as the sum of three components ( $\varepsilon = \varepsilon_1 + \varepsilon_2 + \varepsilon_3$ ) corresponding to mutually orthogonal cracks with normals parallel to the principal stresses  $\sigma_1, \sigma_2, \sigma_3$ , and that the effects of oblique cracks on wave speeds can be vectorially partitioned among the three principal directions. From their elastic wave data, Soga et al. (1978) inferred that all three components of the crack density progressively increased with deformation (Fig. 33). Near the peak stress, the crack density attained a value of  $\varepsilon \approx 0.7$ . If the stress-induced microcracking is axisymmetric about the  $\sigma_1$  direction, then one expects  $\varepsilon_2 = \varepsilon_3$ . The appreciable difference between  $\varepsilon_2$  and  $\varepsilon_3$  in their data was interpreted by Soga et al. (1978) as due to the asymmetric sample bulging that was evident from strain measurements. Comparable increases in crack densities were inferred by Takahashi et al. (1984)

**Fig. 33.**  
Influence of axial strain on three principal components of the crack density tensor inferred from elastic wave velocity data of Westerly granite triaxially compressed at confining pressure of 100 MPa (after Soga et al. 1978)

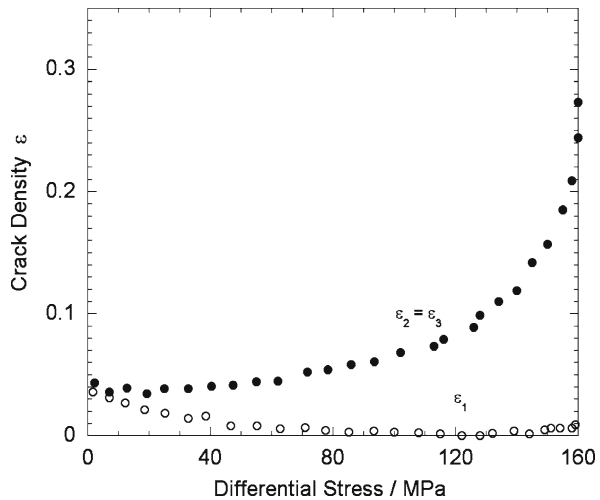


in “true” triaxial compression experiments on Westerly granite at a minimum principal stress of 50 MPa. Kachanov (1993) developed a relatively general model for inferring from elastic wave speed data the crack density as a second-rank tensor. Using this approach on the Ashima and Toki granites, Schubnel et al. (2003) concluded that beyond the onset of dilatancy the crack density was strongly anisotropic and that the magnitude of its trace exceeded 1 when a granite sample had been stressed to near peak stress.

Similar analyses have been performed on porous rocks. Ayling et al. (1995) measured compressional and shear wave speeds in Darley Dale sandstone in the pre- and post-peak stages. Using the approach of Soga et al. (1978), they inferred that the crack density  $\varepsilon_2 (= \varepsilon_3)$  in a sample deformed at confining pressure of 50 MPa decreased slightly at first and then progressively increased from the onset of dilatancy to peak stress. A total increase in  $\varepsilon_2 (= \varepsilon_3)$  of  $\approx 1.0$  was attained at the peak stress. In contrast, the component  $\varepsilon_1$  decreased by about 0.2 in the pre-peak stage. In the post-peak stage, slight increase and decrease were inferred for the crack density components  $\varepsilon_1$  and  $\varepsilon_2 (= \varepsilon_3)$ , respectively. Similar conclusions were drawn by Sayers and Kachanov (1995) in their analysis of the Berea sandstone data of Scott, Ma and Roegiers (1993). Sayers and Kachanov (1995) argued that the use of a second-rank tensor (with principal components  $\varepsilon_1$ ,  $\varepsilon_2$ , and  $\varepsilon_3$ ) would be adequate in this case. The inferred crack densities for Berea sandstone deformed at confining pressure of 20 MPa are shown in Fig. 34. It can be seen that the component  $\varepsilon_2 (= \varepsilon_3)$  initially decreased slightly and then increased from the onset of dilatancy to a value of about 0.3 near the peak stress, whereas the component  $\varepsilon_1$  decreased moderately with deformation.

A major limitation of the theoretical analyses is that they are all based on models that do not account for crack interaction and therefore may not be realistic approximations of the behaviour at relatively high crack densities. Nevertheless, they provide useful insight into the micromechanics of brittle failure. A common feature of the elastic wave speed measurements on both compact and porous rocks is that they imply significant

**Fig. 34.** Influence of differential stress on components of the crack density inferred from elastic wave velocity data of Berea sandstone triaxially compressed at a confining pressure of 20 MPa (after Sayers and Kachanov 1995)



increases in the crack density components  $\varepsilon_1$  and  $\varepsilon_2$ , which probably arise from the development of stress-induced cracking sub-parallel to the  $\sigma_1$  maximum compression direction. The data also indicate an important difference in the evolution of the component  $\varepsilon_3$ . In a compact rock, the development of dilatancy seems to involve appreciable cracking in directions oblique to the  $\sigma_1$  direction, which is manifested by significant increase in  $\varepsilon_3$ . In contrast, the development of volume change in a porous sandstone seems to be accommodated by appreciable compaction of pores aligned perpendicular to the  $\sigma_1$  direction, which is manifested by moderate decrease in  $\varepsilon_3$ .

The wave speeds measured along different paths in a sample being deformed can be used to infer the spatial heterogeneity of stress-induced microcracking (Ganryd, Getting and Spetzlar 1983). Yukutake (1989) used 12 piezoelectric transducers to measure the wave speeds along 20 ray paths in granite samples deformed at confining pressures up to 400 MPa. The tomographic images computed from the sonic data revealed localized regions of relatively high crack densities from where the macroscopic failure nucleated at very near the peak stress. Chow, Meglis and Young (1995) used a similar approach to obtain tomographic images of the progressive development of damage during cyclic, uniaxial compression of Lac du Bonnet granite.

#### 5.4.4 Attenuation

Another property of elastic wave propagation that is sensitive to the presence of cracks and to their degree of fluid saturation is the attenuation, as indicated by the relative amplitude of the received waves or pulses. A quantitative measure of attenuation is given by the specific attenuation factor  $Q^{-1}$  (Knopoff 1964; O'Connell and Budiansky 1978). It is well known that the attenuation of elastic waves in rocks is relatively high compared to that in single crystals or in metals (Nowick and Berry 1972) and is increased when the rock is saturated with water (Birch and Bancroft 1938a,b; Born 1941; Krishnamurthi and Balakrishna 1957; Peselnick and Zietz 1959; Auberger and Rinehart 1961; Peselnick and Outerbridge 1961; Knopoff and Porter 1963; Attewell and Ramana 1966; Gordon and Davis 1968; McKavanagh and Stacey 1974; Birch 1975; Singh 1976; Brennan and Stacey 1977; Wulff and Burkhardt 1997). This high attenuation was at first vaguely attributed to the grain boundaries but it would seem more likely to be associated with the presence of pores and cracks, which would also tend to contribute more significantly to attenuation than would the anelastic processes intrinsic to the solid parts of the rock. The most important mechanisms have not been clearly established but they may involve friction at points of light contact or dissipation processes at crack tips, the scattering of elastic waves if the sonic wavelength is comparable to the crack or pore dimensions, or viscous dissipation in the pore fluid in wet rock; see Knopoff (1964), Walsh (1966, 1968, 1969), White (1966), Gordon and Davis (1968), Jackson and Anderson (1970), Kuster and Toksöz (1974), Gliko (1976), O'Connell and Budiansky (1977), Toksöz and Johnston (1981), Winkler and Murphy (1995), Meglis et al. (1996), Wulff and Burkhardt (1997), and Mavko, Mukerji and Dvorkin (1998).

Conventionally, laboratory measurements of anelastic behaviour and wave attenuation have been based on ultrasonic wave propagation methods (Vassiliou, Salvado and Tittman 1984). However, in view of there being some frequency dependence (dis-

persion), it is also desirable to conduct experiments on elastic properties and attenuation at low frequencies and strain amplitudes comparable to those of seismic waves in the Earth (Peselnick and Liu 1987; Jackson 1993).

That the presence of open cracks in dry rocks contributes importantly to the attenuation was first attested to by the observation that the application of a confining pressure decreases the attenuation (Birch and Bancroft 1938a). The same effect, attributable to the closing of cracks, is observed at low levels of uniaxial loading, coincident with the initial increase in wave speed described above, while at higher applied stresses, even under considerable confining pressure, the attenuation in most cases tends to increase markedly after roughly half the macroscopic fracture stress is exceeded (Balakrishna and Ramana 1964; Balakrishna 1967; Gowd 1970; Rao and Gogte 1972; Thill 1973; Rao and Ramana 1974). Thus, it would appear that the increased attenuation in dry rocks at the higher stresses can be correlated with the proliferation of cracking associated with dilatancy prior to macroscopic fracturing. Rao and Ramana found that the attenuation changes are, in fact, more marked than the wave speed changes under applied stress, although Thill warns that attenuation data should only be used to complement the wave speed data because of the many variables that can influence the attenuation. Lockner, Walsh, and Byerlee (1977), however, found that for  $V_{s31}$  the attenuation in granite decreased with increasing stress up to large stresses, possibly reflecting a continuing predominant influence of the closure of cracks normal to the stress axis on this velocity component. The data of Tao and King (1990) on slate, limestone, sandstone and granite suggest that anisotropy in velocity is generally associated with anisotropy in attenuation.

Ayling, Meredith and Murrell (1995) used the spectral ratio technique to determine the specific attenuation factor  $Q^{-1}$  from ultrasonic measurements of compressional and shear waves during triaxial compression of Darley Dale sandstone. Both  $Q^{-1}$  values exhibit large decreases upon initial loading, followed by rapid increases from the onset of dilatancy to the peak stress. In an experiment at 50 MPa confining pressure, the  $Q^{-1}$  value for compressional waves decreased to almost one half, and then increased by a comparable amount, while the  $Q^{-1}$  value for shear waves decreased by more than a factor of two and then increased by about 60%. In the post-peak stage, slight decreases in  $Q^{-1}$  values were observed. While the overall changes in attenuation followed trends similar to those for elastic wave speeds, the proportional changes observed in the  $Q^{-1}$  values were about an order of magnitude greater. Qualitatively similar behaviour was also observed in spectral ratio measurements conducted on deformed samples of slate (Xu and King 1990) and sandstones (Wulff, Raab and Huenges 2000).

## 5.5 Transport Properties

Transport properties that are dependent on the connected void space in the rock are markedly affected by the opening or closing of microfractures. These effects have been studied mainly in the cases of permeability to fluids and of electrical conductivity.

**Permeability.** Permeability is determined from observations on the passage of a pore fluid through the rock. This fluid is usually either an inert gas (argon) or water. Gas is



a convenient medium when chemical interaction with the rock is to be avoided and the purely geometric aspect of the permeability is being sought, and when the permeability is very low. However, there are potential limitations with the use of gas due to its higher compressibility and to the Klinkenberg effect (Klinkenberg 1941; Guéguen and Palciauskas 1994). The Klinkenberg effect arises when the mean free path of the gas molecules becomes comparable to the pore size, thus introducing a pressure dependence in the apparent viscosity and hence in the determined permeability. The use of water as pore fluid is therefore common and is often more appropriate for application to crustal rocks where the interaction of water with the rock is potentially of interest.

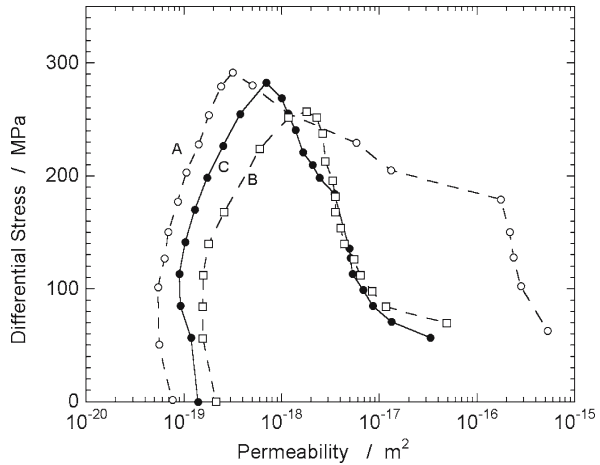
There are three methods of measurement in general use. In the first, the pressure drop for a given rate of steady state flow is measured. In the second, the transient response to an abrupt step in the pore fluid pressure is analysed. In the third, the pore fluid pressure is cycled at one end of the sample and the amplitude and phase of the cyclic response at the other end is analysed. The second and third methods also, in principle, can give the storage capacity of the sample. Details of the application of these methods can be found in Thénoz, (1956); Brace, Walsh, and Frangos, (1968); Hsieh (1981), Neuzil et al. (1981), Trimmer (1981, 1982), Lin (1982), Lin, Pirie and Trimmer (1986), Morin and Olsen (1987), Kranz, Saltzman and Blacic (1990), Fischer (1992), Fischer and Pater-son (1992), Wang and Hart (1993), and Lesnic et al. (1997).

In compact rocks, the permeability may decrease slightly under the application of relatively small stresses but on further increasing the stress there is usually found to be a level above which the permeability increases very markedly, even under confining pressure (Pérami 1965; Mordecai and Morris 1971; Farran and Pérami 1974; Zoback and Byerlee 1975b), although Wilhelmi and Somerton (1967) did not find such an effect. This threshold can be correlated closely with the onset of marked acoustic emission (Pérami and Thénoz 1969), although the exact pattern of behaviour varies with the type of rock. Thus, Farran and Pérami (1974) distinguished, in granite, between one threshold stress for the onset of moderate rates of acoustic emission and increase in permeability and a considerably higher threshold at which there is a transition to markedly greater rates of acoustic emission and permeability increase, accompanied by marked dilatancy. These threshold stresses decreased in further cycles of stress (note that the hysteresis in permeability during the cycling of the stress in granite is very large: Farran and Pérami 1974; Zoback and Byerlee 1975b; Morrow, Zhang and Byerlee 1986; Bernabé 1987). Such effects were much less marked in limestone, although the changes in acoustic emission and permeability with stress can become markedly accentuated in compact limestone or dolomite if it is subjected to a prior heating cycle to 300–500 °C at atmospheric pressure (Pérami 1971a; cf. Sect. 5.7.3).

It is also generally observed in a triaxial compression test on compact rocks that permeability changes are positively correlated with changes in porosity. Application of the confining pressure reduces both the porosity and the permeability due to elastic closure of pre-existing microcracks (Brace, Walsh and Frangos 1968). Similarly the initial application of a stress difference induces both the porosity and permeability to decrease due to elastic compression of the pore space. However, at the onset of dilatancy this trend is reversed with concomitant increases in porosity and permeability (Zoback and Byerlee 1976a,b). A recent study of Kiyama et al. (1996) extended the measurement from the pre-failure to the post-failure stage. In Inada granite, they

**Fig. 35.**

Permeability of Inada granite as a function of differential stress at confining pressure of 10 MPa and pore pressure of 5 MPa. The three samples were cored in three orthogonal directions marked as A, B and C (after Kiyama et al. 1996)



observed an enhancement of permeability by almost an order of magnitude from the onset of dilatancy to the peak stress, after which the permeability and porosity continued to increase while the sample strain softened (Fig. 35).

In contrast, in porous rocks the correlation between porosity and permeability changes is not as well defined. Whereas Mordecai and Morris (1971) measured an increase of ~20% in permeability prior to brittle faulting in Darley Dale sandstone, Gatto (1984) observed that permeability consistently decreased with increasing stress in Berea sandstone. Somerton, Soylemezoglu and Dudley (1975) concluded that, in coal, permeability was primarily dependent on the mean stress and that nonhydrostatic stresses had negligible influence (see also Wilhelmi and Somerton 1967). However, Nelson (1981), Holt (1989) and Rhett and Teufel (1992) observed that permeability evolution in sandstone was very sensitive to loading path through the interplay of hydrostatic and nonhydrostatic loadings.

Zhu and Wong (1997) presented data for several porous sandstones which showed negative correlations between permeability and porosity changes with the onset of dilatancy. This type of permeability evolution is illustrated in Fig. 36 for Berea sandstone. While the porosity and permeability changes were positively correlated for hydrostatic loading and for triaxial loading during the initial elastic compression stage before the onset of dilatancy, permeability was observed to continue to decrease even though the pore space dilated in response to the stress difference beyond  $C'$ . To characterize the fundamentally different evolution paths for permeability in compact and porous rocks during the development of dilatancy and brittle failure, Zhu and Wong (1997) introduced the parameter

$$\xi = \frac{k(\text{peak})}{k(C')} - 1$$

where  $k(C')$  and  $k(\text{peak})$  denote the permeabilities at the onset of dilatancy and at peak stress, respectively. The parameter  $\xi$  gives a measure of the prefailure perme-

**Fig. 36.** Permeability of Berea sandstone as a function of differential stress at pore pressure of 10 MPa and two different confining pressures as indicated. The data were tabulated by Zhu and Wong (1997), and the stress level  $C'$  at onset of dilatancy is marked. Beyond the onset of dilatancy the permeability continued to decrease monotonically, corresponding to a negative correlation between porosity and permeability changes

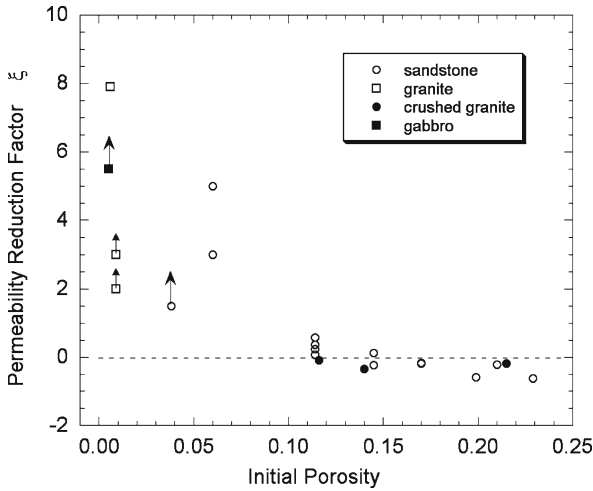
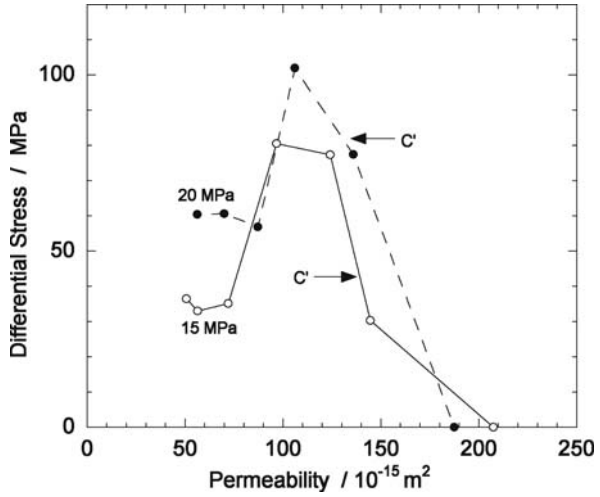


**Fig. 37.** Relative change of permeability from onset of dilatancy to peak differential stress for lithified rocks (sandstone, gabbro, and granite) and granular material (crushed Westerly granite) that fail by brittle faulting. If the factor  $\xi > 0$  then permeability is enhanced with the onset of dilatancy (cf. Fig. 35), and the porosity and permeability changes are positively correlated. If  $\xi < 0$  then permeability decreases in a dilating sample (cf. Fig. 36). A data point marked by an arrow indicates that the permeability was measured before the peak stress had been attained and it probably represents a lower bound (after Wong and Zhu 1999)

ability change which can be correlated with the porosity. A compilation of values of  $\xi$  for several rock types and unconsolidated materials as a function of initial porosity is shown in Fig. 37. There is an overall trend for the correlation between permeability evolution and porosity to change from positive to negative with increasing initial

porosity. In compact crystalline rocks, permeability evolution is positively correlated with porosity (with  $\xi > 0$ ). In contrast, permeability evolution is negatively correlated with porosity (with  $\xi < 0$ ) in a sandstone with porosity  $> 15\%$  or so. Recent data of Keaney, Meredith and Murrell (1998), Main et al. (2000) and Heiland (2003) for sandstone agree with this overall trend.

Data for crushed Westerly granite from Jones (given in Table 1 of Wong and Zhu 1999) suggest that in unconsolidated materials a negative permeability-porosity correlation may persist to porosities down to 11%. Zoback and Byerlee (1976a,b) also studied the influence of stress difference on permeability under confining pressure in Ottawa sand and crushed Westerly granite; very large decreases in permeability occur during straining, especially in the crushed granite in which they suggest that the production of debris may be important. Although it is difficult to extract values of  $\xi$  from their data, the results for crushed Westerly granite and Ottawa sand of Zoback and Byerlee (1976a,b) and for quartz/clay mixture of Brown et al. (1994) indicate qualitatively similar trends. The ultrasonic and permeability measurements of King, Chaudhry and Shakeel (1995) and King, Shakeel and Chaudhry (King, Shakeel and Chaudhry 1997) on several sandstones indicate that the speed of shear waves propagating in a direction perpendicular to the maximum compression direction is correlated with the hydraulic permeability for flow parallel to this direction. Gibson and Toksöz (1990) proposed a theoretical model for such correlation between wave speed anisotropy and permeability.

A decrease in permeability with time has been observed by Summers, Winkler, and Byerlee (1978) in granite at high temperature, possibly from clogging due to solution transfer (see also Moore et al. 1993; Moore, Morrow and Byerlee 1986; Kranz and Blacic 1984; Morrow et al. 1981; Morrow, Moore and Lockner 1997). A further observation of tectonic importance is that the permeability increase associated with the presumed opening of microcracks in the low-porosity rocks is relatively small compared with that associated with macroscopic cracks (Turner and Secor 1974; Zoback and Byerlee 1975a).

**Electrical conductivity.** Effects analogous to those shown in permeability are also shown in the electrical conductivity of water-saturated rock. At temperatures below a few hundred degrees, the electrical conductivity is predominantly determined by the conduction through the pore fluids (for a summary of the factors affecting conductivity of saturated rock, see Brace 1971b). The application of small stress differences tends to reduce the conductivity, but beyond about half the macroscopic fracture stress the conductivity increases, the increase becoming especially marked within 20% of the fracture stress (Brace and Orange 1966, 1968, who also review earlier work pointing to these effects); see also Tomashevskaya and Khamidullin (1972) and Brace (1977). Thus the changes in conductivity closely parallel the dilatancy behaviour and so can also be correlated with the closing and opening of microcracks (Brace and Orange 1968; Trimmer et al. 1980; Lockner and Byerlee 1986; Tomecka-Suchon and Rummel 1992; Glover et al. 1994; Glover et al. 1997; Siddiqi et al. 1997; Glover, Gómez and Meredith 2000). Exceptional behaviour was noted by Brace and Orange in marble but it was attributed to sealing off the connections between cracks in this relatively ductile material. Par-

tially saturated rocks also show increase in conductivity with stress to a similar degree at the higher stresses, although their behaviour under purely hydrostatic pressure is markedly different from that of saturated rocks (Mitchell and Brace 1973; Brace 1975).

In response to an applied stress field, the electrical and hydraulic transport may evolve in a complex manner since these two processes are coupled together. In a porous medium, the flow of a fluid in response to a hydraulic gradient will induce the development of a “streaming potential”. Similarly an electric current in response to a potential difference induces the development of “electro-osmosis” (Mitchell 1991). The electrokinetic phenomena associated with such cross-coupling effects have been proposed to explain low-frequency electromagnetic anomalies observed in seismogenic and geothermal systems (Mizutani et al. 1976; Corwin and Morrison 1977; Fitterman 1979; Corwin and Hoover 1979; Park et al. 1993). Previous laboratory studies have focused on granular materials (Ishido and Mizutani 1981; Morgan, Williams and Madden 1989; Mitchell 1993). Recent measurements on porous claystone and sandstone (Jouniaux, Lallemand and Pozzi 1994; Jouniaux and Pozzi 1995; Yoshida, Clint and Sammonds 1998; Lorne, Perrier and Avouac 1999) indicate the development of appreciable streaming potentials in relation to brittle fracture.

The *thermal conductivity* can also be expected to depend somewhat sensitively on the presence of cracks in dry rock (Walsh and Decker 1966). This property does not seem to have been exploited as a method of detecting stress-induced microcracking. However, deviations from the linear dependence of *remanent magnetization* on stress have been correlated with dilatancy (Ohnaka and Kinoshita 1968; Martin and Wyss 1975; Martin, Habermann and Wyss 1978; Martin 1992).

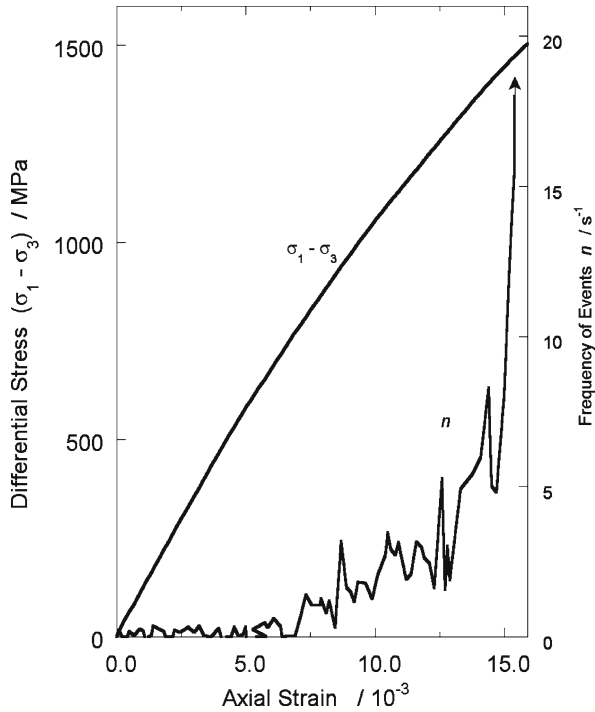
## 5.6 Acoustic Emission

Acoustic emission (AE) in solid bodies results from local strain events that occur with sufficient suddenness to generate acoustic pulses. A well-known example is the “tin-cry” that is heard when polycrystalline tin is strained plastically and which originates from the abrupt occurrence of mechanical twinning in individual grains. Similarly, local microfracturing can give rise to acoustic emission and the study of this topic has therefore become an important tool in rock mechanics, where the effect is often referred to as “microseismic activity”. Acoustic emission from rock stressed near to fracture is sometimes even evident aurally, as in the sharp snapping noises heard from granite, but noise of a much wider range of frequency is detected with a suitable transducer. This noise has been studied both as a precursor for predicting impending failure in practical situations and as an aid in the study of the fundamentals of the mechanical behaviour of rock. We deal only with the latter aspect here. Reviews that deal with practical applications have been given by Hardy (1971, 1972, 1973). Lockner (1993a) has presented a comprehensive review of the role of acoustic emission in the study of rock fracture.

Beginning with the pioneering work of Obert and Duvall (1942, 1945), there have been many experimental studies that show that the number of acoustic events per unit

**Fig. 38.**

Increase in rate of acoustic emission in Westerly granite at 400 MPa confining pressure during loading along stress-strain curve shown (after Scholz 1968d)



stress increment increases with increasing stress, especially as the macroscopic fracture stress is approached (Konstantinova 1960; Mogi 1962c; Goodman 1963; Suzuki et al. 1964; Cook 1965; Brown and Singh 1966; Nagumo and Hoshino 1967; Knill, Franklin and Malone 1968; Mae and Nakao 1968; Scholz 1968d; Kotte et al. 1969; Pérami and Thénoz 1969; Gowd 1970; Barron 1971b; Chugh, Hardy and Stefanko 1972; Tomashevskaya and Khamidullin 1972; Thill 1973; Zvyagintsev, Tomashevskaya and Khamidullin 1974; Reymond 1975; Chen 1979; Gowd 1980; Ohnaka and Mogi 1981; Shimada, Cho and Yukatake 1983; Sammonds et al. 1989; Meredith 1990; Zhang et al. 1990; Zhang, Wong and Davis 1990a; Cox and Meredith 1993; Zang, Wagner and Dresen 1996). These studies have embraced both uniaxial and triaxial compressive loading, as well as loading in tension or bending. The result shown in Fig. 38 for granite loaded in compression at a confining pressure of 400 MPa is typical of the stress dependence. Superimposed on this effect, especially in the case of uniaxial compressive loading, there is often additional acoustic emission at small stresses, which can be attributed to the collapse of pores. Because of the latter effect, it is not always easy to pinpoint a stress threshold for the onset of acoustic emission attributable to microcracking, although such a threshold is often mentioned (e.g., Pérami and Thénoz 1969; Barron 1971b; Thill 1973). However, a great increase in acoustic activity always becomes obvious at some stage in the upper part of the loading range. Mogi (1967a, 1969) has suggested that in homogeneous rocks this stage is not reached until very close to the macroscopic fracture stress, but generally it occurs somewhere above half the macroscopic fracture stress.

In porous rocks, the acoustic emission associated with grain crushing and pore collapse becomes an important feature. This effect is observed already under purely hydrostatic pressure (Zhang et al. 1990) and further acoustic emission is observed during deformation (Ohnaka and Mogi 1982; Zhang, Wong and Davis 1990a). In porous rock the latter activity can be associated with shear-enhanced compaction rather than dilatancy (Lockner et al. 1992; Read et al. 1995; Wong, David and Zhu 1997).

Acoustic emission is also time dependent since it is observed to continue at a given stress level even when the stress is no longer being increased. This effect is most clearly illustrated in creep experiments at room temperature. On first applying the load, there tends to be considerable acoustic emission which may decrease with time to a relatively low level of activity. However, the activity tends to increase markedly again before fracture ensues (Mogi 1962c; Brown and Singh 1966; Wu and Thomsen 1975; Byerlee and Lockner 1976; Atkinson and Rawlings 1981; Sano, Terada and Ehara 1982; Meredith and Atkinson 1983; Ohnaka 1983; Costin 1987; Hirata 1987; Meredith 1990; Baud and Meredith 1997). Hardy et al. (1970), Wu and Thomsen (1975), and Lockner and Byerlee (1977a) have emphasized the close correlation between the creep strain and the accumulated activity (total number of acoustic events to the point of observation). Allied to the time effects is the influence of water on acoustic emission through stress corrosion (Sammonds, Meredith and Main 1992; Aves et al. 1993; Zang, Wagner and Dresen 1996; Seto et al. 1997; Carlson et al. 1998).

Acoustic emission during cyclic straining has also been studied (Goodman 1963; Gramberg 1974; Scholz and Kranz 1974). Here it is sometimes observed that acoustic emission recommences at the maximum stress of previous cycles, an effect known as the "Kaiser effect" (Kurita and Fujii 1979; Lockner 1993a; Yoshikawa and Mogi 1981; Sondergeld and Estey 1981; Rao and Ramana 1992; Holcomb 1993b; Shah and Labuz 1995; Holt et al. 1996; Dai and Labuz 1997). Constitutive and damage models have been developed to interpret this phenomenon (Holcomb 1984, 1993a; Holcomb and Costin 1986; Tang et al. 1997). However, in rocks, the effect cannot be relied upon, especially at higher stresses near the fracture stress (see review by Lockner 1993a).

So far we have only dealt with the counting of the acoustic events, without referring to their nature. Almost all earlier work involved only the counting of events and this has often remained the only aspect considered. However, a number of attempts have been made also to characterize the acoustic emission more fully by determining the frequency components and the energy of the acoustic pulses. This is difficult experimentally because the observations are affected both by the characteristics of the recording equipment and by the acoustic properties of the specimen and the loading machine (see discussion by Knill, Franklin and Malone 1968; Blake and Duvall 1969; Chugh, Hardy and Stefanko 1972).

The use of flat-response transducers and wide-band audio-amplifiers showed that the frequency components towards the ultrasonic end of the audio range were the more dominant (e.g., Suzuki et al. 1964), although this is not always the case (Chugh, Hardy and Stefanko 1972). Scholz (1968d) found, by extending the frequency range of observation to 1 MHz, that most of the acoustic emission in granite was in the 100 kHz to 1 MHz range. The observations of Thill (1973) for granodiorite and marble fall in this range, while Byerlee (1974) has used a range of 10 kHz to 10 MHz. The range of around 100 kHz to 2 MHz is now widely used (Ohnaka and Mogi 1982; Lockner 1993a).

Quantitative studies have been made of the amplitude of the various frequency components, from which the energy distribution can be obtained (for example, Chugh, Hardy and Stefanko 1972; Ohnaka and Mogi 1981, 1982; Read et al. 1995). Another approach, analogous to that used in seismology, is to study the overall magnitude of energy content of the acoustic events as a function of their relative frequency of occurrence. Thus it has been shown that the usual relation found in seismology is obeyed whereby the frequency of occurrence of events decreases as their magnitude increases (Vinogradov 1959, 1962; Mogi 1962b; Mae and Nakao 1968; Scholz 1968b). Specifically the Gutenberg-Richter relation for earthquake statistics is given by

$$\log N(M) = a - bM$$

where  $N$  is the number of earthquakes of magnitude greater than  $M$ , and  $a$  and  $b$  are constants. In fractal geometry (Mandelbrot 1983) this type of power law is considered to be typical of a medium with self-similar geometric attributes, and the fractal dimension is approximately twice the  $b$ -value determined from earthquake size-frequency distribution (Aki 1981; Scholz 1990). For an acoustic emission event, the magnitude is commonly assumed to be proportional to the maximum amplitude of the stress wave recorded by the transducer and the above power law has been shown to apply as well for acoustic emissions in brittle rock, with a  $b$ -value on the order of unity (Weeks, Lockner and Byerlee 1978; Meredith, Main and Jones 1990; Lockner and Byerlee 1995). In a further analogy with seismology, Mogi and Scholz have pointed out the similarity between earthquake after-shock sequences and the acoustic emission observed subsequent to fracturing in a laboratory specimen (for details and references, see Scholz 1968b; Lockner 1993a). Meredith (1990) observed that the  $b$ -value in Darley Dale sandstone first decreased to attain a minimum in the proximity of the peak stress, and then increased in the post-peak stage; when pore fluid pressure was present, a double minimum was observed (Sammonds, Meredith and Main 1992), as predicted theoretically (Main, Meredith and Jones 1989).

The association between acoustic activity and microfracturing has been observed directly in ice (Gold 1960) and in glass (Byerlee and Peselnick 1970); also Harding and Hardy (quoted by Hardy 1972) have shown that in granite under a constant uniaxial compressive stress the more prominent acoustic events are directly correlated with small jumps in the strain. Thus, although other processes may at times be involved (Knill, Franklin and Malone 1968), it is widely accepted that acoustic emission is an effective indicator of the occurrence of microfracturing in rock specimens. This association is further supported by the observation that the onset of marked acoustic emission can be correlated with the onset of dilatancy (Suzuki et al. 1964; Scholz 1968d; Barron 1971b), which has itself been attributed to the onset of proliferation of microcracking, as discussed in the previous section.

By observing the relative arrival times of the pulses at several transducers at different positions on the surface of the specimen, the spatial origin of the microfractures can also be located. In this way, Scholz (1968a) concluded that the sources of acoustic emission are at first distributed throughout the specimen but that at higher loads they become concentrated in the zone in which the macroscopic fracture finally oc-



curs, although Lockner and Byerlee (1977b) in a similar study could not confirm that this clustering preceded the formation of the fracture. Other observations have been made by Byerlee and Lockner (1977) and Lockner and Byerlee (1977c) during the injection of pore water under pressure into a specimen held at constant stress difference and high confining pressure; the acoustic emission, at first widely distributed, became concentrated at the fracture front when a shear fracture began to form.

It should be noted that hypocentre location hinges on the assumption that the wave speed structure is known. Appreciable wave speed anisotropy and attenuation may develop in a stressed rock, and the location may be biased if these effects are not appropriately taken into account (Lockner and Byerlee 1980). In a rock that has a P-wave speed on the order of  $5 \text{ km s}^{-1}$ , the three-dimensional location of acoustic emission hypocentres has an accuracy of about 2 mm if the transducer has a frequency response in the megahertz range and the time measurement has an accuracy on the order of  $0.1 \mu\text{s}$  (Lockner 1993a). With the advent of this technology, acoustic emission location is used to delineate the spatial evolution of microcracking and shear localization in real time (Yanagidani et al. 1985; Nishizawa, Onai and Kusunose 1984; Kusunose and Nishizawa 1986; Hirata, Satoh and Ito 1987; Satoh, Nishizawa and Kusunose 1990; Lockner et al. 1992; Lockner and Moore 1992; Shah and Labuz 1995; Zang, Wagner and Dresen 1996; Zang et al. 1998; Zang et al. 2000). The rate of acoustic emission can simultaneously be used as a feedback signal for servo-controlling of the post-peak deformation (Lockner et al. 1992).

In triaxial compression experiments on a compact rock such as Westerly granite, spatial clustering of acoustic emission activity is not obvious in the pre-peak stage. By contrast, intensive acoustic emission activity in the post-peak stage is observed to cluster along an elongate volume that propagates progressively to develop a through-going shear band across the sample (Fig. 39). Localization of acoustic emission activity follows somewhat different patterns in a porous rock such as Berea sandstone, in which diffuse clusters are observed before the peak stress is attained. Nevertheless, it was only in the post-peak stage that Lockner et al. (1992) observed a planar zone of localized acoustic emission activity that ultimately developed into the macroscopic shear fault. In unconfined compression experiments (Yanagidani et al. 1985; Nishizawa, Onai and Kusunose 1984; Meglis, Chow and Young 1995; Chow, Meglis and Young 1995), there seems to be a tendency for localization to initiate from the exposed sample surface which may be subjected to localized weakening due to the presence of adsorbed water vapour.

The spatial distribution of acoustic emission activity and correlation between event location and size can be used to infer the “correlation exponent”, which is a measure of the fractal dimension (Hirata, Satoh and Ito 1987; Lockner and Byerlee 1995). This approach was used by Lockner and Byerlee (1995) to analyze the data of Lockner et al. (1992) for Westerly granite and Berea sandstone. For the granite, they found a fairly constant value of 2.4 for the correlation coefficient in the pre-peak stage, and it dropped abruptly to a value of 2.0 with the onset and development of localization. In contrast, there was a systematic decrease of the correlation coefficient in the sandstone from approximately 2.6 to 1.6 in the pre-peak stage, indicating a progressive clustering of acoustic emission locations into diffuse clouds.

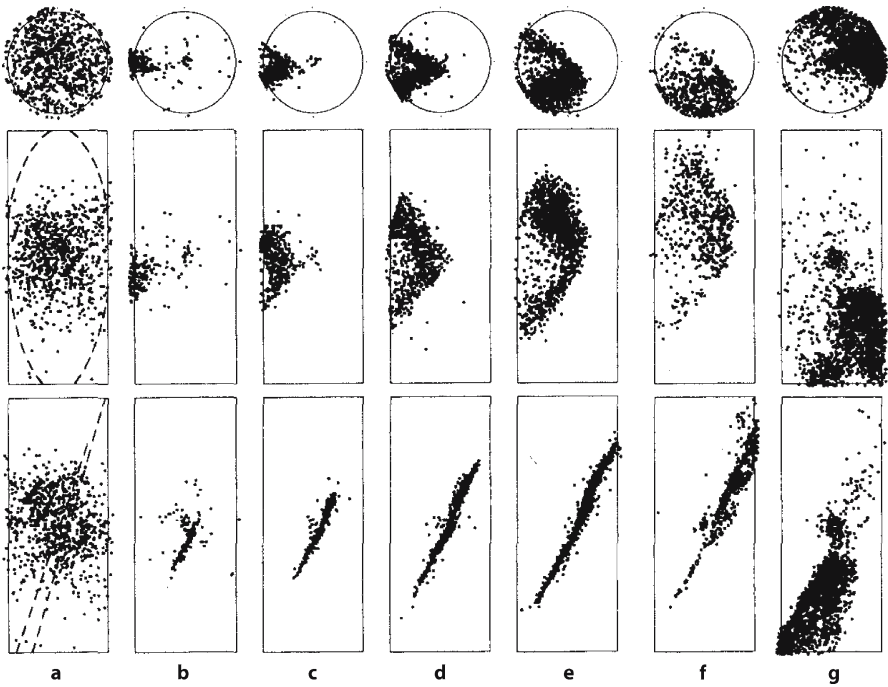


**Fig. 39.** Plot of AE locations for a Westerly granite sample triaxially compressed (with  $\sigma_1$  in the vertical direction) at confining pressure of 50 MPa. Each point represents an AE event. *Bottom plot* of each set is view looking along-strike of eventual fracture plane. *Middle plot* is face-on view of fault in which sample has been rotated counterclockwise by  $90^\circ$ . *Top plot* is view looking down on sample. The data for set (a) were collected in the pre-peak stage when the differential stress increased from about 50 MPa below to the peak. Projections of surface trace of eventual fault plane are shown in (a) for reference. Shear localization initiated in set (b) and developed in the post-peak stage from (b) to (f) (after Lockner et al. 1992)

If a multichannel recording system is used to acquire the full wave forms of acoustic emission events, then polarity data of the first motions can be used to deduce the “focal mechanism” of each event. The focal mechanisms for acoustic emission events that occur during uniaxial compression of granite and andesite have been inferred to be predominantly “double couples”, which are indicative of shear cracking (Sondergeld and Estey 1982; Nishizawa, Onai and Kusunose 1984; Kusunose and Nishizawa 1986). In contrast, significant proportions of acoustic emission events recorded in triaxial compression events have been observed to be associated with all-compressional first motions that are indicative of extensile cracking (Satoh, Nishizawa and Kusunose 1990; Kranz et al. 1990). In a cyclic loading test, Satoh, Nishizawa and Kusunose (1990) reported that about a third of the events were extensile events, 15% were pure shear events, and the rest were “complex” events that could not be classified as pure extensile or shear. See also Shah and Labuz (1995), Satoh et al. (1996); Zang, Wagner and Dresen (1996), and Zang et al. (1998).

## 5.7 Microscopical Observations

### 5.7.1 General

The microscopical study of the processes in the brittle failure of rock was slow in its early development partly from a lack of appropriate techniques of observations, but probably partly also from the inhibiting idea that, since the field of view is very limited at the high magnifications needed for seeing small cracks, it is necessary to know, a priori, the precise location of a highly localized site of cracking, as envisaged in the simple Griffith model. In fact, it turns out that the flaws and the brittle failure processes involving them are, at least initially, rather widely distributed throughout the rock and can be readily observed with the appropriate techniques. In the following sections we deal in turn with the techniques of observation, the initial crack or flaw structure of rocks, and the development of cracking under stress.

### 5.7.2 Observational Methods

The first approach has usually been to use the optical microscope to examine thin sections or ground or polished faces. With conventional methods, only relatively coarse cracks are readily observed in this way, and there is the problem of distinguishing between original cracks and those introduced in the specimen preparation. However, with care this simple approach can give significant information. Also with suitable modification of the conventional techniques, including the use of thicker sections, the problem of artifacts can be reduced and more information gained; see Houpert, Legendre, and Richard (1969), Willard and McWilliams (1969), Simmons, Todd, and Baldrige (1975), Simmons and Richter (1976), Chen, Yao and Xie (1979), Gottschalk et al. (1990), Moore and Lockner (1995) and (Basan et al. 1997) for details of preparation and measuring procedures that have been used for optical studies.

To improve or exaggerate the visibility of cracks, various “decorating” techniques have been used. These include the introduction of fluorescent dyes (Gardner and Pincus 1968; Kotte et al. 1969; D’Andrea and Condon 1971; Thill 1973; Soeder 1990; Nishiyama and Kusuda 1994), electrochemically deposited copper (Simmons and Richter 1976), residual carbon from the charring of organic liquids (Simmons, Todd and Baldrige 1975), and radioactive tracers (Lévéque 1969; Degeldre et al. 1996). Triboluminescence has also been exploited (D’Albissin and Spanjaard 1969; Garten and Head 1971). Such procedures are especially useful in studying the larger-scale distribution of microcracks in laboratory specimens.

With the aid of electron microscopy, the character of cracks and other flaws can be studied in much more detail. Transmission electron microscopy has only been applied to a limited extent in the study of cracks (e.g., Boland and Hobbs 1973; Martin and Durham 1975), but the scanning electron microscope has proved to be very useful in studying the morphology of pores and cracks. The general character of pores and

a limited amount of information about microcracks can be gained from examining fracture surfaces without special preparation; see Gillott (1969), Weinbrandt and Fatt (1969, 1970), Nissen and Wessicken (1970); and Timur, Hempkins, and Weinbrandt (1971) for some of the earlier examples of such observations on pore structures, and Hoskins (1969a), Willard (1969), Willard and Hjelmstadt (1971), Logan et al. (1973), Dengler (1976) and Lloyd and Hall (1981) for crack structures. However, to study the material away from the macroscopic fracture surface a section has to be cut and the question arises again of distinguishing original cracks from artifacts. This difficulty was considered by Brace et al. (1972) to limit severely the usefulness of studies on sections prepared in the standard way, and they introduced the procedure of removing the surface damage by ion bombardment, removing a layer of 30–40  $\mu\text{m}$  after an initial careful mechanical polish. Subsequent observation by scanning electron microscope (or optically) reveals very interesting detail (Sprunt and Brace 1974a,b; Montgomery and Brace 1975; Solberg 1975; Tapponnier and Brace 1976; Kranz 1979b; Durham 1981; Kowallis, Roeloffs and Wang 1982; Wong 1982b; Kowallis and Wang 1983; Caruso, Simmons and Wilkens 1985; Wong and Biegel 1985; Fonseka, Murrell and Barnes 1985; Wong, Fredrich and Gwanmesia 1989; Burns, Cheng and Wilkens 1990; Hirth and Tullis 1994; Menéndez, Zhu and Wong 1996; Siddiqi et al. 1997). There may still be some question regarding the sampling because, although Sprunt and Brace (1974a) found consistency in a granite between porosity deduced from the scanning electron microscope observations and measured independently, Hadley (1976a) could only see cavities accounting for about half the known porosity in another granite; see also further comment by Brace (1977), Kranz (1983) and Wong (1985). However, this procedure appears to be a very powerful aid in reducing artifacts and revealing fine detail. Also the usefulness of the combined application of optical and scanning electron microscopy has been emphasized by Richter, Simmons, and Siegfried (1975). While most microscopic observations are conducted on previously deformed samples, attempts have also been made to conduct *in situ* observations while the rock sample is being actually deformed (Batzle, Simmons and Siegfried 1980; Lindqvist, Lai and Alm 1984; Ichikawa, Wang and Jeong 1995).

In addition to optical and electron microscopy, various other techniques have been used either to reveal the location of microcracks, as in the radiographic technique of Nelson and Wang (1976), or to reveal the local distribution of inelastic strain within the samples. Techniques for the latter include the use of photoelastic coatings to show up grain-to-grain variations (Peng 1976) and of slit diffraction (Liu and Livanos 1976) and holography (Soga, Martin and Spetzler 1976) to reveal the concentration of strain preliminary to forming a shear failure. The acoustic microscope has also been used to delineate the cracks and mineralogical differences (Danburg and Yuhus 1978; Briggs 1992); a resolution of about 1  $\mu\text{m}$  can be obtained at a frequency of 1.6 GHz (Rodríguez-Rey et al. 1989).

Traditional microscopy techniques have the limitation that imaging is done in two dimensions only. Qualitative insights into the complexity of the three-dimensional geometry can be gained from scanning electron microscope observations on pore casts. The pore space is first impregnated with acid-resistant epoxy (Pittman and Duschatko 1970; Wardlaw 1976; Caruso, Simmons and Wilkens 1985; Abdel-Gawad, Bulau and Tittman 1987) or Wood's metal (Dullien and Dhawan 1975; Swanson 1979;

Myer et al. 1992; Yao et al. 1997; Pyrak-Nolte, Montemagno and Nolte 1997; Darot and Reuschlé 1999), and then the solid grains are dissolved away with acid. However, it is difficult to characterize quantitatively the three-dimensional pore structure. Interpolation of two-dimensional images on serial sections can provide such data (Koplik, Lin and Vermette 1984; Lindholm, Yeakley and Nagy 1974), but the procedure is very tedious to implement.

Recently there have been significant advances in several three-dimensional imaging techniques. X-ray computer tomography (Wellington and Vinegar 1987; Raynaud et al. 1989; Kawakata et al. 1999) has been used to characterize the spatial distribution of porosity at a resolution of about 0.5 mm. In situ observations can be made in a testing machine that is transparent to X-rays (Vinegar, de Waal and Wellington 1991; Geraud et al. 1998). The nuclear magnetic resonance technique (Osment et al. 1990; Fukushima 1999) with a resolution of about 25  $\mu\text{m}$  has been used to characterize the pore geometry and image the flow of fluid (Kenyon 1992; Geraud, Caron and Faure 1995). Even higher resolution (of 1 to 10  $\mu\text{m}$ ) is available from synchrotron computed microtomography (Flannery et al. 1987) of cylindrical samples of porous rock with diameters of 5 mm or larger (Spanne et al. 1994; Auzerais et al. 1996; Coker, Torquato and Dunsmuir 1996; Coles et al. 1998). The finest resolution ( $\sim 0.2 \mu\text{m}$ ) is attained by the use of the laser scanning confocal microscope on rock samples impregnated with an epoxy that has been doped with a fluorochrom (Fredrich, Greaves and Martin 1993; Fredrich, Menéndez and Wong 1995; Montoto et al. 1995; Petford, Davidson and Miller 1999). In a porous sandstone, a penetration depth of about 250  $\mu\text{m}$  can be achieved before significant image degradation is apparent (Fredrich 1999).

### 5.7.3

#### Initial Structure

There are various microstructural features initially present in rock that are potentially of vital significance in its brittle behaviour. These features include grain and twin boundaries, the contrast between different types and orientations of grains, and, above all, various sorts of microcavities. Among the microcavities it is useful to distinguish broadly between “pores” and “microcracks” (Habib and Bernaix 1966; Walsh and Brace 1966; Lindborg 1969; Morlier 1971a; Brace 1972b).

*Pores* can have various shapes. They can be more or less equidimensional and represent intergranular spaces in sediments, fluid inclusions in igneous and metamorphic rocks, and so forth. Alternatively, they can be tubular in shape (Richter and Simmons 1977; Shirey, Simmons and Padovani 1980). Connected pores are mainly responsible for the permeability in rocks of medium to high permeability.

Cleavages and other fractures in the mineral grains and partings at originally intact grain boundaries are examples of *microcracks*. Microcracks may be the main source of porosity and permeability in rocks of low porosity. Some writers have distinguished different categories of microcracks (e.g., the microfractures and microfissures of Pérami 1971a), but here we use the term comprehensively to include all cracks on the microscopic scale, from dimensions of several grain diameters down to a fraction of a grain diameter. Kranz (1983) has provided an extensive review of microcrack morphology and classification.

Since it is the microcracks that figure prominently in discussions on the behaviour of brittle rock under stress, particular interest attaches to microscopical observations of the initial microcrack structure in the rock and its role in the structural changes under stress. The properties of the microcrack structure discussed include the lengths, aspect ratio, and connectivity of the cracks and their spacing or number per unit volume.

Optical observations on the initial microcrack structure have most commonly been concerned with the quartz-rich rocks such as granite and quartzite. In these rocks, optically visible microcracks have been reported to occur mainly in the quartz and to have lengths roughly equal to or somewhat less than the grain size (D'Albissin and Spanjaard 1969; Lévêque 1969; Thill, Willard and Bur 1969; Friedman and Logan 1970a; Peng and Johnson 1972). The density of these cracks can be quite high – 340 per mm<sup>2</sup> in a quartzite studied by Baldrige and Simmons (1971) – but the quartz-bearing rocks are said to have higher crack porosities than other rocks (Nur and Simmons 1970). Also the preferred orientation of the optically observed microcracks can be related to the anisotropy in mechanical properties (Aveline et al. 1963; Isnard and Leymarie 1963; McWilliams 1966; Thill, Willard and Bur 1969; Perkins, Green and Friedman 1970; Peng and Johnson 1972; Thill, Bur and Steckley 1973; Friedman and Bur 1974; Simmons, Todd and Baldrige 1975; Solberg 1975).

The scanning electron microscope studies by Brace and co-workers threw much new light on the initial microcrack structures and indicated that the above optical observations must be accepted with reservation. Their more careful preparation procedures (see Sect. 5.7.2) revealed that many of the initial cracks would not be resolved by the optical microscope, a conclusion already arrived at indirectly by Friedman, Perkins, and Green (1970) and Perkins, Green, and Friedman (1970). The cracks commonly studied optically may in varying degrees be artifacts of the preparation procedure, although probably often genetically related to the initial microcracks and so indirectly representing the initial structure. This reservation about the conventional optical observations is thought to be less serious for observations on stressed rocks, to be described later, because the stressing will have caused many of the initial microcracks to grow to microscopic dimensions. However, before dealing with effects of stress, the observations of Brace and co-workers on initial structure must be summarized and some comments made on the origin of the initial structure.

The scanning electron microscope observations on virgin rock reveal a rich variety and abundance of microcavities, especially in granites (Brace et al. 1972; Sprunt and Brace 1974a; Hadley 1976a). The chief findings are:

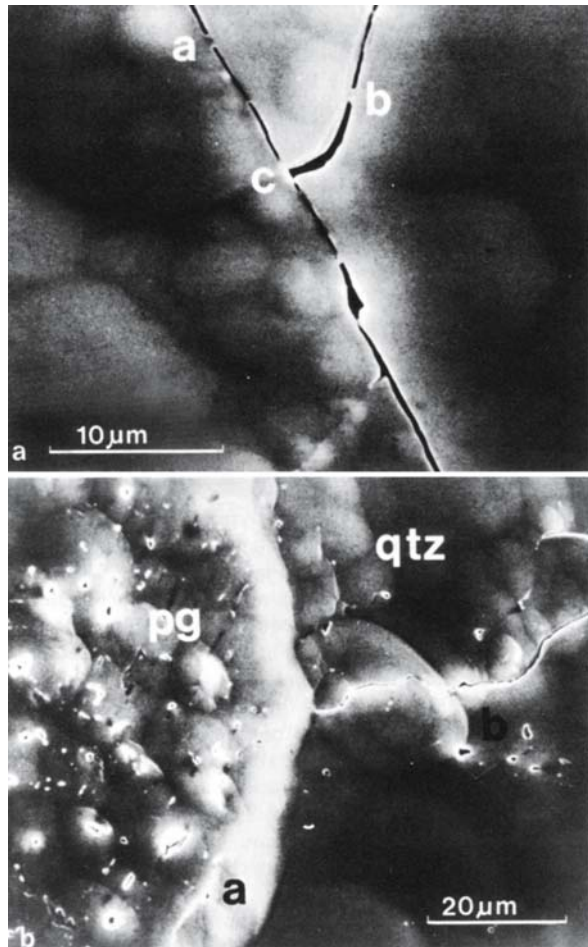
1. Long, narrow, sharp-ended cracks typical of brittle fracture are rarely seen. There is a wide variety of lengths and aspect ratios of cavities but the ratio of length to width is commonly not more than 100, that is, generally rather less than the  $10^3$ – $10^4$  values often deduced indirectly from measurements on physical properties such as compressibility and permeability (e.g., Brace, Walsh and Frangos 1968; Morlier 1971a; Simmons, Siegfried and Feves 1974; Simmons, Todd and Baldrige 1975).
2. The elongate cavities commonly follow grain boundaries, are less than 1  $\mu\text{m}$  in width, and are not more than about one-tenth of the grain size in length, that is, they are an order of magnitude less in length than previously thought. They can occupy a

large proportion of the grain boundary, especially in granites, although in diabase and gabbro the grain boundaries are nearly free of cracks and, indeed, these rocks contain relatively few microcavities altogether. Crack-like cavities are rare within grains; only occasional cracks are seen in quartz, in contrast to the relative abundance reported in more conventional optical studies (above), but somewhat more appear in minerals with good cleavage such as mica and feldspar.

3. The ends of the elongate cavities are typically blunt or rounded and often appear to be formed by the “bridging” of a longer cavity, as if a long crack had been partially healed (Fig. 40a).
4. Nearly equant cavities are also common, many at grain boundaries and some within grains. Intragranular equant cavities are especially common in sodic plagioclase in granite (Fig. 40b); for further observations on plagioclases, see Montgomery and Brace (1975).

**Fig.40.**

Examples of initial cavity structure in granite, as revealed by transmission electron microscopy on ion-etched surfaces. **a** Elongate cavities associated with quartz grains in Westerly granite, showing “bridges” at *a*, *b*, *c*. **b** Intragranular equant cavities in Chelmsford granite, numerous in the sodic plagioclase (*pg*) but not in the quartz (*qtz*) (Sprunt and Brace 1974a)



Sprunt and Brace (1974b) explored the effects of temperature and pressure cycling on these initial microstructures. A cycle of heating leads to breaking of the bridges separating the elongate cavities, increases the amount of grain boundary cracking and, if severe enough, introduces a few sharp-ended new cracks. The first two effects also result from a cycle of hydrostatic pressure but in a much smaller degree; also the effects of temperature cycling are reduced if the cycling is done under pressure.

There have been various views about the genesis of the microcavities in virgin compact rock. Prior to the work of Brace and co-workers, just described, some controversy existed regarding the origin of the optically revealed microcracks, taken as being the characteristic initial feature, especially in quartz grains in granite. On the one hand, it was suggested that the microcracks derive from differences in compressibility and thermal expansion between grains of different minerals giving rise to internal stresses when pressure and temperature are changed in bringing the rock to the Earth's surface (Nur and Simmons 1970; Perkins, Green and Friedman 1970; Simmons and Richter 1976, although the latter distinguish cracks from a number of other causes also); climatic fluctuations have also been invoked (Lévêque 1969). On the other hand, Pérami, Farran, and Capdecemme (1966) concluded that these effects are inadequate to explain fully the microcracks in granite and that tectonic stress has also been important. Internal stresses arising from anisotropy of thermal expansion or linear compressibility can also be expected to give rise to microcracks even in monomineralic rocks, and especially in marble in which cracking along grain boundaries can readily be brought about experimentally (Gamba 1899; Rayleigh 1934; Pater-son 1963; Sage 1966; Rosengren and Jaeger 1968; Barbish and Gardner 1969; Pérami 1971b). However, in the light of their observations, Brace et al. (1972) and Sprunt and Brace (1974a) concluded that, except possibly for microcracks in quartzite, most of the microcavities, both equant and elongate, that they observed in several types of rocks were not predominantly of a late, brittle origin but had largely persisted from the early history of the rock. Sprunt and Brace suggest that possibly many of the elongate cavities represent brittle fractures in the early history, since modified by healing, and that the equant cavities may represent fluid inclusions in igneous rocks or residual sedimentary porosity in others.

In rocks of high porosity, the initial structure of the pore space also includes numerous tubular pores, typically located at interfaces between several grains. Three-dimensional imaging techniques have been employed to characterize the geometry of such tubular pores in porous sedimentary rocks. A fairly complete set of data is available for the Fontainebleau sandstone, which is monomineralic and has a wide variability in porosity (ranging from 3% to 28%) due to different degrees of silicification during its diagenetic evolution (Thiry, Ayrault and Grisoni 1988). Quantitative analysis of synchrotron X-ray tomographic data indicates that the lengths of the tubular pores are comparable to the average grain size, and there is an overall decrease in these lengths with increasing porosity (Lindquist et al. 2000). In comparison, stereological measurements on thin sections show that the effective diameters are less than one-fifth of the grain size (Doyen 1988; Fredrich, Greaves and Martin 1993; Coker, Torquato and Dunsmuir 1996). The coordination number ranges from 3 to 9, with a mean of around 4 (Lindquist et al. 2000). With decreasing porosity and increasing cementation, there is an overall decrease of coordination number and loss of connec-



tivity (Doyen 1988; Fredrich, Menéndez and Wong 1995; Fredrich 1999). The geometric attributes and connectivity of the tubular pores influence significantly the elastic and transport properties (Bernabé 1991; Dullien 1992). However, they are not as important as the microcracks in the development of brittle failure.

#### 5.7.4 Effects of Stressing

Very few direct microscopical observations of significance bearing on the detail of the development of brittle failure in rock under stress were reported prior to 1970, although there had been considerable speculation, and models of crack propagation had been postulated on the basis of supposed analogue studies in homogeneous materials (e.g., Brace and Bombolakis 1963). Since about 1970, notable contributions have come from three avenues of study. The first were the optical microscope studies on conventional sections of specimens that had been loaded to various points on the force-displacement curve and then unloaded; some of these studies encompassed the complete force-displacement curve with the aid of the stiff or servo-controlled testing machines that were now available (Sect. 5.2.1). Second, there were the scanning electron microscope studies at higher resolution, especially on ion-eroded surfaces. Third, there have been preliminary studies of the three-dimensional aspects (Vinegar, de Waal and Wellington 1991; Fredrich, Menéndez and Wong 1995; Geraud et al. 1998; Kawakata et al. 1999). Finally, stereological techniques have been widely used to characterize quantitatively the density and anisotropy of stress-induced cracking (Kranz 1983; Wong 1985). There are data for compact crystalline rocks (Tapponnier and Brace 1976; Hadley 1976a; Wong 1982a; Wong and Biegel 1985; Fredrich, Evans and Wong 1989; Siddiqi et al. 1997; Alber and Hauptfleisch 1999; Homand et al. 2000) and porous sandstones (Menéndez, Zhu and Wong 1996; Wibberley, Petit and Rives 2000; Wu, Baud and Wong 2000; Mair, Main and Elphick 2000). We now summarize the main findings of these studies.

In *uniaxial compression*, optical observations both on granite and on marble show that a proliferation of microcracking is already evident before the maximum force is reached (Wawersik and Fairhurst 1970; Wawersik and Brace 1971; Bombolakis 1973; Peng and Ortiz 1973; Thill 1973; Ui 1976). The cracks are distributed throughout the specimens, but diminish in density somewhat towards the ends (for a study of the dependence of the distribution of microcracking on the nature of the end constraint in granite, see Peng and Johnson 1972). There is at first a predominance of microcrack orientations roughly parallel to the specimen axis but some microcracks are inclined up to 35° or more to the axis. The proportion of the more highly inclined cracks increases as the total crack density increases with progression towards and through the maximum force. The cracks are both intergranular and transgranular. However, Wawersik and Brace comment that they find very few cases of growth of pre-existing cracks exactly in the manner postulated for propagation of a Griffith crack in homogeneous material (Brace and Bombolakis 1963; Hoek and Bieniawski 1965, 1966 – see Chapt. 4).

Initial stages in the development of the microcracking in granite under stress are revealed in more detail in the scanning electron microscope observations of Tapponnier and Brace (1976); see also Sprunt and Brace (1974a), Hadley (1976a) and Kranz (1979a). Qualitatively similar observations have also been made on other types of compact rocks,

such as gabbro, granodiorite, dolerite, gneiss, amphibolite and marble (Chen, Yao and Xie 1979; Wong and Biegel 1985; Fonseka, Murrell and Barnes 1985; Gottschalk et al. 1990; Chang and Haimson 2000; Rawling, Baud and Wong 2002). These observations have been made at various points on the pre-failure stress-strain curve under a small confining pressure. With increasing stress, the first changes in granite are: (1) an increase in the amount of grain boundary cracking, both through rupturing of bridges in the original elongate cavities and through the appearance of new elongate cavities, so that most grain boundaries are almost continuously cracked before the maximum force is reached; (2) completely healed cracks are re-opened (these occur mainly in quartz, Fig. 41a); (3) a few fresh cleavages appear in the microcline. These effects become evident at roughly the stress level at which dilatancy is first detected. At somewhat higher stresses, transgranular axial cracks begin to proliferate, starting at pores, at transverse grain boundaries between different minerals (one of the pair often being biotite, Fig. 41b), and at pre-existing elongate cavities at grain boundaries; axial cracks originating at shear cracks as depicted in Fig. 41c were found to be uncommon. The new cracks were distinguished by their sharp ends and nearly constant width. At the higher stresses the transgranular cracks tend to run from grain boundary to grain boundary. At the maximum stress, nearly all grains contain new transgranular cracks, quartz and microcline containing more than plagioclase. Notwithstanding the intensity of microcracking, localization of damage is not evident in the post-peak stage, in agreement with data from acoustic emission location discussed earlier. Kinking in the biotites is also associated with intense transgranular cracking and Tapponnier and Brace suggest that the maximum stress may in fact be determined as an instability arising out of the kinking process in the biotite. The study of Shea and Kronenberg (1993) of fifteen schists and gneisses indicates that such an instability mechanism increases in importance with increasing mica content.

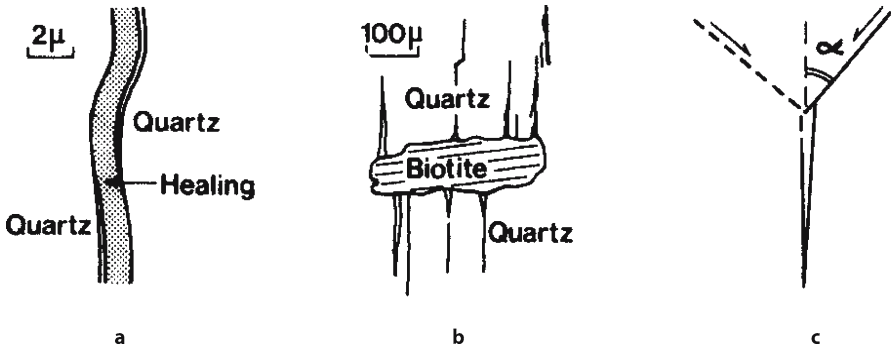


**Fig. 41.** Idealized sketches of microcracking resulting from application of stress in granite, as revealed by transmission electron microscopy on ion-etched surfaces; the maximum compressive stress is vertical. **a** Re-opening of cracks previously formed but healed or cemented during earlier history of the rock; these cracks are the most commonly observed. **b** Transgranular cracking in quartz at biotite grain boundary. **c** Crack formation at shear cracks, often invoked in discussions on dilatancy; this type of cracking is not common (Tapponnier and Brace 1976)

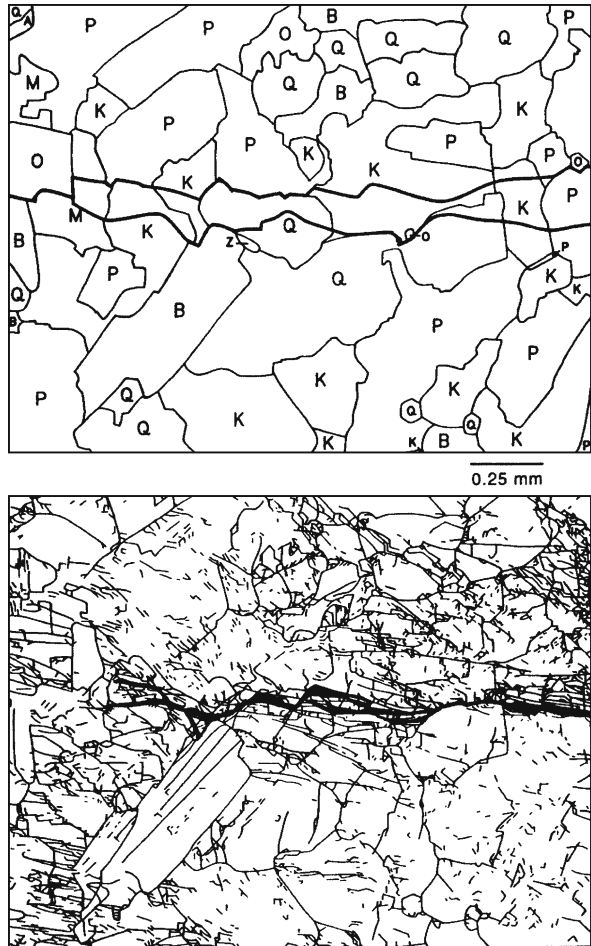
The proliferation of the predominantly axial microcracking seen optically in granite and marble continues to be the predominant process in uniaxial compression as the force passes through its maximum and begins to fall again (Wawersik and Fairhurst 1970; Wawersik and Brace 1971). Thus the failure associated with the stress peak appears to be at first a general weakening of the specimen through the development of a distribution of local cracks rather than the onset of a macroscopic fracture, although refined methods of observing strain distribution first reveal local strain concentration at the site of the eventual macroscopic failure just before the maximum force is reached (Liu and Livanos 1976; Soga, Martin and Spetzler 1976). Only after passing the peak does local shear fracturing become obvious microscopically. The shear fractures develop on a macroscopic scale, in a more pronounced manner in the marble than in the granite, before macroscopic axial fracturing (“slabbing”) occurs as the final stage of collapse of the specimen. It is noteworthy that this sequence was observed in Westerly granite even though it showed Class II post-peak behaviour (Sect. 5.2.2). However, in other, more brittle rocks the preliminary microcracking was less pronounced, possibly due to their greater homogeneity and finer grain size (Houperit 1974a); the most extreme cases were those of basalt and Solnhofen limestone, which appeared to fail initially by shear fracturing.

The use of *confining pressure* on granite in the range up to 150 MPa leads to more profuse pre-failure microcracking but, except at very low confining pressures, this increase results from an increase in the proportion of cracks inclined at  $20^\circ$  or more to the axis of compression (Wawersik and Brace 1971). Below 10 MPa confining pressure, the stress maximum is still associated with proliferation and growth of predominantly axial microcracks but the macroscopic longitudinal slabbing that tends to develop in uniaxial tests is suppressed. At higher pressures, the microcracks (now mainly inclined ones) tend to form inclined zones which develop into the macroscopic shear fracture, often by linking up en echelon inclined fractures (see also Friedman, Perkins and Green 1970). Microstructural observations in granite (Wong 1982b; Moore and Lockner 1995) and gabbro (Wong and Biegel 1985) show that the localized coalescence of microcracks that extends over two or more grains is quite evident in samples stressed to beyond the peak stress (Fig. 42), in agreement with acoustic emission sources that also begin to localize in the post-peak stage (Lockner et al. 1992). Scanning electron microscope observations have revealed that the macroscopic development of shear localization involves at least three geometric instability mechanisms: microbuckling of slender columns in grains that have been segmented by microcrack arrays (Fig. 43a), kinking in biotite grains, and rotation and crushing of micro-blocks formed by pore-emanated cracks in plagioclase. In addition, shear slip along cracks at high angle to  $\sigma_1$  that are favourably oriented for frictional displacement also promotes the development of a continuous shear band across the sample (Fig. 43b).

In marble, increase in the confining pressure introduces features that are related to the brittle-ductile transition (Wawersik and Fairhurst 1970; Thill 1973; Fredrich, Evans and Wong 1989). The pre-failure axial microfractures become suppressed at higher pressures and the stress peak may be associated with the formation of localized shear fractures that subsequently extend and join up to form the macroscopic shear fracture. At the same time, intragranular plastic deformation becomes evident too.

**Fig. 42.**

Propagation of a macroscopic shear fracture in Westerly granite by coalescence of grain boundary and intragranular cracks in the post-peak stage. The sample was triaxially compressed at confining pressure of 50 MPa and retrieved just before the shear fracture had almost propagated to the right end of the sample. The mineralogical and microcrack maps at the top and bottom were determined from a petrographic thin-section oriented with the shear fracture aligned horizontally. The mineral abbreviations are given by: Q - quartz; P - plagioclase; K - microcline/orthoclase; B - biotite; M - muscovite; O - opaque minerals, usually magnetite; A - apatite; Z - zircon (after Moore and Lockner 1995)

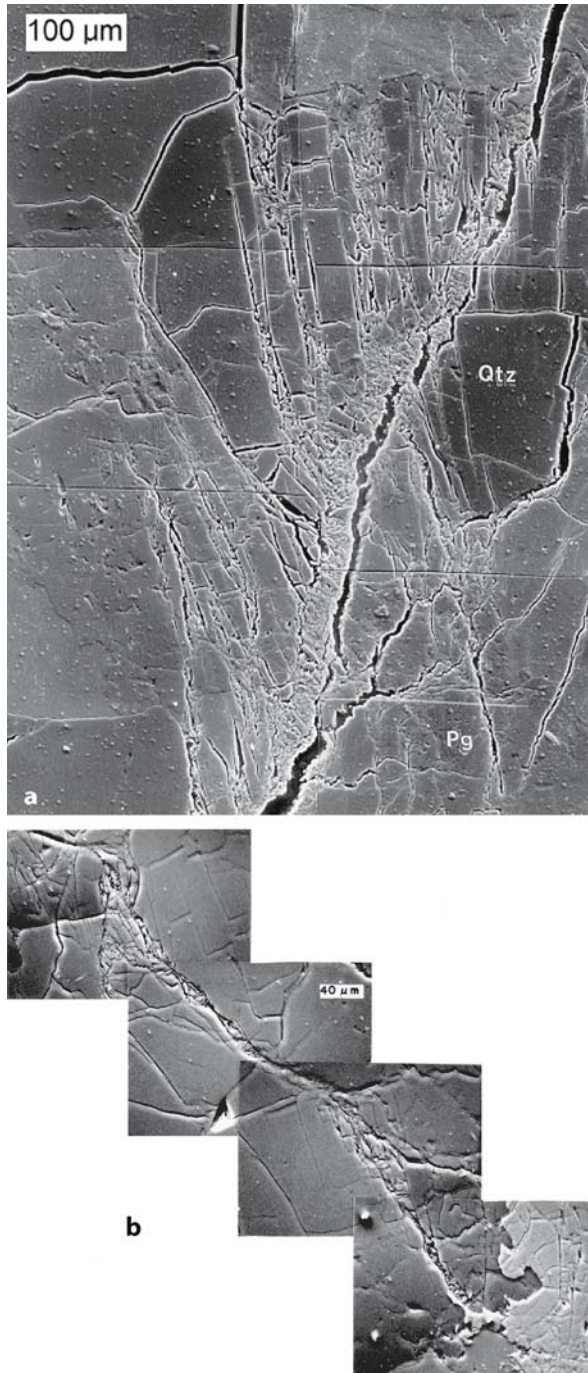


There have also been studies on sandstone and quartzite. Hoshino and Koide (1970) observed microscopically the development of microfracturing in a low-porosity, calcite-cemented sandstone. Here the microfractures occurred both within the cementing matrix and within the sand grains. Their density increased with strain, and they tended to concentrate in inclined zones from which the macroscopic fracture developed. Sangha, Talbot, and Dhir (1974) made similar observations on another sandstone of more argillaceous matrix but found that the microfractures occurred mainly in the matrix. In contrast, in an argillaceous quartzite, Hallbauer, Wagner, and Cook (1973) found the stress-induced microcracks to be mainly transgranular within the quartz grains, mostly close to an axial orientation ( $\pm 10^\circ$ ), and evidently commonly initiated at points of contact between the quartz grains (cf. Gallagher et al. 1974). The macroscopic shear developed by step-wise joining of the microcracks, beginning in the centre of the specimen.

**Fig. 43.**

**a** Coalescence of arrays of microcracks in quartz (*qtz*) and plagioclase (*pg*) grains to form a macroscopic shear fracture in Westerly granite. The sample was triaxially compressed (with  $\sigma_1$  in the vertical direction) at confining pressure of 250 MPa and temperature of 150 °C to the post-peak stage (after Wong 1982b).

**b** An incipient localized zone in San Marcos gabbro that has propagated across a plagioclase grain, with damage concentrated in the vicinity of a preexisting crack aligned favourably for shear slip. The relatively undeformed phase with lighter colour at the bottom is pyroxene. The sample was triaxially compressed (with  $\sigma_1$  in the vertical direction) at confining pressure of 350 MPa to the post-peak stage (after Wong and Biegel 1985)



Dunn, La Fountain, and Jackson (1973) have studied the development from microfracturing to macroscopic fracture in porous sandstones as a function of porosity. A scanning electron microscope study of Berea sandstone samples deformed through the post-peak stages was conducted by Menendez, Zhu and Wong (1996), who concluded that brittle faulting in the weakly cemented sandstone (with initial porosity of 21%) involves micromechanical processes quite different from those in a compact rock. Dilatancy and acoustic emission activity in the pre-failure stage seem to primarily involve intergranular cracking. Very little intragranular cracking was observed, except for isolated clusters of extensile microcracks that radiated from grain contacts in a sample loaded to very near the peak stress (Fig. 44a). Stress-induced anisotropy was not appreciable in pre-failure samples. Shear localization develops by the coalescence of such clusters of damage (Fig. 44b). In contrast, scanning electron microscope observations on Darley Dale sandstone (with initial porosity of 13%) have shown that dilatancy in this more compact siliciclastic rock involves significant contribution from intragranular cracking, which also induces appreciable stress-induced anisotropy (Wu, Baud and Wong 2000). In this sense, the damage evolution is more similar to that documented for a compact granite or gabbro.

Recent studies (Bésuelle, Desrues and Raynaud 2000; Haied, Kondo and Henry 2000; El Bied, Sulem and Martineau 2002; Mair, Elphick and Main 2002) in other

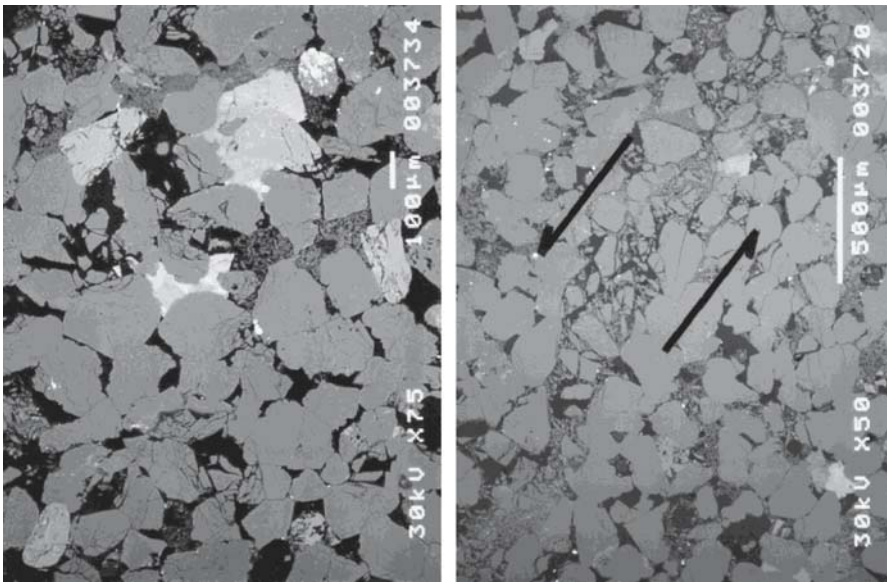


**Fig. 44.** Damage and shear localization in Berea sandstone. The samples were triaxially compressed (with  $\sigma_1$  in the vertical direction) at effective pressure of 20 MPa. **a** Isolated clusters of Hertzian fractures emanating from grain contacts as observed in a sample unloaded immediately after the peak stress had been attained. **b** Coalescence of clusters of damage to form a macroscopic shear band in a sample loaded to the post-peak stage (after Menéndez, Zhu and Wong 1996)

sandstones (all with porosities exceeding 20%) have documented micromechanical behaviour that is qualitatively similar to that in Berea sandstone. Attempts have also been made to investigate the evolution of shear localization by deforming sandstone samples well into the post-peak region. While the evolution of geometric complexity is expected to be sensitively dependent on the boundary conditions, these studies provide a useful analogue for deformation bands that tend to develop as subparallel arrays in sandstone formations. In a relatively large sample of Locharbriggs sandstone (100 mm in diameter) Mair, Main and Elphick (2000) documented the increase in number of shear bands with deformation. In Fontainebleau sandstone deformed at confining pressure of 7 MPa, El Bied, Sulem and Martineau (2002) observed appreciable dilatancy in the shear band. In contrast the sample at 28 MPa pressure had a compacting shear band with intense grain crushing, which was sandwiched between dilatant zones with significant cracking. Relatively complex pattern was documented by Wibberley, Petit and Rives (2000) using a shear box at different normal stresses.

Amongst sundry observations, mention may be made of the following. Friedman and Logan (1970b) and Conrad and Friedman (1976) described “microscopic feather fractures” in granite and quartzite, adjacent to shear failure surfaces or pre-cut sliding surfaces, which are interpreted as extension microfractures forming subsequent to the shear failure in response to the local stress field. Peng and Podnieks (1972) observed the propagation of cracks during stress relaxation tests on tuff, and Peng (1975) made similar observations of the propagation of the fractures in uniaxial tension in sandstone and marble. Mosher, Berger, and Anderson (1975) have studied the cracking within granite thin sections when stressed in tension or compression under the microscope; intergranular fractures predominated in tension and intragranular in compression. For some more detailed studies on limestone and marble in compression, see Olsson (1974b) and Olsson and Peng (1976).

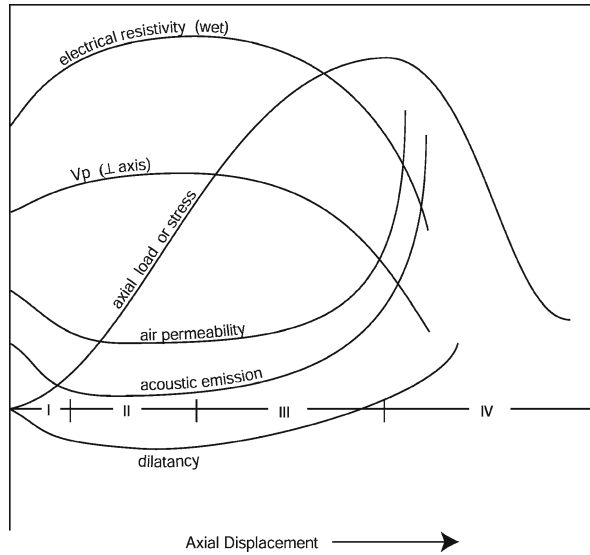
## 5.8 A Synoptic View of Brittle Failure

In the light of the observations reviewed in this chapter, we now attempt to summarise the development of brittle failure in a rock in terms of the processes that eventually lead to macroscopic fracture. We will first discuss the development in a compact rock. The stress-strain behaviour of such a rock in compression in the brittle field can be divided into several stages prior to the macroscopic fracture, as shown in Fig. 45. The basis of such a scheme was first put forward by Brace (1964a) and elaborated by Brace, Paulding, and Scholz (1966) and it has been supported by later work. The main stages distinguished are:

- I. A “settling-down” phase.
- II. Nearly perfect linear elasticity.
- III. Development of microfracturing and dilatancy involving stable microcrack propagation.
- IV. Unstable developments in the pattern of microcracking, involving localization and leading to the growth of a macroscopic fracture.

**Fig. 45.**

Generalized demarcation of four stages in the complete load-displacement curve of a compact rock in a compression test and the corresponding courses of change in various physical properties



A useful summary of the characteristics of these stages, including especially the acoustic characteristics, is given by Thill (1973) but with a somewhat more elaborate subdivision; see also Brace (1971a) and the review by Friedman (1975). Similar schemes have been proposed by many writers, for example, Pérami (1965), Bieniawski (1967a), Brady (1970b), and Hoshino and Koide (1970), although the interpretations have varied somewhat.

*Stage I* is a stage of rapid hardening and is seen most clearly in uniaxial compression. The upward concavity of the stress-strain curve here is usually attributed to the closing of pre-existing cracks, a process that can be more or less completely reversible, that is, non-linearly elastic in its macroscopic effect. An initial hardening can also appear in triaxial tests if the confining pressure is not very high but many of the pre-existing cracks will have already been closed by the application of the confining pressure before the additional axial force has been applied and so the initial non-linear effect is usually not marked. In low porosity rocks, some irreversible collapse of pores may also be expected to contribute here, especially in uniaxial compression, but this effect will not be restricted to Stage I.

*Stage II* can be mainly attributed to the elastic deformation of the grains. Hysteresis has sometimes been detected in this stage (e.g., Cook and Hodgson 1965) and also in uniaxial strain (Walsh and Brace 1972), indicating that some irreversible processes are also occurring to a small extent. Some sliding on pre-existing cracks has been suggested, for example, by Bieniawski (1967a), who relates the shape of the hysteresis loop to the frictional resistance to such sliding, with reference to the theory of Walsh (1965b). However, the microscopical studies have shown little evidence for activity at shear cracks and so the explanation of the hysteresis must remain conjectural. Whatever is occurring is probably premonitory of the developments in Stage III. The sensitivity with which non-linearity in the stress-strain curve can be detected will, of course, influence



the range of strain that is attributed to Stage II, but it is clear that this range also varies considerably with the type of rock and the confining pressure. Thus Pérami (1965) and Pérami and Thénoz (1969) do not explicitly recognize a Stage II in their discussion of uniaxial compression. Since there is rarely a complete absence of acoustic emission at any stage of loading it may be said to be, to some degree, a matter of convention whether to recognize a Stage II in which microcrack activity is negligible. However, especially under high confining pressure, the recognition of such a stage does commonly seem to be useful for compact rock.

In *Stage III*, departures from perfectly elastic behaviour are clearly in evidence from dilatancy, increased acoustic emission, decreased speed of elastic waves, and other changes, as outlined earlier in this chapter. These changes involve the proliferation and propagation of large numbers of microcracks distributed fairly uniformly throughout the specimen. From the elastic wave speed and microscopical studies, there appears to be a general tendency for the cracks to develop predominantly parallel to the maximum principal compressive stress. However, it is difficult to quantify how the damage is partitioned between the microcracks that propagate from smaller ones initially present and the nucleation of new cracks. In contrast to the wave speed and microscopical indications, the acoustic emission source analyses often point to a predominance of shear events, suggesting development of shear cracks rather than axial cracks. Possibly the two types of observation are detecting different aspects of the cracking, the proliferation of axial cracks being often relatively quiet acoustically while the shear events relate to the sudden initiation of small wing cracks at the ends of axial cracks. While further study is needed, the observations may also mean that there is a considerable variety of behaviour at the microscopic level, at the grain scale and below. An important general characteristic is that the propagation of the microcracks in this stage is a stable process in the sense that the cracks only extend by limited amounts in response to given increments in stress (apart from subsidiary time effects) and do not run on to develop a macroscopic fracture. Some writers have distinguished a new stage just pre-peak, characterized by an accelerated development of the already prominent microcracking, possibly with an increase in the proportion of inclined microcracks (cf. Thill 1973) and some degree of localization in the concentration of microcracks. However, it is probably better to acknowledge that there is a certain arbitrariness in distinguishing the transition to Stage IV.

*Stage IV* can be defined by the onset of marked localization of the microcracking development and is here taken to include the complete progression from this point to macroscopic fracture. Microstructural observations indicate that the microcracks continue to be predominantly axial in orientation, but generally an increasing proportion come to be of inclined orientation or “shear” character. As the concentration increases there develops a linking-up of microcracks which leads to the growth of the macroscopic fracture, either of the axial splitting or shear type. Details of this failure progression and its dependence on the nature of the rock need further study. Further, it should be noted that, since the deformation is now macroscopically inhomogeneous, the measurements of the various properties plotted in Fig. 45 are no longer meaningful except as averages.

Various observations indicate that the transition from Stage III to Stage IV occurs somewhere in the vicinity of the peak load. However, the observations are apparently

contradictory as to whether this transition occurs in the pre- or post-peak stage. While acoustic emission location and microstructural observations commonly indicate that onset of localization does not occur until the peak stress has been attained, strain and surface deformation measurements seem to indicate pre-peak localization. Further, there are theoretical reasons based on bifurcation analysis, developed in the next chapter, why initiation of localization is, in general, to be expected to occur in the post-peak stage. Closer study of the initiation of localization and thus of the transition from Stage III to Stage IV integrating different measurement techniques would be useful to resolve this apparent discrepancy.

In porous rocks, most of the studies have focused on sandstone. In a porous sandstone the development of brittle failure is different in at least three aspects. First, while the phenomenological behaviour is qualitatively similar to that illustrated schematically in Fig. 45 the permeability evolution may be significantly different. The data summarized in Fig. 37 show that the permeability may actually decrease while a porous sandstone undergoes dilatancy. For sandstone this transition in permeability evolution occurs at a porosity of about 15%. Second, microscopic studies have shown that stress-induced microcracking is not as pervasive in a porous rock. In Stage III the acoustic emission activity seems to be associated with the rupture of lithified grain contacts, and dilatancy arises primarily from relative movement among grains. The microcracks that proliferate in Stage IV are mostly extensile cracks emanating from grain contacts. Third, while shear localization involves the coalescence of clusters of such Hertzian cracks, its development in Stage IV depends on the interplay of dilatant and compactant processes. So far studies have focused on sandstone, and further study on other rock types would provide a more general understanding of brittle failure in porous rocks.

## Micromechanics of Brittle Fracture

### 6.1 Introduction

In the previous chapter we frequently invoked explanations of the observed behaviour in terms of flaws and heterogeneities in the rock material on the microscopic scale. The direct observations that have been made of these features were also reviewed. These observations provide a basis for micromechanical views of brittle fracture. In this chapter, specific micromechanical theories will first be summarized for compact rock and the view of brittle fracture as a localization in the proliferation of microcracking set out. The theories for development of brittle failure in a porous rock will also be reviewed.

It was emphasized in Chapt. 4 that the Griffith type of theory is only applicable to the initiation of failure on the scale of microcracks whereas the strength observations refer to the macroscopic failure. An adequate theory of failure should therefore provide a fairly complete description of the key mechanical processes from the stage of initiation to the final stage of macroscopic fracture. In this connection, a distinction needs to be made between the sources of initiation of the microcracks, which lie in the initial structure, as described in Sect. 5.7.3, and the growing microcracks themselves, described in Sect. 5.7.4. The former might be referred to as the “source defects” and the latter as the “growing microcracks”. A theory of failure therefore needs to take the following aspects into account:

1. The local initiation of potentially-growing microcracks at source defects.
2. The subsequent individual growth of these microcracks with increased loading.
3. The increase in the number of growing microcracks with increased loading.
4. The interaction between the growing microcracks as their lengths and numbers increase.
5. The stability of the crack proliferation process and the possibility of its localization, leading to macroscopic failure.

In compact rock, it is commonly considered that the sources of microcrack initiation are themselves microcracks already present in the rock and that from the onset of dilatancy  $C'$  to near the peak stress, irreversible deformation involves the growth of stress-induced extensile microcracks. A theoretical model should characterize the nucleation and stable propagation of the multiplicity of stress-induced microcracks in relation to the evolution of dilatancy and strain hardening behaviour. In porous rock, considerations of crack initiation at pores or of intergranular bonding strength also enter.

Micromechanics is a field of mechanics that takes into account the microstructure of a material (Budiansky 1983; Mura 1987). The micromechanical analysis of the inelastic behaviour and brittle failure of rock applies to the microstructure the basics of fracture mechanics, which, as summarized in Appendix 1, derives some of its key concepts from Griffith's (1920) theory. The micromechanical models attempt to capture the important attributes inferred from microstructural and acoustic emission observations, and to arrive at constitutive relations that describe the inelastic and failure behaviour observed in experiments. They advance beyond classical Griffith-type models (summarized in Chapt. 4) by explicitly considering the relationships between the applied stress field, the local tensile stress concentration on the grain scale, and the propagation of a microcrack along a path that may be out of its initial plane.

Under overall compressive loading, final macroscopic failure occurs by shear localization. From a micromechanical view, this final stage is dominated by crack coalescence. The mechanics of the coalescence process hinges on the complex interaction of stress fields of the numerous neighbouring cracks. A comprehensive analysis of the evolution of the instability requires fairly detailed characterization of the microcrack structure in conjunction with intensive computation.

Important advances have also been made in the analysis of shear localization by drawing on the principles of continuum mechanics. If a macroscopic constitutive model has been formulated to describe realistically the inelastic and dilatant behaviour of the brittle rock, then the onset of shear localization can be predicted to occur under critical conditions at which a homogeneous deformation evolves into a pattern that embeds a highly concentrated shear band. At this critical condition, an incremental change in the applied stress field results in a deformation field that is non-unique, with separate solutions corresponding to localized shear within the shear band and relatively homogeneous inelastic deformation outside the band.

## 6.2 Micromechanical Theory for Compact Rock

### 6.2.1 Initiation of Stress-Induced Microcracking

The heterogeneous nature of natural rock gives rise to various types of defects or local stress concentrations that might act as sources for growing microcracks (Kemeny and Cook 1991). On the basis that the most likely sources are the initially-present microcracks, the micromechanical model that has been analyzed most thoroughly is that of the "sliding crack" (Brace and Bombolakis 1963; Brace, Paulding and Scholz 1966; Fairhurst and Cook 1966). This model considers sources of tensile stress concentration that are located at the tips of inclined pre-existing cracks (shown in Fig. 46a) with length  $2c$  and oriented at angle  $\gamma$  to  $\sigma_1$ , the maximum principal compressive stress). The cracks are assumed to be closed under the axisymmetric triaxial loading conditions considered here. The applied stresses induce a shear traction on the crack plane and, if this resolved shear traction is sufficiently high to overcome the frictional resistance along the closed crack, frictional slip results in tensile stress concen-

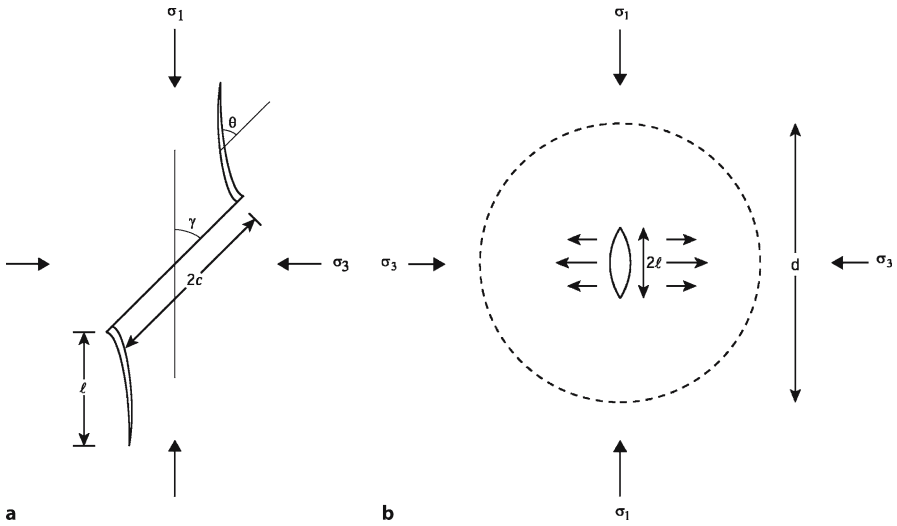


**Fig. 46.** **a** The nucleation and propagation of a wing crack from the tip of a sliding crack. Directions of the maximum and minimum principal stresses are indicated. The sliding and wing cracks are at angles of  $\gamma$  and  $\theta$  with respect to the  $\sigma_1$  direction, respectively. **b** A generic model for the nucleation and propagation of wing crack due to local tensile stress concentration characterized by the parameter  $f'$

trations at the two tips of the sliding crack, which, in turn, may induce “wing cracks” to nucleate there. The driving force for nucleation is characterized by the stress intensity factor  $K_I$  at the site of wing crack initiation. With increased loading,  $K_I$  will attain the critical value  $K_{Ic}$  at which point a wing crack nucleates.

The qualitative behaviour of such a crack system (pre-existing sliding crack plus nucleating wing crack) was first studied by Brace and Bombolakis (1963) in photoelastic material and glass. A first-order solution in closed form for the stress intensity factor of a slightly curved or kinked crack was obtained by Cotterell and Rice (1980). Using their solution, it can be shown that a wing crack nucleates at an angle  $\theta = \cos^{-1} 1/3$  ( $\approx 70.5^\circ$ ) at the stress state given by

$$\sigma_1 = \frac{\sin 2\gamma + \mu(1 + \cos 2\gamma)}{\sin 2\gamma - \mu(1 - \cos 2\gamma)} \sigma_3 + \frac{\sqrt{3}}{\sin 2\gamma - \mu(1 - \cos 2\gamma)} \frac{K_{Ic}}{\sqrt{\pi c}} \quad (6.1)$$

where  $\mu$  is the friction coefficient for the pre-existing sliding crack surface, and the angles  $\gamma$  and  $\theta$  are defined in Fig. 46a (Rawling, Baud and Wong 2002). If the onset of dilatancy  $C'$  is identified with the initiation of wing cracks and if the rock is assumed to contain randomly oriented cracks, then the wing cracks should first nucleate from those sliding cracks oriented at  $\gamma = \frac{1}{2} \tan^{-1}(1/\mu)$  at a stress state given by

$$\sigma_1 = \frac{\sqrt{1 + \mu^2} + \mu}{\sqrt{1 + \mu^2} - \mu} \sigma_3 + \frac{\sqrt{3}}{\sqrt{1 + \mu^2} - \mu} \frac{K_{Ic}}{\sqrt{\pi c}} \quad (6.2a)$$

(Ashby and Sammis 1990). In an anisotropic rock with a preferred orientation of planes of weakness (Sect. 3.7.1), it has been observed that wing cracks first nucleate from sliding cracks aligned along the weakness plane. Rawling, Baud and Wong (2002) show that if the preferred orientation is given by the angle  $\beta$  (between the weakness plane and  $\sigma_1$ ) then wing cracks should first nucleate from those sliding cracks oriented at  $\gamma = \beta$  at a stress given by

$$\sigma_1 = \frac{\sin 2\beta + \mu(1 + \cos 2\beta)}{\sin 2\beta - \mu(1 - \cos 2\beta)} \sigma_3 + \frac{\sqrt{3}}{\sin 2\beta - \mu(1 - \cos 2\beta)} \frac{K_{Ic}}{\sqrt{\pi c}} \quad (6.2b)$$

The model predicts that the principal stresses at the onset of wing crack growth are linearly related. Identifying this stress state with the onset of either dilatancy or acoustic emission activity, Ashby and Sammis (1990) compared experimental data for 9 relatively isotropic rock types with Eq. 6.2a. They showed that the data generally follow approximately linear trends, with slopes corresponding to values of  $\mu$  ranging from 0.55 to 0.64. Figure 27a shows data for granites, gabbro and aplite. Using the anisotropic nucleation condition (Eq. 6.2b), Rawling, Baud and Wong (2002) inferred values of  $\mu$  ranging from 0.2 to 0.3 for the Four-mile gneiss with relatively strong mica foliation.

The sliding crack model has some advantages of analytical tractability and it captures a vital aspect of mean stress dependence through introducing friction on the sliding crack. However, it is only one of a range of possible models which can describe the generation of growing cracks initiated at heterogeneities in the rock (Nemat-Nasser 1985). Some other types of model have been reviewed by Kemeny and Cook (1991), involving reference to tensile stress concentrations induced by cylindrical pores (Sammis and Ashby 1986), elastic mismatch (Dey and Wang 1981), elastic contact of impinging grains (Zhang, Wong and Davis 1990b), and dislocation pile-up (Wong 1990b). Since there are common features to all these models, the essential aspects might be represented by a generic model.

Thus, Costin (1983, 1985) developed a generic model that does not depend explicitly on the sliding crack to initiate extensile cracking. Without specifying the microstructural heterogeneity that acts as the source of local tensile stress concentration, he made the empirical assumption that the local tensile stresses are linearly related to the remotely applied principal deviatoric stresses. Costin's model was modified by Rudnicki and Chau (1996), who provided a more unified constitutive model for multiaxial loading. They introduced the proportionality factor  $f'$  to characterize the tensile stress concentration (Fig. 46b). In their model under triaxial compression, cracks open up preferentially along a direction parallel to  $\sigma_1$  and are initially subjected to a tensile stress concentration of

$$f' \frac{\sigma_1 - \sigma_3}{3} - \sigma_3$$

This type of model again predicts that the principal stresses at the onset of stress-induced cracking are linearly related. For penny-shaped cracks (of initial radius  $a_0$ ), the relation between the principal stresses at the onset of crack growth is given by Rudnicki and Chau (1996) as

$$\sigma_1 = \left( \frac{3}{f'} + 1 \right) \sigma_3 + \frac{3\pi}{2f'} \frac{K_{Ic}}{\sqrt{\pi a_0}} \quad (6.3)$$

Values of  $f'$  ranging from 1.1 to 2.1 were inferred from data on the onset of dilatancy for granite, marble and tuff (Costin 1985; Senseny 1986; Rudnicki and Chau 1996). Another, slightly more elaborate, generic model has been discussed by Kemeny and Cook (1991).

### 6.2.2

#### Microcrack Propagation and Stability

Once nucleated, the wing crack grows out of the initial plane of the sliding crack. The analysis of the propagation behaviour requires the computation of the stress intensity factor at each stage as well as of the wing crack trajectory. The formulation and solution of this fracture mechanics problem is very involved. The technical difficulties were reviewed by Lo (1978), who also presented one of the most thorough analyses. With applications to geologic materials in mind, Nemat-Nasser and Horii (1982) generalized Lo's (1978) approach to the case of compressive loading, and later extended the analysis to an array of interacting wing cracks (Horii and Nemat-Nasser 1985). They implemented the method of "pseudo-traction", by which the stress intensity factors can be evaluated numerically by solving a system of integral equations. For mathematical convenience, several groups adopted analytic approximations to the rigorous numerical results of Nemat-Nasser and Horii (1982) and Horii and Nemat-Nasser (1985) in order to analyze the propagation behaviour of a wing crack (Steif 1984; Nemat-Nasser 1985; Ashby and Hallam 1986; Kemeny and Cook 1987; Fanella and Krajcinovic 1988; Lehner and Kachanov 1996; Baud, Reuschlé and Charlez 1996).

The theoretical propagation of an isolated wing crack in an infinite medium shows two features that agree with experimental and microstructural observations. First, the stress intensity factor decreases with increasing wing crack length  $\ell$  (if both  $\sigma_1$  and  $\sigma_3 > 0$ ). This implies that wing crack growth is stable under all-compressive loading. Second, the wing crack orientation  $\theta$  also decreases with increasing  $\ell$ , from its initial value of  $70.5^\circ$  to approach  $\gamma$ . This implies that the trajectory curves gradually approach an orientation parallel to  $\sigma_1$  (Fig. 46a).

The mechanical basis for the stable propagation behaviour can be illustrated with reference to Horii and Nemat-Nasser's (1985) analytic approximation for the stress intensity factor at the tip of an extending wing crack. Neglecting cohesion on the initial sliding crack, their expression can be written as

$$\frac{K_I}{\sqrt{\pi c}} = \frac{(\sigma_1 - \sigma_3) \sqrt{1 + \mu^2} - (\sigma_1 + \sigma_3) \mu}{\pi \sqrt{L/c}} \sin \theta - \frac{1}{2} \sqrt{\frac{\ell}{c}} (\sigma_1 + \sigma_3 - (\sigma_1 - \sigma_3) \cos 2(\theta - \gamma)) \quad (6.4)$$

(The quantity

$$L = \ell + \frac{8c}{3\pi^2}$$

is an effective wing crack length used in their approximation, the factor  $8/3\pi^2$  being obtained by equating Eq. 6.4 with Eq. 6.2a for the case  $\ell = 0$  and  $\cos \theta = 1/3$ ). The wing crack orientation is obtained by maximizing the above expression for  $K_I$  with respect to  $\theta$ . There are thus two contributions to the stress intensity factor at the tip of a wing crack. The first term on the right of Eq. 6.4 arises from the tensile stress field due to the “wedging” action at the ends of the pre-existing sliding crack. This term decreases with increasing  $\ell/c$  because, as the wing crack gradually grows, its tip propagates further from the local source of tensile stress concentration. The second (negative) term is due to normal traction resolved on the plane of the wing crack. Since this traction is compressive, it tends to inhibit the further propagation of the wing crack and its negative effect becomes greater with increasing  $\ell/c$ . The two processes act cooperatively to stabilize the wing crack propagation. The crack growth behaviour according to this model is illustrated in Fig. 47, where the normalized stress intensity factor and wing crack angle are plotted as functions of the normalized length  $\ell/c$  for fixed  $\mu = 0.3$  and  $\gamma = \frac{1}{2} \tan^{-1}(1/\mu) = 36.7^\circ$ . The wing cracks initiate at an angle of  $\theta = 70.5^\circ$  ( $\cos \theta = 1/3$ ) to the main crack; the angle  $\theta$  then decreases with increasing wing crack length and asymptotically approaches the value of  $\gamma = 36.7^\circ$  for very large  $\ell/c$ .

The stable propagation behaviour is qualitatively similar in other models that do not involve wing cracks (Kemeny and Cook 1991). In Costin’s (1983) generic model, the stress intensity factor is assumed to decrease linearly with crack extension.

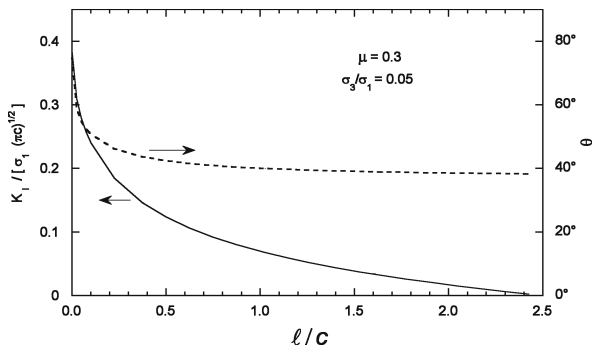
### 6.2.3

#### Microcrack Interaction and Damage Mechanics of Brittle Failure

In the sliding crack model, a consequence of the stability of wing crack growth is the proliferation of stress-induced extensile cracks that propagate along orientations subparallel to  $\sigma_1$  as  $\sigma_1$  is increased. Also, as the applied stress is increased, shorter and less favorably oriented sliding cracks will be activated, thus nucleating an increasing

**Fig. 47.**

The normalized stress intensity factor and wing crack orientation as functions of the normalized wing crack extension according to Eq. 6.4 for stress ratio  $\sigma_3/\sigma_1 = 0.05$  and friction coefficient  $\mu = 0.3$





number of wing cracks distributed throughout the sample. With the progressive increase in both number and dimensions of wing cracks, their stress fields will interact with one another in a complex manner (Horii and Nemat-Nasser 1983). The complexity of the crack interaction process is such that the fracture mechanics analysis of a predominant or representative crack is no longer adequate. The stress intensity factor may be enhanced or reduced relative to that given by Eq. 6.4, which applies only to a non-interactive wing crack system.

Two approaches have been adopted to analyze the mechanics of crack interaction. The first approach is based on continuum damage mechanics (Kachanov 1986; Krajcinovic 1989; Lemaitre 1996). Continuum mechanics treatments of inelastic and failure behaviour can be formulated in terms of the evolution of internal variables that reflect the current microstructural arrangement (Rice 1975). In a micromechanics-based damage mechanics model as applied here, the term “damage” refers to an internal variable characterizing the density and geometry of the multiplicity of microcracks and pores in the brittle rock. The damage parameter evolves with the history of loading.

The second approach is a stochastic one that involves intensive numerical computation of a system of cracks with geometric attributes following certain statistical distributions. This type of model will be discussed in Sect. 6.2.5.

For mathematical convenience, most damage mechanics models consider systems of source microcracks of uniform initial lengths. The microcracks are embedded in a linearly elastic medium, the moduli of which are assumed to remain unchanged even though damage may progressively accumulate. The inelastic behaviour of the cracked solid is directly related to such factors as the shear slip of sliding cracks and the dilation of wing cracks. Unless interaction among the wing cracks is explicitly accounted for, the stable propagation behaviour of an individual wing crack is as discussed in Sect. 6.2.2 and the macroscopic inelastic behaviour of a solid containing many such cracks will be characterized by strain hardening and dilatancy (Kachanov 1982a,b; Nemat-Nasser and Obata 1988; Fanella and Krajcinovic 1988; Yu and Feng 1995).

The interaction between wing cracks arises from the overlap of their local stress fields, which will be a function of the spacing of the cracks or the crack density. For the analysis of this interaction, various idealized geometric configurations, typically involving periodic arrays of wing cracks, have been proposed (Fig. 48). Whereas in the case of the individual crack (Sect. 6.2.1 and 6.2.2), we can think of a representative elementary volume (REV) as containing only one crack, we now have to consider an REV containing at least two cracks. As pointed out by Kemeny and Cook (1991), the extreme cases are those in which the cracks are, respectively, collinear and parallel (a similar situation arises in dislocation theory, where the interaction between dislocations is strongly dependent on whether their relative positions are in the same slip plane or in parallel slip planes (Weertman and Weertman 1992, Ch. 3)). These limiting cases have been analyzed by considering a rectilinear array of wing cracks emanating from sliding cracks (Ashby and Hallam 1986; Kemeny and Cook 1987; Hallam and Ashby 1990; Kemeny and Cook 1991).

We consider now the particular case of interaction in a collinear crack array with wide spacing between the lines of cracks (Fig. 48a), which was analysed by Ashby and Sammis (1990). In this 2-dimensional damage mechanics model, the initial sliding cracks are assumed to have uniform length of  $2c$ . Wing cracks of length  $\ell$  are nucle-

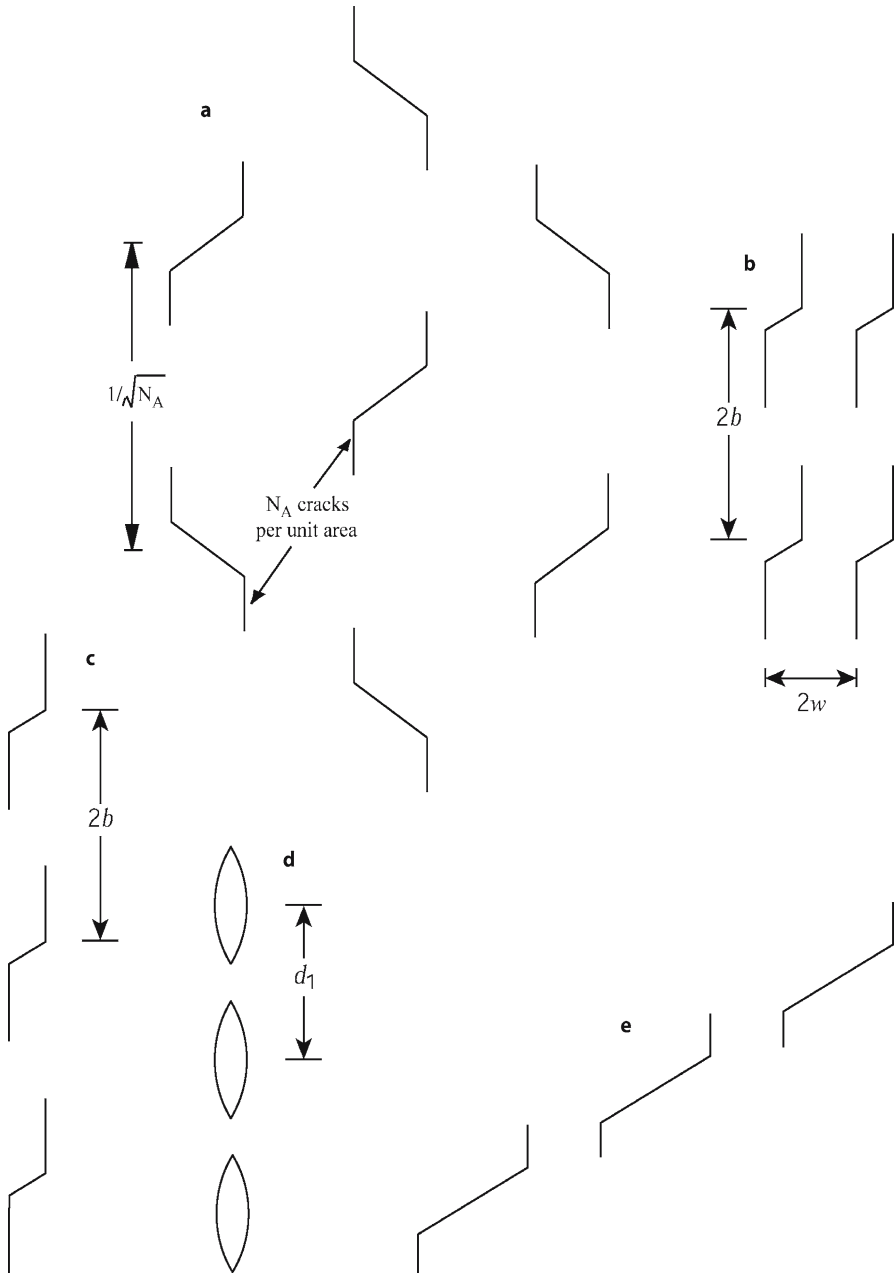


**Fig. 48.** Geometric models of wing crack arrays proposed by (a) Ashby and Sammis (1990), (b,c) Kenney and Cook (1987), (d) Costin (1985), and (e) Horii and Nemat-Nasser (1985) to analyze crack interaction

ated at each sliding crack. The stress intensity tending to cause the nucleation and propagation of a wing crack is calculated and expressed in terms of a quantity

$$D = \pi(\ell + c \cos \gamma)^2 N_A = \pi \left( \frac{\ell}{c} + \cos \gamma \right)^2 \varepsilon_0$$

where  $N_A$  is the number of cracks per unit area and  $\varepsilon_0 = c^2 N_A$  is the 2-dimensional equivalent of the crack density introduced by Budiansky and O'Connell (1976) that was discussed in Sect. 5.4.2. The quantity  $D$  is called the *damage parameter*. Before wing cracks nucleate, the length  $\ell = 0$  and therefore the initial damage is represented by

$$D_0 = \pi(c \cos \gamma)^2 N_A = \pi \varepsilon_0 \cos^2 \gamma$$

Ashby and Sammis (1990) have estimated the additional contribution of the crack interaction to the stress intensity factor, added this to the stress intensity factor for the isolated crack (Eq. 6.4), and concluded that the total stress intensity factor may increase with increasing  $\ell$  over a certain range of crack lengths, implying the possibility of unstable wing crack growth that may lead to coalescence with neighbouring cracks. This analysis leads to the following expression for the relation between the principal stresses as a function of the damage  $D$ :

$$\sigma_1 = \left[ C_1 + \frac{C_4 (\sqrt{D/D_0} - 1)}{1 + \sqrt{\pi D_0} \frac{\sqrt{D/D_0} - 1}{1 - \sqrt{D}}} \right] \sigma_3 + \frac{\sqrt{\sqrt{D/D_0} - 1 + 0.1/\cos \gamma}}{1 + \sqrt{\pi D_0} \frac{\sqrt{D/D_0} - 1}{1 - \sqrt{D}}} \frac{C_4}{\sqrt{\cos \gamma}} \frac{K_{Ic}}{\sqrt{\pi c}} \quad (6.5)$$

where

$$C_1 = \frac{\sqrt{1 + \mu^2} + \mu}{\sqrt{1 + \mu^2} - \mu}$$

and

$$C_4 = \frac{\sqrt{30} \cos \gamma}{\sqrt{1 + \mu^2} - \mu}$$

Although the ultimate failure and instability arise from the interaction and coalescence of numerous microcracks that have nucleated from sliding cracks with a range of  $\gamma$  values, it is implicitly assumed in Ashby and Sammis' (1990) derivation of the above equation that the cooperative effects of the multiplicity of cracks are approximated by choosing an "effective" value of  $\gamma = 45^\circ$ , which implies that  $D_0 = (\pi/2)\varepsilon_0$ , and  $D = D_0 + \pi \ell N_A$ . The loading history is then represented by the evolution of the damage parameter  $D$ .

If one specifies the material parameters  $D_0$  (or equivalently  $\varepsilon_0$ ),  $K_{Ic}/\sqrt{\pi c}$  and  $\mu$ , then the evolution of the principal stress  $\sigma_1$  as a function of damage  $D$  at a fixed confining stress  $\sigma_3$  can be calculated using Eq. 6.5. In the brittle regime, the damage accumulation is manifested first by strain hardening and then by strain softening (Fig. 49). The critical stress state at which instability occurs is identified as the peak value at the transition from hardening to softening for each curve. For example, the unconfined peak stress for the case shown in Fig. 49 is given by  $\sigma_1 = 4.26 K_{Ic}/\sqrt{\pi c}$ . Repeating the calculation for different values of fixed  $\sigma_3$  allows one to map out the brittle failure envelope in the principal stress space (Fig. 50). To a first approximation this failure envelope can be described empirically by a linear relation

**Fig. 49.** Normalized maximum principal stress as function of damage according to Eq. 6.5 for initial damage  $D_0 = 0.1$  and friction coefficient  $\mu = 0.6$ . The curves for three different values of normalized minimum principal stress are shown

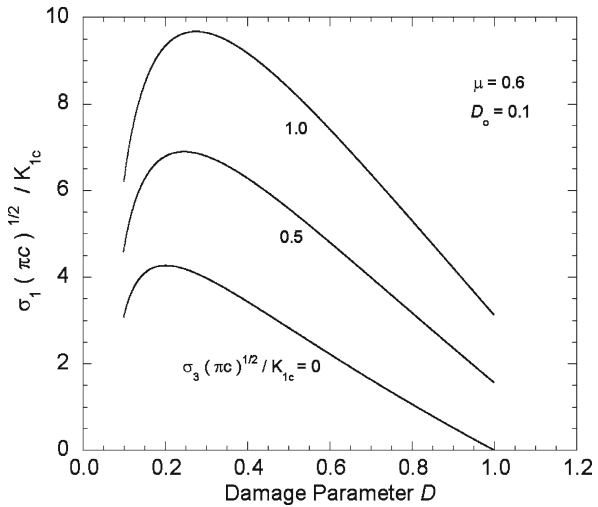
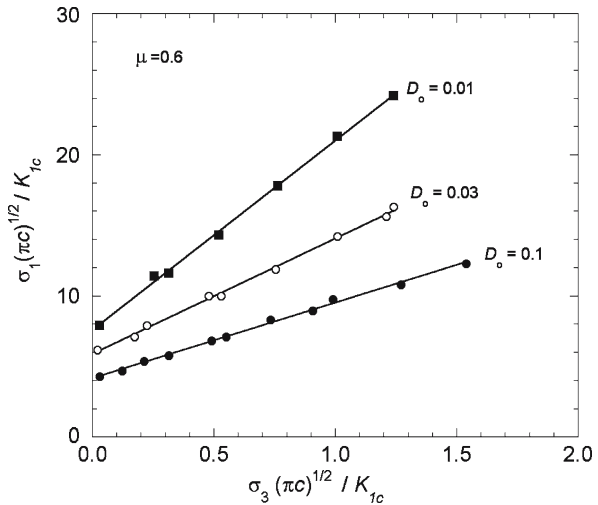


**Fig. 50.** The peak value of the normalized maximum principal stress as function of the normalized minimum principal stress according to Eq. 6.5 for friction coefficient  $\mu = 0.6$  and three different values of initial damage (after Ashby and Sammis 1990)



$$\sigma_1 = A(\mu, \varepsilon_0)\sigma_3 + B(\mu, \varepsilon_0)K_{Ic} / \sqrt{\pi c} \quad (6.6)$$

This model predicts that at the same confining pressure, a lower strength is associated with a sample with higher initial damage (Fig. 50). With reference to Eqs. 3.1 and 3.2, it can be seen that this damage mechanics model connects the empirically determined “coefficient of internal friction”  $\tan \phi$  to the friction coefficient of the sliding crack  $\mu$  and initial damage  $\varepsilon_0$ . In addition the “cohesion”  $\tau_0$  is related also to the third parameter  $K_{Ic}/\sqrt{\pi c}$ . Ashby and Sammis (1990) also developed a 3-dimensional model, with damage characterized by the parameter

$$D = (4\pi/3)(\ell + c \cos \gamma)^3 N_V$$

with  $N_V$  denoting the number of cracks per unit volume. Additional assumptions have to be made to deal with the geometric complexity, and the final expressions are more involved.

If triaxial compression data for the onset of dilatancy and peak stress follow the linear trends described by Eqs. 6.2 and 6.6, then the slopes and intercepts of the two sets of stress data provide four constraints for inferring the three parameters  $\varepsilon_0$ ,  $K_{Ic}/\sqrt{\pi c}$  and  $\mu$ . However the scatter of the data for the dilation stress (Fig. 27) is such that the intercept cannot be easily determined. The more practical approach is to use the dilation stress data and Eq. 6.2 to constrain  $\mu$ , and the peak stress data and Eq. 6.6 to constrain  $\varepsilon_0$  and  $K_{Ic}/\sqrt{\pi c}$ . The parameters so inferred for a variety of rock types are compiled in Table 3.

**Table 3.** Fracture mechanics and microstructural parameters inferred from damage mechanics model of Ashby and Sammis (1990). Ashby and Sammis (1990) used the 3-dimensional version of their model, and their inferred values of the initial damage are converted using the relation  $\varepsilon_0 = c^3 N_V = 3\sqrt{2}(2\pi)D_0$ , whereas the other studies used the 2-dimensional version, and their inferred values are converted using  $\varepsilon_0 = c^2 N_A = 2/\pi D_0$

Rock type	Porosity	$\mu$	$K_{Ic}/(\pi c)^{1/2}$ (MPa)	$\varepsilon_0$	Reference
Akaishi eclogite	0.004	0.60	32.6	0.05	Ashby and Sammis 1990
Murotomisaki gabbro	0.004	0.55	28.2	0.08	Ashby and Sammis 1990
Horoman dunite	0.005	0.60	25.2	0.03	Ashby and Sammis 1990
Four-mile gneiss	0.007	0.24	95.0	0.07	Rawling, Baud and Wong 2002
Westerly granite	0.011	0.64	25.2	0.01	Ashby and Sammis 1990
Carrara marble	0.011	0.60	27.3	0.08	Ashby and Sammis 1990
Solnhofen limestone	0.03	0.53	97.0	0.16	Baud, Schubnel and Wong 2000
Bunter sandstone	0.15	0.60	12.5	0.10	Ashby and Sammis 1990
Darley Dale sandstone (dry)	0.13	0.74	27.0	0.28	Baud, Schubnel and Wong 2000
Darley Dale sandstone (wet)	0.13	0.66	25.0	0.28	Baud, Schubnel and Wong 2000
Berea sandstone (dry)	0.21	0.56	29.0	0.19	Baud, Schubnel and Wong 2000
Berea sandstone (wet)	0.21	0.51	28.5	0.19	Baud, Schubnel and Wong 2000

There seems to be an overall trend for the initial damage  $\varepsilon_0$  to increase with increasing porosity. The inferred values of friction coefficient fall within a relatively narrow range that is comparable to typical values for silicate minerals and rocks, except for the Four-mile gneiss. The relatively low value of  $\mu = 0.24$  was determined from mechanical data of this foliated rock with  $\sigma_1$  inclined at  $45^\circ$  to the foliation. Microstructural observations (Rawling, Baud and Wong 2002) showed that the extensile wing cracks nucleated from sliding cracks predominantly located along cleavages of biotite grains, which are known to have such a low friction coefficient (Horn and Deere 1962). It is commonly postulated that  $c$  should scale as the average grain size, with the implication that the peak stress depends on the inverse square root of grain size (Fanella and Krajcinovic 1988; Fredrich, Evans and Wong 1990; Wong, Chau and Wang 1996; Hatzor and Palchik 1997). If the fracture toughness for wing crack propagation does not vary significantly, then the normalized parameter  $K_{IC}/\sqrt{\pi c}$  is expected to increase with decreasing grain size, which can explain its relatively high value for the ultrafine grained Solnhofen limestone.

The inelastic and failure behaviour is qualitatively similar in other crack interaction models that consider somewhat different geometric configurations. Kemeny and Cook (1987) proposed an interaction model with a doubly periodic array of wing cracks. Since the axial and lateral spacings are  $2b$  and  $2w$  respectively (Fig. 48b), the array has an initial crack density of  $\varepsilon_0 = c^2/(4wb)$ . If the magnitude of  $w$  is comparable to  $b$ , then the post-peak behaviour is relatively stable, corresponding to Class I strain softening (Chapt. 5). On the other hand, Class II behaviour is observed if  $w \gg b$  and Kemeny and Cook (1987) suggested that an alternative interactive model with a collinear crack array (with an initial crack density  $\varepsilon_0 < c^2/(4w^2)$ ) would be more appropriate (Fig. 48c). Similar collinear models with axial wing cracks were adopted by Fanella (1990) and Gambarotta (1993) to analyze the brittle failure of concrete in uniaxial compression. Horii and Nemat-Nasser (1985) and Fanella (1990) analyzed a collinear row of wing cracks aligned at an angle to  $\sigma_1$  (Fig. 48e). Except for Horii and Nemat-Nasser's (1985) numerical simulations, all these interaction models are based on analytic approximations.

Costin (1985), Li and Nordlund (1993), and Rudnicki and Chau (1996) considered the interaction of a collinear row of axial extensile cracks (with axial spacing  $d_1$ ) that were not connected to sliding cracks (Fig. 48d). In Rudnicki and Chau's (1996) model, the tensile stress concentration in a rock subjected to triaxial compression is given by

$$f'g(a)\frac{\sigma_1 - \sigma_3}{3} - \sigma_3$$

where  $a$  is the radius of a penny-shaped crack aligned with  $\sigma_1$  and  $f'$  is the stress concentration factor (Sect. 6.2.1). The function  $g$  evolves with crack extension (from initial radius  $a_0$  to current radius  $a$ ) according to

$$g(a) = \frac{1}{a/a_0} \sqrt{\frac{1 - (a_0/d_1)^2}{1 - (a/d_1)^2}} \quad (6.7)$$

The term  $(a/a_0)^{-1}$  describes the decrease of tensile stress as the crack grows away from the local inhomogeneity, corresponding to the stable propagation behaviour discussed in the previous section. The term

$$\frac{1}{\sqrt{1 - (a/d_1)^2}}$$

which describes the tensile stress enhancement due to crack interaction is an analytic approximation of Horii and Nemat-Nasser's (1983) numerical results.

The interaction models discussed so far focus on specific geometric configurations of cracks in a representative elementary volume of the brittle rock. An alternative approach is to focus on an individual crack that is embedded in an effective medium that corresponds to a cracked solid. The stiffness of the effective medium decreases with increasing damage in the solid, and its evolution can be modelled by a homogenization method that accounts for crack interaction. Lee and Ju (1991) adopted the self-consistent method to evaluate the elastic stiffness tensor as a function of damage, taking into account both stress-induced microcracking and anisotropy. Their self-consistent model predicts enhanced axial and volumetric strains, compared with those evaluated at the same stress level with a model assuming constant elastic moduli. The discrepancy between the two types of models is more pronounced in a solid with higher initial damage.

#### 6.2.4

#### General Comments on Micromechanics-Based Damage Mechanics Models for Compact Rock

The damage mechanics models have provided useful insight into the mechanics of compressive failure in compact rock. They have advanced beyond the Griffith type of models (discussed in Chapt. 4) in several important aspects. First, the micromechanical basis for the development of dilatancy and brittle faulting is established in terms of the nucleation, propagation, and coalescence of stress-induced microcracks. Second, the models predict stress-strain and hysteretic behaviours that are in reasonable agreement with experimental data. Lastly, the fracture mechanics and microstructural parameters that control these micromechanical processes are identified. For reference, these parameters and values that have been adopted to model the inelastic (Fig. 27) and failure (Fig. 9) behaviour of Westerly granite are compiled in Table 4.

An advantage of the wing crack model is the mathematical convenience by which the local stress field can be related to the remotely applied stresses. However, it has been criticized on the ground that wing cracks which nucleate from pre-existing sliding cracks are seldom observed in deformed samples under the microscope (Tapponnier and Brace 1976; Holcomb and Stevens 1980; Kranz 1983), although Moore and Lockner (1995) observe a zig-zag propagation of shear fracture in granite that has some points of resemblance to the wing-crack model. Nemat-Nasser (1985) argued that since the growth behaviour of a wing crack is qualitatively similar to that induced by stress concentrations arising from other mechanisms (such as elastic mismatch or equidimen-

**Table 4.** Fracture mechanics and microstructural parameters used in wing crack models for development of dilatancy and brittle failure in Westerly granite

Reference	$\mu$	$K_{Ic}$ (MPa m <sup>1/2</sup> )	$c$ ( $\mu\text{m}$ )	$K_{Ic}/\sqrt{\pi c}$ (MPa)	$\epsilon_0$
Moss and Gupta 1982	0.65	1.86	375	54	0.07
Nemat-Nasser and Obata 1988	0.1	0.7	250	25	0.34
Ashby and Sammis 1990; Gupta and Bergström 1997	0.64	1.0	500	25	0.01
Kemeny and Cook 1991	0.4	1.0	150	46	<0.02
Okui and Horii 1997	0.2–0.4	1.0	20	126	0.3
Lockner and Madden 1991b	0.5	1.0	$\ell_0$ ( $\mu\text{m}$ ) = 100	$K_{Ic}/\sqrt{\pi \ell_0} = 56$ MPa	
Costin 1985; Rudnicki and Chau 1996	$f' = 1.14$	1.23	$a_0$ ( $\mu\text{m}$ ) = 700	$K_{Ic}/\sqrt{\pi a_0} = 26$ MPa	$d_1 = 2.3$ mm

sional voids), it provides a useful mathematical analogue for analyzing the propagation and coalescence of a multiplicity of stress-induced cracks in a compact rock. Indeed the qualitative agreement between theoretical predictions of Costin's (1983, 1985) generic model and various wing crack models seem to support this argument.

Since linear elastic fracture mechanics is used to describe the damage process on the microstructural scale, the fracture toughness  $K_{Ic}$  is the key parameter that controls the nucleation and propagation of wing cracks in all these models. The values of  $K_{Ic}$  in most models are comparable to laboratory measurements for the constituent minerals (Appendix 1). Guided by laboratory measurements for tensile fracture of quartz, a  $K_{Ic}$  value on the order of 1 MPa m<sup>1/2</sup> is usually assumed for compact silicate rocks such as granite, aplite, gabbro, and gneiss (Kachanov 1982a,b; Moss and Gupta 1982; Costin 1983, 1985; Wong 1985; Nemat-Nasser and Obata 1988; Ashby and Sammis 1990; Kemeny and Cook 1991; Li and Nordlund 1993; Okui and Horii 1997). The only exception seems to be Senseny's (1986) choice of 0.385 MPa m<sup>1/2</sup> for Algeria granite. Somewhat lower values (ranging from to 0.3–0.7 MPa m<sup>1/2</sup>) have been used for porous sandstone and tuff (Costin 1985; Ashby and Sammis 1990; Myer et al. 1992; Pestman and van Munster 1996). Values in the range of 0.3–0.6 MPa m<sup>1/2</sup> have been used for carbonate rocks (Kachanov 1982a,b; Ashby and Sammis 1990; Myer et al. 1992; Wong, Chau and Wang 1996), with the exception of Tennessee marble which seems to require an anomalously high value of  $\sim 2$  MPa m<sup>1/2</sup> (Kachanov 1982a,b; Costin 1985). A value on the order of 0.1 MPa m<sup>1/2</sup> is commonly used for modelling the compressive failure of ice (Schulson et al. 1991).

However, it should be noted that predictions of the wing crack models are not very sensitive to the value of the toughness by itself, but rather to the ratio  $K_{Ic}/\sqrt{\pi c}$  which has the dimension of a stress. As indicated in Table 4, although the models used com-



parable toughness values, the choices for the pre-existing crack length differ significantly. It is commonly postulated that  $c$  should scale as the average grain size, with the implication that the peak stress depends on the inverse square root of grain size (Fanella and Krajcinovic 1988; Fredrich, Evans and Wong 1990; Wong, Chau and Wang 1996; Hatzor and Palchik 1997). The  $c$  values compiled in Table 4 range from about 1 to 0.1 times the average grain size of Westerly granite, and consequently the ratio  $K_{IC}/\sqrt{\pi c}$  varies by a factor of 5 among the models. There are also significant differences among the values adopted for the friction coefficient  $\mu$  and initial damage parameter  $\epsilon_0$ .

These apparent discrepancies may be attributed to the differences in approach by which the compiled parameters were inferred from fitting the model predictions to very different ranges of confining pressure and different aspects of mechanical behaviour. A common feature of the damage mechanics models is their prediction that the failure envelope is linear. If the peak axial stress is plotted versus the confining pressure, the slope increases with increasing friction  $\mu$  and the intercept increases with increasing value of the ratio  $K_{IC}/\sqrt{\pi c}$ . While the observed failure envelope can be approximated as linear over a limited range of pressures, it is nonlinear over a broad range of pressures (Fig. 9), with a slope that decreases with increasing pressure. Therefore it is a limitation intrinsic to this type of model that non-unique values of the two parameters  $\mu$  and  $K_{IC}/\sqrt{\pi c}$  are obtained by fitting the models to peak stress data over different ranges of pressure.

For models that do not consider crack interaction (Moss and Gupta 1982; Nemat-Nasser and Obata 1988), the comparison between theory and experiment focuses on the onset and development of dilatancy. The inelastic volumetric strain increases with decreasing friction  $\mu$  and increasing initial damage  $\epsilon_0$ . Nemat-Nasser and Obata (1988) emphasized that a value of  $\mu = 0.1$  was necessary for fitting the volumetric strain data from triaxial compression experiments, even though this choice is significantly lower than friction coefficients of common minerals (Horn and Deere 1962). While Moss and Gupta (1982) managed to fit uniaxial compression data for dilatancy development with a relatively high friction coefficient and low initial damage, their model significantly underestimates the volumetric strain at a confining pressure of 50 MPa reported by Zoback and Byerlee (1975a).

A premise of damage mechanics is that the evolution of stress-induced microstructure can be described by a finite number of internal variables or damage parameters. A single scalar parameter is used in most models that have been developed. However, it is probably unrealistic to expect the complexity of pore geometry and micromechanical processes in a brittle rock to be fully captured by a single internal variable over a relatively broad range of stress conditions. Proposals have been made to characterize the evolution of damage and its anisotropy by a tensor variable (e.g., Oda 1982; Krajcinovic and Mastilovic 1995). Such an approach may account for the development of stress-induced anisotropy (Chapt. 5) and strength anisotropy (Sect. 3.7). Wing cracks nucleate and propagate in a 2-dimensional, isotropic medium in most models. New theoretical results on wing crack growth in an anisotropic medium (Gao and Chiu 1992; Azhdari and Nemat-Nasser 1996) are now available. Experimental and theoretical investigations of 3-dimensional wing crack behaviour are also being pursued (Germanovich et al. 1994). To calculate the inelastic strain, analytic approxima-

tions are employed in the models. Jeyakumaran and Rudnicki's (1995) accurate numerical simulations reveal certain complications related to the opening and propagation of wing cracks that have not been included in the approximate models. The models all assume the pre-existing crack length, friction coefficient and fracture toughness to be constant. To analyze the influence of geometric and material heterogeneities would require the development of a stochastic model of brittle failure.

### 6.2.5

#### Stochastic Model of Brittle Failure in Compact Rock

The actual microcrack population of a brittle rock is characterized by a broad range of sizes. In response to an applied stress field, microcracking activity is also distributed heterogeneously in a rock sample. To account for these geometric complexities, two key questions need to be addressed in a micromechanical model. First, what geometric attributes are associated with the pore space at the critical point when the microcracks of different sizes coalesce to form a macroscopic fracture zone? Second, how do the crack geometry and statistics evolve with loading to attain this critical geometry, which corresponds to the onset of shear localization?

Percolation theory (Stauffer and Aharony 1992; Turcotte 1992) can be used to address the first question. As discussed in Chapt. 5, the theory is useful for characterizing the first critical state (called the percolation threshold) at which a continuous connection exists in the pore space. Since the permeabilities of most crustal rocks are greater than zero, the connectivity of the pore space is such that it is above the percolation threshold. As damage accumulates in response to stress, the connectivity increases further until the pore space reaches a second critical state at which an initially intact sample develops a macroscopic fracture zone and fragments into two or more pieces.

Allègre, Le Mouél and Provost (1982) analyzed cubic arrays of many different scales embedded in a volume. They first considered an array of eight cubes, which are either "fragile" or "sound", in accordance with the probabilities  $p_0$  and  $1 - p_0$  respectively. By considering all 22 topologically different configurations, the probability  $p_1$  for the cubic array to be fragmented can be expressed in terms of  $p_0$ . On the next scale, a similar array of eight cubes is considered, with the assumption that each cube has an updated "fragility probability" of  $p_1$ . Using this renormalization group method to analyze the multiple scale problem, Allègre, Le Mouél and Provost (1982) showed that the probability converges to the value 1 (corresponding to the development of a macroscopic fracture) if  $p_0 > 0.896$ .

Madden (1983) analyzed a similar cubic network. To compare with microstructural observations, he related the probability to crack density and clarified the influence of stress-induced anisotropy on mechanical failure. He characterized the crack density by three components ( $\varepsilon_x$ ,  $\varepsilon_y$ , and  $\varepsilon_z$ ), so that the sum is equal to the scalar crack density  $\varepsilon_0$  as defined in previous analyses of elastic properties and damage mechanics. The percolation threshold for the cubic array is at  $\varepsilon_0 = 0.75$ , and therefore hydraulic and electrical conduction in an isotropic array can occur if  $\varepsilon_x (= \varepsilon_y = \varepsilon_z) > 0.25$ . Madden's (1983) renormalization group analysis showed that the inception of mechanical failure in an anisotropic array requires the crack density in a preferred orientation to increase to

more than three times the density at the percolation threshold. For example, if the crack density for a direction transverse to  $\sigma_1$  is 0.4, then mechanical failure is predicted to occur if the crack density in the  $\sigma_1$  direction increases to about 0.85, corresponding to  $\varepsilon_0 \approx 1.45$ . Allègre and Le Mouél (1994) used an analogous approach to analyze the effect of anisotropy on the brittle-ductile transition. Bebbington, Vere-Jones and Zheng (1990) and Guéguen, Chelidze and Le Ravalec (1997) provided further discussion of the use and limitation of percolation theory.

For these models the critical crack density at instability is  $\varepsilon_{cr} \sim 1$ , and since the inelastic dilational strain  $\varepsilon_v^{\text{peak}}$  at peak stress is related to the crack density by

$$-\varepsilon_v^{\text{peak}} \sim \frac{4\pi}{3} \frac{c}{a} \varepsilon_{cr}$$

(if the size and aspect ratio  $c/a$  of the stress-induced cracks are narrowly distributed), one would expect that  $-\varepsilon_v^{\text{peak}} \sim 4/3\pi(c/a)$  near the peak stress. This seems to be in agreement with the experimental observations (compiled in Table 1 in Chapt. 5) that  $-\varepsilon_v^{\text{peak}}$  values for both compact and porous rocks fall in a relatively narrow range of 0.002–0.019 which, according to this simple analysis, correspond to aspect ratios  $c/a$  approximately in the range of  $5 \times 10^{-3}$  to  $5 \times 10^{-4}$ .

While these models analyze the geometric attributes of the pore space necessary for the development of brittle fracture, they do not address the mechanics of cracking that induces the critical damage. Mechanical analysis of the progressive development of damage in a solid that initially contains a stochastic population of microcracks requires intensive computation. One approach is to simulate directly the cooperative behaviour of a large number of wing cracks, assuming that each crack extends in accordance with criteria discussed above. Myer et al. (1992) considered the average response of 10 000 cracks, with orientation  $\gamma$  randomly distributed between 0 and  $90^\circ$  and initial length  $c$  randomly distributed between an upper and a lower limit. This approach has the limitation that spatial development of strain localization cannot be simulated because interaction and coalescence among the cracks are not explicitly accounted for.

Lockner and Madden (1991a,b) considered a triangular network made up of 5 800 elements of dimension  $\ell_0$ . To simulate compressive failure in Westerly granite at confining pressures ranging from 5 MPa to 800 MPa, they used a network with 20% of its elements completely cracked and 80% partially cracked. At a sufficiently high normal stress, a crack may close and provide frictional resistance. Table 4 includes parameters used in this multiple-crack model. A renormalization group method was used to calculate the elastic response of the cracked solid. A limitation of this model is that it assumes that crack growth is always unstable, rupturing the entire length of  $\ell_0$ , contrary to the microstructural observations of stable, incremental growth of stress-induced microcracks. Since the stress field associated with the incremental growth of an individual crack was not computed, the fracture mechanics criterion was not implemented in a rigorous manner. In practice, the criterion was based on a tensile strength that scales as  $K_{Ic} \sqrt{\ell_0}$ . Nevertheless, the model captures some of the key features of brittle failure, including the development of dilatancy and shear localization. If only

mode-I cracking was allowed in the model, the brittle strength would follow a linear trend in principal stress space. To simulate the nonlinear failure envelope (Fig. 9), Lockner and Madden (1991b) had to incorporate mode-II cracking, with the criterion  $K_{IIc} = 15 \text{ MPa m}^{1/2}$ . Their model predicts that the shear mode of microcracking that becomes pervasive under elevated pressures is responsible for the nonlinear curvature of the failure envelope.

Recently Okui and Horii (1997) proposed an “interaction field theory” that accounts for the fracture mechanics and interaction of wing cracks in a more rigorous manner. A continuum model with a statistical distribution of crack density was analyzed. The stress field within the finite-element mesh is characterized by a spatially heterogeneous “interaction field” that evolves with damage (Okui, Horii and Akiyama 1993). This field variable is evaluated by the method of pseudo-tractions (Horii and Nemat-Nasser 1985). The local stress field that drives crack growth at a given location is characterized by the sum of interaction field and the average stress. This continuum model can simulate the development of strain softening as well as shear localization. The parameters used by Okui and Horii (1997) to match the failure behaviour of Westerly granite are also included in Table 4. It can be seen that the value of  $\epsilon_0$  is significantly higher than what was used in damage mechanics models that build in relatively unstable geometric configurations to simulate coalescence (e.g., Ashby and Sammis 1990; Kemeny and Cook 1991). While they modelled the stress field and fracture mechanics in a relatively rigorous manner, Okui and Horii (1997) were restricted by computational constraint to consider a relatively small finite element mesh. Consequently the spatial resolution on the development of shear localization is somewhat less than that of Lockner and Madden (1991a,b).

The models discussed so far are based on the assumption that the local strength and fracture toughness are uniform. However, difference in mineralogy and heterogeneity of grain boundary structure are expected to result in non-uniform strength. McClintock and co-workers have modelled both analytically and numerically the development of a pattern of stable microcracks in a hexagonal array of potential crack sites having an assumed statistical distribution of strengths; in the model, account is taken of the change in the stress distribution as each new crack appears (McClintock and Mayson 1977; McClintock and Zaverl 1979). With increase in stress, unstable macroscopic cracking eventually results from the juxtaposition of enough microcracks to form a crack of critical length, and a stress maximum is reached. It is shown that the value of this maximum is lower the larger the size of the specimen, thus predicting the usual size effect (cf. Sect. 3.5). However, it is also found that the initiation of microcracking occurs at a lower fraction of the maximum stress the larger the specimen.

Gupta and Bergström (1997) adopted a similar approach to analyze a continuum model made up of “crack clusters”. The evolution of damage within an individual cluster was considered to be similar to the model of Ashby and Sammis (1990). Accumulation of damage reduces the elastic moduli of a given cluster, resulting in stress concentration in its vicinity. The stress field was modelled as that due to an elliptical inhomogeneity, and Monte Carlo simulations were conducted on an assembly of 2500 clusters. The development of shear localization was modelled, and the strength envelopes of Westerly granite and several other rock types were simulated using parameters identical to those used by Ashby and Sammis (1990). Although the size effect was not ad-

dressed, it is expected to be analogous to that observed by McClintock and Zaverl (1979) since a Weibull-type of strength distribution was assumed in both models. Indeed a major uncertainty in this type of model is related to the choice of the Weibull parameters, which are relatively unconstrained in the absence of systematic measurements. It should also be noted that most statistical models are limited in being 2-dimensional. More realistic, 3-dimensional modelling requires intensive computation that may be feasible in the future.

## 6.2.6

### Time-Dependent Failure of Compact Rock

The micromechanical models discussed so far are based on the criterion that crack propagation occurs when the stress intensity factor attains the critical value  $K_c$ . These theoretical models neglect subcritical crack growth and its kinetics, which have to be considered in analyzing the time-dependent behaviour of brittle failure (Sect. 3.4). To develop a damage mechanics model applicable to time-dependent behaviour, one of the several subcritical crack growth laws described in Appendix 1 needs to be incorporated. For mathematical convenience, earlier models approximated these laws by relating the crack velocity  $v$  directly to the applied stress field  $\sigma$ , thus neglecting details of the stress concentration that drives crack growth. Assuming a power law of the form  $v \propto \sigma^n$ , Sano, Ito and Terada (1981) developed a model that predicts that the peak stress is related to the stress rate by a power law. Using a similar approach, Spetzler, Sondergeld and Getting (1981) used an exponential law of the form  $v \propto e^{b\sigma}$  to derive a model that predicts the peak stress to depend on logarithm of stress rate.

Analytic solutions are not available for models that account for the fracture mechanics and kinetics in a more rigorous manner. Kemeny (1991) considered the wing crack model assuming a subcritical crack growth law of the form  $v \propto K^n$ . A value of  $n = 31$  was used to match the uniaxial compressive strength of Oshima granite at strain rates from  $10^{-5}$  to  $10^{-8} \text{ s}^{-1}$  (Sano, Ito and Terada 1981). Costin and Mecholsky (1983) started from Costin's (1983) damage mechanics model and incorporated a subcritical crack growth law of the form  $v \propto \exp(\beta K/K_c)$ . A value of  $\beta = 31.3$  was used to match the uniaxial compressive strength of dry and saturated Westerly granite at strain rates from  $10^{-2}$  to  $10^{-8} \text{ s}^{-1}$ . The model predicts that at high strain rates ( $> 10^{-1} \text{ s}^{-1}$  or so) the peak stresses are rate-independent because loading occurs so rapidly that the stress corrosion mechanism has little time to act. At lower strain rates, stress corrosion becomes increasingly important, leading to a progressive decrease in strength with decreasing strain rate. Finally a point is reached where the loading rate is so slow that stress corrosion can completely relax the local tensile stresses, corresponding to a threshold stress below which the rock will not fail. This regime occurs at a relatively low strain rate that was not attained in the experiments.

A similar approach can be adopted to analyze creep behaviour under a constant applied stress. Assuming a power law for subcritical crack growth, Yoshida and Horii (1992) applied the wing crack model using a value of  $n = 30$ . Reasonable agreement was obtained with data on time-to-failure of Barre granite at different stress levels obtained by Kranz (1980) at confining pressures up to 198 MPa. Similar analyses were performed by Kemeny (1991), Costin and Mecholsky (1983), and Lockner (1993b). More

elaborate statistical models were also analyzed by Lockner and Madden (1991b), and Okui and Horii (1997). See also Lyakhovskiy, Ben-Zion and Agnon (1997), Renshaw and Schulson (1998) and Lockner (1998).

## **6.3 Micromechanical Theory for Porous Rock**

### **6.3.1 General**

As noted in Sect. 5.7.3, the term porous rock covers a range of granular materials that can be viewed as extending from the strongly cohesive to the weakly cohesive. The modelling of their behaviour therefore is most simply done by considering these two end members. In strongly cohesive rock the intergranular boundaries play little role and the structure can be idealized in terms of more or less equant pores embedded in an elastic continuum. The pores act as stress raisers for the initiation of microcracking which can then propagate through the porous medium and determine the mechanical behaviour. In contrast, in weakly cohesive rock, the grain boundaries or grain contacts are of primary importance. The bonds at the grain contacts are readily ruptured by applied stress, allowing neighbouring grains to slip and rotate relative to each other. The material can then be idealized as a particulate system in which the particles can be variously viewed as being rigid, elastic, or subject to intragranular fracture. We shall now elaborate on these two types of model for porous rock.

### **6.3.2 Strongly Cohesive Porous Rock**

In strongly cohesive porous rock the representative elementary volume may be idealized as an equant pore embedded in an elastic continuum. Applied macroscopic stress can induce localized stress concentration at the pore and lead to microcrack initiation at the pore surface. Two-dimensional models based on axial cracks emanating from cylindrical pores have been considered by Sammis and Ashby (1986), Isida and Nemat-Nasser (1987a,b) and Wimmer and Karr (1996). The behaviour of such a pore-emanated crack is qualitatively similar to that of a wing crack induced by sliding on an inclined crack. The stable propagation of pore-emanated cracks initially results in dilatancy and strain hardening. As the cracks propagate further, they begin to interact and if their mean spacing is sufficiently small, crack propagation becomes unstable, possibly leading to crack coalescence. To consider the effect of a more acute geometry for crack initiation, Wong (1990a) extended the model to stress-induced cracks emanating from a tubular pore of nearly square cross-section. Although developed for compact rock, the wing crack model has also been adopted to analyze brittle failure behaviour in porous sandstone, limestone, and tuff (Costin 1985; Ashby and Sammis 1990; Myer et al. 1992; Atkinson and Cook 1993; Pestman and van Munster 1996; Gupta and Bergström 1997). The mechanical data can be matched using values of fracture toughness that are somewhat lower and of initial damage that are higher than those in compact rock.

### 6.3.3

#### Weakly Cohesive Porous Rock

When the bonding at grain contacts is easily ruptured and neighbouring grains are enabled to slip and rotate relative to each other, a micromechanical model is needed which accounts for this particulate motion since it plays a dominant role in the development of dilatancy or compaction associated with the brittle failure of weakly cohesive rock. The representative elementary volume now consists of a group of grains that can move relative to each other, exchange neighbours, and undergo dilation, comminution or other processes involved in accommodating the relative motions.

The elastic and inelastic behaviour of a particulate system has been studied extensively in soil mechanics using analytic and numerical models. Analytic models of spheres in elastic contact have also provided useful insight into the mechanical behaviour. In response to a hydrostatic stress, the macroscopic deformation is an integrated average of the localized deformation at all the grain contacts, which can be evaluated from the Hertz (1881) solution for spheres in elastic contact under normal loading. If the spheres are of different sizes or have different elastic properties, the contacts will also be subjected to tangential forces. A deviatoric stress field induces further tangential forces that can exceed the frictional resistance at the grain contacts, which may then undergo two possible modes of slip. Partial slip occurs in an outer annular region of the contact area when the induced tangential force is still insufficient to overcome the frictional resistance at the central region (Mindlin 1949). If the induced tangential force can overcome the frictional resistance at every point on a grain contact, relative particulate motion may then occur.

Elastic solutions for unslipped or partially slipped contacts have been incorporated into theoretical models that analyze the nonlinear elastic and anelastic behaviour of a porous granular aggregate, idealized as regular or random packing of spheres (Brandt 1955; Deresiewicz 1958; Walton 1987). The influence of cohesive bonding on the elastic deformation of a porous rock was considered by Digby (1981).

When the contacts undergo complete slip, the mechanical behaviour involves two complications. First, the deformation has a significant inelastic component due to particulate motion, and the micromechanics is strongly influenced by the kinematics of this relative grain movement. Second, photoelastic and microstructural observations (Drescher and de Josselin de Jong 1972; Oda 1978; Oda, Konishi and Nemat-Nasser 1983; Mehrabadi et al. 1988) have revealed a highly heterogeneous and anisotropic distribution of contact forces in a particulate system stressed to near failure. To be mathematically tractable, most numerical models consider a two-dimensional assembly of elastic circular disks, although some analyses have also been performed on elliptical (Rothenburg and Bathurst 1992) and oval (Konishi, Oda and Nemat-Nasser 1982) elements. Cundall's (1971) distinct element method has been widely used to model the kinematics, force distribution, and development of brittle failure in an assembly of circular disks. The modeller defines the domain in which grains are to be created, and specifies the grain size distribution as well as the friction coefficient and stiffness of the contacts. The computer code will create the assembly of disks by the use of a random-number generator, and then evaluate discrete quantities such as contact forces, slip at contacts, and particle velocities and rotations, as well as average quantities such

as stress, strain, and fabric. The numerical simulations show that the applied stresses are supported primarily by a small proportion of grains forming continuous chains that sustain excessively high contact forces (Cundall, Drescher and Strack 1982). Anisotropy of the applied stress field is reflected by corresponding fabric anisotropy (manifested by an anisotropic distribution of contact normal orientations). Dilatancy initiates at isolated clusters of grains, and the inception of shear localization occurs after dilatancy is pervasive throughout the sample (Thornton and Randall 1988; Jenkins, Cundall and Ishibashi 1989; Bathurst and Rothenburg 1990; Bardet and Proubet 1991). Numerical simulations on circular disks of a wide range of sizes suggest that shear localization and distributed particulate flow are promoted in well and poorly sorted assemblies, respectively (Antonellini and Pollard 1995).

A more realistic model of brittle failure in porous rock should consider cohesive grain contacts and the possibility of intragranular cracking induced by tensile stress concentration at grain contacts. This requires calculation of the intragranular stress field. Liu, Myer and Cook (1993) and Liu, Cook and Myer (1994) first used an energy minimizing method to calculate the stresses and displacement at grain contacts and then the boundary element method to calculate the stress field within a grain by imposing the appropriate boundary conditions and integrating the influences from all the grain contacts. They have considered regular and random packings of circular disks, with uniform or stochastic strength. Separate tensile strength criteria were adopted for debonding and breakage of grains, and a reduction of 25% in the Young's modulus of a crushed grain. The model predictions are in qualitative agreement with experimental and microstructural observations on development of dilatancy, strain softening and shear localization in weakly cohesive porous rock.

The growth of intragranular cracks in a porous rock may either dilate or compact the pore space. Intragranular cracks that emanate from grain contacts to propagate across an initially intact grain can break it into several fragments. The pores in the vicinity of crushed grains may then collapse, resulting in an overall compaction of the pore space. In contrast, stress-induced cracking that is distributed in unfragmented grains is expected to induce dilation.

Some attempts have been made to use fracture mechanics to model this type of stress-induced cracking. Considering a random packing of spheres of different sizes, Zhang, Wong and Davis (1990b) developed a fracture mechanics model to analyze the onset of grain crushing and pore collapse under hydrostatic loading. The tensile stress concentration in the proximity of the grain contact was derived from Hertzian contact theory. Their model predicts that the critical pressure  $P^*$  for grain crushing depends on porosity  $\phi$  and average grain radius  $r$  through a power law:  $P^* \propto (\phi r)^n$ , with an exponent  $n = -3/2$ . The constant of proportionality depends on the fracture toughness, elastic moduli and ratio of the pre-existing crack length to the grain radius. Application of deviatoric stresses enhances the tangential force and tensile stress concentration in the vicinity of a contact, and therefore promotes the development of grain crushing and pore collapse, which may initiate at a mean stress level as low as one-half of  $P^*$ . Mechanical data on sandstone suggest that a rock of lower porosity and smaller grain size requires a higher critical pressure for the onset of grain crushing, and therefore it is considered to be more "brittle" in the sense that dilatancy and shear localization are observed over a wider range of confining pressures (Wong, David and Zhu 1997).



A more comprehensive model would go beyond the initiation stage to analyze the development of grain fragmentation in more detail. Fracture mechanics can be used to model the propagation behaviour of Hertzian fractures in an intact grain under normal and shear loading (Shah and Wong 1997). However, the subsequent comminution and pore collapse processes involve significant geometric and kinematic complexities, the realistic modelling of which would require intensive computation.

## 6.4 Localization Theory

### 6.4.1

#### Application of Plasticity Theory and Bifurcation Analysis

Micromechanical theories analyze the development of a macroscopic fault by appealing to the growth and coalescence of microcracks. In a micromechanical model, the damage evolution and brittle failure processes hinge on local stress concentrations that are related to initial heterogeneity intrinsic to the rock. In contrast, theories of shear localization explore the macroscopic fault formation in a continuum without any explicit consideration of initial non-uniformity of material properties.

Plasticity models are commonly used to describe the macroscopic phenomenology of inelastic volume change and hardening in brittle rock. Plasticity theory is the part of continuum mechanics that deals with the irreversible or “plastic” deformation of solids under general states of stress. Historically plasticity theory was developed for the mechanical analysis of metals, which are fundamentally different from rock and soil in that the yield stresses are not sensitive to pressure and the inelastic deformations generally do not involve significant volumetric strains. Basic plasticity concepts relevant to brittle rock deformation and shear localization are summarized in Appendix 2. In adapting plasticity theory to dilatant, frictional materials, it is necessary to establish the appropriate characteristics of the yield function, the work hardening rule and the flow rule, taking into account the pressure dependence and the dilatancy.

Predictions of shear localization are sensitively dependent on the specific phenomenological model and constitutive parameters that have been chosen to characterize the mechanical behaviour. For a brittle rock, the constitutive model should capture key attributes of its inelastic behaviour, including its pressure sensitivity as well as the progressive development of strain hardening and dilatancy. Starting with phenomenological descriptions of the inelastic deformation, shear localization theories aim to derive conditions under which a uniform (or smoothly varying) deformation field becomes non-unique in the sense that it may have two (or more) solutions, one of which corresponds to deformation concentrated in a shear band (Hill 1962; Mandel 1966; Rice 1976; Vardoulakis and Sulem 1995; Bésuelle and Rudnicki 2004). The mathematical analysis of the bifurcation of continuing deformation into a localized shear band provides a critical condition that can be regarded as setting an upper limit to stability against fault formation (Rice 1980). This bifurcation condition occurs when the constitutive parameters evolve to attain certain critical values at the onset of shear localization.

In the case of many materials, such as ductile metals, the plastic deformation can be described by an “associated flow rule” (Appendix 2, Eq. A2.2). In materials obeying this rule the work done by each stress component can be regarded as being solely associated with the production of an incremental strain component having the same direction as the stress component, relative to the same Cartesian axes. Although laboratory data for carbonate rocks (Elliott and Brown 1985), sandstones (Wong, David and Zhu 1997), and saline ice (Schulson and Nickolayev 1995) deformed in the cataclastic flow regime (Chapt. 9) can show reasonable agreement with the associated flow rule, geomaterials that fail by brittle faulting generally show poor agreement. Laboratory data for soil (Chen 1984; Desai and Siriwardane 1984), compact crystalline rock (Rudnicki and Rice 1975), and porous sandstone (Wong, David and Zhu 1997) deformed in the brittle faulting regime consistently show dilatancy that is significantly lower than that predicted using an associated flow rule.

Therefore it is generally necessary to adopt a “non-associated” flow rule for describing hardening and dilatancy in a pressure-sensitive material such as rock, concrete and soil. As elaborated in Appendix 2, many proposals have been promulgated in the literature. The theoretical predictions of a localization analysis are discussed here with reference to the non-associated formulation due to Rudnicki and Rice (1975). In its simplest form (for the isotropic hardening case), the constitutive equations involve three parameters: an internal friction coefficient  $\mu'$  that characterizes the pressure dependence of the yield stress, a dilatancy factor  $\beta$  that is defined to be the ratio of the plastic volumetric strain to the plastic shear strain, and a hardening modulus  $h$  (which is positive for hardening and negative for softening behaviour). If  $\beta = \mu'$ , the flow law is associative. For brittle rock compressed in confinement, it is often observed that  $\beta < \mu'$  (Rudnicki and Rice 1975; Senseny, Fosum and Pfeifle 1983; Bernabé and Brace 1990; Wong, David and Zhu 1997; Rudnicki and Olsson 1998).

Given the boundary conditions that the loading is uniform and that the rock deforms in accordance with the prescribed constitutive equations, an analysis is performed to seek a solution to the strain field other than the trivial solution corresponding to uniform flow. If indeed such a solution exists, the point in the history of the deformation at which this non-uniqueness phenomenon enters is known as a “bifurcation”. For the Rudnicki and Rice (1975) model, such a bifurcation analysis provides the critical value of the hardening modulus ( $h_{cr}$ ) at the inception of shear localization and the angle  $\theta$  of the shear band (Eqs. A2.23–A2.25), as functions of the three constitutive parameters, the two elastic moduli, and a parameter  $N$  that represents the normalized intermediate principal deviatoric stress. Thus, if the flow stress satisfies a Drucker-Prager condition (Eq. A2.9) and the strain increment is calculated using (Eq. A2.1) with a plastic potential obtained by substituting a dilatancy parameter  $\beta$  for the pressure sensitivity parameter  $\mu'$  in the Drucker-Prager yield function, the Rudnicki and Rice (1975) analysis predicts that shear localization will occur when the condition (Eq. A2.25) for the hardening parameter  $h$  is met.

Figures 51a and 51b plot the theoretical predictions for the critical hardening modulus (normalized by the shear modulus  $G$ ) and the shear band angle as functions of the dilatancy factor  $\beta$  for internal friction coefficient  $\mu' = 0.9$  and Poisson's ratio  $\nu = 0.3$ . (Note that the angles shown are different from those tabulated by Rudnicki and Rice (1975) because a minor error in their calculations, pointed out by Perrin and Leblond

(1993), has been corrected here). A conclusion from the bifurcation analysis that has important implications for the extrapolation of laboratory data to geologic settings is that the critical conditions for the onset of shear localization are sensitively dependent on the loading configuration. The three different configurations shown in Figs. 51a and 51b have values of  $N = 1/\sqrt{3}$  (for axisymmetric compression),  $-1/\sqrt{3}$  (for axisymmetric extension), and 0 (for the shear test,  $\sigma_2 = \frac{1}{2}(\sigma_1 + \sigma_3)$ ), including the special case of  $\sigma_3 = -\sigma_1$ ,  $\sigma_2 = 0$ ), respectively. The parameter  $h_{cr}$  may be positive for brittle rock loaded in simple shear and plane strain, and indeed Ord, Vardoulakis and Kajewski (1991) concluded from their plane strain experiments that the onset of shear localization in Gosford sandstone occurred at the hardening stage. Similar behaviour was reported in a more comprehensive study in Tennessee marble by Holcomb and Rudnicki (2001), who also cautioned that the apparent hardening in a plane strain test can arise from a rapid increase of the mean stress even though the parameter  $h$  may actually be negative.

For a specific loading configuration the critical parameter  $h_{cr}$  is sensitive to both constitutive parameters  $\beta$  and  $\mu'$  (Fig. 51a). The first term in equation (Eq. A2.25) represents the influence of non-normality, but if  $N$  is relatively large (such as in axisymmetric compression) then this term represents a relatively small contribution to  $h_{cr}$ , which is then primarily controlled by the sum of  $\beta$  and  $\mu'$  in the second term. With increasing confining pressure, dilatancy is often inhibited and therefore  $\beta$  decreases, with the consequence that  $h_{cr}$  becomes less negative (assuming the non-normality contribution from the first term remains constant). The three curves for axisymmetric compression shown in Fig. 51a show that  $h_{cr}$  becomes less negative with increasing  $\mu'$ . For reference, Rudnicki and Rice (1975) inferred from triaxial compression data for several compact rocks that  $\mu'$  ranges from 0.4 to 0.9, and Wong, David and Zhu (1997) determined  $\mu'$  values between 0.5 and 1.0 for sandstones with porosities ranging from 15% to 35%.

The shear band angle (Fig. 51b) is also sensitively dependent on the loading configuration. Predictions for axisymmetric compression fall in the range of experimental observations of the fracture angle (summarized in Chapt. 3). For a fixed value of  $\mu'$ , the fracture angle  $\theta$  decreases with increasing dilatancy factor  $\beta$ . According to Eqs. A2.23 and A2.24 this angle is a function of  $\beta$  and  $\mu'$ , and therefore increasing  $\mu'$  is also expected to result in a shear band with a smaller angle. A comprehensive discussion of band orientation was presented recently by Bésuelle and Rudnicki (2004).

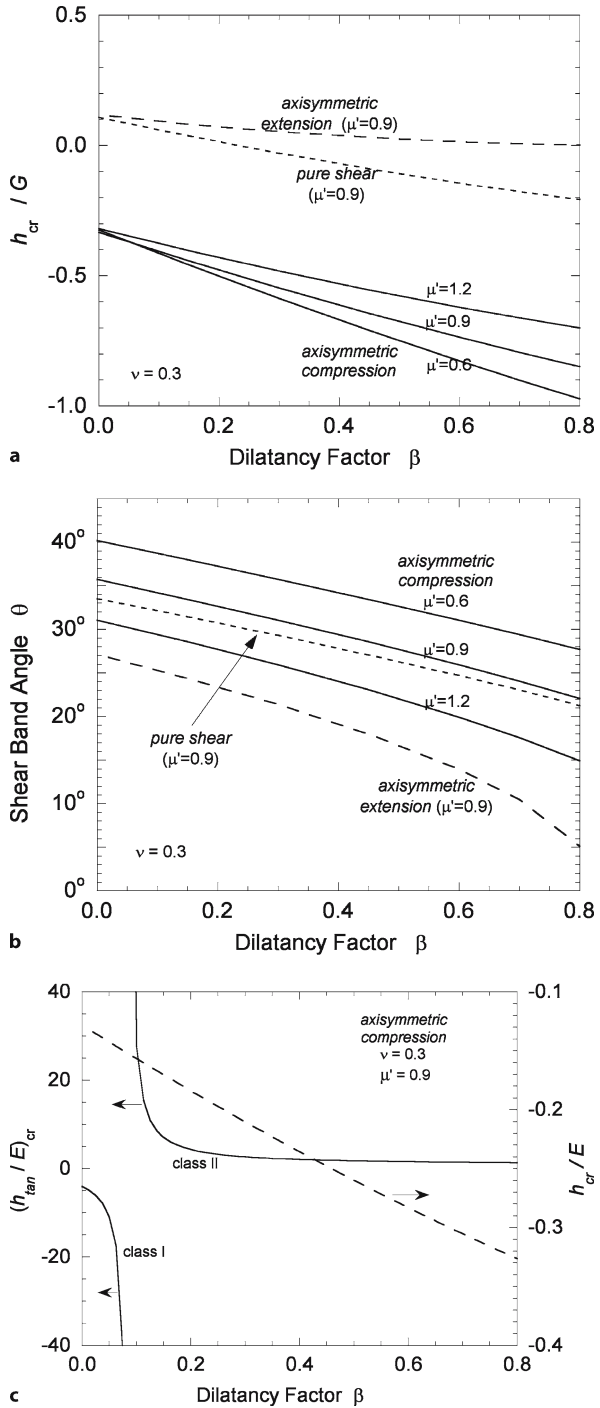
In the case of the axisymmetric triaxial compression test,  $h$  is related to the slope  $h_{tan}$  of the stress-strain curve by Eq. A2.20c). Thus, for this test, combining Eq. A2.20c and Eq. A2.25 and putting  $N = 1/\sqrt{3}$  leads to

$$\left(\frac{h_{tan}}{E}\right)_{cr} = \frac{2(\mu' - \beta)^2 - (1 - \nu)(\mu' + \beta + \sqrt{3})^2}{(1 + \nu)(\mu' - \beta)^2 - (1 - \nu)(6\sqrt{3}(\mu' + \beta) - 9)} \quad (6.8)$$

Figure 51c plots the above expression as a function of the dilatancy factor for  $\mu' = 0.9$  and  $\nu = 0.3$ , as well as the critical hardening modulus  $h_{cr}$  according to Eq. A2.25. Since here the modulus  $h_{cr}$  is normalized by the Young's modulus  $E$  (instead of the shear modulus  $G$ ) the values shown in Fig. 51c are lower relative to those in the corresponding curve in Fig. 51a, by a factor of  $2(1 + \nu)$ .

**Fig. 51.**

**a** The critical hardening modulus (normalized by the shear modulus) at the onset of shear localization. **b** Shear band angle as functions of the dilatancy factor. Three loading configurations are shown, and Eq. A2.25 was used assuming internal friction parameter  $\mu' = 0.9$  and Poisson's ratio  $\nu = 0.3$ . **c** The critical tangent modulus (normalized by Young's modulus) at the onset of shear localization as function of the dilatancy factor, according to Eq. 6.8. Axisymmetric compression and Poisson's ratio  $\nu = 0.3$  were assumed, for three different values of the internal friction parameter  $\mu'$



While the bifurcation analysis predicts that shear localization under triaxial compression will often occur when the hardening modulus  $h$  (defined with respect to the plastic strain) is negative, Fig. 51a shows that the corresponding tangent modulus  $h_{\text{tan}}$  (defined by the local slope of curve of the differential stress versus axial strain including the elastic and plastic components) may be either negative or positive. Laboratory data for the brittle faulting regime indicate that the constitutive parameters  $\mu'$  and  $\beta$  are both positive and, if their values are less than  $\sqrt{3}$ , then it can be observed from Eq. A2.20c that the tangent modulus  $h_{\text{tan}}$  would become unbounded if the absolute value of the hardening modulus  $h$  is given by

$$\frac{|h|}{E} = \frac{(\sqrt{3} - \mu')(\sqrt{3} - \beta)}{9} \quad (6.9)$$

For a modulus  $h$  that is negative with a relatively small magnitude, the corresponding tangent modulus  $h_{\text{tan}}$  is also negative, corresponding to the so-called Class I behaviour (Fig. 21a). However, as the modulus  $h$  becomes more negative its magnitude may attain the threshold value given by Eq. 6.9, at which point the tangent modulus  $h_{\text{tan}}$  undergoes a discontinuous jump in value (from  $-\infty$  to  $\infty$ ) with a concomitant change in sign. Beyond this transition point shear localization is predicted to occur when the differential stress-axial strain curve shows Class II behaviour (Fig. 21a), corresponding to a positive tangent modulus  $h_{\text{tan}}$  in the post-peak stage.

As discussed in Appendix 2, the shear band angle for axisymmetric compression is given by

$$\theta = \frac{\pi}{4} - \frac{1}{2} \arcsin \alpha$$

with

$$\alpha = \frac{2\sqrt{3}}{9} (1 + \nu)(\mu' + \beta) - \frac{(1 - 2\nu)}{3}$$

An enhancement of dilatancy or high pressure-sensitivity of inelastic yield is manifested by a relatively high value of  $\mu' + \beta$ , and the bifurcation analysis predicts in this case a relatively low fracture angle  $\theta$ . If the equality  $\mu' + \beta = \sqrt{3}(2 - \nu)/1 + \nu$  is satisfied then the minimum angle of  $\theta = 0$  is attained. In contrast, if a porous rock is highly compactant and its yield stress has a negative dependence on the mean stress, then there is the possibility of attaining the critical condition of  $\mu' + \beta = -\sqrt{3}$ , corresponding to the maximum angle of  $\theta = \pi/2$  if  $\nu = 0.3$ .

The first scenario corresponds to a localization mode analogous to axial splitting, but the localization analysis predicts that it may occur over a range of loading conditions. Issen and Rudnicki (2000) referred to this failure mode as a “dilation band”. Du Bernard et al. (2002) recently presented field observations of dilation bands, and Engelder (1999) reviewed the experimental uncertainty and geologic implications of such a failure mode. Since earlier bifurcation analyses focused on the development of shear localization in a dilatant material, the possibility of the second scenario with

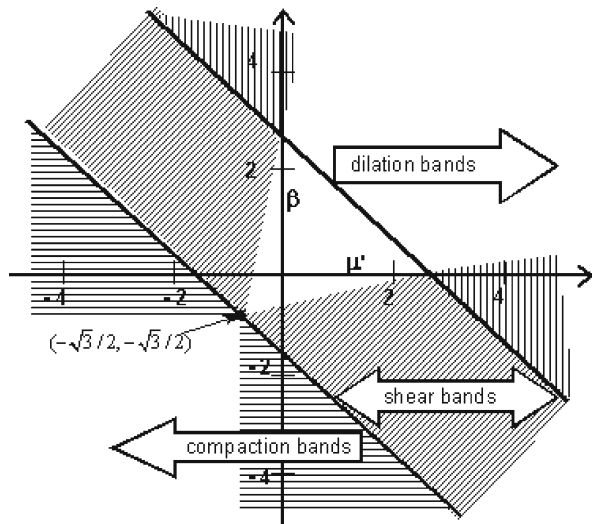
$\theta = \pi/2$  has been neglected until Olsson (1999) demonstrated that the critical condition  $\mu' + \beta = -\sqrt{3}$  can indeed be attained in a porous sandstone. Following Mollema and Antonellini (1996), who first documented similar features in the field, he referred to such a localized structure that is oriented subperpendicular to  $\sigma_1$  as a “compaction band”.

The critical conditions under which dilation or compaction bands develop were elucidated by Issen and Rudnicki's (2000) localization analysis. Figure 52 summarizes their results for axisymmetric compression and maps out the failure mode as a function of the constitutive parameters  $\mu'$  and  $\beta$ . For  $-\sqrt{3} \leq \mu' + \beta \leq \sqrt{3}(2 - \nu)/(1 + \nu)$  shear bands are predicted to develop at the critical hardening modulus values given by Eq. 6.8 above. In this regime, the shear bands may be further categorized as “compacting” or “dilating” (Bésuelle 2001). Issen and Rudnicki (2000) demonstrated that dilation and compaction bands can still develop if  $\mu' + \beta > \sqrt{3}(2 - \nu)/(1 + \nu)$  or  $\mu' + \beta < -\sqrt{3}$ , respectively (Fig. 52). However, if either inequality is satisfied the critical hardening modulus is given by expressions that are somewhat different from Eq. 6.8 for shear bands.

Laboratory observations (Olsson and Holcomb 2000; DiGiovanni et al. 2000; Wong, Baud and Klein 2001) have documented the occurrence of compaction localization in sandstones with porosity ranging from 13% to 28%. Analogous failure involving compaction bands has also been observed in cellular solids such as honeycombs (e.g., Papka and Kyriakides 1999) and metal foams (e.g., Bastawros, Bart-Smith and Evans 2000) and in ice during the I  $\rightarrow$  II transformation (Durham, Heard and Kirby 1983) that involves significant volume decrease. In porous sandstones Wong, Baud and Klein (2001) concluded that the development of compaction localization is commonly associated with stress states in the transition between brittle faulting and cataclastic flow, a topic that will be discussed further in Chapt. 9.

In the further application of bifurcation analysis, it is necessary to take into account the evolution of the constitutive parameters with strain. In the simple case of

**Fig. 52.** Failure mode map derived from bifurcation analysis. The three modes of compaction band, shear band, and dilation band are separated by the diagonal lines  $\beta + \mu = -\sqrt{3}$  and  $\beta + \mu = \sqrt{3}(2 - \nu)/(1 + \nu)$ , where  $\nu$  is the Poisson's ratio. For each failure mode, localization develops during strain hardening in the darkened area and during softening in the unmarked area (after Issen and Rudnicki 2000)



isotropic hardening, the work-hardening parameter  $h$  provides an isotropic expansion of the yield surface which, in effect, implies an increase in the “cohesion” parameter  $k$  (or  $\tau_0$  in the Coulomb model) while not affecting the internal friction  $\mu'$  (or  $\varphi$ ) and dilatancy  $\beta$  (or  $\psi$ ) factors. Thus it is the evolution of  $h$  which can lead to the condition (Eq. A2.25) being met and localization ensuing. However, the values of  $\mu'$  and  $\beta$  can also evolve with straining. In particular, while  $\beta$  can either increase or decrease at small strains, it is likely eventually to approach zero at large strains if the mechanism of deformation is cataclastic or granular flow and the “critical state” is approached. Thus, the onset of localization may occur after various amounts of strain, as observed.

### 6.4.2

#### Comments on Localization Theory

Bifurcation analysis provides an elegant tool for understanding the onset of strain localization as a failure mode of brittle rock. It advances beyond the conventional approach in geology (e.g., Edmond and Paterson 1972; Poirier 1980; White et al. 1980) that identifies the onset of shear localization as the point beyond which the rock no longer behaves as a strain-hardening material. Thus Hobbs, Muhlhaus and Ord (1990) point out that such a stability criterion does not properly deal with the possibility that, even when there is stability in the sense that a continuation of a given mode of deformation may be stable, there may be a non-uniqueness (bifurcation) in the modes of deformation that would satisfy the continuing stress equilibrium conditions. It is also important to note that conditions for uniqueness and stability are not generic and can be derived only when the boundary conditions and loading paths have been specified (Hill 1958, 1961). Nevertheless, bifurcation analysis elucidates the interplay of pressure sensitivity, dilatancy and hardening in the brittle failure process. On the basis of phenomenological observations of the inelastic behaviour of a homogeneously deformed specimen, the analysis can be used to predict the critical deformation state and fracture angle at the inception of shear localization. Laboratory observations of shear localization behaviour for a specific loading configuration can also be used to extrapolate to other configurations.

However, the quantitative comparison between localization theory and experiment is not straight forward because it is difficult to relate an essentially mathematical concept (bifurcation of deformation gradient in a continuum) to the clustering of damage in a polyminerale aggregate. According to the theory, the localization process can be considered as the propagation of a stationary acceleration wave and therefore a shear band should cut through the sample instantaneously once the critical conditions are attained (Thomas 1961; Hill 1962). As summarized in Chapt. 5, acoustic emission and microscopic observations have documented a progressive clustering of damage, and therefore it is difficult to pinpoint the onset of localization as related to the bifurcation point.

Although it is difficult to locate exactly the onset of shear localization in the stress-strain curve, the most negative slope observed in the post-peak stage of a triaxial compression experiment places a lower bound  $h_{\min}$  on the critical hardening parameter that can be compared with theoretical prediction of  $h_{cr}$ . Data on compact and

porous rocks (Rudnicki and Rice 1975; Wong, David and Zhu 1997) indicate that the isotropic hardening model significantly overestimates the amount of softening required for the onset of shear localization. There is significant difference between the theoretical predictions according to Eq. A2.25 and the experimentally observed lower bounds, with the former being less by as much as an order of magnitude. If Eq. A2.23 is used to calculate the fracture angle for shear localization in a triaxial compression test, the theoretical estimates are systematically smaller than the observed angles. The discrepancies suggest that certain key features of constitutive behaviour responsible for the inception and development of brittle faulting have not been captured in the isotropic hardening model assuming a smooth yield surface.

A more comprehensive model requires the introduction of additional constitutive parameters. It is assumed in the isotropic hardening model that all yield surfaces are smooth, but micromechanical considerations (for example, of wing crack growth under multiaxial loading) suggest that vertex-like structures (corners) may develop in subsequent yield surfaces (Kachanov 1982a,b). Also Rudnicki and Rice (1975) argued that the isotropic hardening model overestimates the stiffness of response to stress increments directed tangential to the current yield surface, and they proposed the introduction of a second hardening parameter  $h_1$  ( $< h$ ) to characterize such response to tangential stress increment. Figure 53 plots their theoretical predictions of  $h_{cr}$  and  $\theta$  for  $h_1/G = 0.1$ , which show better agreement with experimental observations.

Rudnicki and Rice (1975) neglected terms of the order stress divided by shear modulus, which may be important in the localization analyses of granular material and weakly cemented porous rock (Vardoulakis 1980; Anand and Spitzig 1982). Their model also neglected stress-induced anisotropy in the inelastic deformation, which can be destabilizing and tends to decrease the magnitude of  $h_{cr}$  (Rudnicki 1977; 2002). A constitutive model and localization analysis incorporating these complexities (e.g.,

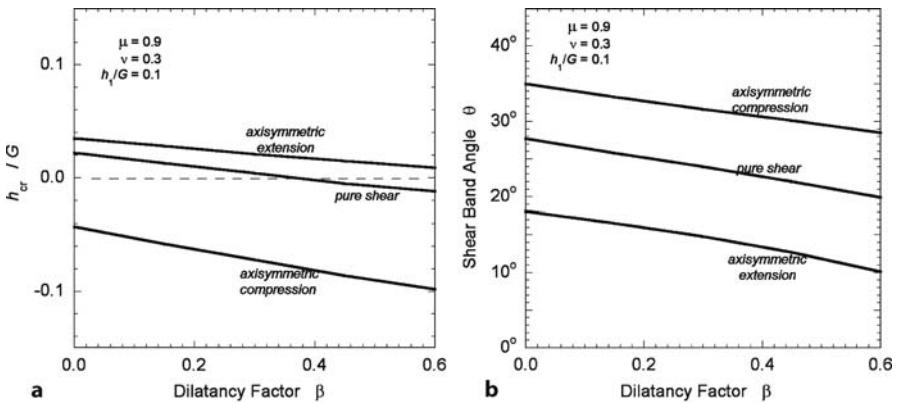


**Fig. 53.** **a** The critical hardening modulus (normalized by the shear modulus) at the onset of shear localization, and **(b)** shear band angle as functions of the dilatancy factor. The constitutive model incorporates a second hardening parameter  $h_1$  that characterizes the inelastic response to tangential stress increment. Three loading configurations are shown, and values of  $\mu' = 0.9$  and  $\nu = 0.3$  are assumed (after Rudnicki and Rice 1975)



Chau and Rudnicki 1990) may provide predictions on the onset of shear localization that are in better agreement with experimental observations. However, characterization of the additional constitutive parameters necessitates the use of loading configurations such as plane strain (e.g., Ord, Vardoulakis and Kajewski 1991; Labuz, Dai and Papamichos 1996; Holcomb and Rudnicki 2001) and rotary shear (e.g., Olsson 1992) in addition to the axisymmetric compression that is commonly used in the rock mechanics laboratory.

As a physical theory, the treatment of shear localization as a bifurcation phenomenon has two intrinsic limitations. As discussed above, it does not consider the progressive evolution of shear localization, involving both the initiation and the propagation of the shear band in a crack-like mode. Furthermore, conventional continuum theories do not have any prescribed length scales other than those associated with the geometry of the solid, so that the bifurcation analysis cannot be used to predict the geometry of the shear band. Geometric attributes (such as the average grain size) have been incorporated into plasticity models that include the effects of strain gradient or couple stress on mechanical behaviour of soil (e.g., Mühlhaus and Vardoulakis 1987; Vardoulakis and Aifantis 1991) and metal (e.g., Zbib and Aifantis 1988; Fleck and Hutchinson 1993) as well as tectonic deformation on a crustal scale (Twiss, Souter and Unruh 1993). Mühlhaus and Vardoulakis (1987) concluded that the prediction of such a theory for the thickness of the shear band is in reasonable agreement with observations of band widths on the order of 10 grain diameters in sand. To what extent this type of theory can be applied to a cohesive rock needs to be investigated in the future.

## The Role of Pore Fluids

### 7.1 Introduction

Almost all rocks are porous to some degree and, under natural conditions, the pores are likely to contain a fluid phase. This fluid will often be water or carbon dioxide, but other fluids such as air, gas, oil, or partial rock melt may also be involved. The presence of the fluid can affect the behaviour of the rock through both chemical and mechanical interactions. The chemical effects are particularly important for geological processes such as metasomatism and metamorphism and they also have some interaction with brittle deformation. However, in this chapter we shall concentrate mainly on the mechanical influence, where it is the pressure of the fluid that is of primary importance, with implications in both geology and engineering, such as in the behaviour of faults (Hickman, Sibson and Bruhn 1995).

The pore structure of rocks has been investigated by a variety of methods, including optical microscopy, X-ray tomography, scanning electron microscopy, and inference from physical properties (see Sect. 5.7.2). In general, a bimodal distinction can be made between pore space that is of more or less equant shape and that which is of markedly non-equant shape (Walsh and Brace 1966). These classes are often distinguished as “pores” and “cracks”, respectively, and their combination can be treated as “double porosity” (Berryman and Wang 1995). However, one can also distinguish a third class of pore space, which consists of “channels” such as those along three-grain junctions in equilibrated polycrystalline structures with dihedral angles between  $0^\circ$  and  $60^\circ$  (Smith 1948; Bulau, Waff and Tyburczy 1979; Hay and Evans 1988). The connectivity of the pore structure is of special relevance for such properties as permeability and electrical conductivity of fluid-saturated rock (Sect. 5.5) and, in this connection, it is common to distinguish between “pores” and “throats”, the latter being of predominating importance in determining the permeability or conductivity.

Many of the ideas about the mechanical role of pore fluid pressure were first developed in soil mechanics but here they are applied to rocks. Before describing the experimental findings and allied theoretical studies, it is necessary to consider briefly the conventions used in describing the stresses when pore fluid pressure is present and to introduce the effective stress notion which underlies many discussions of pore pressure effects.

## 7.2 The Notion of Effective Stress

It is normally convenient and appropriate initially, for experimental work and for applications, to treat as independent measurable stress variables the pore fluid pressure and the total macroscopic stress. The total macroscopic stress components are defined in the conventional way by considering the total forces, including those from any fluid phases, that act on the faces of an elementary cube. The dimensions of the cube are, however, chosen to be sufficiently large compared with the pore dimensions that statistical homogeneity is approximated. This continuum approach has been clearly set out by Biot (1941), Jaeger and Cook (1979, p. 211), Nur and Byerlee (1971), Rice and Cleary (1976), Detournay and Cheng (1991) and Wang (2000). The stresses thus defined are directly measurable.

There are more sophisticated theoretical approaches based on the notion of a mixture treated as a continuum, in which partial stress and deformation measures are defined for the individual components, somewhat as for the variables in chemical thermodynamics of multicomponent systems, but they need not be developed here (see, e.g., Schiffman 1970; Garg 1971; Morland 1972; Berryman 1995; Coussy 1995). An alternative theoretical approach is to try to consider the actual stresses within the solid particles or framework, as in inclusion-based models (for example, Endres 1997; Berryman 1998). However, the following discussion of experimental work will be in terms of the pore pressure and the total macroscopic stress as defined above.

The gross mechanical behaviour of a porous solid, such as in consolidation or in shearing deformation, either elastic or inelastic, depends in general both on the total macroscopic stress and on the pore pressure. In practice, however, this dependence can usually be expressed in terms of an *effective stress*. This is a notional macroscopic stress, which is derived from the measured total macroscopic stress and the pore pressure, and which is treated as the only stress variable governing the behaviour in question. That is, it is the stress that is *effective* in controlling a particular behaviour. This view of effective stress is clearly set out by Skempton (1961), Robin (1973) and Berryman (1992), and is adopted here because of its generality. There is an alternative, widely used approach in which the convention is adopted of *defining* the “effective stress” as  $\sigma_{ij} - p\delta_{ij}$  where  $\sigma_{ij}$  is the total macroscopic stress and  $p$  the pore pressure (e.g., Lambe and Whitman 1969, p. 241; Jaeger and Cook 1979, p. 219); the stress defined more narrowly in this way is better described as the *conventional effective stress* (cf. Garg and Nur 1973).

Experimental observations commonly indicate that, at least for isotropic behaviour, the effective stress can be written in the form  $\sigma_{ij} - \alpha p\delta_{ij}$  where  $\alpha$  is a constant depending on the particular property or situation. The principal effective stress components are then  $\sigma_1 - \alpha p$ ,  $\sigma_2 - \alpha p$ ,  $\sigma_3 - \alpha p$  where  $\sigma_1$ ,  $\sigma_2$ ,  $\sigma_3$  are the principal total macroscopic stress components.

In the case of the shear strength and consolidation properties of soils, it has been well established that  $\alpha$  can generally be taken to be equal to 1 as a very close approximation (references are given below). This condition is often referred to as “Terzaghi’s principle”, or alternatively as the law of effective stress (“conventional effective stress law” in the terminology adopted here). Terzaghi’s rule represented the first introduc-

tion of the notion of effective stress in soil mechanics. It is to be noted that it was introduced on an empirical basis specifically in connection with consolidation and shear strength of soils; see Skempton (1961) for an account of the evolution of Terzaghi's ideas, with reference to his original papers, and of its further verification by Rendulic.

Terzaghi's rule that  $\alpha = 1$  also seems to have a wide empirical validity for the inelastic behaviour of rocks (see Sect. 7.4 for experimental studies). However, it should be borne in mind that it does not have a clear theoretical basis. Values of  $\alpha$  that differ from 1 have been reported in various types of porous rock and in joints (see, for example, Gangi and Carlson 1996; Boitnott and Scholz 1990; Kwon et al. 2001) although Bernabé (1987) showed that, in the case of permeability of a compact rock,  $\alpha$  tended to approach unity after cycling. For a review of values of  $\alpha$  in relation to various properties, see Sect. 7.3.1. If the solid skeleton can be considered to be a single homogeneous constituent, then the value of  $\alpha$  is predicted to be less than or equal to 1 in relation to elastic and transport properties (Nur and Byerlee 1971; Walsh 1981; Berryman 1992). Sometimes  $\alpha$  is substantially greater than 1, for example,  $\alpha = 4$  for permeability in Berea sandstone (Zoback and Byerlee 1975c). Berryman (1992) showed that if the solid skeleton of such a clayey sandstone can be considered to be made up of two or more distinct constituents, then it is plausible for  $\alpha$  to be greater than 1 if the constituent properties are significantly different. The situation may be more complicated when more than one fluid is present, as in unsaturated soils and rocks. Even when  $\alpha = 1$ , there may be advantages in decomposing the effective stress into hydrostatic and deviatoric components (Skempton 1954; Cornet and Fairhurst 1974).

## 7.3 Elastic Properties of Porous Media

### 7.3.1 Linear Poroelasticity

Following Biot (1941), reprinted in Tolstoy (1992), linear elastic deformation of a porous body is conveniently described by

$$\varepsilon_{ij} = \frac{\sigma_{ij} - \sigma_m \delta_{ij}}{2G} + \frac{\sigma_m \delta_{ij}}{3K} - \frac{p \delta_{ij}}{3H} \quad (7.1)$$

where  $\sigma_m = (\sigma_{11} + \sigma_{22} + \sigma_{33})/3$  (see also Jaeger and Cook 1979, pp. 211–214; Rice and Cleary 1976; Kumpel 1991; Wang 2000). The quantities  $\varepsilon_{ij}$  are the macroscopic infinitesimal strain components, determined from the displacement of points in the solid parts of the body, and  $\sigma_{ij}$  are the total macroscopic stress components. The elastic parameters  $G$  and  $K$  are the macroscopic shear and bulk moduli of the porous rock in the absence of a pore pressure or, equivalently, the moduli in a saturated sample determined under drained condition at a constant pore pressure. The additional parameter  $H$  determines the further contribution to the strain that arises when pore pressure  $p$  is introduced. Thus, the macroscopic strain tensor for the porous body is determined by three material constants,  $G$ ,  $K$ , and  $H$ , all of which can be determined by direct laboratory measurement on the porous body. The coefficient  $1/H$  is not

considered in classical elasticity theory. It represents the bulk volume change induced by a pore pressure change while maintaining the applied stress constant. The above description refers, of course, only to statistically homogeneous and isotropic bodies with fully connected porosity and adequate permeability for maintaining a drained condition with uniformity in pore pressure.

The other macroscopic quantity of interest is the change in pore fluid content,  $\zeta$ , defined to be the volume of fluid storage per unit bulk volume of the porous material (Biot 1941; Rice and Cleary 1976; Wang 2000). In response to the macroscopic stress or pore pressure, the change in fluid content is given by

$$\zeta = \frac{\sigma_m}{H} - \frac{p}{R} \quad (7.2)$$

where  $R$  is a fourth material constant which can be directly measured in the laboratory by monitoring the change in fluid storage induced by a pore pressure change while maintaining the applied stress constant. The storage change arises due to the concomitant changes in porosity  $\phi$  and fluid volume  $V_f$ . If  $K_f$  is the bulk modulus of the fluid, then the storage change is  $\zeta = \Delta\phi - \Delta V_f/V$  where  $V$  is the reference bulk volume and  $\Delta V_f = \Delta p V_f / K_f$  (Berryman 1992; Wang 2000).

The elastic behaviour of the porous solid and its fluid content are therefore determined as functions of the macroscopic stresses and the pore pressure by four material constants,  $G$ ,  $K$ ,  $H$ , and  $R$ , treating the porous material statistically as an isotropic continuum. If the porosity  $\phi$  and the bulk modulus  $K_s$  of the material forming the solid parts of the porous body as well as the bulk modulus  $K_f$  of the fluid are known, they can be related to the two poroelastic constants by:

$$\frac{1}{H} = \frac{1}{K} - \frac{1}{K_s} \quad (7.3)$$

$$\frac{1}{R} = \frac{1}{H} + \phi \left( \frac{1}{K_f} - \frac{1}{K_s} \right) = \frac{1}{K} - \frac{1+\phi}{K_s} + \frac{\phi}{K_f} \quad (7.4)$$

These relations are readily derived by considering the behaviour when the macroscopic stress is a hydrostatic pressure equal to the pore pressure  $p$  (Nur and Byerlee 1971; Wang 2000). Here we have assumed that the bulk and pore compressibilities of an unjacketed sample are equal to that of the solid material forming the skeleton of the porous body. This widely used assumption is valid if every part of the void space is continuous and accessible to fluid, the solid phase is homogeneous and isotropic, and the fluid is chemically inert with respect to the solid phase (Rice and Cleary 1976; Rudnicki 2001).

This choice of a set of four independent coefficients for characterizing the linear poroelastic behaviour is not unique. For instance, instead of the two coefficients  $H$  and  $R$  one may use two dimensionless numbers introduced by Biot and Willis (1957) and Skempton (1961). In terms of  $H$  and  $R$  the Biot-Willis coefficient is given by

$$\alpha_m = \frac{K}{H} = 1 - \frac{K}{K_s} \quad (7.5)$$

and Skempton's coefficient by

$$B = \frac{R}{H} = \frac{1/K - 1/K_s}{1/K - 1/K_s + \phi(1/K_f - 1/K_s)} \quad (7.6)$$

These two parameters are of interest in several "effective stress laws". While the Eqs. 7.1 and 7.2 express completely the macroscopic linear poroelastic behaviour, they can be written more simply in terms of effective stresses  $\sigma'_{ij} = \sigma_{ij} - \alpha p \delta_{ij}$ . The relations for the bulk strains are then given by

$$\varepsilon_{ij} = \frac{\sigma'_{ij} - \sigma'_m \delta_{ij}}{2G} + \frac{\sigma'_m \delta_{ij}}{3K} \quad (7.7a)$$

with  $\sigma'_m = (\sigma'_{11} + \sigma'_{22} + \sigma'_{33})/3$  and  $\alpha$  given by the Biot-Willis coefficient as defined in Eq. 7.5:

$$\alpha = \alpha_m = 1 - \frac{K}{K_s} \quad (7.7b)$$

This relation was derived by Biot (1957) and by Nur (1969a) and the latter supported it by experimental results for Westerly granite, thereby confirming earlier suggestions by Geertsma (1957) and Skempton (1961). In soil mechanics it is commonly observed that the bulk material is significantly more compressible than the solid grains, so that  $K_s \gg K$  and therefore  $\alpha_m$  and the effective stress parameter  $\alpha$  can both be taken to be unity.

Similarly the fluid content  $\zeta$  can be related to the mean effective stress  $\sigma'_m$  by

$$\zeta = \frac{\sigma'_m}{H} \quad (7.8a)$$

where  $\alpha$  in this case is given by the reciprocal of Skempton's coefficient  $B$  as defined in Eq. 7.6

$$\alpha = \frac{1}{B} = 1 - \phi \frac{(1/K_f - 1/K_s)}{(1/K - 1/K_s)} \quad (7.8b)$$

One can isolate that part of the fluid content change that arises from porosity change by considering an incompressible fluid (with  $K_f \rightarrow \infty$ ), which then gives the effective stress parameter  $\alpha$  for porosity change (Robin 1973; Berryman 1992)

$$\alpha = 1 - \frac{\phi}{\alpha_m} \frac{K}{K_s} = 1 - \frac{\phi}{K_s(1/K - 1/K_s)} \quad (7.8c)$$

In soil for which the solid material can be considered as incompressible ( $K_s$  infinitely large), then the  $\alpha$ 's in Eqs. 7.8a and 7.8c for bulk and pore volume changes can both be taken to be unity.

Note that the expressions for  $\alpha$  in the effective stresses differ in Eq. 7.7b for the bulk strains, in Eq. 7.8b for fluid content, and in Eq. 7.8c for the pore volume. This illustrates

the statement of Nur and Byerlee (1971) that different elastic processes can be controlled by different “effective stress laws”.

So far, only the open system, in which the pore pressure is an independent variable, has been considered. For the undrained case, the amount of pore fluid in the body is fixed (Gassmann 1951; Brown and Korringa 1975) and therefore the change in fluid content  $\zeta = 0$ . Under undrained condition, significant pore pressure excess may develop in response to compressive loading. This limiting case is of interest as a reasonable approximation for certain tectonic deformations, such as the instantaneous response of groundwater levels to the static strain field of an earthquake and the hydrologic response of a confined aquifer to earth tides (Roeloffs 1996). It can be seen from Eqs. 7.2 and 7.6 that with  $\zeta = 0$  Skempton's coefficient gives the ratio between the change in pore pressure under undrained condition and the change in mean stress, so that  $\Delta p = -B \Delta \sigma_m$ . In soil mechanics, it is commonly assumed that Skempton's pore pressure coefficient  $B = 1$  for soil saturated with water (Holtz and Kovacs 1981) since the bulk medium is much more compressible than either the water or the solid grains ( $K_s > K_f \gg K$ ). For such an unconsolidated material the storage coefficient  $1/R$  is, according to Eq. 7.4, given by  $1/R = 1/K + \phi/K_f$ , a definition that is widely adopted in hydrology (Domenico and Schwartz 1998). Fredrich, Martin and Clayton (1995) obtained values of  $B$  close to 1 at effective pressures up to 50 MPa for tuff samples with porosities of 37% and 40%. The tuff is similar to soil in that the bulk compressibility is very high.

### 7.3.2

#### Experimental Measurement of Poroelastic Properties

Complete characterization of the behaviour of an isotropic rock requires the independent measurement of at least four poroelastic constants in drained or undrained tests. There is a paucity of such measurements under controlled conditions of pore and confining pressures (Table 5). However, if two of the drained moduli ( $K$  and  $G$ ) have been measured, then the values of  $R$  and  $H$  can be inferred from Eqs. 7.3 and 7.4 if the bulk moduli  $K_s$  and  $K_f$  and the porosity  $\phi$  are known. Taking such an approach Rice and Cleary (1976) compiled and estimated poroelastic constants for 6 rocks, using the experimental data of Haimson and Fairhurst (1970), Nur and Byerlee (1971), Rummel (1974) and Zoback and Byerlee (1975c). Their compiled data are also included in Table 5.

Berryman (1992) pointed out that the Biot-Willis coefficient is bounded by the porosity and unity, so that  $\phi \leq \alpha_m \leq 1$ . While the experimental data in Table 5 fall within these bounds, the coefficient  $\alpha_m$  seems not to be systematically related to the porosity  $\phi$ . This is not surprising since the bulk constants  $G$  and  $K$  themselves cannot, in general, be expressed in terms of the porosity and the elastic constants of the solid material because they also depend on the shape of the pores; (cf. Walsh 1965a,b; Warren 1973; Zimmerman 1991). In Fig. 54a we compile data on the Biot-Willis coefficient as a function of the conventional effective pressure for a granite, marble, limestone and sandstone. We calculated the  $\alpha_m$  values from the bulk moduli data of Mesri, Adachi and Ullrich (1976) using Eq. 7.5. The recent data of Lockner and Beeler (2003b) for Berea sandstone at higher effective pressures are also included. At relatively low effective

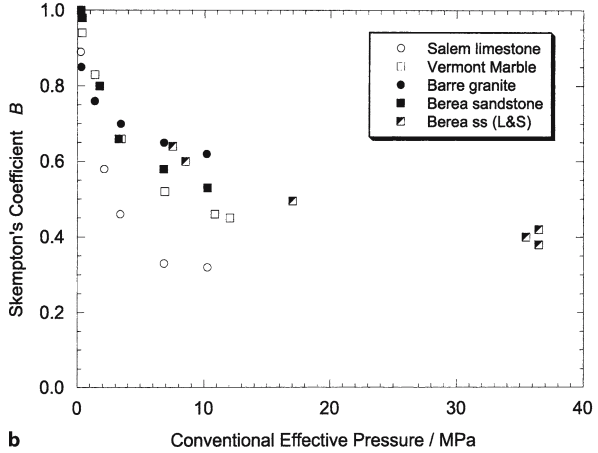
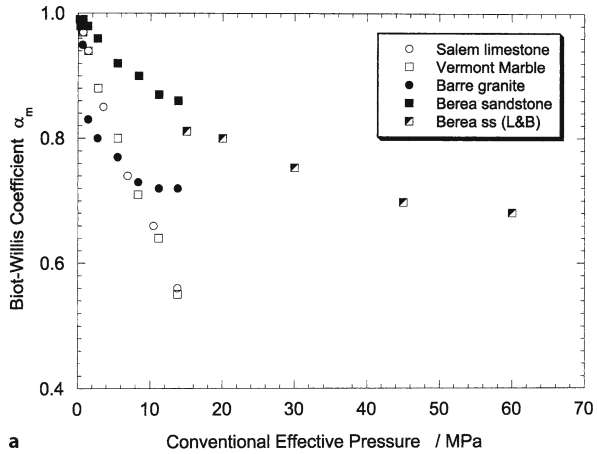
**Table 5.** Laboratory data on poroelastic constants for compact and porous rocks

Rock	$\phi$	$K$ (GPa)	$K_s$ (GPa)	$\alpha_m$	$B$	Pressure (MPa)	Reference
<b>Granite</b>							
Westerly	0.01	25	45	0.47	0.85		Rice and Cleary 1976
Charcoal	0.02	35	45	0.27	0.55		Rice and Cleary 1976
Barre	0.027	15	53	0.72	0.62	$P_c - p \sim 10$	Mesri et al. 1976
<b>Carbonate</b>							
Tennessee marble	0.02	40	50	0.19	0.51		Rice and Cleary 1976
Vermont marble	0.021	25	69	0.64	0.46	$P_c - p \sim 10$	Mesri et al. 1976
Salem limestone	0.126	13	38	0.66	0.32	$P_c - p \sim 10$	Mesri et al. 1976
Indiana limestone	0.13	21.2	72.6	0.71	0.46	$P_c - \alpha_m p \sim 20-35$	Hart and Wang 1995
Tonnerre limestone	0.13	19.3	41.4	0.53	0.20		Fabre and Gustkiewicz 1997
Chauvigny limestone	0.165	16.3	52.6	0.69	0.20	$P_c \sim 100$	Fabre and Gustkiewicz 1997
Lavoux limestone	0.219	13.8	58.9	0.77	0.30	$P_c \sim 50$	Fabre and Gustkiewicz 1997
Lixhe chalk	0.428	3.8	42.5	0.91	0.35		Fabre and Gustkiewicz 1997
<b>Sandstone</b>							
Ruhr	0.02	13	36	0.65	0.88		Rice and Cleary 1976
Weber	0.06	13	36	0.64	0.73		Rice and Cleary 1976
Fontainebleau	0.06	30.9	35.2	0.12	0.25	$P_c = 90$	Fabre and Gustkiewicz 1997
Vosges (yellow)	0.17	17.4	42.5	0.91	0.46		Fabre and Gustkiewicz 1997
Vosges (red)	0.18	13.9	38.6	0.64	0.35		Fabre and Gustkiewicz 1997
Berea	0.19	8	36	0.79	0.62		Rice and Cleary 1976
Berea	0.19	6.6	28.9	0.77	0.75	$P_c - \alpha_m p = 10$	Hart and Wang 1995
Berea	0.203	4.7	36.3	0.87	0.53	$P_c - p \sim 10$	Mesri et al. 1976



**Fig. 54.**

**a** The Biot-Willis coefficient and **(b)** the Skempton coefficient as function of conventional effective pressure. The Berea sandstone data at elevated pressures are from Lockner and Beeler (2003b) and Lockner and Stanchits (2002). All other data are from Mesri et al. (1976)



pressures the bulk modulus  $K$  is very small due to the presence of numerous open cracks and pores, and consequently the values of  $\alpha_m$  are close to unity. At elevated pressures crack closure results in appreciable decrease of the Biot-Willis coefficient.

Skempton's coefficient  $B$  is expected to fall between 0 and 1, and the laboratory data compiled in Table 5 are within this range. The  $B$  values seem not to be systematically correlated with porosity. We compile in Fig. 54b the data of Mesri, Adachi and Ullrich (1976) on Skempton's coefficient of water-saturated samples as a function of the conventional effective stress, as well as the data of Lockner and Stanchits (2002) for Berea sandstone at higher effective pressures.  $B$  values close to 1 were measured at low effective pressures, but they fall to values between 0.33 and 0.69 at effective pressures of 10 MPa or so. Similar behaviour was observed in saturated dolomite and sandstone (Berge, Wang and Bonner 1993; Fredrich, Martin and Clayton 1995; Green and Wang 1986). The rapid decrease of  $B$  with increasing effective pressure can again be attributed to the increase of the bulk modulus  $K$  induced by crack closure.

In the case of an anisotropic porous body, the scalar coefficients  $\alpha_m$  and  $B$  are replaced by a second rank tensor (cf. Brown and Korringa 1975; Carroll 1979). Cheng (1997) presented explicit relations for these tensor coefficients. In undrained triaxial compression experiments on two sandstones, Lockner and Stanchits (2002) observed that stress-induced anisotropy can be so significant that both the Biot-Willis and Skempton's coefficients cannot be approximated as scalar quantities. Their data show that in Berea sandstone Skempton's coefficient for the undrained response to an increase in the axial stress can be as much as four times that for corresponding response to the transverse stress. Such a poroelastic response to deviatoric stresses seems to arise from the anisotropic stiffening from crack closure.

The simple theory of the elastic deformation of porous solids given above serves to illustrate in principle the approach to the inclusion of pore pressure effects in terms of effective stress. Similar considerations can be extended to the influence of pore pressure on the velocities of elastic wave propagation; see Banthia, King and Fatt (1965) and Todd and Simmons (1972) for some observations and for references to theory. However, this type of theory is limited to small strains, beyond which non-linear effects soon become important; for introduction to the non-linear aspects, see Walsh (1971a), Biot (1973), Garg and Nur (1973) and Guéguen, Dormieux and Buotéca (2004).

## 7.4 Brittle Failure – Experimental

### 7.4.1 Drained Tests

There have been many experimental studies on the influence of pore pressure on brittle fracture in rocks because of its importance in fields such as tectonics, seismology and geotechnical engineering. The experimental work has normally focused on situations in which the fluid-containing pores are interconnected, so that the pore fluid pressure can be changed or controlled by introducing or removing some fluid. This is done by connecting the specimen to an external pressure source (see Chapt. 2). Most of the work on rocks has been done with the external pressure source connected continuously to the pore system of the rock, with the aim of maintaining constancy of pore pressure; this is the arrangement known in soil mechanics as the “drained test”. The alternative arrangement (“undrained test”), in which the specimen is isolated from any external fluid systems during the test, has been used less often. The undrained condition implies that, in the absence of hydration/dehydration reactions or other internal fluid consumption/generation, the amount of fluid in the specimen is held constant during the test but the pore fluid pressure will tend to change (see further under Sect. 7.4.2).

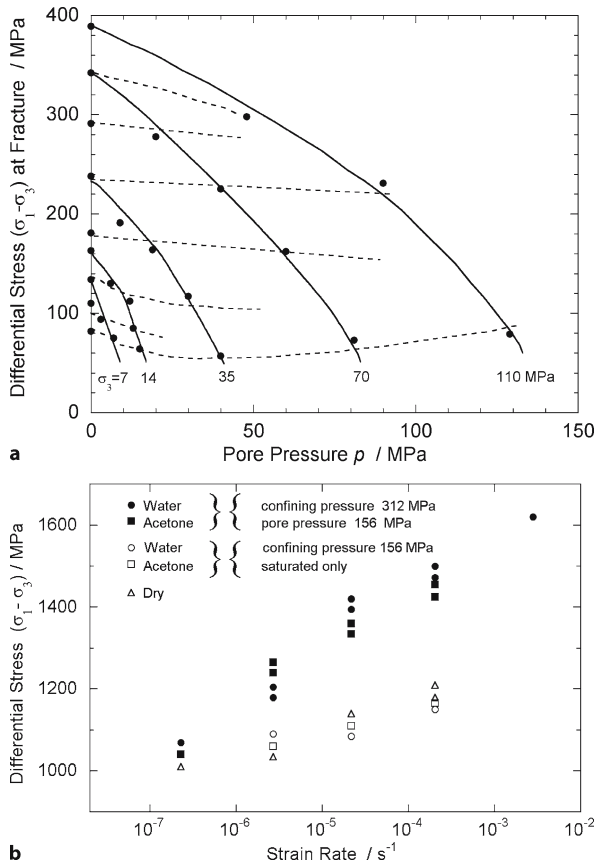
Experimental details covering such aspects as saturation of specimens, control of pore pressure, and measurement of the amount of fluid moving in or out of pores during testing have been given by Robinson (1959), Heard (1960), Handin et al. (1963), Murrell (1965), Donath (1966), Neff (1966), Lane (1970), Heck (1972) and Chiu, Johnston and Donald (1983). The pore fluid used has normally been water except when the

chemical activity of water was to be avoided or when the influence of different viscosities was to be tested. Pre-saturation of the specimen by evacuating the air while the specimen is immersed in the fluid helps to minimize complications from incomplete saturation (e.g., Neff 1966; Heck 1972; Rutter 1972b). However, there remains the frequent problem of attaining equilibrium in pore pressure through the sample when the permeability is low. Connecting the pore pressure pumping system to both ends of the specimen is sometimes done to alleviate this problem (Robinson 1959; Murrell 1965; Neff 1966; Heck 1972).

There is a considerable body of experimental work showing that to a fairly good approximation Terzaghi's effective stress rule governs the shear failure of a wide variety of rocks, including sandstone, limestone, dolomite, shale, and siltstone (Robinson 1959; Serdengecti and Boozer 1961; Handin et al. 1963; Murrell 1965; Dunn, LaFountain and Jackson 1973; Byerlee 1975; Gowd and Rummel 1977; Dropek, Johnson and Walsh 1978; Schmitt and Zoback 1989). An example is given in Fig. 55a. That is, in general, the differential stress for shear failure of a particular rock is approximately the same at the same "effective confining pressure" when the latter is taken to be the total confining

**Fig. 55.**

**a** Influence of pore pressure  $p$  on differential stress at fracture in triaxial compression tests at various confining pressures  $\sigma_3$  for a sandstone of 21% porosity, showing approximate conformity with the Terzaghi effective stress rule; the broken lines are lines of constant "effective pressure"  $\sigma_3 - p$  (after Murrell 1965).  
**b** Differential stress at fracture of Westerly granite as a function of strain rate at two confining pressures but at the same "effective pressure", showing departure from Terzaghi's effective stress rule at strain rates above  $10^{-6} \text{ s}^{-1}$  (after Brace and Martin 1968)



pressure minus the pore pressure ( $\alpha = 1$ ). However, apparent exceptions have been noted. Heard (1960) found that the differential stress for brittle failure in Solnhofen limestone increased with total confining pressure even though the conventional effective pressure was held constant. Robinson's (1959) results for Indiana limestone showed a similar trend, as did also the results of Handin et al. (1963) for Hasmark dolomite, a shale, and a siltstone (but only with water in the latter case, not with kerosene). Thus, it was concluded by Handin et al. (1963) that "the important mechanical properties – ultimate strength and ductility – are functions of the [conventional] *effective stresses*, provided that (a) the interstitial fluid is inert relative to the mineral constituents of the rock so that pore pressure effects are purely mechanical, (b) the permeability is sufficient to allow pervasion of the fluid and furthermore to permit the interstitial fluid to flow in or out of the rock during the deformation so that the pore pressure remains constant and uniform throughout (the test is "drained"), and (c) the rock is a sandlike aggregate with connected pore space, the configuration of which insures that the pore ("neutral") pressure is transmitted fully throughout the solid phase."

The conclusion of Handin et al. (1963) about the role of permeability has been confirmed by detailed work on low permeability rocks at slow strain rates by Brace and Martin (1968); see also Brace (1969b) and Martin (1980). They compared fracture strengths at zero pore pressure and 156 MPa confining pressure with those at 156 MPa pore pressure and 312 MPa confining pressure – the conventional effective pressure in both cases being 156 MPa. Several igneous rocks of 0.7% or less porosity and a sandstone of 2.6% porosity were tested. The porosities were measured at pressure, presumably by fluid take-up, so as to ensure comparable conditions of crack closure. Typical results for Westerly granite (porosity 0.7%) are given in Fig. 55b, showing that when the strain rate is reduced to  $10^{-7} \text{ s}^{-1}$  Terzaghi's effective stress rule is clearly obeyed; this strain rate is called the "critical strain rate". The apparent departures from Terzaghi's rule at higher strain rates were found to be independent of the chemical nature of the fluids (water and acetone) provided the viscosities were similar. The influence of viscosity is illustrated in tests on the sandstone, for which the critical strain rate is  $10^{-4} \text{ s}^{-1}$  when water is used as pore fluid and  $10^{-7} \text{ s}^{-1}$  when a silicone fluid of nearly three orders of magnitude greater viscosity is used; this relative change in critical strain rate is, therefore, consistent with the predicted relative change in the rate at which pressure equilibration with an external source could be established. The failures, single major faults with subsidiary small fractures in all cases, had the same appearance regardless of pore pressure conditions.

In a similar study of Solnhofen limestone near its brittle-ductile transition, Rutter (1972a) found a critical strain rate of  $10^{-6} \text{ s}^{-1}$  for the apparent validity of Terzaghi's effective stress rule when water is the pore fluid; the porosity, measured by saturating with water at atmospheric pressure, was 5.3%. In a study of Nevada Test Site tuff, Christensen, Green and Jones (1973) found a critical strain rate of  $10^{-3} \text{ s}^{-1}$ . It is to be noted, however, that, as emphasized by Ladanyi (1970), the behaviour above the critical strain rate in these observations need not represent a real failure of Terzaghi's effective stress rule within the specimens; it may be entirely due to the actual pore pressures being different from the fluid pressure applied and measured at the surface of the specimen, this disequilibrium being accentuated by any concurrent dilatancy (cf. Gowd and Rummel 1977).

In the case of specimens without jackets to exclude the confining pressure fluid, the specimen is potentially subject to a pore fluid pressure equal to the confining pressure and the conventional effective pressure equal to zero, provided there is sufficient permeability for the penetration of the fluid to establish the pressure in the pores. Thus, in triaxial tests on specimens without jackets, brittleness tends to persist to higher confining pressures, and fracture strengths or flow stresses tend to be lower, than when jackets are used (Griggs 1936; Goguel 1948; Handin 1953; Bredthauer 1957; Heard 1960). However, only in specimens of high permeability is the strength of unjacketed specimens equal to or near that found in atmospheric pressure tests, in accord with Terzaghi's rule; the sandstone tested at 500 MPa confining pressure by Handin et al. (1963) is an example. More usually, and especially when using fairly viscous confining pressure fluids, such as kerosene at the higher pressures, the strengths of unjacketed specimens show intermediate values and tend to increase appreciably as the confining pressure increases, indicating that some effective confining pressure is being established; Solnhofen limestone (Griggs 1936) and Muddy Shale (Handin et al. 1963) are examples. Also, in such cases, the strength of unjacketed specimens is likely to appear anomalously sensitive to strain rate because of the time dependence of penetration of the fluid (Jaeger 1963).

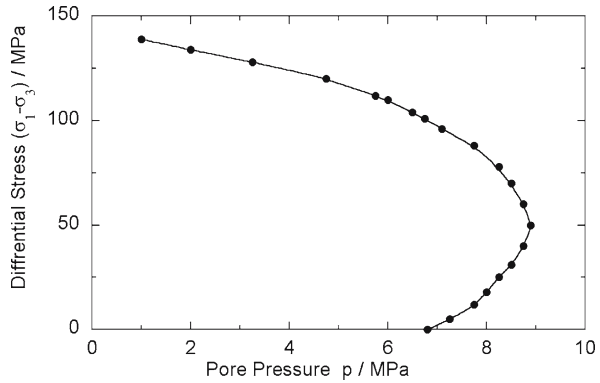
While most of the above examples of the effects of pore fluid pressure have involved triaxial compression tests, there have also been observations confirming the approximate validity of Terzaghi's effective pressure principle in extension tests, especially in Bridgman pinching-off tests in which the conventional effective pressure is zero if the specimen is unjacketed (Jaeger 1963; Jaeger and Cook 1963; Schmitt and Zoback 1989; Bruno and Nakagawa 1991). However, this conclusion is again dependent on there being adequate permeability for establishing pore pressure equilibrium throughout the specimen (Schmitt and Zoback 1992).

#### 7.4.2 Undrained Tests

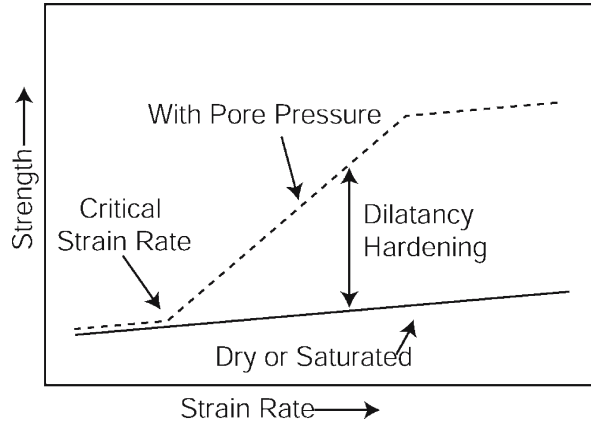
Pore pressure effects can be substantially modified by changes in porosity during an experiment. These changes may involve dilatation or compaction, either during application of confining pressure or during deformation under differential stress (see Chapt. 6), and they are likely to be accompanied by significant changes in permeability. If the permeability is adequate and the specimen is continuously connected to the pore fluid reservoir ("drained" test), the only effect may be movement of fluid into or out of the specimen; such an effect has been widely observed (Robinson 1959; Handin et al. 1963; Rutter 1972b), and it has sometimes been monitored to give a measure of change in porosity (Read and Meredith 1989; Chiu, Johnston and Donald 1983; Zhang, Cox and Paterson 1994; Zhang, Paterson and Cox 1994; Read et al. 1995; Bernabé and Brace 1990; Wong 1990a). On the other hand, if the specimen is saturated and then isolated from the reservoir ("undrained" test), changes in pore pressure will be induced by changes in porosity accompanying deformation, as shown by Neff (1966), Aldrich (1969), Heck (1972), (also in Lane 1970), Dropek, Johnson and Walsh (1978), and Green and Wang (1986); see Fig. 56 and previous discussions in Sect. 7.3.1. Similar changes have been inferred by Ismail and Murrell (1976) to explain the behaviour in

**Fig. 56.**

Changes in pore pressure with application of differential stress in an undrained triaxial compression test on Berea sandstone (18% porosity) at 14 MPa confining pressure, 7 MPa initial pore pressure (after Heck 1972)

**Fig. 57.**

The concepts of dilatancy hardening and critical strain rate associated with it, deriving from observations of the type shown in Fig. 56 (after Brace and Martin 1968)



undrained tests of rocks of various porosities when water was added in excess of that needed for initial saturation.

Induced changes in pore pressure similar to those in “undrained” tests can also be expected in nominally “drained” tests when the permeability is inadequate for the maintenance of equilibrium between the pressure in the pores and in the reservoir, that is, when the strain rate is above the critical strain rate defined by Brace and Martin (1968) and mentioned in Sect. 7.4.1. An increase in porosity can then lead to a decrease in the actual pore pressure within the specimen, so that greater differential stress is needed for deformation than when constancy of actual pore pressure can be maintained. This effect, known as “*dilatancy hardening*”, has been discussed by Brace and Martin (1968) and depicted by them as in Fig. 57; see also Rutter (1972a), Ismail and Murrell (1976), Chiu, Johnston and Donald (1983), and Schmitt and Zoback (1992). The effect is similar to the effect in granular media discussed by Reynolds (1885; 1887) and Mead (1925), and it can be expected to affect sliding on fault surfaces or cataclastic deformation whenever permeability is low in relation to the strain rate and dilatation accompanies the deformation. Its relevance to seismicity has been discussed by Frank (1965, 1966) and it is an important aspect of the models for the mechanism of earth-

quakes of Nur (1972), and Scholz, Sykes and Aggarwal (1973), which have figured in discussions on earthquake predictions (for example, Mogi 1977; Sibson 1981; Crampin, Evans and Atkinson 1984).

### 7.4.3 Chemical Effects

An active role of the interstitial fluid through chemical or other processes independent of the applied pore pressure has often been observed. The apparent exception to Terzaghi's rule for siltstone with water as pore fluid, observed by Handin et al. (1963) and noted above, was attributed to the swelling of montmorillonite clays, which greatly reduces the permeability. However, it has been widely observed, especially in quartz-rich rocks but also in limestone, that water, including even that adsorbed from a humid atmosphere, has a specific weakening effect relative to behaviour after careful drying (Hirschwald 1912, pp. 192–196; Jaeger 1943; Terzaghi 1945; Price 1960; Serdengecti and Boozer 1961; Colback and Wiid 1965; Murrell 1965; Aldrich 1969; Podnieks, Chamberlain and Thill 1972; Rutter 1972b; Christensen, Green and Jones 1973; McCarter and Willson 1973; Parate 1973; Atkins and Peng 1974; van Eeckhout 1976; Seto et al. 1997). Alkaline solutions have also been observed to lower the fracture stress of both quartzite and quartz crystals (Griggs and Bell 1938; Fairbairn 1950), and aluminium and ferric iron-bearing solutions have a similar or even more marked effect which can be rationalized in terms of zeta-potentials (Swolfs 1972). Such observations call to mind the Rehbinder effect (Rehbinder, Schreiner and Zhigach 1948). Thus, Boozer, Hiller and Serdengecti (1963) observed weakening effects with a number of surface-active liquids on both sandstone and limestone, independently of any pore pressure effect; for example, oleic acid and water weakened both rocks, whereas *n*-hexadecane produced no effect. Robinson (1967) confirmed and extended the observations of Boozer et al. but pointed out that the additional weakening by solutions or organic chemicals over that due to water alone applied only to the yielding, not to brittle strength. Colback and Wiid (1965) also reported observations on uniaxial strength of quartzitic sandstone in a number of liquids, which show a correlation between the degree of weakening and the surface tension of the liquid (see also Vutukuri 1974, for limestone). However, as seen from the relative effects with oleic acid and water, such a correlation does not apply in the results of Boozer, Hiller and Serdengecti (1963), who make the more likely suggestion that it is the surface energy of the mineral when wetted with the fluid that is important (see also van Eeckhout 1976; Baud, Zhu and Wong 2000). On the other hand, studies of the influence of water on crack propagation in quartz (Charles 1959; Scholz 1968c; Martin 1972) suggest a specific chemical role for water in silicate rocks in assisting to break Si-O bonds (see also Swolfs 1972). These effects can be viewed as examples of crack propagation controlled by stress corrosion; see reviews by Anderson and Grew (1977), Atkinson and Meredith (1987b) and Costin (1987).

The effects of adsorbed moisture can also be treated from a point of view commonly adopted in soil mechanics for unsaturated soils. In clay soils, there are important variations in strength with variations in moisture content when no free water is present. Relative to the saturated condition, reduction in water content gives a strengthening which has been variously dealt with in terms of notions of suction, soil mois-

ture tension, pressure deficiency, negative pore pressure, etc., introduced into effective stress theory; see, e.g., papers in British National Society (1961) or Lambe (1969). This approach has not been applied much in rock mechanics but it could be relevant in fine grained rocks, especially in argillaceous rocks. Thus, Chenevert (1970) treated the strength of argillaceous shales in terms of an adsorptive pore pressure, defined as  $(RT/v) \ln(p/p_0)$ , where  $p$  and  $p_0$  are the vapour pressures of water in equilibrium with the rock and with free water, respectively,  $v$  is the specific volume of water,  $R$  is the gas constant and  $T$  the absolute temperature; the relative humidity of the atmosphere in equilibrium with the rock is taken as the measure of  $p/p_0$  (see also Schmitt, Forsans and Santarelli 1994). The adsorptive pore pressure, which is negative, that is, of the same sign as tensile stress, is then used in the same way as the pore pressure in a saturated rock to derive conventional effective stresses (for relation to swelling in shales, see Huang, Aughenbaugh and Rockaway 1986). Chenevert found that the compressibility, swelling and strength of several shales exposed to atmospheres of various relative humidities behaved as if controlled by effective stresses obtained in this way, and the same correlation was shown to apply to the quartzitic shale and quartzitic sandstone of Colback and Wiid (1965), mentioned above. The strength of granular materials containing amounts of water below the level of saturation is also of concern in the technology of such materials and has been discussed in terms of “capillary bonds” between grains (cf. Carr 1967; Frank 1971, 1972, and other references given by them).

## 7.5

### Brittle Failure – Theory of Pore Pressure Effects

The theory of the influence of pore pressure on brittle failure has encountered a number of difficulties. In particular, discussion of the theoretical basis of the dominant role of the conventional effective stress has been marked by a good deal of controversy and some confusion. Fundamentally, the theoretical problem is to relate the stresses and attendant failure phenomena on the microscopic scale (scale of the pores) to the macroscopic stress state and the macroscopic failure.

In theoretical discussion, it is important to keep clearly in mind the various ways in which stresses are defined (cf. Sect. 7.2). Firstly, there are the total macroscopic stresses, involving the totality of forces, in both solid and fluid parts, acting across a hypothetical macroscopically plane surface, the area of which is taken to include both the solid material and the pore space intersected by the surface. Secondly, there are local stresses, based on the forces acting on local parts of this hypothetical surface lying entirely within a uniform region (either solid material or pore space). Finally, there are quantities which can be described as partial macroscopic stresses, defined by considering the forces acting on only those parts of the surface that intersect either solid or fluid but dividing the measure of the forces by the total area of the macroscopic surface.

It is also important to consider brittle failure specifically since it is already evident from the previous sections on elastic deformation and on the experimental study of brittle failure that there is no simple universal definition of “effective stress” which permits a uniform treatment of all phenomena affected by pore fluid pressure. Thus, the discussion of so-called buoyancy forces and their role in sliding friction on sur-



faces between separate bodies, which dominated much of the paper and subsequent discussion of Hubbert and Ruby (1959), is not necessarily directly relevant in understanding the role of the conventional effective stress in brittle failure of initially intact rock. It should also be noted (cf. Moore 1961) that mathematically the particular decomposition of the total stress into a “neutral stress”  $p$  and a conventional effective stress has no special uniqueness. Emphasis has sometimes been put on the “neutral” character of the pore pressure, which is said to give a uniform hydrostatic reference state through the whole of the material if the pressure is transmitted to all the pores, but this concept is useful only as long as either infinitesimal elastic deformation alone is involved or elastic deformation is entirely neglected.

A common approach to rationalizing the apparent role of the conventional effective stresses in brittle failure has been to consider some sort of average value of the local stresses in the solid parts of the specimen. Considering the stress components on a potential plane of failure, it is readily shown (e.g., Skempton 1961; Jaeger and Cook 1979, p. 222) that the total normal stress component  $\sigma$  can be written as

$$\sigma = p + (1 - f)(\sigma_s - p) \quad (7.9)$$

where  $\sigma_s$  is the average value of the local normal stress in the solid parts intersected by the macroscopic element of area upon which the stress  $\sigma$  is calculated,  $f$  is the fraction of this area occupied by the pore space, and  $p$  is the pore pressure. The quantity  $f$  is generally taken to be equal to the porosity and is often called the “boundary porosity” (e.g., Robinson and Holland 1970). Equation 7.9 can be re-written as

$$(1 - f)\sigma_s = \sigma - fp \quad (7.10)$$

The quantity  $(1 - f)\sigma_s$  is equal to the total normal force transmitted through the solid parts divided by the total area; that is, it is a partial stress. By a similar consideration to that leading to Eq. 7.9, the total shear stress  $\tau$  can be written as

$$(1 - f)\tau_s = \tau \quad (7.11)$$

where  $\tau_s$  is the average value of the local shear stress in the solid parts intersected.

If it is now assumed that shear failure will occur on the surface under consideration when the average stresses in the solid parts satisfy a Coulomb condition similar to that applying to the same material with no pores, then

$$\tau_s = \tau_0 + \sigma_s \tan \varphi$$

where  $\tau_0$  and  $\tan \varphi$  are the cohesion and coefficient of internal friction of the solid material itself, or closely related parameters. Substituting from Eqs. 7.10 and 7.11 gives

$$\tau = (1 - f)\tau_0 + (\sigma - fp) \tan \varphi \quad (7.12)$$

Therefore,  $\sigma - fp$  appears in the Coulomb condition for the porous specimen instead of  $\sigma$ , that is, the “effective” shear stress is still  $\tau$ . This or similar arguments (Terzaghi

1945; Skempton 1961) have thus led to the prediction that brittle failure should be governed by effective stresses  $\sigma'_{ij} = \sigma_{ij} - \alpha p \delta_{ij}$  where  $\alpha = f$ , the “boundary porosity”.

However, the observed behaviour generally corresponds to  $\alpha = 1$ , even in rocks of low porosity, so that if the porosity is taken as the measure of  $f$  the above prediction is not obeyed (see also Robin 1973). To reconcile this discrepancy, it has become customary in soil mechanics to view the potential failure surface as a wavy surface following only in an approximate way the plane surface considered in the definition of the stresses in the above argument (e.g., Lambe and Whitman 1969, p. 242). It is then said that, since such a wavy surface can lie almost entirely within pore space by going around the grains, its boundary porosity  $f$  is close to unity. A similar view can be applied to rock but it leads to the conclusion that “the voids must consist of very narrow but continuous slits” (Terzaghi 1945, p. 786).

Such an explanation of how the conventional effective stresses ( $\alpha = 1$ ) apply to brittle failure is not very satisfying for rocks. Its deficiency probably lies mainly in treating the stresses within the solid parts as uniform, that is, in taking into account only the average value of the local stresses, and in neglecting to consider the local and propagating nature of a brittle failure. The latter point has been raised by Laubscher (1960) who suggests that during the approach to failure there is a changing microscopic geometry involving the development of a series of local fractures, so that the effective boundary porosity of a potential fracture surface increases during this development and approaches unity just before the macroscopic movement on the fracture surface begins. The analysis of such a situation is most simply approached through the Griffith model for brittle fracture.

The Griffith model has been described in Chapt. 4. It takes into account the actual stress state around an ellipsoid-shaped crack, assuming elastic behaviour prior to the local failure whereby the crack is extended, and it postulates that the crack will extend when the extra work of creating new crack surface can be provided from elastic strain energy available. If the crack contains a fluid under pressure, the theory shows that the failure condition remains of the same form provided conventional effective stresses  $\sigma_{ij} - p \delta_{ij}$  are used instead of the total stresses  $\sigma_{ij}$ , this applies in both the two-dimensional model (Murrell 1964; Jaeger 1969, p. 169; Jaeger and Cook 1979, p. 279) and the three-dimensional (Murrell and Digby 1970). Thus, Griffith theory *predicts*  $\alpha = 1$ , and, insofar as it is applicable, gives justification for the use of the conventional effective stresses in predicting brittle failure. Of course, as discussed in Chapt. 4, Griffith theory is only strictly relevant to the initiation of fracture, but similar considerations presumably apply at each stage of the propagation of the fracture and it seems plausible that the macroscopic failure of a brittle porous material with pore pressure should similarly be governed by the conventional effective stresses ( $\alpha = 1$ ).

Indeed this is the approach usually adopted to incorporate pore pressure effects into the various micromechanical models of brittle failure discussed in Chapt. 6. Underlying the fracture mechanics treatment is the usual presumption that the pore fluid is always in hydrostatic equilibrium. However, in a crack growing sufficiently rapidly, viscous drag may prevent continuous fluid penetration to the crack tip, a situation discussed by Abé, Mura, and Keer (1976) in the context of hydraulic fracturing, which represents another aspect of the critical strain rate (Sect. 7.4.1). Atkinson and Cook (1993) have modelled such a situation microdynamically.

## Friction and Sliding Phenomena

### 8.1 Introduction

Sliding at discrete discontinuities in rocks is of interest from many points of view. In particular, studies have been directed to the following topics:

1. The physics of friction in rocks, viewed as a distinctive class of materials.
2. The “residual” strength of rock after shear failure.
3. The mechanical behaviour of jointed or crushed rock.
4. The mechanics of geologic faulting and the generation of structures such as slickensides.
5. Dynamical behaviour, especially in relation to earthquake mechanisms.

No attempt is made to survey all these topics here. However, since friction is a very important factor in the brittle behaviour of rocks, especially under predominantly compressive conditions, a resumé of the basics must be given as part of the fundamentals of the mechanical behaviour of rocks.

Associated with friction there is the important phenomenon of wear at the sliding surfaces, which leads to the formation of *gouge*, the name given to the granular material that is the product of wear. Although sliding on clean surfaces may be the ideal frictional situation, it is rarely the case in studies on rocks. The formation of gouge and its role in the physics and mechanics of the sliding process are therefore intimately bound up with the study of friction in rocks. Further, because of the variable amounts of gouge that may be involved, a distinction arises between cases where the sliding rock surfaces make actual contact, through the gouge layer if present, and cases where the relative motion of the rock faces is entirely accommodated within gouge.

As with the study of fracture, there are broadly two approaches to the study of friction, (1) the phenomenological, and (2) the physical and micromechanical:

1. The phenomenology of friction consists mainly of the relationships between the macroscopic forces and relative displacements to which contacting bodies are subjected. The simplest, classic approach deals with the coefficient of friction as a steady state property. However, there have also been many studies of dynamical aspects, especially in more recent years, focussing on the transient responses to changes in rate of displacement or loading and on the role of time. Stick-slip instability is another aspect of dynamic behaviour, which arises from the mechanical interaction of the loading system and frictional behaviour of the sliding surface. These topics are dealt with in Sect. 8.2 and 8.3.

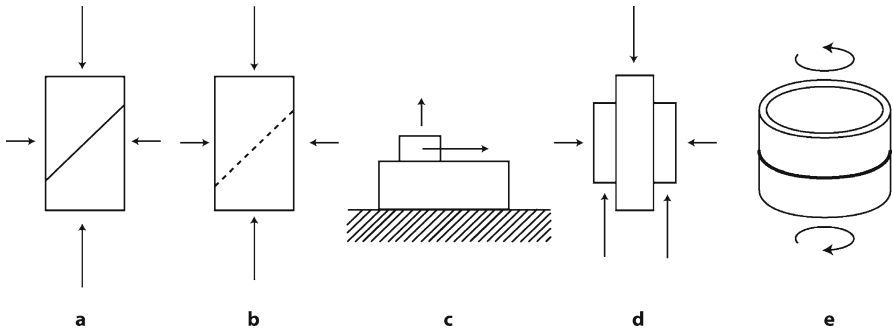


**Fig. 58.** Common types of friction tests. **a** Sliding on saw cut; **b** sliding on previously induced shear fracture; **c** conventional shear test; **d** double shear test; **e** rotary shear test

- The physical and micromechanical studies are concerned with evidence bearing on the physical mechanisms of friction and with the wear that rubbing surfaces tend to undergo. Considerable geological interest attaches to the formation and properties of gouge as a product of wear. The study of surface topography is also linked to the mechanisms of friction and wear. These topics are dealt with in Sect. 8.4.

Early reviews of friction studies were given by Jaeger (1971), Jaeger and Cook (1979, Ch. 3), Brace (1974) and Logan (1975). These reviews can also be consulted for an introduction to the experimental techniques (the common experimental arrangements are shown schematically in Fig. 58). For more recent reviews, see Byerlee and Wyss (1978), Tullis (1986), Marone and Blanpied (1994a,b), and Marone (1998b).

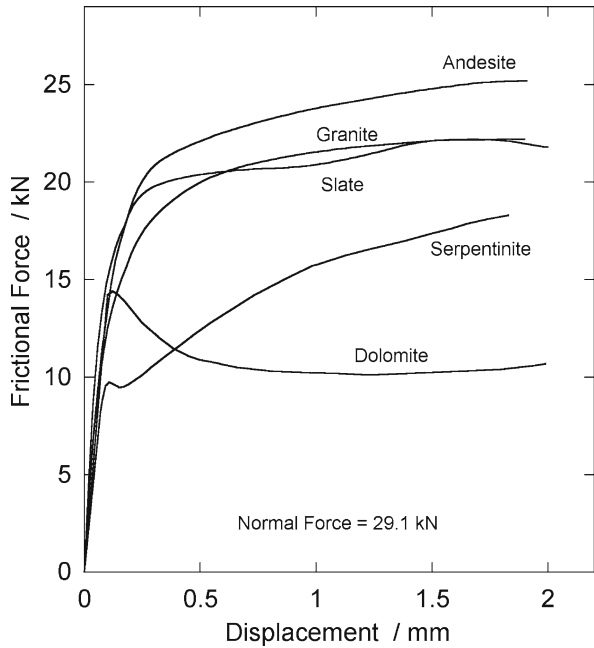
## 8.2 Coefficient of Friction

### 8.2.1 General

The resistance to sliding at an interface is usually expressed in terms of the *coefficient of friction*,  $\mu$ , defined as the ratio of shear force to normal force necessary either to initiate sliding (the coefficient of static friction) or to maintain continuing sliding (the coefficient of kinetic or dynamic friction). In the classic view,  $\mu$  is a constant, reflecting the laws enunciated by Leonardo da Vinci and Amontons that the friction force is proportional to the normal load and is independent of the area of contact. However, the frictional resistance tends to change with amount of sliding (Fig. 59), presumably due to wear processes and so a specified coefficient of friction can be taken as referring either to a steady state reached after a certain amount of sliding or to a transient state at a given stage in the history of sliding. In this section, a steady state is implied. It is also often convenient to normalize the normal and frictional forces to the apparent contact area, specifying them as the normal stress and shear stress, respectively.

**Fig. 59.**

Dependence of friction on amount of sliding for several types of rocks in the double shear test at the same normal force; the area of contact is approximately 600 mm<sup>2</sup> (after Ohnaka 1975)



Values of  $\mu$  for various rocks have been collated by Jaeger and Cook (1979, p. 59), and further values are given by Barton (1973), Ohnaka (1975), Barton and Choubey (1977), Byerlee (1978), Einstein and Dowding (1981), and Lockner (1995). The range is from about 0.2 to 0.8, the majority of values falling within 0.4 to 0.7. No clear dependence on rock type emerges, since the variations between the results of different workers on a given type of rock tend to be comparable to the differences between different types reported by a given worker. Under low normal stresses ( $< 2$  MPa or so), significant variation arises because friction is sensitively dependent on the surface roughness (Barton 1976; Byerlee 1978).

The following values  $\mu$  may be taken as typical, covering static and dynamic friction:

■ Granite	0.5–0.7
■ Gabbro	0.2–0.7
■ Sandstone and quartzite	0.5–0.7
■ Marble	0.4–0.8
■ Serpentinite	0.3–0.5

Individual minerals have been reported as commonly having lower values of  $\mu$  than do the rocks containing them. Thus Horn and Deere (1962) found  $\mu = 0.1–0.2$  for quartz, microcline, and calcite when air-dry, rising markedly to 0.3–0.7 when wet; on the other hand, various hydrous minerals had  $\mu = 0.3–0.7$  when dry and only one-half

these values when wet. Brace and Byerlee (1967) suggested that the difference between mineral and rock can be explained by difference in surface roughnesses used, but it should also be noted that the measurements of Horn and Deere were made with a slider of small area moving over a large surface so that the same conditions for build-up of gouge may not apply.

While the values of  $\mu$  for rocks given above serve as a rough guide for a variety of conditions, the values for a given rock are subject to influence by many factors, the more important of which are now considered.

### 8.2.2

#### Influence of Variables

**Normal pressure.** Although the laws of da Vinci and Amontons are obeyed to a rough approximation, measurements show that the coefficient of friction tends to become somewhat smaller as the normal stress is increased, especially beyond about 100–200 MPa (Maurer 1965; Raleigh and Paterson 1965; Byerlee 1967a, 1968, 1978; Hoskins, Jaeger and Rosengren 1968; Handin 1969; Abey and Heard 1973; Edmond and Murrell 1973; Olsson 1974a; Jaeger and Cook 1979, p. 60). This non-linearity leads to various types of expressions being used for the relationship between shear stress  $\tau$  and normal stress  $\sigma$ . Two such expressions are  $\tau = \mu' \sigma^m$  and  $\tau = S_0 + \mu'' \sigma$ , where  $\mu'$ ,  $m$ ,  $\mu''$ , and  $S_0$  are empirical constants. By analogy with the Coulomb condition for macroscopic failure in intact rock,  $S_0$  is often called the cohesion and in practice it can commonly be assigned a value of the order of tenths to tens of a megapascal (Hoskins, Jaeger and Rosengren 1968; Jaeger and Cook 1979, p. 60; Byerlee 1967a, 1970). The constant  $\mu''$  is sometimes termed the coefficient of friction (for example, Engelder 1974b), but this usage departs from normal usage in physics and it would seem better to define the coefficient of friction as  $\mu = \mu'' + S_0/\sigma$  (Byerlee 1978).

In view of the insensitivity of the coefficient of friction of rock at room temperature to the nature of the rock, and of the slight non-linearity with normal stress, Byerlee (1978) has proposed that for many geologic applications (with normal stresses greater than 2 MPa or so) the friction between rocks can be described by the expressions

$$\tau = 0.85\sigma \quad \text{for} \quad \sigma < 200 \text{ MPa} \quad (8.1)$$

$$\tau = 50 \text{ MPa} + 0.6\sigma \quad \text{for} \quad 200 < \sigma < 1700 \text{ MPa}$$

This empirical rule has often been invoked in the geological literature, where it is referred to as Byerlee's law. As shown in Fig. 60, the bilinear relation is applicable to saw cut and fractured surfaces, as well as to surfaces separated by a layer of simulated gouge.

However, it was also noted by Byerlee (1978) that certain clay (illite, montmorillonite and vermiculite) and serpentinite gouges have anomalously low coefficients of friction. Because illite, montmorillonite and serpentine are common constituents of fault gouges, the frictional strengths of these gouges have implications for the limiting shear stresses along fault zones. Extensive studies on these materials have been

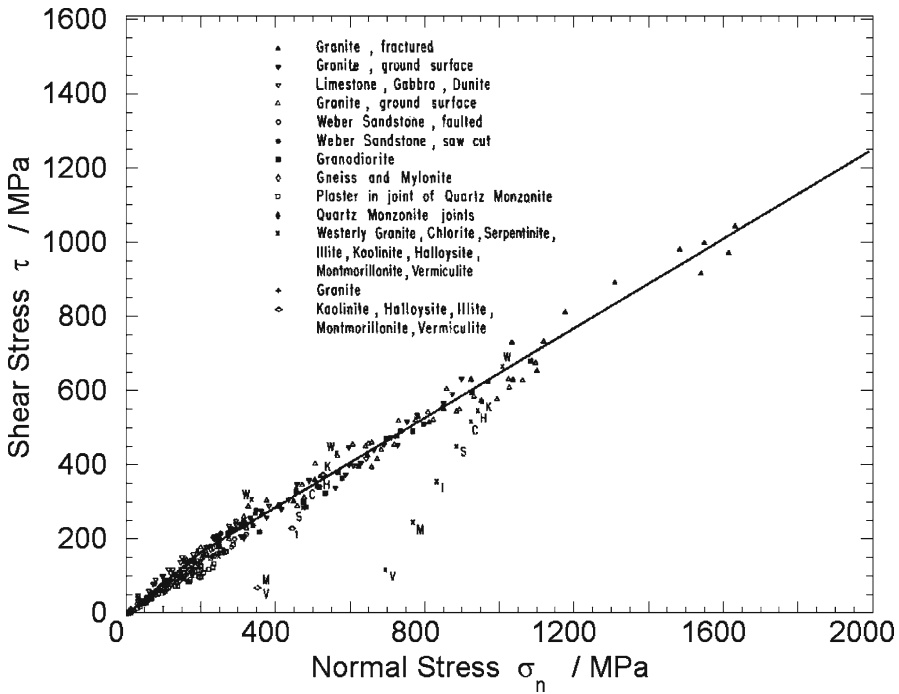
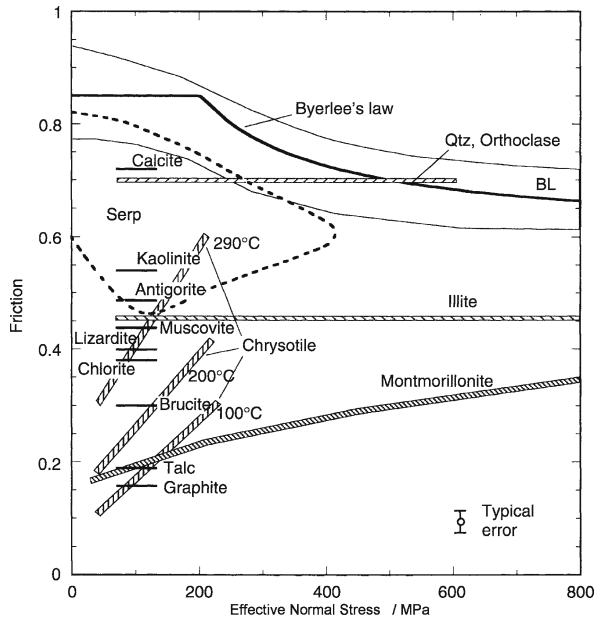


**Fig. 60.** Dependence of friction on normal stress for a wide variety of rocks and gouges (after Byerlee 1978)

conducted in the past two decades. Shimamoto and Logan (1981a) determined the friction coefficient of nominally dry illite gouge to be 0.48, and Logan and Rauenzahn (1987) observed a coefficient as low as 0.08 for nominally dry montmorillonite. Both studies showed that the friction coefficient of a mixed gouge decreased with increasing clay content. Tests under drained conditions showed that clay gouges saturated with water are consistently weaker than the dry gouges (Morrow, Radney and Byerlee 1992). The coefficient of friction for various clay-rich gouges from the San Andreas and Hayward fault zones in California ranged from 0.21 to 0.55 under saturated, drained conditions (Morrow, Shi and Byerlee 1982).

Very low friction has also been documented in certain serpentinite gouges. There are three major varieties of serpentine (lizardite, antigorite and chrysotile). A compilation including serpentinite data is shown in Fig. 61. The lowest values of friction coefficient (0.15–0.35) were determined by Reinen, Weeks and Tullis (1994) for a chrysotile (identified incorrectly as lizardite). Even though higher friction coefficients have been measured in lizardite, the values for both chrysotile and lizardite are lower than the predictions of Byerlee's law over a wide range of pressure. In contrast, the high-temperature form antigorite has friction coefficients that agree with Byerlee's law. In a recent study Moore and Lockner (2004) compared the frictional strengths of 17 sheet

**Fig. 61.** Frictional resistance of simulated gouge of crushed rock and minerals sheared between driving blocks of granite or sandstone (after Lockner and Beeler 2003a)



structure mineral powders. Adding water causes the friction coefficient to decrease for every mineral tested except graphite, and the dry coefficient of friction ranges upward from 0.2 for graphite, leveling off at 0.8 for margarite, clintonite, gibbsite, kaolinite, and lizardite. Moore and Lockner’s (2004) data also indicate that the dry coefficient correlates directly with calculated (001) interlayer bond strengths of the minerals.

**Surface conditions.** In many rock engineering problems, the maximum effective normal stress acting across discontinuities considered critical for stability range from 0.1 to 2.0 MPa (Barton 1976). At such stress levels, the coefficient of friction is sensitively dependent on surface roughness, and a number of empirical relations for geotechnical applications have been developed (Goodman 1976). For example, Barton (1973) proposed that the frictional strength is related to the normal stress by

$$\tau = \sigma \tan \left[ \text{JRC} \log \left( \frac{\text{JCS}}{\sigma} \right) + \phi_b \right] \tag{8.2}$$

In this expression, the “joint roughness coefficient” JRC is a scale of roughness that varies from 0° (for the very smooth surfaces) to 20° (for the roughest surfaces); thus the frictional strength increases with increasing roughness. The “joint wall compressive strength” JCS is equal to the unconfined compressive strength of the dry rock, but may reduce to as low as 1/4 of this strength for a joint with significant weathering and moisture content. The “basic friction angle”  $\phi_b$  determined from tests on smooth,



unweathered rock surfaces lies between 25° to 35°, and an average value of 30° is commonly assumed (Barton and Choubey 1977).

At higher stresses of interest in geological applications, the coefficient of friction is, in general, not strongly dependent on surface conditions. There are some indications that the coefficient of friction on prepared surfaces increases with increasing surface roughness (Horn and Deere 1962, on minerals; Byerlee 1967a,b, using granite), although Logan (1972, using sandstone) found that the coefficient of friction at first decreased with increasing roughness before going through a minimum. However, the situation is complicated by the wear brought about by the sliding itself, because of which the coefficient of friction changes in the course of sliding, commonly increasing to a steady value. The wear tends to produce a flattening of the surfaces, increasing the area of contact, and to produce a layer of “gouge” or rock flour between the surfaces. Both effects have been said to contribute to an increase in the coefficient of friction (Byerlee 1967a; Dieterich 1972a; Drennon and Handy 1972; Scholz, Molnar and Johnson 1972). In natural joints the friction often shows a pronounced peak on initial sliding, dropping to lower values as sliding is continued (Jaeger 1971). The role of a layer of gouge produced by wear on the sliding surfaces is considered in more detail in Sect. 8.4.3.

The friction on artificial shear fracture surfaces, formed in initially intact rock in triaxial or shear tests, has often been obtained from the final, post-failure part of the load-displacement curve from those tests (Paterson 1958; Jaeger 1959; Maurer 1965, 1966; Murrell 1965; Raleigh and Paterson 1965, and many others; Byerlee 1967a, 1968; Engelder 1974a). The values of  $\mu$  are commonly in the range 0.6 to 1, increasing at lower normal stresses; these values are not markedly different from those measured on cut surfaces, perhaps generally a little higher. Maurer (1965, 1966) and Byerlee (1968) have emphasized that there is remarkable similarity in the friction on fracture surfaces in different types of rocks.

**Moisture and pore pressure.** No clear pattern is evident in the effect on friction of wetting the sliding surfaces, perhaps in part due to insufficient attention to establishing a truly dry reference condition, free of adsorbed water. Sometimes wetting produces no effect (Jaeger and Rosengren 1969, for quartzite; Hoskins, Jaeger and Rosengren 1968, for trachyte); possibly more often there is a slight decrease in the coefficient of friction (Jaeger 1959; Hoskins, Jaeger and Rosengren 1968, for sandstone; Byerlee 1967a, for granite), while increases have been reported in other rocks (Jaeger 1971) and in minerals (Horn and Deere 1962, but not in the platy minerals). Dieterich and Conrad (1984) found that, under conditions of careful drying, the friction between quartzite surfaces was substantially higher than under humid conditions ( $\mu$  of 0.85 to 1.00 against 0.55 to 0.65), while Drennon and Handy (1972) suggest that adsorbed water films may have an important influence on frictional behaviour at low normal stresses.

The influence of fluid chemistry has been investigated to a limited extent. Feucht and Logan (1990) studied the frictional behaviour of a sandstone saturated with aqueous solutions of NaCl, CaCl<sub>2</sub> and Na<sub>2</sub>SO<sub>4</sub> at varying ionic strengths and pH values. Their data suggest that the frictional strength seems to be primarily controlled by the

ionic strength of the pore fluid. Dunning and Miller (1984) observed that the frictional strengths of Berea sandstone saturated with surfactants (surface-active agents) were somewhat higher than samples saturated with distilled water.

The presence of water under pressure at the interface strongly affects the frictional resistance. Although there may be some influence of the wetting itself (for example, Murrell 1965), it is usually found that the resistance to sliding is determined to a first approximation by an effective normal stress  $\sigma_n - p$  where  $\sigma_n$  is the total normal stress and  $p$  is the pressure in the water (Hubbert and Rubey 1959; Byerlee 1967a; Jaeger and Rosengren 1969; Byerlee and Brace 1970). The practical importance of this in geology has been emphasized by Rubey and Hubbert (1959) and its relevance to earthquakes by Healy et al. (1968, 1972). Apparent deviations from the effective pressure principle for friction in serpentinite and clay gouges were reported by Wang and Mao (1980) and Moore et al. (1984) but it is unclear whether fully drained conditions were attained in these experiments in the relatively impermeable gouge materials. However, a comprehensive series of drained tests on illite and montmorillonite gouges by Morrow, Radney and Byerlee (1992) showed that the effective pressure law for friction holds over a wide range of conditions. Their data indicate that loosely bonded interlayer water in an expandable clay such as montmorillonite does not modify the mechanical effect of pore pressure on the frictional behaviour.

**Temperature and sliding rate.** As in the case of composition and surface conditions, there also appears generally to be no strong dependence of friction on rate of sliding or on moderate changes in temperature under dry conditions. Thus, in experiments on a variety of igneous or metamorphic rocks, including granite, gabbro, peridotite, and quartzite, the shear stress needed to cause sliding on a shear fracture previously introduced at low temperature has been found to be not greatly affected by increase in temperature up to around 700 or 800 K although substantial decreases are often seen at higher temperatures (Stesky and Brace 1973; Stesky et al. 1974; Stesky 1978b, and various early triaxial test results quoted by them). In the case of gouge-filled sawcuts in granite, a relative decrease in friction is observed with temperature increase above about 600 K if water is present but not under dry conditions (Blanpied, Lockner and Byerlee 1991, 1995; Lockner, Summers and Byerlee 1986; Chester 1994). In contrast, heating to a temperature of about 473 K caused the frictional strength of serpentinite gouges to increase appreciably, possibly by removal of the adsorbed water (Moore et al. 1996; Moore et al. 1997). Similar strengthening behaviour was also observed in clay and gypsum gouges (Shimamoto 1986a). Donath, Fruth, and Olsson (1973) and Olsson (1974a) found a slight decrease in  $\mu$  up to 573 K in experiments on a limestone, while, Friedman, Logan, and Rigert (1974) found an increase in resistance to sliding on a saw cut in a sandstone as the temperature increased.

To a first approximation, increase in the rate of sliding has been variously found to have no influence or to result in a small increase or decrease in the coefficient of friction in rocks such as granite, gabbro and limestone (Scholz, Molnar and Johnson 1972; Scholz and Engelder 1976; Brace and Stesky 1973; Donath, Fruth and Olsson 1973; Olsson 1974a). However, the small variations in frictional resistance with change in rate of sliding have received much attention in connection with establishing the constitutional relationships for friction dynamics, as will be discussed in the next sections.

## 8.3 Phenomenology of Frictional Behaviour

### 8.3.1 General

It has long been known that the force to set into relative motion two surfaces initially at relative rest is often greater than the force to maintain motion. Conventionally, two coefficients of friction are distinguished: the static coefficient  $\mu_s$  which corresponds to the force to initiate motion, and the kinetic coefficient  $\mu_k$  which is operative for moving surfaces (Rabinowicz 1951). A striking feature of frictional sliding, frequently observed, is an unsteady motion of the sliding surfaces, described graphically as “stick-slip”. The effect has been observed with many materials but in the case of rocks it has attracted particular attention because of the possibility that an understanding of it may throw light on the mechanism of earthquakes (Brace and Byerlee 1966). The fundamental problem of stick-slip is to identify the nature of the instability underlying the fluctuating displacement and sliding speed in response to the applied loading. Although the instability arises from the mechanical interaction of the loading system and sliding surface, the primary source of the phenomenon must lie in the intrinsic properties of the sliding surfaces whereby the resistance to sliding varies during the experiment.

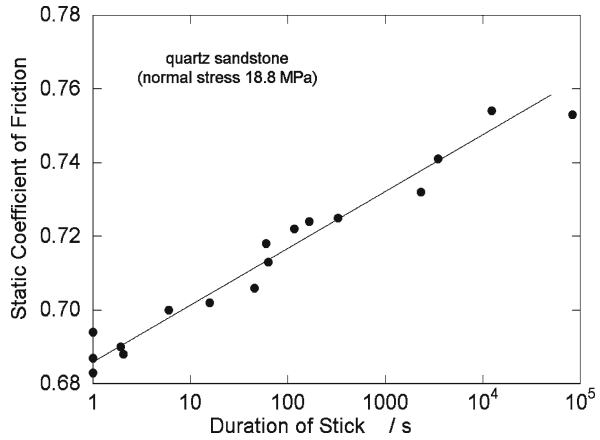
Simply to distinguish between coefficients of static and kinetic friction allows simple models to be set up for theoretical treatments of the stick-slip phenomenon (Jaeger 1971; Jaeger and Cook 1979, p. 63; Johnson and Scholz 1976) but it fails to account for certain complexities of frictional behaviour. Studies of metals (Dokos 1946; Brockley and Davis 1968; Richardson and Nolle 1976) and rocks (Dieterich 1972a, 1981; Scholz and Engelder 1976) have shown that the static coefficient increases with time of contact and the kinetic coefficient is sensitively dependent on the sliding velocity. Furthermore Rabinowicz’s (1958) analysis of metal data indicates that in practice the kinetic coefficient is dependent not only on velocity but also on “the sliding history of a preceding critical distance” which for metals is on the order of 100  $\mu\text{m}$ . These characteristics of friction, first investigated systematically in rocks by Dieterich (1978, 1979a,b, 1981), have provided the experimental bases for development of the rate- and state-dependent friction model. In Appendix 3, constitutive laws for frictional sliding are summarized and constitutive parameters of the rate- and state-dependent friction model are defined.

Phenomenological observations on time dependence of static friction and velocity dependence of kinetic friction are reviewed below. Experimental data on rate- and state-dependence are then summarized. Experimental observations on stick-slip and implications of friction constitutive behaviour on the stick-slip phenomenon will be discussed in Sect. 8.3.5 and 8.3.6, respectively.

### 8.3.2 Time Dependence of Static Friction

Conventionally the static coefficient is determined by comparing the frictional behaviour in two sequential stages of loading. The frictional surface is first held in stationary contact with the shear stress maintained at a level below the static friction. In

**Fig. 62.**  
Increase in static friction  
during static contact in  
quartz sandstone (after  
Dieterich 1972a)



the second stage the shear stress is rapidly increased until the contacting surface moves. The normal stress is maintained constant in both stages. The static coefficient of friction corresponds to the peak frictional resistance attained in the second stage, beyond which the dynamics of the sliding surface may involve stable sliding or stick-slip. By varying the duration of stationary contact, Dieterich (1972a) studied the time dependence of the static coefficient in several porous and compact rocks at normal stresses ranging from 2 to 85 MPa. As illustrated in Fig. 62 the static coefficient generally increases with contact time, and the data follow an approximately linear relation between the coefficient of static friction  $\mu_s$  and the logarithm of the time  $t_s$  of stationary contact.

Subsequent measurements on initially bare surfaces (Johnson 1981; Dieterich and Conrad 1984; Kato et al. 1992; Beeler, Tullis and Weeks 1994; Nakatani and Mochizuki 1996) and on gouge layers (Dieterich 1981; Beeler and Tullis 1995; Nakatani 1998; Marone 1998a) show similar behaviour. This phenomenon has been referred to as time-dependent healing, strength recovery, or ageing. The experimental data can be described by the empirical relation

$$\mu_s = \mu_{s0} + \beta \ln(1 + t_s / \tau) \quad (8.3)$$

where the two coefficients  $\mu_{s0}$  and  $\beta$  are relatively insensitive to normal stress. According to this relationship, the static coefficient of friction approaches a constant value equal to  $\mu_{s0}$  for  $t_s \ll \tau$ . Since Dieterich's (1972a) data showed that no time-dependency was observed for durations of 1 second and less, the cutoff time  $\tau$  is considered to be on the order of 1 s.

Reported values of the coefficient  $\beta$  for rock surfaces and gouges are compiled in Table 6. The data suggest that time-dependent healing is more rapid for initially bare surfaces than gouge layers. While similar behaviour has also been observed in other materials, the healing rates are quite different. For polymer (PMMA and PS) surfaces, the coefficient  $\beta$  ranges from 0.01 to 0.03 at room temperature, and values up to 0.13 were measured at temperatures near the glass transition temperature (Berthoud et al.

**Table 6.** Time-dependent healing coefficient for initially bare surface and gouge layer at room temperature

Rock/gouge type	Time-dependent strengthening coefficient ( $\beta$ )	Normal stress (MPa)	Reference
Initially bare surface			
Porous sandstone	0.007	2 – 48	Dieterich 1972
Granite	0.010	6 – 69	Dieterich 1972
Quartzite	0.009	9 – 85	Dieterich 1972
Graywacke	0.005	10 – 30	Dieterich 1972
Granite	0.009	25	Beeler, Tullis and Weeks 1994
Quartzite	0.005	25	Beeler, Tullis and Weeks 1994
Granite	0.004–0.011	5	Nakatani and Mochizuki 1996
Granite, quartzite and quartz (vacuum dry)	0	1.7	Dieterich and Conrad 1984
Simulated gouge layer			
Crushed granite	0.003–0.004	10	Dieterich 1981
Crushed granite and quartzite	0.004	25	Beeler and Tullis 1995
Crushed granite	0.004	25	Marone 1998a
Crushed granite	0.001–0.004	10	Nakatani 1998

1999). A relatively high value of about 0.03 was observed for steel surfaces (Dokos 1946; Rabinowicz 1958). Since Dieterich and Conrad (1984) have observed that the static coefficients in a very dry environment were essentially independent of contact time, it is inferred that a humid environment is necessary for the occurrence of time-dependent healing. Mechanisms that have been proposed for time-dependent healing will be discussed in Sect. 8.4.5.

Although the empirical relation (Eq. 8.3) is widely used for rock and gouge, it should be noted that other relations (such as power law) have been proposed for metals (Richardson and Nolle 1976). While the empirical relation describes the static friction as a function of contact time, recent data have demonstrated that the static coefficient also depends on at least two other factors. First, the previous loading history influences the subsequent healing behaviour. As discussed in the next section, the coefficient  $\mu_{s0}$  depends on the velocity that the sliding surface has experienced before it was held in stationery contact. To acquire data of comparable loading paths, a standardized “slide-hold-slide” procedure has been adopted in most recent tests. The load point is first displaced at a relatively slow velocity until a “steady state” kinetic friction is attained, and then it is locked so that the sliding surface is held in nominally stationery contact. After a specific time of hold during which the stress may relax somewhat, the load point is reactivated at a relatively high velocity and the peak stress

attained is measured. Second, it has also been observed that the stress state during the “hold” stage can influence the strengthening rate appreciably. By varying the shear stresses during this stage from zero to near the static friction strength, an increase of the strengthening rate by a factor of 2 or more has been observed in initially bare surfaces of rock (Nakatani and Mochizuki 1996) and polymer (Berthoud et al. 1999). Similar studies in gouge layers (Nakatani 1998; Karner and Marone 1998) show very complex dependence of frictional healing on the shear load. Richardson and Marone (1999) also observed that oscillatory perturbation of the normal stress increased the strengthening rate.

### 8.3.3 Velocity Dependence of Kinetic Friction

It has long been known that the kinetic friction  $\mu_k$  of a metal is sensitive to the sliding speed  $V$  (Rabinowicz 1958; Brockley and Davis 1968; Richardson and Nolle 1976). Empirical relations for kinetic friction and sliding speed have been used in theoretical models for stick-slip (Sampson et al. 1945; Stoker 1950; Brockley, Cameron and Potter 1967) which predict that an instability may occur if  $\mu_k$  decreases with increasing  $V$ . Some of the earliest measurements on rocks were conducted by Scholz and Engelder (1976) who showed that  $\mu_k$  of Westerly granite, Solnhofen limestone and Twin Sisters dunite decreases with increasing  $V$ , for speeds varying over three orders of magnitude.

When a sliding speed is imposed on a frictional interface, it is commonly observed that, after kinetic motion has initiated, the frictional resistance first undergoes transient adjustments before attaining a “steady state” friction. In order to avoid confusion from this transient variation of kinetic friction, a coefficient of friction  $\mu_{ss}(V)$  is defined with reference to steady state sliding. Depending on whether  $\mu_{ss}$  increases or decreases with increasing  $V$ , the sliding behaviour is referred to as “velocity strengthening” or “velocity weakening”.

For a broad range of materials the steady state coefficient has been observed to have an approximately linear dependence on the logarithm of the sliding speed (Dieterich and Kilgore 1994, 1996a,b). Hence the velocity dependence can be characterized by the derivative

$$\frac{\partial \mu_{ss}}{\partial \ln V}$$

which in most geologic materials has values on the order of  $10^{-3}$  to  $10^{-2}$ . Because of its relation to the mechanics of stick-slip and earthquake rupture, the velocity-dependent frictional behaviour has been intensively studied. For a velocity weakening material, since the derivative  $\partial \mu_{ss} / \partial \ln V < 0$ , any perturbation that causes the fault to accelerate can potentially result in strength degradation and slip instability. Conversely it is unlikely that earthquake instability may develop in a velocity strengthening material.

In earlier studies using a double-direct shear apparatus, velocity weakening was observed in initially bare surfaces of granite (Dieterich 1978) and crushed granite gouge (Dieterich 1981) at relatively low normal stresses. In contrast, triaxial tests under

elevated normal stresses indicated velocity-strengthening behaviour in similar materials (Stesky 1978a; Solberg and Byerlee 1984; Logan and Rauen Zahn 1987). Since then, significant efforts have been made to build test machines that can attain relatively long slip distances and a wide range of slip velocities at elevated normal stress and temperature. High-pressure rotary shear experiments have been conducted at speeds ranging over 5 orders of magnitude and cumulative slip distances up to 700 mm (Beeler et al. 1996; Blanpied, Tullis and Weeks 1998). Normal stresses up to 150 MPa have been attained in the double-direct shear apparatus (Kilgore, Blanpied and Dieterich 1993), and triaxial tests have been used to study the velocity dependence under hydrothermal conditions (Blanpied, Lockner and Byerlee 1991; Chester 1994). While the new measurements have shown that velocity weakening may occur over a wide range of normal stress and temperature conditions, they also indicate that whether the quantity  $\partial\mu_{ss}/\partial\ln V$  is positive or negative depends sensitively on the slip displacement and sliding velocity. The velocity dependence is also sensitive to fluid-rock interaction, surface roughness, and gouge particle size. Selected measurements of  $\partial\mu_{ss}/\partial\ln V$  are compiled in Table 7.

The complex influence of slip displacement and sliding speed on velocity dependence of frictional sliding is illustrated in Figs. 63 and 64. For an initially bare granite surface, Beeler et al. (1996) observed a transition from velocity strengthening to weakening at a slip distance of about 10 mm, beyond which  $\partial\mu_{ss}/\partial\ln V$  remained fairly constant (Fig. 63a). Similar transition for a relatively rough surface of gabbro was observed at a distance of about 40 mm (Marone and Cox 1994).

While the coefficients in Fig. 63a were characterized at a limited range of speeds ( $1\text{--}10\ \mu\text{m s}^{-1}$ ), measurements of Kilgore, Blanpied and Dieterich (1993) for granite surface at sliding rates ranging over 7 orders of magnitude showed more complicated behaviour (Fig. 64). In tests conducted at normal stresses ranging from 5 to 150 MPa, velocity weakening was observed at velocities between  $10^{-4}$  and  $1\ \mu\text{m s}^{-1}$ . However, at rates above  $10\ \mu\text{m s}^{-1}$ , velocity weakening was observed only at normal stresses of 30, 70 and 150 MPa, while velocity neutral and strengthening were observed at normal stresses of 15 MPa and 5 MPa, respectively. Blanpied, Tullis and Weeks (1998) also observed a transition from velocity weakening to strengthening with increasing sliding rate for granite surface at a normal stress of 25 MPa. Their data at sliding distances greater than 50 mm showed that  $\partial\mu_{ss}/\partial\ln V$  became positive as the speed increased to above  $1\ \text{mm s}^{-1}$ . Their data for normal stresses ranging from 5 to 25 MPa also suggest an increase of  $\partial\mu_{ss}/\partial\ln V$  by  $10^{-3}$  per decade increase of normal stress.

The evolution of velocity dependence with slip distance in a simulated gouge layer seems to be more complicated. Beeler et al. (1996) observed that even though a transition from velocity strengthening to weakening also occurred in crushed granite at a slip distance of about 10 mm, the trend reversed with  $\partial\mu_{ss}/\partial\ln V$  becoming less negative with further slip (Fig. 63b). In simulated quartz gouge, Mair and Marone (1999) observed a transition from strengthening to weakening at a slip distance of about 5 mm, but the slip weakening trend persisted without any reversal up to a maximum slip distance of 20 mm. Measurements on halite (Shimamoto 1986b; Shimamoto and Logan 1986) and ice (Jones, Kennedy and Schulson 1991) also show several regimes of velocity strengthening and weakening over different ranges of sliding speeds.

**Table 7.** Velocity dependence of the friction coefficient for steady state sliding at room temperature

Rock/gouge type	Normal stress (MPa)	Velocity dependence	Maximum $\left  \frac{\partial \mu_{ss}}{\partial \ln V} \right $	Slip displacement (mm)	Sliding speed ( $\mu\text{m s}^{-1}$ )	Reference
Initially bare surface						
Granite	2	-	0.009	< 10	$10^{-1}$ – $10$	Dieterich 1978, 1981
Granite	25	+	0.002	0 – 10	1–10	Beeler et al. 1996
	25	-	0.005	15 – 400	1–10	
Granite	5	-	0.003	6 – 24	$10^{-3}$ –1	Kilgore, Blanpied and Dieterich 1993
	5	+	0.003	6 – 24	$10^{-10^3}$	
	30 – 150	-	0.005	6 – 24	$10^{-3}$ – $10^3$	
Granite	25	-	0.006	50 – 500	$10^{-2}$ – $10^2$	Blanpied, Tullis and Weeks 1998
	25	+	0.009	50 – 500	$10^3$ – $3.2 \times 10^3$	
Granite (water saturated)	100	-	0.002	< 13	$2 \times 10^{-1}$ –10	Marone, Raleigh and Scholz 1990
Quartzite	3	-	0.009	< 10	0.01–2	Ruina 1980
Dolomite	75	+	0.005	2.5 – 4.7	$10^{-2}$ –1	Weeks and Tullis 1985
Gabbro (smooth)	5	-	0.002	10 – 60	$10^{-1}$ –10	Marone and Cox 1994
Gabbro (rough)	5	-	0.006	2 – 38	$10^{-1}$ –10	
	5	+	0.001	54 – 62	$10^{-1}$ –10	
Serpentine (antigorite)	25 – 125	+	0.018	< 400	$3.2 \times 10^{-3}$ – $3.2 \times 10^2$	Reinen et al. 1991
	25 – 125	-	0.005	< 400	$10^{-1}$ –10	

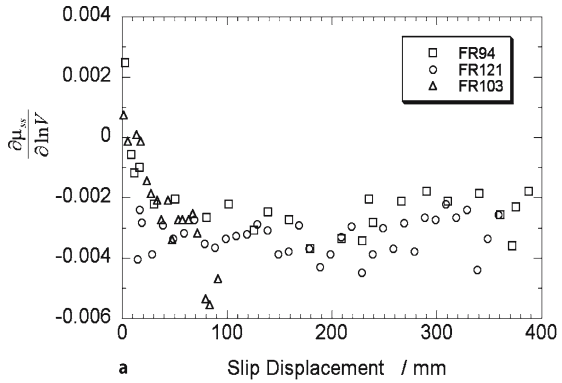


Table 7. Continued

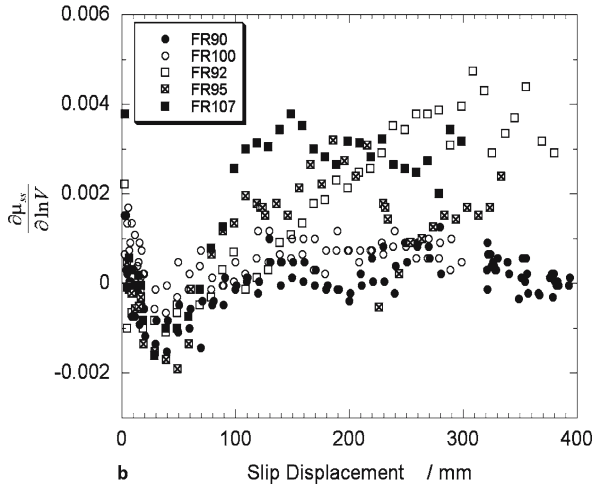
Rock/gouge type	Normal stress (MPa)	Velocity dependence	Maximum $\left  \frac{\partial \mu_{ss}}{\partial \ln V} \right $	Slip displacement (mm)	Sliding speed ( $\mu\text{m s}^{-1}$ )	Reference
Simulated gouge layer						
Crushed granite	10	+	0.004	< 2.5	$2.5 \times 10^{-1}$ –25	Dieterich 1981
	10	-	0.005	2.5 – 8	$2.5 \times 10^{-1}$ –25	
Crushed granite	25	-	0.002	20 – 60	1–10	Beeler et al. 1996
	25	+	0.004	100 – 400	1–10	
Crushed granite	50 – 600	+	0.007	< 10	$7 \times 10^{-3}$ –7	Solberg and Byerlee 1984
Feldspar	25	-	0.008	30 – 170	$10^{-3}$ –10	Scruggs and Tullis 1998
Quartz	25 – 70	+	0.014	2 – 4	$10^{-3}$ –10	Mair and Marone 1999
	25 – 70	-	0.007	8 – 16	$10^{-3}$ –10	
Quartz (water saturated)	50 – 190	+	0.004	< 13	$10^{-1}$ –30	Marone, Raleigh and Scholz 1990
Illite, montmorillonite, and mixture (saturated)	360 – 400	+	0.007	< 8	$10^{-2}$ –1	Morrow, Radney and Byerlee 1992
Quartz–montmorillonite mixture (saturated)	55 – 81	+	0.008	< 12	$3 \times 10^{-3}$ – $2 \times 10^2$	Logan and Rauenzahn 1987
Muscovite	25 – 150	+	0.006	< 200	$10^{-3}$ –10	Scruggs and Tullis 1998
Biotite	25	-	0.006	< 150	$10^{-3}$ –10	Scruggs and Tullis 1998
Serpentine (antigorite, chrysotile)	25	+	0.04	< 276	$10^{-3}$ – $10^{-1}$	Reinen, Weeks and Tullis 1994
	25	-	0.01	< 276	1–32	

**Fig. 63.**

Velocity dependence of steady-state friction as a function of displacement, showing (a) a transition from initial velocity strengthening to steady velocity weakening for initially bare granite surfaces; (b) a similar transition for gouge layers but with more complicated subsequent behaviour (after Beeler et al. 1996)



a



b

**Fig. 64.**

Velocity dependence of steady-state friction as a function of the logarithm of velocity at various normal stresses for sliding granite surfaces (after Kilgore, Blanpied and Dieterich 1993)

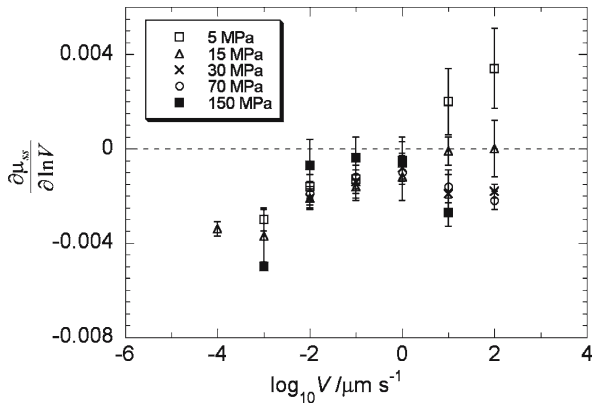
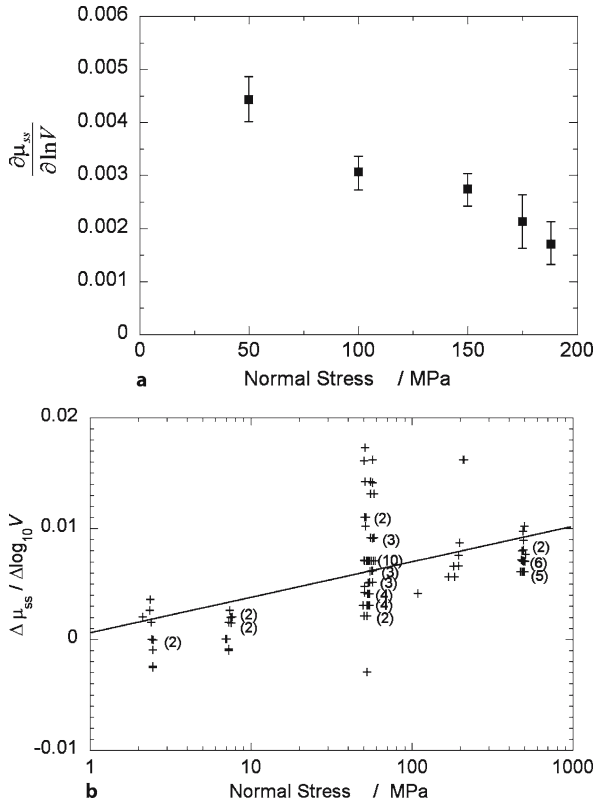


**Fig. 65.**

**a** Velocity dependence of steady-state friction decreasing as a function of normal stress in quartz gouge (after Marone, Raleigh and Scholz 1990). **b** Velocity dependence of steady-state friction as a function of normal stress in crushed granite, showing the opposite trend (after Solberg and Byerlee 1984)



The data of Mair and Marone (1999) also indicated that the velocity dependence is not significantly influenced by either sliding velocity or normal stress. In contrast, Marone, Raleigh and Scholz (1990) observed that  $\partial \mu_{ss} / \partial \ln V$  decreased with increasing normal stress in quartz gouge (Fig. 65a), whereas Solberg and Byerlee (1984) observed that  $\partial \mu_{ss} / \partial \ln V$  of crushed granite increased by  $9 \times 10^{-4}$  per decade increase of normal stress (Fig. 65b).

Experimental data on other rock types indicate significant variability. Measurements on initially bare surfaces and gouges of serpentinite show that, while  $\partial \mu_{ss} / \partial \ln V$  is sensitive to sliding speed, it follows a trend opposite to that for granite (Fig. 64). At relatively low speeds the frictional behaviour is velocity strengthening, switching to velocity weakening or velocity neutral at speeds greater than  $0.1 \mu\text{m s}^{-1}$  or so (Reinen, Weeks and Tullis 1991, 1994; Moore et al. 1997). High-pressure measurements on simulated gouges show that velocity weakening does not occur in either expandable or non-expandable types of clay (Logan and Rauenzahn 1987; Morrow, Radney and Byerlee 1992). However, results at relatively low normal stresses indicate complex and potentially unstable frictional behavior in partially saturated smectite (Saffer et al. 2001; Saffer and Marone 2003).

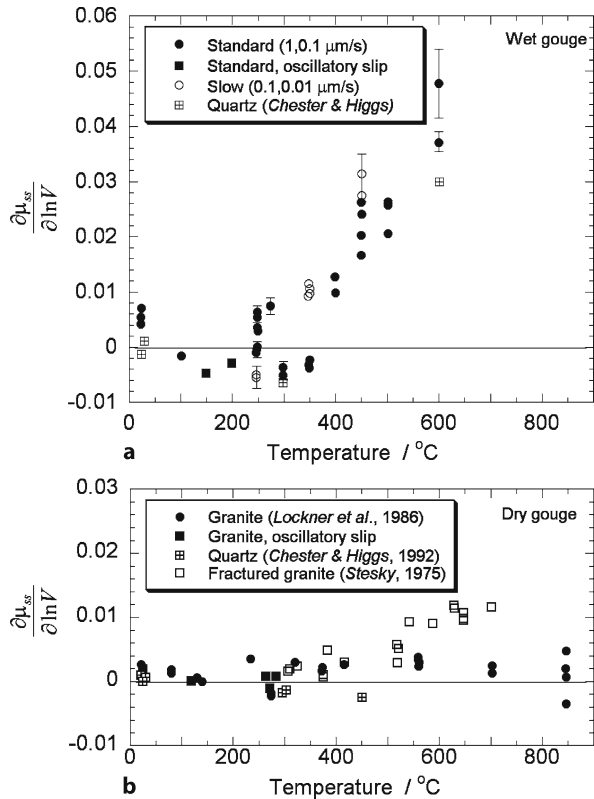
The influence of temperature has been studied in granite, quartz gouge and serpentinite. At elevated temperatures velocity strengthening and neutral behaviour were observed in the prefractured surface of granite (Stesky 1975), granite gouge (Lockner, Summers and Byerlee 1986) and quartz gouge (Chester and Higgs 1992) that were nominally dry (Fig. 66). In the presence of water, more pronounced and complex changes of velocity dependence have been observed in quartz (Chester and Higgs 1992) and granite (Blanpied, Lockner and Byerlee 1995) gouges. While velocity weakening was observed at intermediate temperatures between 373 and 623 K, significant increase of velocity strengthening was measured at temperatures up to 873 K. The influence of temperature on velocity dependence in serpentinite gouges is just as complex (Moore et al. 1997). Velocity strengthening was observed in a limited range of velocities that shifted to faster values at elevated temperatures.

In an earthquake mechanics model, velocity weakening can be used as a criterion for slip instability and, on the basis of laboratory data for specific rock and gouge types, the derivative  $\partial\mu_{ss}/\partial\ln V$  can then be prescribed as a function of temperature, normal stress and pore pressure for the analysis of spatio-temporal development of seismicity (Rice 1983; Scholz 2002; Marone 1998b; Lockner and Beeler 2003a). While the experimental data have demonstrated the significant influence of slip and sliding

**Fig. 66.**

Velocity dependence of steady-state friction as a function of temperature for quartz and granite gouges, wet and dry.

**a** The standard and slow (velocity step) and oscillatory slip tests were from data for granite gouge, while the ultrafine quartz data were inferred from relaxation tests. **b** Except for the oscillatory slip data, the measurements were from velocity-step tests (after Blanpied, Lockner and Byerlee 1995)



speed, our understanding of these phenomena is so limited that they have not been accounted for in most earthquake models. In this context it is particularly essential to investigate frictional sliding at speeds on the order of  $1 \text{ m s}^{-1}$ , that is, comparable to coseismic slip velocities. This aspect of rock friction poses a major challenge to the experimentalist, and many important questions remain unanswered. Preliminary data suggest the activation of mechanisms at high sliding speeds that are quite different from those for quasi-static slip. In unconfined rotary shear experiments on gabbro (Tsutsumi and Shimamoto 1997) reported that the frictional coefficient drops to the range of 0.4–0.5 at sliding speeds of 0.43–1.3  $\text{m s}^{-1}$ . They attributed the degradation of frictional strength to the development of shear melting on the sliding surfaces. Recently Goldsby and Tullis (2002) found that the coefficient of friction for quartz rocks decreases markedly, by a factor of three or so, when the rate of sliding was increased from  $10 \text{ } \mu\text{m s}^{-1}$  to  $100 \text{ } \mu\text{m s}^{-1}$  and finally  $3.2 \text{ mm s}^{-1}$ . While their thermal calculations indicate that the temperatures in the samples were not sufficiently high for melting to occur on the entire sliding surface or localized asperities, they suggest that the anomalously low friction coefficient may arise from the presence of a silica gel layer on the quartz surface. It should also be noted that while this “dynamic weakening” phenomenon was observed in a novaculite, it did not occur in Westerly granite which has a lower quartz content (DiToro, Goldsby and Tullis 2004).

#### 8.3.4

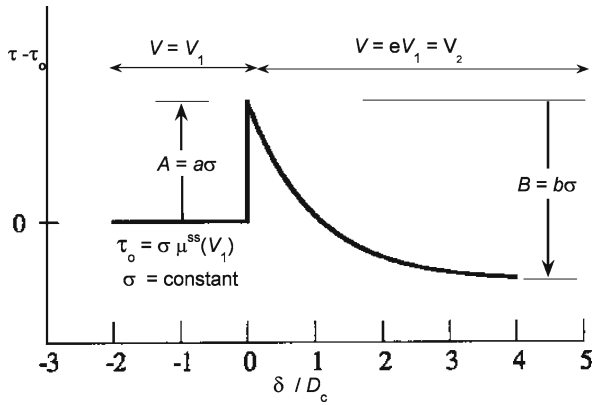
#### Rate- and State-Dependent Friction

The experimental observations summarized above would suggest that a model which independently prescribes a static coefficient that is time-dependent and a kinetic coefficient that is velocity-dependent can capture the attributes of many frictional phenomena. However, such a model may not be adequate for describing the complete evolution of a stick-slip cycle. Experiments have shown that the phenomena of time-dependent healing and velocity-dependent sliding are not unrelated to one another, and therefore the static and kinetic coefficients should not be considered as independent material constants. A model that provides a consistent description of both phenomena should connect the time scale of healing with the velocity of sliding, which naturally suggests introducing a characteristic length scale. Rabinowicz (1958) observed that, in the metal surfaces he studied, a critical slip distance on the order of  $100 \text{ } \mu\text{m}$  was always involved in the transient change of frictional resistance that led to steady state sliding. Presumably this critical slip distance is related to the roughness and characteristic dimension of asperities on the sliding surface. Recognizing the importance of investigating both the transient and steady state behaviour, Dieterich (1978, 1979a, 1981) proposed an experimental methodology which has been adopted extensively in rock friction studies and has provided the experimental bases for development of the rate- and state-dependent friction model.

The rate- and state-dependent model does not distinguish between a static and kinetic coefficient. Instead, it considers the friction coefficient to be a function of the current sliding speed and a state variable that represents a memory of past sliding history. As summarized in Appendix 3, the rate- and state-dependent friction model in its simplest form involves three constitutive parameters  $a$ ,  $b$ , and  $D_c$ . The state variable

**Fig. 67.**

Experimental methodology for measuring the rate- and state-dependent friction parameters



concept was introduced explicitly by Ruina (1980) The methodology for measurement of these constitutive parameters is illustrated in Fig. 67. With the normal stress maintained constant during the test, the frictional system initially slides at a prescribed speed  $V^*$  until steady state is attained at a resistance corresponding to the frictional coefficient  $\mu_{ss}(V^*)$ . A step change of sliding speed is then imposed and the frictional resistance as a function of slip is measured. In response to the step change, the frictional resistance typically undergoes an instantaneous jump, which is followed by a displacement-dependent decay, and finally by stabilization at a steady state friction characteristic of the new sliding speed  $V$ . According to the rate- and state-dependent model, the “direct” effect is described by the instantaneous jump in friction coefficient given by  $a \ln(V/V^*)$ , and the evolution effect is associated with an approximately exponential decay of frictional resistance over a characteristic slip distance  $D_c$  needed to attain the steady-state friction. The net change in frictional coefficient during the evolution stage is given by  $b \ln(V/V^*)$ , and the step change in sliding speed results in a change in steady-state friction given by

$$\mu_{ss}(V) - \mu_{ss}(V^*) = (a - b) \ln(V/V^*)$$

This type of frictional response has been documented in various rock surfaces and gouges, as well as in metals, polymers, wood and paper (Dieterich and Kilgore 1996b). As indicated in Appendix 3, the quantity  $a - b$  can readily be determined as the value of the derivative  $\partial \mu_{ss} / \partial \ln V$  of the steady state frictional strength. All the constitutive parameters can be specified if independent measurements of  $a$  and  $D_c$  are also available. However, since these two parameters characterize the transient responses to velocity perturbation which involve the mechanical interaction between the frictional sliding and loading systems, the contribution of the elastic loading system has to be appropriately separated from the experimental data on the stress and slip before one obtains the intrinsic frictional resistance and slip of the sliding surface. Both forward modelling and inverse method have been employed to derive these constitutive parameters from experimental data (Reinen and Weeks 1993).

**Table 8.** Room-temperature measurements of the friction constitutive parameter *a*

Rock/gouge type	Normal stress (MPa)	Value of <i>a</i>	Reference
Initially bare surface			
Granite (smooth)	2	0.003 – 0.005	Dieterich 1981 inferred by Gu et al. 1984
Granite (rough)	2	0.006 – 0.008	Dieterich 1981 inferred by Gu et al. 1984
Granite	5 – 150	0.011 – 0.020	Kilgore, Blanpied and Dieterich 1993
Granite	25	0.010 – 0.014	Blanpied, Tullis and Weeks 1998
Granite (water saturated)	100	0.024	Marone, Raleigh and Scholz 1990
Quartzite	3	0.011	Ruina 1980
Dolomite	75	0.080 – 0.200	Weeks and Tullis 1985
Gabbro (smooth)	5	0.006 – 0.015	Marone and Cox 1994
Gabbro (rough)	5	0.005 – 0.019	
Serpentinite (antigorite)	25 – 125	0.002	Reinen, Weeks and Tullis 1991
Simulated gouge layer			
Crushed granite	10	0.015	Dieterich 1981 inferred by Gu et al. 1984
Crushed granite	10 – 25	0.004 – 0.024	Biegel, Sammis and Dieterich 1989
Quartz	25 – 70	0.001 – 0.027	Mair and Marone 1999
Quartz (water saturated)	50 – 190	0.007 – 0.016	Marone, Raleigh and Scholz 1990
Montmorillonite	52 – 76	0.001 – 0.095	Logan and Rauenzahn 1987
Quartz-montmorillonite mixture (water saturated)	55 – 81	0.002 – 0.017	Logan and Rauenzahn 1987
Serpentinite (antigorite, chrysotile)	25	0.003 – 0.008	Reinen, Weeks and Tullis 1994

Selected measurements of the direct effect parameter *a* are compiled in Table 8. In most geologic materials, this parameter has values on the order of  $10^{-3}$  to  $10^{-2}$ . The data show that there tends to be more scatter in measurements for a gouge layer than those for initially bare surfaces. While most studies do not indicate any systematic dependence of the direct effect on slip distance or sliding speed, Mair and Marone (1999) reported that the coefficient *a* for quartz gouge was sensitive to slip distance at relatively high sliding speeds (above  $0.1 \text{ mm s}^{-1}$ ). Data of Biegel, Sammis and Dieterich (1989) for crushed granite also indicate that the coefficient *a* increases with surface roughness of the sliding block.

The values for serpentinite in Table 8 are for relatively high velocities with velocity weakening. At relatively low speeds ( $< 0.1 \text{ } \mu\text{m s}^{-1}$  or so), Reinen, Weeks and Tullis (1994) observed velocity strengthening with negligible evolution effect (corresponding to  $b = 0$ ) in response to a velocity change, and they concluded that the deformation was accom-

modated by plastic flow within the serpentinite gouge layer. If one assumes that the rate- and state-dependent model can still be applied in this regime, then a relatively high value in the range of 0.02–0.03 has to be assigned to  $a$ . Chester (1995) and Blanpied, Lockner and Byerlee (1995) adopted a similar approach to model the “frictional” strength of quartz and granite gouge under hydrothermal conditions. At elevated temperatures, the gouge deformation is by plastic flow that is sensitive to strain rate and temperature, which can be approximated by a frictional system with the constitutive parameters  $b \approx 0$  and  $a$  also in the range of 0.02–0.03.

It should be noted that the direct effect is a unique feature of the rate- and state-dependent friction model that had not been accounted for in any previous friction models (Nakatani 2001). Rice, Lapusta and Ranjith (2001) have also emphasized that the parameter  $a$  plays a critical role in the consistent development of a constitutive model for quasi-static sliding and dynamic earthquake instability, which should be able to realistically capture the transition from elastodynamic to quasi-static sliding. For example, their elastodynamic analysis for an anti-plane system can be passed to a quasi-static limit only if the direct effect is nonzero; specifically such a transition requires the sliding velocity

$$V \ll \frac{2\sqrt{a(b-a)}\sigma V_s}{G}$$

(where  $V_s$  is the shear wave speed and  $G$  is the shear modulus), and therefore a non-imaginary value for  $V$  is obtained in a velocity weakening material (with  $b - a > 0$ ) only if  $a > 0$ .

Unlike the dimensionless parameters  $a$  and  $b$ , the third parameter  $D_c$  has dimension of length. Since it characterizes the length scale for the transient evolution of frictional strength, this parameter is expected to be related to geometric attributes of the sliding system, such as surface roughness and gouge particle size. Selected measurements of the constitutive parameters  $D_c$  are compiled in Table 9. For initially bare surfaces of rock,  $D_c$  is on the order of 1–10  $\mu\text{m}$ , whereas measurements on metals (Rabinowicz 1958) and polymers (Baumberger, Berthoud and Caroli 1999) show values on the order of 100  $\mu\text{m}$  and 0.1–1  $\mu\text{m}$ , respectively. The influence of roughness was demonstrated by Dieterich (1978, 1979a) who observed an increase of  $D_c$  with increasing roughness in granite and granodiorite surfaces. Values in the ranges of 10–24  $\mu\text{m}$ , 5–15  $\mu\text{m}$  and 1–3  $\mu\text{m}$  were measured in granodiorite surfaces lapped with #60, #240 and #600 abrasives, respectively.

A wider range of  $D_c$  values have been measured in gouge layers. It seems that the characteristic length depends on surface roughness of the sliding block, gouge particle size, as well as the contact arrangement of the granular system which in turn depends on normal stress, gouge thickness, slip distance and sliding speed. Dieterich (1981) first observed that both surface roughness and particle size affect  $D_c$ , and his data for crushed granite also indicated that  $D_c$  may be larger for the thicker layers. A more systematic study by Marone and Kilgore (1993) showed that at a given displacement, the value of  $D_c$  for a quartz gouge scales with the layer thickness. Other data also suggest that  $D_c$  increases with increasing normal stress (Biegel, Sammis and Dieterich 1989) and sliding velocity (Mair and Marone 1999).



**Table 9.** Room-temperature measurements of the characteristic slip displacement  $D_c$ 

Rock/gouge type	Normal stress (MPa)	Value of $D_c$ ( $\mu\text{m}$ )	Reference
Initially bare surface			
Granite	< 45	1 – 5	Dieterich 1978
Granodiorite	6	1 – 24	Dieterich 1979a
Granite	5 – 150	1 – 10	Kilgore, Blanpied and Dieterich 1993
Granite <sup>a</sup>	25	1 – 4 (5–60)	Blanpied, Tullis and Weeks 1998
Granite (water saturated)	100	3 (71)	Marone, Raleigh and Scholz 1990
Quartzite <sup>a</sup>	3	0.3 (5)	Ruina 1980
Dolomite <sup>a</sup>	75	0.03 – 0.05 (5–100)	Weeks and Tullis 1985
Gabbro	5	1 – 5	Marone and Cox 1994
Serpentinite (antigorite) <sup>a</sup>	25 – 125	6 – 8 (85–180)	Reinen, Weeks and Tullis 1991
Simulated gouge layer			
Crushed granite	10	13 – 275	Dieterich 1981
Crushed granite	10 – 25	5 – 130	Biegel, Sammis and Dieterich 1989
Quartz	25	4 – 183	Mair and Marone 1999
Quartz (water saturated)	50 – 190	1 – 12	Marone, Raleigh and Scholz 1990
Montmorillonite	52 – 76	50 – 300	Logan and Rauenzahn 1987
Quartz-montmorillonite mixture (water saturated)	55 – 81	20 – 400	Logan and Rauenzahn 1987
Serpentinite (antigorite, chrysotile) <sup>a</sup>	25	5 – 14 (119–590)	Reinen, Weeks and Tullis 1994

<sup>a</sup> Data which have been interpreted using two characteristic distances. Values of the second distance  $D_{c2}$  are in brackets.

In its simplest formulation, the rate- and state-dependent model considers a single state variable, the evolution of which is characterized by the parameters  $b$  and  $D_c$ . In response to a velocity step, the transient decay of frictional strength in such a system can be approximated by a single exponential function of slip distance (Appendix 3). However, there are many studies for which the transient decay cannot be described by a single exponential function. In most such cases, the experimental data can be represented by the superposition of two exponential decay functions, characterized by two independent sets of constitutive parameters:  $(b_1, D_{c1})$  and  $(b_2, D_{c2})$ . In this scenario, the velocity dependence of steady state sliding friction is described by

$$\frac{\partial \mu_{ss}}{\partial \ln V} = a - (b_1 + b_2)$$

Measurements for a variety of materials show that the distance  $D_{c2}$  is usually greater than  $D_{c1}$  by an order of magnitude (Table 9). Under elevated temperatures Chester (1994) determined characteristic distances on the order of 100  $\mu\text{m}$  for nominally dry and saturated quartz gouge, and he suggested that these relatively high values possibly correspond to  $D_{c2}$  since the evolution associated with  $D_{c1}$  might not have been resolved.

Additional complications were revealed by two recent studies, which suggest that the characteristic weakening distance can be significantly larger than the quasi-static measurements in relatively small samples. Chambon, Schmittbuhl and Carfdir (2002) conducted gouge shear experiments on a ring-shaped sample of quartz sand, with a thickness and diameter of about 100 and 600 grains, respectively. They also observed appreciable slip-weakening over a characteristic distance of about 0.5 m. While this overall weakening occurred over a large slip distance, a secondary velocity-weakening behaviour was also observed with a  $D_c \sim 100 \mu\text{m}$ . In rotary shear experiments on initially bare surfaces of a quartzite and a novaculite, Goldsby and Tullis (2002) also reported a weakening distance  $D_c \sim 0.5 \text{ m}$  at relatively high speeds (up to  $3.2 \text{ mm s}^{-1}$ ). Such high slip distances are comparable to values of  $D_c$  inferred by some seismologists from dynamic modelling of strong motion data, as discussed later in Sect. 8.3.7.

### 8.3.5

#### Experimental Observations on the Occurrence of Stick-Slip

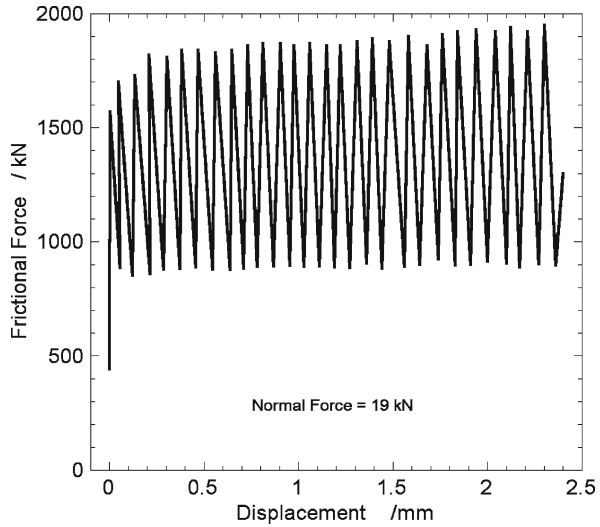
The stick-slip phenomenon is manifested by an intermittently unsteady relative motion of the sliding surfaces. This type of frictional instability has been observed with many materials (Bowden and Tabor 1950; Jaeger 1971; Rabinowicz 1995; Persson 2000). In the case of rocks it has attracted particular attention because of the possibility that an understanding of it may throw light on the mechanism of earthquakes. Here we shall summarize the observations and ideas relating to the stick-slip phenomenon. For possible relevance to earthquakes, see the following papers and reviews: Brace and Byerlee (1966, 1970); Brace (1968, 1969c, 1972a); Byerlee (1968); Rikitake (1968); Walsh (1971b); Dieterich (1972b), Scholz, Molnar and Johnson (1972); Johnson, Wu and Scholz (1973); Weeks, Lockner and Byerlee (1978); Ohnaka (1978, 1996); Rice (1983); Ohnaka et al. (1986); Scholz (1992, 1998); Dieterich and Kilgore (1996b); Marone (1998); Rice et al. (2001); Lockner and Beeler (2003b). We shall first review early rock mechanic investigations that have centred on the factors which determine whether or not stick-slip occurs in a given experimental arrangement.

Stick-slip behaviour has been observed in various experimental arrangements, those commonly used being depicted in Fig. 58. Examples of how the registered shearing force varies with sliding displacement are given in Figs. 68 and 69 for various situations involving stick-slip. It will be noted that the amplitude of the force fluctuation, usually referred to as the stress drop when normalized to unit surface area, varies widely. However, the chief interest of early studies has centred on the factors that determine whether or not stick-slip occurs in a given experimental arrangement. These factors are as follows:

1. *Type of rock and gouge.* Stick-slip behaviour has at one time or another been reported for almost all of the common types of rocks – acid and basic igneous rocks,

**Fig. 68.**

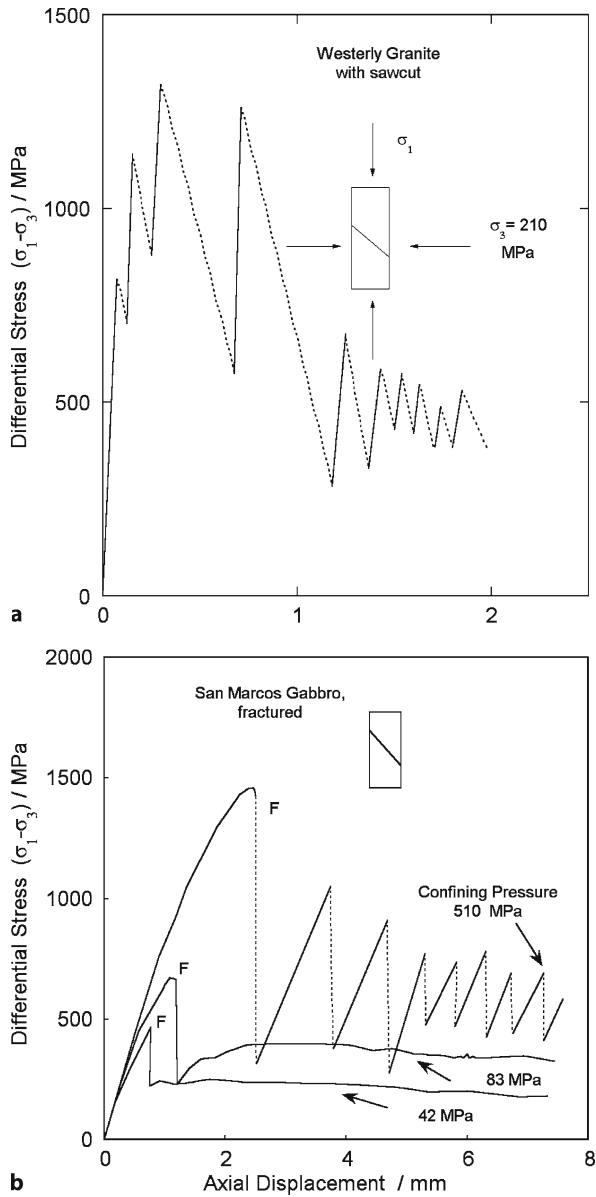
Stick-slip oscillations during frictional sliding in a “soft” double shear apparatus, using quartzite with worn ground surface of 3.3 micrometre initial average roughness; the area of contact is 5800 mm<sup>2</sup> (after Jaeger and Cook 1971)



calcareous rocks, quartzites, and others – provided the porosity is not high. However, under given conditions there are definite trends with mineral content. The presence of quartz seems to be especially conducive to stick-slip. This trend is revealed by the wide-spread use of granite, quartzite, and sandstone in stick-slip studies (Brace and Byerlee 1966; Byerlee 1967a, 1970; Byerlee and Brace 1968; Hoskins, Jaeger and Rosengren 1968; Jaeger and Cook 1971; Dieterich 1972a; Humston and Logan 1972; Scholz, Molnar and Johnson 1972; Logan et al. 1973; Ohnaka 1973a; Engelder 1974c, 1976; Friedman, Logan and Rigert 1974; Stesky et al. 1974, and others). The same trend is revealed in a comparative study of gneisses by Jackson and Dunn (1974), who observed an increasing tendency to stick-slip with increasing quartz content (and decreasing mica content), and it is further consistent with the observations on minerals by Horn and Deer (1962), who encountered stick-slip only in quartz although only when the surfaces had been wetted. Another factor that has been observed to influence stick-slip behaviour is the orientation of the surface with respect to the foliation in a gneiss (Jackson and Dunn 1974; La Fountain and Dunn 1974).

In contrast, the presence of serpentine has been found to inhibit stick-slip (Byerlee and Brace 1968; Brace 1972a), while chlorite and mica are said by the same authors to have little influence. However, there are also many studies of initially bare surfaces and gouge layers of serpentinites that exhibit unstable sliding (Ohnaka 1975; Summers and Byerlee 1977; Dengo and Logan 1981). The sliding behaviour of clay gouges has been investigated extensively, and most of these studies indicate the absence of stick-slip (Summers and Byerlee 1977; Wang and Mao 1979; Shimamoto and Logan 1981a; Morrow, Shi and Byerlee 1982). Stick-slip also occurs less readily in carbonate rocks (Byerlee and Brace 1968) but can still be found under suitable conditions, as shown by other observations on marble, compact limestone, and composite sandstone-dolomite specimens (Hoskins, Jaeger and Rosengren 1968; Drennon and Handy 1972; Logan et al. 1973; Ohnaka 1973a, 1975; Olsson 1974a).

**Fig. 69.** Stick-slip oscillations observed during frictional sliding in triaxial apparatus at confining pressures shown (a) on ground saw cut surface in granite (after Brace and Byerlee 1966); (b) on previously induced shear fracture in gabbro, *F* denoting the point of fracture (after Byerlee and Brace 1968)



2. *Surface finish and gouge accumulation.* Surface conditions have usually been recognized as having a primary influence on whether or not stick-slip occurs but because of apparently contradictory observations the specific roles of surface roughness and gouge have not always been clear. For example, some workers have demonstrated stick-slip on shear fracture surfaces (Brace and Byerlee 1966; Byerlee

1967a; Byerlee and Brace 1968) while others have found only stable sliding on such surfaces (Jaeger 1959; Jaeger and Cook 1971); and the presence of gouge has variously been said to increase and to decrease the tendency to stick-slip. However, as further observations accumulated, the following trends emerged more clearly.

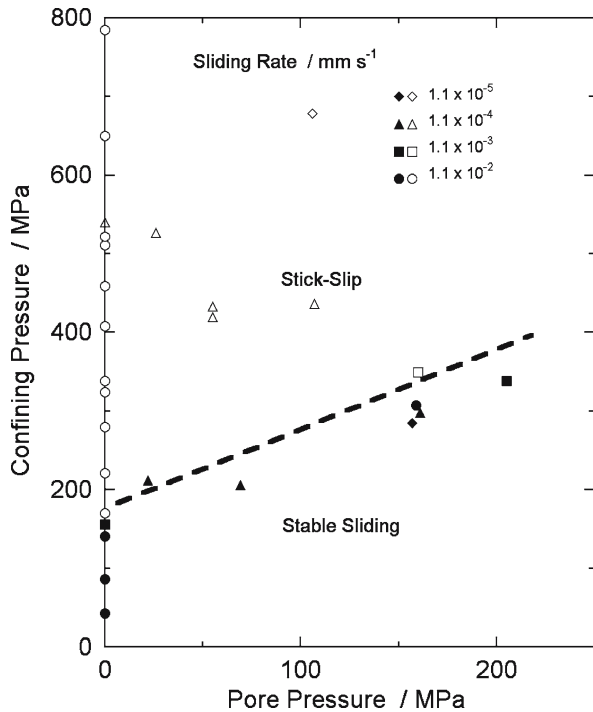
At relatively low normal stresses and in the absence of complication from the accumulation of gouge, insofar as this factor can be dissociated, it appears that stick-slip occurs more readily on smooth surfaces (e.g., finely ground or polished saw cuts, especially if carefully flattened and mated) than on rough surfaces (such as unground or roughly ground saw cuts and shear fracture surfaces) (Hoskins, Jaeger and Rosengren 1968; Logan 1972; Dieterich 1972a; Ohnaka 1973a). Ohnaka also showed that a finer finish was needed for stick-slip behaviour in softer rocks. In the cases just quoted the normal stress did not exceed 100 MPa and generally was much less. The reports of stick-slip on rough surfaces and on shear fracture surfaces have been mainly from experiments under high confining pressure where the normal stress has been at least several hundred megapascals (Byerlee 1967a; Byerlee and Brace 1968). However, the development of gouge may also be closely involved in these distinctions between surface finishes.

There are many observations pointing to stick-slip being inhibited or reduced in amplitude by the build-up of a layer of gouge (Hoskins, Jaeger and Rosengren 1968; Byerlee 1970; Brace 1972a; Drennon and Handy 1972; Scholz, Molnar and Johnson 1972; Jackson and Dunn 1974; Byerlee and Summers 1976). However, gouge does not always inhibit stick-slip. Dieterich (1972a) found stick-slip on coarsely-ground surfaces only if there was an accumulation of gouge, and Johnson (1975) found that gouge appeared to enhance stick-slip on dunite although the stress drops were smaller than those in similar experiments on Westerly granite in which Scholz, Molnar and Johnson observed an inhibiting influence of gouge. There are also observations in which a stable sliding regime is succeeded by a stick-slip regime as sliding is continued where the accumulation of gouge may be involved or artificial gouge is being "conditioned" (e.g., Jaeger and Rosengren 1969; Logan et al. 1973; Engelder 1974b; Engelder, Logan and Handin 1975). Thus the presence of gouge in itself cannot be correlated uniquely with the presence or absence of stick-slip. Its influence presumably depends on the nature and specific behaviour of the gouge layer, for example, possibly on its propensity to develop local or boundary shears, or on its degree of induration; in particular, the nature of the sliding in case of artificial gouge depends strongly on the nature of the minerals constituting the gouge, especially on their Mohr hardness (Shimamoto and Logan 1981b).

3. *Normal Stress.* There is wide agreement that increase in normal stress favours stick-slip. If stable sliding occurs at low normal stresses, there is commonly a transition to stick-slip at higher normal stresses, provided the rock remains brittle; and in the stick-slip regime the stress-drop increases as the normal stress increases (Byerlee and Brace 1968; Brace 1969a, 1972a; Byerlee 1970; Drennon and Handy 1972; Humston and Logan 1972; Scholz, Molnar and Johnson 1972; Abey and Heard 1973; Christensen, Swanson and Brown 1974; Engelder 1974b,c, 1976; Engelder, Logan and Handin 1975). If pore pressure is present, the same trend is found to be valid with respect to the effective confining pressure (Byerlee and Brace 1972; Stesky et al. 1974; Fig. 70), although there may be some complications (Wang and Haimson 1974). The reversed

**Fig. 70.**

Influence of confining pressure and pore pressure on occurrence of stick-slip; experiments on San Marcos gabbro at the various strain rates shown. *Closed symbols:* stable sliding; *open symbols:* stick-slip; the *broken line*, representing an “effective pressure” (confining pressure minus pore pressure) of 160 MPa, coincides with the boundary between the two sliding regimes (after Byerlee and Brace 1972)

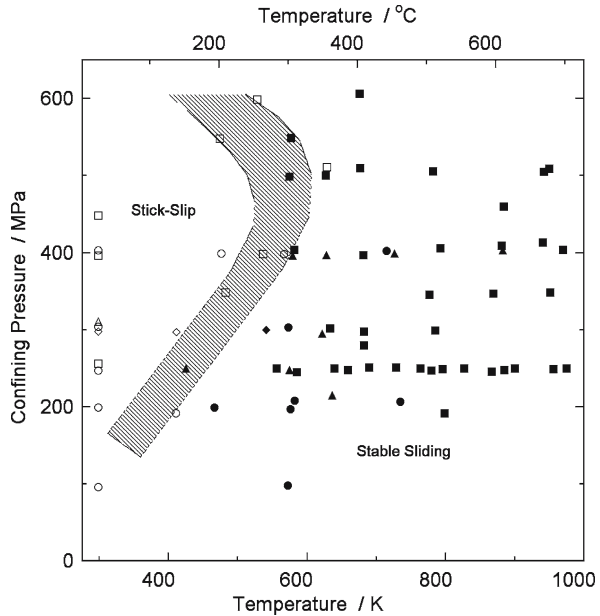


trend, from stick-slip to stable sliding with increased confining pressure, has also been observed by Engelder and co-workers (Engelder 1974c; Engelder, Logan and Handin 1975) and by Olsson (1974a); in the first case, the transition is correlated with a brittle-ductile transition in the compacted quartz powder constituting artificial gouge, and in the second case, it occurs in limestone at 300 °C. Similarly in granite there tends to be a transition back from stick-slip to stable sliding, including on shear fracture surfaces, but at very high confining pressures (Brace and Byerlee 1970; Brace 1972a; Stesky et al. 1974).

4. *Temperature.* With increasing temperature stick-slip behaviour is generally observed to be replaced by stable sliding, under moderate to high normal stresses. Under confining pressures of 300–400 MPa, this transition occurs at 200–300 °C for Westerly granite (Fig. 71), rather higher for quartzite and somewhat lower for gabbro, anorthosite, and dunite (Brace and Byerlee 1970; Brace 1972a; Stesky et al. 1974). In the case of a sandstone, stick-slip behaviour at room temperature was found to give way to episodic sliding at 150–250 °C and to stable sliding at 400 °C (Friedman, Logan and Rigert 1974). In limestones under low normal stresses, on the other hand, moderate increase in temperature appears to promote stick-slip. Thus Olsson (1974a) found stick-slip in limestone in the temperature range 200–300 °C at confining pressures up to 60 MPa, and Drennon and Handy (1972) found that increase in temperature around 100 °C promoted stick-slip in limestone under very light loads, an effect which they attributed to driving off adsorbed water films that are favourable to stable sliding.

**Fig. 71.**

Influence of temperature on occurrence of stick-slip: experiments on Westerly granite in triaxial apparatus using saw cut (*circles*), shear fracture formed at room temperature (*squares*, or *diamonds* in a few cases of pore pressure plotted at the corresponding “effective pressure”), or shear fracture formed at test temperature (*triangles*). *Closed symbols*: stable sliding; *open symbols*: stick-slip (after Stesky et al. 1974)



5. *Dynamical Aspects.* Close observation shows that the sticking intervals in the stick-slip sequence are not necessarily intervals of no motion at all; rather, the slip movements represent fairly abrupt increases in velocity succeeding a measurable slower motion. Sometimes it has been implied that the slower motion is a continuous one on which the slip motion is superimposed (Humston and Logan 1972); otherwise it is seen as a premonitory creep preceding the slip phase, no creep being discernible immediately after the slip phase (Jaeger and Cook 1971; Scholz, Molnar and Johnson 1972; Byerlee and Summers 1975; Johnson 1975; Scholz and Engelder 1976). For granite, Johnson reports that the prior creep displacement was usually 5–15  $\mu\text{m}$ , in part reversible and in part not, while the abrupt slip displacement was about 50–100  $\mu\text{m}$ . Further details of the displacement history in stick-slip episodes, including the effect of temporarily reducing the shear stress, are given by Jaeger and Cook (1971) and Johnson (1975).

Another variant of unsteady sliding motion is that in which the faster rate of sliding is still relatively slow and is not accompanied by acoustic effects, that is, in which there is alternation between intervals of steady creep of moderate rate and intervals of little or no sliding; this phenomenon has been called “*episodic sliding*” (Scholz, Molnar and Johnson 1972; Friedman, Logan and Rigert 1974; Johnson 1975). It has been observed in granite, dunite, and sandstone and appears to be intermediate between stable and stick-slip behaviour in terms of properties and the conditions for its occurrence.

Johnson and Scholz (1976) have shown that there is a great difference between the rupture velocity and the particle velocity in the slip events. The rupture velocity is the rate of propagation of the boundary of the region of rapid slipping into the region where this slipping has not yet begun; its value is approximately that of

the elastic shear wave velocity and it may even slightly exceed this velocity. The particle velocity is defined as half the velocity of one of the sliding surfaces with respect to the other; it depends on the stress drop but has values of the order of tens of  $\text{cm s}^{-1}$ , compared with several  $\text{km s}^{-1}$  for the rupture velocity. Thus the onset of sliding is very quickly established over the whole surface and then most of the sliding itself occurs more or less homogeneously over a much longer period. For a given experimental arrangement, Ohnaka (1973a) and Johnson and Scholz (1976) found that the duration of the sliding event was approximately constant (about 1 ms) independent of the amount of displacement that occurred during it.

Although Byerlee and Brace (1968) found stick-slip to be insensitive to machine stiffness in the range investigated by them, Jaeger and Cook (1971), using machines of higher stiffness, found that stick-slip gave way to stable sliding with increase in machine stiffness. Ohnaka (1973a) showed that increase in stiffness reduces the stress drop and the duration of slipping, the latter effect being predicted to be inversely proportional to the square root of the stiffness. Ohnaka also found that the stress drop was less sensitive to stiffness at high normal load and at slow velocity, and he suggests that this may explain Byerlee and Brace's observation. A further point of interest here is that stick-slip was not observed in triaxial extension tests under similar conditions to those that produced stick-slip in compression or shear tests (Handin, Logan and Ting 1973). This observation suggests a role for coupling between normal and shearing forces through the loading machine and so, by further inference, a possible application to thrust and normal faults (for a discussion of the relative effective stiffnesses of laboratory machines and geological fault environments, see Walsh 1971b).

### 8.3.6

#### Influence of Friction Constitutive Behaviour and Machine Stiffness on Stick-Slip

These laboratory observations indicate that stick-slip is a frictional instability phenomenon that arises from the mechanical interaction between the loading system and the frictional sliding surface. Therefore, the dynamics of stick-slip is expected to be influenced by the machine stiffness and friction constitutive parameters. While stick-slip and stable sliding correspond to two end members of the nonlinear dynamical responses of a frictional system, the transition between these two sliding modes may not occur abruptly, but instead involve complex oscillatory phenomena.

The stability of frictional sliding in small laboratory samples can be analyzed by a spring-slider system with a single degree of freedom (Appendix 3, Fig. 86). The predictions of this analysis for stick-slip depend on the specific friction law assumed, as set out in Appendix 3. It is shown that the rate- and state-dependent friction law allows the most satisfactory interpretation of experimental observations of repeated stick-slip as "limit cycles". In particular, it is predicted from linear stability analysis that there is a critical stiffness

$$k_{\text{cr}} = \frac{(b - a)\sigma}{D_c} \quad (8.4)$$



below which stick-slip may occur in a velocity weakening material (Rice and Ruina 1983). According to this interpretation intrinsic factors (such as rock and gouge type, surface roughness, gouge size distribution, fluid chemistry) and extrinsic variables (such as temperature and strain rate) that favour velocity weakening behaviour (with negative values of  $\partial\mu_{ss}/\partial\ln V$  in Table 7) would promote stick-slip instability. Similarly instability is promoted if the frictional response is associated with a relatively long slip distance (corresponding to a large value of  $D_c$  in Table 9). Whether a stick-slip event such as those reviewed in the previous section would actually occur in a particular test system would ultimately hinge on the machine being sufficiently soft such that its stiffness  $k$  is less than  $k_{cr}$  as given by Eq. 8.4. Even if the frictional sliding behaviour is velocity weakening, stick-slip would be inhibited in a relatively stiff system with  $k > k_{cr}$ . Indeed this critical interaction between the test machine and frictional sliding surfaces has been emphasized in the earlier observations of Jaeger and Cook (1971).

If cyclic stick-slip events were to occur while a constant loading velocity  $V_0$  is applied to the system, the rate- and state-dependent model predicts that the stress drop amplitude is a function of  $\ln V_0$  and  $\ln(k/k_{cr})$ , and it also scales with  $(b - a)\sigma$  (Gu and Wong 1991; He, Wong and Beeler 2003). This prediction is in qualitative agreement with earlier laboratory observations that document the influence of loading velocity, stiffness and normal stress on the development of stick-slip (Rabinowicz 1958; Ohnaka 1973a; Engelder, Logan and Handin 1975; Teufel and Logan 1978; Shimamoto and Logan 1986). It is also in agreement with recent investigations (Wong and Zhao 1990; Karner and Marone 2000) that specifically address the influence of these factors. These studies have important implications for the scaling of seismic stress drop with earthquake recurrence time (Kanamori and Allen 1986; Beeler, Hickman and Wong 2001; Scholz 2002).

Between the two end members of stable sliding and cyclic stick-slip, very complex dynamical behaviour can arise from the nonlinear coupling between the test machine and frictional system (Gu et al. 1984). If the equality  $k = k_{cr}$  is satisfied, then the sliding motion is predicted to involve quasi-static oscillations with a period of

$$2\pi \frac{D_c}{V_0} \sqrt{\frac{a}{b-a}}$$

Such self-sustained oscillations are akin to the “*episodic sliding*” phenomenon described in earlier studies (Scholz, Molnar and Johnson 1972; Friedman, Logan and Rigert 1974; Johnson 1975), as well as recent studies in silicate and dolomite rocks (Weeks and Tullis 1985; Wong et al. 1992). In the “neutral stability” regime where the stiffness  $k$  is comparable to the critical value  $k_{cr}$ , even if the stiffness is slightly higher than the critical value (Eq. 8.4) and the system is predicted to be stable from a linearized analysis, stick-slip instability may actually occur if the frictional sliding system is significantly perturbed (Gu et al. 1984). Laboratory studies have also documented the occurrence of period-doubling and apparently chaotic oscillations in the transition from stable sliding to cyclic stick-slip, which is predicted by numerical simulations for spring-slider system that obeys a friction law with more than one state variable (Ruina 1980; Gu and Wong 1994b).

### 8.3.7

#### Nucleation and Propagation of Dynamic Shear Rupture

In a relatively small sample the slip occurs almost simultaneously on the whole surface, and therefore its development can be modelled satisfactorily by a system with a single degree of freedom. However, frictional sliding experiments on such a sample do not provide any information on how slip initiates and propagates dynamically along the surface. To resolve details of the nucleation and propagation of frictional instability, a biaxial system with a sliding surface 2 m long was used by Okubo and Dieterich (1981, 1984) and a somewhat smaller surface 0.4 m long was studied by Ohnaka et al. (1986) and Ohnaka and Kuwahara (1990). These studies have demonstrated that slip initiates from stress concentration possibly associated with a localized structural heterogeneity along the sliding surface. Once nucleated the localized slip grows quasi-statically to a patch of finite dimension  $L_c$ , and then dynamic motion sets in with the inertia-controlled rupture propagating away from the nucleation patch at a speed comparable to that for shear wave propagation.

At a fixed point on the surface, the incipient arrival and subsequent propagation of the dynamic instability are manifested initially by a quasi-static increase of the shear stress to attain a maximum  $\tau^P$ , after which the shear stress decreases with slip until it attains a residual value. The strength degradation process occurs over a characteristic slip distance  $D_0$  and can be described by the slip-weakening model (Ida 1972; Palmer and Rice 1973) (Appendix 3). For a large granite sample Okubo and Dieterich (1984) determined average  $D_0$  values of 25  $\mu\text{m}$  and 5  $\mu\text{m}$ , respectively for rough and smooth surfaces.

The effective shear fracture energy  $G_c$  in mode II (Appendix 1) can also be determined by an integration under the slip-weakening curve in excess of the residual friction (Rice 1980; Wong 1982c) corresponding to the hatched area in Fig. 21b. Values of  $G_c$  so determined range from 0.1–1  $\text{J m}^{-2}$  for smooth sawcut surfaces under low normal stresses (Okubo and Dieterich 1981; Ohnaka et al. 1986) to  $10^4$ – $10^5$   $\text{J m}^{-2}$  for shear fracture of initially intact rocks under elevated pressures and temperatures (Wong 1982c; Cox and Scholz 1988; Lockner et al. 1991; Kato, Ohnaka and Mochizuki 2003). There is an overall trend for the shear fracture energy to increase with normal stress and structural complexity of the shear (Okubo and Dieterich 1986; Wong 1986; Li 1987; Ohnaka and Shen 1999), possibly related to their effects on the stress drop and characteristic slip distance. While the laboratory measurements for shear fracture of initially intact rocks are comparable to  $G_c$  values for relatively small earthquakes inferred seismologically, significantly higher values on the order of 1–10  $\text{MJ m}^{-2}$  have been reported from strong motion modelling of large earthquakes. In relation to the slip-weakening model, the seismological data imply that the characteristic slip distance  $D_0$  for large earthquakes can range up to 1 m or so (Mikumo et al. 2003). Numerical simulations using a rate- and state-dependent model (Okubo 1989; Bizzarri and Cocco 2003) have shown that the dynamic rupture process can effectively be represented by a slip-weakening curve with a weakening distance  $D_0$  that is an order of magnitude larger than the constitutive parameter  $D_c$  (Appendix 3, Table 9). Hence the seismological data seem to suggest that the characteristic distance  $D_c$  can be up to 0.1 m or so for large earthquakes.

A direct shear system (Fig. 58d) with a surface 0.29 m long was used by Ohnaka and Shen (1999) to investigate the nucleation of frictional instability. Unless one has a dense array of transducers on the large frictional surface, it is difficult to measure accurately the nucleation zone dimension. Nevertheless Ohnaka and Shen (1999) inferred from their data for granite surfaces with different degrees of roughness that slip first nucleated quasi-statically on a patch with characteristic dimension  $L_c$  on the order of 10–100 mm. The patch size increases with increasing roughness and seems to be linearly related to the slip distance  $D_0$ . For a linear slip-weakening law such that the frictional stress  $\tau$  decreases linearly with the slip  $\delta$ , Uenishi and Rice (2003) presented a 2-dimensional analysis of the nucleation of instability on a slip-weakening fault subjected to a heterogeneous, locally peaked “loading” stress. They proved that the nucleation length  $L_c$  is independent of the shape of the loading stress distribution, with a “universal” value given by

$$L_c = 1.158 \frac{G}{W} \quad (8.5a)$$

where  $G$  is the shear modulus and  $W = d\tau/d\delta$  is the slip-weakening rate, with the implication that the nucleation patch size  $L_c$  is proportional to  $D_0$ .

Alternatively one can use a rate- and state-dependent friction model to analyze the nucleation process. If slip has developed over a patch of characteristic dimension  $L$  embedded in an infinite elastic medium, the effective shear stiffness of such a patch can be approximated by  $k = \eta G/L$ , where  $\eta$  is a geometric factor with numerical value on the order of 1 (Walsh 1971b; Dieterich 1992). Dieterich (1986) pointed out that frictional instability would develop when the stiffness attains the critical value given by Eq. 8.4, which implies that the patch has the critical size

$$L_c = \eta \frac{GD_c}{\sigma(b-a)} \quad (8.5b)$$

Once the critical condition is attained, dynamic instability propagates away from the nucleation patch with a rupture speed on the order of the shear wave speed  $V_s$ . The maximum speed for the propagation of a crack tip during dynamic rupture is a fundamental question in mechanics (Rosakis 2002) and seismology (Das 2003). Theory predicts that in an ideally elastic solid the maximum rupture speed is given by the Rayleigh wave speed for mode I and mode II crack propagation and by the shear wave speed for a mode III crack (Kostrov and Das 1988; Freund 1990). These limiting speeds were derived assuming that there is no friction on the crack surface. However, if friction on the crack surface and the inelastic yielding in the vicinity of the crack tip are accounted for, numerical simulations (e.g., Andrews 1976b) have shown that the rupture speed of an in-plane shear crack could exceed the Rayleigh wave speed. Freund (1979) presented an asymptotic solution which shows that a mode II crack may propagate by the rupture jumping ahead of the primary rupture front to propagate at a “super-shear” speed equal to  $\sqrt{2}V_s$ . Such a scenario in brittle polyester resin was resolved in detail by Rosakis, Samudrala and Cokjer (1999) using dynamic photoelasticity measurements.

In Okubo and Dieterich's (1984) study, representative rupture speeds were 2.5–4.0 km s<sup>-1</sup> for the smooth fault and 0.5–1.5 km s<sup>-1</sup> for the rough fault. Since the Sierra white granite they used has a  $V_s = 3$  km s<sup>-1</sup>, super-shear rupture speeds were observed in many of their tests on the smooth fault. Okubo and Dieterich (1984) also observed that the slip velocity was approximately proportional to the stress drop and shear wave speed. The slip velocities were on the order of 1 cm s<sup>-1</sup>, with higher values recorded on the smooth fault. Qualitatively similar observations were reported by Ohnaka, Kuwahara and Yamamoto (1987) in smaller samples. Notwithstanding these laboratory observations, seismological data indicate that the rupture speeds of most earthquakes are lower than the Rayleigh wave speed (Madariaga and Olsen 2000; Das 2003). However, there are also reports from localized areas which show that super-shear rupture may have occurred during the 1979 Imperial Valley (Archuleta 1984), the 1992 Landers (Olsen, Madariaga and Archuleta 1997), and the 1999 Izmit (Bouchon et al. 2000) earthquakes.

## 8.4 Physical Aspects of Rock Friction

### 8.4.1 Frictional Slip, Wear and the Formation of Gouge

The most obvious effects at sliding rock surfaces are the development of grooves, pits, or other unevenness and the formation of gouge. Gouge is a product of wear and is nearly always present, although under mild conditions on smooth surfaces the amount may be very small (Hoskins, Jaeger and Rosengren 1968). Under light loads or after small amounts of sliding, surfaces may show evidence of damage only in localized spots near which debris can be seen, indicating only isolated areas of contact. However, under heavier loads and after greater amounts of sliding, the surfaces tend to become entirely covered with gouge; the larger asperities or other features of large-scale unevenness are worn down or filled with gouge so that the area of contact becomes relatively large (Byerlee 1967a; Jaeger 1971). In this section, we deal first with the features such as grooves that develop on the sliding surfaces and then with the characteristics of the gouge itself.

Since no surface is ideally flat, the contact between two surfaces is limited initially to isolated spots at which high contact stresses occur. The relative movement of the surfaces then tends to give rise to *striations and grooves* of various types as the points of contact or asperities move over the opposing surface. Such wear tracks have, of course, long been known (e.g., Jaeger 1971) and they have been examined more closely by Engelder (1974c, 1976), Jackson and Dunn (1974), La Fountain, Swain and Jackson (1975), and Engelder and Scholz (1976).

On the sliding surfaces of rocks such as granite and quartzite, microscopic grooves are formed which have a tapered or carrot-like shape when viewed normal to the surface; the grooves deepen towards the wide end, which is also in the direction in which the opposing block moved. In highly polished Westerly granite, Engelder (1974c) found that such grooves only form when the confining pressure in the triaxial tests on saw-cut specimens exceeds 300 MPa, the pressure at which transition from stable to

stick-slip sliding occurs; the length of the grooves was equal to or less than the amount of the individual slips in the stick-slip progression. A similar situation held for quartzite. However, wear grooves have been observed associated with stable sliding as well as with stick-slip (J. M. Logan, pers. comm.). Macroscopic wear grooves seen on a gneiss when the gouge is removed are described by Jackson and Dunn (1974) and La Fountain, Swain and Jackson (1975); here the lengths of the grooves correspond to the total displacement and the effects depend on the orientation of the gneissic foliation, which affects plucking of grains. Very rough surfaces subjected to large relative displacements develop a more-or-less continuous grooving or corrugation parallel to the movement (Jaeger 1971).

Evidently wear tracks are of various sorts and have various mechanisms of formation, depending on such variables as relative hardness and normal load. Thus Engelder and Scholz (1976) distinguish three types of wear tracks in experiments in which small indenters of chosen hardnesses are drawn over various substrates including polished quartz, microcline, fused silica, and limestone. These types are: (1) a trail of debris when a relatively soft indenter is drawn over a harder surface; (2) a trail of fractures when the hardnesses are equal; (3) a groove when a harder asperity ploughs into the surface (the change from sliding to ploughing with increased indenter hardness also leads to an increase in coefficient of friction). A similar distinction was made by Engelder (1976) in the wear tracks on granite and on quartz and feldspar grains rubbed by asperities of these minerals. The partial ring fractures produced along wear tracks are shown by Engelder and Scholz (1976) to be more prolific as the normal load is increased. They identify the fractures as Hertzian fractures formed under the indenter in a way similar to that described by Jaeger (1971), Graham (1972), and La Fountain, Swains, and Jackson (1975). Presumably this and similar microfracturing in the grains adjacent to the sliding surfaces is an essential part of the process of forming gouge (see, e.g., Hoskins, Jaeger and Rosengren 1968; Engelder 1974a; Conrad and Friedman 1976).

Gouge is the detrital material that is usually formed in greater or lesser amounts during the sliding of rock surfaces. The amount of gouge can be very small and restricted to isolated patches, or it may be present in considerable quantities, including to the extent of forming a continuous layer completely separating the sliding surfaces. The rate of build-up of the gouge might be expected to increase with increasing normal load but in practice this trend is complicated by other factors (Jackson and Dunn 1974). Engelder (1974a) showed that on the fracture surface of a sandstone at a given normal load the thickness of the gouge initially increases linearly with displacement.

In many experimental studies aiming to elucidate the role of gouge in frictional sliding, simulated gouge has been generated by placing a layer of crushed or granular material within a saw cut in the rock and, preferably, giving it a preliminary shearing. Such artificial or simulated gouge has been shown to have structure and properties similar to true gouge produced experimentally by extensive shearing, say on a fracture surface, as well as to natural gouge (Engelder 1974a; Engelder, Logan and Handin 1975).

Optical and electron-microscopical examination of gouge shows that the broken fragments constituting it may be angular or rounded, the latter shape indicating further wear of the particles themselves during further sliding (e.g., Engelder and McKee 1973; Engelder 1974a). The particle sizes reported vary widely, from less than  $0.1 \mu\text{m}$  to  $100 \mu\text{m}$  and are widely distributed in a given sample. The mean particle size also de-

creases and the gouge becomes more compact with increasing normal load and with the presence of water (Jaeger 1959; Engelder 1974a; Engelder, Logan and Handin 1975). Although gouge is commonly a loose powder, it can also develop an “indurated” character, and several types of indurated gouge have been distinguished (Friedman, Logan and Rigert 1974; Jackson and Dunn 1974). Glass has been reported in indurated gouge in quartz-bearing rocks by these authors, the amount of glass increasing when the ambient temperature is raised to 500 °C. The attainment of melting temperatures is not surprising in view of estimates of the heat generated at sliding surfaces (Jaeger 1942, 1959; Bowden and Tabor 1950; McKenzie and Brune 1972), and temperatures of up to 1150 °C have been registered at asperities on sandstone with the use of “thermodyes” (Teufel and Logan 1975a,b).

When the rock surfaces at which relative sliding has taken place are parted, coarse striations or *slickensides* are often observed (Paterson 1958; Jaeger 1959; Riecker 1965; Hoskins, Jaeger and Rosengren 1968; Norris and Barron 1969; Einstein, Baecher and Hirschfeld 1970; Gay 1970; Müller and Siemes 1972). The slickensides occur on both saw cuts and shear fractures but especially when substantial amounts of gouge are formed. Associated with the slickensides are steps which have been observed to face either way but which commonly face the direction of motion of the block on which they appear (that is, so as to oppose the motion). Presumably the steps are release features produced during unloading and parting of the surfaces but their origin must be related to some aspect of the original shearing process. This origin has been discussed by Norris (1969), Gay (1970), Lindström (1974), Ui (1973), and Byerlee et al. (1978); discussion of possible geologic relevance (with further references) will be found in these papers also.

#### 8.4.2 Gouge Deformation

We now give a brief resumé of some of the principal observations on the structure and behaviour of gouge layers, although noting that, at the scale of the layer, the deformation is essentially a plastic deformation rather than a brittle phenomenon and so it is somewhat outside the scope of this monograph. In the case of relatively thick gouge layers, including “artificial gouges”, the relative movement between the opposing surfaces may be entirely accommodated within the gouge layer. Then frictional sliding at the bounding solid surfaces, or friction in a strict sense, is not involved. Nevertheless, in many studies of shearing in gouge layers, the shearing is still viewed as a frictional phenomenon and discussed in terms of one-dimensional shearing displacement between the bounding surfaces, with an effective friction coefficient. Alternatively, since gouge is a layer of granular material of finite thickness, the deformation within such a layer can be treated as the shearing deformation of a granular medium and discussed in terms of the strain in the gouge layer and its associated heterogeneities.

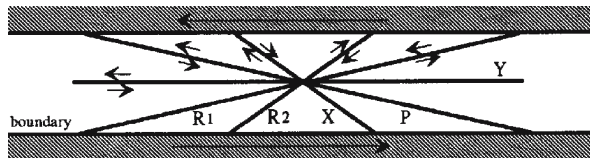
In sufficiently thick gouge layers, internal structures have been observed which evidently derive from the flow and failure processes within the gouge. These structures include both microfractures within the particles of the gouge and larger-scale bands of intense shearing within the gouge body. The microfractures correspond to extension fractures with respect to the local macroscopic stress field (Engelder 1974a) and their opening and closing have been related to changes in elastic velocities in the

gouge (Peselnick et al. 1976). The microfracturing leads to grain size reduction, often with a self-similar or fractal size distribution (Sammis, King and Biegel 1987; Sammis and Biegel 1989), and even down to grain sizes less than 10 nm (Yund et al. 1990).

The larger-scale shear bands may be oblique or parallel to the boundary of the gouge (Engelder, Logan and Handin 1975; Byerlee et al. 1978). The oblique bands have been likened to the shear failures recognized by Riedel (1929) in the sheared clay models of Cloos (Jackson and Dunn 1974; Byerlee et al. 1978). A classification of the various shear bands that have been recognized is shown in Fig. 72, where  $R_1$  represents the classic Riedel shears and the  $R_2$  shears are conjugate to these with respect to the probable maximum principal compressive stress direction. The bands forming parallel to the boundaries are known as  $Y$ -shears, and the  $P$ -shears are conjugate to the  $R_1$ -shears with respect to the  $Y$  direction. The shear bands can be viewed as representing localization instabilities in the deformation of the gouge layer, and are commonly interpreted as Coulomb failure planes (Mandl, de Jong and Maltha 1977; Byerlee and Savage 1992). Such Riedel shears have been observed widely in simulated gouge layers (Byerlee et al. 1978; Rutter et al. 1986; Moore, Summers and Byerlee 1989; Logan et al. 1992; Gu and Wong 1994a; Beeler et al. 1996; Mair, Frye and Marone 2002) although the detailed development of each localization mode as a function of shear deformation may vary in gouges of different composition and grain size. Typically the inception of shear localization is marked by the  $R_1$ -shears, and the accumulation of shear deformation is accommodated collectively by the  $R_1$ -shears and the progressive development of  $R_2$ -shears in the conjugate direction as well as  $X$ - and  $P$ -shears. A through-going  $Y$ -shear may ultimately develop along the rock-gouge interface through the coalescence of a multiplicity of such shear structures (Moore, Summers and Byerlee 1989; Logan et al. 1992; Gu and Wong 1994a; Beeler et al. 1996; Mair, Frye and Marone 2002).

Since gouge is a granular material, its deformation can be viewed at the continuum mechanics level as the plastic deformation of a rate-independent, dilatant, pressure-sensitive material of Drucker-Prager or Coulomb type (Appendix 2) (Byerlee and Savage 1992; Scott, Marone and Sammis 1994), possibly with a cap representing volumetric yielding (Schofield and Wroth 1968; DiMaggio and Sandler 1971; Wong, David and Zhu 1997; Olsson 1999). At higher temperatures and in the presence of fluids, this picture has to be modified to take into account temperature-dependent plastic processes such as pressure solution (Chester 1994; Bos, Peach and Spiers 2000; Bos and Spiers 2002b; Kronenberg et al. 2002). Alternatively, at the microphysical level, there have been a number of studies simulating the deformation behaviour of gouge in terms of particle movements, emphasizing the important role of the evolution of particle bridges or “force chains” (Sammis and Steacy 1994; Morgan and Boettcher 1999; Morgan 1999; Losert et al. 2000; Abe et al. 2002). However, even at ambient temperatures, the deformation of the gouge tends to show rate and state dependence analogous to the rela-

**Fig. 72.**  
Classification of shear zones in  
gouge (after Logan et al. 1992)



tively small effects observed in conventional friction studies. Therefore, the analysis of the deformation of gouge has commonly been cast in terms of rate and state dependence (Appendix 3, for example, Sleep 1997; Sleep, Richardson and Marone 2000).

In common with granular materials, gouge can show dilatancy during deformation. It is observed that the porosity of the gouge decreases initially upon shearing but shows dilatation at larger shear strains (Teufel 1981; Raleigh and Marone 1986; Morrow and Byerlee 1989; Marone, Raleigh and Scholz 1990; Beeler et al. 1996; Marone 1998b; Lubert and de Ryck 2001). The amount of dilatation is dependent on the velocity of sliding (Morrow and Byerlee 1989; Beeler et al. 1996). It has also been observed that dilatancy is associated with stick-slip events (Nasuno et al. 1998; Lubert and de Ryck 2001).

In soil mechanics a conceptual model proposed by Rowe (1962) is often used to analyze the effect of dilatancy on shear strength. The frictional strength is considered to arise from the interplay of frictional resistance at grain contacts, particle rearrangement and dilatation. If the contribution from the first two mechanisms is denoted by  $\mu_f$ , then the overall friction coefficient can be expressed as

$$\mu = \mu_f + \frac{d\phi}{d\gamma}$$

where the rate of change of porosity  $\phi$  with shear strain  $\gamma$  corresponds to the contribution from volume expansion against the imposed normal stress (Mitchell 1993). Marone, Raleigh and Scholz (1990) postulated that this conceptual model can be adopted to analyze the effect of dilatancy on the velocity dependence of friction. If the “dilatancy rate”  $d\phi/d\gamma$  of a gouge layer is positively correlated with the sliding velocity  $V$ , then velocity strengthening is enhanced and the volume expansion would contribute a component

$$\frac{d}{d \ln V} \left( \frac{d\phi}{d\gamma} \right)$$

toward the velocity dependence of steady-state friction  $\partial\mu_{ss}/\partial \ln V$  (Scott, Marone and Sammis 1994). Whereas Marone, Raleigh and Scholz (1990) concluded that such a contribution from dilatancy rate can explain the velocity strengthening behaviour observed in their quartz gouge tests, Beeler et al. (1996) determined in their experiments on granite gouge (Fig. 63b) that the maximum contribution from dilatancy rate was about 0.005. This contribution is too small to account for the pronounced velocity strengthening observed at large displacements in these tests.

Since the permeation of fluids along fault zones is a topic of considerable interest in connection both with earthquake genesis and with ore deposition, there have been a number of experimental studies of permeability of gouge layers (Morrow, Shi and Byerlee 1981, 1984; Teufel 1987; Zhang, Tullis and Scruggs 1999). Associated with the changes in permeability are changes in the porosity of the gouge; an initial compaction can give way to later dilatation (Raleigh and Marone 1986). Also, when aqueous fluids are present, there is the possibility of deformation being influenced by solution-precipitation processes (Bos, Peach and Spiers 2000; Bos and Spiers 2002a; Kanagawa, Cox and Zhang 2000) and at high temperatures there may be significant weakening due to the presence of water (Masuda et al. 2002).



### 8.4.3

#### Physical Factors Determining the Frictional Strength

In considering the factors that determine the friction coefficient we seek first to identify the nature of the obstacles to sliding and the manner of surmounting the obstacles. In the absence of substantial amounts of gouge, there are in general at least three cases to be considered:

1. *Welded contacts and plastic flow.* With metals, the resistance to sliding is believed to involve plastic deformation and indentation at local areas of contact at which welding has probably occurred (Bowden and Tabor 1950, 1964). Whether local plastic deformation or welding is important in the case of rocks is not clear, but it cannot be dismissed a priori as a contributory factor in view of the local high temperatures that arise (see above, Sect. 8.3.5). Bowden and Tabor's adhesion model predicts that the coefficient of friction is given simply by the ratio between the shear strength and indentation hardness. While this ratio depends only on mechanical properties, it is independent of any geometric attributes of the sliding surface. However, both experimental and theoretical studies indicate that geometric constraints may play a role, as follows.
2. *Riding over topographic highs.* Here the frictional resistance arises from the irreversible work done against the normal load through the dilatational component of the displacement. This factor has been discussed mainly in relation to sliding on joints (see, e.g., Jaeger 1971; Goodman and Dubois 1972; Barton 1973, 1976; Barton and Choubey 1977). To override the topographic obstacles the sliding surface needs to dilate and this process may enhance the "effective" friction coefficient  $\mu$  of a rough surface relative to the "basic" coefficient  $\mu_b (= \tan \phi_b)$  for a smooth, unweathered rock surfaces. For an idealized obstacle in the form of a rigid wedge inclined at an angle  $\theta$  to the direction of the applied shear stress, frictional sliding is accompanied by dilatancy with an effective coefficient  $\mu = \tan(\theta + \phi_b)$  (Rowe 1962; Jaeger 1971; Goodman 1976). In an attempt to incorporate additional effects due to geometric complexity and weathering, Barton (1973) replaced  $\theta$  by the empirical factor

$$\text{JRC} \log \left( \frac{\text{JCS}}{\sigma} \right)$$

as discussed in Sect. 8.2.2. Recently, advances have been made in the quantitative characterization of surface topography and numerical simulation of frictional sliding on a rough surface (for example, Biegel et al. 1992). In the absence of inelastic deformation and failure, the local deformation can be described by elastic contact theory (Johnson 1985). On the basis of surface profile measurements a rough surface can be represented by a statistical distribution of asperity summits (Greenwood and Williamson 1966; Greenwood and Tripp 1971; Yamada et al. 1978). Numerical simulations can then be used to determine the population of asperities that are in contact under an applied normal stress, as well as the population that would slip in response to an applied shear stress. The macroscopic stresses can be

evaluated by integrating the normal and shear forces sustained at the contacting asperities (Brown and Scholz 1985; Yoshioka and Scholz 1989a,b).

3. *Local brittle fracture.* From the observations summarized in the preceding section it is clear that brittle behaviour is involved in an essential way at sliding rock surfaces, and it is common to attribute friction in rocks to the resistance to brittle failure within or under the surface asperities. Byerlee (1967b) developed a theory of friction based on the fracture of asperities and has thereby been able to account for many of the observed properties of rock friction. Jaeger (1971) suggested that Byerlee's approach could be simplified by postulating simple shear failure of the asperities rather than tensile failure under the stress distribution assumed by Byerlee. It has also been pointed out that the complete shear stress versus displacement characteristic of the material failure should be taken into account, together with a distribution in the stages of failure in the many asperities involved (Jaeger and Cook 1971). However, fracture of the asperity itself is not the only process involved. The presence of wear grooves suggests that a ploughing mode of failure is also involved, which has been analysed by Scholz and Engelder (1976). Associated with these processes are also time-dependent effects that may represent either time-dependent cracking or a component of plastic flow giving rise to asperity creep (Dieterich 1972a; Scholz, Molnar and Johnson 1972; Scholz and Engelder 1976; Teufel and Logan 1976). Loose particles generated from the wear processes may also contribute to friction in the same way as asperities.

When substantial amounts of gouge are present so as to separate the rock surfaces completely, the preceding pictures of friction may need substantial modification. If the relative movement is accommodated within the gouge, the friction will represent the resistance to cataclastic or other deformation of the gouge. This deformation may be distributed more or less uniformly throughout the gouge or it may be concentrated in bands oblique to or along the boundaries of the gouge, as discussed in the previous section. The frictional behaviour will then depend directly on the properties of the gouge itself. Also the stress field within the gouge may not coincide with the nominal stress field applied to the country rock. Although equilibrium would require that the normal and shear tractions at the interface to be continuous, the stress tensors in the country rock and gouge layer may be quite different (Rice 1992), as manifested by microstructure and shear localization observed in sheared gouge layers (Gu and Wong 1994a; Savage and Lockner 1997). Nevertheless, Byerlee and Savage (1992) and Lockner and Byerlee (1993) demonstrated that a simple relation exists between the friction coefficient and failure parameters of the gouge material. If the gouge material undergoes Coulomb failure at shear and normal stresses obeying Eq. 3.2 with a coefficient of internal friction  $\tan \phi$ , and if the coefficient of friction (defined as the ratio between the shear and normal stress applied to the country rock) is denoted by  $\mu$ , then it can be shown by Mohr circle analysis that  $\mu = \sin \phi$ . Since  $\sin \phi < \tan \phi$  this implies that the coefficient of friction  $\mu$  of the country rock-gouge system is always smaller than the coefficient of internal friction. For example, if  $\tan \phi$  of the gouge ranges from 0.75 to 1.35, then  $\mu$  is predicted to fall within a much narrower range of 0.6 to 0.8. This relation partly explains the narrow range of  $\mu$  values observed in gouge systems with very different compositions (Byerlee 1978).

#### 8.4.4 Physical Basis for the Direct Effect (Velocity Parameter $a$ )

The above discussion underscores the fact that surfaces are rough on a microscopic scale. When two such surfaces are pressed together by a normal force  $W$  the real area of contact  $A_c$  can be significantly smaller than the nominal area  $A$ . The average normal stress sustained at a contacting asperity is given by  $\sigma_c = W/A_c$ , and application of a shear force  $F$  induces an average shear stress of  $\tau_c = F/A_c$  at the contacts. These local stresses can be significantly higher than the nominal stresses  $\sigma = W/A$  and  $\tau = F/A$ . The coefficient  $\mu$  is a macroscopic measure of friction given by the ratio  $F/W = \tau/\sigma$ , which corresponds to the ratio  $\tau_c/\sigma_c$  at the contacting asperities. A micromechanical model of rate- and state-dependent friction aims to describe how the second-order effect arises from the interplay of real area of contact, local shear stress and normal stress in response to velocity perturbation, stationary contact and frictional sliding.

To a first approximation the real area of contact  $A_c$  is directly proportional to the applied load  $W$  and independent of the nominal area  $A$ . In the adhesion model of Bowden and Tabor (Bowden and Tabor 1950, 1964) the local stress  $\sigma_c$  is considered to be so high that plastic yield occurs uniformly in all the contacts. This requires that the average normal stress  $\sigma_c = p_m$ , the indentation hardness, and therefore the real area contact is directly proportional to the applied load according to  $A_c = W/\sigma_c = W/p_m$ . Contrary to earlier ideas that this important result is valid only for a plastic rheology, Archard (1957) pointed out that it can also apply to purely elastic contact. In their analysis of asperities with random distributions of heights that are in Hertzian contact, Greenwood and Williamson (1966) showed that an increase in the normal load would induce the size of an individual contact spot to increase in area but that at the same time new contacts are established with relatively small areas, and there is a perfect balance which leaves the average normal stress unchanged. In the elastic scenario the local stress  $\sigma_c$  is not related to plastic yield, but instead is a function of the elastic moduli and geometric attributes of the surface (including the radius of curvature and standard deviation of the height distribution of the asperities).

In the past decade a consensus seems to have emerged that the “direct effect” in the rate- and state-dependent friction model arises from a thermally activated rate process in connection with creep that occurs at asperity contacts. As reviewed by Nakatani (2001) and Rice, Lapusta and Ranjith (2001), such a micromechanical framework was implicit in earlier studies of Stesky (1978a) and Chester (1994) and it has since been elaborated in many analyses of the frictional behaviour of rock, metal and polymer (e.g., Heslot et al. 1994; Bréchet and Estrin 1994; Sleep 1997; Persson 1998; Baumberger, Berthoud and Caroli 1999). A similar treatment was also developed by Briscoe and Evans (1982) in their analysis of the sliding friction between two highly oriented monolayers embedded between mica substrates.

In such a model of frictional sliding as a thermally activated process, the localized creep deformation at an asperity contact is considered to arise from discrete processes involving small number of molecules, whose motion is constrained by potential barriers that arise from interaction with the neighbours. The potential barrier can be overcome by the local shear stress  $\tau_c$  in conjunction with the random thermal fluctuations (at the absolute temperature  $T$ ), with a distribution described by the

Boltzmann relation. Accordingly the average time  $t'$  for a mobile molecule to pass across the barrier is inversely proportional to its effective vibration frequency  $\nu$  multiplied by the Boltzmann factor (Eyring 1936; Glasstone, Laidler and Eyring 1941)

$$\frac{1}{t'} = \nu \exp\left[-\frac{(Q' - \tau_c \Omega)}{kT}\right]$$

where  $k$  is the Boltzmann constant, and  $Q'$  and  $\Omega$  are activation energy and volume, respectively, for the rate process.

If one considers only forward motion down the potential gradient and assumes that the potential barriers are separated by an average distance  $\delta$ , then the average velocity of a mobile molecule is given by  $\delta/t'$ . Even though this is not the velocity one measures during frictional sliding, the sliding velocity  $V$  is expected to be proportional to  $\delta/t'$  and will accordingly follow an Arrhenius relation

$$V = V^* \exp\left[-\frac{(Q' - \tau_c \Omega)}{kT}\right]$$

where  $V^*$  is a reference velocity that is bounded by (but may actually be significantly lower than) the shear wave speed  $V_s$  (Briscoe and Evans 1982; Baumberger, Berthoud and Caroli 1999; Rice, Lapusta and Ranjith 2001). After transposing, the above relation becomes

$$\tau_c = \frac{Q'}{\Omega} + \frac{kT}{\Omega} \ln\left(\frac{V}{V^*}\right)$$

The nominal shear stress  $\tau$  is related to the local stress  $\tau_c$  by  $\tau = (\sigma/\sigma_c)\tau_c$  because of the equality among the three ratios  $A_c/A = \sigma_c/\sigma = \tau_c/\tau$ ; consequently we can express the friction coefficient as

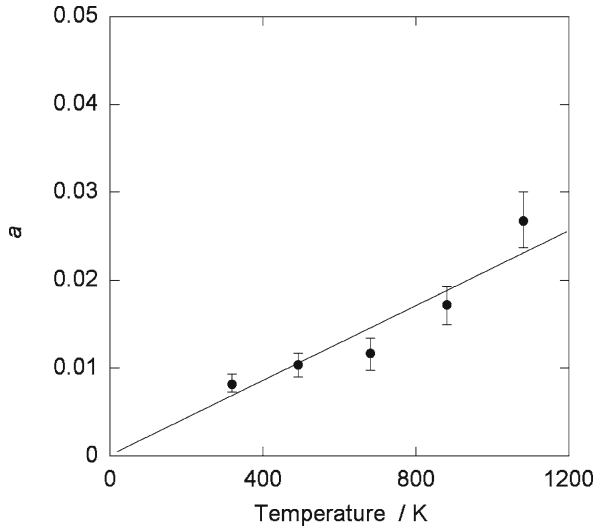
$$\mu = \frac{\tau}{\sigma} = \frac{Q'}{\sigma_c \Omega} + \frac{kT}{\sigma_c \Omega} \ln\left(\frac{V}{V^*}\right)$$

Comparison of the above with Eq. A3.1b shows that the constitutive parameter  $a$  which characterizes the direct velocity dependence is simply given by

$$a = \frac{kT}{\sigma_c \Omega} \tag{8.6}$$

Nakatani (2001) conducted measurements on feldspar gouge at elevated temperatures in a direct shear apparatus. His data for the parameter  $a$  as a function of temperature show an approximately linear trend (Fig. 73). Using a value of  $a = 0.01$  (Table 8) and guided by optical (Dieterich and Kilgore 1994, 1996a) and surface profile measurements (Boitnott et al. 1992), Rice, Lapusta and Ranjith (2001) estimated that the local normal stress  $\sigma_c \sim 0.2G$  (where  $G$  is the shear modulus)  $\sim 6$  GPa and

**Fig. 73.**  
Velocity parameter  $a$  for  
feldspar gouge as a function  
of temperature (after Naka-  
tani 2001)



therefore  $\Omega \sim 0.4 \text{ nm}^3$  for quartzite and granite, with the implication that several atomic volumes are involved in the rate process.

If a plausible value of  $V^*$  is assumed, the activation energy  $Q'$  can then be inferred from measurement of the friction parameters  $\mu$  and  $a$  at a given sliding velocity  $V$ . Given the logarithmic dependence, such an estimate is not very sensitive to the exact choice of  $V^*$  (Briscoe and Evans 1982). Rice, Lapusta and Ranjith (2001) suggested a value of  $V^* \sim 10^{-6} V_s \sim 3 \text{ mm s}^{-1}$ , which, assuming  $\mu = 0.54$  and  $a = 0.1$ , then gives  $Q' \sim 170 \text{ kJ mol}^{-1}$  for quartzite. For feldspar gouge, Nakatani (2001) showed that his data can be interpreted assuming a single mechanism with  $Q' \sim 200 \text{ kJ mol}^{-1}$ , or alternatively two different mechanisms with  $Q' \sim 90 \text{ kJ mol}^{-1}$  and  $500 \text{ kJ mol}^{-1}$  at temperatures below and above  $T = 673 \text{ K}$ , respectively. While pointing out that the low- and high-temperature values are roughly comparable to the activation energies cited for stress corrosion (Atkinson 1984) and dislocation creep (Carter and Tsenn 1987), respectively, Nakatani (2001) also cautioned that there have not been sufficient constraints to identify specific mechanisms without some uncertainty. While the estimates of activation volume seem to be of the right order of magnitude, it is unclear how localized the thermally activated process is and why similar estimates have been obtained for initially bare surfaces as well as gouge layers. Many details of such a micromechanical model need to be clarified in future work.

#### 8.4.5

##### Physical Basis for the Ageing and Evolution Effects (Parameters $\beta$ and $b$ )

While the direct effect can be interpreted as a rate process that is active on asperities with relatively constant contact area, the time-dependent strengthening under stationary contact and the evolution of frictional strength during slip are commonly inter-

preted as due to changes in the contact area. The area of indentation in many materials has been observed to increase approximately with the logarithm of time (Bowden and Tabor 1964; Scholz and Engelder 1976; Dieterich and Conrad 1984). Such an “indentation creep” phenomenon has also been directly observed in contacting asperities in optically transparent materials (Dieterich and Kilgore 1994, 1996a).

Under stationary contact the static coefficient is observed to increase with time, and this time-dependent strengthening or ageing effect is characterized by the coefficient  $\beta$  (Eq. 8.1 and Table 6). Bréchet and Estrin (1994) argued that the ageing coefficient  $\beta$  is directly related to the strain-rate sensitivity of the indentation creep process. Their original analysis was for metals, but since then Estrin and Bréchet (1996) and Berthoud et al. (1999) have applied a similar model to rock and polymer.

Bréchet and Estrin (1994) considered a constitutive model that relates the creep strain rate  $\dot{\epsilon}$  to the local normal stress  $\sigma_c$  by  $\dot{\epsilon} \propto \exp(\sigma_c S)$ , whereas Berthoud et al. (1999) assumed a power law of the form  $\dot{\epsilon} \propto \sigma_c^n$ , where  $S$  and  $n$  are parameters that characterize the strain-rate sensitivity of the operative creep process. If the assumption is made that the contact area is inversely proportional to the asperity height (so that volume is locally conserved), then the average contact area is predicted to increase with time such that  $A_c \propto [1 + (1/n) \ln(1 + t/t_c)]$ , and, if no additional asperity contacts develop during the ageing time, then the static coefficient of friction will increase with time according to

$$\mu_s = \mu_{s0} \left[ 1 + \frac{\ln(1 + t/t_c)}{n} \right] \quad (8.7)$$

with the cutoff time  $1/t_c = n \exp(n) \dot{\epsilon}_0$ , where  $\dot{\epsilon}_0$  is the initial strain rate. Comparison with the empirical Eq. 8.1 shows that the ageing coefficient  $\beta$  is inversely proportional to strain-rate sensitivity  $n$  according to  $\beta = \mu_{s0}/n$ .

Berthoud et al. (1999) measured the time-dependent increase of static coefficient as well as the strain-rate sensitivity of creep in two polymer glasses from room temperature up to the glass transitions. Their data show reasonable agreement with the theoretical prediction, but appreciable discrepancy was observed as the glass transitions were approached. Estrin and Bréchet (1996) proposed that elastic-brittle as well as strain hardening behaviour should be incorporated in such a model, but then the analysis becomes rather involved and it is difficult to make quantitative comparison with experimental data.

Such a micromechanical model for ageing under stationary contact can be generalized to the evolution effect during steady-state sliding. At a sliding velocity of  $V$ , a new population of asperity contacts is replenished and memory of prior state removed after slip has occurred over a characteristic distance  $D_c$ . This implies an average ageing time of  $D_c/V$  during steady-state sliding, and if indeed there is a direct correspondence with the time under stationary contact then one may speculate that  $-\partial\mu_{ss}/\partial \ln V$  (at constant  $D_c$ ) is comparable to  $\partial\mu_s/\partial \ln t$  (under stationary contact), and therefore  $(b - a) \sim \beta$  (Scholz 1990). However, frictional sliding experiments on rock (Marone 1998a) and polymer (Baumberger, Berthoud and Caroli 1999) suggest that the interplay of the evolution and direct effects is such that the data follow more closely the

trend  $b \sim \beta$ , and accordingly Baumberger et al. (1999) proposed that the evolution parameter  $b$  and the ageing parameter  $\beta$  should both be considered as inversely proportional to the strain-rate sensitivity  $n$ , as discussed above.

While such a model focuses on the change of contact area due to indentation creep, there are also proposals that the time-dependent effect may arise from degradation of the “quality” of the contact due to fluid-rock interaction. Experiments on bare surfaces (Dieterich and Conrad 1984) and gouge layers (Frye and Marone 2002) have demonstrated that the phenomena of time-dependent strengthening under stationary contact as well as velocity dependence under steady-state sliding can occur only in the presence of humidity. It is plausible that a temporal decrease of  $\tau_c$  in the presence of chemically reactive fluid contributes to the ageing and evolution effects, but to our knowledge a systematic analysis of such a process has not been presented in the literature.

## Brittle-Ductile Transition

### 9.1 Introduction

So far we have been concerned mainly with brittle behaviour culminating in gross brittle fracture, that is, in failure involving marked strain softening (Chapt. 5) and strain localization (Chapt. 6). However, under suitable conditions, rock can also exhibit ductility. This is an aspect of behaviour that becomes of central importance in many geologic situations but which may also have relevance in some engineering contexts. Ductility in rock can be achieved in the laboratory with the aid of sufficiently high confining pressure and temperature. In this chapter, we are concerned with bridging the two fields of laboratory study, the brittle and the ductile behaviour, and particularly with setting out the essential factors involved in the transition from brittleness to ductility (for early comment on this transition, see Griggs and Handin 1960).

The term “ductility” is used here to denote the capacity for substantial change of shape without gross fracturing on the scale of the specimen. This definition is an essentially macroscopic or phenomenological one, taking no account of the microscopical mechanisms whereby the deformation occurs. These mechanisms include crystal plasticity, diffusional flow, and granular flow. In the ductile regime, rock may therefore exhibit a wide range of macroscopic characteristics, deriving from the variety of microscopical flow mechanisms and being reflected in a wide variety of behaviour under various loading conditions, thermodynamic environments and rock characteristics. This complexity has, incidentally, given rise to a hybrid terminology based on distinguishing the nature of the mechanisms, such as “semibrittle” and “plastic” (Carter and Kirby 1978; Rutter 1986; Evans, Frederich and Wong 1990; Murrell 1990).

We consider first the characteristics of the brittle-ductile transition and the variables influencing it, and then the nature of the transition in terms of possible deformation mechanisms and stabilizing factors. The first sections therefore deal with the stress-strain properties and certain other macroscopic observations such as those on porosity change. In the later sections, the types of microscopical mechanisms that are potentially of relevance in rocks are listed and the brittle-ductile transition discussed in terms of these. Finally some special cases of opposite trends in ductility with increase in pressure or temperature are reviewed.



## 9.2 Experimental Observations

### 9.2.1 Role of Confining Pressure

Since the pioneering experiments of von Kármán (1911) on Carrara marble, there have been many studies on the role of confining pressure in achieving ductility (or on the role of effective confining pressure if pore fluid is present; note that the presence of a jacket on the specimen is normally implied in connection with rock deformation experiments under confining pressure). However, the nature of the brittle-ductile transition with increasing pressure is still most conveniently demonstrated in experiments on marble at room temperature (Figs. 74 and 75, cf. also Fig. 23). Figure 74 shows that with increasing confining pressure there are three important effects in the stress-strain curves of marble:

1. The strain reached before macroscopic failure increases very markedly when the confining pressure exceeds about 20 MPa. This change from the occurrence of macroscopic fracture at strains of less than a few percent to a capacity for undergoing

**Fig. 74.** Progression in the nature of the stress-strain curve in triaxial compression of Wombeyan marble as confining pressure is increased as shown (after Paterson 1958)

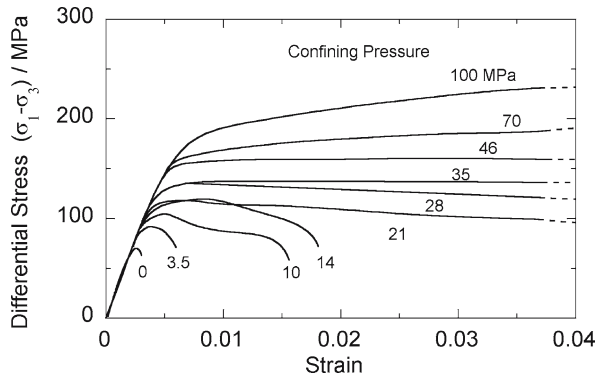
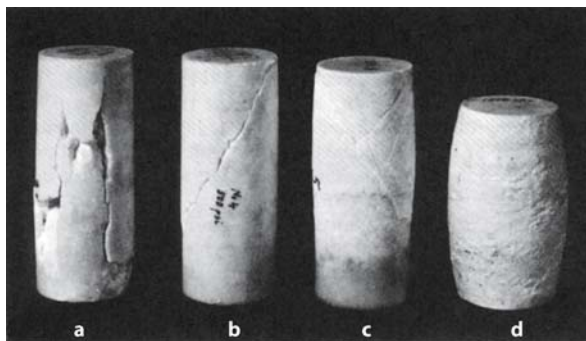


**Fig. 75.** Types of fractures or flow in Wombeyan marble at various confining pressures. **a** Axial splitting failure at atmospheric pressure; **b** single shear failure at 3.5 MPa; **c** conjugate shears at 35 MPa; **d** ductile behaviour at 100 MPa (cf. Paterson 1958)



distributed strains of larger magnitudes is taken as defining the brittle-ductile transition. In particular, following Heard (1960) and Evans, Fredrich and Wong (1990), the value of 3–5% strain to failure is often taken as defining the transition, that is, an order of magnitude greater than the elastic range (Bates and Jackson 1987).

2. The over-all level of the stress-strain curves becomes higher at higher confining pressures.
3. There is an increasing tendency for the stress-strain curve to continue rising up to large strains and with greater slope, that is, there is a greater extent and degree of strain-hardening at higher pressures.

Figure 75 shows the appearance of the marble specimens at the end of the stress-strain tests in the series from which the curves of Fig. 74 were taken. The suppression of longitudinal splitting occurs at relatively low confining pressures compared with the brittle-ductile transition (cf. Sect. 3.2). Therefore the brittle range is mainly characterised by a single macroscopic shear fracture (Fig. 75b). At confining pressures in the upper part of the brittle range a conjugate pair of shear fractures sometimes forms (Fig. 75c); however, this occurrence is considerably influenced by end conditions (thus, the use of a spherical seat favours the formation of only a single shear fracture). The main effects towards the upper end of the brittle range are the broadening of the zone of shear failure and the appearance of appreciable deformation outside the shear zone. Insofar as these two effects can be separated, the broadening of the shear zone is a change from a sharply defined shear fracture to a narrow zone of intense deformation, described by Donath and coworkers as a “ductile fault” (Donath and Faill 1963; Donath, Faill and Tobin 1971). The deformation occurring outside the shear zone itself is evident macroscopically in bulging or barrelling of the specimen and in other surface effects. Its existence suggests that distributed deformation precedes the localized shear failure. This effect is presumably also reflected in the stress-strain curve by the substantial strain reached before the strong downward plunge of final failure.

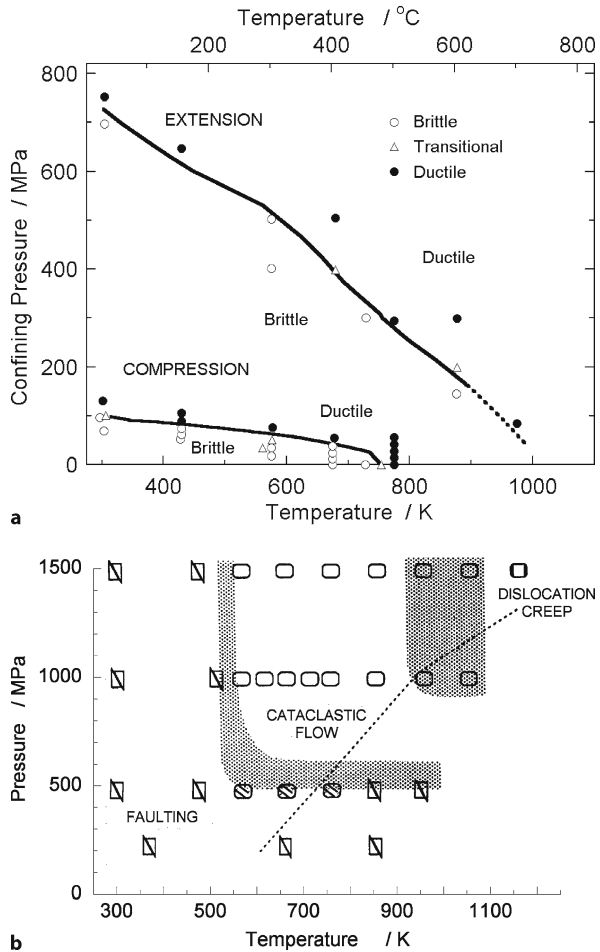
As the ductile field is entered further with increase in confining pressure, the macroscopic deformation becomes more pervasively distributed throughout the volume of the specimen so that at confining pressures of several hundred megapascals the deformation is essentially uniform except for some restriction, due to frictional end effects, in the immediate vicinity of the ends. However, even in the ductile field, there may be a finer-scale heterogeneity within the macroscopic deformation, analogous to Lüders’ bands, as described by Heard (1960) and Friedman and Logan (1973). The pattern of deformation also depends on the amount of strain; in particular, the macroscopic shear failure zone appears after an amount of strain that increases with increase in confining pressure, an effect studied by Donath and coworkers (Donath 1970b; Donath, Faill and Tobin 1971; Tobin and Donath 1971) and represented by them in “deformational mode fields” in plots of strain versus confining pressure.

Other marbles and limestones show similar transitions with increasing confining pressure (e.g., von Kármán 1911; Griggs 1936; Heard 1960; Byerlee 1968; Donath 1970b; Mogi 1972a; Rutter 1972a; Fredrich, Evans and Wong 1989, 1990; Dresen and Evans 1993; Renner and Rummel 1996). However, the transition pressure tends to be higher when

the rock is finer-grained or less pure (Fredrich, Evans and Wong 1990). Thus, for the very fine-grained Solnhofen limestone, the brittle-ductile transition occurs at about 100 MPa instead of 20–30 MPa for pure coarse-grained marbles (Heard 1960). There is also a trend for the transition pressure in limestones to decrease with increasing porosity (Vajdova, Baud and Wong 2004). The brittle-ductile transition in marble has also been studied with the aid of stiff testing machines, which reveal detail of the changes in the complete load-displacement curves through the transition (Sect. 5.2.2).

A thorough study of many aspects of the brittle-ductile transition in Solnhofen limestone was made by Heard (1960). He showed that if the specimens were loaded in extension, ductility was only attained at confining pressures greater than 700 MPa, compared with a transition pressure of 100 MPa in compression tests. He also showed that for both types of tests the transition pressure decreased as the temperature was raised (Fig. 76a); lowering the strain rate would be expected to have a similar effect,

**Fig. 76.** Brittle-ductile transition as a function of temperature. **a** In Solnhofen limestone, in compression and in extension (after Heard 1960); **b** in Bushveld anorthosite in compression at a strain rate of  $10^{-5} \text{ s}^{-1}$ , with transitions shown by stippled regions (after Tullis and Yund 1992)



although at room temperature the effect is relatively small (Rutter 1972a). Heard further showed that when a pore fluid pressure was applied as well to the Solnhofen limestone, the brittle-ductile transition occurred at a higher confining pressure; however, Terzaghi's effective stress principle did not hold in determining the transition pressure, either with water or carbon dioxide as confining fluid, presumably because of low permeability of the limestone in relation to the strain rate ( $10^{-4} \text{ s}^{-1}$ ) used (cf. Sect. 5.4.1). The latter conclusion was confirmed by Rutter (1972a) who found that Terzaghi's principle did hold for his more permeable sample of Solnhofen limestone if the strain rate did not exceed  $10^{-6} \text{ s}^{-1}$ .

The macroscopic nature of the progression through the brittle-ductile transition just described for marble and limestone can probably be taken as being more or less typical for other rocks as well. However, the pressures required for the transition are often rather different from those for marble and limestone and the microscopical mechanisms involved may vary substantially. Some examples of transitions that can be observed in triaxial compression tests at room temperature are listed in Table 10. Examples for sedimentary rocks are given by Hoshino et al. (1972) and Logan (1987) and other rocks are discussed below.

**Table 10.** Brittle-ductile transitions: some examples observed in triaxial compression tests at room temperature

Rock	Approx. pressure at transition (MPa)	Reference
Limestones and marbles	30 – 100	See text
Limestone (0.16 porosity)	10 – 20	Vajdova, Baud and Wong 2004
Chalk (0.43 porosity)	< 10	Homand and Shao 2000
Dolomite	100 – 200 or higher	Handin and Hager 1957; Mogi 1971b
Gypsum	40	Murrell and Ismail 1976a
Anhydrite	100	Handin and Hager 1957
Rocksalt	< 20	Handin 1953
Talc	400	Edmond and Paterson 1972
Serpentinite	300 – 500	Raleigh and Paterson 1965 Escartin, Hirth and Evans 1997
Chloritite	300	Murrell and Ismail 1976a
Quartzite (0.07 porosity)	600	Hadizadeh and Rutter 1983; Hirth and Tullis 1989
Sandstone (~0.10 porosity)	200 – 300	Edmond and Paterson 1972; Hoshino et al. 1972; Schock, Heard a. Stephens 1973; Bergues et al. 1974
Sandstone (~0.20 porosity)	< 100	Wong, David and Zhu 1997
Siltstones and shales of medium to high porosity	< 100	Handin and Hager 1957; Hoshino et al. 1972
Basalt (0.05 porosity)	300	Shimada and Yukutake 1982
Porous lavas	30 – 100	Mogi 1965; Hoshino et al. 1972

Nonporous and unaltered igneous and metamorphic silicate rocks, such as granite and quartzite, are, in general, brittle at room temperature over the whole of the normal range of laboratory confining pressures up to 1000 MPa or more. Granites have been found to be still brittle at pressures up to 3000 MPa at room temperature (Schock and Duba 1972; Schock, Heard and Stephens 1973; Schock and Heard 1974; Bergues et al. 1974; Shimada and Yukutake 1982; Shimada, Cho and Yukutake 1983), as are also dunite, gabbro and eclogite (Shimada and Yukutake 1982; Shimada, Cho and Yukutake 1983) and anorthosite (Hadizadeh and Tullis 1986). Compact quartzite is also brittle up to at least 1200 MPa at room temperature (Hirth and Tullis 1994). Where transitions to ductility at less than 1000 MPa have been reported for compact silicate rocks at room temperature, the rocks have contained alteration products, such as serpentine in dunite and gabbro (Byerlee 1968) and altered feldspars in granite (Paterson 1964b), or they have been composed mainly of hydrous silicate minerals, such as serpentinite (Raleigh and Paterson 1965; Murrell and Ismail 1976a; Escartin, Hirth and Evans 1997), and chloritite (Murrell and Ismail 1976a). Phyllites and schists of high phyllosilicate content and strong anisotropy form ductile shear zones or kinks under high confining pressure (Donath 1964; Paterson and Weiss 1966; Shea and Kronenberg 1993; McLamore and Gray 1967).

The application of high confining pressure is more effective in promoting ductility in porous rocks. Thus, while at room temperature in the absence of significant porosity, quartzite is brittle up to 1200 MPa (above), a brittle-ductile transition is already observed at 600 MPa when a porosity of 0.07 is present (Hadizadeh and Rutter 1983; Hirth and Tullis 1989). Similarly, in contrast to the behaviour of nonporous basic rocks, basalts of 0.07–0.08 porosity show a brittle-ductile transition at around 300 MPa (Mogi 1965; Shimada 1986; Shimada and Yukutake 1982; Shimada, Cho and Yukutake 1983). However, the most extensive studies of the role of porosity in the brittle-ductile transition have been on sandstones and similar rocks (von Kármán 1911; Handin and Hager 1957; Handin et al. 1963; Robinson 1959; Serdengecti and Boozer 1961; Edmond and Paterson 1972; Schock, Heard and Stephens 1973; Logan 1987; Gowd and Rummel 1980; Bernabé and Brace 1990; Hadizadeh and Rutter 1983; Scott and Nielson 1991; Wong 1990a; Wong, Szeto and Zhang 1992; Jamison and Teufel 1979; Wong, David and Zhu 1997; Menéndez, Zhu and Wong 1996). In these rocks, the transition from brittle to ductile behaviour is generally found to be in the range 100–200 MPa for porosities of around 0.2 to 0.1. Higher porosity favours a lower brittle-ductile transition pressure, but the transition is also sensitive to grain size, as well as to the nature of the cement and to the presence of clay minerals or alteration products. Wong, David and Zhu (1997) compiled data for 13 siliciclastic rocks with porosities ranging up to 0.35, which indicate that the transition pressure for a rock with porosity  $\phi$  and grain size  $D$  scales with  $(\phi D)^{1.5}$ . When pore fluid is present, the brittle-ductile transition is determined by the Terzhagi effective pressure provided the permeability is adequate for fluid pressure equilibrium at the strain rate used (Robinson 1959; Rutter 1972a; Bernabé and Brace 1990; Handin et al. 1963).

Mogi (1965, 1966a) has pointed out that, as a general rule, the brittle-ductile transition is related to the strength of the rock. In silicate rocks in compression, it occurs when the confining pressure becomes equal to roughly one-third of the stress differ-

ence at failure, and in carbonate rocks at about one-quarter. Ductility in extension requires much higher confining pressures (cf. Heard 1960, above). In the case of porous sandstone, Wong, David and Zhu (1997) find that the transition to ductility occurs at an effective confining pressure of about 0.15 times the critical effective pressure for the onset of grain crushing under hydrostatic pressure.

### 9.2.2

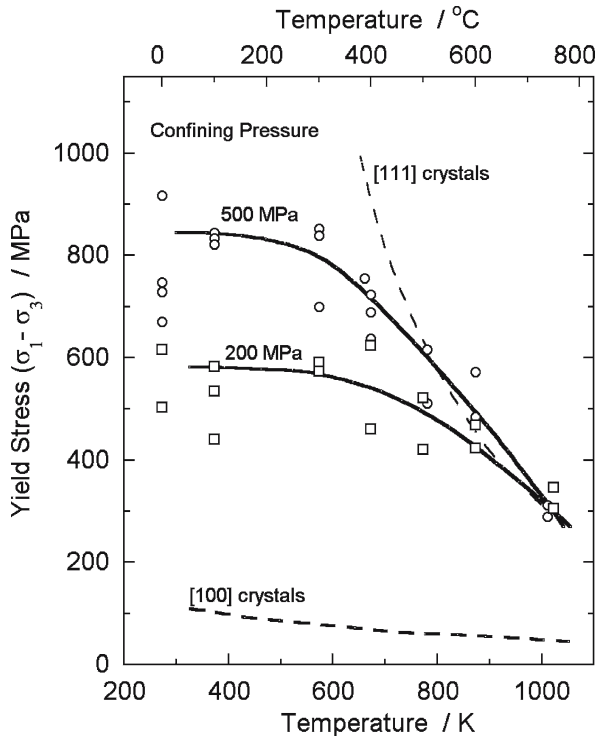
#### Role of Temperature and Strain Rate

Increase in temperature has, in general, a very important role in promoting ductility in rocks. Thus, if a sufficiently high temperature is used, ductility can usually be achieved in compression tests at confining pressures of considerably less than 1000 MPa. However, increase in temperature alone at atmospheric pressure is normally ineffective in attaining ductility. For example, Murrell and Chakravarty (1973) found that dolerite, microgranodiorite and peridotite were brittle up to 1323 K, beyond which temperature partial melting occurred in the first two rocks; the maximum strains reached in creep tests were of the order of one percent. An exceptional case is Solnhofen limestone, which Heard (1960) showed can be strained up to 5% at 773 K without confining pressure; the very fine grain size may be a favourable factor here but decomposition would prevent much higher temperatures being used. A greater range of ductility can be expected in single crystals of minerals, as shown by the well known twinning of calcite even at room temperature and pressure. However, for rocks, it is generally necessary to apply some confining pressure, as well as raise the temperature, in order to achieve ductility. The influence of strain rate is also important at high temperature and so a complete depiction of the brittle-ductile transition would require a three-dimensional diagram.

For given strain rate, a temperature-pressure field for ductility can be mapped as shown in Fig. 76a for Solnhofen limestone (Heard 1960; Evans, Frederich and Wong 1990). The pressure sensitivity of the resistance to flow may also reflect the nature of the deformation mechanism. Thus if the flow stress at a given strain, say 5 or 10%, is taken as being characteristic of the general level of the stress-strain curve and plotted against the confining pressure, the slope  $\tan \psi$  of the plot, or alternatively the slope  $\tan \phi$  of the equivalent Mohr envelope (cf. Sect. 3.3), can be taken as a measure of the pressure sensitivity. The use of these measures of pressure sensitivity is adequate in examples such as that illustrated in Fig. 77 for polycrystalline magnesium oxide; here there is a change from a relatively high to low pressure sensitivity as the temperature increases, which can be explained in terms of a transition from partly cataclastic to fully crystal-plastic deformation mechanisms (Paterson and Weaver 1970). Other examples are discussed by Paterson (1967). Similar plots have been made for a few other materials, including molybdenum (Galli and Gibbs 1964), quartzite (Hirth and Tullis 1994), granite (Tullis and Yund 1977; Evans, Frederich and Wong 1990), diabase (Kronenberg and Shelton 1980; Caristan 1982) and anorthosite (Tullis and Yund 1992; Fig. 76b). It is found that, for ductility in nonporous siliceous rocks, temperatures of at least 600–800 K are generally required, depending somewhat on the confining pressure. Thus, limited ductility was demonstrated in dunite, pyroxenite, basalt and granite

**Fig. 77.**

Influence of confining pressure on differential stress at initial yielding of polycrystalline magnesium oxide in triaxial compression test, as a function of temperature. Also shown are the yield stresses for single crystals of magnesium oxide compressed, respectively, along the [110] and [111] directions (after Paterson and Weaver 1970)



at 873–1173 K in compression tests at 500 MPa confining pressure and strain rates between  $10^{-1}$  and  $10^{-3} \text{ s}^{-1}$  (Griggs, Turner and Heard 1960) but higher temperatures or lower strain rates are required for a high degree of ductility. Tullis and Yund (1977) found that, at a strain rate of  $10^{-6} \text{ s}^{-1}$ , dry granite became ductile at about 800 K at 1500 MPa confining pressure and at about 1200 K at 800 MPa. At strain rates of around  $10^{-5} \text{ s}^{-1}$ , quartzite is marginally ductile at 800 MPa confining pressure and 1200–1300 K, or, in the presence of added water, at 300 MPa and 1300 K (Heard and Carter 1968; Mainprice and Paterson 1984), but fine-grained “wet” quartz aggregates already have high ductility at around 300 MPa, 1100 K (Kronenberg and Tullis 1984; Luan and Paterson 1992).

As examples of the influence of strain rate, Tullis and Yund (1980) found that for wet albite at 1073 K and 1500 MPa confining pressure, the deformation changed from ductile at  $10^{-6} \text{ s}^{-1}$  to brittle at  $10^{-4} \text{ s}^{-1}$ , while the results of Caristan (1982) show that, for diabase at 1273 K, the brittle-ductile transition pressure decreased from around 400 MPa at  $10^{-3} \text{ s}^{-1}$  to around 150 MPa at  $10^{-5} \text{ s}^{-1}$  strain rate. Grain size may also be important; for example, Hacker and Christie (1990) found that at strain rates of around  $10^{-5} \text{ s}^{-1}$  fine-grained (75–100  $\mu\text{m}$ ) synthetic amphibolite was ductile at 1023–1223 K and 1000 MPa confining pressure, while natural amphibolite of 0.2–1.2 mm grain size was brittle under the same conditions.

Occasionally opposite trends with pressure or temperature have been reported. Cases of negative pressure sensitivity have been reviewed by Evans, Fredrich and Wong (1990), while a case with negative temperature dependence in limestone was reported by Olsson (1974b). Embrittlement associated with dehydration is dealt with in Sect. 9.4.2.

### 9.2.3

#### Physical Properties and Pressure Sensitivity

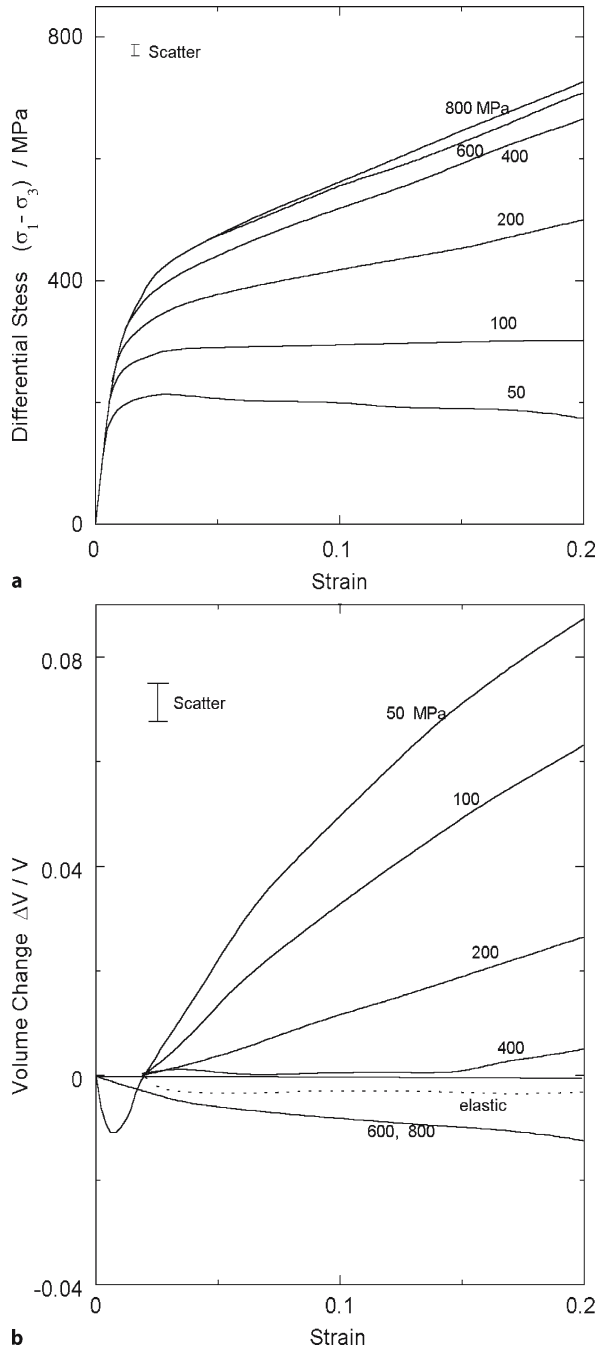
Measurements on physical properties such as dilatancy, acoustic emission, and permeability also point to the involvement of a cataclastic component of deformation in the brittle-ductile transition. Volume changes that occur during deformation derive from two opposing effects. On the one hand, the formation and propagation of microcracks will lead to increase in volume, that is, to dilatancy. On the other hand, the collapse of pores under the combined effect of the high pressure and the deviatoric stress field will lead to decrease in volume, sometimes called shear-enhanced compaction. The observation of volume change in itself may therefore be ambiguous of interpretation. However, if the rock has negligible initial porosity, the dilatancy observed at relatively low temperatures can usually be safely attributed to the occurrence of microcracking (the formation of voids by cavitation in creep is normally seen only at relatively low pressures and at temperatures where diffusion is rapid, for example, Raj 1993; Wiederhorn, Luecke and French 1995; Chokshi 1993). Edmond and Paterson (1972) deformed marble and other rocks up to 20% shortening at room temperature and observed dilatancy at confining pressures much greater than the brittle-ductile transition pressure (Fig. 78). Similar effects have been observed by Scholz (1968d), Crouch (1970), Schock, Heard, and Stephens (1973), Schrodtr and Holder (1983), Fredrich, Evans and Wong (1989), and Zhang, Cox and Paterson (1994). Fluid flow measurements in marble (Zhang, Cox and Paterson 1994) and halite (Peach and Spiers 1996; Popp, Kern and Schulze 2001) show that the permeability would increase while such a compact rock dilates and deforms in a ductile mode. Further evidence that microcracking occurs on both the brittle and ductile sides of the transition comes from observations of acoustic emission and of decrease in elastic waves speeds in marble (Thill 1973).

If the ductile failure of a compact rock involves porosity change, this change is likely to consist of dilatancy due to microcracking and related cataclastic mechanisms. In contrast, significant inelastic compaction is associated with ductile failure in a porous rock (Wong, David and Menéndez 2004). The phenomenon of shear-enhanced compaction has been systematically investigated in sandstones (Wong, David and Zhu 1997; Wong and Baud 1999) and carbonate rocks (Xiao and Evans 2003; Vajdova, Baud and Wong 2004). In a sandstone pore collapse initiates from Hertzian cracking and grain crushing, which are manifested by significant acoustic emission activity, decreases in sound speeds (Ayling, Meredith and Murrell 1995), and significant permeability reduction of up to 3 orders of magnitude (Zhu and Wong 1997; Zhu, Montesi and Wong 2002). However, in calcite rock, there may be no evidence of microcracking (Xiao and Evans 2003).



**Fig. 78.**

Dilatancy in relation to the brittle-ductile transition in Carrara marble. **a** Stress-strain curves at confining pressures shown. **b** Corresponding relative volume changes versus strain; *dotted line* shows the elastic change to be expected in a non-porous calcite aggregate at stresses corresponding to the 200 MPa stress-strain curve (after Edmond and Paterson 1972)



### 9.2.4

#### Microstructural Observations

The microstructural changes preceding and accompanying macroscopic brittle fracture, especially those changes involving microfracturing, have been described in Sect. 5.7.4. We now review the microscopical evidence relating to deformation processes that may be involved in the transition to ductile behaviour.

In case of marble at room temperature, the distributed microcracking that precedes macroscopic shear failure in the brittle field continues to develop up to larger strains as the confining pressure increases (Wawersik and Fairhurst 1970; Thill 1973), and the sharply defined shear fracture that forms at low pressure broadens into a macroscopic shear zone before becoming completely suppressed at the transition to ductile behaviour. The microcracking continues to be an important feature of the microstructure into the ductile field but reports on its characteristics vary somewhat. In a low-porosity oolitic limestone, Olsson (1974b) found that the sub-axial microcracks continued to predominate, while, in Carrara marble, Fredrich, Evans and Wong (1989) found the disappearance of intergranular cracks extending over three or four grains to be the most notable observation as the ductile field was entered. An increase in the density of twins is also noted and it is evident that there is some dislocation glide; Fredrich et al. show TEM evidence for this, and X-ray colouration also points to the occurrence of dislocation glide (Paterson 1958). It has not been established what are the fractional contributions to the total strain from the relative movement of grains and from twinning and dislocation glide as the ductile field is entered but it does appear that the transition to ductile behaviour involves a capacity for the microcracking to continue developing in a stable manner up to larger strains and that near the transition an essential difference between the brittle and ductile fields lies in the uniformity of the microcracking. As confining pressure is further increased, the microfracturing is progressively inhibited and crystal plastic processes become predominant (see also Dresen and Evans 1993; Siddiqi, Liu and Evans 1997 for two-phase marbles).

In the brittle to ductile transition in porous quartzite and sandstone at room temperature the microstructural development clearly does not involve any crystal plasticity in the quartz grains. Much cracking is observed both within and between grains, leading to comminution of the original grains and formation of gouge-like material in local micro-shear zones (Handin et al. 1963; Hoshino and Koide 1970; Hadizadeh and Rutter 1982, 1983; Bernabé and Brace 1990; Hirth and Tullis 1989). Thus, Hadizadeh and Rutter (1982, 1983) describe a “loosening” of the structure by the formation of gouge-filled microshears on grain boundaries, resulting in a lozenge-like structure. The fracturing within the grains and the resultant pore collapse in these rocks is often similar to that seen in sand; it appears to result from Hertzian contact stresses at the impinging grain contacts (Borg et al. 1960; Gallagher et al. 1974; Bernabé and Brace 1990; Zhang, Wong and Davis 1990a,b; Zhang et al. 1990; Menéndez, Zhu and Wong 1996). As the ductile field is approached with increasing pressure, the zone of concentration of microcracking broadens and its inclination to the compression axis increases, until the microcracking is more or less uniformly distributed (Handin et al. 1963; Hoshino and Koide 1970; Wong, David and Menéndez 2004). The larger strains in the ductile field then result mainly

from the relative movement of grains or grain fragments (“granular flow”). The term “cataclastic flow” refers to this combination of microcracking and granular flow.

In the case of nonporous silicate rocks for which increase in pressure at room temperature fails to achieve ductility and the transition is brought about by increasing the temperature as well, the microstructural observations often reveal evidence of a combination of cataclastic and crystal-plastic processes at the transition with increase in temperature at a given pressure. Thus, in granite, Tullis and Yund (1977) observe gouge-filled microshears in both quartz and feldspar grains at 500 to 1500 MPa, 573 to 773 K and  $10^{-6} \text{ s}^{-1}$  strain rate and in the feldspar grains still up to 973 K, but the amount of dislocation activity appears to increase through this range until it is predominant at higher temperatures. That is, there is a gradual mechanism change from cataclastic to crystal-plastic deformation over this range, the transition being completed at higher temperature in the feldspar than in the quartz (see also Dell’Angelo and Tullis 1996; Tullis 1990; Carter et al. 1981). The role of temperature is evidently more important than that of pressure in determining the mechanism of the brittle-ductile transition but water can also have an important effect (Tullis and Yund 1980). The intermediate cataclastic flow mechanism is particularly important in feldspar, as shown in studies on pure feldspar aggregates (Tullis and Yund 1987; Tullis 1990; Tullis and Yund 1992; Marshall and McLaren 1977). Other observations of an intermediate regime as temperature and pressure are increased have been made on quartzite (Hirth and Tullis 1994), diabase (Kronenberg and Shelton 1980; Caristan 1982), clinopyroxenite (Kirby and Kronenberg 1984; Boland and Tullis 1986), peridotite (Boland and Hobbs 1973), and shale (Ibanez and Kronenberg 1993). In general, with further increases in temperature and/or pressure, the strain comes to derive mainly from crystal plasticity within the grains. However, for very fine-grained rocks, especially at higher temperatures, there may be a transition to another type of granular flow in which the strain derives from the relative movement of grains that is accommodated by the deformation of the grains themselves, either by diffusion or crystal-plastic processes (the so-called “diffusion creep” regime).

## 9.3 Physical Basis of the Brittle-Ductile Transition

### 9.3.1 Preliminaries

Before considering the physical explanation of the brittle-ductile transition, it is useful to recall the various deformation processes that may be involved in ductile behaviour and some geometric constraints associated with their activity. Which combination of processes will be involved in a particular case will depend greatly on the conditions of pressure, temperature and strain rate. In general, two classes of deformation mechanism in polycrystalline materials can be distinguished according to whether:

1. the deformation of the individual grains is approximately the same as the macroscopic deformation, that is, the deformation is approximately homogeneous down to the grain scale and neighbouring grains remain neighbours, or

2. the macroscopic deformation results mainly from a reconfiguration of grain positions, that is, the deformation results from the relative movement of the grains so that the grains can change neighbours and any deformation of individual grains (or group of grains), as required for intergranular compatibility, can be markedly different from the macroscopic deformation.

In the first class, the intragranular deformation mechanisms are the same as those of single crystals and are of two types:

- *Crystal plasticity.* The term “crystal plasticity” or “dislocation flow” is used to denote permanent deformation by slip and twinning within the grains. For an introduction to these processes and to the mechanical behaviour that reflects their activity, with special reference to minerals and rocks, see, for example, Nicolas and Poirier (1976), Poirier (1985) or Barber (1990). Crystal plasticity is essentially volume-constant deformation and so tends to be independent of confining pressure (see review by Paterson 1967). However, there can be a small degree of pressure dependence of the flow stress, arising from the pressure dependence of the elastic moduli, which appear in most formulae in dislocation theories, or from the pressure dependence of diffusion rates where the dislocation motion is dependent on climb or jog-dragging. These effects may become significant at very high confining pressures, as in the Earth’s mantle (Béjina, Jaoul and Lieberman 1999).

If the macroscopic deformation of a non-porous rock is to be achieved entirely by crystal plasticity in the grains, the strains in neighbouring grains must be mutually compatible if the grain boundaries are to remain intact. The simplest way of ensuring compatibility of strain across all grain boundaries is to specify homogeneous deformation, in which each grain undergoes the same strain as the aggregate. To meet such a requirement with deformation by slip, five independent slip systems are needed, in accordance with the criterion of von Mises (1928); see also Taylor (1938), Bishop (1953), and Groves and Kelly (1963, 1969). In applying the von Mises criterion, it is implicit that the slip is interpenetrating and pervasive on the scale of the grain, and it is understood that a slip system, that is, a particular combination of slip direction and slip plane that gives the equivalent of a simple shear, is “independent” if it can produce strains that are impossible to produce with any combination of the other available slip systems.

When von Mises’ criterion is applied to rocks, it is commonly the case that more slip systems are required in the constituent minerals than are known from experimental studies to operate readily (Paterson 1969). For example, in olivine the reported slip systems are all based on the slip directions  $[100]$ ,  $[010]$ , and  $[001]$  (Phakey, Dollinger and Christie 1972) and accordingly, regardless of how many slip planes are involved, it can be shown that the maximum number of independent slip systems cannot exceed three. There are two ways in which the constraints from the von Mises criterion can be circumvented. First, the requirement of five independent slip systems can be partially relaxed when some heterogeneity of strain is allowed, as when some grains deform more than others, or the deformation within the grains is heterogeneous. The extent to which this heterogeneity relaxes the von Mises requirement is not clear but, intuitively, it would seem likely that, at least, the lack of

a fifth independent slip system could be accommodated and that the presence of porosity would also help. Second, other types of deformation mechanism may be active in a supplementary way, such as cataclastic flow at low temperatures and dislocation climb or diffusional flow at high temperatures.

- *Diffusional flow.* Diffusional flow (“diffusion creep”) consists of change in shape of a grain brought about by diffusion of material from one part of its surface to another. The diffusion path may be through the grain or around the boundary. Nabarro-Herring and Coble creep are simple models based, respectively, on these two paths (Nabarro 1948; Herring 1950; Coble 1963). More possibilities may be introduced by taking into account specific diffusion mechanisms such as dislocation climb or diffusion along dislocations or dislocation arrays; for surveys, see Weertman and Weertman (Ch. 16 in Cahn 1970), Weertman (Weertman 1970, 1975), or Nicolas and Poirier (1976). In porous rocks, the diffusion path may also be through a fluid phase in intergranular spaces, as in the “pressure solution” process often invoked in geologic writing (for example, Durney 1972, 1976; Elliott 1973; Stocker and Ashby 1973; Weyl 1959; Lehner 1995; Rutter 1976; de Meer and Spiers 1995; Paterson 1995b).

In diffusional flow in the polycrystalline aggregate, intergranular strain compatibility is readily achieved at all scales provided no restriction is placed on possible diffusion directions. However, there is necessarily a certain amount of grain boundary sliding (Lifshitz 1963). Like dislocation flow, diffusional flow is relatively insensitive to confining pressure.

In the second class of deformation mechanisms listed above, two further categories can be distinguished, based on intergranular movement and accommodation processes:

- *Cataclastic flow or microbrittle granular flow.* Cataclastic flow is a term, largely peculiar to the literature of rock deformation (Bates and Jackson 1987), which describes the permanent straining achieved by (1) distributed fracturing whereby the material is broken into fragments (the “brittle” or “cataclastic” aspect) and (2) the relative movement of the fragments (the “granular flow” aspect). The first aspect involves the proliferation of local cracking without the development of shear localization so that the originally intact material is fragmented more or less uniformly, and it is this aspect that is specifically associated with situations in rock deformation where high confining pressures and other constraints apply (Tullis and Yund 1992; Wong, David and Zhu 1997). The second aspect is analogous to the flow of a particulate material such as sand and so involves concepts analogous to many in soil mechanics but with additional intergranular accommodation considerations (see, for example, papers in Jenkins and Satake 1983; Vermeer and Luger 1982; Satake and Jenkins 1988; Shen et al. 1993). Important properties of cataclastic flow arise from two factors, (1) the friction between the sliding parts and (2) the changes in porosity and hence in specimen volume associated with the re-arrangement of the fragments. Because the confining pressure contributes to the normal forces acting on the sliding interfaces or cracks and hence to the friction, cataclastic flow tends to be strongly pressure sensitive. Further, if the rock is of very low porosity, the internal cracking and internal re-arrangements will give rise to considerable dilatancy and add to the

pressure sensitivity. However, if there is substantial initial porosity, the tendency to dilatancy may be counter-balanced through collapse of this porosity during the deformation and in such cases cataclastic flow may be accompanied by compaction rather than dilation.

It is not yet possible to give a comprehensive theory of cataclastic flow. The primary difficulty is to treat adequately the stabilization of the distributed microcracking that must occur initially in the intact rock, leading to fragmentation of the rock. Then the deformation arising from the relative movement of the fragments has to be described. The latter process consists of a type of granular flow in which the resistance to deformation arises from friction between the fragments and some further crushing of the fragments. These theoretical questions are pursued further in Sect. 9.3.2.

- *Microplastic (high temperature) granular flow.* This term is introduced to denote flow that occurs by the relative movement of grains without fracture and without disruption of the grain boundaries. Maintaining contact at the grain boundaries requires accommodation processes that may involve either diffusion along the boundaries or dislocation flow within the grains. Such flow is characterized by the primary role of grain-boundary sliding, in contrast to its secondary role in diffusional flow (Ashby and Verrall 1973; Arieli and Mukherjee 1980; Paterson 1990b, 1995a; Nieh, Wadsworth and Sherby 1997). Microplastic granular flow is favoured by high temperature, low strain rate, and fine grain size. Also, since the diffusional or dislocation flow accommodation processes will be rate limiting, microplastic granular flow will tend to be relatively insensitive to pressure.

The term “superplastic flow” has sometimes been used in geological writing to denote the microplastic granular flow mechanism, both in relation to naturally-deformed rocks (for example, Boullier and Gueguen 1975; Boullier and Nicolas 1975; Gueguen and Boullier 1976) and to experimental deformation (for example, Schmid 1976; Schmid, Boland and Paterson 1977). However, this term is generally used in materials science in a macroscopic sense to refer to extensile deformation to very large elongations without necking and is better reserved for that usage, even though microscopically the microplastic granular flow mechanism is thought to be active (often referred to as the grain boundary sliding mechanism).

### 9.3.2

#### **Brittle-Ductile Transition with Increasing Pressure**

In view of the variety of potential deformation mechanisms in the ductile field one can expect a corresponding variety in the character of the brittle-ductile transition when the physical mechanisms are considered. Thus no single mechanistic view of the brittle-ductile transition can be valid under all conditions. Here we consider first the nature of the transitions that can occur with increasing confining pressure at relatively low temperatures. Within the wide range of possibilities, it is useful to distinguish two end-members or extreme cases in which the deformation mechanisms in the ductile field are, respectively, purely cataclastic and purely crystal plastic; characterized as B-type and A-type transitions by Mogi (1972b, 1974a) (cf. also the transitions of second and first kind of Murrell 1967b).

- *Brittle-to-cataclastic transition* (Fig. 79a). The properties of a shear failure have been invoked by various writers to explain the brittle-ductile transition in a way that implies a transition to cataclastic flow (Orowan 1960; Maurer 1965; Mogi 1966a, 1972b, 1974a; Murrell 1967b; Byerlee 1968; Barton 1976); but note that the case of marble quoted by Orowan probably involves plastic flow to a large degree since the extensive cracking that he described in von Kármán's specimens could have arisen in a large part during pressure release (Paterson 1963). It is assumed that the trend of the fracture stress is less pressure dependent or more strongly non-linear than that of the frictional sliding stress so that the cross-over depicted in Fig. 79a will actually occur. However, this picture is to some extent merely an alternative macroscopic description of the transition, and it does not clearly identify the stabilizing factors involved in cracking on the microscopical scale that are fundamental to cataclastic flow. For fuller understanding of the brittle-ductile transition it is necessary to consider the way in which the microscopical developments leading to the macroscopic shear fracture become suppressed as the pressure rises. Increase in confining pressure not only makes microcrack growth more difficult but the growth that is produced under the higher stresses now applied tends to be stabilized, eventually leading to sufficient disintegration or fragmentation of the specimen by proliferation of stable microcracks that a purely cataclastic mode of deformation becomes possible, as, for example, envisaged by Mitra (1978).

Thus, an understanding of the brittle-ductile transition with increasing confining pressure requires further consideration of the effect of pressure in stabilizing the propagation and proliferation of microcracking. Early approaches by Dower (1967) and, in more detail, by François and Wilshaw (1968), refer to the transition in brittle metals in tension (for references to relevant experimental work see François and Wilshaw 1968; Carpentier and François 1971). François and Wilshaw (1968) considered two specific dislocation models for the nucleation of cracks and predicted that, because the additional stress from a confining pressure is small compared with the local stresses in the cores of dislocations, the stress for microfracture initiation will be nearly independent of pressure while crack propagation across a grain and through a grain boundary would show important dependence on pressure. Using energy balance calculations, they deduced that as confining pressure is increased the stress for propagation of cracks across grains increases but at first remains above the stress for propagation across grain boundaries so that the cracks remain unstable; however, at higher pressures, propagation across a grain boundary becomes more difficult than propagation within a grain and so the crack is stabilized. This approach has been further developed by Wong (1990b) who emphasizes the importance of taking into account the Peierls stress in the case of minerals. Another view of the stabilization of microcracking derives from the wing crack model, as set out in Chapt. 6. This model does not take into account the grain structure but assumes the prior existence of a population of cracks in a continuum. It predicts that wing cracks nucleate at the pre-existing cracks and propagate at a stress difference that increases as the confining pressure increases. However, such cracks change their orientation during propagation in such a way as to become stabilized.

In compact rock and in strongly cohesive porous rock, the stabilization of the propagating cracks permits the initiation of further cracking as loading is increased,

leading to the intersection of cracks and their increasing connectivity, and eventually to the breaking down or “cataclasis” of the rock into a granular mass. In weakly cohesive porous rock, the cataclasis will arise more from grain crushing, as modelled with Hertzian fracture mechanics (Zhang, Wong and Davis 1990b; Wong, David and Menéndez 2004). As the cataclasis develops, the mechanism of strain can change from predominantly elastic distortion, with minor contributions from the opening of cracks and some sliding on cracks, to predominantly granular flow resulting from the relative movement of the fragments produced by the cataclasis. Such a development is supported by observations in some compact rocks, notably

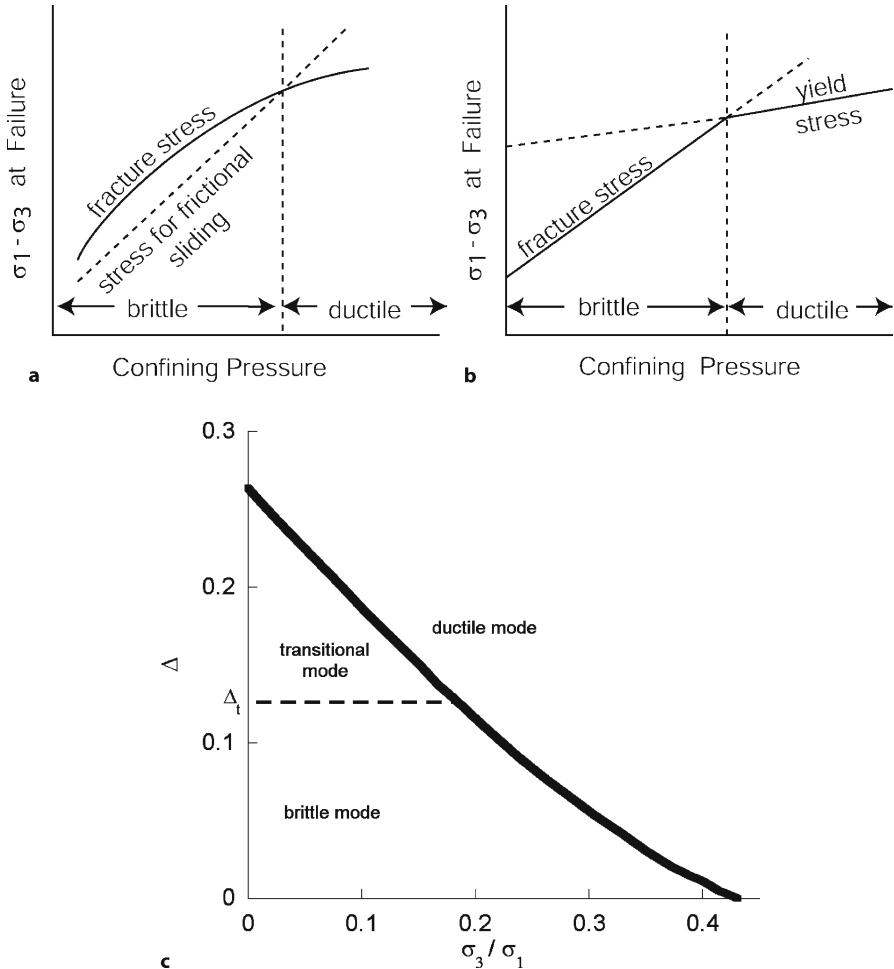


**Fig. 79.** Simple models for the brittle-ductile transition. **a** Transition to cataclastic flow; **b** transition to plastic flow; **c** failure mode as function of the stress ratio  $\sigma_3/\sigma_1$  and the ratio  $\Delta$  between normalized fracture toughness and yield stress (after Horii and Nemat-Nasser 1986)



in feldspar rocks at intermediate temperatures, but it is more commonly observed in porous rocks and the most extensive observations relate to the latter (Sect. 9.2.3). However, although the early evolution of strain hardening will be mechanically different in compact rock, strongly cohesive porous rock, and weakly cohesive porous rock, it can be expected that at large strains the various types of behaviour will tend to converge towards a similar “critical state” condition of constant volume and constant flow stress.

- *Brittle-to-crystal-plastic transition* (Fig. 79b). For simplicity, we consider the situation in which the plastic deformation is rate-independent. If increasing the confining pressure raises the brittle fracture strength of the rock to a level exceeding the yield stress for crystal plastic flow, then the application of stress will lead to deformation by crystal plasticity (there could, of course, be an intermediate regime in which a transition of the type depicted in Fig. 79a first occurs). The transition to crystal-plastic flow can come about because the required stress for flow tends to be less sensitive to confining pressure than is that for brittle fracture or cataclastic flow (Fig. 79b).

A simple model for a brittle-crystal plastic transition has been given by Horii and Nemat-Nasser (1986). In this two-dimensional model (Fig. 79c), brittle behaviour is said to result under given stressing if a crack propagates in preference to a plastic zone, and ductile behaviour in the reverse case. The transition depends both on the value of  $\Delta = \sigma_c / \tau_y$  (where

$$\sigma_c = \frac{K_{Ic}}{\sqrt{\pi c}}$$

is the far-field stress giving rise to the critical stress intensity  $K_{Ic}$  at the crack tip for crack extension and  $\tau_y$  is the yield stress for extending the plastic zone) and on the ratio  $\sigma_3 / \sigma_1$  of lateral stress or “confining pressure”  $\sigma_3$  to axial stress  $\sigma_1$ . The model reproduces the general character of observed brittle-crystal plastic transitions but is over-simplistic from the micromechanical point of view. A more sophisticated model needs to relate the transition to the evolution of strain hardening associated, on the one hand, with microcrack proliferation and, on the other hand, with crystal-plastic deformation within the grains, and to examine the conditions for suppression or localization of these processes. Assuming that the proliferation of microcracking has been suppressed by raising the confining pressure, the emphasis shifts to suppressing localization of plastic deformation. As in the case of the brittle-cataclastic transition discussed above, this question again becomes one of stabilizing the plastic flow through strain hardening.

### 9.3.3 Continuum Models and Localization Analysis

As discussed above, the pressure sensitivity of the resistance to flow may reflect the nature of the deformation mechanism. If there are significant volume changes, the resistance to flow is more fully represented by the rate at which work  $W$  is done on the specimen rather than by the stress difference itself. Thus, in the triaxial test, in which

the axial strain  $\varepsilon_1$  is usually regarded as the independent variable, the resistance to flow is most fully specified by  $dW/d\varepsilon_1$ , designated  $\sigma_w$ . It is easily shown (Edmond and Paterson 1972) that

$$\sigma_w = \frac{dW}{d\varepsilon_1} = (\sigma_1 - \sigma_3) + \sigma_3 \frac{d\varepsilon_v}{d\varepsilon_1}$$

where  $\sigma_1 - \sigma_3$  is the stress difference,  $\sigma_3$  is the confining pressure and  $\varepsilon_v = -\Delta V/V_0$  is the volumetric strain (following the convention of compressive stress and strain being positive, relative decrease in volume is taken as positive volumetric strain). The pressure sensitivity of the resistance to flow is then given by the slope of the plot of  $\sigma_w$  at a given strain versus the confining pressure. It can also be noted that a work-hardening rate is correspondingly given by

$$\frac{d\sigma_w}{d\varepsilon_1} = \frac{d(\sigma_1 - \sigma_3)}{d\varepsilon_1} + \sigma_3 \frac{d^2\varepsilon_v}{d\varepsilon_1^2}$$

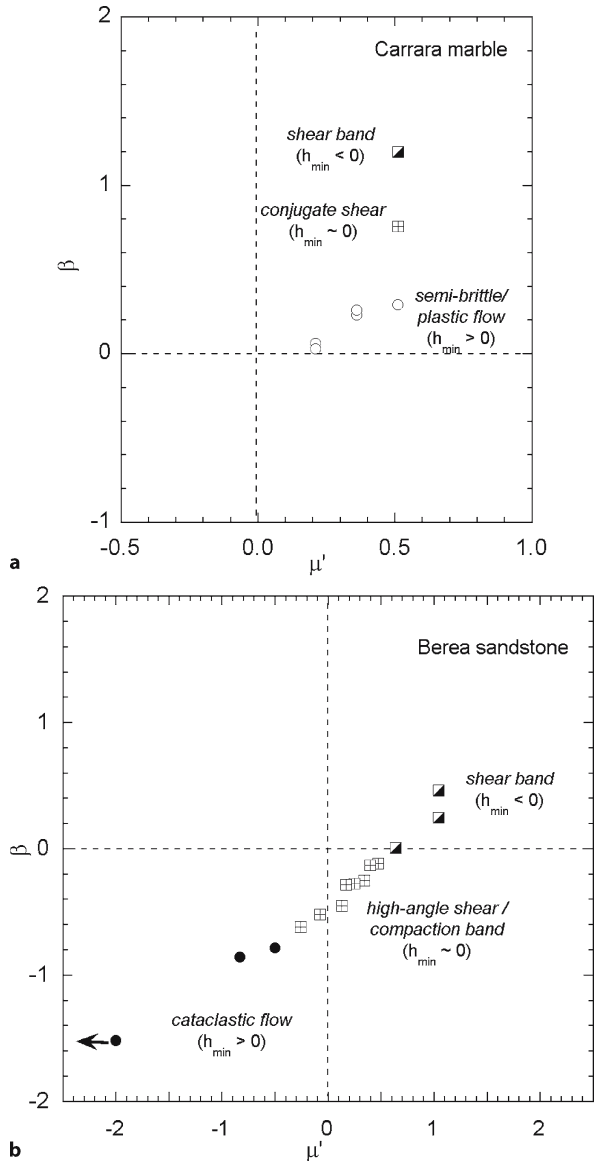
Thus change in porosity during a triaxial test also gives rise to an apparent work-hardening or work-softening through the  $d^2\varepsilon_v/d\varepsilon_1^2$  term if the plot of  $\varepsilon_v$  versus  $\varepsilon_1$  is non-linear. This approach to the analysis of pressure effects was applied by Edmond and Paterson (1972), Hadizadeh and Rutter (1982) and Renner and Rummel (1996) to observations on various rocks in which the flow mechanism involves inelastic volume changes. However, as pointed out by Hobbs, Muhlhaus and Ord (1990), the suggestion of Edmond and Paterson that localization of deformation would set in when the apparent work-hardening term  $d^2\varepsilon_v/d\varepsilon_1^2$  reduces to zero is not universally valid (see Sect. 6.4.1 and 9.3.2).

In a more comprehensive continuum model, the effects of the evolution of the microcracking and cataclastic flow are subsumed in macroscopic yield criterion and stress-strain relationships. Whether early localized failure, and hence brittleness, can be expected depends on the nature of this stress-strain relationship. Therefore, localization theory such as developed by Rudnicki and Rice (1975) can, in principle, be applied in helping to understand the brittle-ductile transition (Evans, Frederick and Wong 1990; Dresen and Evans 1993; Wong, David and Zhu 1997). A full description of the evolution of the yield or loading function  $f(\sigma_{ij})$  and of the flow law or plastic potential  $g(\sigma_{ij})$ , as defined in Appendix 2, is needed for such an approach, which deals with the brittle-ductile transition in terms of potential shear localization. Using incremental plasticity theory, Rudnicki and Rice (1975) proceeded initially with assuming a Drucker-Prager form of loading function and an analogous form for the plastic potential (Appendix 2, Eqs. A2.9 and A2.16). Their analysis involves three material parameters, namely, the hardening modulus  $h$ , the pressure sensitivity parameter  $\mu'$ , and the dilatancy parameter  $\beta$ . Each of these parameters can be evaluated experimentally in tests such as the axisymmetric triaxial test, with associated volumetry.

Fredrich, Evans and Wong (1989) determined the constitutive parameters  $\mu'$  and  $\beta$  for Carrara marble (Fig. 80a). Their data illustrate the evolution of pressure sensitivity and volume change associated with the brittle to crystal plastic transition. At pressures of 5 and 40 MPa the samples failed by brittle faulting along a single shear band and

**Fig. 80.**

**a** The dilatancy factor  $\beta$  and internal friction parameter  $\mu'$  for Carrara marble (Fredrich, Evans and Wong 1989). Relatively high positive  $\beta$  values were measured for samples that failed by shear faulting under low confinement. With increasing pressure both  $\beta$  and  $\mu'$  progressively decreased, and the failure mode evolved to semi-brittle and ultimately plastic flow (at constant volume with  $\beta \sim 0$ ). **b** In Berea sandstone the data of Wong, David and Zhu (1997) show progressive decreases in both  $\beta$  and  $\mu'$  with increasing pressure, as the failure mode evolved from brittle faulting to high-angle shear or compaction bands, and ultimately to cataclastic flow. Negative values of  $\beta$  and  $\mu'$  are associated with inelastic compaction and negative pressure sensitivity



conjugate bands, respectively. Appreciable dilatancy was observed and the pressure sensitivity of these samples were characterized by a value of 0.5, in the range of  $\mu'$  values for compact crystalline rocks compiled by Rudnicki and Rice (1975). The sample that failed at 5 MPa with a single shear band had the highest dilatancy value of  $\beta = 1.20$ . At higher pressures microcracking was inhibited and the deformation was progressively dominated by crystal plasticity mechanisms including mechanical twinning and dis-

location slip. This is manifested by a progressive decrease of the dilatancy parameter with increasing pressure, and, ultimately, negligible volumetric change was observed at a confining pressure of 300 MPa (with a  $\beta$  of 0.03). The pressure sensitivity parameter  $\mu'$  decreased progressively to a small positive value at high pressures, in agreement with the conceptual model shown in Fig. 79a.

As discussed in Sect. 6.4.1, bifurcation analysis using Rudnicki and Rice's (1975) constitutive model for Carrara marble with the range of  $\mu'$  and  $\beta$  values plotted in Fig. 80a would predict that shear localization can develop only if the hardening parameter  $h$  attains a very large negative value. In this sense the continuum model agrees with experimental observation, since brittle faulting was inhibited in samples that strain hardened (with a positive  $h$ ) and failed by semi-plastic flow. Thus localization analysis can provide a useful framework for understanding the interplay of strain hardening, pressure sensitivity and porosity change in controlling the mode of failure during the brittle-ductile transition. However, it should also be noted that the theory has its limitations in that quantitative agreement with experimental data ultimately rests on the validity of the assumed forms of the loading potential and potential functions, not just on the values of the parameters appearing in particular forms. In particular, if one uses Rudnicki and Rice's (1975) constitutive model with three inelastic parameters, the predicted values of the critical hardening parameter at the onset of shear localization are often more negative than the experimental observations, and indeed this was the case for Carrara marble, as noted by Fredrich, Evans and Wong (1989).

For the brittle to cataclastic transition the evolution of pressure sensitivity and volume change can be significantly different. Figure 80b shows the data for Berea sandstone determined by Wong, David and Zhu (1997). In the brittle faulting regime the pressure sensitivity parameter  $\mu'$  attained a relatively high value of 1.0, which is comparable to those of compact rocks. In a porous rock this parameter also decreases with increasing pressure, but instead of approaching a limiting value of 0 its value can become negative in the cataclastic flow regime, corresponding to the onset of shear-enhanced compaction when the sign of the dilatancy parameter  $\beta$  switches from positive to negative. That the yield stresses at elevated pressures can only be described by a "cap" with negative pressure sensitivity is not captured in the conceptual model shown in Fig. 79a, which is a pertinent only to a compact rock.

As discussed in Sect. 6.4.1 and Appendix 2, Rudnicki and Rice's (1975) model predicts that the shear band angle for axisymmetric compression is given by  $\theta = \pi/4 - \arcsin \alpha/2$  with

$$\alpha = \frac{2\sqrt{3}}{9}(1+\nu)(\mu' + \beta) - \frac{(1-2\nu)}{3}$$

If the parameters  $\mu'$  and  $\beta$  have negative values, then there is the possibility that the band angle  $\theta$  becomes so large that it exceeds  $\pi/4$  and at the critical condition of  $\mu' + \beta = -\sqrt{3}$  attains the maximum value of  $\theta = \pi/2$ , corresponding to the development of a localized compaction band perpendicular to  $\sigma_1$ . Indeed recent laboratory tests (DiGiovanni et al. 2000; Olsson and Holcomb 2000; Wong, Baud and Klein 2001; Baud, Klein and Wong 2004) have revealed a whole spectrum of compaction localization phenomena associated with the brittle to cataclastic transition in porous sandstones.

In practice, the transition will tend to be less sharp than depicted in Fig. 79b because of microyielding effects, since some yielding of individual grains can occur already in the brittle field at stresses below the macroscopic failure stress (Sect. 6.2.3). In the case of quartz aggregates at somewhat elevated temperatures, Hirth and Tullis (1994) have noted that there can even be considerable dislocation activity in early stages of deformation in quartz aggregates before the onset of cataclastic deformation. As the fracture stress rises with increasing confining pressure, yielding in more grains and on more slip systems in individual grains can be expected until a stage is reached when sufficient slip systems are active in a sufficient number of grains to satisfy intergranular strain compatibility requirements. If the confining pressure is now high enough to suppress all cataclastic effects at the required flow stress, and if the work-hardening extends over a sufficiently large range of strain, then a transition to ductility will have been achieved.

More generally, the brittle-ductile transition with increase in pressure at relatively low temperatures will commonly involve some combination of crystal plastic and cataclastic flow mechanisms. In the transitional region, stable cataclastic processes may be active at stress differences at which some slip is also occurring but not yet enough grains or on enough slip systems to satisfy intergranular strain compatibility requirements with slip alone. In this case, potential misfit between grains resulting from the slip could be accommodated at first by relative movement on microcracks, with a greater degree of involvement of crystal plasticity at higher pressures. However, in the case of rocks, especially silicate rocks, the role of crystal plasticity will be very limited unless the temperature is raised substantially. Also strain rate effects will not generally become important until the higher temperatures. These aspects are dealt with in the next section.

### 9.3.4

#### **Influence of Temperature, Strain Rate and Water**

The influences of temperature and strain rate on the brittle-ductile transition are mainly important in relation to the transition to crystal plasticity. There are two aspects. First, many minerals, especially silicates, have a high Peierls stress that prevents any crystal plasticity at or near ambient temperature, but they may show crystal plasticity at higher temperatures. Second, even if some slip systems can be activated at relatively low temperatures, the number of independent systems may still be inadequate to satisfy the von Mises criterion (Sect. 9.3.1), but, as the temperature increases, the number of independent systems tends to increase or other accommodating mechanisms become active. Thus, for a given confining pressure, it can be expected that, as the temperature is raised, the mechanistic nature of the brittle-ductile transition will change progressively away from depending mainly on transition to cataclastic flow towards depending mainly on crystal plasticity.

The Peierls stress aspect is illustrated in the case of dunite (polycrystalline olivine). Even under 3000 MPa confining pressure, this rock is still brittle at room temperature (Shimada and Yukutake 1982; Shimada, Cho and Yukutake 1983) but it becomes ductile at temperatures above about 1200 K, where the Peierls stress is reduced and thermal activation facilitates slip.

The second aspect is probably widely important in rocks but the principle is well illustrated in the progression to predominance of crystal plasticity at higher temperatures in polycrystalline magnesium oxide deformed under high confining pressures (Paterson and Weaver 1970). Figure 77 shows how the macroscopic yield stress falls when the critical stress for yielding on the “hard” non-dodecahedral planes (reflected in the yield stresses for the [111]-oriented crystals) becomes comparable to the applied stress, so that non-dodecahedral slip can take the place of cataclasis in compensating for the inadequacy of dodecahedral slip in achieving intergranular strain compatibility (the “easy” dodecahedral slip, reflected in the yielding of [111] crystals, can contribute only two independent slip systems). The simultaneous disappearance of the marked pressure dependence of the macroscopic yielding further demonstrates the change from mixed cataclastic-crystal plastic deformation to fully crystal-plastic deformation in the ductile field as the temperature is increased.

Another illustration of the importance of intergranular accommodation is seen in olivine aggregates (Hirth and Kohlstedt 1995; Kohlstedt and Zimmerman 1996). The high strength of the coarse-grained aggregates corresponds to that of the “hard” [010] slip systems that are presumably needed for their contribution to satisfying the von Mises criterion. However, the lower strength of the fine-grained aggregates corresponds to that of the “soft” [100] slip systems; evidently grain-boundary sliding or diffusional accommodation processes are contributing sufficiently in the latter case that the requirement for multiple slip processes under the von Mises criterion is more relaxed.

In the case of quartz and similar minerals in which dislocation glide involves breaking silicon-oxygen bonds, raising the temperature is in itself insufficient for achieving ductile behaviour by crystal plasticity at moderate confining pressures since even at 1700 K dry quartz is still exceedingly strong (see review by Paterson 1989). However, in the presence of water, the yield stress can be sufficiently lowered at high temperatures that a transition to ductile behaviour by crystal plasticity becomes possible. Natural quartzites contain water and the brittle-crystal plastic transition can be observed in these in the laboratory (Hirth and Tullis 1994). A similar water-weakening effect at high temperatures is observed in feldspar aggregates but these also show an extensive regime of cataclastic deformation at intermediate temperatures, thought to be related to easy cleavage (Tullis and Yund 1980, 1987, 1992).

## 9.4 Ductile to Brittle Transitions

### 9.4.1 High Pressure Embrittlement

Although increase in confining pressure is normally conducive to increased ductility, exceptional cases have been reported in which rocks that are ductile in a certain range of confining pressures become brittle again at higher pressures (Byerlee and Brace 1969). Such a transition from ductility to brittleness with increasing confining pressure is illustrated for crushed granite in Fig. 81. Byerlee and Brace observed similar transitions in serpentinized gabbro and dunite and in a sandstone of 15% porosity. A similar transition has also been observed by Giardini et al. (1968) in altered granodiorite but

no such effect has been reported in limestones. Byerlee and Brace comment that this behaviour in triaxial tests somewhat resembles the onset of the “snapping” instability observed in shearing tests by Bridgman (1935, 1936, 1937); see also Riecker and Seifert (1964a,b), who attributed the snapping to stick-slip between specimen and piston, and Giardini and Abey (1972, 1973), who attribute it to instability within the specimen itself. Byerlee and Brace further point to a similarity to the transition from stable sliding to stick-slip in friction experiments on several unaltered silicate rocks with increased normal stress, relating this behaviour to the properties of the gouge (cf. Sect. 6.4.2 and 6.4.4).

Hirth and Tullis (1989) have observed that a quartzite of 0.07 porosity can deform in a ductile cataclastic mode to substantial strains at 600 MPa confining pressure but fail in a brittle manner after a strain of 25%. They associate the termination of the ductile phase with a stage at which the pore collapse no longer dominates over the dilatancy arising from continuing microcracking. Similar observations have been made on a porous sandstone (Zhang, Wong and Davis 1990a; Wong, Szeto and Zhang 1992) and eclogite (Shimada 2000).

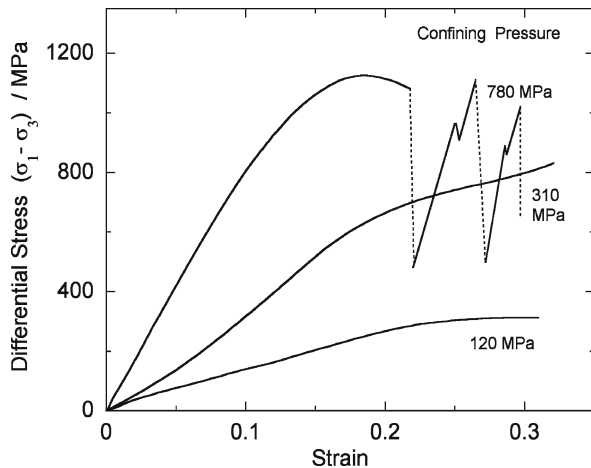
### 9.4.2 High Temperature Embrittlement

Where mineralogical change occurs with the release of a fluid phase, there are departures from the general rule of increasing ductility with increasing temperature. Thus, a transition to brittleness at higher temperatures has been observed in rocks containing serpentinite, gypsum, or other hydrated minerals.

Figure 82 shows that the undrained strength falls markedly in a serpentinite when the temperature is reached for the reaction



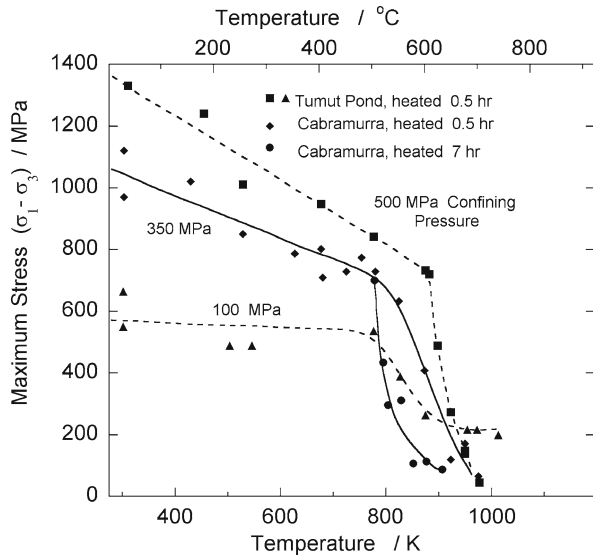
**Fig. 81.** Transition to unstable deformation in compacted, crushed granite as confining pressure is increased (after Byerlee and Brace 1969)



At 350 and 500 MPa confining pressure, specimens are ductile at temperatures below 500 °C and deform fairly uniformly. The fall in strength at higher temperatures coincides with a transition to brittle behaviour, expressed in a discrete shear fracture. In the transitional region, the behaviour depends considerably on the duration of heating prior to the test, showing that the reaction responsible for the embrittlement and weakening is relatively sluggish at these temperatures (see curves for 350 MPa confining pressure in Fig. 82). This behaviour has been demonstrated in both serpentine and serpentinized olivine-rich rocks by several workers (Handin 1964; Raleigh and Paterson 1965; Riecker and Rooney 1966; Sclar and Carrison 1966; Murrell and Ismail 1976a). Dehydration embrittlement has been proposed as a mechanism for intermediate depth earthquakes (Green and Houston 1995; Kirby et al. 1996; Wiens 2001).

Heard and Rubey (1966), Murrell and Ismail (1976a), Ko, Olgaard and Briegel (1995) and Olgaard, Ko and Wong (1995) demonstrated a similar weakening in gypsum accompanying its dehydration to the hemihydrate; an associated development of narrow shear zones shows this to be another example of embrittlement with increase in temperature through a dehydration reaction. Further examples of weakening through dehydration reactions have been found in zeolitized tuff, hornblende, and amphibolite (Riecker and Rooney 1967, 1969) and in chloritite and granodiorite (Murrell and Ismail 1976a,b). Embrittlement was found to accompany the weakening in the chloritite and granodiorite except when additional water had been added, leading to substantial partial melting; embrittlement can only be presumed in the cases studied by Riecker and Rooney because the nature of the tests was not well suited for showing it. Riecker and Rooney's tests on hornblende show the curious effect that at 600 °C, a temperature below that at which the weakening appeared in tests at 1000 MPa confining pressure, the stress-strain curves rose with increasing confining pressure up to 1500 MPa

**Fig. 82.** Strength of two antigorite-chrysotile serpentinites as a function of temperature at various confining pressures and after periods of preheating at test temperature as shown (Raleigh and Paterson 1965)





but then showed a marked fall to 2000 MPa; possibly this is due to the amphibole stability boundary looping back to lower temperatures at higher pressures, as discussed by Essene, Hensen, and Green (1970).

In the case of talc, in which a weakening and embrittlement could be expected from dehydration at about 1073 K, such an effect was not obvious in some experiments of Edmond and Paterson (1971); instead, in all tests above about 773 K the specimens were fairly brittle and had substantially reduced strength. At least two factors may be obscuring the expected effect in talc in these experiments: (1) the specimens had not been oven-dried, and comparative tests on oven-dried specimens at 873 K gave markedly higher strengths, suggesting that there had been sufficient adsorbed water in the other specimens to give appreciable pore pressure already at 773 K or so, thus obscuring the effects of mineral dehydration at 1073 K; (2) the amount of water released in the dehydration of talc is relatively small compared with that for most of the examples above, and so the effect in any case may be less marked, especially in view of the initial low strength of talc.

A primary factor in explaining the above embrittlement and weakening with increasing temperature is the generation of a pore pressure through the release of a fluid phase in the reaction. The fluid is water in the examples cited, but a similar pore pressure effect could be expected with released carbon dioxide. Beyond the temperature threshold for appreciable decomposition, the pore pressure in the undrained jacketed sample soon rises to become equal to the confining pressure, in a way that can be derived from the phase diagram (Raleigh and Paterson 1965), provided that the total fluid phase available is sufficient in relation to the existing pore volume. As shown in Chapt. 7, the effect of a given pore pressure is commonly equivalent to reducing the confining pressure by the same amount; hence when the pore pressure is equal to the confining pressure, the specimen behaves as if under zero confining pressure and consequently in a brittle manner. The important role of the pore pressure is also indicated by the finding of dilatancy hardening effects by Murrell and Ismail (1976a). Ko, Olgaard and Wong (1997) and Wong, Ko and Olgaard (1997) have studied in detail the factors governing the pore pressure generated by dehydration and the influence of permeability and drainage. Acoustic emission activity has also been observed in association with dehydration embrittlement (Meade and Jeanloz 1991; Dobson, Meredith and Boon 2002). However, the effects of the decomposition may not lie entirely in the generation of a pore pressure. The zero-pressure strength itself is probably affected by factors such as destruction of cohesion at old grain boundaries, lack of cohesion between new grains, and hydrolytic weakening in silicate phases (Raleigh and Paterson 1965; Griggs 1967). Further factors that may, in general, affect ductility at high temperatures include the localization of flow in zones of very fine-grained reaction products (Rutter and Brodie 1988), localization associated with partial melting (van der Molen and Paterson 1979; Rutter and Neumann 1995; Fredrich and Evans 1992), and the production of cracking due to differential thermal expansion between the grains when the temperature is raised at low effective confining pressures (pers. comm. from M. Friedman and I. van der Molen). It should also be noted that Jung, Green and Dobrzhinetskaya (2004) recently reported embrittle-

---

ment in an antigorite serpentinite at pressures of 1–6 GPa even though the dehydration reaction involves negative volume change, and they argued that dehydration embrittlement may provide a viable mechanism for nucleating earthquakes independent of depth, as long as there are hydrous minerals breaking down under a differential stress.

## Fracture Mechanics

The subject called “fracture mechanics” originated as an essentially macroscopic approach to the solution of engineering problems involving the likelihood of fracture from the unstable propagation of pre-existing cracks. Fracture mechanics derives largely from Griffith’s (1920) theory of brittle failure, generalized in a more or less empirical way to include in the “surface energy” term other types of energy absorption. However, the main impetus for the current development stems from the work of Irwin (Irwin 1948, 1958, and other papers), and the field now comprises a considerable body of literature covering both theoretical studies and experimental work on many types of materials, including rocks.

Succinct introductions to the general principles of fracture mechanics have been given by Eshelby (1971) and Evans and Langdon (1976). More detailed accounts may be found in the books of Tetelman and McEvily (1967), Knott (1973), Lawn and Wilshaw (1975b), Kanninen and Popelar (1985), Broek (1986), and Lawn (1993) and in the seven-volume treatise edited by Liebowitz (1968). Early applications in rock mechanics were made by Bieniawski (1967a,b, 1968b, 1972) and Hardy, Hudson, and Fairhurst (1973), and more recent applications on various scales have been summarized by Rudnicki (1980), Rice (1980), Pollard (1987), Atkinson (1987), Meredith (1990) and Gueguen, Reuschlé, and Darot (1990).

There are two aspects to fracture mechanics. The first is the treatment of the local stress distribution in the neighbourhood of the crack tip and the relation of this stress field to the external loading of the body. The second aspect is the response of the material of the body to the state of stress at the crack tip. It is therefore appropriate to discuss fracture mechanics under the two headings, (1) stress intensity analysis and (2) critical parameters for failure, while further comments are added under a third heading, (3) dynamic and kinetic effects.

### A1.1 Stress Intensity Analysis

Although it is clearly acknowledged that non-elastic effects are involved at crack tips in most materials, and that even the elastic behaviour in the most highly stressed regions may be non-linear, the practical analysis of the stress distribution in the neighbourhood of the crack tip is usually done on the basis of the classical linear theory of elasticity. The term linear elastic fracture mechanics is sometimes used to indicate this basis. The linear elastic approach is valid provided that the region of

non-linear behaviour is negligibly small compared with the length of the crack and other dimensions of the body. In this case the intensity of deformation in the proximity of the crack tip is controlled by the singular elastic fields. Some progress has also been made in treating the more complex problems that arise when the plastic region around the crack tip is not negligibly small; in these cases, elastic-plastic, viscoelastic, or fully plastic analyses are applied (McClintock and Irwin 1965; Williams 1965; Rice 1968; Hellan 1976). Here we shall only consider the linear elastic analysis.

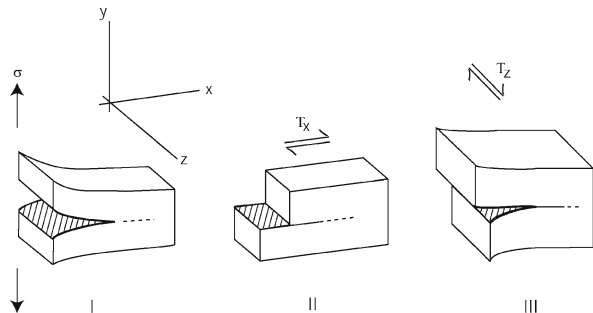
The object of stress intensity analysis is to give a measure of the “loading” applied to the crack tip, which is in effect the driving force for crack propagation. The analysis is done in two stages. First, the nature of the stress distribution in the crack tip region alone is considered and, second, the influence on this region of the external loading on the body and of its geometry is taken into account. We now discuss these two aspects in turn.

a *Stress distribution in the crack tip region.* We assume an ideal flat, perfectly sharp crack of zero thickness (the “mathematical crack”, cf. Jaeger and Cook 1979, p. 273). The analysis of the stress distribution in the neighbourhood of the crack tip is approached by first considering three basic plane modes of distortion around the crack tip. These modes, designated I, II, and III, are defined with respect to a reference plane that is normal to a straight-line crack edge. Modes I and II are the plane strain distortions in which the points on the crack surface are displaced in the reference plane, normal and parallel, respectively, to the plane of the crack. Mode III is the anti-plane strain distortion in which the points on the crack surface are displaced normal to the reference plane. The three modes are depicted in Fig. 83, together with commonly used Cartesian coordinate axes. In each case, the displacements are independent of the  $z$  coordinate, that is, of the position, along the crack edge, of the reference plane used in defining the distortion modes.

The stress and displacement fields around the crack tip can be decomposed into three basic modes of distortion that can be considered as resulting from the application of uniform loadings at infinity, which correspond, in the absence of the perturbations due to the crack, respectively to a uniform tensile stress  $\sigma$  normal to the crack (*I*), a uniform shear stress  $\tau_x$  parallel to the crack in the  $x$  direction (*II*), and a uniform shear stress  $\tau_z$  parallel to the crack in the  $z$  direction (*III*), as shown also in Fig. 83. A variety of mathematical methods can then be applied to calculate

**Fig. 83.**

The three basic plane modes of distortion at a crack tip. *Mode I:* displacement normal to crack plane; *mode II:* displacement parallel to crack plane and normal to crack edge; *mode III:* displacement parallel to crack plane and to crack edge



the local stress and displacement fields around the crack tip (for resumés of the methods, see Paris and Sih 1965; Rice 1968; Sih and Liebowitz 1968; Jaeger and Cook 1979). The calculations show that the stress components all vary inversely as the square root of the distance from the crack tip in all radial directions from the crack tip. This, of course, implies singularities at the crack tip but the strain energy at any finite volume surrounding the crack tip is bounded.

For each mode of distortion, each of the stress components and displacements can be expressed as a product of a spatial distribution function that is independent of the actual value of the applied stress and a scaling factor that depends only on the applied stress and the crack length. The same scaling factor applies for each of the stress components and displacements components in a given mode and is known as the *stress intensity factor* for that mode. The stress intensity factors are designated respectively  $K_I$ ,  $K_{II}$ , and  $K_{III}$ . The formalism can be simply demonstrated with the particular case of the values of the  $\sigma_{yy}$  stress component in mode I at points near the crack tip within the material in the plane of the crack; the elastic solution is

$$\sigma_{yy} = \sigma \sqrt{\frac{c}{2x}}$$

where  $2c$  is the length of the crack (the body being assumed to be large compared with the crack length),  $x$  is the distance from the crack tip, and  $\sigma$  is the macroscopic stress applied normal to the crack. This expression can be written in the form

$$\sigma_{yy} = \frac{K_I}{\sqrt{2\pi x}} \quad \text{where} \quad K_I = \sigma\sqrt{\pi c}$$

The factor

$$1/\sqrt{2\pi x}$$

is the distribution function along the  $x$  axis and

$$K_I = \sigma\sqrt{\pi c}$$

is the scaling factor or stress intensity factor. The full expressions for all the components of stress and displacement at all points in the reference plane in each of the three basic modes of distortion can be found in Paris and Sih (1965), Sih and Liebowitz (1968), Eshelby (1971), and many other papers on fracture mechanics, as listed above.

- b *Stress intensity factors.* So far, we have only considered the general modes of distortion I, II, and III that arise under the particular systems of uniform loading at infinity defined above. Because of the linear properties of elastic behaviour, all more general cases of distortion around crack tips can be treated as combinations of these basic modes. Even in three-dimensional problems, the same consideration applies at each point along a crack edge. Therefore, in the general case, the elastic stress and displacement fields around the crack tip can be obtained from a superposition of

the fields for the three basic modes, scaled according to an appropriate set of three stress intensity factors,  $K_I$ ,  $K_{II}$ , and  $K_{III}$ . The stress intensity factors thus can be said to give a measure of the intensity of loading of the crack tip.

The values of  $K_I$ ,  $K_{II}$ , and  $K_{III}$  in a particular case depend both on the external loading or macroscopic stress field and on the geometry of the specimen (external dimensions and crack dimensions). They have been calculated for many practical cases; a few cases are described by Sih and Liebowitz (1968) and by Eshelby (1971) and comprehensive listings are given by Paris and Sih (1965), Rooke and Cartwright (1976), and Tada, Paris and Irwin (1985).

## A1.2 Critical Parameters for Failure

The type of analysis just given thus enables us, for a particular loading on a specimen of particular shape, to describe the mechanical situation around a crack tip in terms of stress intensity factors and the basic distortion modes. The question next arises as to what aspect of this local situation around the crack tip determines when the crack will begin to spread under the action of increasing the external loading. The simplest view is that the crack will begin to spread when a certain critical intensity of loading is reached at its tip, as measured by the stress intensity factors. That is, the failure criterion is expressed in terms of *critical stress intensity factors*. These factors are material parameters, depending on the type of material, its particular physical condition of grain size, strain-hardening, etc., and the conditions of temperature and pressure. They are designated by  $K_{Ic}$ ,  $K_{IIc}$ , and  $K_{IIIc}$ . Practical procedures for determining the critical parameters for various materials have been extensively developed and codified (e.g., ASTM 1964; Srawley and Brown 1965; International Society for Rock Mechanics Commission on Testing Methods 1988). Typical values are listed by McClintock and Argon (1966, p. 539) and Ashby and Jones (1980). Data for minerals and rocks have been compiled by Atkinson and Meredith (1987a) and, more briefly, by Scholz (1990, p. 24). The value of  $K_{Ic}$  is of the order of 0.1 to 1 MPa m<sup>1/2</sup> for most minerals and rocks.

For practical purposes, the approach in terms of critical loading at the crack tip is a very powerful one since it avoids having to describe the details of the situation at the crack tip; provided the physical identity of the crack is assured and the crack is characterized by its dimensions, all aspects of the precise behaviour at the crack tip (local yielding, non-linear elasticity, atomic configuration, etc.) are subsumed in the empirically determined critical stress intensity factors. The power of the approach stems from the ability to isolate the description of the loading in the crack tip region. Then, for a given material, characterized with respect to its tendency to fail under these local loading conditions by the critical parameters, the local situation of the crack tip can be compared from one type of external loading or specimen to another in terms of the crack tip loading since any singularities or non-linearities will also be comparable; the use of the critical stress intensity factors simply implies that “like causes lead to like effects” (Eshelby 1971). The actual details of behaviour in the singular region at the crack tip are of interest only to those who seek fundamental explanations in atomic terms for the observed values of the critical stress intensity factors and elucidation of the fracture mechanisms at the submicroscopic or subcrack scale.

Various other critical parameters have also been proposed for use as criteria of local failure instead of the critical stress intensity factors. If such criteria are expressed in terms of a single parameter (such as critical relative displacement or energy release rate) then for small-scale yielding they can all be considered to be equivalent in the context of linear elastic fracture mechanics. One of the most widely quoted is the critical energy release rate or crack extension force  $G_c$ . The energy release rate  $G$  is the rate at which the sum of the potential energy of the loading system and the elastic strain energy of the specimen decreases with crack extension. A thermodynamic criterion for crack extension is established by balancing the mechanical energy release against the crack resistance energy (or fracture surface energy)  $R$ :

$$G_c = R$$

The critical energy release rate is related to Griffith's (1920) surface energy term  $\gamma$  (the work of reversible separation of the surfaces to be fractured). In an "ideally" brittle solid,  $R = 2\gamma$ . As first suggested by Orowan (1949) and Irwin (1948),  $R$  may include the work of plastic deformation at the crack tip, and, similarly, it is also directly related to the "modulus of cohesion" of Barenblatt (1962). However, since in simple cases (Sanders 1960; for the restrictions, see Swedlow 1965; Key 1969) the energy release rate can be derived from the elastic analysis of the crack tip loading,  $G$  can also be related to the stress intensity factors by expressions such as

$$G = \frac{1-\nu^2}{E} K_I^2$$

for the mode I plane strain crack tip distortion. Thus, in the general case of a combination of the basic plane modes, the critical parameters for failure are related by

$$G_c = \frac{1-\nu^2}{E} (K_{Ic}^2 + K_{IIc}^2) + \frac{1}{2G} K_{IIIc}^2$$

where  $E$ ,  $G$ , and  $\nu$  are Young's modulus, the shear modulus, and Poisson's ratio, respectively (e.g., Rice 1968, p. 230). The quantity  $G_c$  can also be expressed in terms of a path-independent line or surface integral, such as the J-integral (Sanders 1960; Rice 1968; Eshelby 1971).

The critical condition for crack extension can, further, be alternatively specified in terms of a critical crack opening displacement through the same elastic analysis as is used in defining the stress intensity factors.

In simple cases (Key 1969) all of the critical parameters for crack extension mentioned above are basically equivalent in linear elastic fracture mechanics and have variously been referred to as measures of the "fracture toughness" of a material. However, it should be emphasized that this equivalence is only valid under the basic assumption of linear elastic fracture mechanics that the body is behaving elastically except in a negligibly small region at the crack tip. The term "process zone" is commonly used to describe the region in the vicinity of the crack tip that involves non-linear and irreversible deformation in the form of distributed microcracking or crys-

tal plasticity. In situations where the process zone is relatively large, the various fracture mechanics parameters are no longer equivalent, and emphasis is usually placed on certain parameters chosen as the most significant, such as the crack opening displacement,  $J$ -integral, or plastic zone size (see McClintock and Irwin 1965; Rice 1968, for discussion of difficulties in choosing suitable parameters). The crack resistance  $R$  may also evolve with the crack extension, and the  $R$ -curve can be used to characterize the nonlinear behaviour due to the presence and growth of the process zone (Lawn 1993).

### A1.3 Dynamic and Kinetic Effects

The discussions under the previous two headings apply to quasi-static situations in which the state of stress is assumed to be that for a stationary crack, and no kinetic energy or time-dependent processes are taken into account. In practice, spreading cracks can accelerate to high velocities, comparable to the velocity of sound, or they can spread very slowly.

To analyse the dynamic situation, the stress distribution around the crack tip must be calculated using the equations of motion in place of the equations of equilibrium. This analysis leads to the definition of dynamic stress intensity factors, analogous to the static stress intensity factors considered above; the dynamic stress intensity factors can then be equated to critical values to give failure conditions. Alternatively, the elastic analysis, together with a proper account of the kinetic energy, can be used to calculate an energy release rate which is equated to a critical value  $G_c$  representing the absorption of energy at the crack tip as the crack extends. An introduction to the substantial literature on dynamic crack propagation can be gained through the following references: Erdogan (1968); Rice (1968, p. 235); Eshelby (1971); Rose (1976); Freund (1990). The dynamic theories have potential application in seismology for treating sliding on a fault and the accompanying generation of seismic waves (see, e.g., Kostrov 1966; Ida 1972, 1973; Ida and Aki 1972; Takeuchi and Kikuchi 1973; Andrews 1976a,b; Madariaga 1977; Kostrov and Das 1988) or in rock breakage studies (Swan 1975a). For experimental studies on crack propagation velocities in rocks, see Bieniawski (1968b), Swan (1975b), Henry, Paquet, and Tancrez (1977), Xu and Needleman (1994), Marder and Gross (1995), and Gao (1996).

Stress corrosion in a chemically active environment is another factor potentially of importance in determining the kinetics of crack propagation. Compared with behaviour in a chemically inert environment, stress corrosion leads to rate-dependent crack growth that occurs at a lower stress level and at a crack speed  $v$  that is significantly lower than sonic speed. Since the Griffith theory is based on thermodynamic equilibrium, it cannot predict the kinetics of a crack system that is perturbed from the equilibrium state. This restriction was overcome by Rice (1978), who showed that, in the framework of irreversible thermodynamics, subcritical crack growth and healing are governed by the inequality

$$(G - 2\gamma) v \geq 0$$



In a chemically active environment, adsorption may significantly lower the value of  $\gamma$  (Orowan 1944), which may result in subcritical crack growth. The inequality implies that quasi-static extension or healing may occur, depending on the relative magnitudes of the strain energy release rate  $G$  and the fracture surface energy  $\gamma$ .

Subcritical crack growth is characterized in the laboratory by measuring the crack speed  $v$  as a function of  $G$  or  $K$  (Fig. 84). From experimental data of “model” brittle materials (transparent glasses and single crystals), several distinct regions can be identified (Lawn 1993). The threshold region O defines a temperature-insensitive region in which subcritical crack growth is inhibited. Above this threshold is region I in which the crack speed  $v$  depends strongly on the applied stress, temperature and chemical environment. In region II the crack speed becomes insensitive to applied stress, suggesting control by a transport process whereby the access of the active environmental species to the advancing crack front is increasingly attenuated as  $K$  or  $G$  is increased. This intermediate branch “connects” region I to region III, the latter identifying with the speed response in a chemically inert environment.

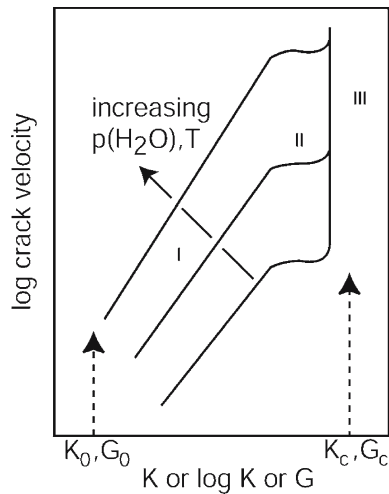
Several relations between  $v$  and  $K$  or  $G$  have been proposed for region I. On purely empirical grounds, the simple power-law relation

$$v \propto K^n$$

has been used (Charles 1958; Atkinson and Meredith 1987b). Such a relationship can be rationalized in terms of a viscous behaviour of material in the vicinity of the crack tip (Maugis 1985; Lawn 1993). However, if subcritical crack growth is modelled as being due to adsorption-induced reduction in bond strength, with the crack speed controlled by the rate of reaction (adsorption) at the crack tip, then  $v$  is proportional to the reaction rate and the subcritical crack growth is governed by an exponential relation

**Fig. 84.**

Three regions of sub-critical crack growth as a function of propagation velocity and stress intensity factor



$$v \propto \exp(bK)$$

(Charles and Hillig 1962; Wiederhorn and Bolz 1970). A further relationship, derived from the classical theory of rate processes (Lawn 1975; Lawn 1993), gives an exponential relation in terms of  $G$ :

$$v \propto \exp(\alpha G) \propto \exp(\beta K^2)$$

In each case, the temperature dependence can be introduced as an Arrhenius factor in the proportionality “constant”.

The scatter in experimental data and the steepness of the  $v$ - $K$  curves in region I are such that it is often difficult to determine which relation is in the best agreement with experimental data. While Gueguen, Reuschlé and Darot (1987) prefer the exponential relation in terms of  $G$ , Atkinson and coworkers (1984, 1987b) advocate the use of the power law for geologic materials. The subcritical crack growth index  $n$  is then determined from a log-log plot of the crack speed versus stress intensity factor. A compilation of values of  $n$  and of the Arrhenius activation energy are given by Atkinson and Meredith (1987a).

## Plasticity Theory and Localization Analysis

### A2.1

#### Introduction

Plasticity theory is the part of continuum mechanics that deals with the irreversible or “plastic” deformation of solids under general states of stress (Hill 1950; Fung 1965; Martin 1975; Chen and Han 1988; Wood 1990). The deforming material is viewed as a continuum with given properties. These properties are here assumed to be strain-rate independent and are expressed in the following empirical or phenomenological relations:

- a A “yield function”  $f(\sigma_{ij})$ , a scalar quantity which describes the yield behaviour of the material and depends only on the stress components  $\sigma_{ij}$ . The material deforms elastically while  $f < 0$  and is assumed to yield when  $f = 0$ . The yield function is represented by a surface in stress space.
- b A “work hardening rule”, which allows for progressive change in the yield function as the deformation proceeds, that is,  $f$  becomes  $f(\sigma_{ij}, \varepsilon_{ij}^p, h)$  where  $\varepsilon_{ij}^p$  is the plastic strain,  $h$  is a hardening parameter, and  $f$  is now called the “loading function”. The case in which the loading surface enlarges uniformly in stress space with continued plastic deformation is known as “isotropic hardening”. The parameter  $h$  determines the rate of hardening and is a function of the plastic strain.
- c A “flow rule”, which determines the deformation that results when the yield condition is met. Since the elastic strain tensor can be determined by differentiation of the elastic potential energy with respect to the stress tensor, it was postulated that the plastic strain increments can be viewed as being derived similarly from a “plastic potential” function  $g(\sigma_{ij})$  according to the equation

$$d\varepsilon_{ij}^p = d\lambda \frac{\partial g}{\partial \sigma_{ij}} \quad (\text{A2.1})$$

where  $d\lambda$  is a positive scalar constant, sometimes called the “loading parameter” (Chen and Han 1988, p. 250). The magnitude of  $d\lambda$  and hence of the strain increments and the strain rates will be determined by the plastic work rate. In a work-hardening material,  $d\lambda$  is inversely related to the hardening parameter  $h$ . However, the full determination of  $d\lambda$  involves the use of the “consistency condition”  $df = 0$  according to which the stress state is required to remain on the yield or loading surface during the plastic flow. The quantity  $d\lambda$  therefore depends on  $f$  as well as

on  $h$  and so generally also involves the parameters that appear in  $f$ . In the case of isotropic hardening (Chen and Han 1988, p. 269),

$$d\lambda = \frac{1}{h} \frac{\partial f}{\partial \sigma_{ij}} d\sigma_{ij} \quad (\text{A2.1a})$$

Under uniaxial loading, work hardening results in the flow stress increasing monotonically with plastic strain. To generalize this concept to a continuum that is subjected to a homogeneous state of stress  $\sigma_{ij}$  and strain  $\varepsilon_{ij}$ , Drucker (1951) proposed the following conditions of “material stability”:

$$d\sigma_{ij} d\varepsilon_{ij}^p > 0 \quad \text{upon loading} \quad (\text{A2.2})$$

$$d\sigma_{ij} d\varepsilon_{ij}^p \geq 0 \quad \text{upon completing a loading-unloading cycle} \quad (\text{A2.3})$$

Drucker’s postulate imposes several constraints on the hardening and flow rules of a work hardening material (Fung 1965; Desai and Siriwardane 1984; Charlez 1991; Fjaer et al. 1992; Chen and Han 1988). In particular, the initial and all subsequent yield surfaces must be convex. However, it should be noted that Drucker’s postulate is more restrictive than is required thermodynamically and that there are materials, discussed later, that do not conform to it (Mroz 1963; Mandel 1966; Chen and Han 1988, p. 255).

## A2.2 Constitutive Relations for a Material without Pressure Dependence or Dilatancy

In the case of many materials, such as ductile metals that deform at constant volume, the plastic potential  $g$  can be assumed to be identical with the yield function  $f$  and the flow rule becomes

$$d\varepsilon_{ij}^p = d\lambda \frac{\partial f}{\partial \sigma_{ij}} \quad (\text{A2.4})$$

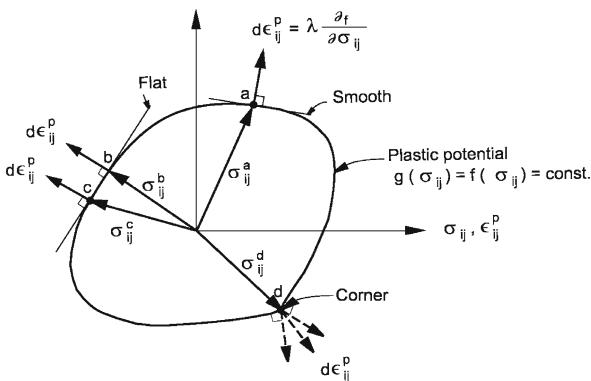
This expression is known as the “associated flow rule”. It is a necessary result of Drucker’s material stability conditions for a work-hardening material. Then, if the strain components and the yield function are plotted in parallel nine-dimensional spaces, the strain increment vector will have the same direction as the normal to the yield function surface at the given stress components (Fig. 85). Thus the relation A2.4 is also known as the “normality rule”.

For non-dilatant materials without pressure dependence, there are two widely-used yield criteria, described by the following yield functions (Chen and Han 1988, p. 74):

a The von Mises criterion, which can be written as

$$f(\sigma_{ij}) = \sqrt{J_2} - k = 0 \quad (\text{A2.5})$$

**Fig. 85.**  
 Illustrating the relationship of strain increments and stresses at yielding (see text)



where

$$J_2 = \frac{1}{6} \left( (\sigma_{11} - \sigma_{22})^2 + (\sigma_{22} - \sigma_{33})^2 + (\sigma_{33} - \sigma_{11})^2 \right) + \sigma_{12}^2 + \sigma_{23}^2 + \sigma_{31}^2$$

is the second invariant of the stress deviation tensor, and  $k$  is a material constant. In terms of the principal stresses,  $\sigma_1$ ,  $\sigma_2$  and  $\sigma_3$ , the von Mises criterion becomes

$$(\sigma_1 - \sigma_2)^2 + (\sigma_2 - \sigma_3)^2 + (\sigma_3 - \sigma_1)^2 = 6k^2 \tag{A2.6}$$

The von Mises criterion effectively states that yielding occurs when the distortional strain energy reaches a certain limit. In the special case of the axisymmetric triaxial condition of  $\sigma_2 = \sigma_3$ , the von Mises criterion becomes

$$\sigma_1 - \sigma_3 = \sqrt{3}k \tag{A2.7}$$

b The Tresca criterion which, in terms of principal stresses, is

$$\sigma_1 - \sigma_3 = 2\bar{k} \quad \text{for } \sigma_1 \geq \sigma_2 \geq \sigma_3 \tag{A2.8}$$

where  $\bar{k}$  is a material constant. Thus the Tresca criterion says that yielding occurs when a limiting value of the maximum shear stress is reached. The Tresca criterion can also be written in terms of the second and third invariants of the stress deviator tensor (Fung 1965, p. 139), but the expression is complex and not very useful.

Since the yield surfaces for the two criteria are of different shape, the relative values of  $k$  and  $\bar{k}$  in Eqs. A2.6 and A2.8 can be chosen differently according to the particular stress conditions under which it is desired to make the yield surfaces coincide (Martin 1975, p. 206; Fung 1965, p. 139; Hill 1950, p. 21). Following Hill (see Chen and Han 1988, p. 74), we here choose

$$\bar{k} = \frac{\sqrt{3}}{2} k = \tau_0$$

where  $\tau_0$  is the yield stress in pure shear ( $\sigma_1 = -\sigma_3 = \tau_0$ ,  $\sigma_2 = 0$ ). Then, in uniaxial stress ( $\sigma_2 = \sigma_3 = 0$ ), the Tresca criterion predicts a yield stress of  $2\tau_0$  and the von Mises criterion predicts a yield stress of  $\sqrt{3}\tau_0$  or 0.866 of that predicted by the Tresca criterion.

### A2.3 Constitutive Model for Dilatant, Pressure-Sensitive Materials

We now consider the application of plasticity theory to the phenomenology of deformation involving dilatancy and hardening in brittle rock. In adapting plasticity theory to such dilatant, “frictional” materials, it is necessary to establish the appropriate characteristics of the yield function, the work hardening rule and the flow rule, taking into account the pressure dependence and the dilatancy.

In principle, the yield point should be identified with the elastic limit, the stress state beyond which the material would retain permanent deformation after a cycle of loading and unloading, and so the onset of plastic yield ought to be delineated in the stress space by cyclic loading to various stress levels (Elliott and Brown 1986). However, it is common in rock and soil mechanics studies to circumvent such a time-consuming procedure by conducting a continuous loading test and identifying the yield points with certain critical points that may be determined conveniently from the data, such as the stress states at the onset of dilatancy or acoustic emission activity (Senseny, Fosum and Pfeifle 1983; Desai and Siriwardane 1984; Holcomb and Costin 1986; Khan, Xiang and Huang 1991; Wong, David and Zhu 1997). In compact rocks that can be approximated as linearly elastic, plastic yield may also be identified with the onset of nonlinearity in the stress-strain curve.

A yield function has commonly been arrived at by generalizing the von Mises and Tresca criteria, giving rise to the Drucker-Prager and Coulomb yield criteria, respectively. Thus, for an initially isotropic material, Drucker and Prager (1952) proposed the yield criterion

$$f(\sigma_{ij}) = \sqrt{J_2} - k - \mu' \frac{I_1}{3} = 0 \quad (\text{A2.9})$$

where  $I_1 = \sigma_{11} + \sigma_{22} + \sigma_{33}$  is the first invariant of the stress tensor (compressive stress positive),  $J_2$  is the second invariant of the stress deviation tensor, and  $\mu'$ ,  $k$  are material parameters. The parameter  $\mu'$  is a measure of the mean-stress sensitivity of the yield stress and  $k$  determines the locus of the yield stress when its hydrostatic component is zero. In the special case of the axisymmetric triaxial compression test, with principal stresses  $\sigma_1$ ,  $\sigma_2$ , and  $\sigma_3 (= \sigma_2)$ , Eq. A2.9 becomes

$$\sigma_1 - \sigma_3 = \frac{3k}{\sqrt{3} - \mu'} + \frac{3\mu'}{\sqrt{3} - \mu'} \sigma_3 \quad (\text{A2.10})$$

In the case of the shear test ( $\sigma_{13} = \sigma_{31} = \tau$ ; all other  $\sigma_{ij} = 0$ ), Eq. A2.9 becomes

$$\tau = k \quad (\text{A2.10a})$$

The parameters  $\mu'$  and  $k$  can be derived from the slope and intercept of the straight line that fits laboratory data from axisymmetric triaxial compression tests (Fig. 27). If the material is insensitive to hydrostatic loading, so that  $\mu' = 0$ , then Eq. A2.9 reduces to the von Mises yield criterion.

As an alternative to the Drucker-Prager criterion, we have the Coulomb yield criterion, according to which the shear stress is linearly related to the normal stress acting on the yield plane. Now the yield function is independent of the intermediate principal stress and in the case of the axisymmetric triaxial test can be expressed in terms of the maximum and minimum principal stresses ( $\sigma_1$  and  $\sigma_3$ ) as

$$\sigma_1 - \sigma_3 = \frac{2\tau_0 \cos \varphi}{1 - \sin \varphi} + \frac{2\sin \varphi}{1 - \sin \varphi} \sigma_3 \quad (\text{A2.11})$$

where  $\tau_0$  is a “cohesion” and  $\varphi$  is an “angle of internal friction”, analogous to the quantities defined for the peak stress state for macroscopic fracture (Sect. 3.3). If the material is insensitive to hydrostatic loading, so that  $\varphi = 0$ , then Eq. A2.11 reduces to the Tresca yield criterion.

If the parameters in the Drucker-Prager and Coulomb criteria in Eqs. A2.10 and A2.11 are to give the same fit to given data from axisymmetric triaxial compression tests, then they are related by

$$\mu' = \frac{2\sqrt{3} \sin \varphi}{3 - \sin \varphi} \quad \text{and} \quad k = \frac{2\sqrt{3}\tau_0 \cos \varphi}{3 - \sin \varphi} \quad (\text{A2.12})$$

Laboratory data for brittle rock (Rudnicki and Rice 1975; Lockner 1995) show that  $\mu'$  ranges in value from 0.4 to 0.9 at the onset of dilatancy and from 0.8 to 1.3 at peak stress, corresponding, respectively, to ranges in  $\varphi$  from 18° to 38° and 35° to 55° (tan  $\varphi$  from 0.3 to 0.8 and 0.7 to 1.4).

For general states of stress, the Drucker-Prager yield surface is continuously curved but the Coulomb yield surface has singular points (“corners” or “vertices”) at locations of the stress space such as  $\sigma_2 = \sigma_3$ , at which the curvature is discontinuous and therefore the normal can not be uniquely defined. Drucker’s postulate constrains the plastic strain increment to lie between adjacent normals to the yield surface at such corners.

**Associated flow rule.** We first consider the situation in which the normality rule holds and the plastic potential has the same form as the yield function, leading to the flow rule (Eq. A2.4), and we focus on the axisymmetric triaxial compression test. If the Drucker-Prager yield function (Eq. A2.10) is assumed, it can be shown that a volume change is predicted according to

$$R = \frac{d\varepsilon_{ii}^p}{d\varepsilon_{11}^p} = \frac{-3\mu'}{\sqrt{3} - \mu'} \quad (\text{A2.13})$$

(Desai and Siriwardane 1984) where  $R$  is the ratio between the volumetric and axial plastic strain increments. The value of  $R$  is always non-zero if  $\mu'$  is non-zero and an axial shortening of the sample will induce dilatancy if  $R$  is negative ( $\mu' > 0$ ).

If the Coulomb yield function (Eq. A2.11) is assumed with principal stresses  $\sigma_1 > \sigma_2 > \sigma_3$  (“true” triaxial stress state), then the associated flow rule implies plane strain deformation ( $d\varepsilon_2^p = 0$ ) with a volume change according to

$$R = \frac{d\varepsilon_{ii}^p}{d\varepsilon_{11}^p} = \frac{-2\sin\varphi}{1 - \sin\varphi} \quad (\text{A2.14})$$

Laboratory data (Chapt. 6) show that, although some materials do show the amount of dilatancy predicted by Eq. A2.13 or A2.14, there are many, including soils, rocks and concrete, that often show a smaller amount. Thus it can be concluded that the latter materials do not satisfy the normality condition and that a non-associated flow rule is commonly required to describe the evolution of dilatancy and hardening in them.

**Non-associated flow rule.** When the plastic potential  $g$  can no longer be identified with the yield function  $f$ , the material is said to follow a “non-associated flow rule”. The normality rule whereby the strain increment vector is parallel to the normal to the yield function surface no longer applies, although the strain increment is still necessarily normal to the plastic potential surface. Many proposals for constitutive relations for non-associated flow and accompanying hardening have been promulgated in the literature for such materials as soils, rocks and concrete (Desai and Siriwardane 1984; Chen and Han 1988).

One of the simplest versions of a non-associated flow model assumes a Coulomb yield function of the form of Eq. A2.11 but with a plastic potential function derived from it by replacing the angle of internal friction  $\varphi$  by an “angle of dilatancy”  $\psi$ :

$$g = (\sigma_1 - \sigma_3) - \sigma_3 \frac{2\sin\psi}{1 - \sin\psi} - \frac{2\tau_0 \cos\psi}{1 - \sin\psi} \quad (\text{A2.15})$$

Dilatancy is controlled by the parameter  $\psi$  and is positive if  $\psi > 0$ . Normality results if the angles of internal friction  $\varphi$  and dilatancy  $\psi$  coincide. As a practical example, Ord, Vardoulakis and Kajewski (1991) reported an average value of  $20^\circ$  for the angle  $\psi$  in Gosford sandstone prior to failure in plane strain, which is smaller than the angle  $\varphi = 44^\circ$  for this material and thus demonstrates non-normal behaviour in this rock.

We now summarize an analysis formulated by Rudnicki and Rice (1975) for non-associated flow and hardening behaviour in a dilatant frictional material, an analysis that has been widely used in shear localization studies. The yield surface is assumed to be smooth, and both the yield and plastic potential functions depend on only the first and second stress invariants. If the constitutive parameters in the Rudnicki and Rice model are assumed to be constants independent of the stress state then the yield criterion can be considered to be analogous to that of Drucker-Prager (Eq. A2.9), and the plastic potential is of the form

$$g(\sigma_{ij}) = \sqrt{J_2} - k - \beta \frac{I_1}{3} \quad (\text{A2.16})$$



where  $\beta$  is a “dilatancy factor” deriving from the ratio of the plastic volumetric strain to the plastic shear strain, and  $\beta > 0$  if axial shortening induces dilatancy. If  $\beta = \mu'$ , the flow law is associative and Eq. A2.16 reduces to Eq. A2.10. Rudnicki and Rice also assume isotropic hardening with a hardening parameter  $h$  (defined with reference to a stress configuration of pure shear with constant mean stress) which is positive for hardening and negative for softening behaviour. Then Eq. A2.1a can be applied and gives

$$d\lambda = \frac{1}{h} \left( \frac{\sigma'_{kl}}{2\sqrt{J_2}} - \frac{\mu'}{3} \delta_{kl} \right) d\sigma_{kl} \quad (\text{A2.17})$$

with the deviatoric stress tensor

$$\sigma'_{ij} = \sigma_{ij} - \frac{\sigma_{kk}}{3} \delta_{ij}$$

The parameters  $\mu'$ ,  $\beta$ , and  $h$  evolve with the inelastic deformation, that is, they are functions of the plastic strain.

Starting with the material at a stress on the yield surface (Eq. A2.9), then, from Eqs. A2.1, A2.1a, A2.9, A2.16, and A2.17, an outward increment of stress  $d\sigma_{ij}$  will give a plastic strain increment of

$$d\varepsilon_{ij}^p = \frac{1}{h} \left( \frac{\sigma'_{kl}}{2\sqrt{J_2}} - \frac{\mu'}{3} \delta_{kl} \right) \left( \frac{\sigma'_{ij}}{2\sqrt{J_2}} - \frac{\beta}{3} \delta_{ij} \right) d\sigma_{kl} \quad (\text{A2.18})$$

(Rudnicki and Rice 1975; Rudnicki 1984; Chen and Han 1988, p. 374; Holcomb and Rudnicki 2001).

In the particular case of an axisymmetric triaxial compression test at constant confining pressure, the incremental principal plastic strain components are

$$d\varepsilon_1^p = \frac{(\sqrt{3} - \beta)(\sqrt{3} - \mu')}{9h} d(\sigma_1 - \sigma_3) \quad (\text{A2.19})$$

$$d\varepsilon_2^p = d\varepsilon_3^p = \frac{\left( -\frac{\sqrt{3}}{2} - \beta \right) (\sqrt{3} - \mu')}{9h} d(\sigma_1 - \sigma_3) \quad (\text{A2.20})$$

and the dilatancy  $R$  is

$$R = \frac{d\varepsilon_v^p}{d\varepsilon_1^p} = \frac{d\varepsilon_1^p + 2d\varepsilon_2^p}{d\varepsilon_1^p} = \frac{-3\beta}{\sqrt{3} - \beta} \quad (\text{A2.20a})$$

These relations allow the value of  $\beta$  to be determined from the experimentally measured  $R$  through

$$\beta = \frac{-\sqrt{3}R}{3-R} \quad (\text{A2.20b})$$

and the value of  $h$  from

$$\frac{h}{E} = \frac{(\sqrt{3} - \mu')(\sqrt{3} - \beta)}{9} \left( \frac{h_{\tan}}{E - h_{\tan}} \right) \quad (\text{A2.20c})$$

where  $E$  is the Young's modulus and  $h_{\tan}$  is the tangent modulus or local slope of the differential stress versus axial strain curve.

Rudnicki and Rice (1975) also consider an alternative to isotropic hardening in which the yield surface develops a vertex at the loading point. This model is suggested from mechanistic considerations akin to those of the wing crack model, focussing on the slip-like activity on sliding cracks. The presence of the vertex at the loading stress state introduces an additional degree of freedom in the hardening behaviour, which is described by introducing extra terms involving an additional hardening parameter  $h_1$  in Eq. A2.18.

## A2.4 Bifurcation, Instability and Shear Localization

So far we have considered the factors determining the stress-strain relationships in plastic deformation at a point in a continuum. Now we consider the distribution of the deformation through a body of finite dimensions. In particular, the question arises of whether, under uniformly applied loading, the deformation will develop uniformly through the body or tend to concentrate locally.

Bifurcation analysis for the onset of shear localization was first developed by Hill (1962) and Mandel (1966) for elastic-plastic solids with rate-insensitive associated-flow constitutive relations. Rudnicki and Rice (1975) later derived the critical conditions for the onset of shear localization in the case of the Drucker-Prager constitutive model described in the previous section. From considerations of compatibility and equilibrium across a shear band, they conclude that the possibility of localization is determined from solutions to an equation

$$(n_i L_{ijkl} n_j) g_k = 0 \quad (\text{A2.21})$$

where  $n_i$  are the components of the unit vector normal to the band,  $L_{ijkl}$  are the components of the "incremental modulus" in the constitutive relation

$$d\sigma_{ij} = L_{ijkl} d\epsilon_{kl} \quad (\text{A2.22})$$

and  $g_k$  are the components of a vector specifying the nonuniformity of deformation across the band. The  $L_{ijkl}$  are functions of the elastic moduli as well as of the constitutive parameters  $h$ ,  $\mu'$  and  $\beta$  defined in the above section, and they can be obtained

by inverting expressions of the type of Eq. A2.18. Localization is predicted when there are solutions of Eq. A2.21 giving non-zero  $g_k$ , that is, when the determinant of the quantity in brackets in Eq. A2.21 is zero. This critical condition is then optimized over all possible orientations of the shear band to identify the deformation state for the first occurrence of such bifurcation (corresponding to the maximum  $h$ ).

Rudnicki and Rice (1975; see also Rudnicki and Olsson 1998) showed that, for the isotropic hardening case, the critical orientation of the shear band lies in the plane of  $\sigma_1$  and  $\sigma_3$ , at an angle  $\theta$  (between the plane and the  $\sigma_1$  direction) given by

$$\theta = \frac{\pi}{4} - \frac{1}{2} \arcsin \alpha \quad (\text{A2.23})$$

where

$$\alpha = \frac{\frac{2}{3}(1+\nu)(\mu' + \beta) - N(1-2\nu)}{\sqrt{4-3N^2}} \quad (\text{A2.24})$$

Here  $\nu$  is the Poisson ratio and the parameter

$$N = \frac{-\left(\sigma_2 - \frac{\sigma_1 + \sigma_2 + \sigma_3}{3}\right)}{\sqrt{J_2}}$$

represents the normalized intermediate principal deviatoric stress;  $N = 1/\sqrt{3}$  in axisymmetric compression,  $N = -1/\sqrt{3}$  in axisymmetric extension, and  $N = 0$  in pure shear. Equation A2.23 is valid for  $-1 \leq \alpha \leq 1$  (Perrin and Leblond 1993; Rudnicki and Olsson 1998), which is satisfied for  $-\sqrt{3} \leq \mu' + \beta \leq \sqrt{3}$ . If  $\alpha > 1$  then  $\theta = 0^\circ$ , and if  $\alpha < -1$  then  $\theta = 90^\circ$ , corresponding to a failure mode of axial splitting.

The corresponding value of the critical hardening parameter  $h_{\text{cr}}$  at bifurcation is

$$\frac{h_{\text{cr}}}{E} = \frac{(\mu' - \beta)^2}{18(1-\nu)} - \frac{(\mu' + \beta + 3N)^2}{36} \quad (\text{A2.25})$$

where  $E$  is the Young's modulus.

For non-isotropic hardening when the yield surface may include a vertex structure and the hardening behavior involves an additional constitutive parameter  $h_1$ , the failure angle and critical hardening parameter can no longer be obtained as simple analytic expressions. However, these factors can have important consequences for the onset of localization (see Chapt. 6).

Localization analyses for a material that obeys the Coulomb yield criterion with a non-associative flow rule were reviewed by Hobbs, Mühlhaus and Ord (1990). The predictions are similar to those of Rudnicki and Rice (1975). In relation to the failure angle, Vardoulakis (1980) concluded that it can be approximated by

$$\theta = \frac{\pi}{4} - \frac{\varphi + \psi}{4} \quad (\text{A2.26})$$

A comprehensive review of recent advances in bifurcation analysis of shear localization in geomechanics was presented by Vardoulakis and Sulem (1995).

## Constitutive Relations for Friction

### A3.1 Introduction

The simplest constitutive relation for friction is the classical one stating that the frictional resistance is represented by two constant friction coefficients. These coefficients apply when the contacting surfaces are initially stationary and moving, respectively, and the static coefficient is normally greater than the kinetic. Although this model agrees qualitatively with many experimental observations, it proves to be inadequate in dealing with stability in friction experiments. Since the frictional resistance is represented as decreasing instantaneously and discontinuously when movement is initiated, the classical model predicts that in any real experiment there would be instability regardless of the stiffness of the system, which is in contradiction of the observation that stick-slip can be controlled in a testing machine of high but finite stiffness (Jaeger and Cook 1971).

To account for the sensitivity of frictional instability to system stiffness, Rabinowicz (1958) proposed that friction is dependent either on the slip displacement (slip-weakening model) or on the slip rate (velocity-weakening model). In the *slip-weakening model*, the frictional strength  $\tau$  is given by a monotonically decreasing function of the amount of slip  $\delta$  (Ida 1972; Palmer and Rice 1973). As discussed in Sect. 8.3, the slope of the slip weakening curve  $\tau(\delta)$  defines a critical stiffness such that instability will occur if the machine stiffness is below this critical value. The slip-weakening behaviour has been characterized during dynamic instability in saw-cut rock samples (Rummel, Alheid and John 1978; Li 1987; Ohnaka et al. 1986, 1990, 1996). Although it is quite adequate for modelling a single instability event, the slip-weakening model has been criticized as being incomplete in that it cannot be used to analyze the occurrence of repeated stick-slip instabilities (Ruina 1985). In the alternative *velocity-weakening model*, the frictional strength  $\tau$  is expressed as a function of the slip rate  $V$ . While such a model can describe aspects of the transient response to perturbations in slip rate, instability would always occur independent of the stiffness if  $d\tau/dV < 0$ . Such a velocity-weakening model has been used extensively in earthquake mechanics models (e.g., Carlson and Langar 1989), even though Rice (1993) argued that such models may not have a well-defined fracture energy or continuum limit.

To capture the complexity of frictional sliding and stability behaviours, the friction constitutive model must take into account laboratory observations on the dependence of friction on both loading rate and history. Assuming that friction depends on slip rate and has memory (reflected in its “state”), Dieterich (1979a) and Ruina (1983) proposed and developed the *rate- and state-dependent friction model*. Since these publications,

this framework has been widely adopted for the interpretation of rock friction data. In the rate- and state-dependent model, friction is characterized by two nonlinear constitutive equations, designated respectively as a friction law and an evolution law. These laws have been defined in various ways, as described in the following sections.

### A3.2 Friction Law

A friction law specifies the frictional strength  $\tau$  (or the friction coefficient  $\mu$ ) as a function of the slip rate  $V$  and the “state” of the sliding surface, characterized by a state variable commonly denoted by  $\Psi$ , or  $\theta$ . The functional form of this law is chosen empirically so as to reproduce laboratory data from velocity stepping experiments (such as depicted schematically in Fig. 67). In response to a perturbation in the slip rate from the reference value  $V^*$  to a new value  $V$ , the frictional strength is commonly observed to change instantaneously by an amount that is proportional to  $\ln(V/V^*)$ . Such a “direct” effect can therefore be described by a rate-dependent term  $A \ln(V/V^*)$ , where  $A$  is a constitutive parameter. As sliding continues at the rate  $V$ , the frictional strength typically changes as a function of time  $t$  (or slip  $\delta$ ) to approach ultimately a “steady state” value  $\tau_{ss}(V)$  that is independent of time. This transient can be characterized by the evolution of a state variable  $\Psi$  with time (or slip). The simplest empirical form of a rate- and state-dependent friction law is therefore

$$\tau = \tau^* + A \ln \frac{V}{V^*} + \Psi \quad (\text{A3.1a})$$

where  $\tau^*$  is the frictional strength at the reference slip velocity  $V^*$ . In this form both the state variable  $\Psi$  and the constitutive parameter  $A$  describing the “direct” velocity effect have dimensions of stress. On the basis of the evolution of state being tied to the time or distance of sliding, the state variable  $\Psi$  can be alternatively represented as

$$\Psi = B \ln \frac{V^* \theta}{D_c}$$

where  $B$  is a second constitutive parameter with dimension of stress,  $\theta$  is a state variable with dimension of time, and  $D_c$  is a characteristic sliding distance for the evolution to steady state. It should be noted that the quantities  $\mu$ ,  $V$ ,  $\Psi$  and  $\theta$  can be functions of time.

The friction law can also be expressed in terms of dimensionless parameters. At a given normal stress  $\sigma$ , one can use the friction coefficient  $\mu = \tau/\sigma$  as the variable, with reference value  $\mu^* = \tau^*/\sigma$ , and define two dimensionless constitutive parameters  $a = A/\sigma$  and  $b = B/\sigma$ . In terms of these parameters and the state variable  $\theta$ , the friction law (Eq. A3.1a) becomes

$$\mu = \mu^* + a \ln \frac{V}{V^*} + b \ln \frac{V^* \theta}{D_c} \quad (\text{A3.1b})$$

### A3.3 Evolution Law

The evolution law is a differential equation that specifies the rate of change of the state variable with respect to time or slip. In more complex scenarios, more than one state variable is invoked to characterize the state of the frictional sliding surface, in which case their evolution is described by a system of differential equations. The laboratory observations suggest that the frictional strength at a given rate  $V$  will always converge to a steady state value  $\tau_{ss}(V)$ , no matter how complicated the previous sliding history has been. To capture this phenomenon of “fading memory”, the state variable is expected to approach within a given fraction of an asymptotic limit after the surface has slipped at the constant velocity  $V$  over a characteristic distance  $D_c$ .

A variety of evolution laws have been proposed. For mathematical convenience we will only consider a single state variable, and discuss two such laws that have been widely used. The first law was introduced by Ruina (1983) as a simplification of an earlier model proposed by Dieterich (1979a). It has often been referred to as the “slip law” (Beeler, Tullis and Weeks 1994; Perrin, Rice and Zheng 1995; Marone 1998b). In terms of the state variable  $\Psi$ , this law can be written as

$$\frac{d\Psi}{dt} = -\frac{V}{D_c} \left( \Psi + B \ln \frac{V}{V^*} \right) \quad (\text{A3.2a})$$

The slip law can alternatively be expressed in terms of the state variable  $\theta$  as

$$\frac{d\theta}{dt} = -\frac{V\theta}{D_c} \ln \frac{V\theta}{D_c} \quad (\text{A3.2b})$$

Note that for steady state sliding,  $d\theta/dt = 0$ . In most experimental studies, the friction constitutive parameters are reported in the dimensionless form  $a$  and  $b$ . For this reason we will primarily use these quantities in our discussion here, in conjunction with the forms of Eqs. A3.1b and A3.2b.

The functional form of the slip law was chosen to match experimental observations from velocity stepping experiments since it is commonly observed that the progressive change in frictional strength with slip distance can be approximated as an exponential function. For a frictional surface initially undergoing steady state sliding at constant velocity  $V_1$ , the initial conditions at  $t = 0$  are given by  $V = V_1$ ,  $\theta = \theta_1 = D_c/V_1$  (from  $d\theta/dt = 0$ ) and

$$\mu(0) = \mu_{ss}(V_1) = \mu^* + (a-b) \ln \frac{V_1}{V^*}$$

If the slip rate is changed to a value  $V_2$ , then according to Eq. A3.1b, the friction coefficient will instantaneously change by an amount  $a \ln(V_2/V_1)$ . Subsequent time-dependent change of friction arises from evolution of the state variable according to Eq. A3.2b, which can be integrated to give

$$\theta(t) = \frac{D_c}{V_2} \left( \frac{V_2}{V_1} \right)^{\exp\left(\frac{-V_2 t}{D_c}\right)} \quad (\text{A3.3a})$$

On substituting into Eq. A3.1b, we obtain an expression that describes the evolution of friction

$$\mu(t) = \mu^* + (a-b) \ln \frac{V_2}{V^*} + b \ln \frac{V_2}{V_1} \exp \frac{-V_2 t}{D_c} \quad (\text{A3.3b})$$

The slip law predicts an exponential change of frictional strength with a characteristic distance  $D_c$ . The friction coefficient has a fading memory of the slip history, and it ultimately attains the steady state value of

$$\mu_{ss}(V_2) = \mu^* + (a-b) \ln \frac{V_2}{V^*}$$

A second evolution law that has been widely used is called the “slowness law”,

$$\frac{d\theta}{dt} = 1 - \frac{V\theta}{D_c} \quad (\text{A3.4})$$

The law was first used in a number of studies of Dieterich (1981, 1986, 1992). For the velocity stepping experiment described above, the slowness law can be integrated to describe the evolution of the state variable

$$\theta(t) = \frac{D_c}{V_2} + \left( \frac{D_c}{V_1} - \frac{D_c}{V_2} \right) \exp \frac{-V_2 t}{D_c} \quad (\text{A3.5})$$

It predicts an exponential evolution with a characteristic distance of  $D_c$ . The state variable (and therefore the friction coefficient) has a fading memory of the slip history, ultimately attaining the steady state value of  $D_c/V_2$  which corresponds to the friction coefficient

$$\mu_{ss}(V_2) = \mu^* + (a-b) \ln \frac{V_2}{V^*}$$

When Eq. A3.5 is substituted into Eq. A3.1b, it predicts an evolution of the friction coefficient that is qualitatively similar to Eq. A3.3b.

Data from velocity stepping tests can be fitted equally well with either evolution law. Other evolution laws have also been proposed (Rice 1983; Ruina 1985; Perrin, Rice and Zheng 1995; Marone 1998b). Although they have somewhat different functional forms for the evolution rate (especially in the high- and low-velocity limits), these evolution laws have two common attributes. First, they all predict that an instantaneous change



of friction coefficient  $a \ln(V_2/V_1)$  in response to a velocity jump  $V_2 - V_1$ . Second, they all predict that with prolonged sliding at a constant velocity  $V$ , the friction coefficient will converge to the steady state value of  $\mu^* + (a - b) \ln(V/V^*)$ . Accordingly, experimental studies have focused on determining the constitutive parameters  $a$  and  $a - b$  from the derivative  $\partial\mu/\partial(\ln V)$  for data from the instantaneous and steady state responses to velocity steps.

### A3.4 Time-Dependent Evolution during Stationery Contact

Although the rate- and state-dependent friction law (Eq. A3.1b) provides reasonable fit to experimental data from velocity stepping experiments, it cannot be extrapolated to the two limiting cases corresponding to slip rate  $V = 0$  and  $\theta \rightarrow 0$  because the logarithmic terms are undefined. Dieterich (1979a, 1981) was aware of this problem, and his original formulation was in the form

$$\mu = \mu^* + a \ln\left(1 + \frac{V}{V^*}\right) + b \ln\left(1 + \frac{V^* \theta}{D_c}\right) \quad (\text{A3.6})$$

The reference slip rate  $V^*$  can be arbitrarily chosen, and if the slip rate and state variable have magnitudes such that  $(V/V^*) \gg 1$  and  $(V^* \theta/D_c) \gg 1$ , then Eq. A3.6 reduces to Eq. A3.1b (Dieterich 1992).

The slip law (Eq. A3.2b) is also not defined for truly stationery contact (with  $V = 0$ ). In proposing the evolution law, Ruina (1983) argued that this may not pose a serious problem since in an experiment one cannot be certain that a sliding surface is perfectly motionless. One can only control the motion of a load point that is connected to the sliding surface by means of a loading device that is deformable, and therefore, even if the load point is held stationery, stress relaxation will induce the loading device and sliding surface to move concomitantly. Because of mathematical convenience, the slip law was widely adopted in many studies in the eighties (e.g., Gu et al. 1984; Blanpied and Tullis 1986; Tullis and Weeks 1986; Rice and Tse 1986; Tse and Rice 1986; Marone, Raleigh and Scholz 1990; Marone, Scholz and Bilham 1991; Gu and Wong 1991). However, subsequently experimental and theoretical studies indicate that it is necessary to allow for an evolution effect during truly stationery contact. Beeler, Tullis and Weeks (1994) studied the time-dependent strengthening of granite and quartzite surfaces in nominally stationery contact and, after accounting for relaxational slip in these slide-hold-slide tests conducted in loading systems with different stiffnesses, they concluded that the slowness law provides a moderately better fit to their data than the slip law. Also, based on seismological observations, Heaton (1990) postulated that earthquake rupture occurs by radiation of slip pulses; but Perrin, Rice and Zheng (1995) concluded in their theoretical study that a dynamic fault model based on a rate- and state-dependent friction law does not produce such "Heaton pulses" unless the evolution law allows for rapid strengthening in truly stationery contact.

### A3.5 Analysis of Frictional Stability – Stick-Slip

A rock friction experiment is commonly modelled as a spring-slider system with a single degree of freedom (Fig. 86). The sliding surface is idealized as a block with unit area moving over a planar surface, and the loading system as an elastic spring with stiffness  $k$ . A constant stress  $\sigma$  is applied normal to the frictional surface. The spring is continually compressed with the load point advancing at a velocity  $V_0$ . Displacements of the load point and the frictional surface are denoted by  $\delta_0$  and  $\delta$ , respectively.

As the shear stress progressively builds up, the frictional response at the interface between the block and the planar surface obeys a specified friction law (Fig. 87). For the classical friction law with a static coefficient  $\mu_s$  and kinetic coefficient  $\mu_k$ , stick-slip instability will always occur if  $\mu_k < \mu_s$ . As soon as the shear stress builds up to the level  $\mu_s \sigma$ , a dynamic instability instantaneously occurs independent of the stiffness.

**Fig. 86.** Spring and slider model for friction experiment

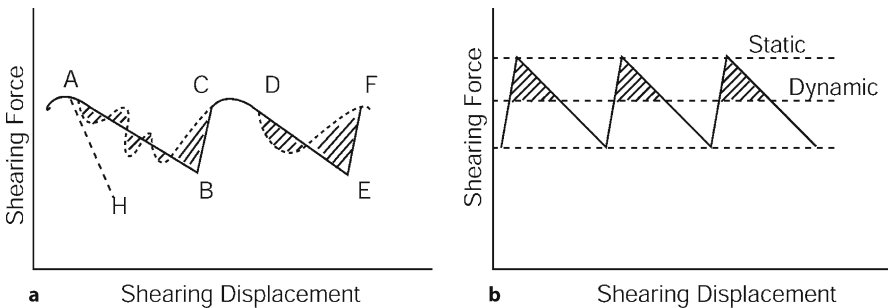
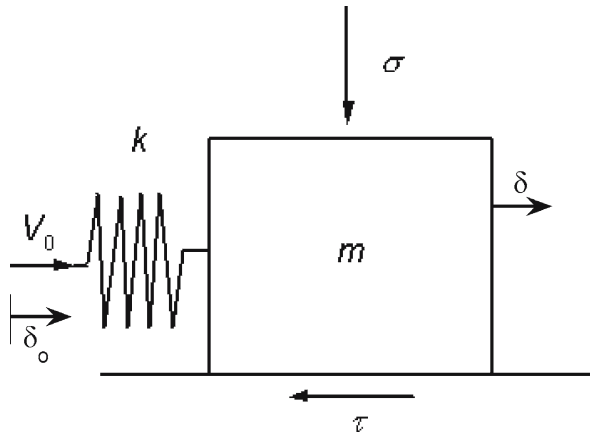


**Fig. 87.** Models for force-displacement characteristics giving rise to stick-slip (see text for details). **a** Case of irregular fluctuation in a slip-weakening model; **b** case of sharply defined coefficients of static and kinetic friction (steeping sloping lines represent elastic distortion only)

For a displacement-dependent friction law  $\tau(\delta)$ , the frictional sliding is always stable if  $d\tau/d\delta > 0$ . In the slip-weakening case with  $d\tau/d\delta < 0$ , dynamic instability occurs only if  $-(d\tau/d\delta) > k$ . For a velocity-dependent friction law  $\tau(V)$ , the frictional sliding is always stable if  $d\tau/dV > 0$ . In the velocity-weakening case, dynamic instability occurs independent of the stiffness if  $d\tau/dV < 0$  at  $V = V_0$  (Stoker 1950).

For the rate- and state-dependent friction law (with a single state variable), some general results were derived by Rice and Ruina (1983). Their linearized stability analysis shows that sliding at a steady load point velocity  $V_0$  is stable if  $d\tau_{ss}/dV > 0$ . This corresponds to a steady state friction that is velocity-strengthening, with the constitutive parameters satisfying the inequality  $a - b > 0$ . In contrast, if  $d\tau_{ss}/dV < 0$  (and therefore  $a - b < 0$ ) the stability behaviour is dependent on the stiffness. The slip is stable if  $k > k_{cr}$ , and unstable if  $k < k_{cr}$  where the critical stiffness is given by

$$k_{cr} = \frac{(b-a)\sigma}{D_c}$$

In the latter case, the stress drop amplitude for cyclic stick-slip events is predicted to scale with  $(b-a)\sigma$ . Furthermore the stress drop increases with increasing loading point velocity and stiffness (Cao and Aki 1986; Gu and Wong 1991), in agreement with laboratory data on a wide range of materials (Rabinowicz 1958; Ohnaka 1973a; Engelder, Logan and Handin 1975; Teufel and Logan 1978; Shimamoto and Logan 1986; Wong and Zhao 1990; Karner and Marone 2000).

If  $k = k_{cr}$  the quasi-static motion is oscillatory with a period

$$2\pi \frac{D_c}{V_0} \sqrt{\frac{a}{b-a}}$$

Such self-sustained oscillations have been observed by Scholz, Molnar and Johnson (1972), Weeks and Tullis (1985), and Wong et al. (1992) in silicate and dolomite rocks. Laboratory studies have also documented the occurrence of period-doubling and apparently chaotic oscillations in the transition from stable sliding to cyclic stick-slip, which is predicted by numerical simulations for a friction law with more than one state variables (Ruina 1980; Gu and Wong 1994b).

### A3.6 Influence of Normal Stress and Temperature

The friction constitutive parameters ( $a$ ,  $b$  and  $D_c$ ) are expected to depend on pressure and temperature. In addition, it has been observed that the frictional sliding behaviour is also sensitive to transient changes in either normal stress or temperature. Linker and Dieterich (1992) conducted experiments in which the normal stress was perturbed while the load point was advancing at a constant velocity. They observed a transient perturbation in the frictional stress which is analogous to that observed in velocity stepping tests. If the normal stress is increased from  $\sigma_1$  to  $\sigma_2$ , the friction coefficient instantaneously increases by an amount that is proportional to  $\ln(\sigma_2/\sigma_1)$ . While the

normal stress is maintained at the new level  $\sigma_2$ , the friction coefficient decays and approaches the steady state friction value that is characteristic of the slip rate. The characteristic distance for memory of the normal stress history to fade is about the same as  $D_c$  for slip history. Linker and Dieterich (1992) argued that the frictional responses to normal stress variation can be interpreted as solely due to the evolution of a state variable that is sensitive to normal stress rate  $\dot{\sigma}$ . Specifically they introduced a constitutive parameter  $\alpha$  and incorporated an additional term

$$-\frac{\alpha\theta\dot{\sigma}}{b\sigma}$$

into the evolution laws, such that the slip and slowness laws respectively become

$$\frac{d\theta}{dt} = -\frac{V\theta}{D_c} \ln \frac{V\theta}{D_c} - \frac{\alpha\theta\dot{\sigma}}{b\sigma} \quad (\text{A3.7a})$$

$$\frac{d\theta}{dt} = 1 - \frac{V\theta}{D_c} - \frac{\alpha\theta\dot{\sigma}}{b\sigma} \quad (\text{A3.7b})$$

If the normal stress is increased from  $\sigma_1$  to  $\sigma_2$  at  $t = 0$  with the slip rate maintained constant at  $V$ , then the normal stress rate is given by  $\dot{\sigma} = (\sigma_2 - \sigma_1)\delta(t)$ , where  $\delta(t)$  is the Dirac delta. According to the evolution law, the state variable will instantaneously be increased by an amount given by

$$\Delta \ln \theta = \frac{\alpha}{b} \ln \frac{\sigma_2}{\sigma_1}$$

and the friction coefficient by  $\alpha \ln(\sigma_1/\sigma_2)$ . Since  $\dot{\sigma} = 0$  for  $t > 0$ , the state variable increment decays exponentially over the characteristic distance  $D_c$  to approach zero and accordingly the friction coefficient approaches the same steady state value as when the normal stress was at the initial level of  $\sigma_1$ .

In this formulation, both the steady state friction (and hence the constitutive parameter  $a - b$ ) as well as the characteristic slip distance  $D_c$  are independent of normal stress. While available data for a relatively limited range of normal stresses seem to be in agreement with these assumptions, a more extensive range should be investigated to validate them. Further, stability analysis of a spring-slider system under conditions of gradually varying normal stress shows that the critical stiffness depends also on the parameter  $\alpha$  (Dieterich and Linker 1992; He, Ma and Huang 1998).

Analogous experiments were conducted by Chester (1994) to investigate the influence of temperature changes on rate- and state-dependent friction. If the temperature is increased from  $T_1$  to  $T_2$  while the load point is advancing at a constant velocity, the friction coefficient instantaneously decreases by an amount that is proportional to  $1/T_1 - 1/T_2$ . While the temperature is maintained at the new level  $T_2$ , the friction coefficient gradually increases and approaches a new steady state value that is somewhat lower than the one at  $T_1$ . The characteristic distance for memory of the temperature

history to fade is about the same as  $D_c$  for slip history. Elevated temperature data for granite and quartz (Stesky 1978a; Chester and Higgs 1992) indicate that the steady state friction scales as  $1/T$ , the reciprocal of temperature, with the implication that micromechanisms of friction are thermally activated and follow an Arrhenius relationship. Chester (1994) postulated that the influence of temperature can be characterized by introducing activation energies  $Q_a$  and  $Q_b$  that are associated with the direct and evolution effects of rate- and state-dependent friction. Specifically he modified the friction and slip law as

$$\mu = \mu^* + a \left( \ln \frac{V}{V^*} + \frac{Q_a}{R} \left( \frac{1}{T} - \frac{1}{T^*} \right) \right) + b \ln \frac{V^* \theta}{D_c} \quad (\text{A3.8a})$$

$$\frac{d\theta}{dt} = -\frac{V\theta}{D_c} \left( \ln \frac{V\theta}{D_c} + \frac{Q_b}{R} \left( \frac{1}{T} - \frac{1}{T^*} \right) \right) \quad (\text{A3.8b})$$

where  $\mu$  is the friction coefficient at the reference slip rate  $V^*$  and temperature  $T^*$ . Unlike Linker and Dieterich's (1992) proposal that the steady state friction coefficient is independent of normal stress, the above friction law predicts that the steady state friction does depend on temperature, following an Arrhenius type of relationship:

$$\mu^{ss} = \mu^* + (a-b) \ln \frac{V}{V^*} + \frac{aQ_a - bQ_b}{R} \left( \frac{1}{T} - \frac{1}{T^*} \right) \quad (\text{A3.9})$$

This relationship has been adopted to infer the frictional strength along localized fault zones in the upper crust (Chester 1995; Blanpied, Lockner and Byerlee 1995).

---

## References

- Abdel-Gawad M, Bulau J, Tittman B (1987) Quantitative characterization of microcracks at elevated pressure. *J Geophys Res* 92:12911–12916
- Abé H, Mura T, Keer LM (1976) Growth rate of a penny-shaped crack in hydraulic fracturing of rocks. *J Geophys Res* 81:5335–5340
- Abe S, Dieterich JH, Mora P, Place D (2002) Simulation of the influence of rate- and state-dependent friction on the macroscopic behavior of complex fault zones with the lattice solid model. *Pure Appl Geophys* 159:1967–1983
- Abey AE, Heard HC (1973) Frictional characteristics of granite and granite/serpentine to high pressures. *EOS Trans AGU* 54:464 (abstract)
- Adams LH, Williamson ED (1923) On the compressibility of minerals and rocks at high pressures. *Franklin Inst J* 195:475–529
- Akai K, Mori H (1967) Study on the failure mechanism of a sandstone under combined compressive stresses. *Proc Japan Soc Civ Eng* 147:11–24
- Akai K, Yamamoto K, Arioka M (1970) Experimentelle Forschung über anisotropische Eigenschaften von kristallinen Schiefen. In: *Proc. 2<sup>nd</sup> Congr. Int. Soc. Rock Mech.*, Belgrade 2, pp 181–186
- Aki K (1981) A probabilistic synthesis of precursory phenomena. In: *Simpson DW, Richards PG (eds) Earthquake prediction. An international review.* American Geophysical Union, Washington, D.C., pp 566–574
- Al-Chalabi M, Huang CL (1974) Stress distribution within circular cylinders in compression. *Int J Rock Mech Min* 11:45–56
- Alber M, Hauptfleisch U (1999) Generation and visualization of microfractures in Carrara marble for estimating fracture toughness, fracture shear and fracture normal stiffness. *Int J Rock Mech Min* 36:1065–1071
- Albert RA, Rudnicki JW (2001) Finite element simulations of Tennessee marble under plane strain laboratory testing: Effects of sample-platen friction on shear band onset. *Mech Mater* 33:47–60
- Aldrich MJ (1969) Pore pressure effects on Berea sandstone subjected to experimental deformation. *Geol Soc Am Bull* 80:1577–1586
- Alexeyev AD, Nedodaev NV, Chekhova GG (1974) The limiting condition for sedimentary rocks under non-equal triaxial compression (in Russian). *Fizicheskie svoystva gornik porod i mineralov pri viisokikh davleniyakh i temperaturakh, Materialli IV Vsesoyuznovo soveshchanie* 9–13 Oct 1974 g.g Tbilisi: Inst. Geophys. Acad. Sci., G.S.S.R., 1974, 249–251
- Alexeyev AD, Osiika EI, Todoseychuk AL (1974) Installation for testing prismatic specimens in triaxial compression (in Russian). U.S.S.R. Description of Invention Certificate No. 394692; Application 12 Oct 1970, Publication 22 Aug 1973, Bulletin No. 34; Publication of Description 3 Jan, 1974
- Alheid H-J (1982) Friction processes on shear surfaces in granite at high pressure and temperature. In: *Schreyer W (ed) High-pressure researches in geoscience. Behaviour and properties of earth materials at high pressures and temperatures.* Schweizerbart'sche Verlagbuchhandlung, Stuttgart, pp 95–102
- Allègre CJ, Le Mouél JL (1994) Introduction of scaling techniques in brittle failure of rocks. *Phys Earth Planet In* 87:85–93
- Allègre CJ, Le Mouél JL, Provost A (1982) Scaling rules in rock fracture and possible implications for earthquake prediction. *Nature* 297:47–49

- Amadei B, Robison J (1986) Strength of rock in multi-axial loading conditions. In: Proc. 27<sup>th</sup> U.S. Symp. Rock Mech., Tuscaloona, Alabama, pp 47–55
- Anand L, Spitzig WA (1982) Shear-band orientations in plane strain. *Acta Metall* 30:553–561
- Anderson OL, Grew PC (1977) Stress corrosion theory of crack propagation with applications to geophysics. *Rev Geophys Space Phys* 15:77–104
- Anderson OL, Lieberman RC (1968) Sound velocities in rocks and minerals: Experimental methods, extrapolation to very high pressures, and results. In: Mason WP (ed) *Physical acoustics. Applications to quantum and solid state physics*. Academic Press, New York, IV, Part B, pp 329–472
- Anderson DL, Minster B, Cole D (1974) The effect of oriented cracks on seismic velocities. *J Geophys Res* 79:4011–4015
- Anderson DL, Whitcomb JH (1973) The dilatancy-diffusion model of earthquake prediction. In: Kovach RL, Nur A (eds) *Proc. Conf. on Tectonic Problems of the San Andreas Fault System*. Stanford Univ Publ Geol Sci 13:417–426
- Andrews DJ (1976a) Rupture propagation with finite stress in antiplane strain. *J Geophys Res* 81:3575–3582
- Andrews DJ (1976b) Rupture velocity of plane strain shear cracks. *J Geophys Res* 81:5679–5687
- Antonellini MA, Pollard DD (1995) Distinct element modeling of deformation bands in sandstone. *J Struct Geol* 17:1165–1182
- Archard JF (1957) Elastic deformation and the laws of friction. *P Roy Soc Lond A Mat* 243:190–205
- Archuleta RJ (1984) A faulting model for the 1979 Imperial Valley earthquake. *J Geophys Res* 89:4559–4585
- Argon AS, Orowan E (1964) Crack nucleation in MgO single crystals. *Phil Mag* 9:1023–1039
- Arieli A, Mukherjee AK (1980) A model for the rate-controlling mechanism in superplasticity. *Mater Sci Eng* 45:61–70
- Ashby MF, Hallam SD (1986) The failure of brittle solids containing small cracks under compressive stress states. *Acta Metall* 34:497–510
- Ashby MF, Jones DRH (1980) *Engineering materials. An introduction to their properties and applications, materials science and technology*. Pergamon Press, Oxford, 278 pp
- Ashby MF, Sammis CG (1990) The damage mechanisms of brittle solids in compression. *Pageoph* 133:489–521
- Ashby MF, Verrall RA (1973) Diffusion-accommodated flow and superplasticity. *Acta Metall* 21:149–163
- ASTM (1964) Progress in measuring fracture toughness and using fracture mechanics (ASTM Special Committee on Fracture Testing of High-Strength Materials). *Mater Res Stand* 4:107–119
- Atkins JO, Peng SS (1974) Compression testing of rock in simulated lunar environment. *U.S. Bur. Mines Rep. Invest.* 7983, 21 pp
- Atkinson BK (1984) Subcritical crack growth in geological materials. *J Geophys Res* 89:4077–4114
- Atkinson BK (ed) (1987) *Fracture mechanics of rock*. Academic Press Geology Series, Academic Press, London, 534 pp
- Atkinson C, Cook JM (1993) Effect of loading rate on crack propagation under compressive stress in a saturated porous material. *J Geophys Res* 98:6383–6395
- Atkinson RH, Ko H-Y (1973) A fluid cushion, multiaxial cell for testing cubical rock specimens. *Int J Rock Mech Min* 10:351–361
- Atkinson BK, Meredith PG (1987a) Experimental fracture mechanics data for rocks and minerals. In: Atkinson BK (ed) *Fracture mechanics of rock*. Academic Press, London, pp 477–525
- Atkinson BK, Meredith PG (1987b) The theory of subcritical crack growth with applications to minerals and rocks. In: Atkinson BK (ed) *Fracture mechanics of rock*. Academic Press, London, pp 111–166
- Atkinson BK, Rawlings RD (1981) Acoustic emission during stress corrosion cracking in rocks. In: Simpson DW, Richards PG (eds) *Earthquake prediction. An international review*. American Geophysical Union, Washington, D.C., Maurice Ewing Series 4, pp 605–616
- Attewell PB, Farmer IW (1973) Fatigue behaviour of rock. *Int J Rock Mech Min* 10:1–9
- Attewell PB, Ramana YV (1966) Wave attenuation and internal friction as functions of frequency in rocks. *Geophysics* 31:1049–1056
- Attewell PB, Sandford MR (1974) Intrinsic shear strength of a brittle, anisotropic rock. I. Experimental and mechanical interpretation. II. Textural data acquisition and processing. III. Textural interpretation of failure. *Int J Rock Mech Min* 11:423–430, 431–438, 439–451
- Auberger M, Rinehart JS (1961) Ultrasonic velocity and attenuation of longitudinal waves in rocks. *J Geophys Res* 66:191–199

- Auzerais FM, Dunsmuir J, Ferréol BB, Martys N, Olson J, Ramakrishnan TS, Rothman DH, Schwartz LM (1996) Transport in sandstone: a study based on three-dimensional microtomography. *Geophys Res Lett* 23:705–708
- Aveline M, Baudran A, Habib P, Isnard P, Leymarie P, Morlier P (1963) Résultats expérimentaux sur les relations entre la microfissuration et la vitesse de propagation des ultra-sons dans les granites du Sidobre (Tarn). *Science de la Terre (Nancy)* 9:441–448
- Aves P, Meredith PG, Sammonds PR, Murrell SAF (1993) Influence of water on cracking in rocks monitored by pore volumetry and acoustic emission measurements during triaxial deformation. In: Parnell J, Ruffield AH, Moles NR (eds) *Geofluids '93*. British Gas, London, pp 166–168
- Avramova E, Stancheva T (1966) An example of mechanical anisotropy (in Russian). *Bulgarian Acad. Sci., Works on the Geology of Bulgaria, Series Eng Geol and Hydrogeol* V:235–241
- Ayling MR, Meredith PG, Murrell SAF (1995) Microcracking during triaxial deformation of porous rocks monitored by changes in rock physical properties. I. Elastic-wave propagation measurements on dry rocks. *Tectonophysics* 245:205–221
- Azhdari A, Nemat-Nasser S (1996) Hoop stress intensity factor and crack-kinking in anisotropic brittle solids. *Int J Solids Struct* 33:2023–2037
- Babb SE (1970) The measurement of hydrostatic pressure. In: Pugh HLD (ed) *Mechanical behaviour of materials under pressure*. Elsevier, Amsterdam, pp 119–152
- Balakrishna S (1967) Experimental study of fracture mechanism in sandstones. *Geophys J Roy Astr S* 14:119–128
- Balakrishna S, Gowd TN (1965) Compressional wave velocities in sandstones under uniaxial pressure. *Bull Nat Geophys Res Inst (India)* 3:147–163
- Balakrishna S, Ramana YV (1964) Effect of uniaxial stress on elastic behaviour of rocks. *Bull Nat Geophys Res Inst (India)* 2:123–141
- Baldrige S, Simmons G (1971) Progress in micro-crack decoration. *EOS Trans AGU* 52:342 (abstract)
- Balla A (1960) Stress conditions in triaxial compression. *J Soil Mech Found Div, Proc Am Soc Div Engrs* 86:57–84
- Balmer GG (1953) Physical properties of some typical foundation rocks. U.S. Bureau of Reclamation, Denver, Concrete Lab Report No SP-39
- Banthia BS, King MS, Fatt I (1965) Ultrasonic shear-wave velocities in rocks subjected to simulated overburden pressure and internal pore pressure. *Geophysics* 30:117–121
- Barber DJ (1990) Régimes of plastic deformation – processes and microstructures: an overview. In: Barber DJ, Meredith PG (eds) *Deformation processes in minerals, ceramics and rocks*. Unwin Hyman, London, pp 138–178
- Barbish AB, Gardner GHF (1969) The effect of heat on some mechanical properties of igneous rocks. *J Soc Petrol Eng AIME* 9:395–402
- Bardet JP, Proubet J (1991) A numerical investigation of the structure of persistent shear bands in granular media. *Géotechnique* 41:599–613
- Barenblatt GI (1959) Concerning equilibrium cracks forming during brittle fracture. *J Appl Math Mech (PMM)* 23:1273–1282
- Barenblatt GI (1962) The mathematical theory of equilibrium cracks in brittle fracture. *Adv Appl Mech* 7:55–129
- Barla G, Goffi L (1974) Direct tensile testing of anisotropic rocks. In: *Advances in Rock Mechanics, Proc. 3<sup>rd</sup> Congr. Int. Soc. Rock Mech.*, Denver, 1974. Washington, D.C., Nat. Acad. Sci., II, Part A, pp 93–98
- Barla G, Innaurato N (1973) Indirect tensile testing of anisotropic rocks. *Rock Mech* 5:215–230
- Barnard PR (1964) Researches into the complete stress-strain curve for concrete. *Mag Concrete Res* 16:203–210
- Barron K (1971a) Brittle fracture initiation in and ultimate failure of rocks. I. Isotropic rock. II. Anisotropic rocks, theory. III. Anisotropic rocks, experimental results. *Int J Rock Mech Min* 8:541–551, 553–563, 565–575
- Barron K (1971b) Detection of fracture initiation in rock specimens by the use of a simple ultrasonic listening device. *Int J Rock Mech Min* 8:55–59
- Barton N (1973) Review of a new shear-strength criterion for rock joints. *Eng Geol* 7:287–332
- Barton N (1976) The shear strength of rock and rock joints. *Int J Rock Mech Min* 13:255–279



- Barton N, Choubey V (1977) The shear strength of rock joints in theory and practice. *Rock Mech* 10:1–54
- Basan PB, Lowden BD, Whattler PR, Attard JJ (1997) Pore-size data in petrophysics: a perspective on the measurement of pore geometry. In: Lovell MA, Harvey PK (eds) *Developments in petrophysics*. The Geological Society, London, Special Publication No. 122, pp 47–67
- Bastawros A-F, Bart-Smith H, Evans AG (2000) Experimental analysis of deformation mechanisms in a closed-cell aluminum alloy foam. *J Mech Phys Solids* 48:301–322
- Bates RL, Jackson JA (eds) (1987) *Glossary of geology*. American Geological Institute, Alexandria, Virginia
- Bathurst RJ, Rothenburg L (1990) Observations on stress-force-fabric relationships in idealized granular materials. *Mech Mater* 9:65–80
- Batzle M, Simmons G, Siegfried RW (1980) Microcrack closure in rocks under stress. *J Geophys Res* 85:7072–7090
- Baud P, Klein E, Wong T-f (2004) Compaction localization in porous sandstones: spatial evolution of damage and acoustic emission activity. *J Struct Geol* 26:603–624
- Baud P, Meredith PG (1997) Damage accumulation during triaxial creep of Darly Dale sandstone from pore volumetry and acoustic emission. *Int J Rock Mech Min* 34:368 (abs + CD ROM)
- Baud P, Reuschlé T, Charlez P (1996) An improved wing crack model for the deformation and failure of rock in compression. *Int J Rock Mech Min* 33:539–542
- Baud P, Schubnel A, Wong T-f (2000) Dilatancy, compaction and failure mode in Solnhofen limestone. *J Geophys Res* 105:19289–19303
- Baud P, Zhu W, Wong T-f (2000) Failure mode and weakening effect of water on sandstone. *J Geophys Res* 105:16371–16389
- Bauer SJ, Friedman M, Handin J (1981) Effects of water-saturation on strength and ductility of three igneous rocks at effective pressures to 50 MPa and temperatures to partial melting. *Proc. 22<sup>nd</sup> U.S. Rock Mechanics Symposium*, pp 73–78
- Baumberger T, Berthoud P, Caroli C (1999) Physical analysis of the state- and rate-dependent friction law. II Dynamic friction. *Phys Rev B* 60:3928–3939
- Bazant ZP, Kazemi MT (1990) Size effect in fracture of ceramics and its use to determine fracture energy and effective process zone length. *J Am Ceram Soc* 73:1841–1853
- Bebbington M, Vere-Jones D, Zheng X (1990) Percolation theory: a model for rock fracture. *Geophys J Int* 100:215–220
- Becker GF (1893) Finite homogeneous strain, flow and rupture of rocks. *Geol Soc Am Bull* 4:13–90
- Bednar HH (1985) *Pressure vessel design handbook*. Van Nostrand Reinhold, New York, 431 pp
- Beeler NM, Hickman SH, Wong T-f (2001) Earthquake stress drop and laboratory-inferred interseismic strength recovery. *J Geophys Res* 106:30701–30713
- Beeler NM, Tullis TE (1995) Implications of Coulomb plasticity for the velocity dependence of experimental faults. *Pure Appl Geophys* 144:252–276
- Beeler NM, Tullis TE, Weeks JD (1994) The roles of time and displacement in the evolution effect in rock friction. *Geophys Res Lett* 21:1987–1990
- Beeler NM, Tullis TE, Blanpied ML, Weeks JD (1996) Frictional behavior of large displacement experimental faults. *J Geophys Res* 101:8697–8715
- Béjina F, Jaoul O, Lieberman RC (1999) Activation volume of Si diffusion in San Carlos olivine: implications for upper mantle rheology. *J Geophys Res* 104:25529–25542
- Berg CA (1965) Deformation of fine cracks under high pressure and shear. *J Geophys Res* 70:3447–3452
- Berge PA, Fryer GJ, Wilkens RH (1992) Velocity-porosity relationships in the upper oceanic crust: theoretical considerations. *J Geophys Res* 97:15239–15254
- Berge PA, Wang HF, Bonner BP (1993) Pore pressure buildup coefficient in synthetic and natural sandstones. *Int J Rock Mech Min* 30:1135–1142
- Bergues J, Derlich S, Habib P, Massat H, Vodar B (1974) Études de quatre roches sous très hautes pressions. In: *Advances in Rock Mechanics, Proc. 3<sup>rd</sup> Congr. Int. Soc. Rock Mech.*, Denver, 1974. Washington, D.C., Nat. Acad. Sci., II, Part A, pp 493–498
- Bernabé Y (1987) The effective pressure law for permeability during pore pressure and confining pressure cycling of several crystalline rocks. *J Geophys Res* 92:649–657
- Bernabé Y (1991) Pore geometry and pressure dependence of the transport properties in sandstones. *Geophysics* 56:436–446

- Bernabé Y, Brace WF (1990) Deformation and fracture of Berea sandstone. In: Duba AG, Durham WB, Handin JW, Wang HF (eds) *The brittle-ductile transition in rocks. The Heard Volume.*: American Geophysical Union, Washington, D.C., *Geophys Monograph* 56, pp 91–101
- Berryman J (1969) New laboratory methods of studying the mechanical properties of rock. *Int J Rock Mech Min* 6:43–90
- Berntsson L, Hedberg B, Malinkowski R (1971) Triaxial deformations by uniaxial compressive load on heat-cured and high-strength concrete. In: Te'eni M (ed) *Structure, solid mechanics and engineering design. Proc. Southampton 1969 Civil Eng. Materials Conf.* Wiley-Interscience, London, pp 799–813
- Berry JP (1960) Some kinetic considerations of the Griffith criterion for fracture. I. Equations of motion at constant force; II. Equations of motion at constant deformation. *J Mech Phys Solids* 8:194–206, 207–216
- Berry JP (1963) Determination of fracture surface energies by the cleavage technique. *J Appl Phys* 34:62–68
- Berryman JG (1992) Effective stress for transport properties of inhomogeneous porous rock. *J Geophys Res* 97:17409–17424
- Berryman JG (1995) Mixture theories for rock properties. In: Ahrens TJ (ed) *Rock physics and phase relations. A handbook of physical constants.* American Geophysical Union, Washington, D.C., *AGU Reference Shelf* 3, pp 205–228
- Berryman JG (1998) Rocks as poroelastic composites. In: Thimus, J-F, Abousleiman Y, Cheng, A H-D, Coussy O, Detournay E (eds) *Poromechanics.* A. A. Balkema, Rotterdam, pp 11–16
- Berryman JG, Wang HF (1995) The elastic coefficients of double-porosity models for fluid transport in jointed rock. *J Geophys Res* 100:24611–24627
- Berthoud P, Baumberger T, G'Sell C, Hiver J-M (1999) Physical analysis of state- and rate-dependent friction law: static friction. *Phys Rev B* 59:14313–14327
- Bésuelle P (2001) Compacting and dilating shear bands in porous rock: theoretical and experimental conditions. *J Geophys Res* 106:13435–13442
- Bésuelle P, Desrués J, Raynaud S (2000) Experimental characterization of the localisation phenomenon inside a Vosges sandstone in a triaxial cell. *Int J Rock Mech Min* 37:1223–1237
- Bésuelle P, Rudnicki JW (2004) Localization: shear bands and compaction bands. In: Guéguen Y, Boutéca M (eds) *Mechanics of fluid-saturated rocks.* Elsevier Academic Press, Amsterdam, pp 219–321
- Bhattacharya K, Ortiz M, Ravichandran G (1998) Energy-based model of compressive splitting in heterogeneous brittle solids. *J Mech Phys Solids* 46:2171–2181
- Biegel RL, Sammis CG, Dieterich JH (1989) The frictional properties of a simulated gouge with fractal particle distribution. *J Struct Geol* 11:827–846
- Biegel RL, Wang W, Scholz CH, Boitnott GN, Yoshioka N (1992) Micromechanics of rock friction. 1. Effects of surface roughening on initial friction and slip hardening in Westerly granite. *J Geophys Res* 97:8951–8964
- Bieniawski ZT (1967a) Mechanism of brittle fracture of rock. Part I. Theory of the fracture process; Part II. Experimental studies; Part III. Fracture in tension and under long-term loading. *Int J Rock Mech Min* 4:395–430
- Bieniawski ZT (1967b) Stability concept of brittle fracture propagation in rock. *Eng Geol* 2:149–162
- Bieniawski ZT (1968a) The effect of specimen size on compressive strength of coal. *Int J Rock Mech Min* 5:325–335
- Bieniawski ZT (1968b) Fracture dynamics of rock. *Int J Fract Mech* 4:415–430
- Bieniawski ZT (1970) Time-dependent behaviour of fractured rock. *Rock Mech* 2:123–137
- Bieniawski ZT (1971) Deformational behaviour of fractured rock under multiaxial compression. In: Te'eni M (ed) *Structure, solid mechanics and engineering design. Proc. Southampton 1969 Civil Eng. Materials Conf.* Wiley-Interscience, London, pp 589–598
- Bieniawski ZT (1972) Propagation of brittle fracture in rock. In: Gray KE (ed) *Basic and applied rock mechanics. Proc. 10<sup>th</sup> Symp. Rock Mech., Austin, Texas, May 1968.* A.I.M.E., New York, pp 409–427
- Bieniawski ZT, Denkhaus HG, Vogler UW (1969) Failure of fractured rock. *Int J Rock Mech Min* 6:323–341
- Bieniawski ZT, van Heerden WL (1975) The significance of in situ tests on large rock specimens. *Int J Rock Mech Min* 12:101–113

- Biot MA (1941) General theory of three-dimensional consolidation. *J Appl Phys* 12:155–164
- Biot MA (1973) Nonlinear and semilinear rheology of porous solids. *J Geophys Res* 78:4924–4937
- Biot MA, Willis DG (1957) Elastic coefficients in the theory of consolidation. *J Appl Mech-T ASME* 24:594–601
- Birch F (1960) The velocity of compressional waves in rocks to 10 kilobars, Part 1. *J Geophys Res* 65:1083–1102
- Birch F (1961) The velocity of compressional waves in rocks to 10 kilobars, Part 2. *J Geophys Res* 66:2199–2224
- Birch F (1975) Velocity and attenuation from resonant vibrations of spheres of rock, glass and steel. *J Geophys Res* 80:756–764
- Birch F, Bancroft D (1938a) The effect of pressure on the rigidity of rocks. *J Geol* 46:59–87, 113–141
- Birch F, Bancroft D (1938b) Elasticity and internal friction in a long column of granite. *B Seismol Soc Am* 28:243–254
- Birch F, Bancroft D (1940) New measurements on the rigidity of rocks at high pressure. *J Geol* 48:752–766
- Bishop JFW (1953) A theoretical examination of the plastic deformation of crystals by glide. *Phil Mag* 44:51–64
- Bizzarri A, Cocco M (2003) Slip-weakening behavior during the propagation of dynamic ruptures obeying rate- and state-dependent friction laws. *J Geophys Res*, 108, 2373, doi: 10.1029/2001JB002198
- Blacic JD, Halleck PH, d'Onfro P, Riecker RE (1981) Thermo-mechanical properties of Galsville sandstone. In: Carter NL, Friedman M, Logan JM, Stearns DW (eds) Mechanical behavior of crustal rocks. The Handin Volume. American Geophysical Union, Washington, D.C., geophysical monograph 24, pp 153–159
- Blake W, Duvall WI (1969) Some fundamental properties of rock noises. *Trans AIME Soc Min Eng* 244:288–290
- Blanpied ML, Lockner DA, Byerlee JD (1991) Fault stability inferred from granite sliding experiments at hydrothermal conditions. *Geophys Res Lett* 18:609–612
- Blanpied ML, Lockner DA, Byerlee JD (1995) Frictional slip of granite at hydrothermal conditions. *J Geophys Res* 100:13045–13064
- Blanpied ML, Tullis TE (1986) The stability and behavior of a frictional system with a two state variable constitutive law. *Pure Appl Geophys* 124:415–444
- Blanpied ML, Tullis TE, Weeks JD (1998) Effects of slip, slip rate, and shear heating on the friction of granite. *J Geophys Res* 103:489–511
- Blanton TL (1981) Effect of strain rates from  $10^{-2}$  to  $10 \text{ sec}^{-1}$  in triaxial compression tests on three rocks. *Int J Rock Mech Min* 18:47–62
- Blekhherman MK, Indenbom VL (1974) The Griffith criterion in the microscopic theory of cracks. *Phys Status Solidi A* 23:729–738
- Boeker R (1915) Die Mechanik der bleibenden Formänderung in kristallinisch aufgebauten Körpern. *Ver Deutsch Ing Mitt Forsch* 175:1–51
- Boitnott GN, Scholz CH (1990) Direct measurement of the effective pressure law: deformation of joints subject to pore and confining pressures. *J Geophys Res* 95:19279–19298
- Boitnott GN, Biegel RL, Scholz CH, Yoshioka N, Wang W (1992) Micromechanics of rock friction. 2. Quantitative modeling of initial friction with contact theory. *J Geophys Res* 97:8965–8978
- Boland JN, Hobbs BE (1973) Microfracturing processes in experimentally deformed peridotite. *Int J Rock Mech Min* 10:623–626
- Boland JN, Tullis TE (1986) Deformation behavior of wet and dry clinopyroxenite in the brittle to ductile transition region. In: Hobbs BE, Heard HC (eds) Mineral and rock deformation: laboratory studies. The Paterson Volume. American Geophysical Union, Washington, D.C., Geophys Monograph 36, pp 35–49
- Bombolakis EG (1964) Photoelastic investigation of brittle crack growth within a field of uniaxial compression. *Tectonophysics* 1:343–351
- Bombolakis EG (1973) Study of the brittle fracture process under uniaxial compression. *Tectonophysics* 18:231–248
- Bonn R, Haupt P (1995) Exact solutions for large elastoplastic deformations of a thick-walled tube under internal pressure. *Int J Plasticity* 11:99–118
- Bonner BP (1974) Shear wave birefringence in dilating granite. *Geophys Res Lett* 1:217–220

- Bonner BP (1975)  $V_p/V_s$  in saturated granodiorite loaded to failure. *Pure Appl Geophys* 113:25–29
- Bonner BP, Benzing WM, Schock RN (1973) Ultrasonic travel-time in rocks under uniaxial compression. *EOS Trans AGU*, 54 467 (abstract)
- Bonner BP, Schock RN (1981) Seismic wave velocity. In: Touloukian YS, Judd WR, Roy RF (eds) *Physical properties of rocks and minerals*. McGraw-Hill Book Co, New York, pp 221–256
- Boozer GD, Hiller KH, Serdengeçti S (1963) Effects of pore fluids on the deformation behavior of rocks subjected to triaxial compression. In: Fairhurst C (ed) *Rock mechanics, 5<sup>th</sup> Symposium on Rock Mechanics*. Pergamon Press, Oxford, pp 579–624
- Bordia SK (1971) The effects of size and stress concentration on the dilatancy and fracture of rock. *Int J Rock Mech Min* 8:629–640
- Borg I, Friedman M, Handin J, Higgs DV (1960) Experimental deformation of St. Peter sand: a study of cataclastic flow. In: Griggs D, Handin J (eds) *Rock deformation*. *Geol Soc Am Mem* 79:133–191
- Born WT (1941) The attenuation constant of earth materials. *Geophysics* 6:132–148
- Bos B, Peach CJ, Spiers CJ (2000) Slip behavior of simulated gouge-bearing faults under conditions favoring pressure solution. *J Geophys Res* 105:16699–16717
- Bos B, Spiers CJ (2002a) Fluid-assisted healing processes in gouge-bearing faults: insights from experiments on a rock analogue system. *Pure Appl Geophys* 159:2537–2566
- Bos B, Spiers CJ (2002b) Frictional-viscous flow of phyllosilicate-bearing fault rock: microphysical model and implications for crustal strength profiles. *J Geophys Res*, 107, 10.1029/2001JB000301 (13 pp)
- Bouchon M, Toksöz N, Karabulut H, Bouin M-P, Dieterich M, Aktar M, Edie M (2000) Seismic imaging of the 1999 Izmit (Turkey) rupture inferred from the near-fault recordings. *Geophys Res Lett* 27:3013–3016
- Boullier AM, Gueguen Y (1975) SP-mylonites: origin of some mylonites by superplastic flow. *Contrib Mineral Petr* 50:93–104
- Boullier AM, Nicolas A (1975) Classification of textures and fabrics of peridotite xenoliths from South African kimberlites. In: Ahrens LH, Dawson JB, Duncan AR, Erlank AJ (eds) *Physics and chemistry of the Earth*. 9, pp 467–475
- Bowden FP, Tabor D (1950) *The friction and lubrication of solids, Part I*. Clarendon Press, Oxford, 337 pp
- Bowden FP, Tabor D (1964) *The friction and lubrication of solids, Part II*. Clarendon Press, Oxford 1964, 544 pp
- Brace WF (1960) An extension of the Griffith theory of fracture to rocks. *J Geophys Res* 65:3477–3480
- Brace WF (1961) Dependence of fracture strength of rocks on grain size. In: *Proc. 4<sup>th</sup> Symposium on Rock Mechanics*, Penn. State Univ., Min. Ind. Exp. Sta. Bull. No. 76, pp 99–103
- Brace WF (1964a) Brittle fracture of rocks. In: Judd WR (ed) *State of stress in the Earth's crust*. American Elsevier, New York, pp 111–174
- Brace WF (1964b) Effect of pressure on electric-resistance strain gages. *Exp Mech* 4:212–216
- Brace WF (1968) Current laboratory studies pertaining to earthquake prediction. *Tectonophysics* 6:75–87
- Brace WF (1969a) Laboratory studies pertaining to earthquakes. *New York Acad Sci Trans* 31:892–906
- Brace WF (1969b) The mechanical effects of pore pressure on fracturing of rocks. In: Baer AJ, Norris DK (eds) *Proc. Conf. on Research in Tectonics (Kink Bands and Brittle Deformation)*, Ottawa, March 1968. *Geol. Surv. Canada, Paper* 68–52, pp 113–123
- Brace WF (1969c) Laboratory studies pertaining to earthquakes. *New York Acad Sci Trans* 31:892–906
- Brace WF (1971a) Micromechanics in rock systems. In: Te'eni M (ed) *Structure, solid mechanics and engineering design*. Wiley-Interscience, London 1971b, pp 187–204
- Brace WF (1971b) Resistivity of saturated crustal rocks to 40 km based on laboratory measurements. In: Heacock JG (ed) *The Structure and physical properties of the Earth's crust*. Am. Geophys. Union, Washington, D.C., *Geophys. Monogr. Series*, Vol. 14, pp 243–255
- Brace WF (1972a) Laboratory studies of stick-slip and their application to earthquakes. *Tectonophysics* 14:189–200
- Brace WF (1972b) Pore pressure in geophysics. In: Heard HC, Borg IY, Carter NL, Raleigh CB (eds) *Flow and fracture of rocks*. Am. Geophys. Union, Washington, D.C., *Geophys. Monogr.* 16, pp 265–273
- Brace WF (1974) Experimental studies of seismic behaviour of rocks under crustal conditions. *Eng Geol* 8:109–127
- Brace WF (1975) Dilatancy-related electrical resistivity changes in rocks. *Pure Appl Geophys* 113:207–217
- Brace WF (1977) Permeability from resistivity and pore shape. *J Geophys Res* 82:3343–3349

- Brace WF (1978) Volume changes during fracture and frictional sliding: a review. *Pure Appl Geophys* 116:603–614
- Brace WF, Bombolakis EG (1963) A note on brittle crack growth in compression. *J Geophys Res* 68:3709–3713
- Brace WF, Byerlee JD (1966) Stick-slip as a mechanism for earthquakes. *Science* 153:990–992
- Brace WF, Byerlee JD (1967) Recent experimental studies of brittle fracture of rocks. In: Fairhurst C (ed) *Proc. 8<sup>th</sup> Symposium on Rock Mechanics*, Univ. Minnesota, Sept. 1966. A.I.M.E., New York, pp 58–81
- Brace WF, Byerlee JD (1970) California earthquakes – why only shallow focus? *Science* 168:1573–1575
- Brace WF, Jones AH (1971) Comparison of uniaxial deformation in shock and static loading of three rocks. *J Geophys Res* 76:4913–4921
- Brace WF, Martin RJ (1968) A test of the law of effective stress for crystalline rocks of low porosity. *Int J Rock Mech Min* 5:415–426
- Brace WF, Orange AS (1966) Electrical resistivity changes in saturated rock under stress. *Science* 153:1525–1526
- Brace WF, Orange AS (1968) Electrical resistivity changes in saturated rocks during fracture and frictional sliding. *J Geophys Res* 73:1433–1445
- Brace WF, Orange AS, Madden TR (1965) The effect of pressure on the electrical resistivity of water-saturated crystalline rocks. *J Geophys Res* 70:5669–5678
- Brace WF, Paulding BW, Scholz C (1966) Dilatancy in the fracture of crystalline rocks. *J Geophys Res* 71:3939–3953
- Brace WF, Riley DK (1972) Static uniaxial deformation of 15 rocks to 30 kb. *Int J Rock Mech Min* 9:271–288
- Brace WF, Stesky RM (1973) Time-dependence of frictional sliding in gabbro at high temperature and pressure. *EOS Trans AGU*, 54, 466 (abstract)
- Brace WF, Walsh JB (1962) Some direct measurements of the surface energy of quartz and orthoclase. *Am Mineral* 47:1111–1122
- Brace WF, Walsh JB, Frangos WT (1968) Permeability of granite under high pressure. *J Geophys Res* 73:2225–2236
- Brace WF, Silver E, Hadley K, Goetze C (1972) Cracks and pores – a closer look. *Science* 178:163–165
- Bradt RC, Newnham RE, Biggers JV (1973) The toughness of jade. *Am Mineral* 58:727–732
- Brady BT (1969a) The nonlinear mechanical behaviour of brittle rock. Part I. Stress-strain behaviour during regions I and II. *Int J Rock Mech Min* 6:211–225
- Brady BT (1969b) The nonlinear mechanical behaviour of brittle rock. Part II. Stress-strain behaviour during regions III and IV. *Int J Rock Mech Min* 6:301–310
- Brady BT (1969c) A statistical theory of brittle fracture for rock materials. Part I. Brittle failure under homogeneous axisymmetric states of stress. *Int J Rock Mech Min* 6:21–42
- Brady BT (1969d) A statistical theory of brittle fracture for rock materials. Part II. Brittle failure under homogeneous triaxial states of stress. *Int J Rock Mech Min* 6:285–300
- Brady BT (1970) Effect of the intermediate principal stress on the fracture of brittle rock. In: Somerton WH (ed) *Rock mechanics – theory and practice*. *Proc. 11<sup>th</sup> Symp. Rock Mech.*, Berkeley, 1970. A.I.M.E., New York, pp 267–279
- Brady BT (1970b) A mechanical equation of state for brittle rock. Part I. The pre-failure behaviour of brittle rock. *Int J Rock Mech Min* 7:385–421
- Brady BT (1971a) The effect of confining pressure on the elastic stress distribution in a radially end-constrained circular cylinder. *Int J Rock Mech Min* 8:153–164
- Brady BT (1971b) Effects of inserts on the elastic behavior of cylindrical materials loaded between rough end plates. *Int J Rock Mech Min* 8:357–369
- Brady BT (1971c) An exact solution to the radially end-constrained circular cylinder under triaxial loading. *Int J Rock Mech Min* 8:165–178
- Brady BT (1971d) Initiation of failure in a radially end-constrained circular cylinder of brittle rock. *Int J Rock Mech Min* 8:371–387
- Brady BT (1974) Theory of earthquakes. I. A scale independent theory of rock failure. *Pure Appl Geophys* 112:701–725

- Brady BT (1975) Theory of earthquakes. II. Inclusion theory of crustal earthquakes. *Pure Appl Geophys* 113:149–168
- Brady BT (1976) Theory of earthquakes. III. Inclusion collapse theory of deep earthquakes. *Pure Appl Geophys* 114:119–139
- Brady BT, Blake W (1972) An elastic solution of the laterally constrained circular cylinder under uniaxial loading. In: Gray KE (ed) *Basic and applied rock mechanics*. 10<sup>th</sup> Symposium on Rock Mechanics, Austin, Texas, May 1968. A.I.M.E., New York, pp 199–214
- Brady BHG, Brown ET (1985) *Rock mechanics for underground mining*. George Allen and Unwin, London, 527 pp
- Brady BT, Duvall WI, Horino FG (1971) A study of the post-failure characteristics of brittle rock. Paper II-21 (22 pp). In: *Rock fracture. Proc. Int. Symp. Rock Mech.*, Nancy, Oct. 1971
- Brady BT, Duvall WI, Horino FG (1973) An experimental determination of the true uniaxial stress-strain behaviour of brittle rock. *Rock Mech* 5:107–120
- Brandes M (1970) Mechanical properties of materials under hydrostatic pressure. In: Pugh HLD (ed) *Mechanical behaviour of materials under pressure*. Elsevier, Amsterdam, pp 236–298
- Brandt H (1955) A study of the speed of sound in porous granular media. *Trans Am Soc Mech Eng* 22:479–486
- Bréchet Y, Estrin Y (1994) The effect of strain rate sensitivity on dynamic friction of metals. *Scripta Metall Mater* 30:1449–1454
- Bredthauer RO (1957) Strength characteristics of rock samples under hydrostatic pressure. *Trans Am Soc Mech Eng* 79:695–706
- Brennan BJ, Stacey FD (1977) Frequency dependence of elasticity of rock – test of seismic velocity dispersion. *Nature* 268:220–222
- Bridgman PW (1912) Breaking tests under hydrostatic pressure and conditions of rupture. *Phil Mag* 24:63–80
- Bridgman PW (1935) Effects of high shearing stress combined with high hydrostatic pressure. *Phys Rev* 48:825–847
- Bridgman PW (1936) Shearing phenomena at high pressure of possible importance for geology. *J Geol* 44:653–669
- Bridgman PW (1937) Shearing phenomena at high pressures, particularly in inorganic compounds. *Proc Am Acad Arts Sci* 71:387–460
- Bridgman PW (1938) Reflections on rupture. *J Appl Phys* 9:517–528
- Bridgman PW (1949a) *The physics of high pressure*. G. Bell and Sons, London, 445 pp
- Bridgman PW (1949b) Volume changes in the plastic stages of simple compression. *J Appl Phys* 20:1241–1251
- Bridgman PW (1952) *Studies in large plastic flow and fracture*. Harvard Univ. Press, Cambridge, Mass., 362 pp
- Briggs A (1992) *Acoustic microscopy*. Clarendon Press, Oxford, 325 pp
- Briscoe BJ, Evans DCB (1982) The shear properties of Lanmuir-Blodgett layers. *P Roy Soc Lond A Mat, Ser. A* 380:389–407
- British National Society, I S o S M F E (1961) Pore pressure and suction in soils. Conf. held at Inst. Civ. Eng., London, March 30–31, 1960. Butterworths, London, 151 pp
- Broch E, Franklin JA (1972) The point-load strength test. *Int J Rock Mech Min* 9:669–697
- Brockley CA, Cameron R, Potter AF (1967) Friction-induced vibration. *J Lubric Tech-T ASME* 89:101–108
- Brockley CA, Davis HR (1968) The time dependence of static friction. *J Lubric Tech-T ASME* 90:35–41
- Broek D (1986) *Elementary Engineering Fracture Mechanics*, 3<sup>rd</sup> ed. Martinus Nijhoff, Dordrecht
- Brown ET (1971) Strength-size effects in rock material. In: *Rock fracture. Proc. Int. Symp. Rock Mech.*, Nancy, 1971, pp Paper II-11 (11 pp)
- Brown ET (1974) Fracture of rock under uniform biaxial compression. In: *Advances in Rock Mechanics, Proc. 3<sup>rd</sup> Congr. Int. Soc. Rock Mech.*, Denver, 1974. Washington, D.C., Nat. Acad. Sci., II, Part A, pp 111–117
- Brown ET (ed) (1981) *Rock characterization, testing and monitoring: ISRM suggested methods*. Pergamon, Oxford

- Brown KM, Bekins B, Clennell B, Dewhurst D, Westbrook G (1994) Heterogeneous hydrofracture development and accretionary fault dynamics. *Geology* 22:259–262
- Brown ET, Gonano LP (1974) Improved compression test technique for soft rock. *J Geotech Eng Div, Proc Am Soc Div Eng* 100:196–199
- Brown ET, Gonano LP (1975) An analysis of size effect behaviour in brittle rock. In: 2<sup>nd</sup> Aust. New Zealand Conf. on Geomechanics, Brisbane, 1975, Inst. Eng. Aust., Nat. Conf. Publ. No. 75/4, pp 139–143
- Brown TA, Heuze FE (1979) A new system for high temperature triaxial creep testing of rocks. In: Gray KE (ed) 20<sup>th</sup> U.S. Symposium on Rock Mechanics. University of Texas, Austin, Texas, pp 51–58
- Brown ET, Hudson JA (1971) The influence of microstructure on rock fracture on the laboratory scale. *Paper II-20* (11 pp). In: Rock fracture. Proc. Int. Symp. Rock Mech., Nancy, Oct. 1971
- Brown ET, Hudson JA, Hardy MP, Fairhurst C (1972) Controlled failure of hollow rock cylinders in uniaxial compression. *Rock Mech* 4:1–24
- Brown RJS, Korringa J (1975) On the dependence of the elastic properties of a porous rock on the compressibility of the pore fluid. *Geophysics* 40:608–616
- Brown SR, Scholz CH (1985) Closure of random elastic surfaces in contact. *J Geophys Res* 90:5531–5545
- Brown JW, Singh MM (1966) An investigation of microseismic activity in rock under tension. *Trans AIME Soc Min Eng* 235:255–265
- Brown ET, Trollope DH (1967) The failure of linear brittle materials under effective tensile stress. *Felsmechanik und Ingenieurgeologie* 5:229–241
- Bruner WM (1976) Comment on “Seismic velocities in dry and saturated cracked solids” by Richard J O’Connell and Bernard Budiansky. *J Geophys Res* 81:2573–2578
- Bruno MS, Nakagawa FM (1991) Pore pressure influence on tensile fracture propagation in sedimentary rock. *Int J Rock Mech Min* 28:261–273
- Budiansky B (1983) Micromechanics. *Comput Struct* 16:3–12
- Budiansky B, O’Connell RJ (1976) Elastic moduli of a cracked solid. *Int J Solids Struct* 12:81–97
- Bulau JR, Waff HS, Tyburczy JA (1979) Mechanical and thermodynamic constraints on fluid distribution in partial melts. *J Geophys Res* 84:6102–6108
- Burchartz H, Saenger G (1931) Der Einfluß der Probengröße und Probenform auf die Ergebnisse der Prüfung von Naturgesteinen auf Druckfestigkeit. *Straßenbau* 22:233–236, 257–262
- Burdine NT (1963) Rock failure under dynamic loading conditions. *J Soc Petrol Eng* 3:1–8 (also appears in *Trans Soc Petrol Eng AIME* 228)
- Burnley PC, Green HW, Prior DJ (1991) Faulting associated with the olivine to spinel transformation in  $Mg_2GeO_4$  and its implications for deep-focus earthquakes. *J Geophys Res* 96:425–443
- Burns DR, Cheng CH, Wilkens RH (1990) Sandstone pore aspect ratio spectra from direct observations and velocity inversion. *Int J Rock Mech Min* 27:315–323
- Byerlee JD (1967a) Frictional characteristics of granite under high confining pressure. *J Geophys Res* 72:3639–3648
- Byerlee JD (1967b) Theory of friction based on brittle fracture. *J Appl Phys* 38:2928–2934
- Byerlee JD (1968) Brittle-ductile transition in rocks. *J Geophys Res* 73:4741–4750
- Byerlee JD (1970) Static and kinetic friction of granite at high normal stress. *Int J Rock Mech Min* 7:577–582
- Byerlee JD (1974) Acoustic emission in rock during fluid injection. In: *Advances in Rock Mechanics. Proc. 3<sup>rd</sup> Congr. Int. Soc. Rock Mech., Denver, 1974. Washington, D.C., Nat. Acad. Sci., II, Part A*, pp 633–637
- Byerlee JD (1975) The fracture strength and frictional strength of Weber sandstone. *Int J Rock Mech Min* 12:1–4
- Byerlee JD (1978) Friction of rocks. *Pure Appl Geophys* 116:615–626
- Byerlee JD, Brace WF (1968) Stick slip, stable sliding, and earthquakes – effect of rock type, pressure, strain rate, and stiffness. *J Geophys Res* 73:6031–6037
- Byerlee JD, Brace WF (1969) High-pressure mechanical instability in rocks. *Science* 164:713–715
- Byerlee JD, Brace WF (1970) Modification of sliding characteristics by fluid injection and its significance for earthquake prevention. *EOS Trans AGU* 51:423 (abstract)
- Byerlee JD, Brace WF (1972) Fault stability and pore pressure. *B Seismol Soc Am* 62:657–660
- Byerlee JD, Lockner D (1976) Measurement of acoustic emission in rock at high confining pressure and differential stress and its relation to creep. *EOS Trans AGU* 57:1011 (abstract)

- Byerlee JD, Lockner D (1977) Acoustic emission during fluid injection into rock. In: Hardy HR, Leighton FW (eds) Proc. First Conf. Acoustic Emission/Microseismic Activity in Geologic Structures and Materials. Penn. State Univ., June 1975. Trans. Tech. Publications, Clausthal, pp 87–89
- Byerlee JD, Mjachkin V, Summers R, Voevoda O (1978) Structures developed in fault gouge during stable sliding and stick-slip. *Tectonophysics* 44:161–171
- Byerlee JD, Peselnick L (1970) Elastic shocks and earthquakes. *Naturwissenschaften* 57:82–85
- Byerlee JD, Savage JC (1992) Coulomb plasticity within the fault zone. *Geophys Res Lett* 19:2341–2344
- Byerlee JD, Summers R (1975) Stable sliding preceding stick-slip on fault surfaces in granite at high pressure. *Pure Appl Geophys* 113:63–68
- Byerlee JD, Summers R (1976) A note on the effect of fault gouge thickness on fault stability. *Int J Rock Mech Min* 13:35–36
- Byerlee JD, Wyss RM (1978) Rock friction and earthquake prediction. *Pure Appl Geophys* 116:583–991
- Cahn RW (1970) *Physical metallurgy*, 2<sup>nd</sup> ed. New-Holland, Amsterdam, 1333 pp
- Cain PJ, Peng SS, Podnieks ER (1974) Rock fragmentation by high frequency fatigue. In: *Advances in Rock Mechanics. Proc. 3<sup>rd</sup> Congr. Int. Soc. Rock Mech.*, Denver, 1974. Washington, D.C., Nat. Acad. Sci., II, Part A, pp 367–372
- Cao T, Aki K (1986) Effect of slip rate on stress drop. *Pure Appl Geophys* 124:515–530
- Caristan Y (1982) The transition from high temperature creep to fracture in Maryland diabase. *J Geophys Res* 87:6781–6790
- Carlson RL, Gangi AF (1985) Effect of cracks on the pressure dependence of P wave velocities in crystalline rocks. *J Geophys Res* 90:8675–8684
- Carlson JM, Langar JS (1989) Properties of earthquakes generated by fault dynamics. *Phys Rev Lett* 62:2632–2635
- Carlson SR, Nishizawa O, Satoh T, Kusunose K (1998) Pore pressure transients, strain and acoustic emission activity during creep in Inada granite. *Int J Rock Mech Min* 35:135–146
- Carpentier D, François D (1971) Mechanical properties of zinc and cobalt under pressure. In: Pugh HLD (ed) *Engineering solids under pressure. 3<sup>rd</sup> Int. Conf. on High Pressure*, Aviemore, Scotland, 1970. Inst. Mech. Eng., London, pp 61–68
- Carr JF (1967) Tensile strength of granular materials. *Nature* 213:1158 (letter)
- Carroll MM (1979) An effective stress law for anisotropic elastic deformation. *J Geophys Res* 84:7510–7512
- Carter NL, Kirby SH (1978) Transient creep and semibrittle behavior of crystalline rocks. *Pure Appl Geophys* 116:807–839
- Carter NL, Tsenn MC (1987) Flow properties of continental lithosphere. *Tectonophysics* 136:27–63
- Carter NL, Anderson DA, Hansen FD, Kranz RL (1981) Creep and creep rupture of granitic rocks. In: Carter NL, Friedman M, Logan JM, Stearns DW (eds) *Mechanical behavior of crustal rocks. The Handin Volume. American Geophysical Union, Washington, D.C., Geophysical Monograph 24*, pp 61–82
- Caruso L, Simmons G, Wilkens R (1985) The physical properties of a set of sandstones – part I. The samples. *Int J Rock Mech Min* 22:381–392
- Casagrande A, Carrillo N (1944) Shear failure of anisotropic materials. *J Boston Soc Civil Engineers* 31:74–87 (reprinted in *Contributions to Soil Mechanics 1941–1953*, Boston Soc. Civ. Eng. 122–135)
- Chambon G, Schmittbuhl J, Corfdir A (2002) Laboratory gouge friction: seismic-like slip weakening and secondary rate- and state-effects. *Geophys Res Lett* 29, 10.1029/2001GL014467
- Chang C, Haimson B (2000) True triaxial strength and deformability of the German Continental Deep Drilling Program (KTB) deep hole amphibolite. *J Geophys Res* 105:18999–19013
- Charles RJ (1958) Static fatigue of glass. *J Appl Phys* 29:1549–1560
- Charles RJ (1959) The strength of silicate glasses and some crystalline oxides. In: Averbach BL, Felbeck DK, Hahn GT, Thomas DA (eds) *Fracture. Proc. Int. Conf. Atomic Mechanisms of Fracture*, Swampscott, April 1959. M.I.T. Press and Wiley, New York, pp 225–249
- Charles RJ, Hillig WB (1962) The kinetics of glass failure by stress corrosion. In: *Symposium sur la Resistance Mechanique du Verre et les Moyens de L'Ameliorer: Charleroi, Belgium, Union Sciences Continentale du Verre*, pp 511–527
- Charlez PA (1991) *Rock mechanics. Vol 1. Theoretical Fundamentals*: Paris, Éditions Technip, 333 pp
- Chau K-T, Rudnicki JW (1990) Bifurcations of compressible pressure-sensitive materials in plane strain tension and compression. *J Mech Phys Solids* 38:875–898



- Chen R (1979) Acoustic emission of rocks under triaxial compression with various stress paths. *Int J Rock Mech Min* 16:401–405
- Chen WF (1984) Soil mechanics, plasticity and landslides. In: Dvorak GJ, Shield RT (eds) *Mechanics of inelastic materials*. Elsevier, Amsterdam, pp 31–58
- Chen WF, Han DJ (1988) *Plasticity for structural engineers*. Springer-Verlag, New York, 606 pp
- Chen R, Yao X-X, Xie H-S (1979) Studies of the fracture of gabbro. *Int J Rock Mech Min* 16:187–193
- Chenevert ME (1970) Adsorptive pore pressures of argillaceous rocks. In: Somerton WH (ed) *Rock mechanics – theory and practice*. Proc. 11<sup>th</sup> Symp. Rock Mech., Berkeley, 1970. A.I.M.E., New York, pp 599–627
- Chenevert ME, Gatlin C (1965) Mechanical anisotropies of laminated sedimentary rocks. *J Soc Petrol Eng* 5:67–77; also appears in *Trans Soc Petrol Eng*, AIME 234
- Cheng CH (1993) Crack models for a transversely isotropic medium. *J Geophys Res* 98:675–684
- Cheng AH-D (1997) Material coefficients of anisotropic poroelasticity. *Int J Rock Mech Min* 34:199–205
- Cherry JT, Larson DB, Rapp EG (1968) A unique description of the failure of a brittle material. *Int J Rock Mech Min* 5:455–463
- Cherry JT, Schock RN, Sweet J (1975) A theoretical model of the dilatant behaviour of a brittle rock. *Pure Appl Geophys* 113:183–196
- Chester FM (1994) Effects of temperature on friction: constitutive equations and experiments with quartz gouge. *J Geophys Res* 99:7247–7261
- Chester FM (1995) A rheological model of wet crust applied to strike-slip faults. *J Geophys Res* 100:13033–13044
- Chester FM, Higgs NG (1992) Multimechanism friction constitutive model for ultrafine quartz gouge at hypocentral conditions. *J Geophys Res* 97:1859–1870
- Chiu HK, Johnston IW, Donald IB (1983) Appropriate techniques for triaxial testing of saturated soft rock. *Int J Rock Mech Min* 20:107–120
- Chokshi AH (1993) Superplasticity in fine grained ceramics and ceramic composites – current understanding and future prospects. *Materials Science & Engineering A* 166:119–133
- Chong KP, Hoyt PM, Smith JW, Paulsen BY (1980) Effects of strain rate on oil shale fracturing. *Int J Rock Mech Min* 17:35–43
- Chow TM, Meglis IL, Young RP (1995) Progressive microcrack development in tests on Lac du Bonnet granite – II. Ultrasonic tomographic imaging. *Int J Rock Mech Min* 32:751–761
- Christensen NI (1965) Compressional wave velocities in metamorphic rocks at pressures to 10 kilobars. *J Geophys Res* 70:6147–6164
- Christensen NI (1966) Shear wave velocities in metamorphic rocks at pressures to 10 kilobars. *J Geophys Res* 71:3549–3556
- Christensen NI (1982) Seismic velocities. In: Carmichael RS (ed) *C.R.C. handbook of physical properties of rocks*. CRC Press Inc., Boca Raton, Florida, II, pp 1–228
- Christensen NI (1985) Measurements of dynamic properties of rock at elevated pressures and temperatures. In: Pincus HJ, Hoskins ER (eds) *Measurement of rock properties at elevated pressures and temperatures*. American Society for Testing and Materials, Philadelphia, ASTM STP 869, pp 93–107
- Christensen RJ, Green SJ, Jones AH (1973) Effect of strain rate in loading porous partially saturated rocks. *EOS Trans AGU* 54:369 (abstract)
- Christensen RJ, Swanson SR, Brown WS (1974) Torsional shear measurements of the frictional properties of Westerly granite. In: *Advances in Rock Mechanics*. Proc. 3<sup>rd</sup> Congr. Int. Soc. Rock Mech., Denver, 1974. Washington, D.C., Nat. Acad. Sci., II, Part A, pp 221–225
- Christensen NI, Wepfer WW (1989) Laboratory techniques for determining seismic velocities and attenuations, with applications to the continental lithosphere. In: Pakiser LC, Mooney WD (eds) *Geophysical framework of the continental United States*. Geological Society of America, Boulder, GSA Memoir 172, pp 91–102
- Chugh YP, Hardy HR, Stefanko R (1972) Investigation of the frequency spectra of microseismic activity in rock under tension. In: Gray KE (ed) *Basic and applied rock mechanics*. Proc. 10<sup>th</sup> Symp. Rock Mech., Austin, Texas, May 1968. A.I.M.E., New York, pp 73–113

- Clarke FJP, Sambell RAJ, Tattersall HG (1962) Mechanisms of microcrack growth in magnesium oxide crystals. *Phil Mag* 7:393–413
- Clarke FJP, Tattersall HG, Tappin G (1966) Toughness of ceramics and their work of fracture. *P Brit Ceramic Soc* 6:163–172
- Cleary MP, Chen IW, Lee SM (1980) Self-consistent techniques for heterogeneous media. *J Eng Mech Div-ASCE* 106:861–887
- Coble RL (1963) A model for boundary diffusion controlled creep in polycrystalline materials. *J Appl Phys* 34:1679–1682
- Coffin LF (1950) The flow and fracture of a brittle material. *J Appl Mech-T ASME* 17:233–248
- Cogan J (1976) Triaxial creep tests of Ophongong limestone and Ophir shale. *Int J Rock Mech Min* 13:1–10
- Coker DA, Torquato S, Dunsmuir JS (1996) Morphology and physical properties of Fontainebleau sandstone via a tomographic analysis. *J Geophys Res* 101:17497–17506
- Colback PSB, Wiid BL (1965) The influence of moisture content on the compressive strength of rocks. In: *Proc. Rock Mechanics Symp. held at Univ. of Toronto, Jan. 1965.*: Ottawa, Dep. Mines Tech. Surv., pp 65–83
- Coles ME, Hazlett RD, Spanne P, Soll WE, Muegge EL, Jones KW (1998) Pore level imaging of fluid transport using X-ray microtomography. *J Petrol Sci Eng* 19:55–63
- Committee on Fracture Characterization and Fluid Flow ea (ed) (1996) *Rock fractures and fluid flow. Contemporary understanding and applications, studies in geophysics.* National Academy Press, Washington, D.C., 551 pp
- Congleton J, Petch NJ (1966) Dislocation movement in the brittle fracture of alumina. *Acta Metall Mater* 14:1179–1182
- Conrad RE, Friedman M (1976) Microscopic feather fractures in the faulting process. *Tectonophysics* 33:187–198
- Cook NGW (1965) The failure of rock. *Int J Rock Mech Min* 2:389–403
- Cook NGW (1970) An experiment proving that dilatancy is a pervasive volumetric property of brittle rock loaded to failure. *Rock Mech* 2:181–188
- Cook NGW (1981) Stiff testing machines, stick slip sliding, and stability of rock deformation. In: Carter NL, Friedman M, Logan JM, Stearns DW (eds) *Mechanical behavior of crustal rocks. The Handin Volume.* American Geophysical Union, Washington, D.C., Geophysical Monograph 24, pp 93–102
- Cook NGW, Heard HC (1981) Berkeley workshop on large scale laboratory testing in geomechanics. *Geophys Res Lett* 8:645–723
- Cook NGW, Hodgson K (1965) Some detailed stress-strain curves for rock. *J Geophys Res* 70:2883–2888
- Cook NGW, Hojem JPM (1966) A rigid 50-ton compression and tension testing machine. *S Afr Mech Eng* 16:89–92
- Cornet FH, Fairhurst C (1974) Influence of pore pressure on the deformation behaviour of saturated rocks. In: *Advances in Rock Mechanics. Proc. 3<sup>rd</sup> Congr. Int. Soc. Rock Mech., Denver, 1974.* Washington, D.C., Nat. Acad. Sci., II, Part A, pp 638–644
- Corwin RE, Hoover DB (1979) The self-potential method in geothermal explorations. *Geophysics* 44:226–245
- Corwin RE, Morrison HF (1977) Self-potential variations preceding earthquakes in central California. *Geophys Res Lett* 4:171–174
- Costin LS (1983) A microcrack model for the deformation and failure of brittle rock. *J Geophys Res* 88:9485–9492
- Costin LS (1985) Damage mechanics in the post-failure regime. *Mech Mater* 4:149–160
- Costin LS (1987) Time-dependent deformation and failure. In: Atkinson BK (ed) *Fracture mechanics of rock.* Academic Press, London, pp 167–215
- Costin LS, Mecholsky JJ (1983) Time dependent crack growth and failure in brittle rock. In: Mathewson CC (ed) *Rock mechanics. Theory – experiment – practice. Proc 24<sup>th</sup> U.S. Symposium on Rock Mechanics, Texas A and M University and Association of Engineering Geologists,* pp 385–394
- Cotterell B, Rice JR (1980) Slightly curved or kinked cracks. *Int J Fracture* 16:155–169
- Coussy O (1995) *Mechanics of porous continua.* Wiley, New York, 472 pp

- Cox SJD (1990) Velocity-dependent friction in a large direct shear experiment on gabbro. In: Knipe RJ, Rutter EH (eds) *Deformation mechanisms, rheology and tectonics*. The Geological Society, London, Special Publication No. 54, pp 63–70
- Cox SJD, Meredith PG (1993) Microcrack formation and material softening in rock measured by monitoring acoustic emissions. *Int J Rock Mech Min* 30:11–24
- Cox BG, Saville G (eds) (1975) High pressure safety code. High Pressure Technol. Assoc. U.K., 47 pp
- Cox SJD, Scholz CH (1988) An experimental study of shear fracture in rocks: mechanical observations. *J Geophys Res* 93:3307–3320
- Craggs JW (1960) On the propagation of a crack in an elastic-brittle material. *J Mech Phys Solids* 8:66–75
- Crampin S (1984) Effective anisotropic elastic constants for wave propagation through cracked solids. *Geophys J Roy Astr S* 76:135–145
- Crampin S, Evans R, Atkinson BK (1984) Earthquake prediction: a new physical basis. *Geophys J Roy Astr S* 76:147–156
- Crawford BR, Smart BGD, Main IG, Liakopoulou-Morris F (1995) Strength characteristics and shear acoustic anisotropy of rock core subjected to true triaxial compression. *Int J Rock Mech Min* 32:189–200
- Crouch SL (1970) Experimental determination of volumetric strains in failed rock. *Int J Rock Mech Min* 7:589–603
- Crouch SL (1972a) A note on post-failure stress-strain path dependence in norite. *Int J Rock Mech Min* 9:197–204
- Crouch SL (1972b) The post-failure behaviour of norite in triaxial compression. *Eng Geol* 6:19–30
- Cundall PA (1971) A computer model for simulating progressive, large-scale movements in block rock systems. In: *Proc. Symp. Int. Soc. Rock Mech.*: Nancy 2, pp 8
- Cundall PA, Drescher A, Strack ODL (1982) Numerical experiments on granular assemblies: measurements and observations. In: Vermeer PA, Luger HJ (eds) *Conference on deformation and failure of granular materials*. A. A. Balkema, Rotterdam, pp 355–370
- Curran JH, Carroll MM (1979) Shear stress enhancement of void compaction. *J Geophys Res* 84:1105–1112
- D'Albissin M, Spanjaard E (1969) Recherches préliminaires sur la triboluminescence des roches et ses applications à l'étude de la microfissuration. In: 2<sup>nd</sup> Coll. Fissuration des Roches, Paris, Jan 1969, *Revue de l'Industrie Minérale, Special Number* (July 1969), pp 68–72
- D'Andrea DV, Condon JL (1971) Dye penetrant studies of fractures produced in laboratory cratering. In: Clark GB (ed) *Dynamic rock mechanics. Proc. 12<sup>th</sup> Symp. Rock Mech.*, Univ. Missouri, Nov. 1970. A.I.M.E., New York, pp 479–495
- D'Appolonia E, Newmark NM (1951) A method for the solution of the restrained cylinder under compression. In: *Proc. 1<sup>st</sup> U.S. Nat. Congress. Appl. Mech.*, Chicago, pp 217–226
- Dai ST, Labuz JF (1997) Damage and failure analysis of brittle materials by acoustic emission. *J Mater Civil Eng* 9:200–205
- Danburg JS, Yuhas DE (1978) Acoustic microscope images of rock samples. *Geophys Res Lett* 5:885–888
- Dandurand JL, Fortuné JP, Pérami R, Schott J, Trollon F (1972a) Considérations nouvelles sur le rôle que le gradient géothermique et les actions tectoniques peuvent avoir dans la formation des concentrations minérales. *CR Acad Sci Paris*, 275, sér. D, 2283–2286
- Dandurand JL, Fortuné JP, Pérami R, Schott J, Trollon F (1972b) On the importance of mechanical action and thermal gradient in the formation of metal-bearing deposits. *Miner Deposita* 7:339–350
- Darot M, Reuschlé T (1999) Direct assessment of Wood's metal wettability on quartz. *Pure Appl Geophys* 155:119–129
- Das S (2003) Dynamic fracture mechanics in the study of the earthquake rupturing process: theory and observation. *J Mech Phys Solids* 51:1939–1955
- Davidson TE, Kendall DP (1970) The design of high pressure containers and associated equipment. In: Pugh HLD (ed) *Mechanical behaviour of materials under pressure*. Elsevier, Amsterdam, pp 54–118
- Davis LA, Gordon RB (1968) Pressure dependence of the plastic flow stress of alkali halide single crystals. *J Appl Phys* 39:3885–3897
- Davis PM, Knopoff L (1995) The elastic modulus of media containing strongly interacting antiplane cracks. *J Geophys Res* 100:18253–18258
- Dayre M, Sirieys PM (1964) Phénomènes de rupture fragile et de viscoélasticité des roches isotropes et anisotropes. *CR Acad Sci Paris* 259:1163–1166

- de Meer S, Spiers CJ (1995) Creep of wet gypsum aggregates under hydrostatic loading conditions. *Tectonophysics* 245:171–183
- Deguelle C, Pleinert H, Maguire P, Lehman E, Missimer J, Hammer J, Leenders H, Bock H, Townsend D (1996) Porosity and pathway determination in crystalline rock by positron emission tomography and neutron radiography. *Earth Planet Sc Lett* 140:213–225
- Deklotz EJ, Brown JW, Stemler OA (1966) Anisotropy of a schistose gneiss. In: Proc. 1<sup>st</sup> Congr. Int. Soc. Rock Mech., Lisbon, 1966, I, pp 465–470
- Dell'Angelo LN, Tullis J (1996) Textural and mechanical evolution with progressive strain in experimentally deformed aplite. *Tectonophysics* 256:57–82
- Dengler L (1976) Microcracks in crystalline rocks. In: Wenk H-R (ed) *Electron microscopy in mineralogy*. Springer-Verlag, Berlin Heidelberg New York, pp 550–556
- Dengo CA, Logan JM (1981) Implications of the mechanical and frictional behavior of serpentinite to seismogenic faulting. *J Geophys Res* 86:10771–10782
- Deresiewicz H (1958) Mechanics of granular matter. In: Dryden, H-L, von Kármán T (eds) *Advances in applied mechanics*. Academic Press V, pp 233–306
- Desai CS, Siriwardane HJ (1984) *Constitutive laws for engineering materials with emphasis on geologic materials*. Prentice-Hall Inc., Englewood Cliffs, NJ, 468 pp
- Detournay E, Cheng, A H-D (1991) Fundamentals of poroelasticity. In: Hudson JA (ed) *Comprehensive rock engineering: principles, practice and projects*. Pergamon Press, Oxford, pp 113–171
- Dey T, Halleck P (1981) Some aspects of size-effect in rock failure. *Geophys Res Lett* 8:691–694
- Dey T, Wang CY (1981) Some mechanisms of microcrack growth and interaction in compressive rock failure. *Int J Rock Mech Min* 18:199–210
- Dhir RK, Sangha CM (1973) Relationships between size, deformation and strength for cylindrical specimens loaded in uniaxial compression. *Int J Rock Mech Min* 10:699–712
- Dieterich JH (1972a) Time-dependent friction in rocks. *J Geophys Res* 77:3690–3697
- Dieterich JH (1972b) Time-dependent friction as a possible mechanism for after-shocks. *J Geophys Res* 77:3771–3781
- Dieterich JH (1978) Time-dependent friction and the mechanism of stick-slip. *Pure Appl Geophys* 116:790–806
- Dieterich JH (1979a) Modeling of rock friction. 1. Experimental results and constitutive equations. 2. Simulation of preseismic slip. *J Geophys Res* 84:2161–2168, 2169–2175
- Dieterich JH (1979b) Modeling of rock friction. 2. Simulation of preseismic slip. *J Geophys Res* 84:2169–2175
- Dieterich JH (1981) Constitutive properties of faults with simulated gouge. In: Carter NL, Friedman M, Logan JM, Stearns DW (eds) *Mechanical behavior of crustal rocks. The Handin Volume*. American Geophysical Union, Washington, D.C., *Geophysical Monograph* 24, pp 103–120
- Dieterich JH (1986) A model for the nucleation of earthquake slip. In: Das S, Boatwright J, Scholz CH (eds) *Earthquake source mechanics, Vol 6*. American Geophysical Union, Washington, D.C., *Geophysical Monograph* 37, pp 36–49
- Dieterich JH (1992) Earthquake nucleation on faults with rate- and state-dependent strength. *Tectonophysics* 211:149–178
- Dieterich JH, Conrad G (1984) Effect of humidity on time- and velocity-dependent friction in rocks. *J Geophys Res* 89:4196–4202
- Dieterich JH, Kilgore BD (1994) Direct observation of frictional contacts: new insights for state-dependent properties. *Pure Appl Geophys* 143:283–302
- Dieterich JH, Kilgore BD (1996a) Imaging surface contacts: power law contact distributions and contact stresses in quartz, calcite, glass and acrylic plastic. *Tectonophysics* 256:219–241
- Dieterich JH, Kilgore BD (1996b) Implications of fault constitutive properties for earthquake prediction. *P Natl Acad Sci USA* 93:3787–3794
- Dieterich JH, Linker MF (1992) Fault stability under conditions of variable normal stress. *Geophys Res Lett* 19:1691–1694
- Digby PJ (1981) The effective elastic moduli of porous granular rock. *J Appl Mech-ASME* 48:803–808
- Digby PJ, Murrell SAF (1975a) The role of shear stress concentrations in the initiation of brittle fracture in bodies containing closed cracks. *B Seismol Soc Am* 65:1163–1171

- Digby PJ, Murrell SAF (1975b) The role of shear stresses in brittle fracture. *J Mech Phys Solids* 23:185–196
- Digby PJ, Murrell SAF (1976) The deformation of flat ellipsoidal cavities under large confining pressures. *B Seismol Soc Am* 66:425–431
- DiGiovanni AA, Fredrich JT, Holcomb DJ, Olsson WA (2000) Micromechanics of compaction in an analogue reservoir sandstone. In: Proc. 4<sup>th</sup> North Am. Rock Mech. Symp., pp 1153–1160
- DiMaggio FL, Sandler IS (1971) Material model for granular soils. *J Eng Mech Div-ASCE* 97:935–950
- DiToro G, Goldsby DL, Tullis TE (2004) Friction falls towards zero in quartz rock as slip velocity approaches seismic rates. *Nature* 427:436–439
- Dobson DP, Meredith PG, Boon SA (2002) Simulation of subduction zone seismicity by dehydration of serpentine. *Science* 298:1407–1410
- Dokos SJ (1946) Sliding friction under extreme pressures – I. *Trans Am Soc Mech Eng* 68A:148–156
- Domenico PA, Schwartz FW (1998) Physical and chemical hydrogeology. John Wiley, New York, 506 pp
- Donath FA (1961) Experimental study of shear failure in anisotropic rocks. *Geol Soc Am Bull* 72:985–990
- Donath FA (1962) Role of layering in geologic deformation. *Trans New York Acad Sci* 24:236–249
- Donath FA (1964) Strength variation and deformational behavior in anisotropic rock. In: Judd WR (ed) State of stress in the Earth's crust. American Elsevier, New York, pp 281–297
- Donath FA (1966) A triaxial pressure apparatus for testing consolidated or unconsolidated materials subjected to pore pressure. In: Testing techniques for rock mechanics. *Am Soc Test Mat STP* 402, pp 41–51
- Donath FA (1970a) Rock deformation apparatus and experiments for dynamic structural geology. *J Geol Educ* 18:3–12
- Donath FA (1970b) Some information squeezed out of rock. *Am Sci* 58:54–72
- Donath FA (1972a) Effects of cohesion and granularity on deformational behaviour of anisotropic rock. In: Doe BR, Smith DK (eds) Studies in mineralogy and Precambrian geology. *Geol Soc Am Mem* 135, pp 95–128
- Donath FA (1972b) Faulting across discontinuities in anisotropic rock. In: Cording EJ (ed) Stability of rock slopes. Proc. 13<sup>th</sup> Symp. Rock Mech., Urbana, Ill., Aug/Sept 1971. New York, Am. Soc. Civ. Eng., pp 753–772
- Donath FA, Faill RT (1963) Ductile faulting in experimentally deformed rocks. *Trans Am Geophys Union* 44:103 (abstract)
- Donath FA, Faill RT, Tobin DG (1971) Deformational mode fields in experimentally deformed rock. *Geol Soc Am Bull* 82:1441–1462
- Donath FA, Fruth LS (1971) Dependence of strain-rate effects on deformation mechanism and rock type. *J Geol* 79:347–371
- Donath FA, Fruth LS, Olsson WA (1973) Experimental study of frictional properties of faults. In: Hardy HR, Stefanko R (eds) New horizons in rock mechanics. Proc. 14<sup>th</sup> Symp. Rock Mech., Penn. State Univ. June 1972. *Am Soc Civ Eng*, pp 189–222
- Donath FA, Güven N (1971) Data reduction in experimental rock deformation. *Contrib to Geol (Univ Wyoming)* 10:89–115
- Dower RJ (1967) On the brittle-ductile transition pressure. *Acta Metall Mater* 15:497–500
- Doyen PM (1988) Permeability, conductivity, and pore geometry of sandstone. *J Geophys Res* 93:7729–7740
- Drennon CB, Handy RL (1972) Stick-slip of lightly loaded limestone. *Int J Rock Mech Min* 9:603–615
- Drescher A, de Josselin de Jong G (1972) Photoelastic verification of a mechanical model for the flow of a granular material. *J Mech Phys Solids* 20:337–351
- Dresen G, Evans B (1993) Brittle and semibrittle deformation of synthetic marbles composed of two phases. *J Geophys Res* 98:11921–11933
- Dreyer W (1958) Über die Bruchfestigkeit mono- und polykristallinen Gesteins in Abhängigkeit von Prüf-körperform, Belastungsgeschwindigkeit und Art der Einspannung. *Bergbauwissenschaften* 5:15–22
- Dreyer W (1966) Quantitative Untersuchungen über die Festigkeit einfach strukturierter Gesteinsarten in Korrelation zu den Gefügeparametern und dem Mineralgehalt der Accessorien. In: Proc. 1<sup>st</sup> Congr. Int. Soc. Rock Mech., Lisbon, 1966, I, pp 133–142

- Dreyer W (1967) Die Festigkeitseigenschaften natürlicher Gesteine insbesondere der Salz- und Karbongesteine. Clausthaler Hefte zur Lagerstättenkunde und Geochemie der mineralischen Rohstoffe, Borntäger, Berlin, 247 pp
- Dreyer W (1972) The science of rock mechanics; part 1, the strength properties of rocks. Series on Rock and Soil Mechanics. Trans. Tech. Publ., Clausthal
- Dreyer W, Borchert H (1962) Ähnlichkeitsmechanik. Ein Beitrag zur Gesteinsphysik und Gebirgsdruckforschung. Bergbauwissenschaften 9:356–361
- Dropek RK, Johnson JN, Walsh JB (1978) The influence of pore pressure on the mechanical properties of Kayenta sandstone. *J Geophys Res* 83:2817–2824
- Drucker DC (1951) A more fundamental approach to plastic stress-strain relations. In: Proc. 1<sup>st</sup> U.S. Nat. Congress. Appl. Mech., Chicago, pp 487–491
- Drucker DC, Prager W (1952) Soil mechanics and plastic analysis or limit design. *Q Appl Math* 10:157–165
- Du Bernard X, Eichhubl P, Aydin A (2002) Dilation bands: a new form of localized failure in granular media. *Geophys Res Lett* 29:2176, doi: 10.1029/2002GL015966 (4 pp)
- Dulaney EN, Brace WF (1960) Velocity behavior of a growing crack. *J Appl Phys* 31:2233–2236
- Dullien FAL (1992) Porous media, fluid transport, and pore structure. Academic Press, San Diego
- Dullien FAL, Dhawan GK (1975) Bivariate pore-size distribution of some sandstones. *J Colloid Interf Sci* 52:129–135
- Dunn DE, LaFountain LJ, Jackson RE (1973) Porosity dependence and mechanism of brittle fracture in sandstones. *J Geophys Res* 78:2403–2417
- Dunning JD, Miller ME (1984) Effects of pore fluid chemistry on stable sliding of Berea sandstone. *Pure Appl Geophys* 122:447–462
- Durand E (1975) L'essai de torsion et la résistance au cisaillement des roches. *Rock Mech* 7:199–230
- Durand E, Comes G (1974) L'essai de torsion et la résistance au cisaillement des roches. In: Advances in Rock Mechanics. Proc. 3<sup>rd</sup> Congr. Int. Soc. Rock Mech., Denver, 1974. Washington, D.C., Nat. Acad. Sci., II, Part A, pp 226–232
- Durelli AJ, Parks V (1962) Relationship of size and stress gradient to brittle failure stress. In: Proc. 4<sup>th</sup> U.S. Nat. Congr. Appl. Mech., Berkeley, June 1962. New York, Am. Soc. Mech. Engrs., pp 931–938
- Durham WB (1981) Direct observation of explosively induced damage in sandstone with application to reservoir simulation. In: Scanning Electron Microscopy I: Chicago, SEM, Inc, pp 585–594
- Durham WB (1990) Capabilities for measuring physical and chemical properties of rocks at high pressure. Lawrence Livermore National Laboratory, Report No. UCID-21754
- Durham WB, Heard HC, Kirby SH (1983) Experimental deformation of polycrystalline H<sub>2</sub>O ice at high pressure and low temperature: preliminary results. *J Geophys Res* 88:B377–B392
- Durney DW (1972) Solution-transfer, an important geological deformation mechanism. *Nature* 235:315–317
- Durney DW (1976) Pressure-solution and crystallization deformation. *Philos T Roy Soc A* 283:229–240
- Edmond O, Murrell SAF (1973) Experimental observations on rock fracture at pressures up to 7 kbar and the implications for earthquake faulting. *Tectonophysics* 16:71–87
- Edmond JM, Paterson MS (1971) Strength of solid pressure media and implications for high pressure apparatus. *Contrib Mineral Petr* 30:141–160
- Edmond JM, Paterson MS (1972) Volume changes during the deformation of rocks at high pressures. *Int J Rock Mech Min* 9:161–182
- Eftis J, Liebowitz H (1976) On surface energy and the continuum thermodynamics of brittle fracture. *Eng Fract Mech* 8:459–485
- Einstein HH, Baecher GB, Hirschfeld RC (1970) The effect of size on the strength of a brittle rock. Proc. 2<sup>nd</sup> Congr. Int. Soc. Rock Mech., Belgrade 2:7–13
- Einstein HH, Dowding CH (1981) Shear resistance and deformability of rock discontinuities. In: Touloukian YS, Judd WR, Roy RF (eds) Physical properties of rocks and minerals. McGraw-Hill Book Co, New York, pp 177–219
- El Bied A, Sulem J, Martineau F (2002) Microstructure of shear zones in Fontainebleau sandstone. *Int J Rock Mech Min* 39:917–932
- Elliott HA (1947) An analysis of the conditions for rupture due to Griffith cracks. *Proc Phys Soc London* 59:208–223

- Elliott D (1973) Diffusion flow laws in metamorphic rocks. *Geol Soc Am Bull* 84:2645–2664
- Elliott GM, Brown ET (1985) Yield of a soft, high porosity rock. *Géotechnique* 35:413–423
- Elliott GM, Brown ET (1986) Further development of a plasticity approach to yield in porous rock. *Int J Rock Mech Min* 23:151–156
- Endres AL (1997) Geometrical models for poroelastic behaviour. *Geophys J Int* 128:522–532
- Engelder JT (1974a) Cataclasis and the generation of fault gouge. *Geol Soc Am Bull* 85:1515–1522
- Engelder JT (1974b) Coefficients of friction for sandstone sliding on quartz gouge. In: *Advances in Rock Mechanics. Proc. 3<sup>rd</sup> Congr. Int. Soc. Rock Mech., Denver, 1974. Washington, D.C., Nat. Acad. Sci., II, Part A*, pp 499–504
- Engelder JT (1974c) Microscopic wear grooves on slickensides: indicators of paleoseismicity. *J Geophys Res* 79:4387–4392
- Engelder JT (1976) Effect of scratch hardness on frictional wear and stick-slip of Westerly granite and Cheshire quartzite. In: Strens GJ (ed) *The physics and chemistry of minerals and rocks*. NATO Institute, Newcastle upon Tyne, April 1974. Wiley, London, pp 139–150
- Engelder T (1994) Deviatoric stressitis: a virus infecting the Earth science community. *EOS Trans AGU* 75:209
- Engelder T (1999) Transitional-tensile fracture propagation: a status report. *J Struct Geol* 21:1049–1055
- Engelder JT, Logan JM, Handin J (1975) The sliding characteristics of sandstone on quartz fault-gouge. *Pure Appl Geophys* 113:69–86
- Engelder JT, McKee TR (1973) Electron microscopical study of indurated quartz gouges. In: *Proc. 31<sup>st</sup> Annual Meeting Electron Microsc. Soc. Am.*, pp 214–215
- Engelder JT, Scholz CH (1976) The role of asperity indentation and ploughing in rock friction. II. Influence of relative hardness and normal load. *Int J Rock Mech Min* 13:155–163
- Epstein B (1948) Statistical aspects of fracture problems. *J Appl Phys* 19:140–147
- Erdogan F (1968) Crack-propagation theories. In: Liebowitz H (ed) *Fracture*. Academic Press, II, New York, pp 497–590
- Erdogan F, Sih GC (1963) On the crack extension in plates under plane loading and transverse shear. *Trans Am Soc Mech Eng* 85:519–525
- Esaki T, Kimura T (1989) Mechanical behavior of rocks under generalized high stress conditions. In: Maury V, Fourmaintraux D (eds) *Rock at great depth*. A. A. Balkema, Rotterdam, 1, pp 123–130
- Escartin J, Hirth G, Evans B (1997) Nondilatant brittle deformation in serpentinites: implications for Mohr-Coulomb theory and the strength of faults. *J Geophys Res* 102:2897–2913
- Eshelby JD (1957) The determination of the elastic field of an ellipsoidal inclusion, and related problems. *P Roy Soc Lond A Mat* 241:376–396
- Eshelby JD (1971) *Fracture mechanics*. *Sci Prog* 59:161–179
- Essene EJ, Hensen BJ, Green DH (1970) Experimental study of amphibolite and eclogite stability. *Phys Earth Planet In* 3:378–384
- Estrin Y, Bréchet Y (1996) On a model of frictional sliding. *Pure Appl Geophys* 147:745–762
- Evans B, Frederich JT, Wong T-f (1990) The brittle-ductile transition in rocks: recent experimental and theoretical progress. In: Duba AG, Durham WB, Handin JW, Wang HF (eds) *The brittle-ductile transition in rocks. The Heard Volume.: American Geophysical Union, Washington, D.C., Geophys Monograph* 56, pp 1–20
- Evans AG, Langdon TG (1976) Structural ceramics. *Prog Mater Sci* 21:171–441
- Evans I, Pomeroy CD (1958) The strength of cubes of coal in uniaxial compression. In: Walton WH (ed) *Mechanical properties of non-metallic brittle materials*. Butterworths, London, pp 5–25
- Evans I, Pomeroy CD, Berenbaum R (1961) The compressive strength of coal. *Colliery Eng* 38:75–80, 123–127, 172–178
- Ewy RT, Cook NGW (1990a) Deformation and fracture around cylindrical opening in rocks, I. Observations and analysis of deformations. *Int J Rock Mech Min* 27:387–407
- Ewy RT, Cook NGW (1990b) Deformation and fracture around cylindrical opening in rocks, II. Initiation, growth and interaction of fractures. *Int J Rock Mech Min* 27:409–427
- Eyring H (1936) Viscosity, plasticity, and diffusion as examples of absolute reaction rates. *J Chem Phys* 4:283–291

- Fabre D, Gustkiewicz J (1997) Poroelastic properties of limestones and sandstones under hydrostatic conditions. *Int J Rock Mech Min* 34:127–134
- Fairbairn HW (1950) Synthetic quartzite. *Am Mineral* 35:735–748
- Fairhurst C (1961) Laboratory measurement of some physical properties of rock. In: Hartman HL (ed) 4<sup>th</sup> Symp. on Rock Mechancis. *Bull Mineral Industries Expt Sta* 76:105–118
- Fairhurst C, Cook NGW (1966) The phenomenon of rock splitting parallel to the direction of maximum compression in the neighbourhood of a surface. In: *Proc. 1<sup>st</sup> Congr. Int. Soc. Rock Mech.*, Lisbon, 1966, I, pp 687–692
- Fairhurst CE, Hudson JA (1999) Draft ISRM suggested method for the complete stress-strain curve for intact rock in uniaxial compression. *Int J Rock Mech Min* 36:279–289
- Fanella DA (1990) Fracture and failure of concrete in uniaxial and biaxial loading. *J Eng Mech* 116:2341–2362
- Fanella D, Krajcinovic D (1988) A micromechanical model for concrete in compression. *Eng Fract Mech* 29:49–66
- Farran J, Pérami R (1974) Microfissuration, déformation et compressibilité des roches sous charges triaxiales. In: *Advances in Rock Mechanics. Proc. 3<sup>rd</sup> Congr. Int. Soc. Rock Mech.*, Denver, 1974. Washington, D.C., Nat. Acad. Sci., II, Part A, pp 138–143
- Fayed LA (1968) Shear strength of some argillaceous rocks. *Int J Rock Mech Min* 5:79–85
- Feucht LJ, Logan JM (1990) Effects of chemically active solutions on shearing behavior of a sandstone. *Tectonophysics* 175:159–176
- Filon LNG (1902) On the elastic equilibrium of circular cylinders under certain practical systems of load. *Philos T Roy Soc A* 198:147–233
- Fischer GJ (1992) The determination of permeability and storage capacity: pore pressure oscillation method. In: Evans B, Wong, T-f (eds) *Fault mechanics and transport properties of rocks. International Geophysics Series. Academic Press, London*, pp 187–211
- Fischer GJ, Paterson MS (1989) Dilatancy during rock deformation at high temperatures and pressures. *J Geophys Res* 94:17607–17618
- Fischer GJ, Paterson MS (1992) Measurement of permeability and storage capacity in rocks during deformation at high temperature and pressure. In: Evans B, Wong, T-f (eds) *Fault mechanics and transport properties of rocks. International Geophysics Series. Academic Press, London*, pp 213–252
- Fitterman DV (1979) Theory of electrokinetic-magnetic anomalies in a faulted space. *J Geophys Res* 84:6031–6040
- Fjaer E, Ruistuen H (2002) Impact of the intermediate principal stress on the strength of heterogeneous rock. *J Geophys Res* 107, 10.1029/2001JB000277 (10 pp)
- Fjaer E, Holt RM, Horsrud P, Raen AM, Risnes R (1992) Petroleum related rock mechanics, developments in petroleum science. Elsevier, Amsterdam, 338 pp
- Flannery BP, Deckman HW, Roberge WG, D'Amico KL (1987) Three dimensional X-ray microtomography. *Science* 237:1439–1444
- Fleck NA, Hutchinson JW (1993) A phenomenological theory for strain gradient effect in plasticity. *J Mech Phys Solids* 41:1825–1857
- Fonseka GM, Murrell SAF, Barnes P (1985) Scanning electron microscope and acoustic emission studies of crack development in rocks. *Int J Rock Mech Min* 22:273–289
- Föppl A (ed) (1900) *Abhängigkeit der Bruchgefahr von der Art des Spannungszustandes. Mith Mech-Tech Lab K Tech Hochsch München* 27:1–35
- Fossum AF, Fredrich JT (2000) Cap plasticity models and dilatant and compactive prefailure deformation. In: A. A. Balkema, Rotterdam, pp 1169–1176
- François D, Wilshaw TR (1968) The effect of hydrostatic pressure on the cleavage fracture of polycrystalline materials. *J Appl Phys* 39:4170–4177
- Frank FC (1965) On dilatancy in relation to seismic sources. *Rev Geophys* 3:485–503
- Frank FC (1966) A further note on dilatancy in relation to seismic sources. *Rev Geophys* 4:405–408
- Frank FC (1971) On the capillary bonds between grains in moist sand. *Trans Br Ceram Soc* 70:105–106
- Frank FC (1972) Contributions to study of capillary bonds between grains in moist sand. *Trans Br Ceram Soc*, 71, 94
- Franklin JA (1971a) Discussion. In: Te'eni M (ed) *Structure, solid mechanics and engineering design. Proc. Southampton 1969 Civil Eng. Materials Conf. Wiley-Interscience, London*, pp 1188–1190



- Franklin JA (1971b) Triaxial strength of rock materials. *Rock Mech* 3:86–98
- Fredrich JT (1999) 3D imaging of porous media using laser scanning confocal microscopy with application to microscale transport processes. *Phys Chem Earth Pt A* 24:551–561
- Fredrich JT, Evans B (1992) Strength recovery along simulated faults by solution transfer processes. In: Tillerson JR, Wawersik WR (eds) *Rock mechanics. Proceedings of the 33<sup>rd</sup> U.S. Symposium*. A. A. Balkema, Rotterdam, pp 121–130
- Fredrich JT, Evans B, Wong T-f (1989) Micromechanics of the brittle to plastic transition in Carrara marble. *J Geophys Res* 94:4129–4145
- Fredrich JT, Evans B, Wong T-f (1990) Effect of grain size on brittle and semibrittle strength: implications for micromechanical modelling of failure in compression. *J Geophys Res* 95:10907–10920
- Fredrich JT, Greaves KH, Martin JW (1993) Pore geometry and transport properties of Fontainebleau sandstone. *Int J Rock Mech Min* 30:691–697
- Fredrich JT, Martin JW, Clayton RB (1995) Induced pore pressure response during undrained deformation of tuff and sandstone. *Mech Mater* 20:95–104
- Fredrich JT, Menéndez B, Wong T-f (1995) Imaging the pore structure of geomaterials. *Science* 268:276–279
- Freiman SW (1988) Brittle fracture behavior of ceramics. *Ceramic Bulletin* 67:392–402
- Freudenthal AM (1975) Shear dilatancy in rock and precursory changes in seismic velocities. *Geophys Res Lett* 2:517–520
- Freund LB (1979) The mechanics of dynamic shear crack propagation. *J Geophys Res* 84:2199–2209
- Freund LB (1990) *Dynamic fracture mechanics*. Cambridge University Press, Cambridge, 563 pp
- Friedman M (1975) Fracture in rock. *Rev Geophys Space Phys* 13, No. 3 (U.S. Nat. Rept. to I.U.G.G.), 352–358, 383–389
- Friedman M (1976) Porosity, permeability, and rock mechanics – a review. In: Brown WS, Green SJ, Hustrulid WA (eds) *Site characterization. Proc. 17<sup>th</sup> Symposium on Rock Mechanics*, Snowbird, Utah, Aug. 25–27, 1976, pre-print proceedings, Utah Engineering Experiment Station, pp 2A1–2A17
- Friedman M, Bur TR (1974) Investigations of the relations among residual strain, fabric, fracture and ultrasonic attenuation and velocity in rocks. *Int J Rock Mech Min* 11:221–234
- Friedman M, Handin J, Alani G (1972) Fracture-surface energy of rocks. *Int J Rock Mech Min* 9:757–766
- Friedman M, Logan JM (1970a) Influence of residual elastic strain on the orientation of experimental fractures in three quartzose sandstones. *J Geophys Res* 75:387–405
- Friedman M, Logan JM (1970b) Microscopic feather fractures. *Geol Soc Am Bull* 81:3417–3420
- Friedman M, Logan JM (1973) Lüders' bands in experimentally deformed sandstone and limestone. *Geol Soc Am Bull* 84:1465–1476
- Friedman M, Logan JM, Rigert JA (1974) Glass-indurated quartz gouge in sliding-friction experiments on sandstone. *Geol Soc Am Bull* 85:937–942
- Friedman M, Perkins RD, Green SJ (1970) Observation of brittle-deformation features at the maximum stress of Westerly granite and Solenhofen limestone. *Int J Rock Mech Min* 7:297–306
- Friedman M, Handin J, Higgs NG, Lantz JR (1979) Strength and ductility of four dry igneous rocks at low pressures and temperatures to partial melting. In: Gray KE (ed) *20<sup>th</sup> U.S. Symposium on Rock Mechanics*. University of Texas, Austin, Texas, pp 35–50
- Frye KM, Marone C (2002) Effect of humidity on granular friction at room temperature. *J Geophys Res* 107, 2309, doi: 10.1029/2001JB000654 (15 pp)
- Fukushima E (1999) Nuclear magnetic resonance as a tool to study flow. *Annual Rev Fluid Mech* 31:95–123
- Fung YC (1965) *Foundations of mechanics*. Prentice-Hall International Series in Dynamics. Prentice-Hall Inc., Englewood Cliffs, NJ, 525 pp
- Fung PK (1975) Instrumentation for measuring load and deformation under high pressure. *Exp Mech* 15:61–66
- Gallagher JJ, Friedman M, Handin J, Sowers GM (1974) Experimental studies relating to microfracture in sandstone. *Tectonophysics* 21:203–247
- Galli JR, Gibbs P (1964) The effect of hydrostatic pressure on the ductile-brittle transition in molybdenum. *Acta Metall Mater* 12:775–778

- Gamba P (1899) Sull'aumento temporaneo e permanente dell'elasticità del marmo portato ad alte temperature. *Accademia Nazionale dei Lincei (Rome), Classe di sci. fis., mat. e nat., Atti: Rendiconti, ser. 5*, 8:264–269
- Gambarotta L (1993) Modeling dilatancy and failure of uniaxially compressed brittle materials by microcrack-weakened solids. *Eng Fract Mech* 46:381–391
- Gangi AF, Carlson RL (1996) An asperity-deformation model for effective pressure. *Tectonophysics* 256:241–252
- Ganryd L, Getting IC, Spetzlar H (1983) Path dependence of acoustic velocity and attenuation in experimentally deformed Westerly granite. *Geophys Res Lett* 10:71–74
- Gao H (1996) A theory of local limiting speed in dynamic fracture. *J Mech Phys Solids* 44:1453–1474
- Gao H, Chiu C (1992) Slightly curved or kinked cracks in anisotropic elastic solids. *Int J Solids Struct* 29:947–972
- Garbin HD, Knopoff L (1973) The compressional modulus of a material permeated by a random distribution of circular cracks. *Q Appl Math* 30:453–464
- Garbin HD, Knopoff L (1975a) Elastic moduli of a medium with liquid-filled cracks. *Q Appl Math* 33:301–303
- Garbin HD, Knopoff L (1975b) The shear modulus of a material permeated by a random distribution of free circular cracks. *Q Appl Math* 33:296–300
- Gardner RD, Pincus HJ (1968) Fluorescent dye penetrants applied to rock fractures. *Int J Rock Mech Min* 5:155–158
- Garg SK (1971) Wave propagation effects in a fluid-saturated porous solid. *J Geophys Res* 76:7947–7962
- Garg SK, Nur A (1973) Effective stress laws for fluid-saturated porous rocks. *J Geophys Res* 78:5911–5921
- Garten VA, Head RB (1971) An experimental model of crack nucleation by slip bands. *Int J Fract Mech* 7:343–344
- Gassmann F (1951) Über die Elastizität poröser Medien. *Vierteljahrsschr Naturforsch Gesellsch Zürich* 96:1–23
- Gatto HG (1984) The effect of various states of stress on the permeability of Berea sandstone [M Sc thesis]: Texas A and M
- Gau Q, Cheng H, Zhuo D (1983) The strength, deformation and rupture characteristics of red sandstone under polyaxial compression. In: *Proc. 5<sup>th</sup> Int. Congr. Rock Mech., Melbourne, Australia A*, pp 157–160
- Gay NC (1970) The formation of step structures on slickensided shear surfaces. *J Geol* 78:523–532
- Geertsma J (1957) The effect of fluid pressure decline on volumetric changes in porous rocks. *Trans AIME Soc Min Eng* 210:331–339
- Gelles SH (1968) Apparatus for mechanical testing of soft crystals at high pressure. *Rev Sci Instrum* 39:1814–1819
- Geraud Y, Caron J-M, Faure P (1995) Porosity network of a ductile shear zone. *J Struct Geol* 17:1757–1769
- Geraud Y, Mazerolle F, Raynaud S, Lebon P (1998) Crack location in granitic samples submitted to heating, low confining pressure and axial loading. *Geophys J Int* 133:553–567
- Germanovich LN, Salganik RL, Dyskin AV, Lee KK (1994) Mechanisms of brittle fracture of rock with pre-existing cracks in compression. *Pure Appl Geophys* 143:117–149
- Giardini AA, Abey AE (1972) Room-temperature shear strengths of rocks under near-hydrostatic confining pressure to 80 kbar. 1. Solnhofen limestone and three Georgia marbles. *Tectonophysics* 14:121–142
- Giardini AA, Abey AE (1973) The torsional shear strength of granodiorite and dunite under near-homogeneous confining stress to about 90 kbar. 2. *Tectonophysics* 18:147–165
- Giardini AA, Lakner JF, Stephens DR, Stromberg HD (1968) Triaxial compression data on nuclear explosion shocked, mechanically shocked, and normal granodiorite from the Nevada Test Site. *J Geophys Res* 73:1305–1320
- Gibson RL, Toksöz MN (1990) Permeability estimation from velocity anisotropy in fractured rock. *J Geophys Res* 95:15643–15655
- Gillott JE (1969) Study of the fabric of fine-grained sediments with the scanning electron microscope. *J Sediment Petrol* 39:90–105
- Gilman JJ (1960) Direct measurements of the surface energies of crystals. *J Appl Phys* 31:2208–2218
- Glasstone S, Laidler KJ, Eyring EH (1941) *The theory of rate processes*. Mc-Graw Hill, New York, 611 pp

- Gliko AO (1976) Effective elastic moduli and the structure of two-phase media. *Izv An SSSR Fiz Zem+* 5:32–45 (Engl. tr.: *Izv Acad Sci USSR, Phys of the Solid Earth*, 1976, 307–313)
- Glover PJW, Gómez JB, Meredith PG, Hayashi K, Sammonds PR, Murrell SAF (1997) Damage of saturated rocks undergoing triaxial deformation using complex electrical conductivity measurements: experimental results. *Phys Chem Earth* 22:57–61
- Glover PWJ, Gómez JB, Meredith PG (2000) Fracturing in saturated rocks undergoing triaxial deformation using complex electrical conductivity measurements: experimental study. *Earth Planet Sc Lett* 183:201–213
- Glover PWJ, Meredith PG, Sammonds PR, Murrell SAF (1994) Measurement of complex electrical conductivity and fluid permeability in porous rocks at raised confining pressures. In: *Eurorock94*. A. A. Balkema, Rotterdam, pp 29–36
- Glücklich J, Cohen LJ (1967) Size as a factor in the brittle-ductile transition and the strength of some materials. *Int J Fract Mech* 3:278–289
- Glücklich J, Cohen LJ (1968) Strain-energy and size effects in a brittle material. *Mater Res Stand* 8:17–22
- Goetze C (1971) High temperature rheology of Westerly granite. *J Geophys Res* 76:1223–1230
- Goguel J (1948) *Introduction à l'Étude Mécanique des Déformations de l'Écorce Terrestre*. Imprimerie Nat., Paris, 530 pp
- Gold LW (1960) The cracking activity in ice during creep. *Can J Phys* 38:1137–1148
- Goldsby DL, Tullis TE (2002) Low frictional strength of quartz rocks at subseismic slip rates. *Geophys Res Lett* 29:1844, doi: 10.1029/2002GL015240; 4 pp
- Goldsmith W, Sackman JL, Ewart C (1976) Static and dynamic fracture strength of Barre granite. *Int J Rock Mech Min* 13:303–309
- Goodman RE (1963) Subaudible noise during compression of rocks. *Geol Soc Am Bull* 74:487–490
- Goodman RE (1976) *Methods of geological engineering in discontinuous rocks*. West, St Paul, 472 pp
- Goodman RE, Dubois J (1972) Duplication of dilatancy in analysis of jointed rocks. *J Soil Mech Found Div, Proc Am Soc Div Engrs* 98:399–422
- Goodman RE, Ohnishi Y (1973) Undrained shear testing of jointed rock. *Rock Mech* 5:129–149
- Gordon RB, Davis LA (1968) Velocity and attenuation of seismic waves in imperfectly elastic rock. *J Geophys Res* 73:3917–3935
- Gottschalk RR, Kronenberg AK, Russell JE, Handin J (1990) Mechanical anisotropy of gneiss: failure criterion and textural sources of directional behavior. *J Geophys Res* 95:21613–21634
- Gowd TN (1970) Changes in absorption of ultrasonic energy travelling through rock specimens stressed to fracture. *Phys Earth Planet In* 4:43–48
- Gowd TN (1980) Factors affecting the acoustic emission response of triaxially compressed rock. *Int J Rock Mech Min* 17:219–223
- Gowd TN, Rummel F (1977) Effect of fluid injection on the fracture behaviour of porous rock. *Int J Rock Mech Min* 14:203–208
- Gowd TN, Rummel F (1980) Effect of confining pressure on the fracture behaviour of a porous rock. *Int J Rock Mech Min* 17:225–229
- Grady DE, Kipp ME (1987) Dynamic rock fragmentation. In: Atkinson BK (ed) *Fracture mechanics of rock*. Academic Press, London, pp 429–475
- Grady DE, Lipkin J (1980) Criteria for impulsive rock fracture. *Geophys Res Lett* 7:255–258
- Grady DE, Hollenbach RE, Schuler KW, Callender JF (1977) Strain rate dependence in dolomite inferred from impact and static compression studies. *J Geophys Res* 82:1325–1333
- Graham J (1972) Damage induced by a sliding diamond – an approach to hard rock drilling. *Rock Mech* 4:191–202
- Gramberg J (1965) Axial cleavage fracturing, a significant process in mining and geology. *Eng Geol* 1:31–72
- Gramberg J (1970) The 'ellipse-with-notch' theory to explain axial cleavage fracturing of rocks (a natural extension to the first Griffith theory). *Int J Rock Mech Min* 7:537–559
- Gramberg J (1974) Internal stresses in rock as a result of granular structure and axial cataclasis: acoustic measurements. In: *Advances in Rock Mechanics*. Proc. 3<sup>rd</sup> Congr. Int. Soc. Rock Mech., Denver, 1974, Washington, D.C., Nat. Acad. Sci., II, Part A, pp 549–556
- Green HW, Burnley PC (1989) A new self-organizing mechanism for deep-focus earthquakes. *Nature* 341:733–737

- Green HW, Burnley PC (1990) The failure mechanism of deep-focus earthquakes. In: Knipe RJ, Rutter EH (eds) *Deformation mechanisms, rheology and tectonics*. The Geological Society, London, Special Publication No. 54, pp 133–141
- Green HW, Houston H (1995) The mechanics of deep earthquakes. *Ann Rev Earth Planet Sci* 23:169–213
- Green SJ, Leasia JD, Perkins RD, Jones AH (1972) Triaxial stress behaviour of Solenhofen limestone and Westerly granite at high strain rates. *J Geophys Res* 77:3711–3724
- Green SJ, Perkins RD (1972) Uniaxial compression tests at varying strain rates on three geologic materials. In: Gray KE (ed) *Basic and applied rock mechanics*. Proc. 10<sup>th</sup> Symp. Rock Mech., Austin, Texas, May 1968. A.I.M.E., New York, pp 35–54
- Green DH, Wang HF (1986) Fluid pressure response to undrained compression in saturated sedimentary rock. *Geophysics* 51:948–956
- Green HW, Young TE, Walker D, Scholz CH (1990) Anticrack-associated faulting at very high pressure in natural olivine. *Nature* 348:720–722
- Green HW, Zhou Y (1996) Transformation-induced faulting requires an exothermic reaction and explains the cessation of earthquakes at the base of the mantle transition zone. *Tectonophysics* 256:39–56
- Greenwood JA, Tripp JH (1971) The contact of two nominally flat rough surfaces. *P I Mech Eng* 185:625–633
- Greenwood JA, Williamson JBP (1966) Contact of nominally flat surfaces. *P Roy Soc Lond A Mat* 295:300–319
- Griffith AA (1920) The phenomena of rupture and flow in solids. *Philos T Roy Soc A* 221:163–198
- Griffith AA (1924) The theory of rupture. In: Biezeno CG, Burgers JM (eds) *Proc. 1<sup>st</sup> Int. Congr. Appl. Mech.*: Delft, Tech. Boekhandel en Drukkerij J. Waltman Jr., pp 54–63
- Griggs DT (1935) The strain ellipsoid as a theory of rupture. *Am J Sci* 230:121–137
- Griggs DT (1936) Deformation of rocks under high confining pressures. *J Geol* 44:541–577
- Griggs DT (1967) Hydrolytic weakening of quartz and other silicates. *Geophys J Roy Astr S* 14:19–31
- Griggs DT, Bell JF (1938) Experiments bearing on the orientation of quartz in deformed rocks. *Geol Soc Am Bull* 49:1723–1746
- Griggs DT, Handin J (1960) Observations on fracture and a hypothesis of earthquakes. In: Griggs D, Handin J (eds) *Rock deformation*. *Geol Soc Am Mem* 79:347–364
- Griggs DT, Miller WB (1951) Deformation of Yule marble. Part I. Compression and extension experiments on dry Yule marble at 10 000 atmospheres confining pressure, room temperature. *Geol Soc Am Bull* 62:853–862
- Griggs DT, Turner FJ, Heard HC (1960) Deformation of rocks at 500 to 800 °C. In: Griggs D, Handin J (eds) *Rock deformation*. *Geol Soc Am Mem* 79:39–104
- Griggs DT, Turner FJ, Borg I, Sosoka J (1951) Deformation of Yule marble. Part IV. Effects at 150 °C. *Geol Soc Am Bull* 62:1385–1406
- Groves GW, Kelly A (1963) Independent slip systems in crystals. *Phil Mag* 8:877–887
- Groves GW, Kelly A (1969) Change of shape due to dislocation climb. *Phil Mag* 19:977–986
- Gu J-c, Rice JR, Ruina AL, Tse ST (1984) Slip motion and stability of a single degree of freedom elastic system with rate and state dependent friction. *J Mech Phys Solids* 32:167–196
- Gu Y-J, Wong T-f (1991) Effects of loading velocity, stiffness, and inertia on the dynamics of a single degree of freedom spring-slide system. *J Geophys Res* 96:21677–21691
- Gu Y, Wong T-f (1994a) Development of shear localization in simulated quartz gouge: effect of cumulative slip and gouge particle size. *Pure Appl Geophys* 142:387–423
- Gu Y, Wong T-f (1994b) Nonlinear dynamics of the transition from stable sliding to cyclic stick-slip in rock. In: Newman WI, Gabrielov AM, Turcotte DL (eds) *Nonlinear dynamics and predictability of geophysical phenomena*. American Geophysical Union, Washington, D.C., Geophysical monograph 83, pp 15–35
- Gueguen Y, Boullier AM (1976) Evidence of superplasticity in mantle peridotites. In: Strens RGJ (ed) *The physics and chemistry of minerals and rocks*. NATO Institute, Newcastle upon Tyne, April 1974. Wiley, London, pp 19–33
- Gueguen Y, Reuschlé T, Darot M (1987) Single-crack behaviour and crack statistics. In: Atkinson BK (ed) *Fracture mechanics of rock*. Academic Press, London, pp 48–71
- Guéguen Y, Chelidze T, Le Ravalec M (1997) Microstructures, percolation thresholds, and rock physical properties. *Tectonophysics* 279:23–36

- Guéguen Y, Dormieux L, Boutéca M (2004) Fundamentals of poromechanics. In: Guéguen Y, Boutéca M (eds) *Mechanics of fluid-saturated rocks*. Elsevier Academic Press, Amsterdam, pp 1–54
- Guéguen Y, Palciauskas V (1994) *Introduction to the physics of rocks*. Princeton University Press, Princeton, 294 pp
- Guéguen Y, Reuschlé T, Darot M (1990) Single-crack behaviour and crack statistics. In: Barber DJ, Meredith PG (eds) *Deformation processes in minerals, ceramics and rocks*. Unwin Hyman, London, pp 48–71
- Gupta IN (1973) Seismic velocities in rock subjected to axial loading up to shear fracture. *J Geophys Res* 78:6936–6942
- Gupta V, Bergström JS (1997) Compressive failure of rocks. *Int J Rock Mech Min* 34:3–4, p. 376; CD-ROM paper No. 112
- Gurney C, Rowe PW (1948a) The effect of radial pressure on the flow and fracture of reinforced plastic rods. Aero. Research Council. London: H.M. Stationary Office, Reports and Memoranda No. 2283, May 1945, 10 pp
- Gurney C, Rowe PW (1948b) Fracture of glass rods in bending and under radial pressure. Aero. Research Council. London: H.M. Stationary Office, Reports and memoranda No. 2284, Nov. 1945, 5 pp
- Gustkiewicz J (1975) Strain fluctuations in heterogeneous rocks. *Int J Rock Mech Min* 12:181–189
- Güven N, Donath FA (1971) A controlled rate automatic scanning data collection program in “PAL 111 Assembler Language” for use with PDP/8-type computers. *Contrib to Geol (Univ Wyoming)* 10:117–130
- Haasen P, Lawson AW (1958) Der Einfluß hydrostatischen Druckes auf die Zugverformung von Einkristallen. *Z Metallkd* 49:280–291
- Habib P, Bernaix J (1966) La fissuration des roches. In: Proc. 1<sup>st</sup> Congr. Int. Soc. Rock Mech., Lisbon, 1966, I, pp 185–190
- Habib P, Vouille G (1966) Sur la disparition de l’effect d’échelle aux hautes pressions. *CR Acad Sci Paris* 262:715–717
- Hacker BR, Christie JM (1990) Brittle/ductile and plastic/cataclastic transitions in experimentally deformed and metamorphosed amphibolite. In: Duba AG, Durham WB, Handin JW, Wang HF (eds) *The brittle-ductile transition in rocks*. The Heard Volume. American Geophysical Union, Washington, D.C., Geophys Monograph 56, pp 127–147
- Hadizadeh J, Rutter EH (1982) Experimental study of cataclastic deformation in quartzite. In: Goodman RE, Heuze FE (eds) *Issues in rock mechanics*. Proc 23<sup>rd</sup> Symposium on Rock Mechanics: New York, AIME, pp 372–379
- Hadizadeh J, Rutter EH (1983) The low temperature brittle-ductile transition in quartzite and the occurrence of cataclastic flow in nature. *Geol Rundsch* 72:493–509
- Hadizadeh J, Tullis J (1986) Transition from fracture to cataclastic flow in anorthosite: both *P* and *T* are required. *EOS Trans AGU* 67:372 (abs)
- Hadley K (1973) Laboratory investigation of dilatancy and motion on fault surfaces at low confining pressures. In: Kovach RL, Nur A (eds) *Proc. Conf. on Tectonic Problems of the San Andreas Fault System*. Stanford Univ Publ Geol Sci 13:427–435
- Hadley K (1975a) Azimuthal variation of dilatancy. *J Geophys Res* 80:4845–4850
- Hadley K (1975b) Dilatancy in rock at elevated temperatures. *EOS Trans AGU* 56:1060 (abstract)
- Hadley K (1975c)  $V_p/V_s$  anomalies in dilatant rock samples. *Pure Appl Geophys* 113:1–23
- Hadley K (1976a) Comparison of calculated and observed crack densities and seismic velocities in Westerly granite. *J Geophys Res* 81:3484–3494
- Hadley K (1976b) The effect of cyclic stress on dilatancy: another look. *J Geophys Res* 81:2471–2474
- Haied A, Kondo D, Henry JP (2000) Strain localization in Fontainebleau sandstone. *Mech Cohes-Frict Mat* 5:239–253
- Haimson BC (1974) Mechanical behaviour of rock under cyclic loading. In: *Advances in Rock Mechanics*. Proc. 3<sup>rd</sup> Congr. Int. Soc. Rock Mech., Denver, 1974. Washington, D.C., Nat. Acad. Sci., II, Part A, pp 373–378
- Haimson BC, Chang C (2000) A new triaxial cell for testing mechanical properties of rock, and its use to determine rock strength and deformability of Westerly granite. *Int J Rock Mech Min* 37:285–296
- Haimson B, Chang C (2002) True triaxial strength of the KTB amphibolite under borehole wall conditions and its use to estimate the maximum horizontal in situ stress. *J Geophys Res* 107:2257, doi: 10.1029/2001JB000647 (14 pp)

- Haimson B, Fairhurst C (1970) In-situ stress determination at great depth by means of hydraulic fracturing. In: Somerton WH (ed) *Rock mechanics – theory and practice*. Proc. 11<sup>th</sup> Symp. Rock Mech., Berkeley, 1970. A.I.M.E., New York, pp 559–584
- Haimson BC, Kim CM (1972) Mechanical behaviour of rock under cyclic fatigue. In: Cording EJ (ed) *Stability of rock slopes*. Proc. 13<sup>th</sup> Symp. Rock Mech., Univ. Ill., Urbana, Aug. 1971. Am. Soc. Civ. Eng., New York, pp 845–863
- Hallam SD, Ashby MF (1990) Compressive brittle failure and the construction of multi-axial failure maps. In: Barber DJ, Meredith PG (eds) *Deformation processes in minerals, ceramics and rocks*. Unwin Hyman, London, pp 84–108
- Hallbauer DK, Wagner H, Cook NGW (1973) Some observations concerning the microscopic and mechanical behaviour of quartzite specimens in stiff, triaxial compression tests. *Int J Rock Mech Min* 10:713–726
- Handin J (1953) An application of high pressure in geophysics: experimental rock deformation. *Trans Am Soc Mech Eng* 75:315–324
- Handin J (1964) Strength at high confining pressure and temperature of serpentinite from Mayaguez, Puerto Rico. In: A study of serpentinite. Nat. Acad. Sci., Nat. Res. Council, Publ. 1188, pp 126–131
- Handin J (1966) Strength and ductility. In: Clark SP (ed) *Handbook of physical constants*. Geol Soc Am Mem 97:223–289
- Handin J (1969) On the Coulomb-Mohr failure criterion. *J Geophys Res* 74:5343–5348
- Handin J, Hager RV (1957) Experimental deformation of sedimentary rocks under confining pressure: tests at room temperature on dry samples. *Am Assoc Petrol Geol Bull* 41:1–50
- Handin J, Hager RV (1958) Experimental deformation of sedimentary rocks under confining pressure: tests at high temperature. *Am Soc Petrol Geol Bull* 42:2892–2934
- Handin J, Heard HC, Magouirk JN (1967) Effects of the intermediate principal stress on the failure of limestone, dolomite, and glass at different temperatures and strain rates. *J Geophys Res* 72:611–640
- Handin J, Higgs DV, O'Brien JK (1960) Torsion of Yule marble under confining pressure. In: Griggs D, Handin J (eds) *Rock deformation*. Geol Soc Am Mem 79:245–274
- Handin J, Logan JM, Ting C (1973) Can normal faults generate large earthquakes? *EOS Trans AGU* 54:466 (abstract)
- Handin J, Stearns DW (1964) Sliding friction of rock. *Trans Am Geophys Union* 43:103 (abstract)
- Handin J, Hager RV, Friedman M, Feather JN (1963) Experimental deformation of sedimentary rocks under confining pressure: pore pressure effects. *Bull Am Assoc Petrol Geol* 47:717–755
- Hardy HR (1971) Recent applications in microseismic activity to experimental rock mechanics. In: *Rock fracture*. Proc. Int. Symp. Rock Mech., Nancy, pp Paper II-10 (20 pp)
- Hardy HR (1972) Application of acoustic emission techniques to rock mechanics research. In: *Acoustic Emission*, Am. Soc. Test. Mat., Sp. Tech. Publ. 505, pp 41–83
- Hardy HR (1973) Microseismic techniques – basic and applied research. *Rock Mech supp*:93–114
- Hardy HR, Chugh YP (1971) Failure of geologic materials under low-cycle fatigue. In: Proc. 6<sup>th</sup> Can. Rock Mech. Symp, Montreal 1970. Dep. Energy, Mines and Resources, Ottawa, pp 33–47
- Hardy MP, Hudson JA, Fairhurst C (1973) The failure of rock beams. Part I. Theoretical studies. *Int J Rock Mech Min* 10:53–67
- Hardy HR, Jayaraman NI (1970) An investigation of methods for the determination of the tensile strength of rock. In: Proc. 2<sup>nd</sup> Congr. Int. Soc. Rock Mech., Belgrade 1970, III, pp 85–92
- Hardy HR, Jayaraman NI (1972) Hoop-stress loading – a new method of determining the tensile strength of rock. *J Soc Petrol Eng* 12:246–252; also appears in *Trans Soc Petrol Eng AIME* 253
- Hardy HR, Kim YS (1970) A clamp-on strain transducer for use on geologic materials. *J Soc Petrol Eng* 10:41–50
- Hardy HR, Kim YS (1971a) Detection of a low-level critical stress in geologic materials using ultrasonic techniques. In: Clark GB (ed) *Dynamic rock mechanics*. Proc. 12<sup>th</sup> Symp. Rock Mech., Rolla, Missouri, Nov. 1970. A.I.M.E., New York, pp 301–328
- Hardy HR, Kim YS (1971b) Monitoring crack closure in geologic materials using ultrasonic techniques. In: *Rock fracture*. Proc. Int. Symp. Rock Mech., Nancy, pp Paper I-3 (17 pp)
- Hardy HR, Stefanko R, Kimble EJ (1971) An automated test facility for rock mechanics research. *Int J Rock Mech Min* 8:17–28

- Hardy HR, et al. (1967) Discussion on uniformity of end loading in session on rock failure. In: Fairhurst C (ed) Failure and breakage of rock. Proc. 8<sup>th</sup> Symp. on Rock Mech. Minnesota, Sept. 1966. A.I.M.E., New York, pp 154–158
- Hardy HR, Kim RY, Stefanko R, Wang YJ (1970) Creep and microseismic activity in geologic materials. In: Somerton WH (ed) Rock mechanics – theory and practice. Proc. 11<sup>th</sup> Symp. Rock Mech., Berkeley, 1970. A.I.M.E., New York, pp 377–413
- Hart DJ, Wang HF (1995) Laboratory measurements of a complete set of poroelastic moduli for Berea sandstone and Indiana limestone. *J Geophys Res* 100:17741–17751
- Hasselman DPH, Coppola JA, Krohn DA, Bradt RC (1972) Nonrecoverable elastic energy and crack propagation in brittle materials. *Mater Res Bull* 7:769–772
- Hatano T (1969) Theory of failure of concrete and similar brittle solid on the basis of strain. *Int J Fract Mech* 5:73–79
- Hatzor YH, Palchik V (1997) The influence of grain size and porosity on crack initiation stress and critical flaw length in dolomites. *Int J Rock Mech Min* 34:805–816
- Hatzor YH, Zur A, Mimran Y (1997) Microstructure effects on microcracking and brittle failure of dolomites. *Tectonophysics* 281:141–162
- Hawkes I, Mellor M (1970) Uniaxial testing in rock mechanics laboratories. *Eng Geol* 4:177–285
- Hawkes I, Mellor M, Gariepy S (1973) Deformation of rocks under uniaxial tension. *Int J Rock Mech Min* 10:493–507
- Hay RS, Evans B (1988) Intergranular distribution of pore fluid and the nature of high-angle grain boundaries in limestone and marble. *J Geophys Res* 93:8959–8974
- He C, Ma S, Huang J (1998) Transition between stable sliding and stick-slip due to variation in slip rate under variable normal stress condition. *Geophys Res Lett* 25:3235–3238
- He C, Wong T-f, Beeler NM (2003) Scaling of stress drop with recurrence interval and loading velocity for laboratory-derived fault strength relations. *J Geophys Res* 108, doi:10.1029/2002JB001890
- Healy JH, Lee WHK, Pakiser LC, Raleigh CB, Wood MD (1972) Prospects for earthquake prediction and control. *Tectonophysics* 14:319–332
- Healy JH, Rubey WW, Griggs DT, Raleigh CB (1968) The Denver earthquakes. *Science* 161:1301–1310
- Heard HC (1960) Transition from brittle fracture to ductile flow in Solenhofen limestone as a function of temperature, confining pressure, and interstitial fluid pressure. In: Griggs D, Handin J (eds) Rock deformation. *Geol Soc Am Mem* 79:193–226
- Heard HC (1963) Effect of large changes in strain rate in the experimental deformation of Yule marble. *J Geol* 71:162–195
- Heard HC, Carter NL (1968) Experimentally induced “natural” intragranular flow in quartz and quartzite. *Am J Sci* 266:1–42
- Heard HC, Duba A (1978) Capabilities for measuring physicochemical properties at high pressure: Lawrence Livermore National Laboratory, Report No. UC11
- Heard HC, Ruby WW (1966) Tectonic implications of gypsum dehydration. *Geol Soc Am Bull* 77:741–760
- Heard HC, Duba A, Abey AE, Schock RN (1973) Mechanical properties of Blair dolomite. Lawrence Livermore Lab, Report No. UCRL-51465
- Heaton T (1990) Evidence for and implications of self-healing pulses in earthquake rupture. *Phys Earth Planet In* 64:1–20
- Heck WJ (1972) Development of equipment for studying pore pressure effects in rock. In: Gray KE (ed) Basic and applied rock mechanics. Proc. 10<sup>th</sup> Symp. Rock Mech., Austin, Texas, May 1968. A.I.M.E., New York, pp 243–266
- Heiland J (2003) Permeability of triaxially compressed sandstone: influence of deformation and strain rate on permeability. *Pure Appl Geophys* 160:889–908
- Hellan K (1976) Griffith-type fracture analysis for large-scale yielding conditions. *Eng Fract Mech* 8:501–506
- Henry JB, Paquet J, Tancrez JP (1977) Experimental study of crack propagation in calcite rocks. *Int J Rock Mech Min* 14:85–91
- Henyei FS, Pomphrey N (1982) Self-consistent elastic moduli of a cracked solid. *Geophys Res Lett* 9:903–906

- Herel J (1966) Festigkeits- und Formänderungsverhalten charakterisierender Eigenschaften der Magnesite, die an den Probekörpern von verschiedenem Schlankheitsgrad festgestellt wurden. In: Proc. 1<sup>st</sup> Congr. Int. Soc. Rock Mech., Lisbon, 1966, I, pp 503–507
- Herget G, Unrug K (1974) In-situ strength prediction of mine pillars based on laboratory tests. In: Advances in rock mechanics. Proc. 3<sup>rd</sup> Congr. Int. Soc. Rock Mech., Denver, 1974. Washington, D.C., Nat. Acad. Sci., II, Part A, pp 151–155
- Herring C (1950) Diffusional viscosity of a polycrystalline solid. *J Appl Phys* 21:437–445
- Hertz H (1881) Über die Berührung fester elastischer Körper. *J Reine Angew Math* 92:156–171; also pp 155–173 in *Gesammelte Werke von Heinrich Hertz*, Bd 1, J A Barth, Leipzig, 1895
- Heslot F, Baumberger T, Perrin B, Caroli B, Caroli C (1994) Creep, stick-slip, and dry friction dynamics: experiments and a heuristic model. *Phys Rev E* 49:4973–4988
- Heuze FE (1980) Scale effects in the determination of rock mass strength and deformability. *Rock Mech* 12:167–192
- Heuze FE (1983) High-temperature mechanical, physical and thermal properties of granitic rocks – a review. *Int J Rock Mech Min* 20:3–10
- Hickman S, Sibson R, Bruhn R (1995) Introduction to special section: mechanical involvement of fluids in faulting. *J Geophys Res* 100:12831–12840
- Hill R (1950) The mathematical theory of plasticity. The Oxford Engineering Science Series. Clarendon Press, Oxford, 355 pp
- Hill R (1958) A general theory of uniqueness and stability in elastic-plastic materials. *J Mech Phys Solids* 6:236–249
- Hill R (1961) Uniqueness in general boundary-value problems for elastic or inelastic solids. *J Mech Phys Solids* 9:114–130
- Hill R (1962) Acceleration waves in solids. *J Mech Phys Solids* 10:1–16
- Hirata T (1987) Omori's power law and aftershock sequences of microfracturing in rock fracture experiment. *J Geophys Res* 92:6215–6221
- Hirata T, Satoh T, Ito K (1987) Fractal structure of spatial distribution of microfracturing in rock. *Geophys J Roy Astr S* 90:369–374
- Hirschwald J (1912) Handbuch der bautechnischen Gesteinsprüfung. Gebr. Borntraeger, Berlin, 923 pp
- Hirth G, Kohlstedt DL (1995) Experimental constraints on the dynamics of the partially molten upper mantle 2. Deformation in the dislocation creep regime. *J Geophys Res* 100:15441–15449
- Hirth G, Tullis J (1989) The effects of pressure and porosity on the micromechanics of the brittle-ductile transition in quartzite. *J Geophys Res* 94:17825–17838
- Hirth G, Tullis J (1994) The brittle-ductile transition in experimentally deformed quartz aggregates. *J Geophys Res* 99:11731–11748
- Hoagland RG, Hahn GT, Rosenfield AR (1973) Influence of microstructure on fracture propagation in rock. *Rock Mech* 5:77–106
- Hobbs DW (1964a) Rock compressive strength. *Colliery Eng* 41:287–292
- Hobbs DW (1964b) The tensile strength of rocks. *Int J Rock Mech Min* 1:385–396
- Hobbs BE, Mühlhaus H-B, Ord A (1990) Instability, softening and localization of deformation. In: Knipe RJ, Rutter EH (eds) Deformation mechanisms, rheology and tectonics. The Geological Society, London, Special Publication No. 54, pp 143–165
- Hodgson K, Cook NGW (1970) The effects of size and stress gradient on the strength of rock. In: Proc. 2<sup>nd</sup> Congr. Int. Soc. Rock Mech., Belgrade, 2, pp 31–34
- Hoek E (1965) Fracture of anisotropic rock. *J S Afr I Min Metall* 64:501–518; also in: *Rock Mechanics and Strata Control in Mines*. Johannesburg: S. Afr. Inst. Min. Metall. 1965, 227–244
- Hoek E (1968) Brittle failure of rock. In: Stagg KG, Zienkiewicz OC (eds) *Rock mechanics in engineering practice*. Wiley, London, pp 99–124
- Hoek E, Bieniawski ZT (1965) Brittle fracture propagation in rock under compression. *Int J Fract Mech* 1:137–155
- Hoek E, Bieniawski ZT (1966) Fracture propagation mechanism in hard rock. In: Proc. 1<sup>st</sup> Congr. Int. Soc. Rock Mech., Lisbon, 1966, I, pp 243–249
- Hoek E, Brown ET (1980) *Underground excavation engineering*. Institute of Mining and Metallurgy, London, 527 pp



- Hoek E, Brown ET (1997) Practical estimates of rock mass strength. *Int J Rock Mech Min* 34: 1165–1186
- Hoek E, Franklin JA (1968) Simple triaxial cell for field or laboratory testing of rock. *Trans/Section A Inst Min Met* 77:A22–A26
- Hoek E, Kaiser PK, Bawden WF (1994) Support of underground excavations in hard rock. A. A. Balkema, Rotterdam, 300 pp
- Hoenig A (1979) Elastic moduli of a non-randomly cracked body. *Int J Solids Struct* 15:137–154
- Hojem JMP, Cook NGW (1968) The design and construction of a triaxial and polyaxial cell for testing rock specimens. *S Afr Mech Eng* 18:57–61
- Hojem JPM, Cook NGW, Heins C (1975) A stiff, two meganewton testing machine for measuring the work-softening behaviour of brittle materials. *S Afr Mech Eng* 25:250–270
- Holcomb DJ (1984) Discrete memory in rock – a review. *J Rheol* 28:725–757
- Holcomb DJ (1993a) General theory of the Kaiser effect. *Int J Rock Mech Min* 30:929–935
- Holcomb DJ (1993b) Observations of the Kaiser effect under multiaxial stress states – implications for its use in determining in-situ stress. *Geophys Res Lett* 20:2119–2122
- Holcomb DJ, Costin LS (1986) Detecting damage surfaces in brittle materials using acoustic emissions. *J Appl Mech-ASME* 108:536–544
- Holcomb DJ, Rudnicki JW (2001) Inelastic constitutive properties and shear localization in Tennessee marble. *Int J Numer Anal Method Geomech* 25:109–129
- Holcomb DJ, Stevens JL (1980) The reversible Griffith crack: a viable model for dilatancy. *J Geophys Res* 85:7101–7107
- Holt RM (1989) Permeability reduction induced by a nonhydrostatic stress field. *Proc Annual Tech Conf of Soc Petrol Eng*, 64, SPE19595
- Holt RM, Fjaer O, Torsaeter O, Baake S (1996) Petrophysical laboratory measurements for basin and reservoir evaluation. *Mar Petrol Geol* 13:383–391
- Holtz RD, Kovacs WD (1981) Introduction to geotechnical engineering. Prentice-Hall, Englewood Cliffs, NJ, 733 pp
- Holzhausen GR, Johnson AM (1979) Analysis of longitudinal splitting of uniaxially compressed rock cylinders. *Int J Rock Mech Min* 16:163–177
- Homand F, Hoxha D, Belem T, Pons M-N, Hoteit N (2000) Geometric analysis of damaged microcracking in granites. *Mech Mater* 32:361–376
- Homand S, Shao JF (2000) Mechanical behaviour of a porous chalk and effect of saturating fluid. *Mech Cohes-Frict Mat* 5:583–606
- Horii H, Nemat-Nasser S (1983) Estimate of stress intensity factors for interacting cracks. In: Yuçeoğlu U, Sierakowski RL, Glasgow DA (eds) *Advances in aerospace structures, materials and dynamics*. ASME, New York, pp 111–117
- Horii H, Nemat-Nasser S (1985) Compression-induced microcrack growth in brittle solids: axial splitting and shear failure. *J Geophys Res* 90:3105–3125
- Horii H, Nemat-Nasser S (1986) Brittle failure in compression: splitting, faulting and brittle-ductile transition. *Philos T Roy Soc A* 319:337–374
- Horn HM, Deere DU (1962) Frictional characteristics of minerals. *Géotechnique* 12:319–335
- Hoshino K (1974) Effect of porosity on the strength of the clastic sedimentary rocks. In: *Advances in Rock Mechanics*. Proc. 3<sup>rd</sup> Congr. Int. Soc. Rock Mech., Denver, 1974. Washington, D.C., Nat. Acad. Sci., II, Part A, pp 511–516
- Hoshino K, Koide H (1970) Process of deformation of the sedimentary rocks. In: Proc. 2<sup>nd</sup> Congr. Int. Soc. Rock Mech., Belgrade, 1970 I, pp 353–359
- Hoshino K, Koide H, Inami K, Iwamura S, Mitsui S (1972) Mechanical properties of Japanese Tertiary sedimentary rocks under high confining pressures. Geological Survey of Japan, Report No. 244, 200 pp
- Hoskins ER (1969a) Examination of rock fracture surfaces with a scanning electron microscope. *EOS Trans AGU* 50:674 (abstract)
- Hoskins ER (1969b) The failure of thick-walled hollow cylinders of isotropic rock. *Int J Rock Mech Min* 6:99–125
- Hoskins ER, Jaeger JC, Rosengren KJ (1968) A medium-scale direct friction experiment. *Int J Rock Mech Min* 5:143–154

- Houpert R (1970) La résistance à la rupture des roches en compression simple. In: Proc. 2<sup>nd</sup> Congr. Int. Soc. Rock Mech., Belgrade 1970, II, pp 49–55
- Houpert R (1972) La rupture fragile des roches contrôlée au moyen d'une machine d'essai asservie. CR Acad Sci Paris A275:233–236
- Houpert R (1974a) Comportement fragile en compression simple et structure des roches. In: Proc. 2<sup>nd</sup> Int. Congr. Int. Assoc. Eng. Geol., Sao Paolo, Aug. 1974, 1, pp IV-25.1–IV-25.10
- Houpert R (ed) (1974b) Le rôle du temps dans le comportement à la rupture des roches. In: Advances in Rock Mechanics. Proc. 3<sup>rd</sup> Congr. Int. Soc. Rock Mech., Denver, 1974. Washington, D.C., Nat. Acad. Sci., 325–329 pp
- Houpert R, Legendre J, Richard P (1969) Un appareil de mesure des fissures des roches. In: 2<sup>nd</sup> Coll. sur la Fissuration des Roches, Paris, Jan. 1969, Revue de l'Industrie Minière, Special Number (July 1969), pp 18–20
- Houpert R, Tisot JP, Thomas A (1971) Le comportement des roches après rupture. In: Rock fracture. Proc. Int. Symp. Rock Mech., Nancy, France, Oct. 1971, pp Paper II-22 (16 pp)
- Hsieh PA, Tracy JV, Neuzil CE, Bredehoft JD, Silliman SE (1981) A transient laboratory method for determining the hydraulic properties of “tight” rocks – 1. Theory. Int J Rock Mech Min 18:245–252
- Huang SL, Aughenbaugh NB, Rockaway JD (1986) Swelling pressure studies of shales. Int J Rock Mech Min 23:371–377
- Hubbert MK, Rubey WW (1959) Role of fluid pressure in mechanics of overthrust faulting. I. Mechanics of fluid-filled porous solids and its application to overthrust faulting. Geol Soc Am Bull 70:115–166; discussion 71:611–628 and 72:1441–1451, 1581–1594
- Hudson JA (1971) Effect of time on the mechanical behaviour of failed rock. Nature 232:185–186
- Hudson JA (1981) Wave speeds and attenuation in material containing cracks. Geophys J Roy Astr S 64:133–150
- Hudson JA (1990) Overall elastic properties of isotropic materials with arbitrary distribution of circular cracks. Geophys J Int 102:465–469
- Hudson JA (1994) Overall properties of anisotropic materials containing cracks. Geophys J Int 116:279–282
- Hudson JA, Brown ET (1973) Studying time-dependent effects in failed rock. In: Hardy HR, Stefanko R (eds) New horizons in rock mechanics. Proc. 14<sup>th</sup> Symp. Rock Mech., Penn. State Univ. June 1972. Am Soc Civ Eng, pp 25–34
- Hudson JA, Brown ET, Fairhurst C (1971) Optimizing the control of rock failure in servo-controlled laboratory tests. Rock Mech 3:217–224
- Hudson JA, Brown ET, Fairhurst C (1972) Shape of the complete stress-strain curve for rock. In: Cording EJ (ed) Stability of rock slopes. Proc. 13<sup>th</sup> Symp. Rock Mech., Urbana, Aug. 1971. New York, Am. Soc. Civ. Eng., pp 773–795
- Hudson JA, Brown ET, Rummel F (1972) The controlled failure of rock discs and rings loaded in diametral compression. Int J Rock Mech Min 9:241–248
- Hudson JA, Crouch SL, Fairhurst C (1972) Soft, stiff and servo-controlled testing machines: a review with reference to rock failure. Eng Geol 6:155–189
- Hudson JA, Fairhurst C (1971) Tensile strength, Weibull's theory and a general statistical approach to rock failure. In: Te'eni M (ed) Structure, solid mechanics and engineering design. Proc. Southampton 1969 Civil Eng. Materials Conf. Wiley-Interscience, London, pp 901–914
- Hudson JA, Hardy MP, Fairhurst C (1973) The failure of rock beams. Part II. Experimental studies. Int J Rock Mech Min 10:69–82
- Hugman RHH, Friedman M (1979) Effects of texture and composition on mechanical behavior of experimentally deformed carbonate rocks. Am Assoc Petrol Geol Bull 63:1478–1489
- Humston JA, Logan JM (1972) Stick-slip in Tennessee sandstone. EOS Trans AGU 53:512 (abstract)
- Hustrulid W, Robinson F (1973) A simple stiff machine for testing rock in compression. In: Hardy HR, Stefanko R (eds) New horizons in rock mechanics. Proc. 14<sup>th</sup> Symp. Rock Mech., Penn. State Univ. June 1972. Am Soc Civ Eng, pp 61–84
- Ibanez WD, Kronenberg AK (1993) Experimental deformation of shale: mechanical properties and microstructural indicators of mechanisms. Int J Rock Mech Min 30:723–734
- Ichikawa Y, Wang J, Jeong G-C (1995) Uniaxial compression test of heterogeneous rock under microscopic observation and its homogeneous analysis. In: Fujii T (ed) Proceedings of the 8<sup>th</sup> International Congress on Rock Mechanics. A. A. Balkema, Rotterdam, 1, pp 227–230

- Ida Y (1972) Cohesive force across the tip of a longitudinal-shear crack and Griffith's specific surface energy. *J Geophys Res* 77:3796–3805
- Ida Y (1973) Stress concentration and unsteady propagation of longitudinal shear cracks. *J Geophys Res* 78:3418–3429
- Ida Y, Aki K (1972) Seismic source time function of propagating longitudinal shear cracks. *J Geophys Res* 77:2034–2044
- Inami K, Ibrahim R, Mizutani H (1969) Variation of ultrasonic wave velocity of marbles under triaxial compression. *J Phys Earth* 17:95–100
- Ingles DG, Lee IK, Neil RC (1973) The influence of stress history on lateral strain. *Rock Mech* 5:203–213
- Inglis CE (1913) Stresses in a plate due to the presence of cracks and sharp corners. *Trans Inst Nav Archit London* 55:219–241
- International Society for Rock Mechanics Commission on Standardization of Laboratory and Field Tests (1978) Suggested methods for determining the strength of rock materials in triaxial compression. *Int J Rock Mech Min* 15:47–51
- International Society for Rock Mechanics Commission on Standardization of Laboratory and Field Tests (1979) Suggested methods for determining the uniaxial compressive strength and deformability of rock materials. *Int J Rock Mech Min* 16:135–140
- International Society for Rock Mechanics Commission on Testing Methods (1988) Suggested methods for determining the fracture toughness of rock. *Int J Rock Mech Min* 25:71–96
- Irwin G (1948) Fracture dynamics. In: *Fracturing of metals*. Ohio, Am. Soc. for Metals, Cleveland, pp 147–166
- Irwin GR (1958) Fracture. In: Flügg S (ed) *Handbuch der Physik, Elastizität und Plastizität*. Springer-Verlag, Berlin Heidelberg New York, VI, pp 551–590
- Irwin GR, Kies JA, Smith HL (1958) Fracture strengths relative to onset and arrest of crack propagation. *P Am Soc Test Mater* 58:640–657
- Ishido T, Mizutani H (1981) Experimental and theoretical basis of electrokinetic phenomena in rock-water systems and its applications to geophysics. *J Geophys Res* 86:1763–1775
- Isida M, Nemat-Nasser S (1987a) On mechanics of crack growth and its effects on overall response of brittle porous solids. *Acta Metall* 35:2887–2898
- Isida M, Nemat-Nasser S (1987b) A unified analysis of various problems relating to circular holes with edge cracks. *Eng Fract Mech* 27:571–591
- Ismail IAH, Murrell SAF (1976) Dilatancy and the strength of rocks containing pore water under undrained conditions. *Geophys J Roy Astr S* 44:107–134
- Isnard P, Leymarie P (1963) Observation sur le fil du granite dans les carrières du Sidobre (Tarn). *Science de la Terre (Nancy)* 9:423–437
- Issen KA, Rudnicki JW (2000) Conditions for compaction bands in porous rock. *J Geophys Res* 105:21529–21536
- Jackson I (1993) Progress in the experimental study of seismic wave attenuation. *Ann Rev Earth Planet Sci* 21:375–406
- Jackson DD, Anderson DL (1970) Physical mechanisms of seismic-wave attenuation. *Rev Geophys Space Phys* 8:1–63
- Jackson RE, Dunn DE (1974) Experimental sliding friction and cataclasis of foliated rocks. *Int J Rock Mech Min* 11:235–249
- Jackson I, Paterson MS (1993) A high-pressure high-temperature apparatus for studies of seismic wave dispersion and attenuation. *Pure Appl Geophys* 141:445–466
- Jaeger JC (1942) Moving sources of heat and the temperature at sliding contacts. *Proc R Soc NSW* 76:203–224
- Jaeger JC (1943) The effect of absorption of water on the mechanical properties of sandstones. *J Inst Eng Aust* 15:164–166
- Jaeger JC (1959) The frictional properties of joints in rock. *Geofiz Pur E Appl* 43:148–158
- Jaeger JC (1960a) Rock failures at low confining pressures. *Engineering-London* 189:283–284
- Jaeger JC (1960b) Shear failure of anisotropic rocks. *Geol Mag* 97:65–72
- Jaeger JC (1963) Extension failures in rocks subject to fluid pressure. *J Geophys Res* 68:6066–6067
- Jaeger JC (1964) Discussion to FA Donath, Strength variation and deformational behavior in anisotropic rock. In: Judd WR (ed) *State of stress in the Earth's crust*. American Elsevier, New York, p 297

- Jaeger JC (1965) Fracture of rocks. In: Osborn DJ (ed) Fracture. Proc. 1<sup>st</sup> Tewksbury Symp., Univ. Melbourne, Aug. 1963. Faculty of Engineering, Univ. Melbourne, pp 268–283
- Jaeger JC (1967) Brittle fracture of rocks. In: Fairhurst C (ed) Failure and breakage of rock. Proc. 8<sup>th</sup> Symp. on Rock Mech. Minnesota, Sept. 1966. A.I.M.E., New York, pp 3–57
- Jaeger JC (1969) Elasticity, fracture and flow. Methuen, London, 268 pp
- Jaeger JC (1971) Friction of rocks and stability of rock slopes. *Géotechnique* 21:97–134
- Jaeger JC (1973) Crushing under non-uniform loading. In: Storr ED (ed) National Symposium on Rock Fragmentation, Adelaide, Feb. 1973. Australian Geomechanics Soc., Inst. Eng. Aust., pp 74–80
- Jaeger JC, Cook NGW (1963) Pinching-off and diskings of rocks. *J Geophys Res* 68:1759–1765
- Jaeger JC, Cook NGW (1971) Friction in granular materials. In: Te'eni M (ed) Structure, solid mechanics and engineering design. Proc. Southampton 1969 Civil Eng. Materials Conf. Wiley-Interscience, London, pp 257–266
- Jaeger JC, Cook NGW (1979) Fundamentals of rock mechanics, 3<sup>rd</sup> ed. Chapman and Hall, London, 593 pp
- Jaeger JC, Hoskins ER (1966a) Rock failure under the confined Brazilian test. *J Geophys Res* 71:2651–2659
- Jaeger JC, Hoskins ER (1966b) Stresses and failure in rings of rock loaded in diametral tension or compression. *Br J Appl Phys* 17:685–692
- Jaeger JC, Rosengren KJ (1969) Friction and sliding of joints. *Proc Aust Inst Min Met* 229:93–104
- Jahns H (1966) Messung der Gebirgsfestigkeit in situ bei wachsendem Maßstabsverhältnis. In: Proc. 1<sup>st</sup> Congr. Int. Soc. Rock Mech., Lisbon, 1966, I, pp 477–482
- Jamison WR, Teufel LW (1979) Pore volume changes associated with failure and frictional sliding of a porous sandstone. In: Gray KE (ed) 20<sup>th</sup> U.S. Symposium on Rock Mechanics. University of Texas, Austin, Texas, pp 163–170
- Jenkins JT, Cundall PA, Ishibashi I (1989) Micromechanical modeling of granular materials with the assistance of experiments and numerical simulations. In: Biarez J, Gourvès R (eds) Powders and grains. Proc Int Conf on Micromechanics of Granular Media, Clermont-Ferrand, 4–8 Sept 1989. A. A. Balkema, Rotterdam, pp 257–264
- Jenkins JT, Satake M (eds) (1983) Mechanics of granular materials – new models and constitutive relations. Elsevier, Amsterdam
- Jeyakumaran M, Rudnicki JW (1995) The sliding wing crack – again! *Geophys Res Lett* 22:2901–2904
- John M (1974) Zeitabhängigkeit der Bruchvorgänge von Gesteinen. In: Advances in Rock Mechanics. Proc. 3<sup>rd</sup> Congr. Int. Soc. Rock Mech., Denver, 1974. Washington, D.C., Nat. Acad. Sci., II, Part A, pp 330–335
- Johnson TL (1975) A comparison of frictional sliding on granite and dunite surfaces. *J Geophys Res* 80:2600–2605
- Johnson TL (1981) Time-dependent friction of granite: implications for precursory slip on faults. *J Geophys Res* 86:6017–6028
- Johnson KL (1985) Contact mechanics. Cambridge University Press, New York
- Johnson DP, Newhall DH (1953) The piston gage as a precise pressure-measuring instrument. *Trans Am Soc Mech Eng* 75:301–310
- Johnson TL, Scholz CH (1976) Dynamic properties of stick-slip friction of rock. *J Geophys Res* 81:881–888
- Johnson T, Wu FT, Scholz CH (1973) Source parameters for stick-slip and for earthquakes. *Science* 179:278–280
- Jones R (1952) A method of studying the formation of cracks in a material subjected to stress. *Br J Appl Phys* 3:229–232
- Jones DE, Kennedy FE, Schulson EM (1991) The kinetic friction of saline ice against itself at slow sliding velocities. *Ann Glaciol* 15:242–246
- Jones C, Murrell SAF (1989) Acoustic compressional wave velocity and dilatancy in triaxially stressed rocks. In: Maury V, Fourmaintraux D (eds) Rock at great depth. A. A. Balkema, Rotterdam, 1, pp 241–247
- Jones ME, Preston RMF (eds) (1987) Deformation of sediments and sedimentary rocks. Geological Society, London, Special Publication No. 29, 350 pp
- Joshi MS, Paul BK (1976) Studies of nucleation and propagation of cracks in natural quartz. *J Gemm* 15:129–135
- Jouniaux L, Lallemand S, Pozzi J-P (1994) Changes in the permeability, streaming potential and resistivity of a claystone from the Nankai prism under stress. *Geophys Res Lett* 21:149–152
- Jouniaux L, Pozzi J-P (1995) Streaming potential and permeability of saturated sandstones under triaxial stress: consequences for electrotelluric anomalies prior to earthquakes. *J Geophys Res* 100:10197–10209

- Jung H, Green HW, Dobrzhinetskaya LF (2004) Intermediate-depth earthquake faulting by dehydration embrittlement with negative volume change. *Nature* 428:545–549
- Kachanov LM (1986) Introduction to continuum damage mechanics. Martinus Nijhoff, Dordrecht, 135 pp
- Kachanov ML (1982a) A microcrack model of rock inelasticity. Part I: Frictional sliding on microcracks. *Mech Mater* 1:19–27
- Kachanov ML (1982b) A microcrack model of rock inelasticity. Part II: Propagation of microcracks. *Mech Mater* 1:29–41
- Kachanov M (1993) Elastic solids with many cracks and related problems. *Adv Appl Mech* 30:259–445
- Kanagawa K, Cox SF, Zhang S (2000) Effects of dissolution-precipitation processes on the strength and mechanical behavior of quartz gouge at high-temperature hydrothermal conditions. *J Geophys Res* 105:11115–11126
- Kanamori H, Allen CR (1986) Earthquake repeat time and average stress drop. In: Das S, Boatwright J, Scholz CH (eds) *Earthquake source mechanics*. American Geophysical Union, Washington, D.C., pp 227–236
- Kanninen MF, Poplear CH (1985) *Advanced fracture mechanics*. Oxford Univ Press, New York, 563 pp
- Karihaloo BL (1979) A note on complexities of compression failure. *P Roy Soc Lond A Mat* 368:483–493
- Karner SL, Marone C (1998) The effect of shear load on frictional heating in simulated fault gouge. *Geophys Res Lett* 25:4561–4564
- Karner SL, Marone C (2000) Effects of loading rate and normal stress on stress drop and stick-slip recurrence interval. In: Rundle JB, Turcotte DL, Klein W (eds) *geocomplexity and physics of earthquakes*. American Geophysical Union, Washington, D.C., *Geophys Monograph* 120, pp 187–198
- Kassir MK, Sih GC (1967) Griffith's theory of brittle fracture in three dimensions. *Int J Eng Sci* 5:899–918
- Kato A, Ohnaka M, Mochizuki H (2003) Constitutive properties for the shear failure of intact granite in seismogenic environments. *J Geophys Res* 108:2060, doi: 10.1029/2001JB000791 (16 pp)
- Kato H, Yamamoto K, Yamamoto H, Hirasawa T (1992) Strain-rate effect on frictional strength and the slip nucleation process. *Tectonophysics* 211:269–282
- Kawakata H, Cho A, Kiyama T, Yanagidani T, Kusunose K, Shimada M (1999) Three-dimensional observations of faulting process in Westerly granite under uniaxial and triaxial conditions. *Tectonophysics* 313:293–305
- Keaney GMJ, Meredith PG, Murrell SAF (1998) Laboratory study of permeability evolution in a “tight” sandstone under non-hydrostatic stress conditions. In: *SPE/ISRM Eurorock '98: Trondheim, Norway*, pp SPE Paper 47 265
- Kemeny JM (1991) A model for non-linear rock deformation under compression due to sub-critical crack growth. *Int J Rock Mech Min* 28:459–467
- Kemeny JM, Cook NGW (1987) Crack models for the failure of rocks in compression. *Proc. International Conference on Constitutive Laws for Engineering Materials* 2:879–887
- Kemeny JM, Cook NGW (1991) Micromechanics of deformation in rocks. In: Shah SP (ed) *Toughening mechanisms in quasi-brittle materials*. Kluwer Academic Publishers, Dordrecht, pp 155–188
- Kenyon WE (1992) Nuclear magnetic resonance as a petrophysical measurement. *Nucl Geophys* 6:153–171
- Key PL (1969) A relation between crack surface displacements and the strain energy release rate. *Int J Fract Mech* 5:287–296
- Khan AS, Xiang Y, Huang S (1991) Behavior of Berea sandstone under confining pressure. Part 1: Yield and failure surfaces, and nonlinear elastic response. *Int J Plasticity* 7:607–624
- Kilgore BD, Blanpied ML, Dieterich JH (1993) Velocity dependent friction of granite over a wide range of conditions. *Geophys Res Lett* 20:903–906
- Kimura T, Esaki T, Kameda N, Nishida T (1987) Experimental and theoretical studies on strain softening behavior of rocks. In: Farmer IW, Daemen JJK, Desai CS, Glass CE, Neuman SP (eds) *Rock mechanics. Proceedings of the 28<sup>th</sup> U.S. Symposium*. A. A. Balkema, Rotterdam, pp 197–202
- King MS, Chaudhry NA, Shakeel A (1995) Experimental ultrasonic velocities and permeability for sandstones with aligned cracks. *Int J Rock Mech Min* 32:155–163
- King MS, Shakeel A, Chaudhry NA (1997) Acoustic wave propagation and permeability in sandstones with systems of aligned cracks. In: Lovell MA, Harvey PK (eds) *Developments in petrophysics*. The Geological Society, London, Special Publication No. 122, pp 69–85

- Kirby SH, Kronenberg AK (1984) Deformation of clinopyroxenite: evidence for a transition in flow mechanisms and semibrittle behavior. *J Geophys Res* 89:3177–3192
- Kirby SH, Stein S, Okal EA, Rubie DC (1996) Metastable mantle phase transformations and deep earthquakes in subducting oceanic lithosphere. *Rev Geophys* 34:261–306
- Kiyama T, Kita H, Ishijima Y, Yanagidani T, Aoki K, Sato T (1996) Permeability in anisotropic granite under hydrostatic compression and triaxial compression including post-failure region. *Proc North Am Rock Mech Symposium* 2:1161–1168
- Klinkenberg LJ (1941) The permeability of porous media to liquids and gases. *Drill Prod Pract API* 200–213
- Knill JL, Franklin JA, Malone AW (1968) A study of acoustic emission from stressed rock. *Int J Rock Mech Min* 5:87–121
- Knopoff L (1964) *Q. Rev Geophys* 2:625–660
- Knopoff L, Porter LD (1963) Attenuation of surface waves in a granular material. *J Geophys Res* 68:6317–6321
- Knott JF (1973) *Fundamentals of fracture mechanics*. John Wiley & Sons, New York, 273 pp
- Ko S-c, Olgaard DL, Briegel U (1995) The transition from weakening to strengthening in dehydrating gypsum: evolution of excess pore pressures. *Geophys Res Lett* 22:1009–1012
- Ko S-c, Olgaard DL, Wong T-f (1997) Generation and maintenance of pore pressure excess in a dehydrating system. 1 Experimental and microstructural observations. *J Geophys Res* 102:825–839
- Kobayashi S (1970) Fracture criteria for anisotropic rocks. *Mem Fac Eng Kyoto Univ* 32:307–333
- Kohlstedt DL, Chopra PN (1987) Measurement of rock deformation at high temperatures. In: Sammis CG, Henyey TL (eds) *Methods of experimental physics*. Academic Press, Orlando, 24, Part A, pp 57–87
- Kohlstedt DL, Zimmerman ME (1996) Rheology of partially molten rocks. *Ann Rev Earth Planet Sci* 24:41–60
- Koide H (1972) Fracture initiation in brittle polycrystalline material such as rocks. *Conf. on Mechanical Behaviour of Materials, Kyoto, 1971. Proc Soc Mater Sci Jpn* 4:455–463
- Koifman MI (1963) The size factor in rock-pressure investigations. In: Protod'yakov MM, Koifman MI, et al. (eds) *Mechanical properties of rocks (English translation by Israel Program for Scientific Translations, Jerusalem, 1968. Akademiya Nauk SSSR, Moscow, pp 109–117)*
- Konishi J, Oda M, Nemat-Nasser S (1982) Inherent anisotropy and shear strength of assembly of oval cross-sectional rods. In: Vermeer PA, Luger HJ (eds) *Conference on deformation and failure of granular materials*. A. A. Balkema, Rotterdam, pp 403–412
- Konstantinova AG (1960) Time distribution of elastic pulse energy during destruction of rocks. *Izvestiya Akad Nauk SSR, Ser Geofiz*, pp 1580–1592 (Engl. tr.: *Bull (Izvestiya) Acad Sci, USSR, Geophys Ser*, pp 1056–1061)
- Koplik J, Lin C, Vermette M (1984) Conductivity and permeability from microgeometry. *J Appl Phys* 56:3127–3131
- Kostak B, Bielenstein HU (1971) Strength distribution in hard rock. *Int J Rock Mech Min* 8:501–521
- Kostrov BV (1966) Unsteady propagation of longitudinal shear cracks. *Prikladnaya Matematika U Mekhanika* 30:1042–1049 (Engl. tr.: *J Appl Math Mech* 30:1241–1248)
- Kostrov BV, Das S (1988) *Principles of earthquake source mechanics*. Cambridge Monographs on Mechanics and Applied Mathematics. Cambridge University Press, Cambridge, 286 pp
- Kotte JJ, Bérczes ZG, Gramberg J, Seldenrath TR (1969) Stress-strain relations and breakage of cylindrical granitic rock specimens under uniaxial and triaxial loads. *Int J Rock Mech Min* 6:581–595
- Kovári K, Tisa A (1975) Multiple failure state and strain controlled triaxial tests. *Rock Mech*, 17–33
- Kowallis BJ, Roeloffs EA, Wang HF (1982) Microcrack studies of basalts from The Iceland Research Drilling Project. *J Geophys Res* 87:6650–6656
- Kowallis BJ, Wang HF (1983) Microcrack study of granite cores from Illinois deep borehole UPH3. *J Geophys Res* 88:7373–7380
- Krajcinovic D (1989) Damage mechanics. *Mech Mater* 8:117–197
- Krajcinovic D, Mastilovic S (1995) Some fundamental issues of damage mechanics. *Mech Mater* 21:217–230
- Kranz RL (1979a) Crack growth and development during creep in Westerly granite. *Int J Rock Mech Min* 16:23–36

- Kranz RL (1979b) Crack-crack and crack-pore interactions in stressed granite. *Int J Rock Mech Min* 16:37–48
- Kranz RL (1980) The effects of confining pressure and stress difference on static fatigue of granite. *J Geophys Res* 85:1854–1866
- Kranz RL (1983) Microcracks in rocks: a review. *Tectonophysics* 100:449–480
- Kranz RL, Blacic JD (1984) Permeability changes during time-dependent deformation of silicate rock. *Geophys Res Lett* 11:975–978
- Kranz RL, Harris WJ, Carter NL (1982) Static fatigue of granite at 200 °C. *Geophys Res Lett* 9:1–4
- Kranz RL, Saltzman JS, Blacic JD (1990) Hydraulic diffusivity measurements on laboratory rock samples using an oscillating pore pressure method. *Int J Rock Mech Min* 27:345–352
- Kranz RL, Scholz CH (1977) Critical dilatant volume of rocks at the onset of creep. *J Geophys Res* 82:4893–4898
- Kranz RL, Satoh T, Nishizawa O, Kusunose K, Takahashi M, Masuda K, Hirata A (1990) Laboratory study of fluid pressure diffusion in rock using acoustic emission. *J Geophys Res* 95:21593–21607
- Krech WM (1974) The energy balance theory and rock fracture energy measurements for uniaxial tension. In: *Advances in Rock Mechanics. Proc. 3<sup>rd</sup> Congr. Int. Soc. Rock Mech., Denver, 1974*. Washington, D.C., Nat. Acad. Sci., II, Part A, pp 167–173
- Krishnamurthi M, Balakrishna S (1957) Attenuation of sound in rocks. *Geophysics* 22:268–274
- Kronenberg AK, Shelton GL (1980) Deformation microstructures in experimentally deformed Maryland diabase. *J Struct Geol* 2:341–353
- Kronenberg AK, Tullis J (1984) Flow strengths of quartz aggregates: grain size and pressure effects due to hydrolytic weakening. *J Geophys Res* 89:4281–4297
- Kronenberg AK, Karner SL, Chester FM, Chester JS (2002) Temperature-dependent deformation of granular quartz sand. *EOS Trans AGU* 83, Fall Meet. Suppl., abstract T11F-08 (p F1347)
- Kumar A (1968) The effect of stress rate and temperature in the strength of basalt and granite. *Geophysics* 33:501–510
- Kümpel H-J (1991) Poroelasticity: parameters reviewed. *Geophys J Int* 105:783–799
- Kurita K, Fujii N (1979) Stress memory of crystalline rocks in acoustic emission. *Geophys Res Lett* 6:9–12
- Kuster GT, Toksöz MN (1974) Velocity and attenuation of seismic waves in two-phase media. *Geophysics* 39:587–618
- Kusunose K, Nishizawa O (1986) AE gap prior to local fracture of rock under uniaxial compression. *J Phys Earth* 34:S45–S56
- Kutter HK (1974) Rotary shear testing of rock joints. In: *Advances in Rock Mechanics. Proc. 3<sup>rd</sup> Congr. Int. Soc. Rock Mech., Denver, 1974*. Washington, D.C., Nat. Acad. Sci., II, Part A, pp 254–262
- Kvapil R, Luffer K (1960) Beitrag zur Frage der Spannungsverteilung in würfelförmigen Probekörpern bei triaxialer Beanspruchung. *Bergakademie Freiberg* 12:587–594
- Kwon O, Kronenberg AK, Gangi AF, Johnson B (2001) Permeability of Wilcox shale and its effective pressure law. *J Geophys Res* 106:19339–19353
- La Fountain LJ, Dunn DE (1973) Growth of microfractures during dilatation. *EOS Trans AGU* 54:368 (abstract)
- La Fountain LJ, Dunn DE (1974) Effect of anisotropy on the coefficient of sliding friction in schistose rocks. *Int J Rock Mech Min* 11:459–464
- La Fountain LJ, Swain MV, Jackson RE (1975) Origin of macroscopic wear grooves generated during sliding friction experiments. *Int J Rock Mech Min* 12:367–371
- Labuz JF (1991) The problem of machine stiffness revisited. *Geophys Res Lett* 18:439–442
- Labuz JF, Biollzi L (1991) Class-I vs class-II stability – a demonstration of size effect. *Int J Rock Mech Min* 28:199–205
- Labuz JF, Bridell JM (1993) Reducing frictional constraint in compression testing through lubrication. *Int J Rock Mech Min* 30:451–455
- Labuz JF, Dai S-T, Papamichos E (1996) Plane-strain compression of rock-like materials. *Int J Rock Mech Min* 33:573–584
- Labuz JF, Shah SP, Dowding CH (1983) Post peak tensile load-displacement response and the fracture process zone in rock. In: Mathewson CC (ed) *Rock mechanics. Theory – experiment – practice. Proc 24<sup>th</sup> U.S. Symposium on Rock Mechanics, Texas A and M University and Association of Engineering Geologists*, pp 421–428

- Ladanyi B (1970) Discussion of W. F. Brace and R. J. Martin's paper "A test of the law of effective stress for crystalline rocks of low porosity". *Int J Rock Mech Min* 7:123–124
- Lajtai EZ (1971) A theoretical and experimental evaluation of the Griffith theory of brittle fracture. *Tectonophysics* 11:129–156
- Lajtai EZ (1972) Effect of tensile stress gradient on brittle fracture initiation. *Int J Rock Mech Min* 9:569–578
- Lajtai EZ, Lajtai VN (1974) The evolution of brittle fracture in rocks. *J Geol Soc London* 130:1–18
- Lajtai EZ, Schmidtke RH, Bielus LP (1987) The effect of water on the time-dependent deformation and fracture of granite. *Int J Rock Mech Min* 24:247–255
- Lama RD, Vutukuri VS (1978) Handbook on mechanical properties of rocks. Trans Tech Publications, Clausthal, 481 pp
- Lambe TW, Whitman RV (1969) Soil mechanics. Wiley, New York, 553 pp
- Lane KS (1970) Engineering problems due to fluid pressure in rock. In: Somerton WH (ed) *Rock mechanics – theory and practice*. Proc. 11<sup>th</sup> Symp. Rock Mech., Berkeley, 1970. A.I.M.E., New York, pp 501–540
- Lane KS, Heck WJ (1964) Triaxial testing for strength of rock joints. In: Stokes EM, Christiansen CR (eds) Proc. 6<sup>th</sup> Symp. Rock Mech., Rolla, Missouri, Oct. 1964, Univ. of Missouri, pp 98–108
- Lankford J (1977) Dynamic strength of oil shale. *J Soc Petrol Eng* 16:17–22
- Lankford J (1981) The role of tensile microfracture in the strain rate dependence of compressive strength of fine-grained limestone – analogy with strong ceramics. *Int J Rock Mech Min* 18:173–175
- Laubscher HP (1960) Role of fluid pressure in mechanics of overthrust faulting: discussion. *Geol Soc Am Bull* 71:611–615
- Lawn B (1993) Fracture of brittle solids. Cambridge Solid State Science Series. Cambridge University Press, Cambridge, 378 pp
- Lawn BR (1975) An atomistic model of kinetic crack growth in brittle solids. *J Mater Sci* 10:469–480
- Lawn B, Wilshaw R (1975a) Indentation fracture: principles and applications. *J Mater Sci* 10:1049–1081
- Lawn B, Wilshaw TR (1975b) Fracture of brittle solids. Cambridge, Cambridge Univ. Press, 204 pp
- Lee X, Ju JW (1991) Micromechanical damage models for brittle solids. II: Compressive loadings. *J Eng Mech* 117:1515–1536
- Lehner FK (1995) A model for intergranular pressure solution in open systems. *Tectonophysics* 245:153–170
- Lehner F, Kachanov M (1996) On modelling of "winged" cracks forming under compression. *Int. J. Fracture* 77:R69–R75
- Lemaitre J (1996) A course on damage mechanics. Springer-Verlag, Berlin, 228 pp
- Lesnic D, Elliott DB, Ingham DB, Clennell B, Knipe RJ (1997) A mathematical model and numerical investigation for determining the hydraulic conductivity of rocks. *Int J Rock Mech Min* 34:741–759
- Lévéque P (1969) Étude de la microfissuration par autoradiographie. In: 2<sup>nd</sup> Coll. Fissuration des Roches, Paris, Jan 1969, Revue de l'Industrie Minière, Special Number (July 1969)
- Li VC (1987) Mechanics of shear rupture applied to earthquake zones. In: Atkinson BK (ed) *Fracture mechanics of rock*. Academic Press, London, pp 351–428
- Li C, Nordlund E (1993) Deformation of brittle rocks under compression – with particular reference to microcracks. *Mech Mater* 15:223–239
- Li HB, Zhao J, Li TJ (1999) Triaxial compression tests on a granite at different strain rates and confining pressures. *Int J Rock Mech Min* 36:1057–1063
- Liebowitz H (ed) (1968) *Fracture, an advanced treatise*. Academic Press, New York, 759 pp
- Lifshitz IM (1963) On the theory of diffusion-viscous flow of polycrystalline bodies. *J Exp Theor Phys+* 44:1349–1367; tr. In: *Soviet Physics JETP* 17(4):909–920
- Lin C (1982) Parametric analysis of the transient method of measuring permeability. *J Geophys Res* 87:1055–1060
- Lin C, Pirie G, Trimmer DA (1986) Low permeability rocks: laboratory measurements and three-dimensional microstructural analysis. *J Geophys Res* 91:2173–2181
- Lindborg U (1969) A statistical model for the linking of microcracks. *Acta Metall Mater* 17:521–526
- Lindholm US, Yeakley LM, Nagy A (1974) The dynamic strength and fracture properties of Dresser basalt. *Int J Rock Mech Min* 11:181–191



- Lindquist WB, Venkatarangan A, Dunsmuir J, Wong T-f (2000) Pore and throat size distributions measured from X-ray tomographic images of Fontainebleau sandstones. *J Geophys Res* 105:21509–21527
- Lindqvist P-A, Lai HH, Alm O (1984) Indentation fracture development observed with a scanning electron microscope. *Int J Rock Mech Min* 21:165–182
- Lindström M (1974) Steps facing against the slip direction: a model. *Geol Mag* 111:71–74
- Linker MF, Dieterich JH (1992) Effects of variable normal stress on rock friction: observations and constitutive equations. *J Geophys Res* 97:4923–4940
- Lipkin J, Grady DE, Campbell JD (1977) Dynamic flow and fracture of rock in pure shear. In: 18<sup>th</sup> U.S. Symposium on Rock Mechanics, pp 3B2–1
- Lipkin J, Jones AK (1979) Dynamic fracture strength of oil shale under torsional loading. In: Proc 20<sup>th</sup> U.S. Symposium on Rock Mechanics, Austin, Texas, pp 601–606
- Liu Z, Cook NGW, Myer LR (1994) Numerical studies relating to micro fracture in granular materials. In: Nelson PP, Laubach SE (eds) *Rock mechanics, models and measurements, challenges from industry. Proceedings of the First North American Rock Mechanics Symposium*. A. A. Balkema, Rotterdam, pp 631–638
- Liu H-P, Livanos ACR (1976) Dilatancy and precursory bulging along incipient fracture zones in uniaxial compressed Westerly granite. *J Geophys Res* 81:3495–3510
- Liu Z, Myer LR, Cook NGW (1993) Micromechanics of granular materials – numerical simulation of the effects of heterogeneities. *Int J Rock Mech Min* 30:1281–1284
- Lloyd GE, Hall MG (1981) Application of scanning electron microscopy to the study of deformed rocks. *Tectonophysics* 78:687–698
- Lo KK (1978) Analysis of branched cracks. *J Appl Mech-T ASME* 45:797–802
- Lockner D (1993a) The role of acoustic emission in the study of rock. *Int J Rock Mech Min* 30:883–900
- Lockner D (1993b) Room temperature creep in saturated granite. *J Geophys Res* 98:475–487
- Lockner DA (1995) Rock failure. In: Ahrens TJ (ed) *Rock physics and phase relations. A handbook of physical constants*. American Geophysical Union, Washington, D.C., AGU Reference Shelf 3, pp 127–147
- Lockner DA (1998) A generalized law for brittle deformation on Westerly granite. *J Geophys Res* 201:5107–5123
- Lockner DA, Beeler NM (2003a) Rock failure and earthquakes. In: Lee WHK, Kanamori H, Jennings PC, Kisslinger C (eds) *International handbook of earthquake and engineering seismology, Part A*. Academic Press, San Diego, pp 505–537
- Lockner DA, Beeler NM (2003b) Stress-induced anisotropic poroelasticity response in sandstone. In: Proc. 16<sup>th</sup> ASCE Engin. Mech. Conf., U Washington, Seattle
- Lockner D, Byerlee JD (1977a) Acoustic emission and creep in rock at high confining pressure and differential stress. *B Seismol Soc Am* 67:247–258
- Lockner D, Byerlee JD (1977b) Acoustic emission and fault formation in rocks. In: Hardy HR, Leighton FW (eds) *Proc. First Conf. on Acoustic Emission/Microseismic Activity in Geologic Structures and Materials*, Penn. State Univ., June 1975. *Trans. Tech. Publ., Clausthal*, pp 99–107
- Lockner D, Byerlee JD (1977c) Hydrofracture in Weber sandstone at high confining pressure and differential stress. *J Geophys Res* 82:2018–2026
- Lockner DA, Byerlee JD (1980) Development of fracture planes during creep in granite. In: Hardy HRJ, Leighton FW (eds) *Proc. of 2<sup>nd</sup> Conf. on AE/Microseismic Activity in Geological Structures, and Materials*. *Trans. Tech. Pub., Clausthal*, pp 11–25
- Lockner DA, Byerlee JD (1986) Changes in complex resistivity during creep in granite. *Pure Appl Geophys* 124:659–676
- Lockner DA, Byerlee JD (1993) How geometrical constraints contribute to the weakness of mature faults. *Nature* 363:250–252
- Lockner DA, Byerlee JD (1995) Precursory AE patterns leading to rock fracture. In: Hardy HR (ed) *Acoustic emission/microseismic activity in geologic structures and materials. Proceedings of the Fifth Conference*. *Trans. Tech. Pub., Clausthal*, pp 45–58
- Lockner DA, Madden TR (1991a) A multiple-crack model of brittle failure. 1. Non-time-dependent simulations. *J Geophys Res* 96:19623–19642
- Lockner DA, Madden TR (1991b) A multiple-crack model of brittle failure. 2. Time-dependent simulations. *J Geophys Res* 96:19643–19654

- Lockner DA, Moore DE (1992) Microcrack interaction leading to shear fracture. In: Tillerson JR, Wawersik WR (eds) Rock mechanics. Proceedings of the 33<sup>rd</sup> U.S. Symposium. A. A. Balkema, Rotterdam, pp 807–816
- Lockner DA, Stanchits SA (2002) Undrained poroelastic response of sandstones to deviatoric stress change. *J Geophys Res* 107:2353, doi: 10.1029/2001JB001460 (14 pp)
- Lockner DA, Summers R, Byerlee JD (1986) Effects of temperature and sliding rate on frictional strength of granite. *Pure Appl Geophys* 124:445–469
- Lockner DA, Walsh JB, Byerlee JD (1977) Changes in seismic velocity and attenuation during deformation of granite. *J Geophys Res* 82:5374–5378
- Lockner DA, Byerlee JD, Kuksenko V, Ponomarev A, Sidorin A (1991) Quasi-static fault growth and shear fracture energy in granite. *Nature* 350:39–42
- Lockner DA, Byerlee JD, Kuksenko V, Ponomarev A, Sidorin A (1992) Observations on quasistatic fault growth from acoustic emissions. In: Evans B, Wong, T-f (eds) Fault mechanics and transport properties of rocks. International Geophysics Series. Academic Press, London, pp 3–32
- Logan JM (1972) The influence of surface roughness and gouge on frictional sliding. *EOS Trans AGU* 53:512 (abstract)
- Logan JM (1975) Friction in rocks. *Rev Geophys Space Phys* 13:358–361, 389–390
- Logan JM (1987) Porosity and the brittle-ductile transition in sedimentary rocks. In: Banavar JR, Koplak J, Winkler KW (eds) Physics and Chemistry of Porous Media II, AIP Conf. Proc. AIP Conference Proceedings. Amer. Inst. Phys. New York, 154:pp 229–242
- Logan JM, Handin J (1971) Triaxial compression testing at intermediate strain rates. In: Clark GB (ed) Dynamic rock mechanics. Proc. 12<sup>th</sup> Symp. Rock Mech., Rolla, Missouri, 1970. A.I.M.E., New York, pp 167–194
- Logan JM, Rauenzahn KA (1987) Frictional dependence of gouge mixtures of quartz and montmorillonite on velocity, composition and fabric. *Tectonophysics* 144:87–108
- Logan JM, Dengo CA, Higgs NG, Wang ZZ (1992) Fabrics of experimental fault zones: their development and relationship to mechanical behavior. In: Evans B, Wong, T-f (eds) Fault mechanics and transport properties of rocks. International Geophysics Series. Academic Press, London, pp 33–67
- Logan JM, Iwasaki T, Friedman M, Kling SA (1973) Experimental investigation of sliding friction in multilithologic specimens. In: Pincus H (ed) Geological factors in rapid excavation. *Geol. Soc. Am., Eng Geol Case History No. 9*, pp 55–67
- Lorne B, Perrier F, Avouac J-P (1999) Streaming potential measurements. 2. Relationship between electrical and hydraulic flow patterns from rock samples during deformation. *J Geophys Res* 104:17879–17896
- Losert W, Bocquet L, Lubensky TC, Gollub JP (2000) Particle dynamics in sheared granular material. *Phys Rev Lett* 85:1428–1431
- Love AEH (1910) Elasticity. In: *Encyclopaedia Britannica*. Encyclopaedia Britannica, Inc., New York, IX, pp 141–160
- Luan FC, Paterson MS (1992) Preparation and deformation of synthetic aggregates of quartz. *J Geophys Res* 97:301–320
- Lubert M, de Ryck A (2001) Slip events and dilatancy in a sheared fine noncohesive powder. *Phys Rev E* 63:021502 (7 pp)
- Lundborg N (1967) The strength-size relation of granite. *Int J Rock Mech Min* 4:269–272
- Lundborg N (1968) Strength of rock-like materials. *Int J Rock Mech Min* 5:427–454
- Lundborg N (1972) A statistical theory of the polyaxial compressive strength of materials. *Int J Rock Mech Min* 9:617–624
- Lundborg N (1974) A statistical theory of the polyaxial strength of materials. In: *Advances in rock mechanics*. Proc. 3<sup>rd</sup> Congr. Int. Soc. Rock Mech., Denver, 1974. Washington, D.C., Nat. Acad. Sci., II, Part A, pp 180–185
- Lyakhovskiy V, Ben-Zion Y, Agnon A (1997) Distributed damage, faulting, and friction. *J Geophys Res* 102:27635–27649
- Madariaga R (1977) Implications of stress-drop models of earthquakes for the inversion of stress drop from seismic observations. *Pure Appl Geophys* 115:301–316
- Madariaga R, Olsen KB (2000) Criticality of rupture dynamics in 3-D. *Pure Appl Geophys* 157:1981–2001

- Madden TR (1983) Microcrack connectivity in rocks: a renormalization group approach to the critical phenomenon of conduction and failure in crystalline rocks. *J Geophys Res* 88:585–592
- Mae I, Nakao K (1968) Characteristics in the generation of micro-seismic noises in rocks under uniaxial compressive load. *J Soc Mater Sci Japan* 17:908–913 (in Japanese, with English summary)
- Main IG, Meredith PG, Jones C (1989) A reinterpretation of the precursory seismic b-value anomaly from fracture mechanics. *Geophys J+* 96:131–138
- Main IG, Kwon O, Ngwenya BT, Elphick SC (2000) Fault sealing during deformation-band growth in porous sandstone. *Geology* 28:1131–1134
- Mainprice DH, Paterson MS (1984) Experimental studies of the role of water in the plasticity of quartzites. *J Geophys Res* 89:4257–4269
- Mair K, Elphick SC, Main IG (2002) Influence of confining pressure on the mechanical and structural evolution of laboratory deformation bands. *Geophys Res Lett* 29, 10.1029/2001GL013964
- Mair K, Frye KM, Marone C (2002) Influence of grain characteristics on the friction of granular shear zones. *J Geophys Res* 107:2219, doi: 10.1029/2001JB000516 (9 pp)
- Mair K, Main I, Elphick SC (2000) Sequential growth of deformation bands in the laboratory. *J Struct Geol* 22:25–42
- Mair K, Marone C (1999) Friction of simulated fault gouge for a wide range of velocities and normal stresses. *J Geophys Res* 104:28899–28914
- Mandel J (1966) Conditions de stabilité et postulat de Drucker. In: Kravtchenko J, Sirieys PM (eds) *Rheology and soil mechanics*. IUTAM Symposium, Grenoble, April 1–8, 1964. Springer-Verlag, Berlin Heidelberg New York, pp 58–68
- Mandelbrot BB (1983) *The fractal geometry of nature*. Freeman, San Francisco, 468 pp
- Mandl G, de Jong LNJ, Maltha A (1977) Shear zones in granular material. An experimental study of their structure and mechanical genesis. *Rock Mech* 9:95–144
- Maranhão N (1974) Observations upon rupture and post-rupture behaviour of rocks under uniaxial compression tests. In: *Proc. 2<sup>nd</sup> Int. Congr. Int. Assoc. Eng Geol*, São Paulo, Aug. 1974, I, pp IV-2.1–IV-2.10
- Marder M, Gross SP (1995) Origin of crack tip instabilities. *J Mech Phys Solids* 43:1–48
- Marone C (1998a) The effect of loading rate on static friction and the rate of fault healing during the earthquake cycle. *Nature* 391:69–72
- Marone C (1998b) Laboratory-derived friction laws and their application to seismic faulting. *Ann Rev Earth Planet Sci* 26:643–696
- Marone CJ, Blanpied MLe (1994a) Faulting, friction, and earthquake mechanisms, Part I. *Pure Appl Geophys* 142:413–808
- Marone CJ, Blanpied MLe (1994b) Faulting, friction, and earthquake mechanisms, Part II. *Pure Appl Geophys* 143:1–511
- Marone C, Cox SJD (1994) Scaling of rock friction constitutive parameters: the effects of surface roughness and cumulative offset on friction of gabbro. *Pure Appl Geophys* 143:359–385
- Marone C, Kilgore B (1993) Scaling of the critical distance for seismic faulting with shear strain in fault zones. *Nature* 362:618–621
- Marone C, Raleigh CB, Scholz CH (1990) Frictional behavior and constitutive modeling of simulated fault gouge. *J Geophys Res* 95:7007–7025
- Marone C, Scholz CH, Bilham R (1991) On the mechanics of earthquake afterslip. *J Geophys Res* 96:8441–8452
- Marshall DB, McLaren AC (1977) Deformation mechanisms in experimentally deformed plagioclase feldspars. *Phys Chem Miner* 1:351–370
- Martin CD, Chandler NA (1994) The progressive fracture of Lac du Bonnet granite. *Int J Rock Mech Min* 31:643–659
- Martin RJ (1972) Time-dependent crack growth in quartz and its application to the creep of rocks. *J Geophys Res* 77:1406–1419
- Martin JB (1975) *Plasticity: fundamentals and general results*. The MIT Press, Cambridge, Mass., 931 pp
- Martin RJ (1980) Pore pressure stabilization of failure in Westerly granite. *Geophys Res Lett* 7:404–406
- Martin RJ (1992) The influence of hydrostatic and uniaxial stress on remanent magnetization. In: Evans B, Wong T-f (eds) *Fault mechanics and transport properties of rocks*. International Geophysics Series. Academic Press, London, pp 325–340

- Martin RJ, Durham WB (1975) Mechanisms of crack growth in quartz. *J Geophys Res* 80:4837–4844
- Martin RJ, Habermann RE, Wyss M (1978) The effect of stress cycling and inelastic volumetric strain on remanent magnetization. *J Geophys Res* 83:3485–3496
- Martin RJ, Wyss M (1975) Magnetism of rocks and volumetric strain in uniaxial failure tests. *Pure Appl Geophys* 113:51–61
- Maso J-C, Lerau J (1980) Mechanical behavior of Darney sandstone (Vosges, France) in biaxial compression. *Int J Rock Mech Min* 17:109–115
- Masuda K (2001) Effects of water on rock strength in a brittle regime. *J Struct Geol* 23:1653–1657
- Masuda K, Mizutani H, Yamada I (1987) Experimental study of strain-rate dependence of failure properties of granite. *J Phys Earth* 35:37–66
- Masuda K, Arai T, Fujimoto K, Shigematsu N (2002) Physical and rheological properties of fault zone rocks, mylonite, under high pressure and high temperature. *EOS Trans AGU* 83, Fall Meet. Suppl., abstract T21A-1076 (p F1372)
- Masure P (1970) Comportement mécanique des roches à anisotropie planaire discontinue. In: Proc. 2<sup>nd</sup> Congr. Int. Soc. Rock Mech., Belgrade, Sept. 1970. I, pp 197–207
- Matsushima S (1960a) On the flow and fracture of igneous rocks and on the deformation and fracture of granite under high confining pressure. *Disaster Prevention Res Inst Kyoto Bull* 36, 20 pp
- Matsushima S (1960b) Variation of the elastic wave velocities of rocks in the process of deformation and fracture under high pressure. *Disaster Prevention Res Inst Kyoto Bull* 32, 8 pp
- Maugis D (1985) Subcritical crack growth, surface energy, fracture toughness, stick-slip and embrittlement. *J Mater Sci* 20:3041–3073
- Maurer WC (1965) Shear failure of rock under compression. *J Soc Petrol Eng AIME* 5:167–176
- Maurer WC (1966) Shear failure of rock under axial and hydrostatic pressure. In: Proc. 1<sup>st</sup> Congr. Int. Soc. Rock Mech., Lisbon, 1966, I, pp 337–341
- Mavko G, Mukerji T, Dvorkin J (1998) *The rock physics handbook: tools for seismic analysis in porous media*. Cambridge University Press, Cambridge, 329 pp
- Mazanti BB, Sowers GF (1966) Laboratory testing of rock strength. In: *Testing techniques for rock mechanics*. Am Soc Test Mat STP 402:207–227
- McCabe WM, Koerner RM (1975) High pressure shear strength investigation of an anisotropic mica schist rock. *Int J Rock Mech Min* 12:219–228
- McCarter MK, Willson JE (1973) Strength versus energy dissipation in sandstone. In: Hardy HR, Stefanko R (eds) *New horizons in rock mechanics*. Proc. 14<sup>th</sup> Symp. Rock Mech., Penn. State Univ. June 1972. Am Soc Civ Eng, pp 223–245
- McClintock FA, Argon AS (1966) *Mechanical behaviour of materials*. Addison-Wesley, Reading, Mass., 770 pp
- McClintock FA, Irwin GR (1965) Plasticity aspects of fracture mechanics. In: *Fracture toughness testing and its applications*. Am Soc Test Mat, Spec Tech Publ 381:84–113
- McClintock FA, Mayson HJ (1977) Principal stress effects on brittle crack statistics. In: Cowin SC, Carroll MM (eds) *The effects of voids on material deformation*. 1976 Appl. Mech. Div. Meeting, Utah: New York, Am. Soc. Mech. Eng., Appl Mech Symp Series AMD 16:31–45
- McClintock FA, Walsh JB (1962) Friction on Griffith cracks in rocks under pressure. In: Proc. 4<sup>th</sup> U.S. Nat. Congr. Appl. Mech.: New York, Am. Soc. Mech. Eng., II, pp 1015–1021
- McClintock FA, Zaverl F (1979) An analysis of the mechanics and statistics of brittle crack initiation. *Int J Fracture* 15:107–118
- McEwen TJ (1981) Brittle deformation in pitted pebble conglomerates. *J Struct Geol* 3:25–37
- McGill GE, Raney JA (1970) Experimental study of faulting in an anisotropic, inhomogeneous dolomitic limestone. *Geol Soc Am Bull* 81:2949–2958
- McKavanagh B, Stacey FD (1974) Mechanical hysteresis in rocks at low strain amplitudes and seismic frequencies. *Phys Earth Planet In* 8:246–250
- McKenzie D, Brune JN (1972) Melting on fault planes during large earthquakes. *Geophys J Roy Astr S* 29:65–78
- McLamore R, Gray KE (1967) The mechanical behaviour of anisotropic sedimentary rocks. *J Eng Ind-T ASME* 89:62–73
- McLaughlin R (1977) A study of the differential scheme for composite materials. *Int J Eng Sci* 15:237–244

- McWilliams JR (1966) The role of microstructure in the physical properties of rock. In: Testing techniques for rock mechanics. *Am Soc Test Mat STP* 402:175–189
- Mead WJ (1925) The geologic role of dilatancy. *J Geol* 33:685–698
- Meade C, Jeanloz R (1991) Deep-focus earthquakes and recycling of water into the earth's mantle. *Science* 252:68–72
- Meglis IL, Chow TM, Young RP (1995) Progressive microcrack development in tests on Lac du Bonnet granite – I. Acoustic emission source location and velocity measurements. *Int J Rock Mech Min* 32:741–750
- Meglis IL, Greenfield RJ, Engelder T, Graham EK (1996) Pressure dependence of velocity and attenuation and its relationship to crack closure in crystalline rocks. *J Geophys Res* 101:17523–17533
- Mehrabadi MM, Nemat-Nasser S, Shodja HM, Subhash G (1988) Some basic theoretical and experimental results on micromechanics of granular flow. In: Satake M, Jenkins JT (eds) *Micromechanics of granular materials*. Proc U.S./Japan Seminar, Sendai-Zao, Japan, Oct 26–30, 1987. Elsevier, Amsterdam, pp 253–262
- Mellor M (1973) Mechanical properties of rocks at low temperatures. In: *Permafrost. The North American Contribution to the Second International Conference*. Washington, D.C., Nat. Acad. Sci., pp 334–344
- Mellor M, Hawkes I (1971) Measurement of tensile strength by diametral compression of discs and annuli. *Eng Geol* 5:173–225
- Menéndez B, Zhu W, Wong T-f (1996) Micromechanics of brittle faulting and cataclastic flow in Berea sandstone. *J Struct Geol* 18:1–16
- Meredith PG (1990) Fracture and failure of brittle polycrystals: an overview. In: Barber DJ, Meredith PG (eds) *Deformation processes in minerals, ceramics and rocks*. Unwin Hyman, London, pp 5–47
- Meredith PG, Atkinson BK (1983) Stress corrosion and acoustic emission during tensile crack propagation in Whin Sill dolerite and other basic rocks. *Geophys J Roy Astr S* 75:1–21
- Meredith PG, Main IG, Jones C (1990) Temporal variations in seismicity during quasi-static and dynamic rock fracture. *Tectonophysics* 175:249–268
- Mesri G, Adachi K, Ullrich CR (1976) Pore-pressure response in rock to undrained change in all-round stress. *Géotechnique* 26:317–330
- Mikumo T, Olsen KB, Fukuyama E, Yagi Y (2003) Stress-breakdown time and slip-weakening distance inferred from slip-velocity functions on earthquake faults. *B Seismol Soc Am* 93:262–282
- Mindlin RD (1949) Compliance of elastic bodies in contact. *J Appl Mech-ASME* 16:259–268
- Mitchell JK (1991) Conduction phenomena: from theory to geotechnical practice. *Géotechnique* 41:299–340
- Mitchell JK (1993) *Fundamentals of soil behavior*. John Wiley, New York, 437 pp
- Mitchell T, Brace WF (1973) Electrical resistivity of partially saturated rocks. *EOS Trans AGU* 54:1209 (abstract)
- Mitra G (1978) Ductile deformation zones and mylonites: the mechanical processes involved in the deformation of crystalline basement rocks. *Am J Sci* 278:1057–1084
- Mizutani H, Ishido T, Yokokura T, Ohnishi (1976) Electrokinetic phenomena associated with earthquakes. *Geophys Res Lett* 3:365–368
- Mjachkin VI, Brace WF, Sobolev GA, Dieterich JH (1975) Two models for earthquake forerunners. *Pure Appl Geophys* 113:169–181
- Mjachkin VI, Sobolev GA, Dolbilkina NA, Morozov VN, Preobrazensky VG (1972) The study of variations in geophysical fields near focal zones of Kamchatka. *Tectonophysics* 14:287–293
- Mogi K (1959) Experimental study of deformation and fracture of marble. I. On the fluctuation of compressive strength of marble and the relation to the rate of stress application. *B Earthq Res I Tokyo* 37:155–170
- Mogi K (1962a) The influence of the dimensions of specimens on the fracture strength of rocks. *B Earthq Res I Tokyo* 40:175–185
- Mogi K (1962b) Magnitude-frequency relation for elastic shocks accompanying fractures of various materials and some related problems in earthquakes. *B Earthq Res I Tokyo* 40:831–853
- Mogi K (1962c) Study of elastic shocks caused by the fracture of heterogeneous materials and its relations to earthquake phenomena. *B Earthq Res I Tokyo* 40:125–173

- Mogi K (1965) Deformation and fracture of rocks under confining pressure (2). Elasticity and plasticity of some rocks. *B Earthq Res I Tokyo* 43:349–379
- Mogi K (1966a) Pressure dependence of rock strength and transition from brittle fracture to ductile flow. *B Earthq Res I Tokyo* 44:215–232
- Mogi K (1966b) Some precise measurements of fracture strength of rocks under uniform compressive stress. *Felsmechanik und Ingenieurgeologie* 4:41–55
- Mogi K (1967a) Earthquakes and fractures. *Tectonophysics* 5:35–55
- Mogi K (1967b) Effect of the intermediate principal stress on rock failure. *J Geophys Res* 72:5117–5131
- Mogi K (1969) Laboratory study of elastic shocks prior to rock failure. *Trans Am Geophys Union* 50:401 (abstract)
- Mogi K (1971a) Effect of the triaxial stress system on the failure of dolomite and limestone. *Tectonophysics* 11:111–127
- Mogi K (1971b) Fracture and flow of rocks under high triaxial compression. *J Geophys Res* 76:1255–1269
- Mogi K (1972a) Effect of the triaxial stress system on fracture and flow of rocks. *Phys Earth Planet Int* 5:318–324
- Mogi K (1972b) Fracture and flow of rocks. *Tectonophysics* 13:541–568
- Mogi K (1974a) On the pressure dependence of strength of rocks and the Coulomb fracture criterion. *Tectonophysics* 21:273–285
- Mogi K (1974b) Rock fracture and earthquake prediction (in Japanese). *J Soc Mater Sci Japan* 23:320–331 (a summary in English of the “dry” dilatancy model is given in: Rikitake T (ed) *Earthquake prediction*. Amsterdam. Elsevier 1976, pp 243–244)
- Mogi K (1977) Dilatancy of rocks under general triaxial stress states with special reference to earthquake precursors. *J Phys Earth* 25:S203–S217
- Mohr O (1900) Welche Umstände bedingen die Elastizitätsgrenze und den Bruch eines Materiales? *Z Verein Deutsch Ing* 44:1524–1530, 1572–1577
- Mollema PN, Antonellini MA (1996) Compaction bands: a structural analog for anti-mode-I cracks in aeolian sandstone. *Tectonophysics* 267:209–228
- Montgomery CW, Brace WF (1975) Micropores in plagioclase. *Contrib Mineral Petr* 52:17–28
- Montoto M (1974) Fatigue in rocks: failure and internal fissuration of Barre granite under loads cyclically applied. In: *Advances in Rock Mechanics*. Proc. 3<sup>rd</sup> Congr. Int. Soc. Rock Mech., Denver, 1974. Washington, D.C., Nat. Acad. Sci., II, Part A, pp 379–384
- Montoto M, Martinez-Nistal A, Rodriguez-Rey A, Fernandez-Merayo N, Soriono P (1995) Microfractography of granitic rocks under confocal scanning laser microscopy. *J Microsc* 177:138–149
- Moore WL (1961) Role of fluid pressure in overthrust faulting: a discussion. *Geol Soc Am Bull* 72:1581–1586
- Moore DE, Lockner DA (1995) The role of microcracking in shear-fracture propagation in granite. *J Struct Geol* 17:95–114
- Moore DE, Lockner DA (2004) Crystallographic controls on the frictional behavior of dry and water-saturated sheet structure minerals. *J Geophys Res* 109, B03401, doi: 10.1029/2003JB002582 (16 pp)
- Moore DE, Morrow CA, Byerlee JD (1986) High-temperature permeability and groundwater chemistry of some Nevada Test Site Tuffs. *J Geophys Res* 91:2163–2171
- Moore DE, Summers R, Byerlee JD (1989) Sliding behavior and deformation textures of heated illite gouge. *J Struct Geol* 11:329–342
- Moore DE, Liu L, Lockner D, Byerlee JD (1993) Permeability of granite at elevated temperatures. *EOS Trans AGU* 74:568
- Moore DE, Lockner DA, Ma S, Summers R, Byerlee JD (1997) Strengths of serpentinite gouges at elevated temperatures. *J Geophys Res* 102:14787–14801
- Moore DE, Lockner DA, Summers R, Ma S, Byerlee JD (1996) Strength of chrysotile-serpentinite gouge under hydrothermal conditions: can it explain a weak San Andreas fault? *Geology* 24:1041–1044
- Moore DE, Ma J, Summers R, Byerlee JD (1984) The effects of strain rate and pore pressure on the strength and stability of a serpentine gouge. In: Dowding F, Singh M (eds) *Rock mechanics in productivity and protection*. Proc 25<sup>th</sup> U.S. Symposium on Rock Mechanics, pp 312–319
- Mordecai M, Morris LH (1971) An investigation into the changes of permeability occurring in a sandstone when failed under triaxial stress conditions. In: Clark GB (ed) *Dynamic rock mechanics*. Proc. 12<sup>th</sup> Symp. Rock Mech., Rolla, Missouri 1970. A.I.M.E., New York, pp 221–239

- Morgan JK (1999) Numerical simulations of granular shear zones using the distinct element method. 2. Effects of particle size distribution and interparticle friction on mechanical behaviour. *J Geophys Res* 104:2721–2732
- Morgan JK, Boettcher MS (1999) Numerical simulations of granular shear zones using the distinct element method. 1. Shear zone kinematics and the micromechanics of localization. *J Geophys Res* 104:2703–2719
- Morgan FD, Williams ER, Madden TR (1989) Streaming potential properties of Westerly granite with applications. *J Geophys Res* 94:12449–12461
- Morgenstern NR, Phukan ALT (1966) Non-linear deformation of a sandstone. In: Proc. 1<sup>st</sup> Congr. Int. Soc. Rock Mech., Lisbon, 1966, I, pp 543–548
- Morgenstern NR, Phukan ALT (1969) Non-linear stress-strain relations for a homogeneous sandstone. *Int J Rock Mech Min* 6:127–142
- Morin RH, Olsen HW (1987) Theoretical analysis of the transient pressure response from a constant flow rate hydraulic conductivity test. *Water Resour Res* 23:1461–1470
- Morland LW (1972) A simple constitutive theory for a fluid-saturated porous solid. *J Geophys Res* 77:890–900
- Morlier P (1971a) Description de l'état de fissuration d'une roche à partir d'essais non-destructifs simples. *Rock Mech* 3:125–138
- Morlier P (1971b) Sur le comportement des roches fragiles avant la rupture. In: Rock fracture. Proc. Int. Symp. Rock Mech., Nancy., pp Paper I-4 (10 pp)
- Morrow CA, Byerlee JD (1989) Experimental studies of compaction and dilatancy during frictional sliding on faults containing gouge. *J Struct Geol* 11:815–825
- Morrow C, Moore D, Lockner D (1997) Permeability reduction in granite under hydrothermal conditions. *EOS Trans AGU* 78:F711
- Morrow C, Radney B, Byerlee J (1992) Frictional strength and the effective pressure law of montmorillonite and illite clays. In: Evans B, Wong T-f (eds) Fault mechanics and transport properties of rocks. International Geophysics Series. Academic Press, London, pp 69–88
- Morrow CA, Shi LQ, Byerlee JD (1981) Permeability and strength of San Andreas fault gouge under high pressure. *Geophys Res Lett* 8:325–328
- Morrow CA, Shi LQ, Byerlee JD (1982) Strain hardening and strength of clay-rich fault gouges. *J Geophys Res* 87:6771–6780
- Morrow CA, Shi LQ, Byerlee JD (1984) Permeability of fault gouge under confining pressure and shear stress. *J Geophys Res* 89:3193–3200
- Morrow CA, Zhang B-C, Byerlee JD (1986) Effective pressure law for permeability of Westerly granite under cyclic loading. *J Geophys Res* 91:3870–3876
- Morrow C, Lockner D, Moore D, Byerlee J (1981) Permeability of granite in a temperature gradient. *J Geophys Res* 86:3002–3008
- Mosher S, Berger RL, Anderson DE (1975) Fracturing characteristics of two granites. *Rock Mech* 7:167–176
- Moss WC, Gupta YM (1982) A constitutive model describing dilatancy and failure in brittle rock. *J Geophys Res* 87:2985–2998
- Mott NF (1948) Brittle fracture in mild-steel plates. *Engineering-London* 165:16–18
- Mraz GJ, Nisbett EG (1980) Design, manufacture and safety aspects of forged vessels for high-pressure services. *J Press Vess-Z ASME* 102:98–106
- Mroz Z (1963) Non-associated flow laws in plasticity. *J Mecanique* 2:21–42
- Mühlhaus H-B, Vardoulakis I (1987) The thickness of shear bands in granular materials. *Géotechnique* 37:271–283
- Mukerji T, Berryman J, Mavko G, Berge P (1995) Differential effective medium modeling of rock elastic moduli with critical porosity constraints. *Geophys Res Lett* 22:555–558
- Müller P, Siemes H (1972) Zur Festigkeit and Gefügeregelung von experimentell verformten Magnetit-erzen. *Neues Jb Miner Abh* 117:39–60
- Mura T (1987) Micromechanics of defects in solids, 2<sup>nd</sup> ed. Nijhoff, The Hague
- Murrell SAF (1958) The strength of coal under triaxial compression. In: Walton WH (ed) Mechanical properties of non-metallic brittle materials. Butterworths, London, pp 123–145
- Murrell SAF (1963) A criterion for brittle fracture of rocks and concrete under triaxial stress, and the effect of pore pressure on the criterion. In: Fairhurst C (ed) Rock mechanics. 5<sup>th</sup> Symp. Rock Mechanics. Pergamon Press, Oxford, pp 563–577

- Murrell SAF (1964) The theory of the propagation of elliptical Griffith cracks under various conditions of plane strain or plane stress. *Br J Appl Phys* 15:1195–1223
- Murrell SAF (1965) The effect of triaxial stress systems on the strength of rocks at atmospheric temperatures. *Geophys J Roy Astr S* 10:231–281
- Murrell SAF (1967a) The effect of triaxial stress systems on brittle fracture and on the brittle-ductile transition. In: *Conf. Physical Basis of Yield and Fracture*, Oxford, 1966, Inst. of Phys. and The Phys. Soc. (London), Conf. Series No. 1, pp 225–234
- Murrell SAF (1967b) The effects of triaxial stress systems on the fracture of rocks and on the nature of faulting and earthquakes. *Geophys J Roy Astr S* 14:81–87
- Murrell SAF (1971) Micromechanical basis of the deformation and fracture of rocks. In: Te'eni M (ed) *Structure, solid mechanics and engineering design*. Proc. Southampton 1969 Civil Eng. Materials Conf. Wiley-Interscience, London, pp 239–248
- Murrell SAF (1990) Brittle-to-ductile transitions in polycrystalline non-metallic materials. In: Barber DJ, Meredith PG (eds) *Deformation processes in minerals, ceramics and rocks*. Unwin Hyman, London, pp 109–137
- Murrell SAF, Chakravarty S (1973) Some new rheological experiments on igneous rocks at temperatures up to 1120 °C. *Geophys J Roy Astr S* 34:211–250
- Murrell SAF, Digby PJ (1970) The theory of brittle fracture initiation under triaxial stress conditions. I and II. *Geophys J Roy Astr S* 19:309–334; 499–512
- Murrell SAF, Digby PJ (1972) The thermodynamics of brittle fracture initiation under triaxial stress conditions. *Int J Fract Mech* 8:167–173
- Murrell SAF, Ismail IAH (1976a) The effect of decomposition of hydrous minerals on the mechanical properties of rocks at high pressures and temperatures. *Tectonophysics* 31:207–258
- Murrell SAF, Ismail IAH (1976b) The effect of temperature on the strength at high confining pressure of granodiorite containing free and chemically-bound water. *Contrib Mineral Petr* 55:317–330
- Musgrave MJP (1970) *Crystal acoustics*: San Francisco. Holden-Day, 288 pp
- Myer LR, Kemeny JM, Zheng Z, Suarez R, Ewy RT, Cook NGW (1992) Extensile cracking in porous rock under differential compressive stress. *Appl Mech Rev* 45:263–280
- Nabarro FRN (1948) Deformation of crystals by the motion of single ions. In: Report of a conference on strength of solids (Bristol). The Physical Society, London, pp 75–90
- Nagumo S, Hoshino K (1967) Occurrence of micro-fracturing shocks during rock deformation with a special reference to activity of earthquake swarms. *B Earthq Res I Tokyo* 45:1295–1311
- Nakatani M (1998) A new mechanism of slip weakening and strength recovery of friction associated with the mechanical consolidation of gouge. *J Geophys Res* 103:27239–27256
- Nakatani M (2001) Conceptual and physical clarification of rate and state friction: frictional sliding as a thermally activated rheology. *J Geophys Res* 106:13347–13380
- Nakatani M, Mochizuki H (1996) Effect of shear stress applied to surfaces in stationary contact on rock friction. *Geophys Res Lett* 23:869–872
- Nasuno S, Kudrolli A, Bak A, Gollub JP (1998) Time-resolved studies of stick-slip friction in sheared granular layers. *Phys Rev E* 58:2161–2171
- Neff TL (1966) Equipment for measuring pore pressure in rock specimens under triaxial load. In: *Testing techniques for rock mechanics*. Am Soc Test Mat STP 402, pp 3–17
- Nelson AC, Wang CY (1976) A new method for examining internal crack structure of stressed rocks. *EOS Trans AGU* 57:159 (abstract)
- Nelson RA (1981) A discussion of the approximation of subsurface (burial) stress conditions in laboratory experiments. In: Carter NL, Friedman M, Logan JM, Stearns DW (eds) *Mechanical behavior of crustal rocks*. The Handin Volume. American Geophysical Union, Washington, D.C., geophysical monograph 24, pp 311–321
- Nemat-Nasser S (1985) Discussion of “Geometric probability approach to the characterization and analysis of microcracking in rocks” by Teng-fong Wong. *Mech Mater* 4:277–281
- Nemat-Nasser S, Horii H (1982) Compression-induced nonplanar crack extension with application to splitting, exfoliation, and rockburst. *J Geophys Res* 87:6805–6821
- Nemat-Nasser S, Obata M (1988) A microcrack model of dilatancy in brittle materials. *J Appl Mech-T ASME* 55:24–35



- Nesetova V, Lajtai EZ (1973) Fracture from compressive stress concentrations around elastic flaws. *Int J Rock Mech Min* 10:265–284
- Neuber H (1958) *Kerbspannungslehre*, 2<sup>nd</sup> ed. Springer-Verlag, Berlin Heidelberg New York, 226 pp
- Neuzil CE, Cooley C, Silliman SE, Bredehoft JD, Hsieh PA (1981) A transient laboratory method for determining the hydraulic properties of “tight” rocks – 2. Application. *Int J Rock Mech Min* 18: 253–258
- Newhall DH (1957) A new high pressure technique. *Ind Eng Chem* 49:1993–1995
- Newman K, Newman JB (1971) Failure theories and design criteria for plain concrete. In: Te’eni M (ed) *Structure, solid mechanics and engineering design*. Proc. Southampton 1969 Civil Eng. Materials Conf. Wiley-Interscience, London, pp 963–995
- Niandou H, Shao JF, Henry JP, Fourmaintraux D (1997) Laboratory investigation of the mechanical behaviour of Tournemire shale. *Int J Rock Mech Min* 34:3–16
- Nicolas A, Poirier JP (1976) *Crystalline plasticity and solid state flow in metamorphic rocks*. Wiley Interscience, London, 444 pp
- Nieh TG, Wadsworth J, Sherby OD (1997) *Superplasticity in metals and ceramics*. Cambridge University Press, New York, 273 pp
- Nishimatsu Y, Heroesewojo R (1974) Rheological properties of rocks under the pulsating loads. In: *Advances in rock mechanics*. Proc. 3<sup>rd</sup> Congr. Int. Soc. Rock Mech., Denver, 1974. Washington, D.C., Nat. Acad. Sci., II, Part A, pp 385–389
- Nishiyama T, Kusuda H (1994) Identification of pore spaces and microcracks using fluorescent resins. *Int J Rock Mech Min* 31:369–375
- Nishizawa O (1982) Seismic velocity anisotropy in a medium containing oriented cracks – transversely isotropic case. *J Phys Earth* 30:331–347
- Nishizawa O, Onai K, Kusunose K (1984) Hypocenter distribution and focal mechanism of AE events during tow stress stage creep in Yugawara andesite. *Pure Appl Geophys* 122:36–52
- Nissen H-U, Wessicken R (1970) Observation of superfine fabrics with the scanning microscope. In: Paulitch P (ed) *Experimental and natural rock deformation*. Springer-Verlag, Berlin Heidelberg New York, pp 263–271
- Niwa Y, Kobayashi S (1967) Failure criterion of cement mortar under triaxial compression. *Mem Fac Eng Kyoto Univ* 29:1–15
- Niwa Y, Kobayashi S, Koyanagi W (1967) Failure criterion of light-weight aggregate concrete subjected to triaxial compression. *Mem Fac Eng Kyoto Univ* 29:119–131
- Norris DK, Barron K (1969) Structural analysis of features on natural and artificial faults. In: Baer AJ, Norris DK (eds) *Proc. Conf. on Research in Tectonics*, Ottawa, March 1968. *Geol Soc Can Paper* 97:68–52, 136–167
- Nowick AS, Berry BS (1972) *Anelastic relaxation in crystalline solids*. Academic Press, New York, 677 pp
- Nur A (1971) Effects of stress on velocity anisotropy in rocks with cracks. *J Geophys Res* 76:2022–2034
- Nur A (1972) Dilatancy, pore fluids and premonitory variations of  $t_s/t_p$  travel times. *B Seismol Soc Am* 62:1217–1222
- Nur A (1975) A note on the constitutive law for dilatancy. *Pure Appl Geophys* 113:197–206
- Nur A, Byerlee JD (1971) An exact effective stress law for elastic deformation of rock with fluids. *J Geophys Res* 76:6414–6419
- Nur A, Simmons G (1969a) The effect of saturation on velocity in low porosity rocks. *Earth Planet Sc Lett* 7:183–193
- Nur A, Simmons G (1969b) The effect of viscosity of a fluid phase on velocity in low porosity rocks. *Earth Planet Sc Lett* 7:99–108
- Nur A, Simmons G (1969c) Stress-induced velocity anisotropy in rock: an experimental study. *J Geophys Res* 74:6667–6674
- Nur A, Simmons G (1970) The origin of small cracks in igneous rocks. *Int J Rock Mech Min* 7: 307–314
- Nur AM, Wang Z (eds) (1989) *Seismic and acoustic velocities in reservoir rocks, vol 1: Experimental studies*. Geophysics reprint series: Society of Exploration Geophysicists, Tulsa, Oklahoma, 405 pp
- O’Connell RJ, Budiansky B (1974) Seismic velocities in dry and saturated cracked solids. *J Geophys Res* 79:5412–5426

- O'Connell RJ, Budiansky B (1977) Viscoelastic properties of fluid-saturated cracked solids. *J Geophys Res* 82:5719–5735
- O'Connell RJ, Budiansky B (1978) Measures of dissipation in viscoelastic media. *Geophys Res Lett* 5:5–8
- Obert L, Brady BT, Schmechel FW (1976) The effect of normal stiffness on the shear resistance of rock. *Rock Mech* 8:57–72
- Obert L, Duvall W (1942) Use of subaudible noises for prediction of rock bursts. Part II. U.S. Bur. Min., Rep. Invest. 3564, 22 pp
- Obert L, Duvall W (1945) Microseismic method of predicting rock failure in underground mining. Part II. Laboratory experiments. U.S. Bur. Min., Rep. Invest. 3803, 14 pp
- Obert L, Windes SL, Duvall W (1946) Standardized tests for determining the physical properties of mine rock. U.S. Bur. Min., Rep. Invest. 3891, 67 pp
- Oda M (1978) Significance of fabric in granular mechanics. In: Cowin SC, Satake M (eds) *Proceedings of the U.S.-Japan Seminar on Continuum-Mechanical and Statistical Approaches in the Mechanics of Granular Materials*. Gakujutsu Bunken Fukyukai, Tokyo, pp 7–26
- Oda M (1982) Fabric tensor for discontinuous geologic materials. *Soils Found* 22:96–108
- Oda M, Konishi J, Nemat-Nasser S (1983) Experimental micromechanical evaluation of the strength of granular materials: effects of particle rolling. In: Jenkins JT, Satake M (eds) *Mechanics of granular materials: new models and constitutive relations*. Elsevier, Amsterdam, pp 21–39
- Odé H (1960) Faulting as a velocity discontinuity in plastic deformation. In: Griggs D, Handin J (eds) *Rock deformation*. Geol Soc Am Mem 79, pp 293–321
- Ofoegbu GI, Curren JH (1992) Deformability of intact rock. *Int J Rock Mech Min* 29:35–48
- Oglesby ML, Gutshall PL, Phillips JM (1976) Cleavage surface energy of selenite. *Am Mineral* 61:295–298
- Ohnaka M (1973a) Experimental studies of stick-slip and their application to the earthquake source mechanism. *J Phys Earth* 21:285–303
- Ohnaka M (1973b) The quantitative effect of hydrostatic confining pressure on the compressive strength of crystalline rocks. *J Phys Earth* 21:125–140
- Ohnaka M (1975) Frictional characteristics of typical rocks. *J Phys Earth* 23:87–112
- Ohnaka M (1983) Acoustic emission during creep of brittle rock. *Int J Rock Mech Min* 20:121–134
- Ohnaka M (1996) Nonuniformity of the constitutive law parameters for shear rupture and quasistatic nucleation to dynamic rupture: a physical model of earthquake generation processes. *P Natl Acad Sci USA* 93:3795–3802
- Ohnaka M, Kinoshita H (1968) Effects of uniaxial compression on remanent magnetization. *J Geomagn Goelectr* 20:93–99
- Ohnaka M, Kuwahara Y (1990) Characteristic features of local breakdown near a crack-tip in the transition zone from nucleation to unstable rupture during stick-slip shear failure. *Tectonophysics* 175:197–220
- Ohnaka M, Kuwahara Y, Yamamoto K (1987) Constitutive relations between dynamic physical parameters near a tip of the propagating slip zone during stick-slip shear failure. *Tectonophysics* 144:109–125
- Ohnaka M, Mogi K (1981) Frequency dependence of acoustic emission activity in rocks under incremental, uniaxial compression. *B Earthq Res I Tokyo* 56:67–89
- Ohnaka M, Mogi K (1982) Frequency characteristics of acoustic emission in rocks under uniaxial compression and its relation to the fracturing process to failure. *J Geophys Res* 87:3873–3884
- Ohnaka M, Shen L-f (1999) Scaling of the shear rupture process from nucleation to dynamic propagation: implications of geometric irregularity of the rupturing surfaces. *J Geophys Res* 104:817–844
- Ohnaka M, Akatsu M, Mochizuki H, Odedra A, Tagashira F, Yamamoto Y (1997) A constitutive law for the shear failure of rock under lithospheric conditions. *Tectonophysics* 277:1–27
- Ohnaka M, Kuwahara Y, Yamamoto K, Hirasawa T (1986) Dynamic breakdown processes and the generating mechanism for high-frequency elastic radiation during stick-slip instabilities. In: *Earthquake source mechanics*. AGU, Washington, D.C., *Geophys Monograph* 37 (Maurice Ewing 6), pp 13–24
- Okubo PG (1989) Dynamic rupture modeling with laboratory-derived constitutive laws. *J Geophys Res* 94:12321–12335
- Okubo PG, Dieterich JH (1981) Fracture energy of stick-slip events in a large scale biaxial experiment. *Geophys Res Lett* 8:887–890
- Okubo PG, Dieterich JH (1984) Effects of physical fault properties on frictional instabilities produced on simulated faults. *J Geophys Res* 89:5817–5827

- Okubo PG, Dieterich JH (1986) State variable fault constitutive relations for dynamic slip. In: Das S (ed) Earthquake source mechanics. AGU, Washington, D.C., Geophys Monograph 37 (Maurice Ewing 6), pp 25–35
- Okubo S, Fukui K (1996) Complete stress-strain curves for various rock types in uniaxial tension. *Int J Rock Mech Min* 33:549–556
- Okubo S, Nishimatsu Y (1985) Uniaxial compression testing using a linear combination of stress and strain as the control variable. *Int J Rock Mech Min* 22:323–330
- Okubo S, Nishimatsu Y, Fukui K (1991) Complete creep curves under uniaxial compression. *Int J Rock Mech Min* 28:77–82
- Okubo S, Nishimatsu Y, He C (1990) Loading rate dependence of class II rock behaviour in uniaxial and triaxial compression tests – an application of a proposed new control method. *Int J Rock Mech Min* 27:559–562
- Okui Y, Horii H (1997) Stress and time-dependent failure of brittle rocks under compression: a theoretical prediction. *J Geophys Res* 102:14869–14881
- Okui Y, Horii H, Akiyama N (1993) A continuum theory for solids containing microdefects. *Int J Eng Sci* 31:735–749
- Okusa S (1971) Experimental study on the strength of rocks with a cutting plane. *J Geol Soc Japan* 77:183–192
- Olgaard DL, Ko S-c, Wong T-f (1995) Deformation and pore pressure in dehydrating gypsum under transiently drained conditions. *Tectonophysics* 246:237–248
- Olsen KB, Madariaga R, Archuleta RJ (1997) Three-dimensional dynamic simulation of the 1992 Landers earthquake. *Science* 278:834–838
- Olsen MP, Brandon MT, Gordon RB (1995) Direct measurement of volume strain during experimental deformation of porous materials. *Int J Rock Mech Min* 32:371–373
- Olsson WA (1974a) Effects of temperature, pressure and displacement rate on the frictional characteristics of a limestone. *Int J Rock Mech Min* 11:267–278
- Olsson WA (1974b) Microfracturing and faulting in a limestone. *Tectonophysics* 24:277–285
- Olsson WA (1975) Energy transfer during tensile fracture propagation in quartzite. *EOS Trans AGU* 56:601 (abstract)
- Olsson WA (1991) The compressive strength of tuff as a function of strain rate from  $10^{-6}$  to  $10^3$ /sec. *Int J Rock Mech Min* 28:115–118
- Olsson WA (1992) The formation of a yield-surface vertex in rock. In: Tillerson JR, Wawersik WR (eds) *Rock mechanics. Proc. of the 33<sup>rd</sup> U.S. Symposium. A. A. Balkema, Rotterdam*, pp 701–705
- Olsson WA (1999) Theoretical and experimental investigation of compaction bands in porous rock. *J Geophys Res* 104:7219–7228
- Olsson WA, Holcomb DJ (2000) Compaction localization in porous rock. *Geophys Res Lett* 27:3537–3540
- Olsson WA, Peng SS (1976) Microcrack nucleation in marble. *Int J Rock Mech Min* 13:53–59
- Ohnaka M (1978) Application of some dynamic properties of stick-slip to earthquakes. *Geophys J R Astr Soc* 53:311–318
- Ord A, Vardoulakis I, Kajewski R (1991) Shear band formation in Gosford sandstone. *Int J Rock Mech Min* 28:397–409
- Orowan E (1944) The fatigue of glass under stress. *Nature* 154:341
- Orowan E (1949) Fracture and strength of solids. *Rep Prog Phys* 12:185–232
- Orowan E (1960) Mechanism of seismic faulting. In: Griggs D, Handin J (eds) *Rock deformation. Geol Soc Am Mem* 79, pp 323–345
- Ortiz M (1989) Extraction of constitutive data from specimens undergoing strain localization. *J Eng Mech Div-ASCE* 115:1748–1760
- Osment PA, Packer KJ, Taylor MJ, Attard JJ, Carpenter TA, Hall LD, Herrod NJ, Doran SJ (1990) NMR imaging of fluids in porous solids. *Philos T Roy Soc A* 333:441–452
- Palmer AC, Rice JR (1973) The growth of slip surfaces in the progressive failure of overconsolidated clay slopes. *P Roy Soc Lond A Mat* 332:527–548
- Papamichos E (1999) Constitutive laws for geomaterials. *Oil Gas Sci Technol* 54:759–771
- Papka SD, Kyriakides S (1999) Biaxial crushing of honeycombs – Part 1: experiments. *Int J Solids Struct* 36:4367–4396
- Parate NS (1973) Influence of water on the strength of limestone. *Trans AIME Soc Min Eng* 254:127–131
- Paris PC, Sih GC (1965) Stress analysis of cracks. In: *Fracture toughness testing and its applications. Am Soc Test Mat, Spec Tech Publ* 381:30–81

- Park SK, Johnston MJS, Madden TR, Morgan FD, Morrison HF (1993) Electromagnetic precursors to earthquakes in the ULF band: a review of observations and mechanisms. *Rev Geophys* 31:117–132
- Paterson MS (1958) Experimental deformation and faulting in Wombeyan marble. *Geol Soc Am Bull* 69:465–476
- Paterson MS (1963) Secondary changes of length with pressure in experimentally deformed rocks. *P Roy Soc Lond A Mat* 271:57–87
- Paterson MS (1964a) Effect of pressure on Young's modulus and the glass transition in rubbers. *J Appl Phys* 35:176–179
- Paterson MS (1964b) Triaxial testing of materials at pressures up to 10 000 kg./sq. cm. (150 000 lb./sq. in.). *J Institution Engineers Australia* 36:23–29
- Paterson MS (1967) Effect of pressure on stress-strain properties of materials. *Geophys J Roy Astr S* 14:13–17
- Paterson MS (1969) The ductility of rocks. In: Argon AS (ed) *Physics of strength and plasticity*. M.I.T. Press, Cambridge, Mass., pp 377–392
- Paterson MS (1970) A high-pressure, high-temperature apparatus for rock deformation. *Int J Rock Mech Min* 7:517–526
- Paterson MS (1989) The interaction of water with quartz and its influence in dislocation flow – an overview. In: Karato, S-i, Toriumi M (eds) *Rheology of solids and of the Earth*: Oxford University Press, Oxford, pp 107–142
- Paterson MS (1990a) Rock deformation experimentation. In: Duba AG, Durham WB, Handin JW, Wang HF (eds) *The brittle-ductile transition in rocks*. The Heard Volume. American Geophysical Union, Washington, D.C., *Geophys Monograph* 56, pp 187–194
- Paterson MS (1990b) Superplasticity in geological materials. In: Mayo MJ, Kobayashi M, Wadsworth J (eds) *Superplasticity in metals, ceramics, and intermetallics*. Materials Research Society, Pittsburgh, Pa, 196:303–312
- Paterson MS (1995a) A granular flow approach to fine-grain superplasticity. In: Bradt RC, Brookes CA, Routbort JL (eds) *Plastic deformation of ceramics*. Plenum Press, New York, pp 279–283
- Paterson MS (1995b) A theory of granular flow accommodated by material transfer via an intergranular fluid. *Tectonophysics* 245:135–151
- Paterson MS, Chopra PN, Horwood GR (1982) The jacketing of specimens in high-temperature, high-pressure rock-deformation experiments. *High Temp–High Press* 14:315–318
- Paterson MS, Olgaard DL (2000) Rock deformation tests to large shear strains in torsion. *J Struct Geol* 22:1341–1358
- Paterson MS, Weaver CW (1970) Deformation of polycrystalline MgO under pressure. *J Am Ceram Soc* 53:463–471
- Paterson MS, Weiss LE (1966) Experimental deformation and folding in phyllite. *Geol Soc Am Bull* 77:343–374
- Paul B (1961) A modification of the Coulomb-Mohr theory of fracture. *J Appl Mech-T ASME* 28:259–268
- Paul B (1968) Macroscopic criteria for plastic flow and brittle fracture. In: Liebowitz H (ed) *Fracture*. Academic Press, IL, New York, pp 313–496
- Paul B, Gangal M (1967) Initial and subsequent fracture curves for biaxial compression of brittle materials. In: Fairhurst C (ed) *Failure and breakage of rock*. Proc. 8<sup>th</sup> Symp. on Rock Mech. Minnesota, Sept. 1966. A.I.M.E., New York, pp 113–141
- Peach CJ, Spiers CJ (1996) Influence of plastic deformation on dilatancy and permeability development in synthetic salt rock. *Tectonophysics* 256:101–128
- Peacock S, McCann C, Sothcott J, Astin TR (1994) Seismic velocities in fractured rocks: an experimental verification of Hudson's theory. *Geophys Prospect* 42:27–80
- Peggs GN (ed) (1983) *High pressure measurement techniques*. Appl Sci Publ, London, 404 pp
- Peng SD (1971) Stresses within elastic circular cylinders loaded uniaxially and triaxially. *Int J Rock Mech Min* 8:399–432
- Peng SS (1973) Time-dependent aspects of rock behaviour as measured by a servo-controlled hydraulic testing machine. *Int J Rock Mech Min* 10:235–246
- Peng SS (1975) A note on the fracture propagation and time-dependent behaviour of rocks in uniaxial tension. *Int J Rock Mech Min* 12:125–127

- Peng SS (1976) A photoelastic coating technique for rock fracture analysis. *Int J Rock Mech Min* 13:173–176
- Peng SS, Johnson AM (1972) Crackgrowth and faulting in cylindrical specimens of Chelmsford granite. *Int J Rock Mech Min* 9:37–86
- Peng SS, Ortiz CA (1973) Crack propagation and fracture of rock specimens loaded in compression. In: Sih GC (ed) *Conf. Dynamic Crack Propagation*. Lehigh Univ., 1972. Noordhoff Int. Publ., Leyden, pp 113–129
- Peng SS, Podnieks ER (1972) Relaxation and the behaviour of failed rock. *Int J Rock Mech Min* 9:699–712
- Peng SS, Podnieks ER, Cain PJ (1974) The behaviour of Salem limestone in cyclic loading. *J Soc Petrol Eng* 14:19–24
- Pérami R (1965) Sur les microfissures de roches soumises à des efforts uniaxiaux. *CR Acad Sci Paris* 260:1209–1212
- Pérami R (1971a) Comportement mécanique sous charge uniaxiale de roches déjà microfissurées thermiquement. In: *Rock fracture. Proc. Int. Symp. Rock Mech.*, Nancy, pp Paper II-14 (13 pp)
- Pérami R (1971b) Formation des microfissures dans les roches sous l'effet de variations homogènes de température. In: *Rock fracture. Proc. Int. Symp. Rock Mech.*, Nancy, pp Paper I-6 (11 pp)
- Pérami R, Farran J, Capdecemme L (1966) Mode de développement des microfissures dans les roches cristallines et notamment dans les granites soumis à des efforts uniaxiaux. In: *Proc. 1<sup>st</sup> Congr. Int. Soc. Rock Mech.*, Lisbon, 1966, I, pp 621–624
- Pérami R, Thénoz B (1969) Comparaison des comportements de divers granites soumis à des essais uniaxiaux de microfissuration. In: 2<sup>nd</sup> Coll. sur la Fissuration des Roches, Paris, Jan. 1969, *Revue de l'Industrie Minérale, Special Number* (July 1969), pp 50–62
- Perkins TK, Bartlett LE (1963) Surface energies of rocks measured during cleavage. *J Soc Petrol Eng AIME* 3:307–313
- Perkins RD, Green SJ, Friedman M (1970) Uniaxial stress behaviour in porphyritic tonalite at strain rates to  $10^3$ /second. *Int J Rock Mech Min* 7:527–535
- Perkins TK, Krech WW (1966) Effect of cleavage rate and stress level on apparent surface energies of rocks. *J Soc Petrol Eng AIME* 6:308–314
- Perrin G, Leblond JB (1993) Rudnicki and Rice's analysis of strain localization revisited. *J Appl Mech-ASME* 60:842–846
- Perrin G, Rice JR, Zheng G (1995) Self-healing slip pulse on a frictional surface. *J Mech Phys Solids* 43:1461–1495
- Persson BNJ (1998) *Sliding friction: physical principles and applications*. NanoScience and technology. Springer-Verlag, New York, 462 pp
- Persson BNJ (2000) *Sliding friction: physical principles and applications*. NanoScience and technology, 2<sup>nd</sup> ed. Springer-Verlag, New York, 515 pp
- Peselnick L, Liu H-P (1987) Laboratory measurement of internal friction in rocks and minerals at seismic frequencies. In: Sammis CG, Henyey TL (eds) *Methods of experimental physics*. Academic Press, Orlando, 24, Geophysics Part A, Laboratory Measurements, pp 31–56
- Peselnick L, Outerbridge WF (1961) Internal friction in shear and shear modulus of Solenhofen limestone over a frequency range of 107 cycles per second. *J Geophys Res* 66:581–588
- Peselnick L, Zietz I (1959) Internal friction of fine-grained limestones at ultrasonic frequencies. *Geophysics* 24:285–296
- Peselnick L, Dieterich JH, Mjachkin VI, Sobolev GA (1976) Variation of compressional velocities in simulated fault gouge under normal and direct shear stress. *Geophys Res Lett* 3:369–372
- Pestman BJ, van Munster JG (1996) An acoustic emission study of damage development and stress-memory effects in sandstone. *Int J Rock Mech Min* 33:585–593
- Petford N, Davidson G, Miller JA (1999) Pore structure determination using confocal scanning laser microscopy. *Phys Chem Earth Pt A* 24:563–567
- Phahey P, Dollinger G, Christie J (1972) Transmission electron microscopy of experimentally deformed olivine crystals. In: Heard HC, Borg IY, Carter NL, Raleigh CB (eds) *Flow and fracture of rocks*. American Geophysical Union, Washington, D.C., geophysical monograph 16, pp 117–138
- Piau M (1980) Crack-induced anisotropy and scattering in stressed rocks: effective moduli and attenuation. *Int J Eng Sci* 18:549–568
- Pickett G (1944) Application of the Fourier method to the solution of certain boundary problems in the theory of elasticity. *J Appl Mech-T ASME* 11:176–182

- Pinto da Cunha A (ed) (1990) Scale effects in rock masses. A. A. Balkema, Rotterdam, 337 pp
- Pittman ED, Duschatko RW (1970) Use of pore casts and scanning electron microscopy to study pore geometry. *J Sediment Petrol* 40:1153–1157
- Podnieks ER, Chamberlain PG, Thill RE (1972) Environmental effects on rock properties. In: Gray KE (ed) Basic and applied mechanics. Proc. 10<sup>th</sup> Symposium on Rock Mechanics, Austin, Texas, May 1968. New York, AIME, pp 215–241
- Poirier J-P (1980) Shear localization and shear instability in materials in the ductile field. *J Struct Geol* 2:135–142
- Poirier J-P (1985) Creep of crystals. Cambridge Univ Press, New York, 260 pp
- Pollard DD (1987) Elementary fracture mechanics applied to the structural interpretation of dykes. In: Halls HC, Fahrig WF (eds) Mafic dyke swarms. Geological Association of Canada, Special Paper 34, pp 5–24
- Pomeroy CD, Hobbs DW, Mahmoud A (1971) The effect of weakness-plane orientation on the fracture of Barnsley Hards by triaxial compression. *Int J Rock Mech Min* 8:227–238
- Popp T, Kern H, Schulze O (2001) Evolution of dilatancy and permeability in rock salt during hydrostatic compaction and triaxial deformation. *J Geophys Res* 106:4061–4078
- Pratt HR, Black AD, Brace WF (1974) Friction and deformation of jointed quartz diorite. In: Advances in rock mechanics. Proc. 3<sup>rd</sup> Congr. Int. Soc. Rock Mech., Denver, 1974. Washington, D.C., Nat. Acad. Sci., II, Part A, pp 306–310
- Pratt HR, Brown WS, Brace WF (1971) In situ determination of strength properties in a quartz diorite rock mass. In: Clark GB (ed) Dynamic rock mechanics. Proc. 12<sup>th</sup> Symp. Rock Mech., Rolla, Missouri, Nov. 1970. A.I.M.E., New York, pp 27–43
- Pratt HR, Black AD, Brown WS, Brace WF (1972) The effect of specimen size on the mechanical properties of unjointed diorite. *Int J Rock Mech Min* 9:513–529
- Pretorius JPG (1972) Weakness correlation and the size effect in rock strength tests. *J S Afr I Min Metall* 72:322–327
- Price DG, Knill JL (1966) A study of the tensile strength of isotropic rocks. In: Proc. 1<sup>st</sup> Congr. Int. Soc. Rock Mech., Lisbon, 1966, I, pp 439–442
- Price NJ (1960) The compressive strength of coal measure rocks. *Colliery Eng* 37:283–292
- Prikryl R (2001) Some microstructural aspects of strength variation in rocks. *Int J Rock Mech Min* 38:671–682
- Protodyakonov MM (1964) Methods of evaluating the cracked state and strength of rocks in situ. In: 4<sup>th</sup> Int. Conf. on Strata Control and Rock Mechanics, Henry Krumb School of Mines, Columbia University, New York City. (Supplementary paper: Transl. by H. Frisch, reproduced by Mines Branch, Dept. Min. Tech. Surv. Ottawa, Can., 1965 (DR FMP 65/11-MRL))
- Pugh SF (1967) The fracture of brittle materials. *Br J Appl Phys* 18:129–162
- Pugh HLD, Gunn DA (1964) A strain gauge load cell for use under high hydrostatic pressures: National Engineering Lab, Report No. 143, 16 pp
- Pyrak-Nolte LJ, Montemagno CD, Nolte DD (1997) Volumetric imaging of aperture distributions in connected fracture networks. *Geophys Res Lett* 24:2343–2346
- Raasch J (1971) On the determination of surface energy from cleavage experiments. *Int J Fract Mech* 7:289–300
- Rabinowicz E (1951) The nature of the static and kinetic coefficients of friction. *J Appl Phys* 22:1373–1379
- Rabinowicz E (1958) The intrinsic variables affecting the stick-slip processes. *Proc Phys Soc* 71:668–675
- Rabinowicz E (1995) Friction and wear of materials. John Wiley and Sons, New York, 315 pp
- Rai CS, Hanson KE (1988) Shear-wave velocity anisotropy in sedimentary rocks: a laboratory study. *Geophysics* 53:800–806
- Raj R (1993) Fundamental research in structural ceramics for service near 2 000 °C. *J Am Ceram Soc* 76:2147–2174
- Raleigh B, Marone C (1986) Dilatancy of quartz gouge in pure shear. In: Hobbs BE, Heard HC (eds) Mineral and rock deformation: laboratory studies. The Paterson Volume. American Geophysical Union, Washington, D.C., Geophys Monograph 36, pp 1–10
- Raleigh CB, Paterson MS (1965) Experimental deformation of serpentinite and its tectonic implications. *J Geophys Res* 70:3965–3985

- Ramana YV, Venkatanarayana B (1973) Laboratory studies on Kolar rocks. *Int J Rock Mech Min* 10:465–489
- Rao MVMS, Gogte BS (1972) Elasticity of some serpentinites. *Geophys Res Bull (India)* 10:41–52
- Rao MVMS, Ramana YV (1974) Dilatant behaviour of ultramafic rocks during fracture. *Int J Rock Mech Min* 11:193–203
- Rao MVMS, Ramana YV (1992) A study of progressive failure of rock under cyclic loading by ultrasonic and AE monitoring techniques. *Int J Rock Mech Min* 25:237–251
- Rawling GC, Baud P, Wong T-f (2002) Dilatancy, brittle strength and anisotropy of foliated rocks: experimental deformation and micromechanical modeling. *J Geophys Res* 107:2234, doi: 10.1029/2001JB000472 (14 pp)
- Rayleigh L (1934) The bending of marble. *P Roy Soc Lond A Mat* 144:266–279
- Raynaud S, Fabre D, Mazerolle F, Geraud Y, Latiere HJ (1989) Analysis of the internal structure of rocks and characterization of mechanical deformation by a non-destructive method: X-ray tomodesitometry. *Tectonophysics* 159:149–159
- Read MD, Meredith PG (1989) Permeability measurement techniques under hydrostatic and deviatoric stress conditions. In: Maury V, Fourmaintraux D (eds) *Rock at great depth*. A. A. Balkema, Rotterdam, 1, pp 211–217
- Read MD, Ayling MR, Meredith PG, Murrell SAF (1995) Microcracking during triaxial deformation of porous rocks monitored by changes in rock physical properties. II. Pore volumetry and acoustic emission measurements on water-saturated rocks. *Tectonophysics* 245:223–235
- Rehbinder PA, Schreiner LA, Zhigach KF (1948) Hardness reducers in drilling. (Translation of 1944 Russian Book). Council for Scientific and Ind. Res., Melbourne, 163 pp
- Reinen LA, Weeks JD (1993) Determination of rock friction constitutive parameters using an iterative least squares inversion method. *J Geophys Res* 98:15937–15950
- Reinen LA, Weeks JD, Tullis TE (1991) The frictional behavior of serpentinite: implications for aseismic creep on shallow crustal faults. *Geophys Res Lett* 18:1921–1924
- Reinen LA, Weeks JD, Tullis TE (1994) The frictional behavior of lizardite and antigorite serpentinites: experiments, constitutive models, and implications for natural faults. *Pure Appl Geophys* 143:317–358
- Renner J, Rummel F (1996) The effect of experimental and microstructural parameters on the transition from brittle failure to cataclastic flow of carbonate rocks. *Tectonophysics* 258:151–170
- Renshaw CE, Schulson EM (1998) Non-linear rate dependent friction under compression due to state variable friction. *Geophys Res Lett* 25:2205–2208
- Reymond MC (1975) Étude de la fissuration des éprouvettes sous contraintes en laboratoire et des massifs rocheux en carrières par une méthode d'émission acoustique. *Rock Mech* 7:1–16
- Reynolds O (1885) On the dilatancy of media composed of rigid particles in contact. *Phil Mag* 20:469–481. Reprinted in *Papers on Mechanical and Physical Subjects* by Osborne Reynolds. Cambridge: Univ. Press 1901, Vol. II, pp 203–216
- Reynolds O (1887) Experiments showing dilatancy, a property of granular material, possibly connected with gravitation. *Proc Roy Instn Great Britain* 11:354–363. Reprinted in *Papers on Mechanical and Physical Subjects* by Osborne Reynolds. Cambridge: Univ. Press 1901, Vol. II, pp 217–227
- Rhett DW, Teufel LW (1992) Stress path dependence of matrix permeability of North Sea sandstone reservoir rock. *Proc US Symp Rock Mechanics* 33:345–354
- Rice JR (1968) Mathematical analysis in the mechanics of fracture. In: Liebowitz H (ed) *Fracture*. Academic Press, II, New York, pp 191–311
- Rice JR (1975) Continuum mechanics and thermodynamics of plasticity in relation to microscale deformation mechanisms. In: Argon AS (ed) *Constitutive equations in plasticity*. The MIT Press, Cambridge, Mass, pp 23–79
- Rice JR (1976) The localization of plastic deformation. In: Koiter WT (ed) *Theoretical and applied mechanics*. North-Holland Publishing Company, Amsterdam, pp 207–220
- Rice JR (1978) Thermodynamics of the quasi-static growth of Griffith cracks. *J Mech Phys Solids* 26:61–78
- Rice JR (1980) The mechanics of earthquake rupture. In: Dziewonski AM, Boschi E (eds) *Physics of the Earth's interior*. Italian Physical Society, Bologna, pp 555–649
- Rice JR (1983) Constitutive relations for slip and earthquake instabilities. *Pure Appl Geophys* 121:443–475

- Rice JR (1992) Fault stress states, pore pressure distributions, and the weakness of the San Andreas fault. In: Evans B, Wong, T-f (eds) *Fault mechanics and transport properties of rocks*. International Geophysics Series. Academic Press, London, pp 475–503
- Rice JR (1993) Spatio-temporal complexity of slip on a fault. *J Geophys Res* 98:9885–9908
- Rice JR, Cleary MR (1976) Some basic stress-diffusion solutions for fluid-saturated elastic porous media with compressible constituents. *Rev Geophys* 14:227–241
- Rice JR, Lapusta N, Ranjith K (2001) Rate and state dependent friction and the stability of sliding between elastically deformable solids. *J Mech Phys Solids* 49:1865–1898
- Rice JR, Ruina AL (1983) Stability of steady frictional slipping. *J Appl Mech-ASME* 50:343–349
- Rice JR, Tse ST (1986) Dynamic motion of a single degree of freedom system following a rate and state dependent friction law. *J Geophys Res* 91:521–530
- Richardson E, Marone C (1999) Effects of normal stress vibrations on frictional healing. *J Geophys Res* 104:28859–28878
- Richardson RSH, Nolle H (1976) Surface friction under time-dependent loads. *Wear* 37:87–101
- Richter D, Simmons G (1977) Microscopic tubes in igneous rocks. *Earth Planet Sc Lett* 34:1–12
- Richter D, Simmons G, Siegfried RW (1975) Combined petrographic and scanning electron microscopy of microstructures in igneous rocks. *EOS Trans AGU* 56:447 (abstract)
- Riecker RE (1965) Fault plane features: an alternative explanation. *J Sediment Petrol* 35:746–748
- Riecker RE, Rooney TP (1966) Weakening of dunite by serpentine dehydration. *Science* 152:196–198
- Riecker RE, Rooney TP (1967) Shear strength and weakening of zeolitized tuffs from the Nevada test site, Nevada. *Am Mineral* 52:1174–1178
- Riecker RE, Rooney TP (1969) Water-induced weakening of hornblende and amphibolite. *Nature* 224:1299
- Riecker RE, Seifert KE (1964a) Olivine shear strength at high pressure and room temperature. *Geol Soc Am Bull* 75:571–574
- Riecker RE, Seifert KE (1964b) Shear deformation of upper-mantle mineral analogs: tests to 50 kilobars at 27 °C. *J Geophys Res* 69:3901–3911
- Riedel W (1929) Zur Mechanik geologischer Brucherscheinungen. *Zbl Mineral Geol Päl B* 354–368
- Rikitake T (1968) Earthquake prediction. *Earth-Sci Rev* 4:245–282
- Risnes R, Flaageng O (1999) Mechanical properties of chalk with emphasis on chalk-fluid interactions and micromechanical aspects. *Oil Gas Sci Technol* 54:751–758
- Robertson EC (1955) Experimental study of the strength of rocks. *Geol Soc Am Bull* 66:1275–1314
- Robin P-YF (1973) Note on effective pressure. *J Geophys Res* 78:2434–2437
- Robinson LH (1959) The effect of pore and confining pressure on the failure process in sedimentary rock. *Quart. Colo. School Min., 3<sup>rd</sup> Symposium on Rock Mechanics* 54:177–199
- Robinson LH (1967) Effect of hardness reducers on failure characteristics of rock. *J Soc Petrol Eng AIME* 7:295–299
- Robinson LH, Holland WE (1970) Some interpretation of pore fluid effects in rock failure. In: Somerton WH (ed) *Rock mechanics – theory and practice*. Proc. 11<sup>th</sup> Symp. Rock Mech., Berkeley, 1970. A.I.M.E., New York, pp 585–597
- Rodrigues FP (1966) Anisotropy of granites. Modulus of elasticity and ultimate strength ellipsoids, joint systems, slope attitudes, and their correlations. In: Proc. 1<sup>st</sup> Congr. Int. Soc. Rock Mech., Lisbon, 1966, I, pp 721–731
- Rodrigues FP (1970) Anisotropy of rocks. Most probably surfaces of the ultimate stresses and of the moduli of elasticity. In: Proc. 2<sup>nd</sup> Congr. Int. Soc. Rock Mech., Belgrade, 1, pp 133–142
- Rodrigues FP, Aires-Barros L (1970) Anisotropy of endogenetic rocks – correlation between micro-petrographic index, ultimate strength and modulus of elasticity ellipsoids. In: Proc. 2<sup>nd</sup> Congr. Int. Soc. Rock Mech., Belgrade, 1, pp 161–164
- Rodriguez-Rey A, Briggs GAD, Field TA, Montoto M (1989) Acoustic microscopy of rock. *J Microsc* 160:21–29
- Roeloffs E (1996) Poroelastic techniques in the study of earthquake-related hydrologic phenomena. In: Dmoska R, Saltzman B (eds) *Advances in Geophysics*, Vol. 37. Academic, San Diego, pp 135–195
- Rooke DP, Cartwright DJ (1976) *Compendium of stress intensity factors*. Her Majesty's Stationery Office, London, 330 pp



- Ros M, Eichinger A (1949) Die Bruchgefahr fester Körper bei ruhender – statischer – Beanspruchung (Ergebnisse der an der Eig. Materialprüfungs- und Versuchsanstalt für Industrie, Bauwesen und Gewerbe von 1925–1949 durchgeführten Untersuchungen). Eidgenössische Materialprüfungs- und Versuchsanstalt für Industrie, Bauwesen und Gewerbe, Zürich, Bericht Nr. 172, 246 pp
- Rosakis AJ (2002) Interersonic shear cracks and fault ruptures. *Adv Phys* 51:1189–1257
- Rosakis AJ, Samudrala O, Cokjer D (1999) Cracks faster than the speed of sound. *Science* 284:1337–1340
- Rose LRF (1976) Recent theoretical and experimental results on fast brittle fracture. *Int J Fracture* 12:799–813
- Rosengren KJ, Jaeger JC (1968) The mechanical properties on an interlocked low-porosity aggregate. *Géotechnique* 18:317–326
- Ross-Brown DM, Walton G (1975) A portable shear box for testing rock joints. *Rock Mech* 7:129–153
- Rothenburg L, Bathurst RJ (1992) Effects of particle shape on micromechanical behavior of granular materials. In: Shen HH, et al. (eds) *Advances in micromechanics of granular materials*. Elsevier Science Publishers, Amsterdam, pp 343–352
- Rothman RL, Greenfield RJ, Hardy HR (1975) Quantitative interpretation of velocity variations caused by stress-induced tension cracks. *EOS Trans AGU* 56:447 (abstract)
- Rothman RL, Greenfield RJ, Hardy HR (1976) Cyclic loading and dilatancy as indicated by P-wave velocity changes. *EOS Trans AGU* 57:1010 (abstract)
- Rowcliffe DJ, Frühauf V (1977) The fracture of jade. *J Mater Sci* 12:35–42
- Rowe PW (1962) The stress-dilatancy relation for static equilibrium of an assembly of particles in contact. *P Roy Soc Lond A Mat* 269:500–527
- Rubey WW, Hubbert MK (1959) Role of fluid pressure in mechanics of overthrust faulting. II. Overthrust belt in geosynclinal area of Western Wyoming in light of fluid-pressure hypothesis. *Geol Soc Am Bull* 70:167–206
- Rudnicki JW (1977) The effect of stress-induced anisotropy on a model of brittle rock failure as localization of deformation. In: *Energy resources and excavation technology; Proc. 18<sup>th</sup> U.S. Symposium on Rock Mechanics: Keystone, Colo.*, pp 1–8
- Rudnicki JW (1980) Fracture mechanics applied to the Earth's crust. *Ann Rev Earth Planet Sci* 8:489–525
- Rudnicki JW (1984) A class of elastic-plastic constitutive laws for brittle rocks. *J Rheol* 28:759–778
- Rudnicki JW (2001) Coupled deformation-diffusion effects in the mechanics of faulting and failure of geomaterials. *Appl Mech Rev* 54:483–502
- Rudnicki JW (2002) Conditions for compaction and shear bands in a transversely isotropic material. *Int J Solids Struct* 39:3741–3756
- Rudnicki JW, Chau K-T (1996) Multiaxial response of a microcrack constitutive model for brittle rock. In: Aubertin M, Hassani F, Mitri H (eds) *Rock mechanics, tools and techniques; Proceedings of the 2<sup>nd</sup> North American Rock Mechanics Symposium*. A. A. Balkema, Rotterdam, pp 1707–1714
- Rudnicki JW, Olsson WA (1998) Reexamination of fault angles predicted by shear localization theory. *Int J Rock Mech Min* 35:512, CD ROM paper No. 088
- Rudnicki JW, Rice JR (1975) Conditions for the localization of deformation in pressure-sensitive dilatant materials. *J Mech Phys Solids* 23:371–394
- Ruina AL (1980) Friction laws and instabilities: a quasistatic analysis of some dry frictional behavior [Ph D thesis]. Brown University, 66 pp
- Ruina A (1983) Slip instability and state variable friction law. *J Geophys Res* 88:10359–10370
- Ruina AL (1985) Constitutive relations for frictional slip. In: Bazant ZP (ed) *Mechanics of geomaterials. Rocks, concretes, soils: numerical methods in engineering*. John Wiley and Sons, New York, pp 169–188
- Rummel F (1972) Bruchausbreitung in Kalksteinproben. In: Blinde A, Müller L (eds) *Veröffentlichungen des Inst. für Bodenmechanik und Felsmechanik der Universität Fridericiana, Karlsruhe*. Heft 55:87–109
- Rummel F (1974) Changes in the P-wave velocity with increasing inelastic deformation in rock specimens under compression. In: *Advances in Rock Mechanics*. Proc. 3<sup>rd</sup> Congr. Int. Soc. Rock Mech., Denver, 1974. Washington, D.C., Nat. Acad. Sci., II, Part A, pp 517–523
- Rummel F (1975) Experimentelle Untersuchungen zum Bruchvorgang in Gesteinen. *Berichte des Inst. für Geophysik der Ruhr-Universität Bochum*, Nr. 4, 144 pp
- Rummel F, Alheid H-J, John C (1978) Dilatancy and fracture-induced velocity changes in rock and their relation to frictional sliding. *Pure Appl Geophys* 116:743–764

- Rummel F, Fairhurst C (1970) Determination of the post-failure behaviour of brittle rock using a servo-controlled testing machine. *Rock Mech* 2:189–204
- Rutter EH (1972a) The effects of strain-rate changes on the strength and ductility of Solenhofen limestone at low temperatures and confining pressures. *Int J Rock Mech Min* 9:183–189
- Rutter EH (1972b) The influence of interstitial water on the rheological behaviour of calcite rocks. *Tectonophysics* 14:13–33
- Rutter EH (1976) The kinetics of rock-deformation by pressure-solution. *Philos T Roy Soc A* 283:203–219
- Rutter EH (1986) On the nomenclature of mode of failure transitions in rocks. *Tectonophysics* 122:381–387
- Rutter EH, Brodie KH (1988) Experimental “syntectonic” dehydration of serpentinite under controlled pore water pressure. *J Geophys Res* 93:4907–4932
- Rutter EH, Neumann DHK (1995) Experimental deformation of partially molten Westerly granite under fluid-absent conditions, with implications for the extraction of granitic magmas. *J Geophys Res* 100:15697–15715
- Rutter EH, Maddock RH, Hall SH, White SH (1986) Comparative microstructures of naturally and experimentally produced clay-bearing fault gouges. *Pure Appl Geophys* 124:3–30
- Ryabinin YN, Vereschagin LF, Balashov DB, Livshitz LD (1958) Apparatus for the mechanical investigation of metals under pressures up to 30 000 kg/cm<sup>2</sup>. *Pribory I Tekhn Eksperim* 2, 79 (English trans. In: *Instr Exp Tech* 2:265–272)
- Sack RA (1946) Extension of Griffith's theory of rupture to three dimensions. *Proc Phys Soc London* 58:729–736
- Saffer DM, Marone C (2003) Comparison of smectite- and illite-rich gouge frictional properties: application to the updip limit of the seismogenic zone along subduction megathrusts. *Earth Planet Sci Lett* 215:219–235
- Saffer DM, Frye KM, Marone C, Mair K (2001) Laboratory results indicating complex and potentially unstable frictional behavior in smectite clay. *Geophys Res Lett* 28:2297–2300
- Sage JD (1966) Deformational response of rock at low stress levels. In: *Proc. 1<sup>st</sup> Congr. Int. Soc. Rock Mech.*, Lisbon, 1966, I, pp 489–493
- Saibel E (1971) Size effect in fracture. In: Te'eni M (ed) *Structure, solid mechanics and engineering design*. Proc. Southampton 1969 Civil Eng. Materials Conf. Wiley-Interscience, London, pp 125–129
- Saint Leu C, Sirieys PM (1970) Déformations des roches fragiles sous champs de contraintes homogènes et hétérogènes. In: *Proc. 2<sup>nd</sup> Congr. Int. Soc. Rock Mech.*, Belgrade, 1, pp 399–404
- Saint Leu C, Sirieys PM (1971) La fatigue des roches. In: *Rock fracture. Proc. Int. Symp. Rock Mech.*, Nancy, pp Paper II-18 (13 pp)
- Sammis CG, Ashby MF (1986) The failure of brittle porous solids under compressive stress states. *Acta Metall* 34:511–526
- Sammis CG, Biegel RL (1989) Fractals, fault gouge, and friction. *Pure Appl Geophys* 131:255–271
- Sammis CG, King G, Biegel RL (1987) The kinematics of gouge deformation. *Pure Appl Geophys* 125:777–812
- Sammis CG, Steacy SJ (1994) The micromechanics of friction in a granular layer. *Pure Appl Geophys* 142:777–794
- Sammonds PR, Meredith PG, Main IG (1992) Role of pore fluids in the generation of seismic precursors to shear fracture. *Nature* 359:228–230
- Sammonds PR, Ayling MR, Meredith PG, Murrell SAF, Jones C (1989) A laboratory investigation of acoustic emission and elastic wave velocity changes during rock failure under triaxial stresses. In: Maury V, Fourmaintraux D (eds) *Rock at great depth*. A. A. Balkema, Rotterdam, 1, pp 233–240
- Sampson JB, Morgan F, Reed DW, Muskat M (1943) Studies in lubrication, XII. Friction behavior during the slip portion of the stick-slip process. *J Appl Phys* 14(12):689–700
- Sanders JL (1960) On the Griffith-Irwin fracture theory. *J Appl Mech-T ASME* 27:352–353
- Sangha CM, Dhir RK (1972) Influence of time on the strength, deformation and fracture properties of a lower Devonian sandstone. *Int J Rock Mech Min* 9:343–354
- Sangha CM, Dhir RK (1975) Strength and deformation of rock subject to multiaxial compressive stresses. *Int J Rock Mech Min* 12:277–282
- Sangha CM, Talbot CJ, Dhir RK (1974) Microfracturing of a sandstone in uniaxial compression. *Int J Rock Mech Min* 11:107–113

- Sano O, Ito I, Terada M (1981) Influence of strain rate on dilatancy and strength of Oshima granite under uniaxial compression. *J Geophys Res* 86:9299–9311
- Sano O, Terada M, Ehara S (1982) A study of the time-dependent microfracturing and strength of Oshima granite. *Tectonophysics* 84:343–362
- Santarelli FJ, Brown ET (1989) Failure of three sedimentary rocks in triaxial and hollow cylinder compression tests. *Int J Rock Mech Min* 26:401–413
- Santhanam AT, Gupta YP (1968) Cleavage surface energy of calcite. *Int J Rock Mech Min* 5:253–259
- Satake M, Jenkins JT (eds) (1988) *Micromechanics of granular materials*. Proc U.S./Japan Seminar on the Micromechanics of Granular Materials, Sendai-Zao, Japan, Oct 26–30 (1987), Elsevier, Amsterdam, 366 pp
- Satoh T, Nishizawa O, Kusunose K (1990) Fault development in Oshima granite under triaxial compression inferred from hypocenter distribution and focal mechanism of acoustic emission. *Tohoku Geophys J* 33:241–250
- Satoh T, Shivakumar K, Nishizawa O, Kusunose K (1996) Precursory localization and development of microfractures along the ultimate fracture plane in amphibolite under triaxial creep. *Geophys Res Lett* 23:865–868
- Savage JC, Lockner DA (1997) A test of the double-shearing model of flow for granular materials. *J Geophys Res* 102:12287–12294
- Savage JC, Lockner DA, Byerlee JD (1996) Failure in laboratory fault models in triaxial tests. *J Geophys Res* 101:22215–22224
- Sayers CM (1993) Comment on “Crack models for a transversely isotropic medium” by C. H. Cheng. *J Geophys Res* 98:14211–14213
- Sayers CM, Kachanov M (1991) A simple technique for finding effective elastic constants of cracked solids for arbitrary crack orientation statistics. *Int J Solids Struct* 12:81–97
- Sayers CM, Kachanov M (1995) Microcrack-induced elastic wave anisotropy of brittle rocks. *J Geophys Res* 100:4149–4156
- Sayers CM, van Munster JG (1991) Microcrack-induced seismic anisotropy of sedimentary rocks. *J Geophys Res* 96:16529–16533
- Sayers CM, van Munster JG, King MS (1990) Stress-induced ultrasonic anisotropy in Berea sandstone. *Int J Rock Mech Min* 27:429–436
- Schiffman RL (1970) The stress components of a porous medium. *J Geophys Res* 75:4035–4038
- Schmid SM (1976) Rheological evidence for changes in the deformation mechanism of Solenhofen limestone towards low stresses. *Tectonophysics* 31:T21–T28
- Schmid SM, Boland JN, Paterson MS (1977) Superplastic flow in fine grained limestone. *Tectonophysics* 43:257–291
- Schmitt L, Forsans T, Santarelli FJ (1994) Shale testing and capillary phenomena. *Int J Rock Mech Min* 31:411–427
- Schmitt DR, Zoback MD (1989) Laboratory tests on the effects of pore pressure on tensile failure. In: Maury V, Fourmaintraux D (eds) *Rock at great depth*. A. A. Balkema, Rotterdam, 2, pp 883–889
- Schmitt DR, Zoback MD (1992) Diminished pore pressure in low-porosity crystalline rock under tensional failure: apparent strengthening by dilatancy. *J Geophys Res* 97:273–288
- Schock RN (1976) A constitutive relation describing dilatant behaviour in Climax Stock granodiorite. *Int J Rock Mech Min* 13:221–223
- Schock RN, Duda AG (1972) Quasistatic deformation of solids with pressure. *J Appl Phys* 43:2204–2210
- Schock RN, Duda AG (1973) Pressure effects on the response of foil strain gages. *Exp Mech* 13:43–44
- Schock RN, Heard HC (1974) Static mechanical properties and shock loading response of granite. *J Geophys Res* 79:1662–1666
- Schock RN, Heard HC, Stephens DR (1973) Stress-strain behaviour of a granodiorite and two graywackes on compression to 20 kilobars. *J Geophys Res* 78:5922–5941
- Schofield A, Wroth P (1968) *Critical state soil mechanics*. McGraw Hill, London, 310 pp
- Scholz CH (1968a) Experimental study of the fracturing process in brittle rock. *J Geophys Res* 73:1447–1454
- Scholz CH (1968b) The frequency-magnitude relation of microfracturing in rock and its relation to earthquakes. *B Seismol Soc Am* 58:399–415
- Scholz CH (1968c) Mechanism of creep in brittle rock. *J Geophys Res* 73:3295–3302

- Scholz CH (1968d) Microfracturing and the inelastic deformation of rock in compression. *J Geophys Res* 73:1417–1432
- Scholz CH (1972) Static fatigue of quartz. *J Geophys Res* 77:2104–2114
- Scholz CH (1990) *The mechanics of earthquakes and faulting*. Cambridge University Press, Cambridge, 433 pp
- Scholz CH (1992) Paradigms or small change in earthquake mechanics. In: Evans B, Wong T-f (eds) *Fault mechanics and transport properties of rocks*. International Geophysics Series: London, Academic Press, pp 505–517
- Scholz CH (1998) Earthquakes and friction laws. *Nature* 391:37–42
- Scholz CH (2002) *The mechanics of earthquakes and faulting*, 2<sup>nd</sup> ed. Cambridge University Press, Cambridge, 471 pp
- Scholz CH, Boitnott G, Nemat-Nasser S (1986) The Bridgman ring paradox revisited. *Pure Appl Geophys* 124:587–599
- Scholz CH, Engelder JT (1976) The role of asperity indentation and ploughing in rock friction. I. Asperity creep and stick-slip. *Int J Rock Mech Min* 13:149–154
- Scholz CH, Koczyński (1979) Dilatancy anisotropy and the response of rock to large cyclic loads. *J Geophys Res* 84:5525–5534
- Scholz CH, Kranz R (1974) Notes on dilatancy recovery. *J Geophys Res* 79:2132–2135
- Scholz C, Molnar P, Johnson T (1972) Detailed studies of frictional sliding of granite and implications for the earthquake mechanism. *J Geophys Res* 77:6392–6406
- Scholz CH, Sykes LR, Aggarwal YP (1973) Earthquake prediction: a physical basis. *Science* 181:803–810
- Schreiber E, Anderson OL, Soga N (1973) *Elastic constants and their measurement*. McGraw Hill, New York, 196 pp
- Schrodt JK, Holder JT (1983) Temperature and strain rate effects on micromechanical behavior in triaxially compressed marbles. In: Mathewson CC (ed) *Rock mechanics. Theory – experiment – Practice*. Proc 24<sup>th</sup> U.S. Symposium on Rock Mechanics, Texas A and M University and Association of Engineering Geologists, pp 449–468
- Schubnel A, Nishizawa O, Masuda K, Lei XJ, Zue Z, Guéguen Y (2003) Velocity measurements and crack density determination during wet triaxial experiments on Oshima and Toki granites. *Pure Appl Geophys* 160:869–887
- Schulson EM, Nikolayev OY (1995) Failure of columnar saline ice under biaxial compression: failure envelopes and the brittle-to-ductile transition. *J Geophys Res* 100:22383–22400
- Schulson EM, Kuehn GA, Jones DE, Fifolt DA (1991) The growth of wing cracks and the brittle compressive fracture of ice. *Acta Metall Mater* 39:2651–2655
- Sclar CB, Carrison LC (1966) High-pressure reactions and shear strength of serpentized dunite. *Science* 153:1285–1287
- Scott TE, Ma Q, Roegiers JC (1993) Acoustic velocity changes during shear-enhanced compaction of sandstone. *Int J Rock Mech Min* 30:763–769
- Scott DR, Marone CJ, Sammis CG (1994) The apparent friction of granular fault gouge in sheared layers. *J Geophys Res* 99:7231–7246
- Scott TE, Nielson KC (1991) The effects of porosity on the brittle-ductile transition in sandstones. *J Geophys Res* 96:405–414
- Scruggs VJ, Tullis TE (1998) Correlation between velocity dependence of friction and strain localization in large displacement experiments on feldspar, muscovite and biotite gouge. *Tectonophysics* 295:15–40
- Secor DT, Montenyohl V (1972) The effective tensile strength of rocks. *EOS Trans AGU* 53:1125 (abstract)
- Seldenrath TR, Gramberg J (1958) Stress-strain relations and breakage of rocks. In: Walton WH (ed) *Mechanical properties of non-metallic brittle materials*. Butterworths, London, pp 79–102
- Senseny PE (1986) A microcrack model for the deformation and strength of Algeria granite. *Proc US Symp Rock Mechanics* 27:11–15
- Senseny PE, Fosum AF, Pfeifle TW (1983) Non-associative constitutive laws for low-porosity rocks. *Int J Numer Anal Method Geomech* 7:101–115
- Serdengecti S, Boozer GD (1961) The effects of strain rate and temperature on the behavior of rocks subjected to triaxial compression. In: Hartman HL (ed) *Proc. 4<sup>th</sup> Symposium on Rock Mechanics*, Pennsylvania State University. *Bull Min Ind Exp Sta* 76:83–97

- Seto M, Nag DK, Vutukuri VS, Katsuyama K (1997) Effect of chemical additives in the strength of sandstone. *Int J Rock Mech Min* 34:691 (abs + CD ROM)
- Seya K, Suzuki I, Fujiwara H (1979) The change in ultrasonic wave velocities in triaxially stressed brittle rock. *J Phys Earth* 27:409–421
- Shah KR, Labuz JF (1995) Damage mechanisms in stressed rock from acoustic emission. *J Geophys Res* 100:15527–15539
- Shah KR, Wong T-f (1997) Fracturing at contact surfaces subjected to normal and tangential loads. *Int J Rock Mech Min* 34:727–739
- Shamina OG, Pavlov AA (1974) Investigations of the development of both tension and shearing cracks. *Izv An SSSR Fiz Zem+* 9:19–25 (Engl. tr.: *Izvestiya Acad Sci USSR, Physics of the Solid Earth*, pp 557–560)
- Shamina OG, Pavlov AA, Kopnichev YF (1973) Investigation of the fracture-development process. *Izv An SSSR Fiz Zem+* 8:17–30 (Engl. tr.: *Izvestiya Acad Sci USSR, Physics of the Solid Earth*, pp 503–511)
- Shea WT, Kronenberg AK (1993) Strength and anisotropy of foliated rocks with varied mica contents. *J Struct Geol* 15:1097–1121
- Shen HH, Satake M, Mehrabadi M, Chang CS, Campbell CS (eds) (1993) *Mechanics of granular materials*. *Mech Mater* 16:1–248
- Sheorey PR, Biswas AK, Choubey VD (1989) An empirical failure criterion for rocks and jointed rock masses. *Eng Geol* 26:141–159
- Shimada M (1981) The method of compression test under high pressure in a cubic press and the strength of granite. *Tectonophysics* 72:343–357
- Shimada M (1986) Mechanism of deformation in a dry porous basalt at high pressure. *Tectonophysics* 121:153–173
- Shimada M (2000) *Mechanical behavior of rocks under high pressure conditions*. Geomechanics research series 2. A. A. Balkema, Rotterdam, 178 pp
- Shimada M, Cho A, Yukatake H (1983) Fracture strength of dry silicate rocks at high confining pressures and activity of acoustic emission. *Tectonophysics* 96:159–172
- Shimada M, Yukatake H (1982) Fracture and deformation of silicate rocks at high pressure in a cubic press. In: Akimoto S, Manghnani MH (eds) *High-pressure research in geophysics*. *Advances in earth and planetary sciences* 12. D Riedel Publishing Company, Dordrecht, pp 193–205
- Shimamoto T (1986a) Strengthening of phyllosilicate and gypsum gouges with increasing temperature: effect of temperature or moisture elimination? *Int J Rock Mech Min* 23:439–443
- Shimamoto T (1986b) Transition between frictional slip and ductile flow for halite shear zones at room temperature. *Science* 231:711–714
- Shimamoto T, Logan JM (1981a) Effects of simulated fault gouge on the sliding behavior of Tennessee sandstone. *Tectonophysics* 75:243–255
- Shimamoto T, Logan JM (1981b) Effects of simulated fault gouge on the sliding behavior of Tennessee sandstone: nonclay gouges. *J Geophys Res* 86:2902–2914
- Shimamoto T, Logan JM (1986) Velocity-dependent behaviors of simulated halite shear zones: an analog for silicates. In: Das S (ed) *Earthquake source mechanics*. American Geophysical Union, Washington, D.C., *Geophys Monograph* 37, pp 49–63
- Shimozuru D (1955) Elasticity of rocks under the initial stresses, with special reference to the fracture problem. *B Earthq Res I Tokyo* 33:437–447
- Shirey SB, Simmons G, Padovani ER (1980) Angular, oriented microtubes in metamorphic plagioclase. *Geology* 8:240–244
- Sibson RH (1981) Fluid flow accompanying faulting: field evidence and models. In: Simpson DW, Richards PG (eds) *Earthquake prediction. An international review*. American Geophysical Union, Washington, D.C., *Maurice Ewing Series* 4, pp 593–603
- Sibson RH (1994) Crustal stress, faulting, and fluid flow. In: Parnell J (ed) *Geofluids: origin, migration and evolution of fluids in sedimentary basins*. Geological Society Special Publications: London, Geological Society Special Publication, 78, pp 69–84
- Siddiqi G, Liu M, Evans B (1997) Strengthening of marbles by stiff inclusions. *EOS Trans AGU* 78:F723
- Siddiqi G, Evans B, Dresen G, Freund D (1997) Effect of semibrittle deformation on transport properties of calcite rocks. *J Geophys Res* 102:14765–14778

- Sih GC, Liebowitz H (1968) Mathematical theories of brittle fracture. In: Liebowitz H (ed) *Fracture*. Academic Press, II, New York, pp 67–190
- Simmons G, Brace WF (1965) Comparison of static and dynamic measurements of compressibility of rocks. *J Geophys Res* 70:5649–5656
- Simmons G, Richter D (1976) Microcracks in rocks. In: Strens RGJ (ed) *The physics and chemistry of minerals and rocks*. NATO Institute, Newcastle upon Tyne, April 1974. Wiley, London, pp 105–137
- Simmons G, Siegfried RW, Feves M (1974) Differential strain analysis: a new method for examining cracks in rocks. *J Geophys Res* 79:4383–4385
- Simmons G, Todd T, Baldrige WS (1975) Toward a quantitative relationship between elastic properties and cracks in low porosity rocks. *Am J Sci* 275:318–345
- Singh VP (1976) Investigations of attenuation and internal friction of rocks by ultrasonics. *Int J Rock Mech Min* 13:69–74
- Singh MM (1981) Strength of rock. In: Toulonkian YS, Judd WR, Roy RF (eds) *Physical properties of rocks and minerals*. McGraw-Hill Book Co, New York, pp 83–121
- Singh J, Ramamurthy T, Rao GV (1989) Strength of rocks at depth. In: Maury V, Fourmaintraux D (eds) *Rock at great depth*. A. A. Balkema, Rotterdam, 1, pp 37–44
- Sirieys PM (1966) Phénomènes de rupture fragile des roches isotropes et anisotropes. In: Kravtchenko J, Sirieys PM (eds) *Rheology and soil mechanics*. Symp. Grenoble, April 1964. Springer-Verlag, Berlin Heidelberg New York, pp 396–404
- Sirieys P, Saint Leu C (1969) Expérience relatives à l'influence du gradient des contraintes sur les lois de la fissuration des roches. In: 2ème Coll. sur la Fissuration des Roches, Paris, Jan. 1969, *Revue de l'Industrie Minérale*, July 1969, pp 41–49
- Skempton AW (1954) The pore-pressure coefficients A and B. *Géotechnique* 4:143–147
- Skempton AW (1961) Effective stress in soils, concrete and rocks. In: *Pore Pressure and suction in soils*. Conference organized by Brit. National Soc. of Int. Soc. Soil Mech. Found. Eng. at Inst. of Civ. Eng., March 30–31, 1960. Butterworths, London, pp 4–16
- Skinner WJ (1959) Experiments on the compressive strength of anhydrite. *Engineer-London* 207:255–259, 288–292
- Sleep NH (1997) Application of a unified rate and state friction theory to the mechanics of fault zones with strain localization. *J Geophys Res* 102:2875–2895
- Sleep NH, Richardson E, Marone C (2000) Physics of friction and strain rate localization in synthetic fault gouge. *J Geophys Res* 105:25875–25890
- Smart BGD (1995) A true triaxial cell for testing cylindrical rock specimens. *Int J Rock Mech Min* 32:269–275
- Smith CS (1948) Grains, phases and interfaces: an interpretation of microstructure. *Trans Am Inst Min Metall Pet Eng* 175:15–51
- Smith E (1971) Note on the growth of a penny-shaped crack in a general uniform applied stress field. *Int J Fract Mech* 7:339–342
- Smith JL, Devried KL, Bushnell DJ, Brown WS (1969) Fracture data and stress-strain behavior of rocks in triaxial compression. *Exp Mech, Proc Soc Exp Stress Anal* 26:348–355
- Sneddon IN (1946) The distribution of stress in the neighbourhood of a crack in an elastic solid. *P Roy Soc Lond A Mat* 187:229–260
- Soeder DJ (1990) Applications of fluorescence microscopy to study of pores in tight rocks. *Am Assoc Petrol Geol Bull* 74:30–40
- Soga N, Martin RJ, Spetzler H (1976) Inhomogeneous strain accumulation on laboratory rock samples prior to failure. *EOS Trans AGU* 57:328 (abstract)
- Soga N, Mizutani H, Spetzler H, Martin RJ (1976)  $V_s$  and  $V_p$  velocities and the orientation of the failure plane in laboratory experiments. *EOS Trans AGU* 57:1010 (abstract)
- Soga N, Mizutani H, Spetzler H, Martin RJ (1978) The effect of dilatancy on velocity anisotropy in Westerly granite. *J Geophys Res* 83:4451–4458
- Solberg PH (1975) The influence of microcracks on sheet jointing in four New England granites. *EOS Trans AGU* 56:444 (abstract)
- Solberg P, Byerlee JD (1984) A note on the rate sensitivity of frictional sliding of Westerly granite. *J Geophys Res* 89:4203–4205

- Somerton WH, Soylemezoglu IM, Dudley RC (1975) Effect of stress on permeability of coal. *Int J Rock Mech Min* 12:129–145
- Sondergeld CH, Estey LH (1981) Acoustic emission study of microfracturing during cyclic loading of Westerly granite. *J Geophys Res* 86:2915–2924
- Sondergeld CH, Estey LH (1982) Source mechanisms and microfracturing during uniaxial cycling of rock. *PAGEOCH* 120:151–166
- Spanne P, Thovert JF, Jacquin CJ, Lindquist WB, Jones KW, Adler PM (1994) Synchrotron computer microtomography of porous media: topology and transports. *Phys Rev Lett* 73:2001–2004
- Spencer JW, Nur AM (1976) The effects of pressure, temperature and pore water on velocities in Westerly granite. *J Geophys Res* 81:899–904
- Spetzler H (1987) Rock fracture and frictional sliding. In: Sammis CG, Henyey TL (eds) *Methods of experimental physics*. Academic Press, Orlando, 24, Part A, pp 131–183
- Spetzler H, Martin RJ (1974) Correlation of strain and velocity during dilatancy. *Nature* 252:30–31
- Spetzler HA, Sobolev GA, Getting IC (1989) Holography in laboratory experiments pertinent to rock deformation. In: Takemoto S (ed) *Laser holography in geophysics*. Ellis Horwood Limited, Chichester, pp 31–105
- Spetzler H, Sondergeld C, Getting JC (1981) The influence of strain rate and moisture content in rock fracture. In: Stacey FD, Paterson MS, Nicholas A (eds) *Anelasticity in the Earth*. American Geophysical Union, Washington, D.C., *Geodynamics Series* vol 4, pp 108–112
- Spiers CJ, Schutjins PMTM, Brzesowsky RH, Peach CJ, Liezenberg JL, Zwart HJ (1990) Experimental determination of constitutive parameters governing creep of rocksalt by pressure solution. In: Knipe RJ, Rutter EH (eds) *Deformation mechanisms, rheology and tectonics*. The Geological Society, London, Special Publication No. 54, pp 215–227
- Sprunt ES, Brace WF (1974a) Direct observation of microcavities in crystalline rocks. *Int J Rock Mech Min* 11:139–150
- Sprunt ES, Brace WF (1974b) Some permanent structural changes in rocks due to pressure and temperature. In: *Advances in Rock Mechanics*. Proc. 3<sup>rd</sup> Congr. Int. Soc. Rock Mech., Denver, 1974. Washington, D.C., Nat. Acad. Sci., II, Part A, pp 524–529
- Rawley JE, Brown WF (1965) Fracture roughness testing methods. In: *Fracture toughness testing and its applications*. Am Soc Test Mat, Spec Tech Publ 381, pp 133–196
- Starfield AM, Wawersik WR (1972) Pillars as structural components in room-and-pillar design. In: Gray KE (ed) *Basic and applied rock mechanics*. Proc. 10<sup>th</sup> Symp. Rock Mech., Austin, Texas, May 1968. A.I.M.E., New York, pp 793–809
- Stauffer D, Aharony A (1992) *Introduction to percolation theory*. Taylor & Francis, London, 181 pp
- Steif PS (1984) Crack extension under compressive loading. *Eng Fract Mech* 20:463–473
- Stesky RM (1975) Acoustic emission during high-temperature frictional sliding. *Pure Appl Geophys* 113:31–43
- Stesky RM (1978a) Mechanisms of high temperature frictional sliding in Westerly granite. *Can J Earth Sci* 15:361–375
- Stesky RM (1978b) Rock friction – effect of confining pressure, temperature and pore pressure. *Pure Appl Geophys* 116:690–704
- Stesky RM, Brace WF (1973) Estimation of frictional stress on the San Andreas fault from laboratory measurements. In: Kovach RL, Nur A (eds) Proc. conf. on tectonic problems of the San Andreas fault system. Stanford Univ Publ Geol Sci 13, pp 206–214
- Stesky RM, Brace WF, Riley DK, Robin P-YF (1974) Friction in faulted rock at high temperature and pressure. *Tectonophysics* 23:177–203
- Stillier H, Wagner FC, Vollstädt H (1977) A two-phase model for the description of cracks on the P- and S-wave velocities in dry and saturated rock samples. *Tectonophysics* 43:181–197
- Stocker RL, Ashby MF (1973) On the rheology of the upper mantle. *Rev Geophys Space Phys* 11:391–426
- Stoker JJ (1950) *Nonlinear vibrations*. Interscience, New York, 273 pp
- Stokes RJ, Johnston TL, Li CH (1959) The relationship between plastic flow and the fracture mechanism in magnesium oxide single crystals. *Phil Mag* 4:920–932
- Stoneley R (1949) The seismological implications of aeolotropy in continental structure. *Mon Not R Astron Soc, Geophys Suppl* 5:343–353

- Stowe RL, Ainsworth DL (1972) Effect of rate of loading on strength and Young's modulus of elasticity of rock. In: Gray KE (ed) Basic and applied rock mechanics. Proc. 10<sup>th</sup> Symp. Rock Mech., Austin, Texas, May 1968. A.I.M.E., New York, pp 3–34
- Stuart WD (1974) Diffusionless dilatancy model for earthquake precursors. *Geophys Res Lett* 1:261–264
- Stuart WD, Dieterich JD (1974) Continuum theory of rock dilatancy. In: Advances in rock mechanics. Proc. 3<sup>rd</sup> Congr. Int. Soc. Rock Mech., Denver, 1974. Washington, D.C., Nat. Acad. Sci., II, Part A, pp 530–534
- Suárez-Rivera FR, Cook NGW, Cooper GA, Zheng Z (1990) Indentation by pore collapse in porous rocks. In: Proc 31<sup>st</sup> U.S. Symposium on Rock Mechanics, pp 671–678
- Summers R, Byerlee J (1977) A note on the effect of fault gouge composition on the stability of frictional sliding. *Int J Rock Mech Min* 14:155–160
- Summers DA, Corwine J, Chen L (1971) A comparison of methods available for the determination of surface energy. In: Clark GB (ed) Dynamic Rock Mechanics. Proc. 12<sup>th</sup> Symposium on Rock Mechanics, Univ. Missouri, Nov. 1970. A.I.M.E., New York, pp 241–261
- Summers R, Winkler K, Byerlee J (1978) Permeability changes during the flow of water through Westerly granite at temperatures of 100 °–400 °C. *J Geophys Res* 83:339–344
- Suzuki T, Sasaki K, Siohara Z, Hirota T (1964) A new approach to the prediction of failure by rock noise. In: 4<sup>th</sup> Int. Conf. on Strata Control and Rock Mechanics, Henry Krumb School of Mines, Columbia University, New York City, May 4–8, 1964, pp 99–107
- Swain MV, Lawn BR (1976) Indentation fracture in brittle rocks and glasses. *Int J Rock Mech Min* 13:311–319
- Swan G (1975a) The numerical solution of certain dynamic crack propagation problems. *Int J Rock Mech Min* 12:295–302
- Swan G (1975b) The observation of cracks propagating in rock plates. *Int J Rock Mech Min* 12:329–334
- Swan G, Cook JM, Bruce S, Meehan R (1989) Strain rate effects in Kimmeridge Bay Shale. *Int J Rock Mech Min* 26:135–149
- Swanson BF (1979) Visualizing pores and nonwetting phase in porous rock. *J Petrol Technol* 31:10–18
- Swanson SR, Brown WS (1971a) The mechanical response of pre-fractured rock in compression. *Rock Mech* 3:208–216
- Swanson SR, Brown WS (1971b) An observation of loading path independence of fracture in rock. *Int J Rock Mech Min* 8:277–281
- Swedlow JL (1965) On Griffith's theory of fracture. *Int J Fract Mech* 1:210–216
- Swolfs HS (1972) Chemical effects of pore fluid on rock properties. In: Cook TD (ed) Underground waste management and environmental implications. Proc. Symp. Dec. 6–9 1971, Houston, Texas. Am. Assoc. Petrol. Geol., Memoir 18, pp 224–234
- Swolfs HS (1983) Aspects of the size-strength relationship of unjointed rock. In: 24<sup>th</sup> U.S. Symposium on Rock Mechanics, pp 501–510
- Tada H, Paris PC, Irwin GR (1985) Handbook for stress analysis of cracks, 2<sup>nd</sup> edition. Del Research Corporation, St Louis
- Takahashi M, Kinoshita S, Nishizawa O, Koide H, Chiba H (1984) Seismic wave velocity anisotropy in Westerly granite under true triaxial compression. *Zisin* 37:67–79, (in Japanese)
- Takei Y (2002) Effect of pore geometry on  $V_p/V_s$ : from equilibrium geometry to crack. *J Geophys Res* 107, 10.1029/2001JB000522 (12 pp)
- Takeuchi H, Kikuchi M (1973) A dynamical model of crack propagation. *J Phys Earth* 21:27–37
- Tan TK, Wu HQ (1989) Creep and time dependent dilatancy of rocks at great depths. In: Maury V, Fourmaintraux D (eds) Rock at great depth. A. A. Balkema, Rotterdam, pp 67–76
- Tang CA, Chen ZH, Xu XH, Li C (1997) A theoretical model for Kaiser effect in rock. *Pure Appl Geophys* 150:203–215
- Tao G, King MS (1990) Shear-wave velocity and Q anisotropy in rocks: a laboratory study. *Int J Rock Mech Min* 27:353–361
- Tapponnier P, Brace WF (1976) Development of stress-induced microcracks in Westerly granite. *Int J Rock Mech Min* 13:103–112
- Taylor GI (1938) Plastic strain in metals. *J Inst Metals (London)* 62:307–324
- Te'eni M (ed) (1971) Structure, solid mechanics and engineering design. Proc. Southampton 1969 Civil Eng. Mater. Conf: London, Wiley-Interscience, 1445 pp



- Terada M, Yanagitani T, Ehara S (1984) A rate controlled compression test of rocks. In: Hardy HR, Leighton FW (eds) Proc 3<sup>rd</sup> Conf. on Acoustic Emission/Microseismic Activity in Geologic Structures and Materials. Trans-Technical, Clausthal-Zellerfeld, pp 159–171
- Terzaghi K (1945) Stress conditions for the failure of saturated concrete and rock. *P Am Soc Test Mater* 45:777–792
- Tetelman AS, McEvily AJ (1967) Fracture of structural materials. Wiley, New York
- Teufel LW (1981) Pore volume changes during frictional sliding of simulated faults. In: Carter NL, Friedman M, Logan JM, Stearns DW (eds) Mechanical behavior of crustal rocks. The Handin Volume. American Geophysical Union, Washington, D.C., geophysical monograph 24, pp 135–145
- Teufel LW (1987) Permeability changes during shear deformation of fractures in rock. In: Farmer IW, Daemen JJK, Desai CS, Glass CE, Neuman SP (eds) Rock mechanics. Proceedings of the 28<sup>th</sup> U.S. Symposium. A. A. Balkema, Rotterdam, pp 473–480
- Teufel LS, Logan JM (1975a) Measurement of temperature generated during frictional sliding. *EOS Trans AGU* 56:447 (abstract)
- Teufel LS, Logan JM (1975b) Time dependent friction in Tennessee sandstone. *EOS Trans AGU* 56:1061 (abstract)
- Teufel LS, Logan JM (1976) Measurement of temperatures generated during frictional sliding. *EOS Trans AGU* 57: 1011 (abstract)
- Teufel LW, Logan JM (1978) Effect of displacement rate on the real area of contact and temperatures generated during frictional sliding. *Pure Appl Geophys* 116:840–865
- Teufel LW, Rhett DW, Farrell HE (1991) Effect of reservoir depletion and pore pressure drawdown on in situ stress and deformation in the Ekofisk field, North Sea. In: Proc U.S. Rock Mech Symp 32, pp 63–72
- Thénoz B (1956) Mesure de la perméabilité et de la porosité des roches très compactes. *CR Acad Sci Paris* 243:289–291
- Thill RE (1973) Acoustic methods for monitoring failure in rock. In: Hardy HR, Stefanko R (eds) *New Horizons in rock mechanics*. 14<sup>th</sup> Symposium on Rock Mechanics, University Park, Penn., June 1972. *Am Soc Civ Eng, New York*, pp 649–687
- Thill RE, Bur TR, Steckley RC (1973) Velocity anisotropy in dry and saturated rock spheres and its relation to rock fabric. *Int J Rock Mech Min* 10:535–557
- Thill RE, Willard RJ, Bur TR (1969) Correlation of longitudinal velocity variation with rock fabric. *J Geophys Res* 74:4897–4909
- Thiry M, Ayrault MB, Grisoni J-C (1988) Groundwater silicification and leaching in sands: examples of the Fontainebleau sand (Oligocene) in the Paris Basin. *Geol Soc Am Bull* 100:1283–1290
- Thomas TY (1961) Plastic flow and fracture in solids. Academic Press, New York, 267 pp
- Thornton C, Randall CW (1988) Applications of theoretical contact mechanics to solid particle system simulation. In: Satake M, Jenkins JT (eds) *Micromechanics of granular materials*. Elsevier, Amsterdam, pp 133–142
- Timur A, Hemphkins WB, Weinbrandt RM (1971) Scanning electron microscope study of pore systems in rock. *J Geophys Res* 76:4932–4948
- Tobin DG, Donath FA (1971) Microscopic criteria for defining deformational modes in rock. *Geol Soc Am Bull* 82:1463–1476
- Tocher D (1957) Anisotropy in rocks under simple compression. *Trans Am Geophys Union* 38:89–94
- Todd T, Simmons G (1972) Effect of pore pressure on the velocity of compressional waves in low-porosity rocks. *J Geophys Res* 77:3731–3743
- Todd T, Simmons G, Baldrige WS (1973) Acoustic double refraction in low-porosity rocks. *B Seismol Soc Am* 63:2007–2020
- Toksöz MN, Cheng CH, Timur A (1976) Velocities of seismic waves in porous rocks. *Geophysics* 41:621–645
- Toksöz MN, Johnston DH (eds) (1981) *Seismic wave attenuation*. Geophysics Reprint Series No. 2. Society of Exploration Geophysics, Tulsa, Oklahoma, 459 pp
- Tolstoy I (ed) (1992) Acoustics, elasticity, and thermodynamics of porous media. *Twenty-one Papers by M. A. Biot*. Woodbury, New York, Acoustical Society of America, 265 pp
- Tomashevskaya IS, Khamidullin YN (1972) Precursors of the destruction of rock specimens. *Izv An SSSR Fiz Zem+* 5:12–20 (Engl. tr.: *Izvestiya Acad Sci USSR, Physics of the Solid Earth*, 1972, pp 276–281)
- Tomashevskaya IS, Volodina SI (1976) Deformation of rock samples under uniaxial compression. *Izv An SSSR Fiz Zem+* 5:101–105 (Engl. tr.: *Izvestiya Acad Sci USSR, Physics of the Solid Earth* 12:348–350)

- Tomecka-Suchon S, Rummel F (1992) Fracture-induced resistivity changes in granite. *Int J Rock Mech Min* 29:583–587
- Tourenq C, Fourmaintraux D, Denis A (1971) Propagation des ondes et discontinuités des roches. In: *Rock fracture. Proc. Int. Symp. Rock Mech., Nancy, 1971*, pp Paper I-1 (15 pp)
- Trimmer D (1982) Laboratory measurements of ultralow permeability of geological materials. *Rev Sci Instrum* 53:1246–1254
- Trimmer DA (1981) Design criteria for laboratory measurements of low permeability rocks. *Geophys Res Lett* 8:973–975
- Trimmer DA, Bonner B, Heard HC, Duba A (1980) Effect of pressure and stress on water transport in intact and fractured gabbro and granite. *J Geophys Res* 85:7059–7071
- Trollope DH (1968) The mechanics of discontinua or clastic mechanics in rock problems. In: Stagg KG, Zienkiewicz OC (eds) *Rock mechanics in engineering practice*. Wiley, London, pp 275–320
- Trollope DH, Brown ET (1966) Effective stress criteria of failure of rock masses. In: *Proc. 1<sup>st</sup> Congr. Int. Soc. Rock Mech., Lisbon, 1966, I*, pp 515–519
- Tse ST, Rice JR (1986) Crustal earthquake instability in relation to the depth variation in frictional slip properties. *J Geophys Res* 91:9452–9472
- Tsutsumi A, Shimamoto T (1997) High-velocity frictional properties of gabbro. *Geophys Res Lett* 24:699–702
- Tullis TE (1986) Friction and faulting. *Pure Appl Geophys* 124:375–608
- Tullis J (1990) Experimental studies of deformation mechanisms in quartzo-feldspathic rocks. In: Barber DJ, Meredith PG (eds) *Deformation processes in minerals, ceramics and rocks*. Unwin Hyman, London, pp 190–227
- Tullis TE, Tullis J (1986) Experimental rock deformation techniques. In: Hobbs BE, Heard HC (eds) *Mineral and rock deformation: laboratory studies. The Paterson Volume*. American Geophysical Union, Washington, D.C., *Geophys Monograph* 36, pp 297–324
- Tullis TE, Weeks JD (1986) Constitutive behavior and stability of frictional sliding of granite. *Pure Appl Geophys* 124:383–414
- Tullis J, Yund RA (1977) Experimental deformation of dry Westerly granite. *J Geophys Res* 82:5705–5718
- Tullis J, Yund RA (1980) Hydrolytic weakening of experimentally deformed Westerly granite and Hale albite rock. *J Struct Geol* 2:439–451
- Tullis J, Yund RA (1987) Transition from cataclastic flow to dislocation creep of feldspar: mechanisms and microstructures. *Geology* 15:606–609
- Tullis J, Yund R (1992) The brittle-ductile transition in feldspar aggregates: an experimental study. In: Evans B, Wong, T-f (eds) *Fault mechanics and transport properties of rocks. International Geophysics Series*. Academic Press, London, pp 89–117
- Turcotte DL (1992) *Fractals and chaos in geology and geophysics*. Cambridge University Press, Cambridge, 221 pp
- Turner CE (1974) Fracture mechanics and its application to high-pressure vessels (a review). *High Temp-High Press* 6:1–19
- Turner WT, Secor DT (1974) Effective confining pressure and fluid discharge along fractures. *EOS Trans AGU* 55:431 (abstract)
- Twiss RJ, Souter BA, Unruh JR (1993) The effect of block rotations on the global seismic moment tensor and the patterns of seismic P and T axes. *J Geophys Res* 98:645–674
- Uenishi K, Rice JR (2003) Universal nucleation length for slip-weakening rupture instability under nonuniform fault loading. *J Geophys Res* 108:2042, doi: 10.1029/2001JB001681
- Ui H (1973) Mechanical properties and fault plane features of Shidara sandstone in uniaxial compression tests. *J Earth Sci Nagoya Univ* 21:59–71
- Ui H (1976) Experimental study of the mechanical properties and microfracturing of some brittle rocks by compression tests. *J Earth Sci Nagoya Univ* 23/24:57–91
- Vajdova VP, Baud P, Wong T-f (2004) Compaction, dilatancy and failure in porous carbonate rocks. *J Geophys Res* 109:B05204, doi: 10.1029/2003JB002508 (16 pp)
- van der Molen I, Paterson MS (1979) Experimental deformation of partially-melted granite. *Contrib Mineral Petr* 70:291–318
- van Eeckhout EM (1976) The mechanisms of strength reduction due to moisture in coal mine shales. *Int J Rock Mech Min* 13:61–67

- Vardoulakis I (1980) Shear band inclination and shear modulus of sand in biaxial tests. *Int J Numer Anal Method Geomech* 4:103–119
- Vardoulakis I, Aifantis EC (1991) A gradient flow theory of plasticity for granular materials. *Acta Metall Mater* 39:197–217
- Vardoulakis I, Sulem J (1995) *Bifurcation analysis in geomechanics*. Blackie, London, 462 pp
- Vassiliou M, Salvado CA, Tittman BR (1984) Seismic attenuation. In: Carmichael RS (ed) *C.R.C. handbook of physical properties of rocks*. CRC Press, Boca Raton, Florida, III, pp 295–328
- Vermeer PA, Luger HJ (eds) (1982) *Deformation and failure of granular materials*. In: *Symposium on Deformation and Failure of Granular Materials*, Delft, 31 August–3 September 1982. A. A. Balkema, Rotterdam
- Vernik L, Bruno M, Bovberg C (1993) Empirical relations between compressive strength and porosity of siliciclastic rocks. *Int J Rock Mech Min* 30:677–680
- Vernik L, Lockner D, Zoback MD (1992) Anisotropic strength of some typical metamorphic rocks from the KTB pilot hole, Germany. *Sci Drill* 3:153–160
- Vinegar HJ, de Waal JA, Wellington SL (1991) CT studies of brittle failure in Castlegate sandstone. *Int J Rock Mech Min* 28:441–448
- Vinogradov SD (1959) On the distribution of the number of fractures in dependence on the energy liberated by the destruction of rocks. *Izvestiya Akad Nauk SSSR, Ser Geofiz*, pp 1850–1852 (Engl. tr.: *Bull (Izvestiya) Acad Sci USSR, Geophys Ser*, pp 1292–1293)
- Vinogradov SD (1962) Experimental study of the distribution of the number of fractures in respect to the energy liberated by the destruction of rocks. *Izvestiya Akad Nauk SSSR, Ser Geofiz*, pp 171–180 (Engl. tr.: *Bull (Izvestiya) Acad Sci USSR, Geophys. Ser*, pp 119–125)
- Volarovich MP (1965) The investigation of elastic and absorption properties of rocks at high pressures and temperatures. *Tectonophysics* 2:211–217
- Volarovich MP, Bayuk YI (1960) Effect of all-sided pressures up to 4 000 kg/cm<sup>2</sup> on the elastic properties of rock specimens. *Dokl Akad Nauk SSSR* 135:65–68 (Engl. tr.: *Doklady Acad Sci USSR Earth Sci Sect* 135:1237–1239, 1961)
- Volarovich MP, Balashov DB, Tomashevskaya IS, Pavlogradskiy VA (1963a) A study of the effect of uniaxial compression upon the velocity of elastic waves in rock samples under conditions of high hydrostatic pressure. *Izv An SSSR Geofiz* 8:1198–1205 (Engl. tr.: *Bull Acad Sci USSR, Geophys Ser*. pp 728–732, 1963)
- Volarovich MP, Balashov DB, Tomashevskaya IS, Pavlogradskiy VA (1963b) Velocities of elastic waves in rock samples simultaneous subjected to hydrostatic pressure and uniaxial compression. *Dokl Akad Nauk SSSR* 149:583–585 (Engl. tr.: *Doklady Acad Sci USSR, Earth Sci Sect* 148:1–3, 1965)
- von Kármán T (1911) Festigkeitsversuche unter allseitigem Druck. *Z Verein deutsch Ing* 55:1749–1757
- von Mises R (1928) Mechanik der plastischen Formänderung von Kristallen. *Z F Angewandte Math Mech* 8:161–185
- Vutukuri VS (1974) The effect of liquids on the tensile strength of limestone. *Int J Rock Mech Min* 11:27–29
- Vutukuri VS, Lama RD, Saluja SS (1974) *Handbook on mechanical properties of rocks – testing techniques and results*, Vol. 1. Series on Rock and Soil Mechanics, Vol. 2 (1974/75), No. 1. Trans Tech Publ, Clausthal, 280 pp
- Wagner H (1969) Über den Zusammenhang zwischen den Festigkeitshypothesen von Mohr und Griffith. *Rock Mech* 1:105–118
- Wagner H, Schümann EHR (1971) The stamp-load bearing strength of rock. An experimental and theoretical investigation. *Rock Mech* 3:185–207
- Walsh JB (1965a) The effect of cracks on the compressibility of rock. *J Geophys Res* 70:381–389
- Walsh JB (1965b) The effect of cracks on the uniaxial elastic compression of rocks. *J Geophys Res* 70:399–411
- Walsh JB (1966) Seismic wave attenuation in rock due to friction. *J Geophys Res* 71:2591–2599
- Walsh JB (1968) Attenuation in partially melted material. *J Geophys Res* 73:2209–2216
- Walsh JB (1969) New analysis of attenuation in partially melted rock. *J Geophys Res* 74:4333–4337
- Walsh JB (1971a) First pressure derivative of bulk modulus for porous materials. *J Appl Phys* 42:1098–1100
- Walsh JB (1971b) Stiffness in faulting and in friction experiments. *J Geophys Res* 76:8597–8598
- Walsh JB (1980) Static deformation of rock. *J Eng Mech Div-ASCE* 106(EM5):1005–1019

- Walsh JB (1981) Effect of pore pressure and confining pressure on fracture permeability. *Int J Rock Mech Min* 18:429–435
- Walsh JB, Brace WF (1964) A fracture criterion for brittle anisotropic rock. *J Geophys Res* 69:3449–3456
- Walsh JB, Brace WF (1966) Cracks and pores in rocks. In: *Proc. 1<sup>st</sup> Congr. Int. Soc. Rock Mech.*, Lisbon, 1966, I, pp 643–646
- Walsh JB, Brace WF (1972) Elasticity of rock in uniaxial strain. *Int J Rock Mech Min* 9:7–15
- Walsh JB, Decker ER (1966) Effect of pressure and saturating fluid on the thermal conductivity of compact rock. *J Geophys Res* 71:3053–3060
- Walton K (1987) The effective elastic moduli of a random packing of spheres. *J Mech Phys Solids* 35:213–226
- Wang HF (2000) *Theory of linear poroelasticity with applications to geomechanics and hydrogeology*. Princeton Series in Geophysics. Princeton University Press, Princeton, 287 pp
- Wang C-Y, Goodman RE, Sundaram PN (1975) Variations of  $V_p$  and  $V_s$  in granite premonitory to shear rupture and stick-slip sliding: application to earthquake prediction. *Geophys Res Lett* 2:309–311
- Wang H, Haimson BC (1974) Sliding behaviour in faulted rock during pore-pressure cycling. *EOS Trans AGU* 55:1194 (abstract)
- Wang HF, Hart DJ (1993) Experimental error for permeability and specific storage from pulse decay measurements. *Int J Rock Mech Min* 30:1173–1176
- Wang C-Y, Lin W (1974) Velocity ratios for rocks with oriented microcracks. *Nature* 248:579–580
- Wang C-Y, Lin W, Wenk H-R (1975) The effect of water and pressure on velocities of elastic waves in a foliated rock. *J Geophys Res* 80:1065–1069
- Wang C-Y, Mao NH (1979) Shearing of saturated clays in rock joints at high confining pressures. *Geophys Res Lett* 6:825–828
- Wang Z, Nur A (eds) (1992) *Seismic and acoustic velocities in reservoir rocks; vol 2, Theoretical and model studies*. Geophysics Reprint Series, Society of Exploration Geophysicists, Tulsa, Oklahoma, 457 pp
- Wang Z, Nur A (eds) (2000) *Seismic and acoustic velocities in reservoir rocks; vol 3, Recent developments*. Geophysics Reprint Series, Society of Exploration Geophysicists, Tulsa, Oklahoma, 633 pp
- Wardlaw NC (1976) Pore geometry of carbonate rocks as revealed by pore casts and capillary pressure. *Am Assoc Petrol Geol Bull* 60:245–257
- Warren N (1973) Theoretical calculation of the compressibility of porous media. *J Geophys Res* 78:352–362
- Wawersik WR (1971) Stress-strain and fracture behaviour of Westerly granite in biaxial compression. *EOS Trans AGU* 52:346 (abstract)
- Wawersik WR (1973) Time-dependent rock behaviour in uniaxial compression. In: Hardy HR, Stefankor R (eds) *New horizons in rock mechanics*. Proc. 14<sup>th</sup> Symp. Rock Mech., Penn. State Univ. June 1972. *Am Soc Civ Eng*, pp 85–106
- Wawersik WR (1974) Time-dependent behaviour of rock compression. In: *Advances in Rock Mechanics*. Proc. 3<sup>rd</sup> Congr. Int. Soc. Rock Mech., Denver, 1974. Washington, D.C., Nat. Acad. Sci., II, Part A, pp 357–363
- Wawersik WR (1975) Technique and apparatus for strain measurements on rock in constant confining pressure experiments. *Rock Mech* 7:231–241
- Wawersik WR, Brace WF (1971) Post-failure behaviour of a granite and a diabase. *Rock Mech* 3:61–85
- Wawersik WR, Fairhurst C (1970) A study of brittle rock fracture in laboratory compression experiments. *Int J Rock Mech Min* 7:561–575
- Wawersik WR, Swenson CE (1972) Implications of biaxial compression tests on granite and tuff. *EOS Trans AGU* 53:513 (abstract)
- Weaver CW, Paterson MS (1969a) Deformation of cube-oriented MgO crystals under pressure. *J Am Ceram Soc* 52:293–302
- Weaver CW, Paterson MS (1969b) Stress-strain properties of rubber at pressures above the glass transition pressure. *J Polymer Sci A-2* 7:587–592
- Weeks JD, Lockner DA, Byerlee JD (1978) Changes in b-value during movement on cut surfaces in granite. *B Seismol Soc Am* 68:333–341
- Weeks JD, Tullis TE (1985) Frictional sliding of dolomite: a variation in constitutive behavior. *J Geophys Res* 90:7821–7826
- Weertman J (1970) The creep strength of the earth's mantle. *Rev Geophys Space Phys* 8:145–168

- Weertman J (1975) High temperature creep produced by dislocation motion. In: Li JCM, Mukherjee AK (eds) Rate processes in plastic deformation of materials. Proc. John E. Dorn Symp., Oct. 1972. Am Soc Metals, Metals Park, Ohio, pp 315–336
- Weertman J, Weertman JR (1992) Elementary dislocation theory. Oxford University Press, Oxford, 213 pp
- Weibull W (1939) A statistical theory of the strength of materials. Ing Vet Akad, Stockholm, Handlinger No. 151, 45 pp
- Weibull W (1951) A statistical distribution function of wide applicability. J Appl Mech-T ASME 18:293–297
- Weibull W (1952) A survey of “statistical effects” in the field of material failure. Appl Mech Rev 5:449–451
- Weidner DJ (1987) Elastic properties of rocks and minerals. In: Sammis CG, Henyey TL (eds) Methods of experimental physics. Academic Press, Orlando, 24, Part A, Laboratory Measurements, pp 1–30
- Weinbrandt RM, Fatt I (1969) A scanning electron microscope study of the pore structure of sandstone. J Petrol Technol 21:543–548
- Weinbrandt RM, Fatt I (1970) Scanning electron microscope study of the pore structure of sandstone. In: Somerton WH (ed) Rock mechanics – theory and practice. Proc. 11<sup>th</sup> Symp. Rock Mech., Berkeley, 1970. A.I.M.E., New York, pp 629–641
- Wellington SL, Vinegar HJ (1987) X-ray computerized tomography. J Petrol Technol 39:885–898
- Weyl PK (1959) Pressure solution and force of crystallization – a phenomenological theory. J Geophys Res 64:2001–2025
- White JE (1966) Static friction as a source of seismic attenuation. Geophysics 31:333–339
- White JE (1976) Elastic dilatancy, fluid saturation, and earthquake dynamics. Geophys Res Lett 3:747–750
- White SH, Burrows SE, Carreras J, Shaw ND, Humphreys FJ (1980) On mylonites in ductile shear zones. J Struct Geol 2:175–187
- Wibberley CAJ, Petit J-P, Rives T (2000) Micromechanics of shear rupture and the control of normal stress. J Struct Geol 22:411–427
- Wichter L (1979) On the geotechnical properties of a Jurassic clay shale. In: Proc 4<sup>th</sup> Int Congr on Rock Mechanics, Montreux, pp 319–326
- Wiebols GA, Cook NGW (1968) An energy criterion for the strength of rock in polyaxial compression. Int J Rock Mech Min 5:529–549
- Wiebols GA, Jaeger JC, Cook NGW (1972) Rock property tests in a stiff testing machine. In: Gray KE (ed) Basic and applied rock mechanics. Proc. 10<sup>th</sup> Symp. Rock Mech., Austin, Texas, May 1968. A.I.M.E., New York, pp 297–329
- Wiederhorn SM, Bolz LH (1970) Stress corrosion and static fatigue of glass. J Am Ceram Soc 53:543–548
- Wiederhorn SM, Luecke WE, French JD (1995) Importance of cavitation to the creep of structural ceramics. In: Bradt RC, Brookes CA, Roubort JL (eds) Plastic deformation of ceramics. Plenum Press, New York, pp 479–494
- Wiens DA (2001) Seismological constraints on the mechanism of deep earthquakes: temperature dependence of deep earthquake source properties. Phys Earth Planet In 127:145–163
- Wilhelmi B, Somerton WH (1967) Simultaneous measurement of pore and elastic properties of rocks under triaxial stress conditions. J Soc Petrol Eng AIME 7:283–294
- Willard RJ (1969) Scanning electron microscope gives researchers a closer look at rock fractures. Min Eng AIME 21:88–90
- Willard RJ, Hjelmstad KE (1971) Effect of moisture and temperature on the fracture morphology of dacite. Int J Rock Mech Min 8:529–539
- Willard RJ, McWilliams JR (1969) Microstructural techniques in the study of physical properties of rock. Int J Rock Mech Min 6:1–12
- Williams ML (1965) Initiation and growth of viscoelastic fracture. Int J Fract Mech 1:292–310
- Wimmer SA, Karr DG (1996) Compressive failure of microcracked porous brittle solids. Mech Mater 22:265–277
- Winkler KW, Murphy WF (1995) Acoustic velocity and attenuation in porous rocks. In: Ahrens TJ (ed) Rock physics and phase relations. A handbook of physical constants. American Geophysical Union, Washington, D.C., pp 20–34
- Winkler KW, Plona TJ (1982) Technique for measuring ultrasonic velocity and attenuation. J Geophys Res 87:10776–10780
- Wolters R (1971) Beginn der Rissbildung beim Gestein im Triaxialversuch. In: Rock fracture. Proc. Int. Symp. Rock Mech., Nancy, pp Paper I-5 (13 pp)

- Wong T-f (1982a) Effects of temperature and pressure on failure and post-failure behavior of Westerly granite. *Mech Mater* 1:3–17
- Wong T-f (1982b) Micromechanics of faulting in Westerly granite. *Int J Rock Mech Min* 19:49–64
- Wong T-f (1982c) Shear fracture energy of Westerly granite from post-failure behavior. *J Geophys Res* 87:990–1000
- Wong T-f (1985) Geometrical probability approach to the characterization and analysis of microcracking in rocks. *Mech Mater* 4:261–276
- Wong T-f (1986) On the normal stress dependence of the shear fracture energy. In: Das S, Boatwright J, Scholz CH (eds) *Earthquake source mechanics*. American Geophysical Union, Washington, D.C., pp 1–11
- Wong T-f (1990a) Mechanical compaction and the brittle-ductile transition in porous sandstones. In: Knipe RJ, Rutter EH (eds) *Deformation mechanisms, rheology and tectonics*. The Geological Society, London, Special Publication No. 54, pp 111–122
- Wong T-f (1990b) A note on the propagation behavior of a crack nucleated by a dislocation pileup. *J Geophys Res* 95:8639–8646
- Wong T-f, Baud P (1999) Mechanical compaction of porous sandstone. *Oil Gas Sci Technol* 54:715–727
- Wong T-f, Baud P, Klein E (2001) Localized failure modes in a compactant porous rock. *Geophys Res Lett* 28:2521–2524
- Wong T-f, Biegel R (1985) Effects of pressure on the micromechanics of faulting in San Marcos gabbro. *J Struct Geol* 7:737–749
- Wong RHC, Chau KT, Wang P (1996) Microcracking and grain size effect in Yuen Long marble. *Int J Rock Mech Min* 33:479–485
- Wong T-f, David C (1992) Grain crushing and pore collapse as controlling mechanisms for the brittle-ductile transition. *EOS Trans AGU* 515
- Wong T-f, David C, Menéndez B (2004) Mechanical compaction. In: Guéguen Y, Boutéca M (eds) *Mechanics of fluid-saturated rocks*. Elsevier Academic Press, Amsterdam, pp 55–114
- Wong T-f, David C, Zhu W (1997) The transition from brittle faulting to cataclastic flow in porous sandstones: mechanical deformation. *J Geophys Res* 102:3009–3025
- Wong T-f, Fredrich JT, Gwanmesia GD (1989) Crack aperture statistics and pore space fractal geometry of Westerly granite and Rutland quartzite: implications for an elastic contact model of rock compressibility. *J Geophys Res* 94:10267–10278
- Wong T-f, Ko S-c, Olgaard DL (1997) Generation and maintenance of pore pressure excess in a dehydrating system. 2. Theoretical analysis. *J Geophys Res* 102:841–852
- Wong T-f, Szeto H, Zhang J (1992) Effect of loading path and porosity on the failure mode of porous rock. *Appl Mech Rev* 45:281–293
- Wong T-f, Zhao Y (1990) Effects of loadpoint velocity on frictional instability behaviour. *Tectonophysics* 175:177–195
- Wong T-f, Zhu W (1999) Brittle faulting and permeability evolution: hydromechanical measurement, microstructural observation, and network modeling. In: Haneberg WC, Mozley PS, Moore JC, Goodmin LB (eds) *Faults and subsurface fluid flow in the shallow crust*. American Geophysical Union, Washington, D.C., Geophysical Monograph 113, pp 83–99
- Wong T-f, Gu Y, Yanagidani T, Zhao Y (1992) Stabilization of faulting by cumulative slip. In: Evans B, Wong, T-f (eds) *Fault mechanics and transport properties of rocks*. International Geophysics Series. Academic Press, London, pp 119–143
- Wood DM (1990) *Soil behaviour and critical state soil mechanics*. Cambridge University Press, Cambridge, 462 pp
- Woronow A (1975) A new technique for determining the preferred failure angle of brittle rock. *Int J Rock Mech Min* 12:289–293
- Wu XY, Baud P, Wong T-f (2000) Micromechanics of compressive failure and spatial evolution of anisotropic damage in Darley Dale sandstone. *Int J Rock Mech Min* 37:143–160
- Wu B, King MS, Hudson JA (1991) Stress-induced ultrasonic wave velocity anisotropy in a sandstone. *Int J Rock Mech Min* 28:101–107
- Wu FT, Thomsen L (1975) Microfracturing and deformation of Westerly granite under creep condition. *Int J Rock Mech Min* 12:167–173

- Wuerker RG (1956) Annotated tables of strength and elastic properties of rocks. Petrol. Branch, A.I.M.E. (also Trans AIME Petrol. Branch), Paper No. 663-G, pp 22
- Wuerker RG (1959) Influence of stress rate and other factors on strength and elastic properties of rock. In: 3<sup>rd</sup> Symposium on Rock Mechanics. Quart Colo School of Min 54:3–31
- Wulff A-M, Burkhardt H (1997) Mechanisms affecting ultrasonic wave propagation in fluid-containing sandstone under high hydrostatic pressure. *J Geophys Res* 102:3043–3050
- Wulff A-M, Raab S, Huenges E (2000) Alteration of seismic wave properties and fluid permeability in sandstones due to microfracturing. *Phys Chem Earth Pt A* 25:141–147
- Wyllie MRJ, Gregory AR, Gardner GHF (1958) An experimental investigation of factors affecting elastic wave velocities in porous media. *Geophysics* 23:459–493
- Wyllie MRJ, Gregory AR, Gardner LW (1956) Elastic wave velocities in heterogeneous and porous media. *Geophysics* 21:41–70
- Xiao X, Evans B (2003) Shear-enhanced compaction during non-linear viscous creep of porous calcite-quartz aggregates. *Earth Planet Sc Lett* 216:725–740
- Xu S, King MS (1990) Attenuation of elastic waves in a cracked solid. *Geophys J Int* 101:169–180
- Xu X-P, Needleman A (1994) Numerical simulations of fast crack growth in brittle solids. *J Mech Phys Solids* 42:1397–1434
- Yamada T, Takida N, Kagami J, Naoi T (1978) Mechanisms of elastic contact and friction between rough surfaces. *Wear* 48:15–34
- Yanagidani T, Ehara S, Nishizawa O, Kusunose K, Terada M (1985) Localization of dilatancy in Ohshima granite under constant uniaxial stress. *J Geophys Res* 90:6840–6858
- Yao J, Thovert J-F, Adler P-M, Tsakiroglou CD, Burganos VN, Payatakes AC, Moulu J-C, Kalaydjian F (1997) Characterization, reconstruction and transport properties of Vosges sandstones. *Rev I Fr Petrol* 52:3–21
- Yoffe EH (1951) The moving Griffith crack. *Phil Mag* 42:739–750
- Yoshida S, Clint OC, Sammonds PR (1998) Electric potential changes prior to shear failure in dry and saturated rocks. *Geophys Res Lett* 25:1577–1580
- Yoshida H, Horii H (1992) A micromechanics-based model for creep behavior of rock. *Appl Mech Rev* 45:294–303
- Yoshikawa S, Mogi K (1981) A new method for estimation of the crustal stress from cored rock samples: laboratory study in the case of uniaxial compression. *Tectonophysics* 74:323–339
- Yoshioka N, Scholz CH (1989a) Elastic properties of contacting surfaces under normal and shear loads. 1. Theory. *J Geophys Res* 94:17681–17690
- Yoshioka N, Scholz CH (1989b) Elastic properties of contacting surfaces under normal and shear loads. 2. Comparison of theory with experiment. *J Geophys Res* 94:17691–17700
- Youash YY (1966) Experimental deformation of layered rocks. In: Proc. 1<sup>st</sup> Congr. Int. Soc. Rock Mech., Lisbon, 1966, I, pp 787–795
- Yu S-W, Feng X-Q (1995) A micromechanics-based damage model for microcrack-weakened brittle solids. *Mech Mater* 20:59–76
- Yudhbir, Lemanza W, Prinzl F (1983) An empirical failure criterion for rock masses. In: Proceedings of the Fifth Congress of the International Society for Rock Mechanics. A. A. Balkema, Rotterdam, 1, pp B1–B8
- Yukutake H (1989) Fracturing process of granite inferred from measurements of spatial and temporal variations in velocity during triaxial deformations. *J Geophys Res* 94:15639–15651
- Yukutake H, Shimada M (1995) A novel triaxial testing apparatus for deformation, fracture and frictional sliding of rocks at high pressure and temperature. *Int J Rock Mech Min* 32:181–184
- Yumlu M, Ozbay MU (1995) A study of the behaviour of brittle rocks under plane strain and triaxial loading conditions. *Int J Rock Mech Min* 32:725–733
- Yund RA, Blanpied ML, Tullis TE, Weeks JD (1990) Amorphous material in high strain experimental fault gouges. *J Geophys Res* 95:15589–15602
- Zang A, Wagner CF, Dresen G (1996) Acoustic emission, microstructure, and damage model of dry and wet sandstone stressed to failure. *J Geophys Res* 101:17507–17521
- Zang AR, Wagner FC, Stanchits S, Dresen G, Andresen R, Haidekker MA (1998) Source analysis of acoustic emissions in Aue granite cores under symmetric and asymmetric compressive loads. *Geophys Res Int* 135:1113–1130

- Zang A, Wagner FC, Stanchits S, Janssen C, Dresen G (2000) Fracture process zone in granite. *J Geophys Res* 105:23651–23661
- Zbib HM, Aifantis EC (1988) On the structure and width of shear bands. *Scripta Metall Mater* 22:703–708
- Zhang S, Cox SF, Paterson MS (1994) The influence of room temperature deformation on porosity and permeability in calcite aggregates. *J Geophys Res* 99:15761–15775
- Zhang S, Paterson MS, Cox SF (1994) Porosity and permeability evolution during hot isostatic pressing of calcite aggregates. *J Geophys Res* 99:15741–15760
- Zhang S, Tullis TE, Scruggs VJ (1999) Permeability anisotropy and pressure dependency of permeability in experimentally sheared gouge materials. *J Struct Geol* 21:795–806
- Zhang J, Wong T-f, Davis DM (1990a) High-pressure embrittlement and shear-enhanced compaction in Berea sandstone: acoustic emission measurement and microstructural observation. In: Hustrulid WA, Johnson GA (eds) *Rock mechanics contributions and challenges. Proc. 31<sup>st</sup> U.S. Symposium*. A. A. Balkema, Rotterdam, pp 653–660
- Zhang J, Wong T-f, Davis DM (1990b) Micromechanics of pressure-induced grain crushing in porous rocks. *J Geophys Res* 95:341–352
- Zhang J, Wong T-f, Yanagidani T, Davis DM (1990) Pressure-induced microcracking and grain crushing in Berea and Boise sandstones: acoustic emission and quantitative microscopy measurements. *Mech Mater* 9:1–15
- Zhu W, Montesi L, Wong T-f (2002) Effects of stress on the anisotropic development of permeability during mechanical compaction of porous sandstone. In: de Meer S, Drury MR, de Bresser JHP, Pennock GM (eds) *Deformation mechanisms, rheology and tectonics. The Geological Society, London, Special Publication No. 200*, pp 119–136
- Zhu W, Wong T-f (1997) The transition from brittle faulting to cataclastic flow: permeability evolution. *J Geophys Res* 102:3027–3041
- Zimmerman RW (1991) *Compressibility of Sandstones*. Elsevier, Amsterdam, 173 pp
- Zisman WA (1933a) Comparison of the statically and seismologically determined elastic constants of rocks. *P Natl Acad Sci USA* 19:680–686
- Zisman WA (1933b) Compressibility and anisotropy of rocks at and near the earth's surface. *P Natl Acad Sci USA* 19:666–679
- Zisman WA (1933c) Young's modulus and Poisson's ratio with reference to geophysical applications. *P Natl Acad Sci USA* 19:653–665
- Zoback MD, Byerlee JD (1975a) The effect of cyclic differential stress on dilatancy in Westerly granite under uniaxial and triaxial conditions. *J Geophys Res* 80:1526–1530
- Zoback MD, Byerlee JD (1975b) The effect of microcrack dilatancy on the permeability of Westerly granite. *J Geophys Res* 80:752–755
- Zoback MD, Byerlee JD (1975c) Permeability and effective stress. *Bull Am Assoc Petrol Geol* 59:154–158
- Zoback MD, Byerlee JD (1976a) Effect of high-pressure deformation on permeability of Ottawa sand. *Bull Am Assoc Petrol Geol* 60:1531–1542
- Zoback MD, Byerlee JD (1976b) A note on the deformational behaviour and permeability of crushed granite. *Int J Rock Mech Min* 13:291–294
- Zvyagintsev LI, Tomashevskaya IS, Khamidullin YN (1974) Formation of cracked structure in crystalline rocks under the influence of non-uniform pressure (in Russian). *Izvestiya Akad Nauk SSSR, Ser Geol* 3:83–93



---

# Index

## A

accommodation  
  -, intergranular 224, 233  
  -, process 224  
acoustic  
  -, emission 89, 93–97, 113, 220  
  -, activity 95, 97  
  -, amplitude 96  
  -, frequency 95, 96  
  -, location 98  
  -, threshold stress 89  
  -, event 93, 95, 98  
  -, microscope 100  
activation energy 206, 207  
anelastic behaviour 87  
anisotropy 38, 40, 41, 131  
  -, angular relationship 43  
  -, degree of 78  
  -, fabric 136  
anorthosite 214  
anti-extrusion ring 12  
apatite 108  
aplite 73  
area of contact 205, 207  
Arrhenius relationship 206, 265  
asperity 203–205  
  -, contact 205, 208  
  -, height 208  
attenuation 76, 77, 79, 81, 83, 85, 87, 88  
  -, specific factor 87, 88  
axial symmetry 78

## B

barrelling 213  
bifurcation 137, 138, 143, 254, 255  
  -, analysis 138, 139, 141–143, 145, 231, 254, 256  
  -, condition 137

Biot-Willis coefficient 150–152, 154  
biotite 108  
Boltzmann relation 206  
boundary porosity 162, 163  
Bourdon gauge 11  
Brazilian test 19, 30, 31, 36  
brittle  
  -, behaviour 1, 2, 211  
  -, -crystal plastic transition 228  
  -, -ductile transition 18, 66, 157, 211, 213–219, 222, 225–227, 232  
  -, failure 59, 99, 111, 114, 128, 161  
  -, evolution, stage I to IV 112, 113  
  -, experimental 155, 157, 159  
  -, stochastic model 130  
  -, faulting 91, 138, 230  
  -, fracture 17, 29, 45, 59, 70, 211  
  -, local 204  
  -, micromechanics 115  
  -, shape 33, 68  
  -, size effect 30, 68  
  -, weakest link theory 30  
  -, -to-cataclastic transition 226  
bulging 213  
bulk  
  -, modulus 149, 152, 154  
  -, of the fluid 78, 150  
  -, of the material 150  
  -, strain 151  
  -, volume 150  
  -, reference 150  
Byerlee's law 168, 169

## C

calcite 218  
capillary bond 161, 188  
cataclasis 227  
cavity  
  -, elliptical 51

- , elongate 102, 103, 106
  - , equant 103
  - , intragranular equant 103
  - , penny-shaped 52
  - , structure 103
- channel 147
- characteristic distance 188, 259–261, 263, 264
- Charcoal granodiorite 28
- chemical weakening 160
- circular disk 135, 136
- Class I post-peak behaviour 64, 126, 141
- Class II post peak behaviour 64, 107, 126, 141
- cleavage 106
  - , axial 20, 34
  - , plane 39, 40
- closed-crack modification of Griffith theory 56
- coefficient
  - , frictional 183, 184
  - , of friction 25, 53, 54, 117, 120, 124–126, 165, 166, 168–173, 176, 183, 184, 202–204, 206, 257–265
  - , of internal friction 24, 27, 43, 54, 125, 138, 162, 204
  - , of static and kinetic friction 173
- cohesion 24, 41, 54, 125, 162, 168, 251
  - , modulus 243
  - , parameter 143
- compactancy 68, 76
- compaction 68, 76
  - , band 76, 142, 230, 231
  - , inelastic 230
  - , localization 142
  - , shear-enhanced 76, 219, 220, 231
- compatibility of strain 223
- compressibility 104
- compression 214
  - , axis 39, 40
  - , axisymmetric 139–141, 231, 255
  - , cycling uniaxial 66
  - , experiment
    - , triaxial 97
    - , unconfined 97
  - , failure 55
  - , hydrostatic 75
  - , test 10, 18, 112
    - , axisymmetric triaxial 250, 251, 253
    - , triaxial 6, 18, 34, 38, 40, 89, 139, 156, 215, 220
    - , undrained triaxial 159
    - , uniaxial 15, 34, 63, 71
  - , triaxial 39, 67, 72, 141, 212
  - , uniaxial 20, 30, 32, 49, 63, 67, 72, 105, 112
  - , testing machine 7
- conductivity 92
  - , electrical 88, 92, 147
  - , thermal 93
- confining pressure 6, 7, 18, 23–25, 27, 28, 31, 40, 44, 66, 67, 71–73, 82, 84–86, 88, 90, 91, 94, 98, 107–109, 156, 157, 159, 190, 192, 212, 213, 216, 218–220, 228, 229, 233–235
- constitutive 263
  - , law 173
  - , model 137
  - , parameter 139, 144, 145, 183, 184, 229, 258, 259, 261, 263
  - , additional 255
- contact
  - , area 205, 207
  - , average 208
  - , stationery 173, 208
  - , time 175
- continuum
  - , approach 148
  - , mechanics 116, 121, 137
  - , model 132, 228, 229
- coordination number 104
- copper 99
- correlation
  - , coefficient 97
  - , exponent 97
- Coulomb
  - , condition 162, 168
  - , criterion 24, 45, 54, 251
  - , criterion of failure 35, 54
  - , -Mohr criterion 24
  - , -Navier criterion 24
  - , relation 25, 38, 42
  - , stress 42
  - , theory 41, 42
  - , type 201
  - , yield criterion 251, 255
  - , yield function 252
- crack 147
  - , axial 83, 106, 113, 126
  - , bridging 103
  - , circular 81
  - , closed 53
  - , cluster 132
  - , coalescence 108–110, 116, 123, 127, 132
    - , microcrack 137
  - , collinear 126
  - , density 77, 80, 85–87, 102, 130–132
    - , critical 131
    - , equivalent of 123
    - , initial 126
    - , parameter 81
    - , scalar 130

- , tensor 85
  - , distribution 79
  - , edge 240
  - , extensile 114
  - , extension 126
    - , force 243
  - , formation 106
  - , geometry 81
  - , growth 120
    - , index 246
    - , subcritical 133, 244, 245
  - , initial 102
  - , initiation 134
  - , interaction 86, 121–123, 126, 127, 129, 132
  - , intragranular 136
  - , length 47, 121, 128
  - , mathematical 240
  - , modes I, II, III 132, 240
  - , nucleation 117, 127
    - , anisotropic condition 118
    - , length 197
    - , patch 197
    - , zone 197
  - , oblique 85
  - , observation 99
  - , open 50
  - , orientation 77, 78, 80
    - , preferred 77
  - , penny-shaped 118, 126
  - , plane 240
  - , population 77
  - , pore-emanated 134
  - , pre-existing 112
  - , proliferation 115
  - , proliferation model 75
  - , propagation 20, 120, 133, 197, 226
  - , re-opening of 106
  - , resistance 244
    - , energy 243
  - , shape 47
  - , shear 106, 113
  - , sliding 116–121, 123, 125, 126
  - , speed 244, 245
  - , spheroidal 78
  - , stress-induced 120, 131
  - , thin ellipsoid 81
  - , tip 47, 239, 240
    - , radius of curvature 47
  - , transgranular 106
  - , velocity 133
  - , wing 117–121, 123, 126, 127, 129
    - , model 127, 128, 133, 226
- cracking 83
- , intergranular 110
  - , intragranular 136
  - , mode-I 132
  - , mode-II 132
  - , stress-induced 87, 105, 118, 136
  - , transgranular 106
- creep 193, 205, 208
- , behaviour 133
  - , strain 95
    - , rate 208
- critical state condition 228
- crushing of micro-blocks 107
- crystal plasticity 211, 221–223, 228, 232, 233
- cyclic straining 95
- D**
- damage 121, 123, 124, 127, 129
- , critical 131
  - , initial 123–126, 129
  - , mechanics 120, 121, 129
    - , model 125, 127
  - , parameter 123
- debris trail 199
- deformation 137, 213
- , brittle rock 137
  - , cataclastic 222
  - , crystal-plastic 222, 233
  - , elastic 112
  - , macroscopic 222, 223
  - , mechanism 222, 224, 225
    - , intragranular 223
  - , plastic 137
  - , rate 67
    - , unstable 234
- deformational mode field 213
- dehydration 236
- , weakening through 235
- diamond core drilling 12
- differential stress 6, 7, 24, 25, 39, 41, 44, 86, 90, 91, 98, 156, 159, 220
- diffusion 224
- , creep 222, 224
- dilatancy 68–76, 83, 85, 106, 111, 113, 128, 136, 137, 143, 202, 218, 219, 224, 230, 250, 252, 253
- , angle of 252
  - , diffusion model 75
  - , factor 138–140, 144, 230, 253
  - , hardening 159, 236
  - , hysteresis loop 74
  - , microcrack 74
  - , negative 68, 76
  - , onset of 72, 86, 89–91, 115, 117
  - , parameter 138, 229, 231
  - , rate 202

- , volume change 218, 219
  - , inelastic 68
- dilatation 202
- dilation 68
  - , band 141, 142
  - , stress 125
- dislocation
  - , climb 224
  - , flow 223
  - , glide 221, 233
  - , motion 223
- displacement 14, 180
  - , axial 13
  - , sequence 61
- dolomite 22
- double couple 98
- drained test 155, 157, 158
- Drucker-Prager
  - , condition 138
  - , constitutive model 254
  - , criterion 251, 252
  - , type 201
  - , yield function 138, 251
- Drucker's postulate 248
- ductile
  - , behaviour 1, 2, 212, 222
  - , fault 213
  - , field 225
- ductility 157, 211, 212, 214, 216, 217, 222, 233, 234
  - , transition to 216

## E

- earthquake
  - , magnitude 96
  - , mechanism 165
  - , model 182
  - , rupture 176
  - , size-frequency distribution 96
  - , statistics 96
- effective pressure 110, 154, 156, 192, 193
  - , conventional 158
  - , law 172
- effective stress 148, 149, 151, 155, 157, 161
  - , conventional 148, 154, 161–163
  - , defining 148
  - , law 148, 151, 152
  - , mean 151
  - , parameter 151
  - , principal 148
- elastic
  - , change 218
  - , modulus 223
  - , reference line 70

- electric resistance strain gauge 69
- electrical conductivity 88, 92, 147
- electro-osmosis 93
- electron microscope 99
  - , scanning 99, 100, 102, 105, 107, 110
  - , transmission 99
- embrittlement 235, 236
  - , dehydration 235–237
  - , high pressure 233
  - , high temperature 234
- energy
  - , activation 206, 207
  - , elastic strain 46
  - , potential 46
  - , release rate 243, 244
    - , critical 243
  - , surface 46, 243
    - , specific 47, 48
    - , term 48
- evolution
  - , law 259–261, 264
  - , of friction 260
  - , parameter 209
- expansion
  - , differential thermal 236
  - , thermal 104
- extension 214
  - , axisymmetric 139, 255
  - , crack 126
  - , failure 37
  - , fracture 37
  - , test 9, 18
    - , triaxial 18

## F

- fabric anisotropy 136
- failure 25
  - , angle 38, 44, 255
  - , axial splitting 212
  - , brittle 59, 99, 111, 114, 128, 161
    - , experimental 155, 157, 159
    - , stochastic model 130
  - , compression 55
  - , criterion 21
    - , local 47
    - , non-linear 26
  - , critical parameters 239
  - , envelope 124, 129
    - , slope of 23
  - , inelastic 55
  - , mode 141, 142, 227, 230
  - , mode map 142
  - , plane 42

- , shear 19, 25, 55, 156, 165, 213
- , time-dependent 133
- fault 19
  - , ductile 213
  - , gouge 168
  - , zone 168
- faulting
  - , brittle 91, 138, 230
  - , geologic 165
  - , shear 230
- feather fracture 111
- feldspar gouge 207
- flow
  - , cataclastic 138, 222, 224–227, 230, 232
  - , crystal plastic 228, 232
  - , diffusional 211, 224
  - , dislocation 223
  - , granular 211, 222, 227
  - , law 229
  - , plastic 203, 227, 230
  - , rule 137, 247
    - , associated 138, 248, 251, 252
    - , non-associated 138, 252
  - , steady state 89
  - , stress 217
  - , superplastic 225
- fluid
  - , content 150, 151
  - , change 151, 152
  - , incompressible 151
  - , interstitial 157, 160
  - , phase 147
  - , volume 150
- fluorescent dye 99
- focal mechanism 98
- foliation 44
  - , plane 80
- force
  - , axial 7, 13, 14, 64
  - , net 7
  - , chain 201
  - , contact 135, 136
  - , -displacement curve 59–61, 65, 66, 105
    - , complete 62
    - , post-peak 62, 64, 66, 68
    - , pre-peak 62
    - , settling down 62, 111
    - , time effect 66
  - , normal 205
    - , total 162
- fractal geometry 96
- fracture 30, 156
  - , angle 139, 141
  - , axial splitting 18
  - , brittle 17, 29, 45, 59, 70, 211
    - , local 204
    - , micromechanics 115
  - , compressive 22
  - , extension 18, 19, 22
  - , hardening 56
  - , Hertzian 110, 137, 199
  - , internal 19
  - , intrusion 19
  - , mechanics 125, 128, 136, 137, 239
    - , linear elastic 239
  - , plane 98
  - , peak 60, 62, 66
  - , shear 18, 23, 27, 36, 40, 107, 108, 190, 193, 196, 213, 221
  - , slabbing 107
  - , stress 17, 22, 30, 38, 72, 83, 84, 92, 94
    - , brittle 17
  - , surface
    - , artificial 171
    - , energy 243, 245
  - , tensile 128
  - , toughness 128, 243
  - , trail 199
  - , type of 18
- friction 129, 165, 167–169, 257, 265
  - , adhesion model 203
  - , ageing
    - , coefficient 208
    - , effect 208
    - , parameter 209
    - , time 208
  - , angle 170
  - , coefficient 25, 53, 54, 117, 120, 124–126, 165–173, 176, 183, 184, 202–204, 206, 257–265
    - , dynamic 166
    - , effective 203
    - , internal 138
    - , kinetic 166
    - , static 174
  - , constitutive model 257
  - , constitutive parameter 185, 194
  - , correction 14
  - , cutoff time 174, 208
  - , decay
    - , function 187
    - , transient 187
  - , direct effect parameter 185
  - , dynamic 167
  - , experiment 262
  - , fading memory 259, 260
  - , force 166
  - , healing

- , behaviour 175
- , coefficient 175
- , rate 174
- , time-dependent 174, 175
- , hold stage 176
- , internal 41, 143
  - , angle of 251, 252
  - , coefficient 24, 27, 43, 54, 125, 138, 162, 204
  - , parameter 230
- , kinetic 173, 176
- , law 258, 259
  - , displacement-dependent 262
  - , rate- and state-dependent 188, 194, 196, 235, 236, 258, 261–263
  - , velocity-dependent 262
- , moisture 171
- , parameter 184, 207
  - , internal 140
- , patch size 197
- , physical factors 203
  - , Byerlee approach 204
  - , riding over topographic highs 203
  - , welded contact 203
- , rate- and state-dependent 264
  - , dynamic weakening 183
  - , model 173, 183, 186, 197, 205, 257
  - , state variable 183, 187, 258, 259, 261, 263, 264
  - , strengthening 176, 262
  - , time of stationery contact 174
  - , velocity parameter 205, 207
  - , velocity perturbation 184
  - , weakening distance 188, 196, 235, 236
- , slowness law 260, 264
- , static 167, 173–175, 208
  - , coefficient of 166, 173–175, 183, 208, 262
  - , time dependence 173
- , stationery contact 175, 208, 261, 262
- , steady state 176, 180–182, 184, 187, 202, 258, 259, 263–265
  - , sliding 208, 259, 260
- , test 166
  - , slide-hold-slide 175
  - , slider model 262
- frictional
  - , instability 188, 196
  - , resistance 166, 170, 172, 176, 184, 203, 257
  - , sliding 173, 177, 183, 189, 190, 194–196, 199, 200, 203, 205, 208, 262, 263
  - , slip 198
  - , stability 262
  - , strength 168–172, 183, 186, 187, 203, 207, 257, 258, 260
  - , surface 262

## G

- gabbro 91, 167, 190
  - , San Marcos 73, 109, 192
- Gibbs potential 46
- gouge 165, 166, 168, 169, 171, 177, 188, 191, 198, 199, 201, 204
  - , accumulation 190, 191
  - , artificial 191, 199, 200
  - , clay 169
  - , deformation 200, 201, 204
  - , -filled microshear 221, 222
  - , formation 198
  - , indurated 200
  - , layer 165, 175, 180, 186, 191, 200–202
  - , pressure 11
  - , serpentinite 169
  - , simulated 170
- grain
  - , boundary 103, 104, 106, 134, 223, 225
  - , contact 134, 136
  - , crushing 75, 136
  - , deformation 222
  - , radius 136
  - , size 33, 126, 129, 216, 219
    - , reduction 201
- granite 25, 28, 78, 91, 103, 106, 167, 190
  - , Chelmsford 103
  - , crushed 181, 234
  - , Westerly 91
  - , gouge 182
  - , Inada 90
  - , Kitashirakwa 73
  - , matrix 78
  - , surface 180
  - , Westerly 32, 37, 71, 73, 84, 85, 94, 98, 103, 108, 109, 128, 156, 193
- granular flow
  - , microbrittle 224
  - , microplastic 225
- Griffith's
  - , crack model 42, 163
  - , criterion 50–52
  - , formula 47–49
  - , theory 25, 42, 46, 49, 55, 56, 115, 116, 163, 239
    - , modified 32, 53
- Gutenberg-Richter relation 96
- gypsum 235
- H
- Heaton pulse 262
- Hertzian
  - , contact stress 221

- , contact theory 136
  - , fracture 110, 137, 199
  - , solution 135
- hydrostat 75
- hypocentre location 97
- I
- indentation
  - , area of 208
  - , creep 208, 209
- initial microstructure 104
- instability snapping 234
- interaction field theory 132
- intergranular movement 224
- internal friction 41, 143
  - , angle of 251, 252
  - , coefficient of 24, 27, 43, 54, 125, 138, 162, 204
  - , parameter 230
- ion
  - , bombardment 100
  - , -etched surface 103, 106
- ionic strength 172
- J
- jacketing 13
- joint 2
  - , roughness coefficient 170
  - , wall compressive strength 170
- K
- Kaiser effect 95
- kinetic
  - , coefficient 173, 183, 262
  - , friction 173, 176
  - , steady state 175
- kinking 107
- Klinkenberg effect 89
- L
- length
  - , initial 131
  - , uniform 121
  - , -diameter ratio 32, 33, 68
- limestone 22, 213, 215
  - , Solnhofen 73, 214
- linear elasticity 111
- load
  - , -bearing capacity 60, 61
  - , cell 13, 14
  - , differential 7
  - , -displacement behaviour 63, 67
    - , post-failure 65
  - , -displacement curve 112, 214
  - , peak 113
  - , point 175, 261, 262, 264
    - , velocity 263
- loading 83, 115, 139, 240
  - , compressive 20, 36, 94
  - , configuration 144
  - , cycle 73
  - , cyclic test 98
  - , function 229, 247
  - , hydrostatic 75, 90
  - , nonhydrostatic 90
  - , parameter 247
  - , point velocity 263
  - , stage 173
  - , uniaxial 20, 71
  - , -unloading cycle 248
  - , velocity 195
- localization
  - , analysis 138, 141, 142, 144, 228, 231, 256
  - , theory 137, 139, 141, 143, 145, 229
- loosening of the structure 221
- M
- magnesium oxide 220
- magnetite 108
- marble 22, 28, 63, 73, 167, 213, 215
  - , Carrara 212, 218, 230
  - , Tennessee 63, 67
  - , Wombeyan 212
- material stability 248
- microbuckling 107
- microcavity 102–104
- microcline 108
- microcrack 46, 59, 99–102, 104, 108, 109, 113–115, 121, 130–132
  - , axial 107
  - , coalescence 137
  - , dilatancy 74
  - , growing 115
  - , growth 137
  - , initial 102
  - , initial structure 102
  - , interaction 120
  - , location 100
  - , propagation 74, 111, 119
  - , stress-induced 108, 115, 127, 131
- microcracking 59, 69–71, 77, 81, 94, 97, 105–107, 111, 219–221, 226
  - , stress-induced 85, 87, 93, 114, 116
- microfracture 88, 108, 111, 200

- microfracturing 59, 96, 108, 111, 221
- micromechanics 116
- microscope
  - , acoustic 100
  - , laser scanning confocal 101
  - , optical 99, 102, 105
- microseismic activity 93
- microstrain 59
- microstructural change 221
- microstructural parameter 125, 128
- microtomography 101
- microyielding effect 232
- modulus
  - , cohesion 243
  - , elastic 223
  - , hardening 229
  - , incremental 254
- Mohr
  - , circle analysis 204
  - , criterion of failure 35
  - , envelope 24–26, 44, 51, 53, 54, 56, 217
  - , fracture theory 26
- multiple-crack model 131
- muscovite 108
- N**
- norite 63, 72
- normal stress 24, 43, 53, 166, 168–170, 174, 180, 181, 191, 205, 259, 263, 264
  - , effective 172
  - , local 162, 208
  - , total 172
- normality rule 248
- nuclear magnetic resonance 101
- O**
- O-ring seal 12
  - , retaining sleeve 12
- opaque mineral 108
- orientation
  - , dependence 40
  - , preferred 78, 80
- orthoclase 108
- oscillation
  - , chaotic 263
  - , self-sustained 263
- P**
- P wave 80
  - , speed 97
- particle
  - , bridge 201
  - , velocity 193, 194
- peak
  - , force 60, 62, 66
  - , load 113
  - , stress 17, 71, 82, 85–87, 90, 91, 107, 114, 129, 131, 133, 175
  - , unconfined 124
- Peierls stress 226, 232
- percolation
  - , theory 130
  - , threshold 130
- permeability 88–92, 147, 157, 158, 202, 220
  - , evolution 91
  - , hysteresis 89
  - , storage coefficient 152
- phyllite 39
- piston, loading 9
  - , compensating 10
  - , seal 12
- plagioclase 103, 108, 109
- plane
  - , mode 240
  - , of minimum shear strength 42, 43
  - , of shearing 42
  - , of weakness 41
  - , theory 42
- plastic mechanism 211
- plastic potential 229, 247, 248, 252
- plasticity
  - , crystal 211, 221–223, 228, 232, 233
  - , hardening 112
  - , isotropic 138, 143, 144, 247, 255
  - , modulus 138–142, 144
  - , non-isotropic 255
  - , parameter 138, 143, 144, 231, 247, 253, 255
  - , model 137
  - , theory 137, 247
  - , consistency condition 247
- Poisson's ratio 47, 52, 53, 138, 140, 142, 243, 255
- pore 101, 147
  - , collapse 136
  - , connectivity 105
  - , emanated crack 134
  - , fluid 89, 92, 155, 157
  - , content 150
  - , gas 88
  - , moisture content 160
  - , pressure 7, 10, 89, 147, 148, 155, 158, 161
  - , viscosity 157
  - , pressure 90, 91, 148–150, 152, 155–160, 162, 171, 172, 192, 193, 236
  - , adsorptive 161



- , effect 158, 161, 163
- , space 130, 147
- , structure 147
- , throat 147
- , tubular 104
- poroelastic
  - , behaviour 150, 151
  - , constant 150, 152, 153
- poroelasticity 149
- porosity 89–92, 104, 126, 136, 150, 152, 157–159, 163, 216, 224
  - , boundary 162, 163
  - , change 211, 220
  - , double 147
  - , initial 91
  - , rate of change 202
- post-peak
  - , behaviour 60, 61, 63–65, 67
  - , curve 66
  - , force-displacement curve 62, 64, 66, 68
  - , stage 86, 97, 98, 108–110
  - , transition slope 65
- power-law relation 245
- pre-peak
  - , behaviour 59–61, 63, 65, 67
  - , force-displacement curve 62
  - , stage 86, 97, 98
- pressure
  - , confining 6, 7, 18, 23–25, 27, 28, 31, 40, 44, 66, 67, 71–73, 82, 84–86, 88, 90, 91, 94, 98, 107–109, 156, 157, 159, 190, 192, 212, 213, 216, 218–220, 228, 229, 233–235
  - , conventional effective 157
  - , critical 136
  - , effective 110, 154, 156, 192, 193
    - , confining 156
  - , fluid 11
    - , confining 158
  - , gauge 11
  - , hydrostatic 81, 82, 150
  - , normal 168
  - , pore 90, 91, 148–150, 152, 155–160, 162, 171, 172, 192, 193, 236
  - , sensitivity 137, 217, 228–230
    - , parameter 138, 229, 231
  - , solution 224
  - , transition 213, 214, 216, 219
- process zone 49, 243
- propagation 127
  - , direction 77, 78
  - , velocity 245
- pump 11
- punching test 31, 36
- pyroxene 109

## Q

- quartz 103, 108, 109, 182
  - , gouge 181
  - , grain 103
  - , ultrafine 182
- quartzite 22, 63, 72, 102, 167, 189

## R

- Rayleigh wave speed 197, 198
- relative humidity 161
- relaxation 68
  - , test 182
- remanent magnetization 93
- renormalization group
  - , analysis 130
  - , method 131
- representative elementary volume 121
- residual carbon 99
- resistance
  - , frictional 166, 170, 172, 176, 184, 203, 257
  - , to flow 228
- Riedel shear 201
- rock
  - , anisotropic 41, 43
  - , compact 2, 73, 112, 116, 117, 119, 121, 123, 125, 127, 129–131, 133, 153
  - , country 204
  - , crushed 165, 170
  - , dry 77
  - , foliated 39
  - , friction 183, 198, 199, 201, 203, 205, 207, 209
  - , igneous 22, 24
  - , jointed 165
  - , lithified 91
  - , mass 2
  - , material 2
  - , metamorphic 22
  - , porous 2, 73, 75, 114, 115, 134, 136, 147, 149, 153
  - , saturated 80, 92
  - , sedimentary 22
  - , strongly cohesive 134
  - , type 188
  - , weakly cohesive 134–136
  - , wet 80
- roughness 170, 186
  - , surface 167, 168, 170, 171
- Rudnicki and Rice model 252
- rupture
  - , dynamic 196, 197
  - , speed 197, 198
  - , super-shear 198
  - , velocity 193, 194

## S

S wave 80, 83

- sandstone 28, 63, 75, 91, 114, 156, 167
- , Arkose 67
  - , Berea 73, 75, 86, 91, 110, 154, 159, 230
  - , Boise 75
  - , Bunt 73
  - , fine-grained 66
  - , Kayenta 75
  - , quartz 174
- scanning electron microscope 99, 100, 102, 105, 107, 110
- semibrittle mechanism 211
- serpentinite 167, 169, 234
- , antigorite-chrysotile 235
  - , gouge 169
  - , weakening 235, 236
- servo-control 61
- shale 28, 39
- shear
- , apparatus 189
  - , band 97, 107, 110, 111, 116, 138, 139, 142, 145, 201, 255
    - , angle 138–141, 144, 231
  - , conjugate 212
  - , crack 106, 113
  - , -dilatancy effect 74
  - , displacement 64
  - , -enhanced compaction 76, 219, 220, 231
  - , failure 19, 25, 55, 156, 165, 213
    - , single 212
    - , surface 26
  - , force 166, 205
    - , increment 64
  - , fracture 18, 27, 36, 40, 107, 108, 190, 193, 196, 213, 221
    - , energy 196
    - , induced 166
    - , surface 190, 191
  - , localization 110, 116, 132, 137–141, 143–145, 254, 256
  - , macroscopic 149
  - , modulus 138–140, 144, 197, 206, 243
  - , pure 250
  - , Riedel 201
  - , stiffness 197
  - , strain 202
  - , strength 202
  - , stress 43, 65, 166, 168, 173, 196, 240
    - , effective 162
    - , increment 64
    - , local 162, 205
    - , nominal 206

- , total 162
  - , structure 201
  - , test 15, 139
    - , conventional 166
    - , double 166, 167
    - , rotary 166
  - , wave 78, 79
    - , speed 84, 186, 197, 206
    - , splitting 79
    - , zone 201, 213, 221
- shearing
- , deformation 200
  - , force 188
- silicification 104
- single-plane-of-weakness model 41
- Skempton's coefficient 151, 152, 154, 155
- slate 39, 40
- slickenside 165, 200
- sliding 165–167
- , crack 116–121, 123, 125, 126
  - , distance 177
    - , characteristic 259
  - , episodic 193, 195
  - , frictional 173, 177, 183, 189, 190, 194–196, 199, 200, 203, 205, 208, 262, 263
  - , grain-boundary 225
  - , on saw cut 166
  - , process 165
  - , rate 172, 177
  - , regime 192
  - , resistance to 166
  - , speed 173, 176, 177, 181, 183, 184
    - , step change 184
  - , stable 192, 193, 195
  - , steady state 208, 259, 260
  - , surface 165, 173, 175, 183, 188, 196–199, 261
  - , to steady state 176
  - , velocity 177, 181, 186, 202, 206, 207
- slip 223
- , amount of 257
  - , complete 135
  - , direction 223
  - , displacement 177
    - , characteristic 187
  - , distance 177, 185, 187, 197
    - , characteristic 184, 196, 264
    - , critical 183
  - , dodecahedral 233
  - , frictional 198
  - , instability 182
  - , law 259–261, 265
  - , oscillatory test 182
  - , partial 135
  - , phase 193

- , plane 121, 223
- , rate 257, 258, 260, 263, 264
  - , reference 261, 265
- , shear 109
- , system 223, 233
- , velocity 198
  - , reference 258
- , weakening 188
  - , behaviour 65
  - , case 262
  - , curve 196, 257
  - , model 64, 65, 68, 196, 257
  - , rate 197
- source defect 115
- specimen
  - , characteristics 60
  - , -machine system 60
  - , size 31
- splitting, axial 20, 34, 255
- stick-slip 173, 176, 188–194, 195, 257, 262
  - , behaviour 188, 192
  - , cycle 183
  - , cyclic 195, 263
  - , instability 165, 195, 262
  - , limit cycle 194
  - , model 176
  - , oscillation 189, 190
  - , phenomenon 173, 188
  - , sequence 193
  - , spring model 262
  - , stability analysis 194
- stiffness 60, 61, 66, 195, 262
  - , critical 194, 257, 263, 264
  - , elastic 65
    - , tensor 127
  - , shear 197
- strain 14, 71, 212, 213, 218, 223
  - , axial 14, 71, 85, 229
  - , bulk 151
  - , circumferential 71
  - , critical extensile 19
  - , compatibility 233
  - , distortion 240
  - , energy 31
    - , release rate 49, 245
  - , hardening 124, 137, 142, 213, 231
  - , heterogeneity 223
  - , increment 138, 249
  - , inelastic dilatational 71, 131
  - , localization 143
  - , macroscopic infinitesimal 149
  - , maximum extensile 34, 45
    - , criterion 19
  - , natural 14
  - , plane 139
  - , plastic 247, 253
    - , increment 251, 253
    - , shear 253
    - , volumetric 253
  - , rate 27–29, 73, 133, 156, 157, 159, 192, 214, 217, 219, 232
    - , critical 157, 159
    - , initial 208
    - , sensitivity 27, 29, 208, 209
  - , softening 124
  - , tensor 149
  - , test
    - , biaxial 16
    - , uniaxial 15
  - , volumetric 69, 70, 74, 84, 229
- streaming potential 93
- strength
  - , brittle tensile 46
  - , fracture 33
  - , frictional 168–172, 183, 186, 187, 203, 207, 257, 258, 260
  - , interatomic cohesive 48
  - , local 132
  - , residual 165
  - , tensile 56
  - , theoretical cleavage 55
  - , theoretical shear 55
  - , uniaxial compressive 22, 23, 28, 31, 32, 54, 56, 133
  - , uniaxial tensile 22, 23, 50, 52, 56
- stress 14
  - , at yielding 249
  - , axial 20, 72, 228
  - , biaxial 49, 51
    - , principal 50
  - , brittle failure 29
  - , compressive 20, 106
    - , critical 53
  - , concentration factor 126
  - , confining 124
  - , corrosion 95, 133, 244
  - , critical state 228
  - , deviation tensor 249, 250
  - , difference 6, 7, 90, 229
    - , compressional 82
  - , differential 6, 7, 24, 25, 39, 41, 44, 86, 90, 91, 98, 156, 159, 220
  - , distribution 20, 240
    - , elastic 32
  - , drop amplitude 195
  - , effective 148, 149, 151, 155, 157, 161
    - , notion 147
  - , failure 71

- , far-field 228
  - , field 133
  - , frictional 197, 263
  - , increment 94
    - , tangential 144
  - , intensity analysis 239
  - , intensity factor 117, 119, 120, 123, 133, 241, 245
    - , critical 242
  - , intermediate principal 35, 45, 56
  - , lateral 20, 228
  - , loading 197
  - , local 161, 162, 205, 206
    - , normal 162, 208
    - , tensile 50
  - , longitudinal 20
  - , maximum 23, 66, 132
    - , compressive principal 26
    - , compressive direction 83
    - , differential 25
    - , principal 51, 124
    - , principal compressive 43
    - , shear 24, 53
    - , tensile 21, 45
  - , neutral 162
  - , normal 24, 43, 53, 166, 168–170, 174, 180, 181, 191, 205, 259, 263, 264
    - , compressive 51
    - , effective 172
    - , local 162, 208
    - , total 172
  - , partial macroscopic 161
  - , peak 17, 71, 82, 85–87, 90, 91, 107, 114, 129, 131, 133, 175
    - , differential 28, 32, 91
  - , principal 5, 6, 18, 21, 23, 26, 52, 53, 73, 85, 117, 118, 123, 124, 250
    - , deviatoric 255
    - , minimum 124
  - , rate 133
    - , normal 264
  - , shear 43, 65, 166, 168, 173, 196, 240
  - , -strain behaviour 111
  - , -strain curve 62, 94, 106, 112, 139, 143, 212, 213, 217, 218
  - , -strain relationship 229
  - , -strain test 213
  - , tectonic 104
  - , tensile 19, 21, 47, 118, 127, 240
    - , concentration 116–118, 120, 126, 136
  - , tensor 250
    - , deviatoric 253
  - , threshold 73, 74, 94
  - , total macroscopic 148, 149, 161
    - , principal 148
    - , total normal 162
    - , transverse 20
    - , triaxial 5
    - , true 14
      - , triaxial 252
    - , uniaxial tensile 47
      - , yield 82, 220, 227, 228, 250
  - sub-critical crack growth, threshold region 245
  - super-shear rupture speed 197, 198
  - surface
    - , energy 46, 243
    - , specific 47, 48
    - , term 48
    - , finish 190
    - , frictional 262
    - , nominal area 205
    - , roughness 167, 168, 170, 171
    - , sliding 165, 173, 175, 183, 188, 196–199, 261
  - swelling in shales 161
- ## T
- talc 236
  - tangent modulus 141, 254
    - , critical 140
  - temperature 28, 29, 66, 73, 172, 192, 193, 207, 214, 217, 220, 232, 235
    - , -pressure field 217
  - tension
    - , cut-off 45
    - , uniaxial 46, 47
      - , test 15, 19
  - Terzaghi's
    - , effective stress rule 156
    - , principle 148, 215
    - , rule 157, 158
  - testing machine 60, 194
    - , manually controlled 63
    - , servo-controlled 61, 67
    - , stiff 61, 63
    - , stiffness 60, 194
    - , use of mercury 61
  - thermodye 200
  - torsion test 15, 35
  - toughness, fracture 128, 132
    - , normalized 227
  - transducer, acoustic emission 95–97
  - transition
    - , brittle-crystal plastic 228
    - , brittle-ductile 18, 66, 157, 211, 213–219, 222, 225–227, 232
    - , A-type and B-type 225

- , brittle-to-cataclastic 226
- , brittle-to-crystal-plastic 228
- , ductile to brittle 233, 235, 237
- transmission electron microscopy 103, 106
- transport property 88
- Tresca criterion 249
- triaxial
  - , apparatus 190, 193
  - , compression 39, 67, 72, 141, 212
  - , experiment 97
  - , test 6, 18, 34, 38, 40, 89, 139, 156, 215, 220
  - , experiment 65
  - , stress 51
  - , test 5, 51, 84, 166, 228
  - , axisymmetric 250, 251, 253
  - , conventional 37
  - , true 5, 37
  - , undrained 159
  - , testing apparatus 7–11
- triboluminescence 99
- twinning 221, 223

## U

- undrained
  - , condition 152
  - , test 155, 158, 159
- uniaxial
  - , compression 20, 30, 32, 49, 63, 67, 72, 105, 112
  - , test 15, 34, 63, 71
  - , tensile strength 22, 23, 50, 52, 56
  - , tension 46, 47
  - , test 15, 19

## V

- vapour pressure 161
- velocity
  - , elastic wave 85, 86
  - , parameter 205, 207
  - , seismic 76
  - , stepping experiment 258, 260, 261
  - , stepping test 182, 261, 263
  - , strengthening 176, 177, 180, 182, 185, 202, 263
  - , strengthening material 176
  - , weakening 176, 177, 180–182, 195
  - , model 257
- von Mises
  - , criterion 223, 233, 248
  - , failure criterion 36
  - , yield criterion 251

## W

- water-weakening effect 233
- wave
  - , attenuation 87
  - , compressional 85, 88
  - , elastic 76, 87
  - , velocity 79, 86
  - , shear 85, 88
  - , speed 80, 81, 83, 85
  - , anisotropy 77
  - , compressional 78, 82, 84
  - , compressional 77, 86
  - , elastic 76, 77, 81, 86
  - , measurement 84
  - , saturation 80, 87
  - , shear 77, 78, 82, 84, 86
- wear 165, 166, 198
  - , groove 199
  - , ploughing 199
  - , striation 198, 200
  - , track 198, 199
- Weibull parameter 133
- wing crack 117–121, 123, 126, 127, 129
  - , angle 120
  - , array 122
  - , extension 120
  - , length 119, 120
  - , model 127, 128, 133, 226
  - , orientation 119, 120
- work hardening
  - , parameter 143
  - , rate 229
  - , rule 137, 247
  - , term 229

## X

- X-ray computer tomography 101

## Y

- yield
  - , criterion 229, 250
  - , function 229, 247, 250–252
  - , stress 231, 233
  - , surface 144
  - , vertex 254
- Young's modulus 47, 64, 139, 140, 243, 254, 255

## Z

- zircon 108